Durham University

Durham E-Theses

The geochemistry and petrogenesis of the Mull and Morvern Tertiary lava succession, Argyll, Scotland.

Andrew Craig Kerr

How to cite:

Kerr, Andrew Craig (1993) The geochemistry and petrogenesis of the Mull and Morvern Tertiary lava succession, Argyll, Scotland. Doctoral thesis, Durham University.

Use policy

The full-text may be used and/or reproduced, and given to third parties in any format or medium, without prior permission or charge, for personal research or study, educational, or not-for-profit purposes provided that:

- a full bibliographic reference is made to the original source
- a https://etheses.durham.ac.uk/id/eprint/1564/ is made to the metadata record in Durham E-Theses
- the full-text is not changed in any way

The full-text must not be sold in any format or medium without the formal permission of the copyright holders.

Please consult the full Durham E-Theses policy for further details.

Academic Support Office, The Palatine Centre, Durham University, Stockton Road, Durham, DH1 3LE
e-mail: e-theses.admin@durham.ac.uk Tel: +44 0191 334 6107
https://etheses.durham.ac.uk

The copyright of this thesis rests with the author.
No quotation from it should be published without
his prior written consent and information derived
from it should be acknowledged.

The Geochemistry and Petrogenesis of the Mull and Morvern Tertiary Lava Succession, Argyll, Scotland.

By

Andrew Craig Kerr B.Sc. Hons (St. Andrews)

A thesis submitted in partial fulfilment of the
requirements for the degree of
Doctor of Philosophy

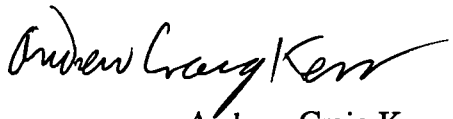
Department of Geological Sciences
University of Durham
September 1993



14 JAN 1994

DECLARATION

I declare that this thesis, which I submit for the degree of Doctor of Philosophy at the University of Durham, is my own work and is not substantially the same as any which has previously been submitted for a degree at this, or any other university.



Andrew Craig Kerr

University of Durham

September 1993

Copyright © 1993 Andrew Craig Kerr

The copyright of this thesis rests with the author. No quotation or data from it should be published without Andrew C. Kerr's written consent, and any information derived from it should be acknowledged.

ABSTRACT

The Geochemistry and Petrogenesis of the Mull and Morvern Tertiary Lava Succession, Argyll, Scotland.

Andrew Craig Kerr, University of Durham 1993

The 840km^2 lava field of the Isle of Mull, Scotland, represents only a small part of the North Atlantic Tertiary Igneous Province. The cause of this igneous activity at approximately 60 Ma, was the arrival and decompression melting of a hot mantle plume. The aim of this study is to gain an insight into the magmatic processes involved in the evolution of the Mull lava succession, through a flow-by-flow study of their geochemistry. 500 lava samples have been analysed from 15 locations across the lava field. Distinctive chemical units of flows have been identified up the succession, and it is possible to correlate these laterally. During the development of the Mull Plateau Group (MPG), the most Mg-rich magmas underwent fractional crystallisation and crustal contamination by acidic Lewisian lower crust, during turbulent ascent through thin dyke- and sill-like magma chambers. In contrast, the more evolved magmas (<8% MgO), which probably fractionated at sub-crustal levels, were not hot enough to assimilate much crust. The MPG lavas become more evolved up the succession culminating in trachytes near the top of Ben More. These seem to have undergone concomitant fractionation and contamination (AFC) at mid-crustal depths. At the base of the succession in several parts of the island, an input to the MPG magmas from a small-fraction-melt derived from the lithospheric mantle, and enriched in the incompatible trace elements, has also been observed. The mostly basal tholeiitic Staffa Magma sub-Type (SMT) lavas, are derived from the same parental magmas as the MPG lavas. However, they have been extensively contaminated with Moine schist during AFC-type processes in *upper* crustal magma chambers. In addition to the MPG, several other magma types are found within the Mull lava succession: the Coire Gorm (CG) magma type, and the later Central Mull Tholeiites (CMT). These owe their chemical differences to processes within the mantle source region. The MPG lavas were probably derived through decompression melting of depleted upwelling mantle in the spinel-garnet lherzolite transition zone. The later tholeiitic lavas are more depleted in the incompatible elements and have flatter heavy rare-earth element (HREE) patterns, reflecting an increasing degree of mantle melting, at shallower (spinel lherzolite) depths, beneath a progressively thinning lithosphere. When lavas free from lithospheric contamination are considered, it can be seen that incompatible element depleted lavas are a feature not only of the British Tertiary Igneous Province, but also of the early Tertiary volcanism *throughout* the North Atlantic region. This strongly suggests that the initial North Atlantic plume had a "depleted" composition.

To my parents

The mountains melt like wax before the Lord,

before the Lord of all the earth.

Psalm 97 v 5

Acknowledgements

I would like to thank my supervisor Bob Thompson, for being brave enough to take me on as his student (despite my eccentricities!), and for his interest and help during the course of this thesis, the financial support of DENI was also greatly appreciated. Thanks must also go to; Henry Emeleus, Sally Gibson and Richard England for numerous discussions on the geology and geochemistry of the British Tertiary Igneous Province; Ian Parkinson (Parky) and Mark Wharton, the geochem "old boys"; Kate Lawson, Sue Loughlin and Sarah Acland, the "new wave" of geochemistry girlies; and Jon (we know a song about that) Freeman, the "centre of geochemical excellence's" latest recruit.

George Randall, Ron Lambert and Julie Harrison are thanked for their production of well over 500 thin and probe sections. Alan Carr and Gerry Dresser ably provided photographic services at various points throughout the course of the thesis. Carol and Lynne, the Departmental secretaries are also to be thanked, as is Dave Asbury for all his help and assistance, and A. Peckett for help with the Durham electron microprobe. Neville Hallam is thanked for his patience with my seemingly endless ability to encounter hitherto unheard of computer problems.

Ron Hardy, well what more can I say, what a star with the XRF and the XRD. Over the last three years Ron has helped the geochemists at to turn the Durham XRF into a force to be reckoned with - cheers Ron!

J. Wills provided technical assistance with the ICP-MS at Royal Holloway. Thanks also to P. Kempton and the staff at the NERC Isotope Geosciences Laboratory, for help with isotopic analyses; Ed Stephens at St. Andrews for allowing me machine time on their wonderful **new** probe, and to Donald Herd for analysing some of my probe sections at St. Andrews.

Jon Seedhouse and Colin Donaldson were lively company in the field on several of my forays to the Isle of Mull. Colin's driving was also quite lively on one occasion! Still, I survived, and their company was much appreciated.

Thanks are also due to; Godfrey Fitton for analysing several of my samples; Ann Morrison for access to her unpublished Mull data, for advice on various interesting locations on Mull, and again analysing several samples; Colin Donaldson for some of his Skye dyke samples, and for reading some parts of my thesis; Brian Upton for his advice on Scottish mantle and crustal xenoliths, and Ray Kent for access to his NATIP database.

My friends at Aidans, James Saunders, Sue Edwards and Troy Meritt are also well deserving of a mention, as are the Ph.D. geologists due to finish this year; Steve Edwards, Jane Keeton, Tim Allsop, Andy Steele, Kate Lawson, Peter Robotham, Paul

Field, Nilpf, Michele McErlean and Guy Spence. Also Gary Ingram, Mikey Curtis, Billy Butler, Zoe Sayer, and Ivan Sansom (I hope his hair falls out, as quickly as mine did!).

A special thank you to Vicky for all her help and support over the last eight months and for preventing me from working *too* hard. The help and support of my very close colleague "John Bole" is also deeply appreciated. It is I think fair to say that without John this thesis would not nave been written!

My parents and grandfather, are thanked for their continued support throughout the course of my education. My sister could never really grasp the finer points of geology, however, her perceptive comment; "The only thing I want to know about rocks, is how far you can throw them!" has strangely stayed with me!

The geochemistry and petrogenesis of the Mull and Morvern Tertiary lava succession, Argyll, Scotland.

Chapter 1 - Introduction		Page
	Aims	1
1.1	Previous work on the Mull Lava Sequence	2
1.2	Tectonic and global setting	7
1.3	The Tertiary Geology of Mull and Morvern	9
Chapter 2 - Field observations and sampling		
2.1	The commencement of Tertiary Volcanic activity	11
2.1.1	Burg	14
2.1.2	Ardtun	16
2.1.3	Malcolm's Point	17
2.1.4	Columnar jointing	17
2.2	The development of the lava succession.	21
2.2.1	Pyroclastics and weathered flow tops	21
2.3	The lava flows	26
2.3.1	Sampling Procedures	26
2.3.2	Lava flow features	30
2.4	Surface weathering and its relationship to geochemistry	35
2.4.1	Platy weathering	35
2.4.2	Pustular, spheroidal and blocky weathering	38
Chapter 3 - Petrography and mineral chemistry.		
3.1	Petrography	39
3.1.1	Mull Plateau Group basalts	39
3.1.2	Mull Plateau Group basaltic-hawaiites	45
3.1.3	Mull Plateau Group hawaiites	48
3.1.4	Mull Plateau Group mugearites	49
3.1.5	Mull Plateau Group benmoreites/trachytes	50
3.1.6	Coire Gorm magma type (CG)	52
3.1.7	Central Mull Tholeiites (CMT)	53
3.1.8	The Staffa Magma sub-Type (SMT)	56
3.2	Mineral Chemistry	56
3.2.1	Olivine	57
	Minor element variation in olivines	57
3.2.2	Clinopyroxene	60

	Minor element variations in pyroxenes	62
3.2.3	Feldspar	66
	Minor element variation in feldspars	69
3.2.4	Oxide minerals	70
	Oxide minerals enclosed in olivines	70
	Oxide minerals within the groundmass	73

Chapter 4 - Petrogenetic processes; magmatic plumbing

4.1	Post-magmatic alteration effects and elemental mobility	75
4.1.1	Factors governing elemental mobility	76
4.1.2	Previous alteration studies	76
	Eastern Iceland	76
	Archean metavolcanics, Abitibi Greenstone Belt, Quebec	77
	Ordovician Cliefden volcanics, New South Wales, Australia	77
	Upper Carboniferous Basalts, New Brunswick, Canada	78
	Oceanic basalts	78
	The influence of rock crystallisation history	78
4.1.3	Trace element mobility within the Mull lava succession	79
4.1.4	Sampling, sample preparation procedures and geochemical interpretation - - in light of the alteration studies.	85
4.1.5	Potential isotopic mobility	85
4.2	Classification of the Mull Plateau Group (MPG) lavas	86
4.3	Fractional crystallisation	90
4.3.1	Basalt to hawaiite	90
	Selection of parental MPG magmas	94
	Modelling of fractional crystallisation	97
	Least squares mass balance calculations	103
4.3.3	Fractionation of evolved lavas (>6.5% total alkalis)	103
	The late differentiates - fractionation processes	106
	The late differentiates - possible crustal contamination processes	110
	Fractionation of the early differentiates	112
4.3.4	Fractional crystallisation - conclusions	117
4.4	The extent and processes of crustal contamination in basic to intermediate MPG lavas	118
4.4.1	Introduction	118
4.4.2	The possible mechanisms of contamination	119
4.4.3	The nature of the crust beneath Mull	121
4.4.4	Contamination of the MPG lavas	122

	Crustal contamination - elemental evidence	127
	Isotopic evidence for crustal contamination	134
4.3.5	Implications for magmatic plumbing systems	140
4.5	Contamination by an enriched small-fraction-melt from the lithospheric mantle	144
4.5.1	Introduction	144
4.5.2	The enriched MPG flows	146
4.5.3	Possible mechanisms of enrichment	149
4.5.3	Wider implications	155

Chapter 5 - The Petrogenesis of the Staffa Magma sub-Type 158

Chapter 6 - Mantle melting, and possible mantle sources

6.1	Introduction	166
6.1.1	Types of mantle melting processes	169
6.1.2	Previous work on mantle melting processes in the BTIP	170
6.2	The magma types of the Mull lava succession	171
6.2.1	The Central Mull Tholeiites	174
6.2.2	The Coire Gorm magma type.	178
6.3	Modelling of mantle melting processes	179
6.3.1	The Mull Plateau Group	179
	Evidence for a melting column beneath Mull	179
	The nature of the mantle source region	185
	Conclusions	191
6.3.2	The Coire Gorm magma type	192
	Major elements	192
	Trace elements	193
	Conclusions	195
6.3.3	The Central Mull Tholeiites	196
	Major elements	196
	Trace elements	196
	Conclusions	198
6.3.4	Modelling conclusions	198
6.4	Comparison with the rest of the NATIP	199
6.4.1	Skye	199
6.4.2	Ulster	201
6.4.3	Faeroe Islands	201

6.4.4 Voring Plateau 202
6.4.5 East Greenland 202
1. Wollaston Foreland / Hold with Hope 202
2. Scoresby Sund 202
3. Blosseville Kyst 203
6.4.6 West Greenland / Baffin Island 203
6.5 Concluding remarks 204

Chapter 7 - Lava sequences and geochemical correlations
7.1 Geochemical correlations 207
Correlation between the primitive crustally contaminated flows 208
Correlations between more evolved (~5-8% MgO) uncontaminated flows 210
Correlation of individual flows 210
7.2 Geochemical variation during the development of the lava succession 210
7.3 Eruptive vents 213
7.4 Conclusions 214

Chapter 8 - Concluding discussion
8.1 Summary 216
8.2 The initial composition of proto-North Atlantic plume . . depleted or what? 219
1. A contribution from depleted lithospheric mantle? 220
2. Interaction with MORB-source upper mantle? 220
3. A depleted plume from the lower mantle? 221
8.2.1 Compositional variation of the North Atlantic plume, with time 221
8.3 Possible future work 222

References cited in the text 223

Appendix 1 - Sample locations and petrographic notes 246

Appendix 2 - Analytical methods and data accuracy
A2.1 Sample preparation 281
A2.2 X-Ray Fluorescence (XRF) 281
Data accuracy and precision 282
A2.3 Inductively Coupled Plasma - Mass Spectrometry (ICP-MS) 284
Data accuracy 284

Comparison with XRF 285
A2.4 Electron microprobe analysis 286
A2.5 Analysis of radiogenic isotopes 287

Appendix 3 - CIPW norms 288

Appendix 4 - Analytical results
A4a - XRF data 301
Mull Plateau Group lavas 302
Staffa Magma sub-Type lavas 325
Coire Gorm type lavas 326
Central Mull Tholeiite lavas 328
Plugs and minor intrusions 329
Skye lavas and dykes 330
Other rocks 331
A4b - ICP-MS data 333
A4c - Radiogenic isotope data 339
A4d - Electron microprobe data 341
Olivines 342
Pyroxenes 347
Feldspars 351
Oxides 356

Publications

KERR, A.C. 1993. Elemental evidence for an enriched small-fraction-melt input into Tertiary Mull basalts. *Journal of the Geological Society; London.* **150,** 763-769.

KERR, A.C. 1993. Current research in the British Tertiary Igneous Province (Conference report). *Journal of the Geological Society; London.* **150,** In press.

Talks

January 1992. Volcanic Studies Group meeting, Lancaster University "The Mull lava succession: a new perspective"

January 1993. Volcanic Studies Group meeting, Open University. "Elemental evidence for an enriched small-fraction-melt input into Tertiary Mull basalts"

May 1993. Current research in the British Tertiary Igneous Province meeting, Durham University. "Crustal assimilation during turbulent magma ascent (ATA); New isotopic evidence from the Mull Tertiary lava succession, N.W. Scotland"

Poster

September 1993. International Association of Volcanology and Chemistry of the Earths Interior, General Assembly, ANU Canberra. "The geochemistry of the Mull Tertiary lavas, Western Scotland; An insight into magmatic plumbing during volcano growth.

Chapter 1

Introduction

The Isle of Mull lies off the west coast of Scotland, about 6 miles west of Oban. The island covers an area of 941 km^2 and, apart from pre-Tertiary lavas and sediments around the coasts and Moine schists and Caledonian granite in the south west, is composed of Tertiary igneous rocks (figure 1.1).

The aims of this Ph.D are basically two-fold;

1.) Flow-by-flow sampling over the entire vertical height of the lava succession. This has chiefly involved the lava sequence from the coast to the top of Ben More (970m asl), in order to assess the nature of the changes in magmatic plumbing and mantle processes during volcano growth.

2.) Collection of samples from different parts of the lava field, in an attempt to try and correlate various sections across the lava succession on a geochemical basis.

1.1 Previous work on the Mull Lava Sequence

The ancient volcanic edifice of Mull has long attracted the curiosity of man, indeed it was the polygonal columns at the base of the Mull lava pile which led the Vikings to name the small adjoining island, Staffa ; 'The Isle of Pillars'.

Many of the early geological observations on the Isle of Mull were made by John MacCulloch in the years 1811-1820. Among his more notable achievements was the discovery of an excellently preserved fossilised tree in the columnar lavas of the cliffs of Burg (NM402278). In 1851, the Mull igneous centre was propelled to the forefront of geological debate with the announcement by the Duke of Argyll of the discovery, at Ardtun (NM379478) of fossilised Tertiary leaves from an interbasaltic sedimentary horizon.

In the latter half of the nineteenth century, discussions over the igneous geology of Mull came to be dominated by two influential geologists; Sir Archibald Gekie and Professor John Judd. The main point of contention between them concerned the mode of eruption of the lavas. Gekie believed that they chiefly ascended and erupted through fissures, which were now represented by the great swarm of Mull Tertiary dykes. He also maintained that preferential eruption along a localised portion of the

UNIV DUNEDIN

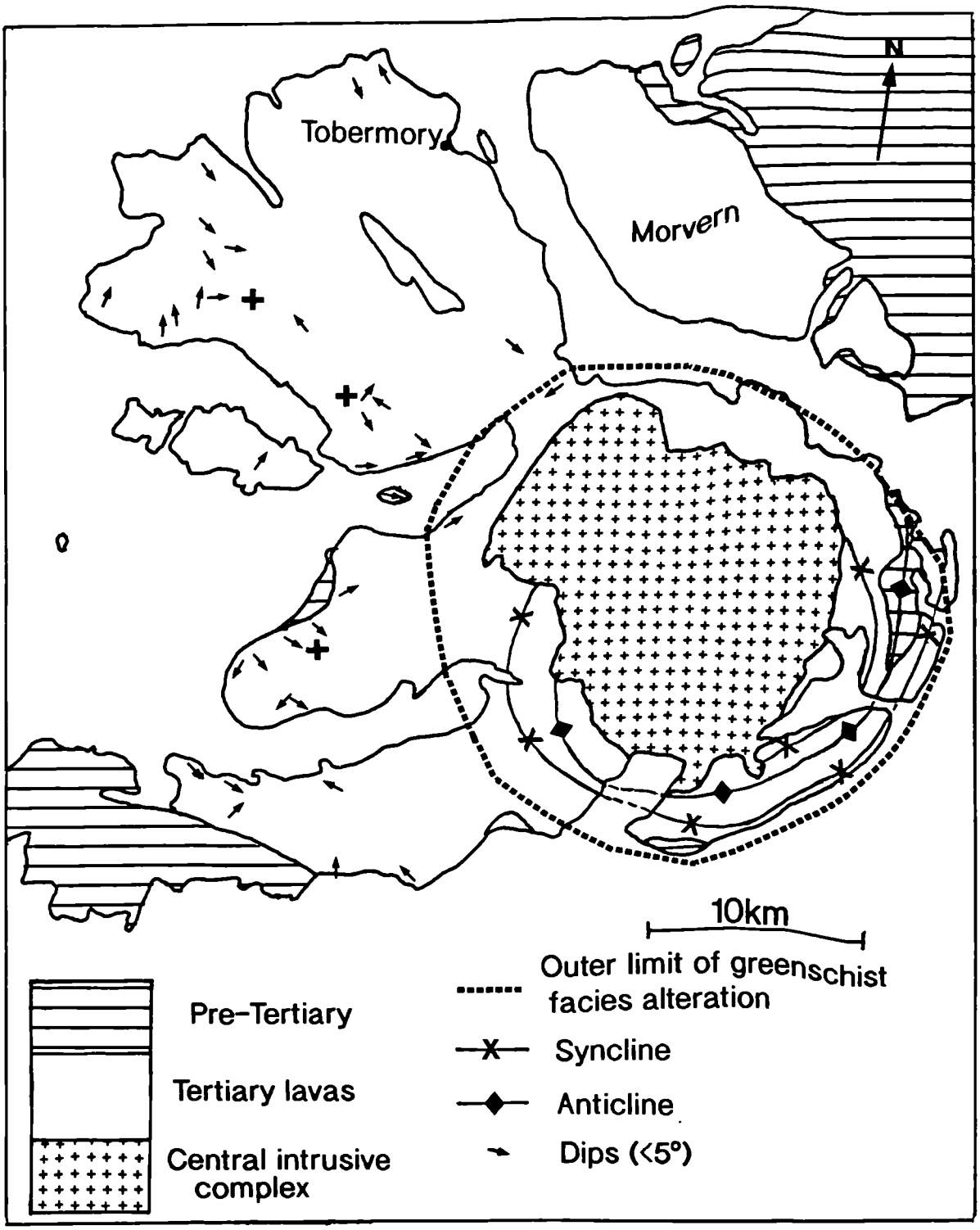


Figure 1.1 The structure of the Mull lava field. Also shown is the outer limit of greenschist-facies alteration, as defined by Walker 1970a.

dyke, could, in time lead to the development of near circular vents (Gekie 1867, 1888).

Judd, on the other hand, asserted that the igneous complexes of Western Scotland (Mull, Skye, Ardnamurchan, Arran and Rhum) were the eroded basal wrecks of Tertiary volcanoes. He doubted the sufficiency of the fissures were to supply the vast pile of Mull lavas and adopted instead the idea that most of the lavas issued from one large central vent with a few parasitic side vents (Judd 1874, 1889).

The publication of the Mull memoir of the Geological Survey of Scotland (Bailey *et al.* 1924) was a milestone in the history of igneous petrology. It established for the first time the concept of **magma types** and **magma series**, based on the igneous rocks of Mull. The two main magma types identified during the study -- the **NON-PORPHYRITIC CENTRAL TYPE (NPC)** and the **PLATEAU TYPE** -- were to dominate petrological thinking in the years to come. The memoir, although quite a lengthy exposition, contains many useful notes and observations. But one of its more astute comments reads as follows: "Individual dykes of the Mull swarm are regarded as a response to regional tension ..... which opened or helped to open fissures" (op. cit., p10). This is hardly a remarkable statement in today's world, however, when one considers that it was made forty years before the concepts of plate-tectonics came to the fore, it becomes quite noteworthy.

For the next forty years a debate raged in petrological circles on the relationship between the NPC (tholeiitic) Type and the Plateau (alkali basalt) Type, and Mull - where the two lava types had first been identified - was to feature prominently in these discussions. Bowen (1928) held to the view that the alkali basalt was the primary Mull magma, from which the tholeiitic type could be produced by differentiation. Kennedy (1933) suggested that one type did not have to be derived from the other, suggesting instead that they could both arise from a common parent, but he did not specify the nature of this parent.

Tilley (1950) compared the Hebridean lava fields with those on Hawaii and concluded that the Alkali Basalt Type was derived from the Tholeiitic Type with differentiation being the dominant process. Wager (1956) in a study of Hawaiian and Hebridean lavas, set forth the view that the basal tholeiitic lavas of the Mull sequence were due to partial melting of a layer of peridotite at quite a high structural level and the overlying alkali basalts were derived by partial melting at a much deeper level. Wager therefore, proposed depth of melting as a critical factor in determining magma type.

Tilley & Muir (1962) attempted to re-assess the normative characteristics of the Mull Plateau Magma type. They noted that most of the available analyses of Mull lavas were of rocks which were mostly hydrothermally altered. They therefore

analysed some unaltered pyroxene and found it to be *Ne* normative. On this basis they proposed that all the Mull Plateau lavas were originally *Ne* normative but that alteration had caused some of them to become *Hy* normative. Fawcett (1961) on the basis of new major element data from the Mull lava succession, tried to distinguish between the tholeiitic and alkalic types, however he found that the analyses spread across the fields of both types. Thompson *et al.* (1972) proposed that the Hebridean Plateau Magma Type - of which Mull forms a part - was both *Ne* and *Hy* normative prior to alteration, ie. transitional in character. It was the nature of this alteration and the extent to which it modified the primary igneous chemistry of the lavas, that was to become important in the following years.

Walker (1970a) mapped five zones of lava amygdale minerals, in Mull and Morvern (figure 1.2). He proposed that the observed secondary mineral assemblage was dependant on the temperature and pressure of the hydrothermal fluids. His work showed that the lowest temperature amygdale infillings were found furthest from the central complex. Forrester and Taylor (1976) similarly demonstrated that the basalts closest to the Mull central intrusive complex were more depleted in $d^{18}O$ than those further away. This change was attributed to $d^{18}O$ exchange associated with the hydrothermal circulation of low $d^{18}O$ meteoric water.

Morrison (1978, 1979) studied the effects of the hydrothermal fluids on the mobility of a wide range of elements as well as Sr and Nd isotopes. In many ways her work has prepared the ground for this present study, because any investigation of igneous petrogenesis requires an intimate knowledge of both the sub-solidus mobility of elements and also which aspects of the chemistry of the lavas retain their original igneous signature. (Morrisons work is described in more detail in section 4.1).

Beckinsale et. al. (1978) in a study of 17 [*sic.*] of the Mull lavas, subdivided them into three groups on the basis of their geochemistry;

Group 1, Alkali basalts;
Group 2, Tholeiitic basalts;
Group 3, Mixtures between groups 1 & 2.

They rejected fractional crystallisation as a major cause of the diversity within each group. They instead advocated varying degrees of partial melting of a "vertically heterogeneous mantle" as the *sole* mechanism to account for the differences between groups one and two.

Morrison *et al.* (1980) and Thompson *et al.* (1982) alternatively, proposed partial melting of a "laterally heterogeneous mantle" below the Hebrides. This process combined with extensive fractional crystallisation and crustal contamination formed the basis of their model.

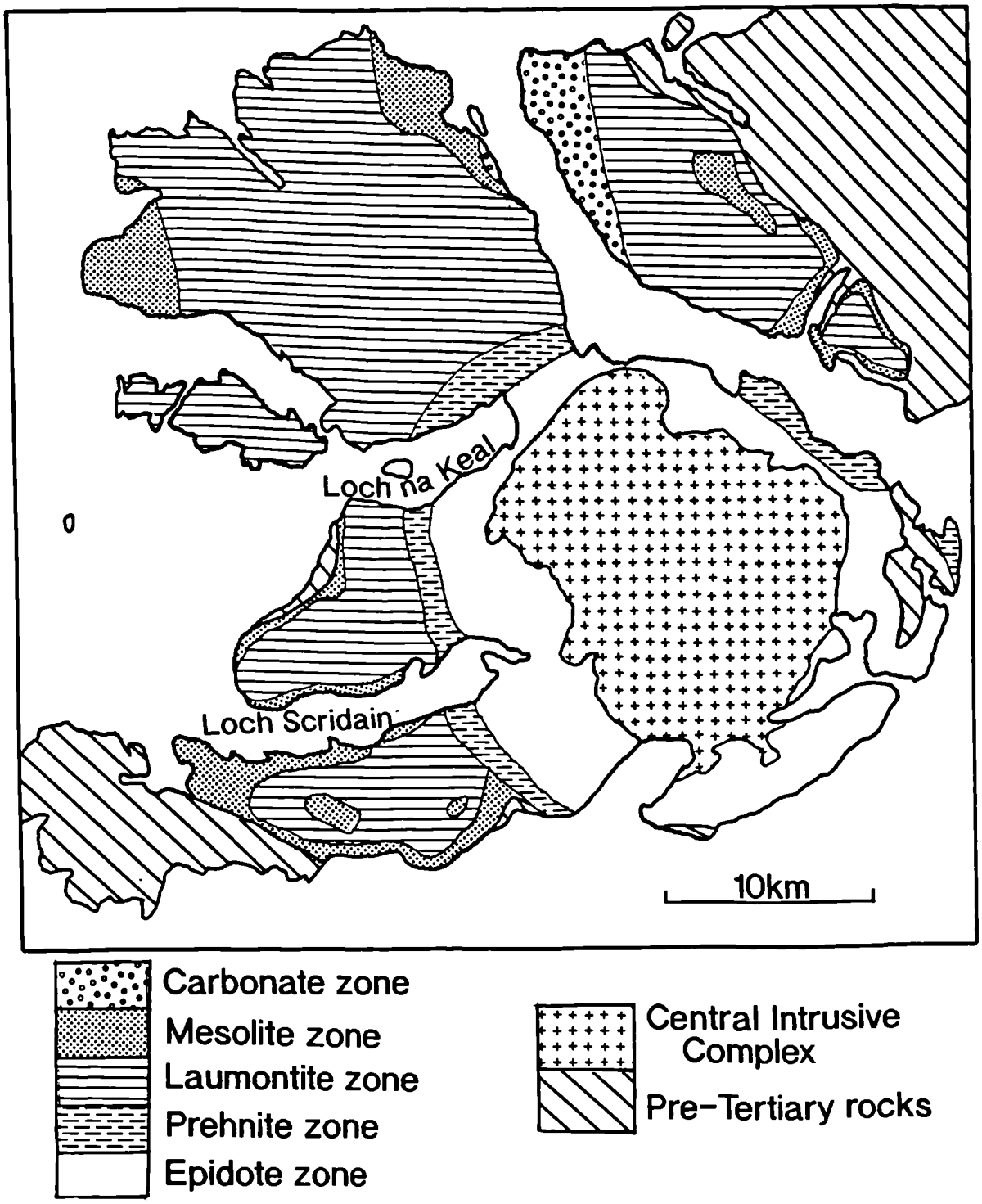


Figure 1.2 The amygdale mineral zones of the Mull lava field (after Walker 1970a), grading outward from the higher temperature epidote zone, closest to the central complex, to the lower temperature mesolite zone, on the periphery of the island.

The relative merits of these two models, along with the most recent work on the geochemistry of the Staffa type lavas at the base of the Mull succession, will be discussed in Chapters 4 & 5.

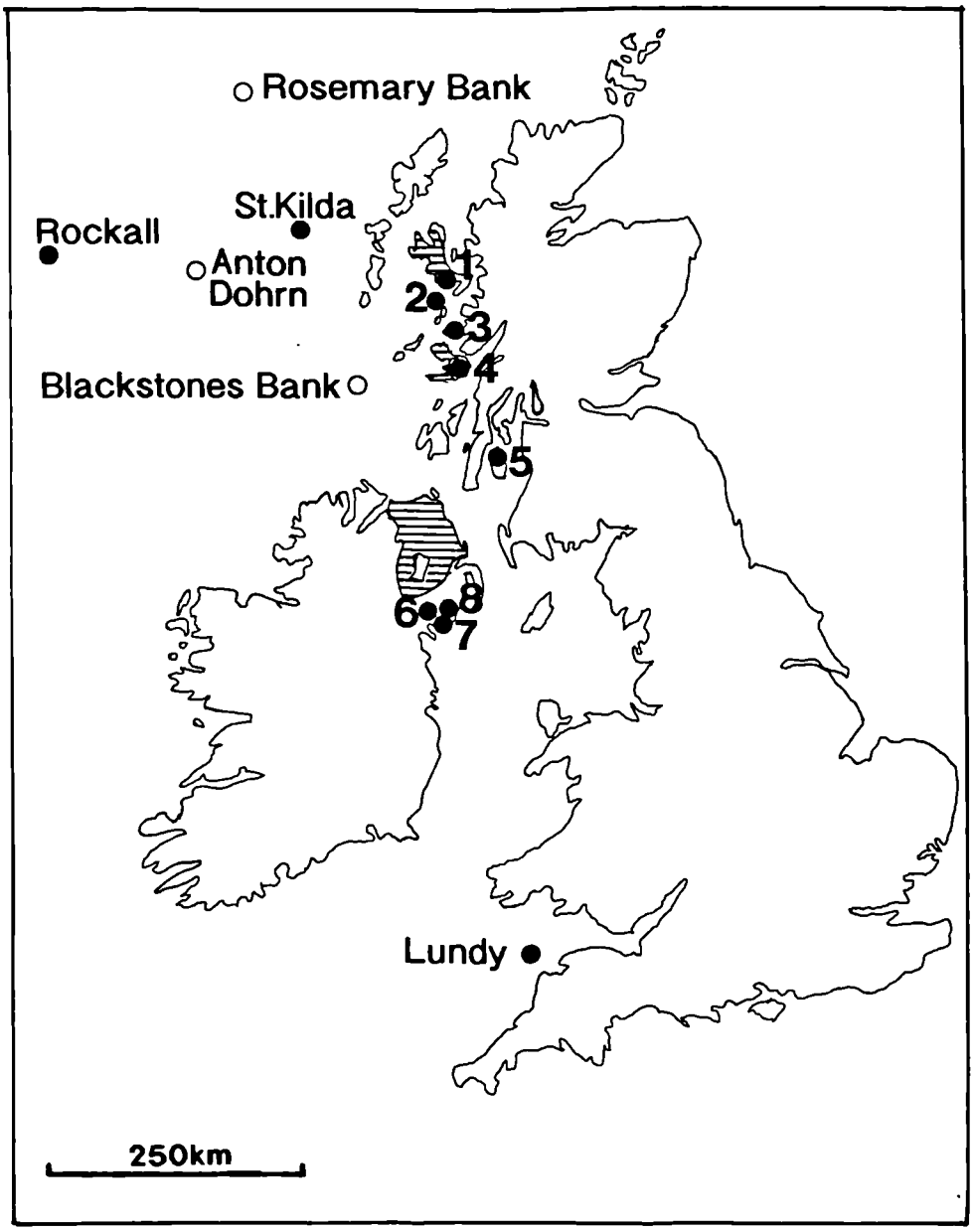


Figure 1.3 The Tertiary Igneous centres of Britain. Hollow circles represent submerged centres, and the horizontal shading shows the main lava fields. [**Key to numbered centres;** 1 - Skye, 2 - Mull, 3 - Rum, 4 - Mull, 5 - Arran, 6 - Slieve Gullion, 7 - Carlingford, 8 - Mourne].

1.2 Tectonic and global setting

The Mull volcanic complex represents only one of a chain of Tertiary igneous centres which lie along the west coast of Britain (figure 1.3).

This British Tertiary Igneous Province (BTIP) forms the eastern portion of the larger North Atlantic Tertiary Igneous Province (NATIP). This province is associated with the initial stages of rifting of the North Atlantic and a pre-drift reconstruction is shown in (figure 1.4). The existence of an Icelandic plume, producing compositionally distinctive melts has long been recognised eg. Schilling (1973) and much recent work has focused attention on the geophysical evidence for such a feature (White 1988; Bott 1988).

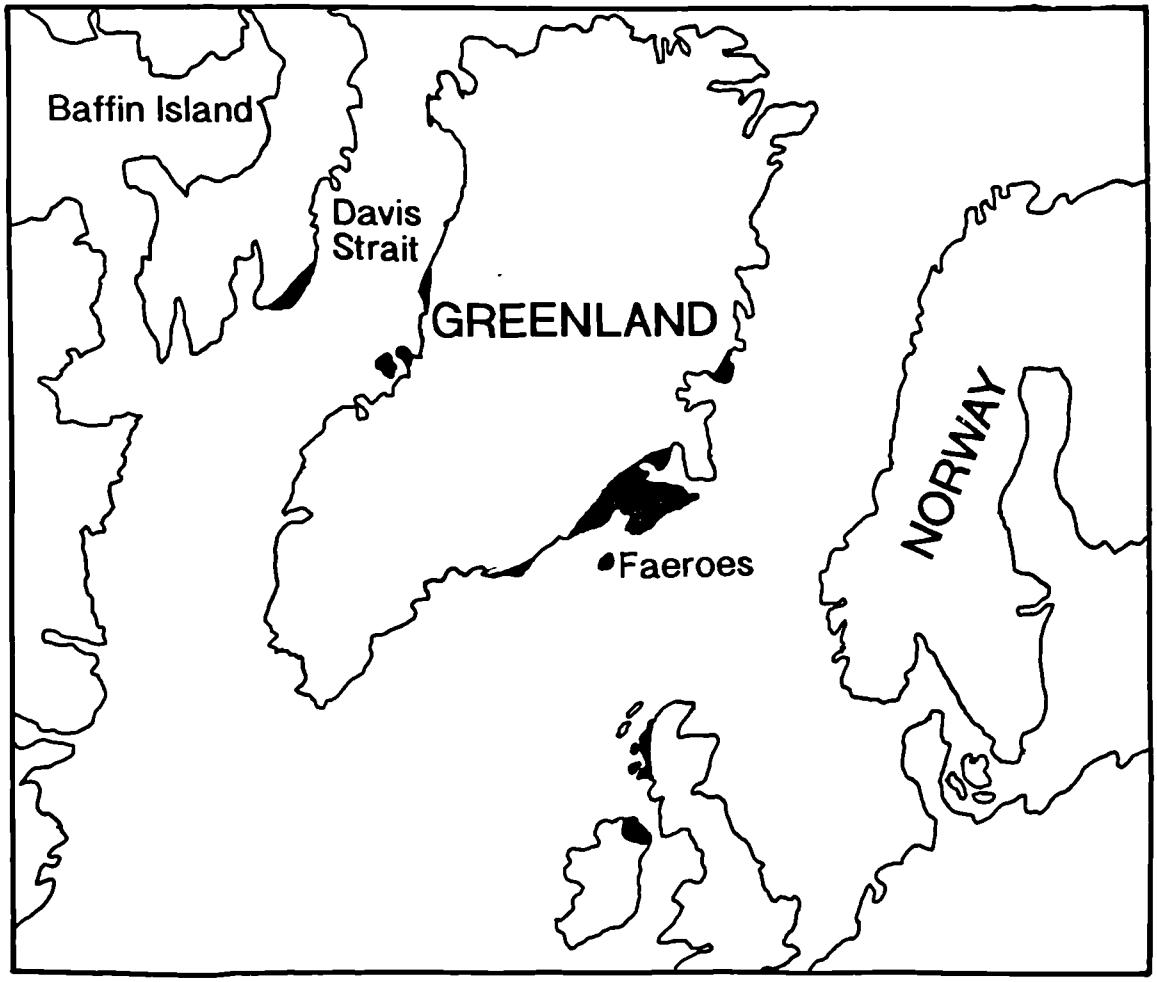


Figure 1.4 Pre-drift reconstruction of the North Atlantic region (ca. 60Ma) after White 1992b. The Tertiary lava fields are shaded in black.

It has been proposed that a narrow (150km diameter; White op.cit) conduit of hot plume material ascended from the core-mantle boundary (Bott op. cit.) and when this

jet of hot material impinged on the base of the lithospheric mantle it spread out laterally, so forming a mushroom shaped head. Prior to the Tertiary, the North Atlantic area had under gone long periods of stretching and basin formation (White 1992a). Part of this involved the propagation of a rift between Greenland and North America, leading to the opening of the Labrador Sea by ~92Ma. However, the arrival of the North Atlantic plume ~60Ma resulted in ridge jumping, and initiation of rifting between Greenland and Europe, (Hill 1991).

Thompson & Gibson (1991) observed a close coincidence between Mesozoic subsiding basins, and the sites of the main lava fields and central intrusive complexes of the BTIP. They proposed that the volcanic centres of the BTIP were focused on pre-existing lithospheric thin-spots, i.e. the sites of Mesozoic basins. It was under these thin-spots that decompression melting of the mantle was greatest. Emeleus (1991) noted that the British Tertiary igneous centres also tended to lie along the line of major faults. Thus the intersection of a Mesozoic basin by a major fault would have been a very favourable location for magma to ascend to the surface, and this has found an expression in the substantial volcanism and intrusive activity, of the BTIP.

On the pre-drift reconstruction map (figure 1.4), West Greenland and the BTIP -- two of the earliest areas in which volcanism occurred -- are 2400km apart. As has been pointed out by Thompson & Gibson (op. cit.) the proposed centre of the plume in East Greenland could not have been displaced very far from this site; otherwise it would have been too great a distance to account for the volcanic activity in either West Greenland or NW Scotland.

The assumptions made so far suppose that the plume ascended from depth in a narrow axisymmetric conduit, impinged on the base of the lithosphere and spread out laterally from this centre. However, volcanism occurs contemporaneously at around 60Ma in East and West Greenland, the Faroes and the BTIP. If the model outlined above is accepted, then one would expect to see the first Tertiary volcanism near the supposed centre of the plume. At the periphery of the plume the first manifestation of igneous activity should be much later, but this is *not* what is observed.

According to White (1992b) plumes of hot material can sometimes take the form of rising sheets, leading to "linear regions of volcanism which would exhibit essentially the same age of volcanism along their lengths". The early Tertiary volcanism in the North Atlantic region occurs in a broad, elongated, elliptical band from W Greenland to the North Sea (figure 1.4) and it may well be that this NW-SE trend can be explained by a sheet of hot material ascending below the region.

1.3 The Tertiary Geology of Mull and Morvern

The Mull Igneous centre (figure 1.1) consists of a central region of later intrusive igneous rocks of both felsic and mafic compositions, of which Bailey *et al.* (1924) commented "Mull includes the most complicated igneous centre as yet accorded detailed examination anywhere in the world" This central intrusive complex is chiefly composed of cone sheets, ring dykes and larger intrusive bodies. Abundant vent and surface agglomerates in this central region contain rhyolitic fragments, indicative of acidic explosive activity, during the later stages of volcano development. Three distinct igneous centres (figure 2.2) have been noted (Skelhorn 1969) and they are the result of a north-westerly migrating focus of intrusion. Associated with these foci of intrusion are two calderas; an early one centred on Beinn Chaisgidle (NM605332) and a later one with its margin delimited by the Loch Ba ring dyke, which is itself the latest major intrusion on Mull.

The rest of Mull, and the adjoining mainland area of Morvern, is chiefly composed of a great pile of basalt, covering an area of 840 km^2. The approximate aggregate thickness of the Mull lava succession is put at about 1800m by Emeleus (1991) but the maximum thickness developed now in any one section around is 1000m on Ben More (NM526331). Over the last 60Ma erosion of the lava succession by the action of ice and water has probably significantly reduced its original thickness. On the basis of amygdale mineral assemblages Walker (1970a) estimated the original total thickness of the succession to be in excess of 2200m.

At the base of the lava pile, mostly in south west Mull, a few columnar flows of tholeiitic composition known as the Staffa Magma sub-Type can be found (Chapter 5). The lava pile is however, for the most part, made up of olivine basalts overlain by the more evolved, so called "Pale Group" of Ben More (Bailey *et al.* 1924). Preserved mostly within the central parts of the island are the fine grained, tholeiitic, so called Non-Porphyritic Central type of lavas, which are interleaved with a magma sub-type, known as the "Porphyritic Central" type, which Bailey *et al.* defined - and identified in the field - by their abundance of plagioclase phenocrysts. However, the division of the central lavas into these two types is not as simple as Bailey *et al.* envisaged and detailed geochemical analysis, of a section of mostly "central type" lavas (samples CA1-20) has revealed that their assumptions were in error (See Chapter 6).

Structurally, the lava pile consists of two parts, Morrison (1979), figure 1.1

a. A peripheral area of gently dipping lavas (<5°) in north and west Mull and Morvern. The lavas dip in varying directions.

b. An area enclosing the intrusive complex in central and south east Mull, where dips are in the range 5-20°. The lavas here have been up-domed by repeated intrusions and as a result arcuate folds have developed.

The intrusion of the central complex supplied heat and fluids to the surrounding lavas and a convective hydrothermal system was established, which resulted in the development of zones of alteration grading outwards with decreasing intensity from the intrusive complex. This led Bailey *et al.* (1924) to delimit a "zone of pneumatolysis" around the complex, inside which no fresh olivine can be found and the amygdales are chiefly infilled with epidote. Outside this zone fresh olivine can be found, with increasing abundance, away from the "zone of pneumatolysis" and amygdales are largely filled with zeolites of varying types. Walker (1970a) noted a zonation outwards of different zeolite minerals and he related this to a lessening of the effect of the hydrothermal alteration, with increasing distance from the intrusive centre (figure 1.2).

Cutting the lava pile is a series of NW trending dykes. These are clearly related to extensional tectonics associated with the opening of the North Atlantic. Speight *et al.* (1982) observed that more dykes occur close to the central complexes. In Mull they calculated the crustal extension, based on aggregate dyke thickness, to be approximately 10%. It has long been held that these dykes represent the consolidated feeders of the lavas, but Beckinsale *et al.* (1978) suggested that pipe-like vents, now represented by plugs, also played a significant role in supplying the lava field.

Mussett (1986) dated various Tertiary igneous rocks from Mull using ^{40}Ar-^{39}Ar techniques. This work revealed that extrusion of the lavas began at 60±0.5 Ma, while igneous activity associated with the central complex, lasted until 57±1 Ma. Dykes appear to have been continually emplaced throughout this 3 Ma. period and indeed the Loch Ba ring dyke - the last major intrusive event - is itself cut by several late basic dykes. Late basic dykes also cut the Beinn Dearg granite on Skye (Thompson and Morrison 1988) which, like the Loch Ba ring dyke, is a late-stage event in the development of the Skye igneous centre.

Chapter 2

Field Observations and sampling.

Sampling of vertical sections on a flow-by-flow basis, has formed the main-stay of the fieldwork. This was because the Ph.D was chiefly concerned with noting and explaining the geochemical changes which occurred as the volcano developed. Consequently no formal mapping of the lava field has been attempted, nevertheless an effort has been made to trace and sample some flows laterally.

In the field, various lava flow features and morphologies have been noted, and it is these observations which form the basis of this chapter. While this is a generalised account, a systematic description of the field occurrences and grid references of all the samples collected and analysed can be found in Appendix 1.

2.1 The commencement of Tertiary Volcanic activity.

The base of the lava succession on Mull is invariably marked by a fine grained, reddened ash, which mostly overlies Mesozoic sediments of varying types. The ash is quite altered, but it does contain some small (3-4mm) angular fragments of quartz. These have probably been derived from the underlying partially silicified Cretaceous chalk. Thin beds of ash can be found at Carsaig (NM534221) Craignure (NM720370) Tobermory (NM505552) and on the shores of Loch Aline in Morvern and, according to Bailey *et al.* (1924), the thickness of this layer of ash rarely exceeds 2m. At Gribun (NM454330) however, 2.5m of basal ash is exposed (plate 2.1), which may suggest the close proximity of an explosive vent.

Some of the first lavas to erupt were of the, Staffa Magma sub-Type[1]. These columnar basalts with their distinctive tholeiitic composition, are a useful marker horizon in the assessment of the pre-eruptive topography. Where the base of the lava pile is at or near sea level, these Staffa sub-type lavas can be found eg. Malcolm's Point (NM500168), Ardtun (NM380249), Burg (NM405270), Ulva Ferry (NM448397) and Bloody Bay (NM493573). No tholeiitic, columnar basalts have been found at the base of the lava section collected in Morvern (NM647545) nor at Gribun, where the lowest lavas overlie Mesozoic sediments 50m above sea level.

[1] The chemistry of this magma sub-type will be reviewed in Chapter 5.

Assuming little post eruptive uplift, these observations are suggestive of an undulating, pre-volcanic topography, with the early lavas ponding in the valleys.

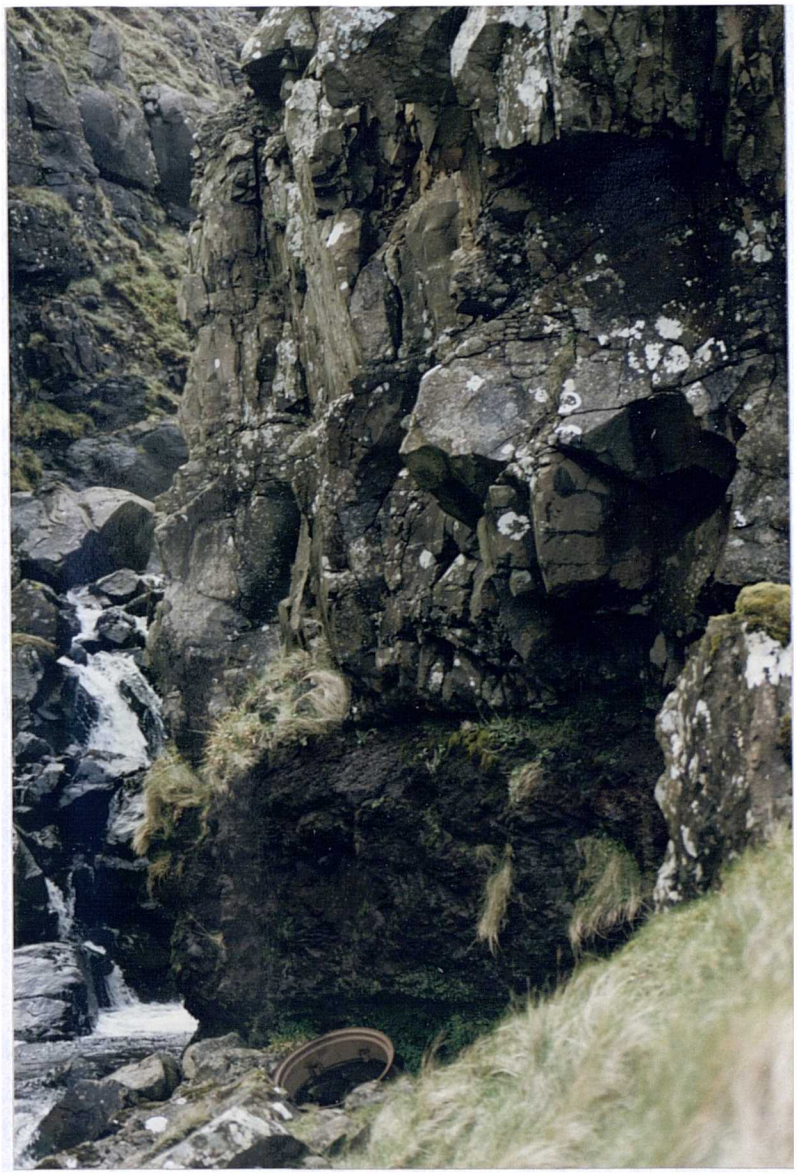


Plate 2.1 The base of the lava succession at Gribun, with a basaltic flow overlying a red/brown bed of ash.

All of the *exposed* basal columnar flows occur around the coast but it is highly likely that unexposed paleo-valleys, with their ponded columnar flows, also exist inland. An excellent localised example of the pre-eruptive topography occurs at Bloody Bay, where some of the early lavas have flowed around a sandstone knoll 15m high and 30m wide (figure 2.1).

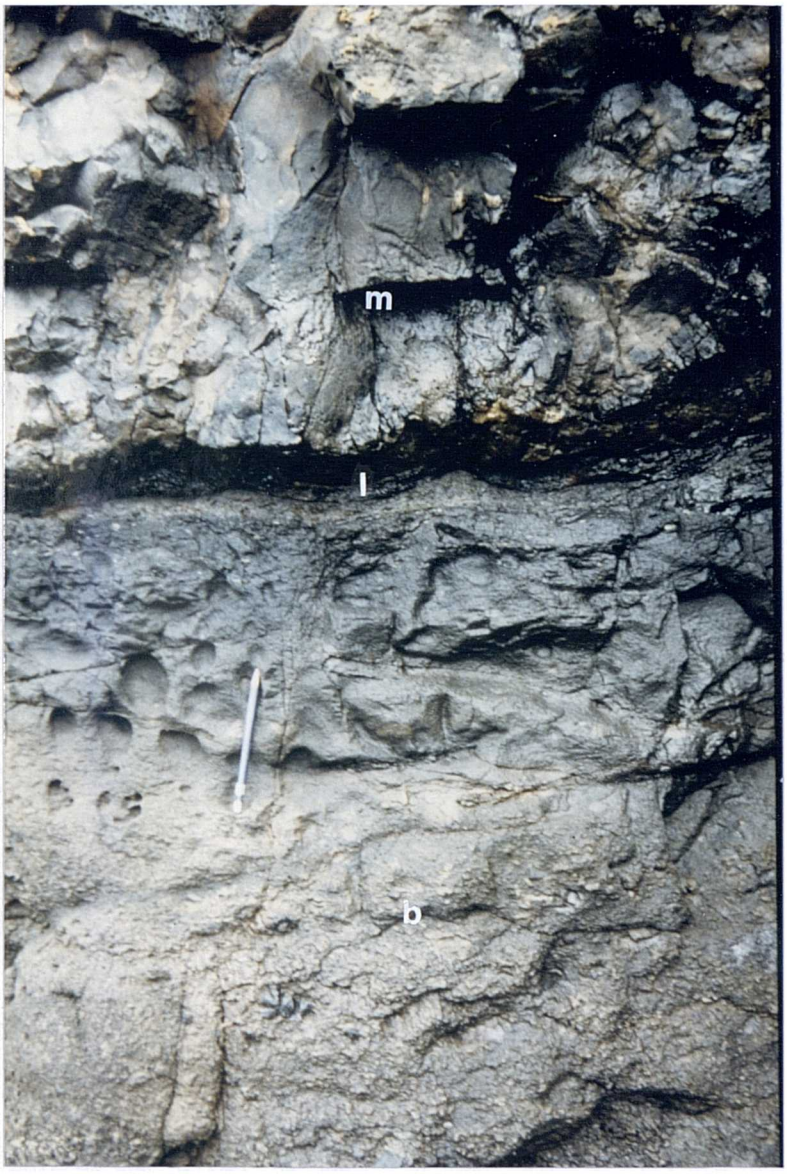


Plate 2.2 A bed of volcanic breccia (b) becoming finer and darker towards its top, and culminating in a thin bed of lignite (l). The basaltic lava overlying these beds is the flow that encloses MacCulloch's tree (m).

A lava is seen filling a valley at (NM403277), several flows above the MacCulloch's tree flow. Along the coast from Carsaig to Malcolm's Point the base of the lavas dip from 100m above sea level at Carsaig, to below sea level near Malcolm's point. The great thickness of some of these early flows, (eg. the lava which encloses MacCulloch's famous fossilised tree) supports this valley filling hypothesis.

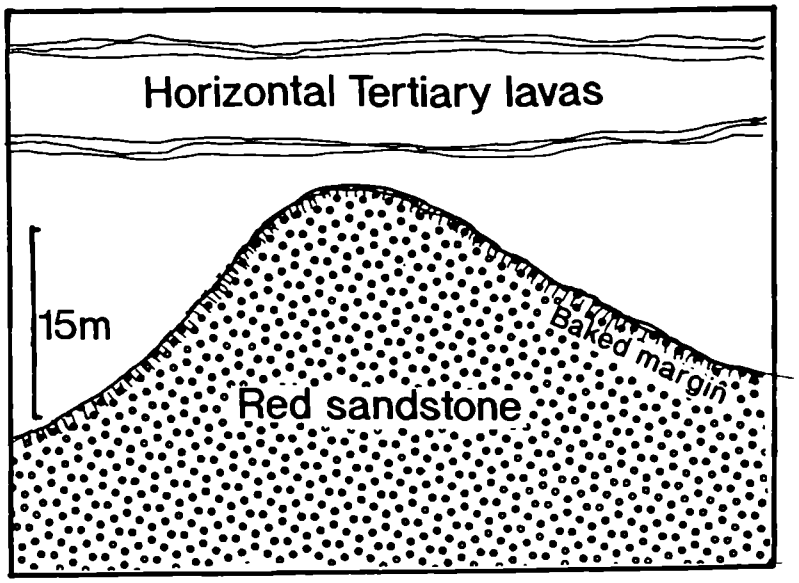


Figure 2.1 A sandstone knoll overlain by horizontal Tertiary lavas, at Bloody Bay (NM477582), after Bailey *et al.* (1924)

Within these paleo-valleys at Burg, Malcolm's Point and Ardtun various types of sediments and pyroclastic debris can be found intercalated with the early lavas and these will be discussed briefly;

2.1.1 Burg

Underlying the thick flow which encloses MacCulloch's tree, a bed of volcanic breccia is exposed, the base of which is below sea-level. It is composed of angular basalt blocks up to 15cm in diameter, along with numerous fragments of wood and other organic material set in fine-grained matrix. The bed gradually becomes finer and darker towards the top, and it culminates in a thin (2-3cm) band of black lignite-like mud (plate 2.2). In places the columns of the overlying flow descend right to its base with the mud (plate 2.3), while in other nearby locations the base of the basalt is quite altered and non-columnar, and ill defined pillow-like structures can be seen (plate 2.4)



Plate 2.3 This shows the columns of the flow enclosing MacCulloch's tree descending right to its basal contact with the underlying breccia.



Plate 2.4 Pillow structures at the base of the MacCulloch's tree flow.

These observations may be interpreted in the following way;

The Burg paleo-valley may have been occupied by a shallow loch or swamp, into which poured or erupted a basaltic flow. The explosive reaction of the water with the molten lava destroyed most of the vegetation (among which were obviously trees) associated with the swamp. This first flow was probably not as voluminous as the overlying flow, and a period of relative quiescence followed this initial explosive phase.

During this phase a thin, black, lignite mud accumulated in the swampy loch. This area of wetland was, however, beginning to dry out. By the time the overlying flow arrived on the scene, parts of the swamp were completely desiccated, and when the lava cooled, columns were able to develop right at its base. Nevertheless, in other places quite deep pools of water still remained, and it was when the same lava poured into these that the pillow structures probably developed.

The earliest Tertiary volcanic activity on Skye similarly consists of dust, ash, lapilli and bombs ejected with explosive force from vents and deposited in shallow lakes. They are closely associated with shales, plant debris and pillow basalts (Anderson and Dunham 1966)

Thin (seldom more than a few centimetres thick) lenticular beds of lignite also occasionally occur, higher up the succession within the main body of the lava field.

2.1.2 Ardtun

At this locality some of Tertiary sediments are exposed between two columnar basalts (Gardiner 1887). They are composed chiefly of gravels with rounded pebbles, along with thinner beds of sandstone, limestones and clay. Associated with these clastic sediments are several intercalations of dark organically-derived material and it is in these beds that fossilised leaves - for which Ardtun became famous - may be found. This sedimentary horizon extends for several kilometres around Ardtun head. It is for the most part 2-3m thick, but locally it is well over 10m thick..

The pebbles in the gravel mentioned above have not been sampled during the present study, but Bailey *et al.* (1924) noted that the clasts were composed of chalk flints (presumably from the Cretaceous), porphyritic augite andesites (which they suggested may be of Old Red Sandstone age), sanidine-felsites of an intrusive origin and Tertiary basalts. Elsewhere in the British Tertiary Province valuable information about directions of river flow, and the relative ages of different Tertiary centres, has been derived from a detailed study of similar inter-lava conglomerates (Emeleus 1973; Meighan *et al.* 1982). A future study of the clasts in the Ardtun gravels may well provide similar useful information.

This whole deposit, including the gravel, sandstones and leaf beds, was interpreted by Bailey *et al.* (op.cit.) as a fluvio-lacustsrine series, and this still seems a very reasonable hypothesis.

2.1.3 Malcolm's Point

A section at this locality (samples C1-10) is exposed as detailed in the stratigraphic succession in table 2.1.

The processes involved in the formation of this sequence are probably similar to those at Ardtun. However, the larger and more angular nature of the fragments, indicates a shorter transport time; the 0.5m diameter boulders would also require transportation by quite a large and powerful torrent of water. The scenario envisaged is one of a loch - developing in a valley which had been blocked by newly erupted lava flows - with typical lake sediments forming on its floor. The deposition of these sediments was interrupted rather abruptly by the dumping of a massive pile of angular and some quite large pieces of debris into the loch. This appears to have been a one-off event and could well be due to a local flash flood, or alternatively the sudden release of water which had perhaps become ponded behind a lava flow or pile of ash.

columnar (tholeiitic) flow, 5m thick. **TOP**
dark shaley, mud, 15cm thick,
breccia, with flint and basalt (tholeiitic, C5) blocks at the base, which are up to 0.5m in diameter (plate 2.5). The clasts become finer towards the top of the bed, (plate 2.6) where it eventually becomes more grit-like with occasional coarser bands. 6-8m thick.
thin, dark, coally, mudstone horizon, 0.5m thick,
5 extremely weathered flows of Mull Plateau Group Basalt, 12-15m thick, **BASE**

Table 2.1 Stratigraphic succession at Malcolm's point (NM501168), Mull.

2.1.4 Columnar Jointing

As has previously been noted, a few of the early flows are tholeiitic basalts with well developed columnar jointing. The thickest development of these columnar flows is at Aird na h-lohaire (NM404289) where 5 flows (samples W2-5) attain an aggregate thickness of approximately 100m.

A very common feature of these basal tholeiitic flows is the tendency for a three-tiered structure to develop. This is comprised of a bottom layer of thick well-formed



Plate 2.5 Flint and basalt blocks up to 0.5m in diameter, set in a matrix of finer material composed of the same type of fragments, at Malcolm's point (NM500168).



Plate 2.6 Showing the same flint and basalt breccia as plate 2.5. The grain size becomes finer towards the top, however, occasional coarser bands of breccia can also be seen.



Plate 2.7 An example of a tiered columnar jointed flow from the Isle of Staffa, composed of a bottom layer of regular well formed columns (the colonnade), and an upper layer of narrower more chaotic columns (the entablature).



Plate 2.8 Columnar jointing in the MacCulloch's tree flow showing regular straight columns at the base giving way to curved columns nearer the top.

columns, known as the *colonnade,* (plates 2.7 & 2.8). These columns often approach 0.5-0.75m across, and project at right angles from the lower cooling surface. They are overlain by a layer of narrower, less regular, often chaotic, but sometimes regularly curved columns, called the *entablature,* (plates 2.7 & 2.8). The columns observed beside the jetty on the Isle of Staffa (NM326351) tend to be regularly curved. The third and top-most layer, is slaggy, vesicular and non-columnar.



Plate 2.9 Close-up view of the sharp junction between the lower colonnade part of the main Staffa flow and the upper entablature (see plate 2.7).

The reason for the development of this three-tier structure probably has much to do with the nature of the cooling surfaces and the fact that columns form at right angles to these cooling surfaces, (Cas and Wright 1987). The lower well formed layer of columns develops as a slow, regular cooling front moves upwards from the base of

the flow. Meanwhile, at the top of the flow, an irregular, front of rapid cooling develops, allowing no time for a columnar structure to develop. Only when the cooling front has advanced significantly downwards into the flow, does the rate of cooling slow down enough to allow small columns to develop. These columns are not usually regular, like those at the base of the flow, because the descending cooling front is much more likely to be of an irregular nature. Therefore columns developing at right angles to this cooling front will also be irregular. Water percolation from the flow surface, down cracks during cooling can also promote the formation of irregular columns (De Graff & Aydin 1987). The two sets of columns ultimately meet and more often than not they form a sharp junction within the flow (plate 2.9).

These columnar flows have vesicles which are infilled with agates and this clearly reflects the tholeiitic character of the host. The abundance of zeolitic infills within the rest of the rest of the Mull lava flows (outside the central region) is likewise indicative of their transitional to alkalic composition. These transitional basaltic flows do sometimes possess a crude type of columnar jointing, but nowhere do they show the well developed columns displayed by the basal tholeiitic lavas on Mull.

2.2 The development of the lava succession.

As has been noted above, the basal columnar flows probably ponded in paleo-valleys and therefore do not have a wide lateral extent. This process of valley filling by the early flows would have soon roughly evened out the topography, so that later flows had the potential to cover a wider area. This potential will of course only be realised if the flows are voluminous enough and have a low viscosity combined with a high extrusion rate (Walker 1970b).

2.2.1 Pyroclastics and weathered flow tops

The chief intercalations found between these later lava flows are red horizons, rarely more than 5cm thick. The post-volcanic weathering on Mull is, however, such that the weathered material falling off the face of each flow tends to obscure its base. As a consequence of this flow junctions and red horizons are not often seen. (The observed occurrences of red horizons or "boles" as they are referred to by Bailey et al (1924) are noted in Appendix 1)

These red boles are usually well exposed in stream sections (eg. flows BM1-12 which are observed in Allt Chreaga Dubah, on the road from Gribun to Loch Scridain, NM469318) or where a small landslip has removed some of the soil covering from the hillside. Although these red boles are commonly less than 5cm

thick, a few are thicker (see table 2.2). Bailey *et al.* (1924) note the occurrence of a red horizon 2.5m thick, on the lower slopes of Beinn Bhuidie (NM383491) "partly made up of rotted lava in situ" (p117), but they do not speculate on the composition of the rest of the bole. This outcrop was not visited by the present author and so the exact nature of this horizon remains in doubt. A thick red horizon - called the "red streak" by the local boatmen - can be seen on the northern cliffs of Ulva, from the boat which sails to Staffa (M.A. Morrison, pers. comm.). An attempt was made to find this exposure but, since the exact location is not known, it met with little success.

Underlying flow	Thickness of red horizon	Grid Reference
BM7	10cm	NM468317
B8	10cm	NM414264
BCH5	20cm	NM408379
BCH9	>25cm	NM413368
BHL35	>40cm	NM451320
BR14	15cm	NM363458

Table 2.2 Showing the locations of red horizons thicker than 10cm.

In the Hebrides these red boles have, for the most part, been interpreted as thin fossil soils resulting from tropical weathering on the surface of basaltic flows (Bailey *et al.* 1924). While in some instances this may be the case, a closer examination of these boles has revealed the presence of fragmental crystals of clinopyroxene and pseudomorphs of zeolite, possibly after feldspar. These are set in a matrix which, although it is very altered and oxidised, preserves - in thin section - a ghost structure reminiscent of streaked-out and bent glass shards. The angular, fragmental nature of the crystals and crystal pseudomorphs, is strongly suggestive of their derivation from an explosive eruption.

Some of the red horizons contain irregular clots of highly altered and zeolitic basalt, up to 10cm in diameter, with a frilly and lobate margin (plate 2.10). These clots of basalt have been noted in two localities during the present study: 1.) above flow BHL35, and 2.) in the lower part of the Beinn Reudle sequence. In both instances, the clots have a chilled, finer grained margin, 1-2mm thick. They contain reasonably well formed pseudomorphs after olivine microphenocrysts and numerous small spheroidal zeolites, which are secondary infills of gas bubbles. Bailey *et al.* (1924) p105 make the following very telling statement ". . . a reddened top is exposed, in which the *amygdales are grouped in bunches,* quite a common arrangement" (my italics). The feature that Bailey *et al.* observed could well have been the clots of

basalt described above. These would have formed with the eruption of a relatively gassy, olivine-rich magma. Such an eruption would have thrown up clots and spatters of molten basalt into the air and the margins of these clots obviously cooled rapidly. The size of these clots strongly suggests that the vent or fissure from which they were erupted was not too far away. These observations lead one to the conclusion that at least some of the thicker boles and perhaps even some thinner ones on Mull are not weathered lava tops - as Bailey *et al.* supposed - rather they represent a pyroclastic tephra deposit.

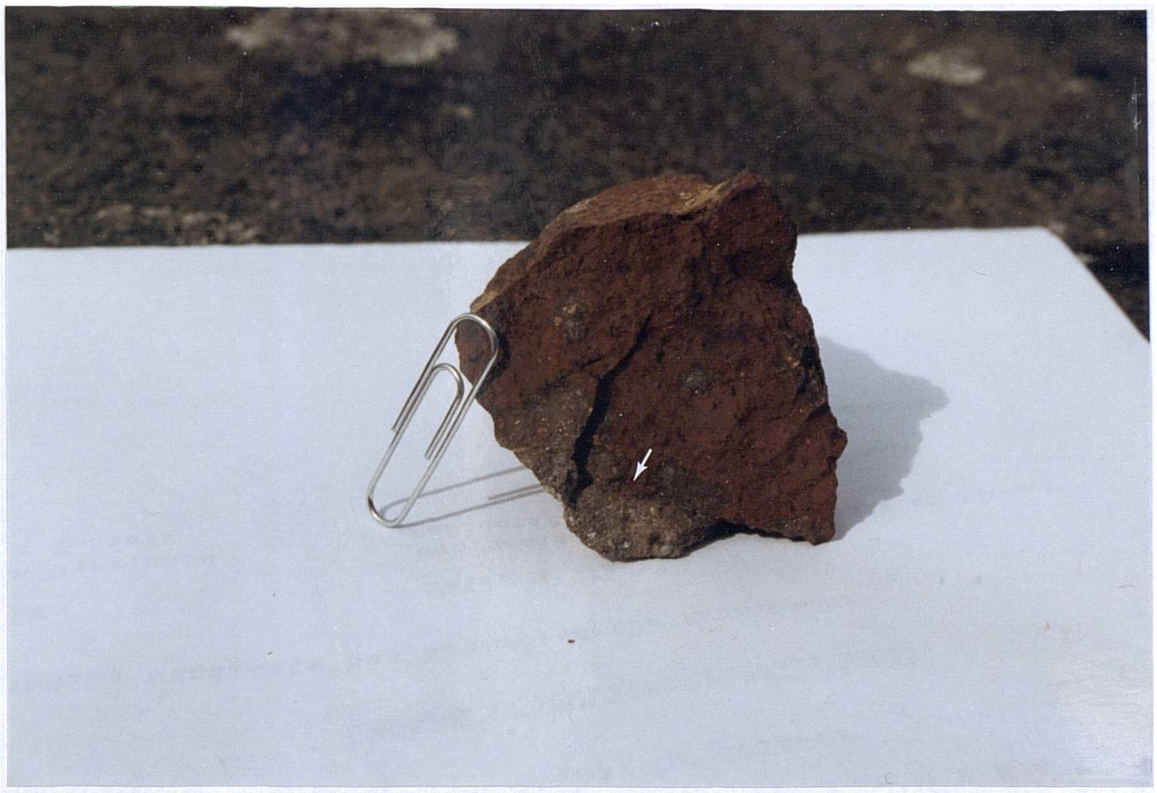


Plate 2.10 Sample of a red horizon containing basalt clots with frilly, lobate margins (arrowed).

It only became apparent to the writer during the later stages of the present study that some of the boles in the Hebrides are in fact of a pyroclastic origin. Because of this the red boles were not assiduously sampled or studied during the initial phase of the project, since they were all assumed to be simply fossil soil horizons. Similar red pyroclastic deposits have also recently been noted in other Hebridean locations; the author and colleagues discovered a red bole, containing both fresh eudhedral crystals and vesicular basalt clots with lobate chilled margins, on the Isle of Skye, within a landslipped block north of Staffin. A pyroclastic deposit has also been found near the base of the lava succession on the Isle of Muck, and again it contains of angular fresh crystals (C.H. Emeleus pers. comm.)

After Bailey *et al.* (1924) most subsequent workers in the area seem to have assumed a weathering origin for the red boles, and indeed the most recent generalised account of the geology of Skye (Bell & Harris 1986) do not even discuss the possibility of a pyroclastic origin. Preston (1981) accedes that, while some boles in the British Tertiary province are undoubtedly formed by surface weathering and mark a distinctive inter-flow interval (eg the thick red, lateritic, Interbasaltic beds so spectacularly visible at the Giants Causeway in North Antrim), others are in sharp contact with the underlying flow and contain fragments of fresh phenocrysts. Preston (op. cit.) concludes that they must be wind-blown dusts, probably the glassy spray from lava fountains. Allwright (1980) proposed that some of the red horizons in the lava successions of Eigg and Muck, were also of a pyroclastic origin.

The recognition of the pyroclastic nature of some of these Hebridean boles has important implications for the development of the lava sequence. If one assumes a solely weathering origin for the boles then each red horizon must represent a reasonably significant time period to allow even for tropical weathering to occur. This need for a significant time gap is, however lessened, if a pyroclastic origin is invoked.

On Mull sharp contacts are not always observed between the bole and the underlying flow, and often one is seen to grade into the other, so implying a weathering origin. There are thus two components of red boles on Mull ie. a component derived from the tropical weathering of a basaltic flow, during a period of volcanic quiescence *and* material of pyroclastic origin, caused by the initial explosive phase of a new eruption. One can immediately see that the possibility exists for the formation of "composite boles" eg. a period of quiescence which allows a weathered red top to develop, followed by a pyroclastic deposit, resulting from the initial explosive phase of a new volcanic eruption. Cas and Wright (1987) note that lavas can often be the terminal event of many explosive eruptions and they cite Mt. St. Helens as an example.

Explosive activity - associated with more silicic eruptions - has been well documented by the early workers in the Hebridean area (Harker 1904; Bailey *et al.* 1924). A red volcanic ash underlies an early, thick mugearitic flow (sample UV2) at Ulva Ferry on Mull. This ash rapidly decreases in thickness away from a nearby plug (samples P10, & 11). This plug is of identical composition to the Ulva ferry mugearite and it is clear that the ash and the lava were in all probability both expelled from this vent. The four trachytes collected from the upper slopes of Ben More (samples BM60-63 in this study) are associated with what Bailey *et al.* (1924) call a "fissile black shale abounding in mugearite [sic] fragments", 1-2ft thick. This occurs

at three localities 6-700m above sea level, according to Bailey's field slips (NM520338, NM525336 and NM532335) plate 2.11.

On the northern face of Ben More (NM520338) the clasts are composed of fine grained, plagioclase-rich fragments up to 10cm in diameter. Some of these are angular, while others seem to have still been molten when erupted. Rounded clasts have also been noted, suggesting that some may have been deposited by water. These clasts, along with individual fragments of larger plagioclases, are set in a highly altered, black, fine grained matrix. Bailey *et al.* (1924) offer little explanation for these exposures, but it seems certain that they are pyroclastic deposits resulting from a build up and violent release of gas from the evolved magmas. The black matrix was probably originally volcanic ash and dust, but since this region lies within the central greenschist-facies alteration zone, its red volcanic ash has been extensively oxidised and altered. Boles within this central region also lose their red colour and commonly turn dark green. This makes their appearance in the field much less conspicuous and, as a result, few boles have been observed within this central zone.



Plate 2.11 Volcanoclastic deposit which occurs below the trachytes on Ben More. It contains both angular and rounded fragments which show a crude alignment, and are set in a fine grained matrix.

Relatively little work has been done on the Central Group of lavas, as defined by Bailey *et al.* (op.cit). These lavas mostly occur with in the central region but Bailey *et al.* also reported their occurrence on the Croggan peninsula (NM705273) and a

section has been collected here (samples CA1-20). A few of these outcrops, which were originally mapped as lava flows, contain some angular fragmental clasts and broken feldspar phenocrysts, visible in thin section (see section 3.1 plate 3.15). Again this feature is not apparent in the field due to the severe hydrothermal alteration of the lavas in this region.

2.3 The lava flows

2.3.1 Sampling Procedures

As has previously been outlined, the chief aim of the fieldwork in this study is to collect - as far as possible - complete vertical sections of lavas on a flow-by-flow basis; that is the collection of every exposed flow on a traverse up a hillside.

Such a study requires good exposure of the lava flows, and the succession on Mull and Morvern is undoubtedly one of the best exposed and thickest British Tertiary lava sequences. It is these two factors which render it ideal for such a study as this.



Plate 2.12 The characteristic terraced appearance of the Mull lava succession, with each terrace usually representing a separate flow. This plate shows the Bearraich section (NM404276 - NM417275)

The lava succession outside the central zone of intense alteration (as defined by Bailey *et al.* (1924) and Walker 1970a) is marked by a very distinctive terraced structure (plate 2.12) which enables individual lava flows to be picked out even though the flow margins are not often observed. This distinctive type of topography is known as "trap" or "step" topography. Having said this, exposure is *not* perfect and sampling gaps in the succession occur were there is a grassy or scree rise with no exposure. These poorly exposed slopes average about 5m thick, and it is possible that another flow could well exist in any one of these gaps. Sometimes, however, a stream can provide an excellent exposure on an otherwise grassy slope between two flows. Likewise a short walk along contour can reveal an exposure of the "missing" flow, such that the sections listed in table 2.3 represent zigzag routes up hillsides to maximise the number of flows collected, as opposed to a straight traverse up the hillside.

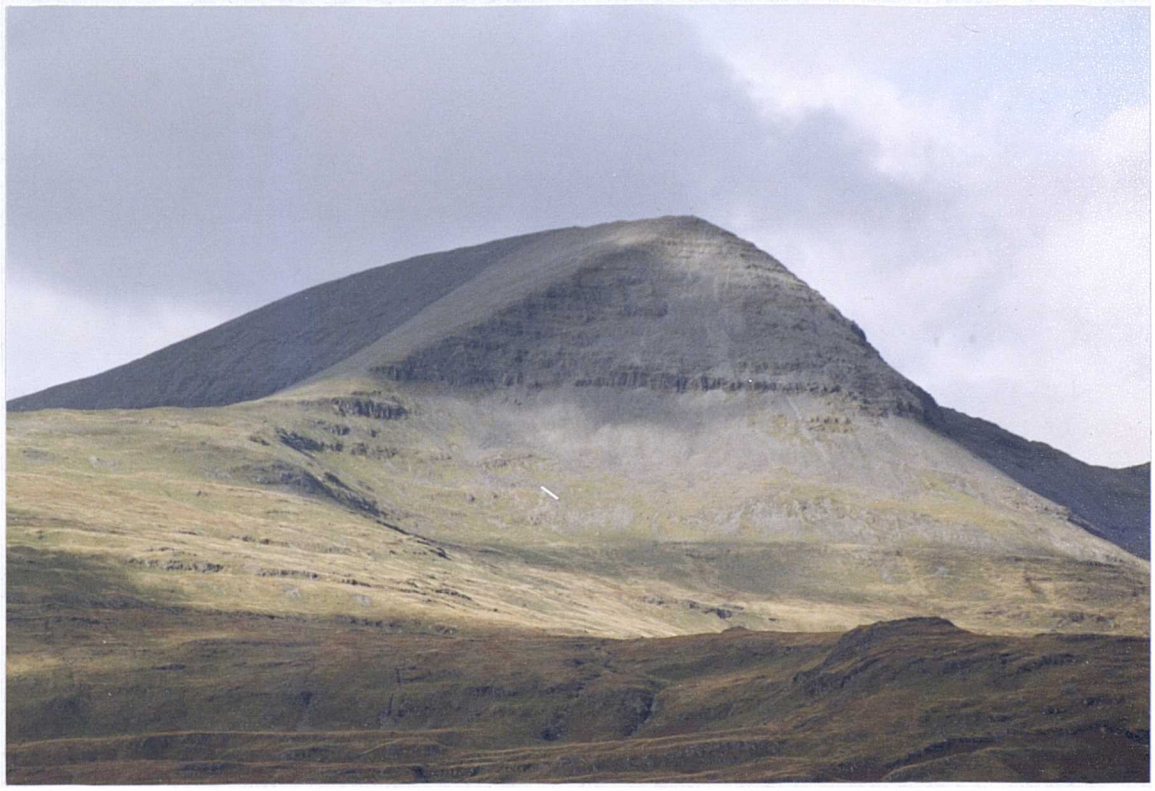


Plate 2.13 A view of the summit of Ben more from the south west, showing the ridge along which samples BM65-89 were collected.

Only two sections have been collected partially or wholly within the central zone of greenschist facies alteration (samples BM37-99 and CA1-20). Within this zone the terraced weathering structure of the lavas is much less pronounced and gives way to a more massive type of weathering, which makes identification and thus sampling of individual flows more difficult. The most troublesome portion of the BM section to

sample were the flows above the evolved lavas (samples BM60-66) and these problems were compounded by the abundance of scree on the top third of the mountain. The best place to collect this portion of the Ben More section was found to be the south-west ridge, where the western face meets sharply with the southern face (NM523323). Here it was relatively easy to pick out individual flows (plate 2.13).

Grid reference	Section name	Abbreviation	Number of samples	Section thickness (m)
NM381249-386232	Ardtun	A	6	20
NM454328-461326	A Mhaol	AM	16	130
NM404276-417275	Bearraich	B	32	430
NM362483-375439	Beinn Bhuidie	BB	25	200
NM412378-404403-411401	Beinn Creagach	BCH	52	310
NM656569-658574	Beinn Ghormaig	BG	8	70-80
NM454328-451320	Beinn na h-Iolaire	BHL	36	300
NM468317-490323-508324-520320-526331	Ben More	BM	100	800
NM363455-363464	Beinn Reudle	BR	33	230
NM501187	Carsaig	C	8	~50
NM699273-696254	Croggan Peninsula	CA	21	~250
NM545420-542413	Killiechronan	K	4	~50
NM644548-636527	Morvern (Sidhean na Raplaich)	MR	41	450
NM493574-484564	Tobermory	T	15	150
NM449397-461311	Ulva Ferry	UV	11	100
NM404284-406285	Wilderness	W	8	70-80
Other lavas	----------	EX/P/STA	17	----------

Table 2.3 Locations of the studied lava successions, sample abbreviations, number of samples collected, and vertical height of the section

A number of lava flows have been traced for several kilometres and samples have been collected at regular intervals along these flows to test intra-flow chemical variation (samples UV2A-F and EBM13A-G). Samples have also been collected

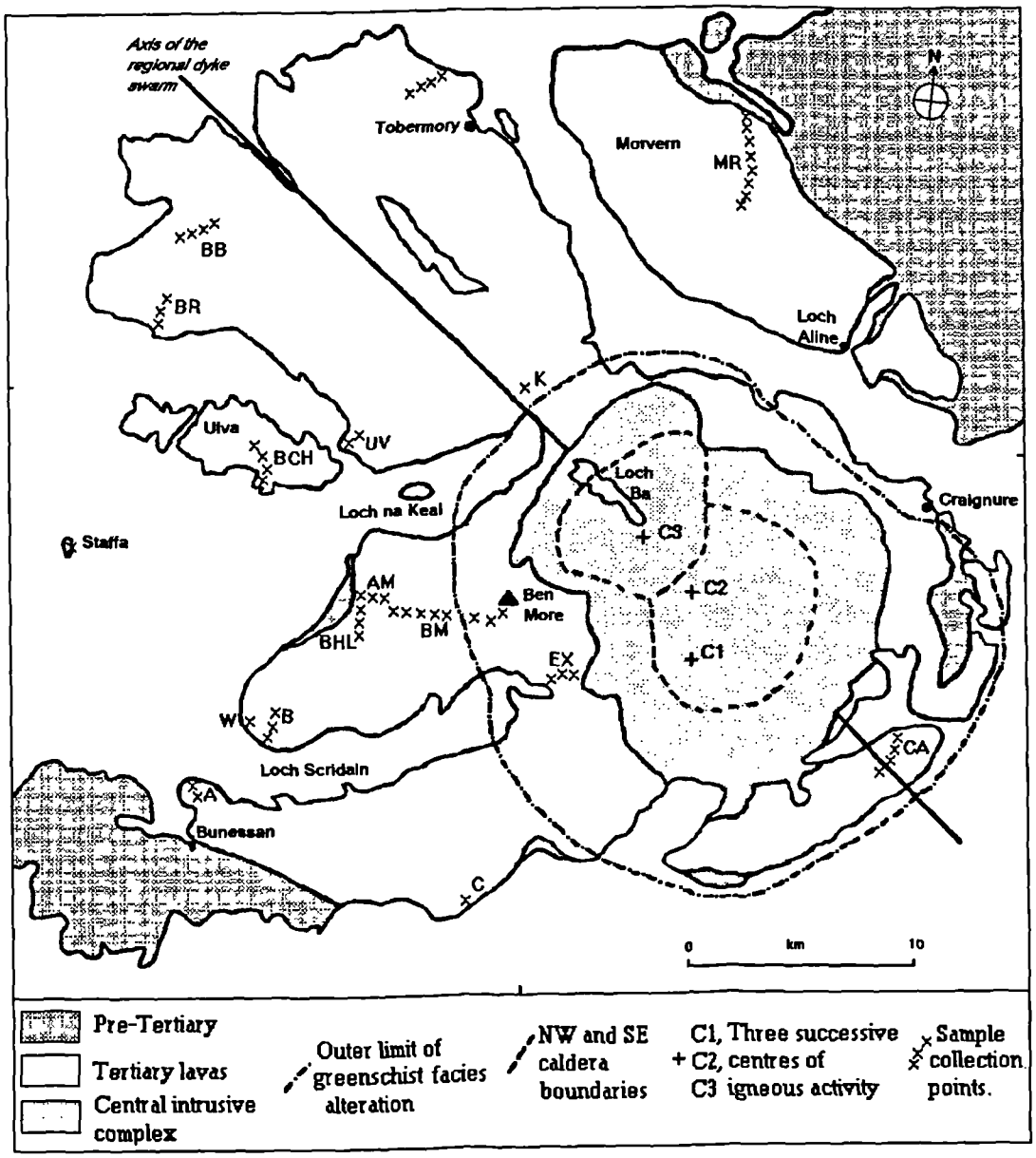


Figure 2.2 Map of the Mull Tertiary lava field showing the locations of the sections studied. For further details see table 2.3 and Appendix 1.

from varying heights within individual flows (AM2 & BM29). These results are presented in Appendix 4a.i. For the most part intra-flow chemical differences are quite small. Samples UV2A-F display quite a marked variation, and it is possible that this may represent several overlapping flows.

Occasional minor faults cut the lava succession, most especially on the Bearraich section (samples B1-30). The down-throw on these faults is seldom more than 5m, and where they have interfered with sample collection their presence has been noted. (Appendix 1)

Figure 2.2 and table 2.3 show the locations of the lava sections collected during the present study. These sections were chosen so as to give as wide a coverage of the lava succession as possible, in order to permit some degree of correlation across the area (Chapter 7). The quality of the exposure and the vertical height of the section were also major factors in choosing sample sites.

2.3.2 Lava flow features

The tops and bottoms of the flows were at one time vesicular but now these vesicles contain numerous secondary alteration minerals; zeolites, outside the central alteration zone, and epidote, albite and calcite within it. Minerals such as these were precipitated by the hydrothermal fluids circulating through the lava pile during the emplacement and cooling of the central complex. These fluids sought out the most permeable horizons along which to migrate, and in the young lava pile these where inevitably the vesicular tops and bottoms of the lava flows. As a result, the vesicular margins of the flows are also the most altered. These altered amygdoidal tops and bases usually enclose a central, generally non-vesicular, and less petrographically altered region of the flow.

Every possible effort was made to try and collect samples from the fresher central portion of the flow. With thin flows this was not always possible and, on a few occasions, quite an amygdoidal sample had to be taken. Several flows encountered during the study were riddled with countless numbers of such amygdales and flows of this type were not sampled. (The locations of such flows are noted in Appendix 1)

As was mentioned in Chapter one, in the areas outside the central greenschist alteration zone the lavas dip gently in varying directions (figure 1.1). These dips may represent the original flow of magma down a hillside, but it is more probable that they are caused by the emplacement of the central complex, or by non-uniform rates of isostatic uplift following the last glacial period.

In a field and petrographic study of the Mull lavas Fawcett (1961), studied, amongst others, the series of flows from the basal ash deposit at Gribun to the top of Beinn na Iolaire (NM452314). A near-identical section was collected during the present study

(Samples BHL1-36). Fawcett claims that the average flow thickness in this section is 80ft (25m) thick but the present author found little evidence to substantiate this claim. Fawcett nowhere defines the criteria which he used to identify flows in the field. In this study, it was assumed that each terrace represented a separate flow and on this basis average flow thickness - in this section - was estimated to be only of the order of 5m.

How valid then was this assumption - based on field observations - given the vast difference in the estimates of flow thickness for this section, between this study and Fawcett (1961)? The argument could well be advanced that several of these terraces, taken together, may well just represent individual flow-units of the same massive flow. An obvious way to assess this proposal is to look at the chemistry of the individual terraces to see if any which overlie each other are identical, so signifying they belong to the same flow. A cursory glance at the geochemical data for the BHL section (Appendix 4.a) reveals that, with the exception of a few pairs of flows, which are *perhaps* units of the same flow (samples BHL17-18, BHL21-22 and BHL35-36) each terrace represents a separate and chemically distinct flow. The average flow thickness encountered during the present study is of the order of 5-7m. I would therefore suggest that Fawcett's conclusions regarding flow thickness on Mull are *seriously* in error..

Bailey *et al.* (1924) noted that the lowest flows on the west side of Loch Aline seemed to thin northwards and be overlapped by upper members of the sequence. A distinct thinning of the flows has also been noted above the four trachytes on Ben More (Appendix 1). Flows which die out laterally are a relatively common phenomenon on Mull, and occasionally the overlying flow is seen to over-step the "nose" of the previous flow, (eg. BCH3 & 4, BCH28 & 29 and MR26 & 27). Occasionally quite thick flows (10-15m) have been found, but they do not have any great lateral extent. These probably were caused by the ponding of magma in surface hollows of the lava field (eg. flow BR6). The ponding of lavas in hollows and valleys has also been reported from the Tertiary lava successions of West-Central Skye (Williamson 1976) and Rum (Emeleus 1985).

As was noted above, the amygdales from without the central zone of alteration are for the most part composed of zeolitic material. According to Walker (1970a) the common minerals are mesolite, thompsonite, analcite and laumontite. These amygdales are usually less than 20mm in diameter, but in once-gassy flows they can be up to 40-50cm long. Fibrous zeolite varieties are most conspicuous in the field and they probably are mesolite or laumontite.

Inside the central zone, the amygdales consist of the higher temperature minerals, prehnite, epidote, feldspar and calcite, along with some high temperature zeolites. A

notable feature of these amygdales is the fact that they are larger than those outside the central alteration zone. This is probably due to more intense hydrothermal activity, promoting rock dissolution (Morrison 1979). These amygdales have a tendency to be elongated parallel to the flow base and some are up to 10cm long.

The larger amygdales are occasionally zoned from green epidote at the margin to zeolitic material in the centre. Such an order of precipitation, from high to lower temperature minerals, reveals the presence of a cooling hydrothermal system (Morrison op.cit.). Within this region thin (up to 5mm) veins often cross cut the flows and they have been observed to "feed" the amygdale pods in places.

Usually the dampness of the ground was sufficient only to promote the formation of a vesicular base to the overlying flow, comprised of sub-spherical vesicles. Occasionally however the surface of the preceding lava flow must have been quite wet, and this has resulted in the formation of brecciated, disrupted flow bases and sometimes pipe vesicles, as jets of steam have tried to escape upwards. These, like their sub-spherical counterparts, have been infilled with zeolitic material (plate 2.14). If the flow is still advancing as the jets of steam rise, then the pipes tend to become stretched in the direction of flow and this can provide a useful indicator of paleo-flow direction.



Plate 2.14 Inclined pipe amygdales at the base of flow BR9.

Good pipe vesicles have been found at several localities on Mull, and they may be anything up to 10cm long. At the base of flows BM29 and AM5 the pipes show no preferred orientation, however in BCH2 they indicate an eastwards paleo-flow direction. Flows BR7-13 are a series of thin (0.5m) vesicular flows, (see below) several of these flows contain inclined pipe amygdales. In flow BR7 the pipes indicate a westwards flow direction, but two flows above this (BR9) the flow direction would seem to be eastwards.

In places groups of vesicles form cone-like structures which can be up to 30cm in length, emanating from the base of the flow. The base of flow B3 (NM404276) shows this feature rather well. These are probably formed by the action of steam shooting rapidly upwards from the wet ground over which the flow had passed. Similar gas pipes have also been noted from the Tertiary lava field in East Greenland (Larsen *et al.* 1989).

Groups of amygdales can also form distinct bands within individual flows (plate 2.15; BCH23) these bands are up to 15cm thick and alternate with more massive bands of lava. They tend to be parallel to the base of the flow and are therefore probably related to the initial flow regime of the molten magma.

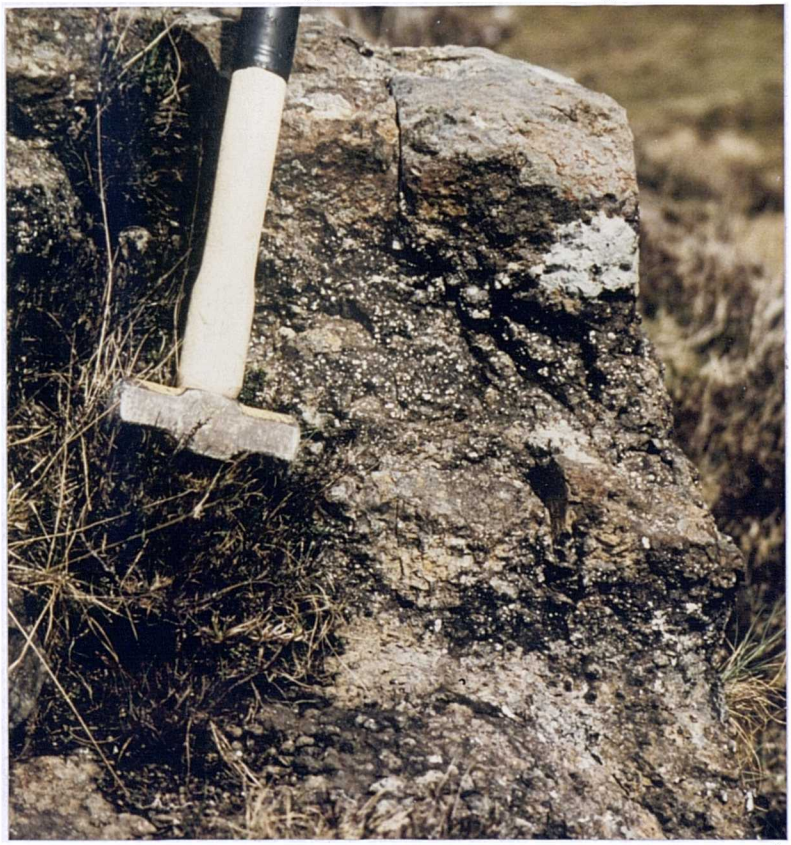


Plate 2.15 Flow BCH23 with bands of amygdaloidal basalt, between layers of more massive, amygdale-free lava

Walker (1970b) sub-divided the lavas into two types depending on whether they were *simple* (ie. not divisible into distinct flow units) or *compound* (ie. they contained distinct flow units). Walker maintained that the type of flow which formed was critically dependant on the extrusion rate of the magma, with simple flows forming when the extrusion rate is high, and compound flows when the rate is low. The banded amygdaloidal flows on Mull obviously belong to the latter category and were probably formed when tongues of lava from the same flow built up on top of one another due to a low extrusion rate. The relationship to *pahoehoe* and *aa* lava types and viscosity is summarised in figure 2.3. Since most of the flows on Mull are, a/ simple flows and b/ low-viscosity basalts, it would seem that the extrusion rate for individual flows must have been quite high.

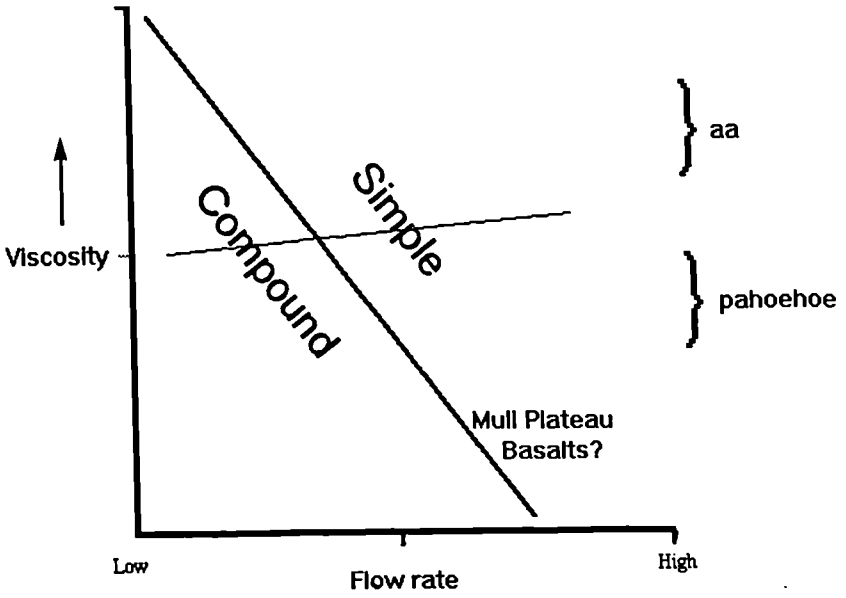


Figure 2.3 The relationship between lava viscosity and flow rate, showing how these two variables influence the morphology of the lava flow (after Walker 1970b). The possible position of the Mull Tertiary basalts is also shown on this diagram.

The series of thin flows mentioned above (BR7-13) are quite amygdoidal (therefore they were originally quite frothy) and altered and several of the available flows were not sampled, simply because they were too altered. These flows are quite olivine rich, each has a distinctive chemistry and more often than not they are separated by a thin red bole. One of these flows (BR11) is composed of small pahoehoe toes each 5-10cm thick.

2.4 Surface weathering and its relationship to geochemistry

In an ancient lava succession, such as Mull, the surface weathering style can often provide clues about the whole rock chemistry - most especially the degree of evolution of the lava flow. Two main types of weathering have been noted;

2.4.1 Platy weathering (plate 2.16)

Such weathering is caused by the microscopic flow-al ignment of plagioclase needles within the rock. This platy type of surface weathering, has in the past been used as a criteria for the identification of more evolved flows in the field. But how valid is this criterion?

Of the flows collected during the present study, 109 have platy surface weathering and the MgO contents of these are listed in table 2.4.

MgO (wt. %)	Number of platy flows	Percentage of the platy flows
>10%	14	13
8-9.99	10	9
6-7.99	23	21
4-5.99	52	48
<3.99	10	9

Table 2.4 The relationship of MgO content to platy weathering

From this table it can be seen that approximately 80% of the flows noted as platy in the field have less than 8% MgO and, in terms of Hebridean lavas, can be described as "more evolved". The platy weathering is never very prominent in the higher MgO lavas but, nonetheless it can be an obvious feature. The reason for this becomes apparent in thin section where these high-MgO, platy lavas often consist of well-formed olivine microphenocrysts, set in a groundmass of sub-aligned plagioclase and ophitic augite. Nine flows with less than 7% MgO, but which show little evidence of platy weathering, have also been discovered within the lava succession. Therefore, it would appear that, although the presence or absence of platy weathering may be used to make a tentative decision in the field about the degree of evolution of a Mull lava flow, it is by no means a foolproof method and it should always be confirmed by chemical and petrographic analysis.

Sometimes these platy flows can develop a convoluted flow-banded structure (plate 2.17) Such features are very striking and again probably reflect an alignment of



Plate 2.16 Platy weathering as shown by flow BM61.



Plate 2.18 Spheroidal weathering in flow BM29.

plagioclase during the forward advance of the flow. Similar convoluted flow-banding has been observed by Lyle & Patton (1989) within the Upper Basalt Formation of the Tertiary Antrim lavas.

On Mull these platy flows are occasionally noticeably feldspar-phyric. These feldspars sometimes have rounded corners, a feature which is very strongly suggestive of resorption (section 3.1; plate 3.9). They have an average length of about 2cm but at Laec an Staoin (NM557242) Bailey *et al.* (1924) report the occurrence of a feldspar phyric basalt with feldspars up to 20cm in length. As well as varying in size, these phenocrysts also vary in abundance from flow to flow, with some flows containing only very sparse phenocrysts, while others (eg. flows MR36-39) contain up to 20% phenocrysts.



Plate 2.17 Convoluted flow banded texture as shown by flow BR27.

Bailey *et al.* classified *all* the big-feldspar lavas they found as "central" types, simply because the three porphyritic lavas they analysed came only from the central area and had higher CaO and Al_2O_3 than the Mull Plateau lavas. Outside the central area, this generalisation was based *only* on field observations, and it is clear from this study that it is incorrect. The present study has shown that the feldspar-phyric lavas which are interdigitated with the Mull Plateau Group basalts are more chemically similar to the MPG basalts than they are to the "Porphyritic Central Magma Type" defined by Bailey *et al.*

2.4.2 Pustular, spheroidal and blocky weathering

The more olivine rich flows have a greater tendency to weather in one or more of the above ways.

Pustular weathering occurs when less-resistant olivines and plagioclase are weathered away leaving the more-resistant ophitic augites upstanding, to form a nobbly or pimply surface. **Blocky weathering** and its more advanced form, **spheroidal weathering** (plate 2.18), probably originate through the exploitation of cooling fractures by the agents of weathering. A common surface weathering feature of these flows is the frequent appearance of small, rusty-red pseudomorphs after original olivine microphenocrysts

The Mull lava flows occasionally contain segregation veins and patches of more-evolved material. This material is generally coarser than the rest of the flow and it represents some of the last material to crystallise. Such features are more readily observable in thin section and consequently these coarser segregations will be discussed in more detail in the petrology and mineral chemistry chapter.

Although some plugs were studied and chemically analysed, no dykes were sampled during the present study. Nevertheless, a limited amount of petrographic and chemical information is available in Lamacraft (1978) and this information has been utilised.

Chapter 3

Petrography and mineral chemistry.

In this chapter some petrographic aspects of the lavas will be described and microprobe analyses of the main mineral phases will be discussed. Since this study is essentially geochemical in nature, no formal attempt has been made to *petrographically* subdivide the basalts. Rather they have been grouped on a *geochemical* basis (Chapter 4). These different basaltic chemical groups have been defined on the basis of incompatible trace elements and each geochemical group possesses a variety of textural features.

3.1 Petrography

In the following section the main petrographic features of each of the (chemically identified, section 4.2) rock types - basalt, basaltic-hawaiite, hawaiite, mugearite, benmoreite/trachyte, Coire Gorm magma type, Central Mull Tholeiites and the Staffa Magma sub-Type - will be discussed. Any notable petrographic features of individual samples are mentioned in Appendix 1.

3.1.1 Mull Plateau Group basalts (>7% MgO; <4% total alkalis)

The dominant phenocryst phase in these basalts is olivine. These crystals vary from being euhedral, to subhedral, skeletal (plate 3.1) and anhedral in form. They can be up to 3mm in length and have core compositions of $Fo_{75\text{-}89}$. (Occasionally, olivine is not in equilibrium with the groundmass, and this has been investigated in more detail in section 4.3). Even away from the central zone of alteration these olivine phenocrysts have a tendency to be quite altered around their margins and along cracks. The alteration products of the olivines include green serpentine/chlorite, orange-brown iddingsite and black oxide material. However, where alteration has not effected the edges of the crystals, they are frequently seen to be zoned, with more fayalitic compositions towards the margins (section 3.2). Within the central greenschist zone of alteration (figure 1.1) no fresh olivine has been found, a feature which Bailey *et al.* (1924) also noted.

The olivine phenocrysts sometimes group together to form glomeroporphyritic crystal clusters (plate 3.1[1]). In the more MgO rich basalts these olivine phenocrysts

[1] All photomicrographs have been taken in cross-polarised light.



Plate 3.1 Showing subhedral to skeletal olivine phenocrysts, along with a glomeroporphyritic cluster of olivine crystals [sample B25B]. Field of view - 13.8mm)

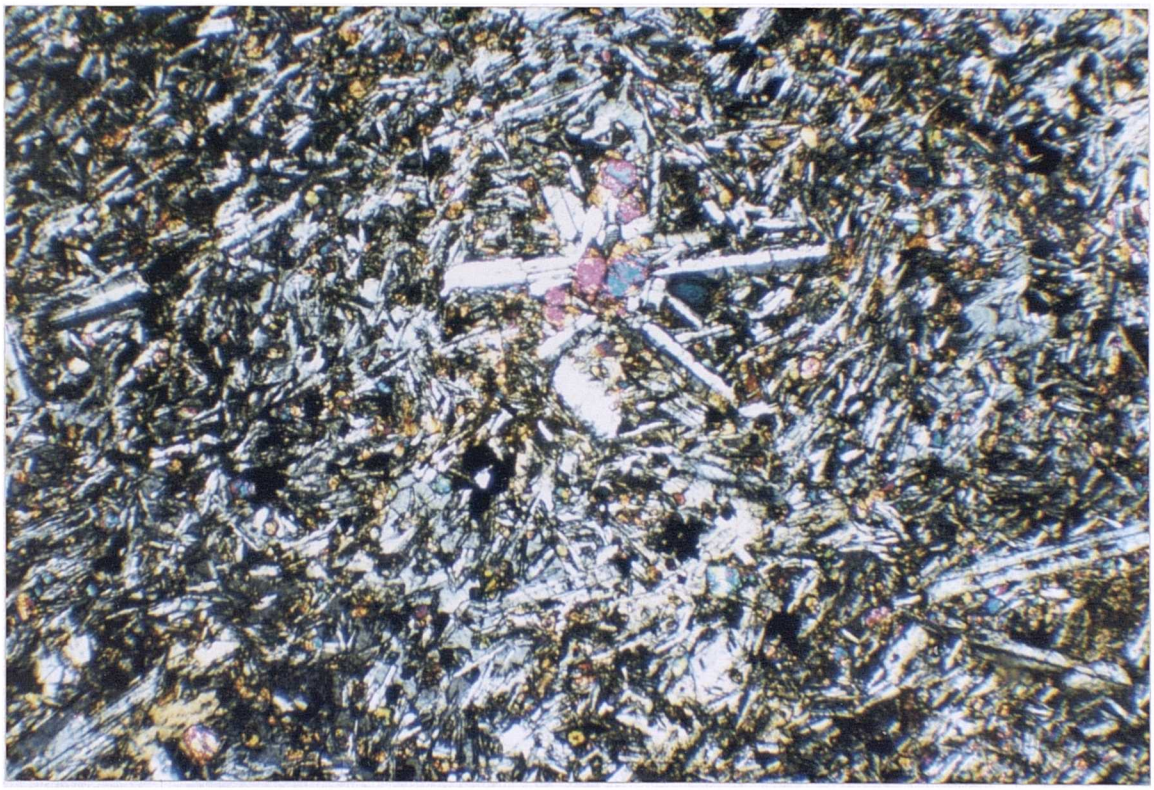


Plate 3.2 A spherulite from flow BR22, composed of plagioclase laths radiating outwards from a central olivine crystal. Field of view 4.5mm.

frequently enclose small (<0.3mm) octahedral, deep brown, chrome spinels. This petrographic feature is reflected in the high (>500ppm) whole rock Cr contents of the more MgO rich lavas (section 4.3).

With lower MgO content, plagioclase phenocrysts begin to appear along with the olivine phenocrysts. These plagioclases form tabular laths, up to 2-3mm in length and are mostly of labradorite composition. They have been variably altered by percolating, subsolidus, hydrothermal fluids to sericite along with thin veinlets and patches of pale green-to-yellow chloritic material.

Sometimes the plagioclase and olivine phenocrysts form glomerocrysts (plate 3.2). These tend to take the form of spherulites, with plagioclase crystals radiating outwards from a central olivine crystal. These early olivine crystals therefore seem to have acted as nuclei on which the later plagioclases grew.

Pyroxene phenocrysts are, for the most part, conspicuous by their absence in the MPG basalts. This is despite considerable *chemical* evidence that clinopyroxene has been a major fractionating phase (section 4.3). Several flows do however, have a few sparse augite phenocrysts (eg. BG5, BG6 & BCH40). Plate 3.3 shows one such typical pyroxene phenocryst, with both oscillatory and sector zoning. This lack of pyroxene phenocrysts is generally true of the BTIP, eg. Bailey *et al.* (1924); Thompson *et al.* (1972) and Williamson (1979).

Pyroxene therefore occurs chiefly as a groundmass phase in these lavas. In all but the most heavily altered and oxidised flows this pyroxene remains fresh, even when the crystals and groundmass around it have been quite badly altered. As would be expected the pyroxenes in these basaltic rocks are quite Mg and Ca rich. (The chemistry of these pyroxenes will be discussed in section 3.2). Two broad forms of interstitial pyroxene can be identified within the MPG lavas;

1/ ophitic to subophitic crystals (plate 3.4) which enclose, or partially enclose groundmass plagioclase laths, olivine and oxide crystals. Sometimes very few crystals are enclosed within the interstitial pyroxene (plate 3.4), suggesting that they may have started life as small phenocrysts within the magma. Upon cooling, further growth of these crystals would have been restricted by the simultaneous growth of other crystals, effectively "hiding" the original pyroxene phenocrysts. However these types of pyroxene are not particularly common, and so other explanations for the lack of pyroxene phenocrysts must be sought (section 4.3). Occasionally, especially in the more fine-grained lavas, the pyroxenes take on a more granular form.

2/ The augite crystals sometimes form oikocrysts within the groundmass (plate 3.5), so giving the lava an 'ophimottled' texture (MacKenzie 1982). This texture sometimes results in the rock having a speckled appearance in hand specimen.

The augites are characterised by varying shades of pale brown to pale purple,



Plate 3.3 A twinned augite phenocryst from flow BCH40 showing both oscillatory and sector zoning. Field of view - 7mm.

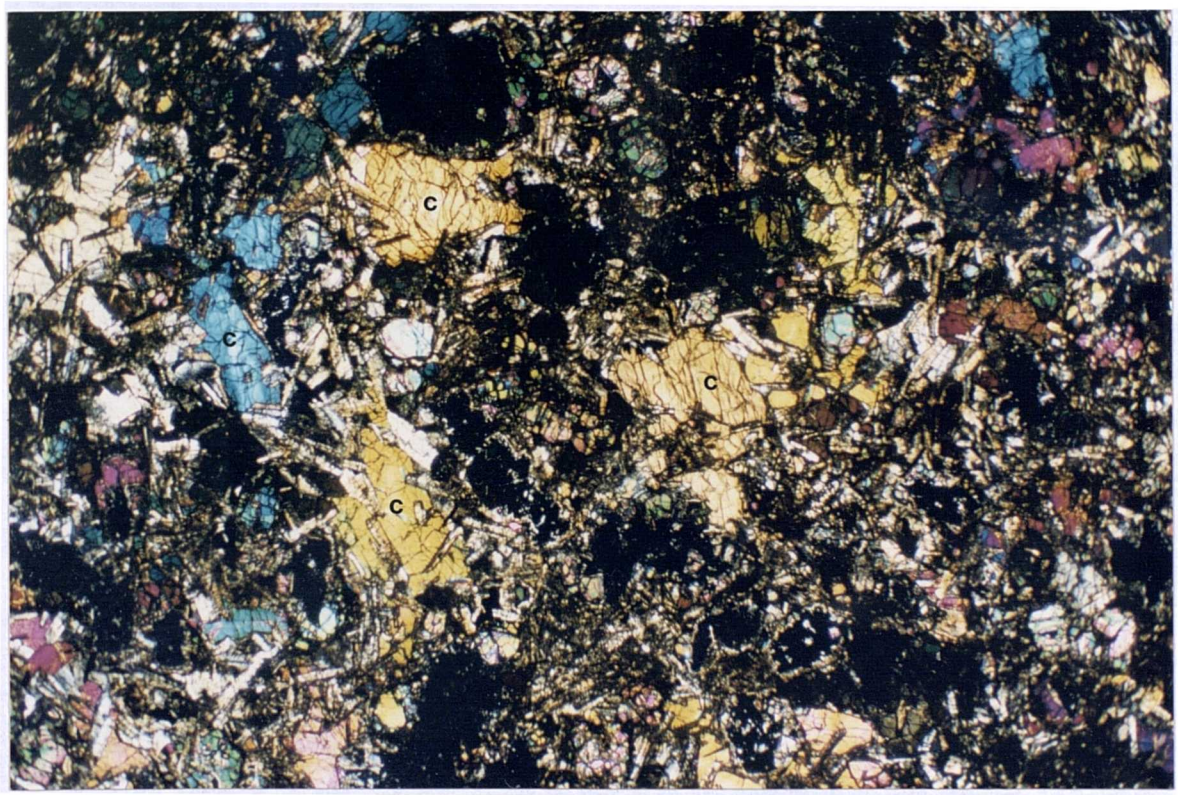


Plate 3.4 Subophitic crystals of clinopyroxene (c), partially enclosing plagioclase laths in flow BM10. Field of view - 13.8mm.

reflecting increasing Ti contents of the crystals (Deer *et al.* 1966). They often show zoning from pale colours in the centres of the crystals to darker, more purple colours at the margin.



Plate 3.5 Photomicrograph showing oikocrysts (o) of clinopyroxene in flow BB9. These impart an 'ophimottled' texture to the lava. Field of view - 13.8.

The size of crystals in the groundmass varies from very fine-grained (<0.3mm; plate 3.6) to medium grained (≤1mm; plate 3.7)) with a doleritic texture. In the more medium-grained lavas it becomes difficult to distinguish between phenocrysts and groundmass olivines since the sizes of the two crystals tend to overlap. Relatively few of these basalts can be described as truly aphyric, since most contain at least a few olivine or plagioclase phenocrysts. *It is important to note that these different textures do not appear to be related to the bulk chemistry of the rock, since high MgO basalts with both fine and medium-grained groundmass have been found.*

The groundmass of these basalts, as has previously been mentioned, contains substantial amounts of variably coloured, fresh, interstitial pyroxene. Small subhedral to anhedral olivines also occur in the groundmass. These are however, mostly altered to pale green serpentine, orange-brown iddingsite, and oxides. Poorly formed laths of plagioclase (bytownite/labradorite) also make up the groundmass material. These tend to be more altered (to chlorite and sericite) than their phenocryst counterparts. Although mostly of labradorite composition, they tend to have lower An contents than the phenocrysts. Subophitic and granular Fe-Ti oxides are also

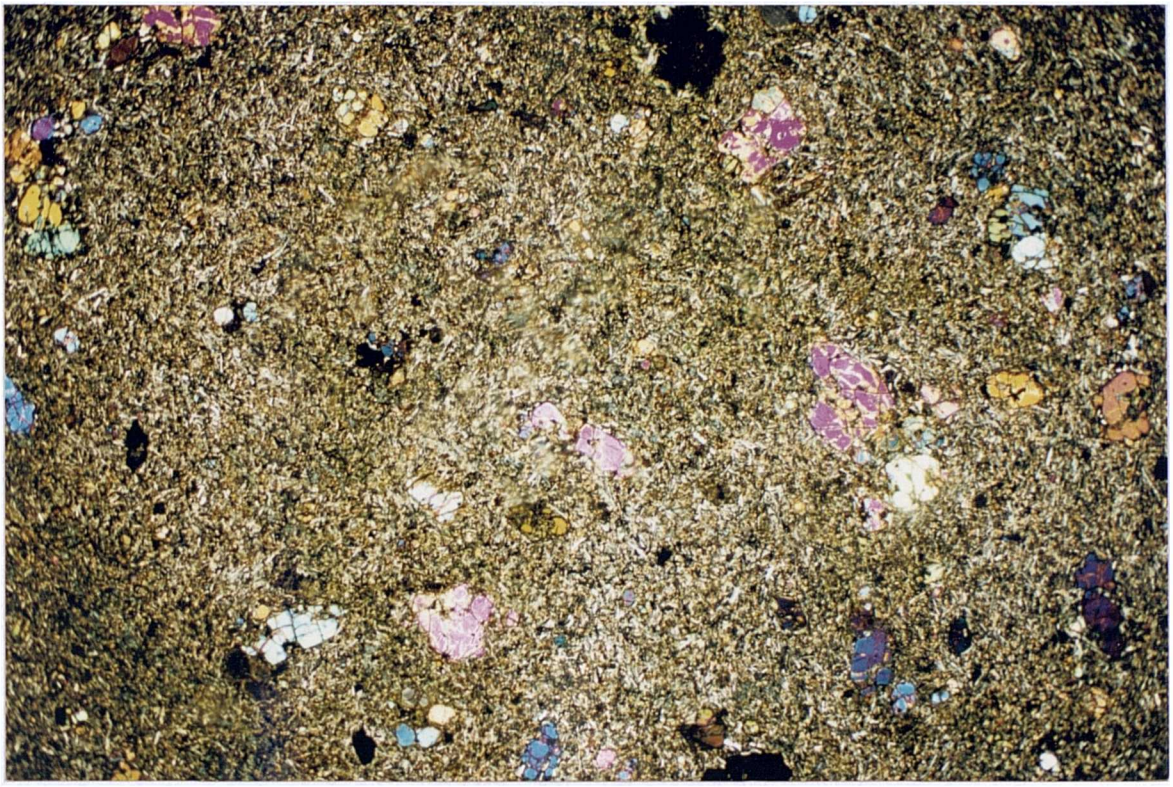


Plate 3.6 Flow BM13 with olivine phenocrysts set in a fine-grained groundmass. Field of view - 13.8mm.



Plate 3.7 Photomicrograph of flow BR9, showing a fine to medium-grained texture. Field of view - 13.8mm.

found in the groundmass. These tend to be mostly titano-magnetite however, they can contain up to 0.5% Cr_2O_3 (section 3.2.4), a feature which reflects the Cr-rich nature of the magma from which they crystallised. Analysis by electron microprobe has also revealed the presence of rare illmenite (section 3.2.4). Small apatite needles can also be found within the groundmass.

The rest of the interstitial material is of secondary origin, and includes chloritic to serpentinitic material, along with various types of zeolites. These zeolites can either form fibrous radiating fibrous masses, or less commonly, more massive crystals, both occupy interstitial regions within the groundmass and also frequently infill amygdales[2]. Morrison (1979) detected the presence of small amounts of fresh glass in the interstitial regions of some of the MPG basalts, and it is therefore probable that some of these secondary minerals have replaced original glass or small crystals. Inside the central zone of alteration, interstitial crystals are much more altered, and frequently only the pyroxene survives. Granular, green-yellow epidote, and chlorite are the most common alteration products

Several basalts display more medium-grained segregation features which represent some of the last material to crystallise from the basalt. These areas are obviously more evolved than the surrounding host basalt from which they are derived, since they contain no olivine. These segregations are composed of large (up to 1mm), zoned, strongly coloured, subophitic pyroxenes, laths of andesine-oligoclase plagioclase, skeletal and subhedral Fe-Ti oxides, numerous acicular apatite needles, interstitial analcite and perhaps biotite. The contact zone between the pegmatite segregation and the olivine rich host basalt is not well marked but it is partially gradational. A similar observation, also from a MPG lava, led Morrison (1979) to suggest that the pegmatite segregation formed *before* the enclosing basalt was totally crystallised.

3.1.2 Mull Plateau Group basaltic-hawaiites (7-5% MgO; 4-5% total alkalis)

The most notable feature of the lavas is their almost uniform tendency to be very fine-grained, only rarely does the crystal size of the groundmass exceed 0.5mm, and several flows have a grainsize of less than 0.25mm (eg BR23). Several of these flows are aphyric (eg. BR23) but more usually they possess predominantly plagioclase

[2] Several large pods of zeolites have been analysed by XRD during the present study; One from within flow BR2 contains analcite (isotropic), mesolite (fibrous habit), thompsonite (radiating, columnar aggregates) with minor amounts of scolecite and natrolite (fibrous); another from flow AM14 contains natrolite, scolecite, with a small amount of analcite, thompsonite! and laumontite (fibrous).

phenocrysts, with variable amounts of olivine phenocrysts, which are more fayalitic than those in the basalts.

The plagioclase microphenocrysts are seldom over 2mm in length and can form good lath shaped, twinned and oscillatory (normal) zoned, andesine-labradorite crystals. The plagioclase phenocrysts and the groundmass plagioclase in these more evolved lavas also have a tendency to become aligned (plate 3.8), so developing a fluxion texture. As was pointed out in Chapter 2, this microscopic feature can sometimes, *but not always,* impart a platy weathering texture to these lavas.



Plate 3.8 Alignment of phenocryst and groundmass plagioclase as shown by flow BR1. Field of view - 13.8mm.

The plagioclase phenocrysts in the more sparsely porphyritic lavas display evidence for crystal resorption and regrowth of new material (plates 3.9 & 3.10 show two excellent examples of this). A notable feature of both these crystals is the presence of inclusions, marking the edge of the resorped portion of the crystal in plate 3.9 and occupying the central part of the resorped crystal (plate 3.10). Closer examination of the marginal inclusions reveals that they are composed mostly of opaques, pyroxene, and chloritic patches (pseudomorphs after olivine). The central inclusions appear to be mostly clear and probably represent partial melting of the crystal during resorption.

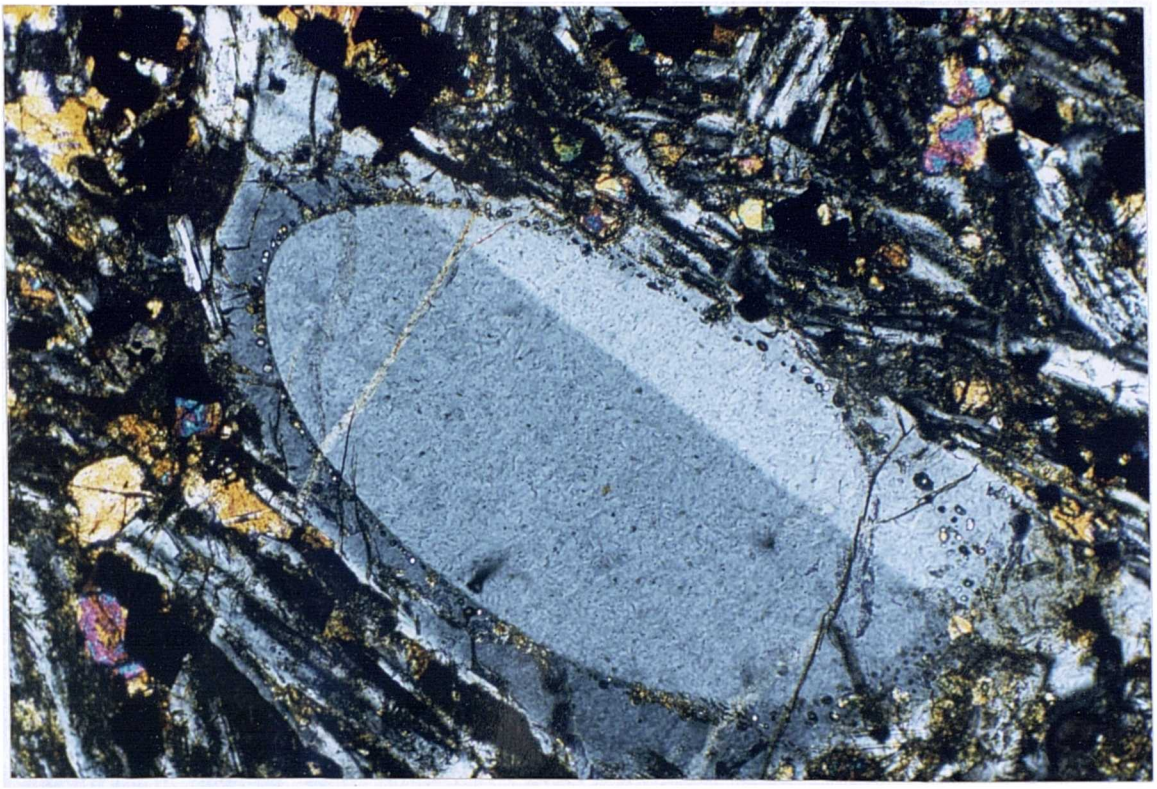


Plate 3.9 Resorption and regrowth of a plagioclase phenocryst from flow BR29. Note the rim of inclusions marking the edge of the resorped portion of the crystal. Field of view - 4.5mm.



Plate 3.10 Extensively resorped plagioclase phenocryst, showing marginal regrowth. The central resorped part of the crystal contains numerous melt? inclusions. Field of view - 4.5mm.

With these type of phenocrysts being quite sparse it was quite difficult to capture one on a an electron microprobe slide. However, a slide of BR22 has yielded a resorbed and regrown phenocryst. The composition of core of this crystal is An_{64}, while the regrown margin is composed of An_{70} (Appendix 4d). These observations strongly support the idea that some kind magma mixing has occurred (eg. Sparks & Huppert 1984) whereby a crystal of plagioclase is brought into contact with hotter magma, than that from which it crystallised. The plagioclase is therefore out of equilibrium with its host liquid and will consequently be melted and resorped by it. In a magma chamber which is continually fractionating, resorption will eventually give way to re-growth on the surface of the eroded crystal.

As was noted above the groundmass of these lavas is quite fine-grained. It is composed of plagioclase laths (sometimes aligned) of andesine-labradorite composition, poikilitic to subophitic and occasionally granular pale brown to lilac clinopyroxene, and small partially altered groundmass olivines. Fe-Ti oxides (mostly titano-magnetite) are more abundant than in the basalts of the MPG. They sometimes are well formed and occasionally form phenocrysts, however they also exist as subophitic, interstitial crystals. Apatite needles also appear to be more abundant in these more evolved lavas. The groundmass and phenocrysts are variably altered to the same assemblage (chlorite, serpentine iddingsite and oxides) as the basalts, while clinopyroxene remains essentially unaltered at the lower grades of alteration.

3.1.3 Mull Plateau Group hawaiites (5-4% MgO; 5-6% total alkalis)

These lavas are petrographically quite similar to the previous group, they are mostly fine-grained (<0.4mm) although several hawaiites have been found that have a more medium-sized (0.5-0.75mm) groundmass texture (eg. BCH12). These lavas also possess sparse rounded, resorbed and zoned labradorite/andesine phenocrysts. Some of these may be up to 10mm in length, although 3-4mm is more common. Although these phenocrysts are resorbed, there is much less of a tendency for them to show signs of regrowth, than in the basaltic hawaiites. Flow MR36 contains over 15% plagioclase phenocrysts, and it seems likely that these represent a flotation cumulate at the top of a magma chamber, that was subsequently erupted. The origin of highly plagioclase phyric MORB has also been explained in terms of flotation cumulates (Bryan 1983), as have basalts from the Deccan Traps which contain numerous plagioclase phenocrysts (Cox & Mitchell 1988).

Olivine has a tendency to form subhedral microphenocrysts in some of the more primitive hawaiites, but the lower MgO character of the hawaiites means that plagioclase (and clinopyroxene; see section 4.3) fractionation are more important.

The groundmass of these lavas essentially contains the same minerals and alteration products as the groundmass of the basaltic-hawaiites. The plagioclase laths have developed a fluxion texture and are mostly of andesine composition An <50 and Fe-Ti oxides are generally more abundant than in the less evolved rocks. These oxides are more inclined to take on euhedral to subhedral forms, implying that they are an earlier crystallising phase in these more evolved lavas. Small granular groundmass olivines are variably altered to chloritic material, iddingsite and oxide. Clinopyroxene is generally coloured pale brown to lilac and contains more Fe than the basaltic flows. It exists as interstitial granules, subophitic plates or oikocrysts up to 0.75mm in diameter, which give the rock an ophimottled appearance. Apatite needles are more abundant, small traces of biotite have also been noted in these hawaiites.

3.1.4 Mull Plateau Group mugearites (3-4% MgO; 6-8% total alkalis)

Most of the mugearitic lavas of the MPG lie within the central zone of greenschist facies alteration, where they are quite highly altered and oxidised. This makes petrographic observations of the primary igneous features more difficult. However, some mugearites lie outside this central zone of alteration (eg. UV2, MR28, MR38, B4a & B5) and consequently their primary igneous mineralogy is reasonably well preserved.

The main phenocryst phase which can be found in these rocks is plagioclase. These andesine-oligoclase phenocrysts can form good lath shaped crystals up to 4-5mm in length, and in some lavas a seriate texture exists among the plagioclase crystals (eg. CA4). Like the hawaiites several lavas have been found (MR37 & MR38) which contain abundant (15-20%) partially resorbed plagioclase (andesine-oligoclase) macrophenocrysts (up to 15mm in length, but more commonly around 5-7mm) set in a fine-grained groundmass (<0.3mm). These, like their plagioclase phyric hawaiite counterparts, may well represent flotation cumulates, and it is therefore unlikely that these flows represent a composition which was originally liquid. The major and trace element chemistry of these lavas (Appendix 4a) does not appear to have been *radically* affected by the addition of these phenocrysts. They have slightly lower levels of incompatible trace elements and higher Al_2O_3 than their aphyric analogues. Occasional olivine phenocrysts can also be found in the more basic mugearites (eg. UV3).

Euhedral phenocrysts (up to 0.7mm) of titanomagnetite are much more common in these lavas than in the hawaiites, a fact which supports the chemical evidence for the fractionation of a Ti-rich oxide phase (section 4.3). Numerous euhedral to subhedral

octahedra make up a significant proportion of the groundmass in these lavas, and the oxide grains frequently group together in small clumps.

The groundmass of these lavas can be exceedingly fine-grained, sometimes <0.15mm (eg. BM66 and MR38) although more medium grained (0.5-0.75mm) mugearites have also been found (eg. B4a). As well as titanomagnetite the groundmass minerals include small granular olivines, abundant apatite needles, pale brown, subophitic clinopyroxene and some interstitial biotite. All these minerals are set in a mass of sub-aligned oligoclase crystals which are zoned towards more potassic compositions. Interstitial alkali feldspar has started to become optically noticeable, and microprobe analysis of the groundmass of sample MR29 has detected the presence of some anorthoclase. This trend towards more alkali feldspar compositions means that fluxion textures - which are principally caused by the alignment of plagioclase feldspars - within these lavas become less pronounced. In some of the lavas the plagioclase crystals are aligned in two directions. The groundmass minerals are essentially altered to the same assemblage of minerals as the less evolved magmas.

3.1.5 Mull Plateau Group benmoreites/trachytes (<3% MgO; >8% total alkalis)

Only a handful of lavas from the MPG fall into these evolved categories. However they *all* occur within the central zone of intense alteration, which has made petrographic observations on these sometimes very fine-grained (<0.15mm) rocks quite difficult. These rocks are essentially aphyric, although occasional phenocrysts of albite and euhedral (sodic alkali feldspar ?; plate 3.11) can be found.

The groundmass of these lavas occasionally preserves a more medium-grained texture (up to 0.4mm; eg. BM63). Thompson *et al.* (1972) and Williamson (1979) noted amphibole and biotite within the groundmass of highly evolved rocks from Skye. However, the extensively altered nature of these lavas to mineral assemblages including epidote, chlorite and serpentine, has meant that biotite and amphibole have not been positively identified in the benmoreite/trachyte lavas during the present study. Nevertheless, these minerals probably did exist as part of the primary igneous mineralogy of these evolved lavas. The appearance of biotite in the groundmass of some MPG mugearites, and the fact that biotite (±amphibole) occurs in several trachytic, Tertiary plugs from Mull, bears witness to this proposal.

The groundmass of these lavas is principally composed of sub-aligned albite-oligoclase laths (plate 3.12), with interstitial areas of sodic alkali feldspar, subhedral or anhedral clear to pale green clinopyroxene and numerous small apatite needles. Abundant euhedral octahedra of magnetite, contain less Ti and more Fe^{3+} than the



Plate 3.11 Photomicrograph of flow CA7 with occasional phenocrysts of sodic alkali feldspar. Field of view - 7mm.

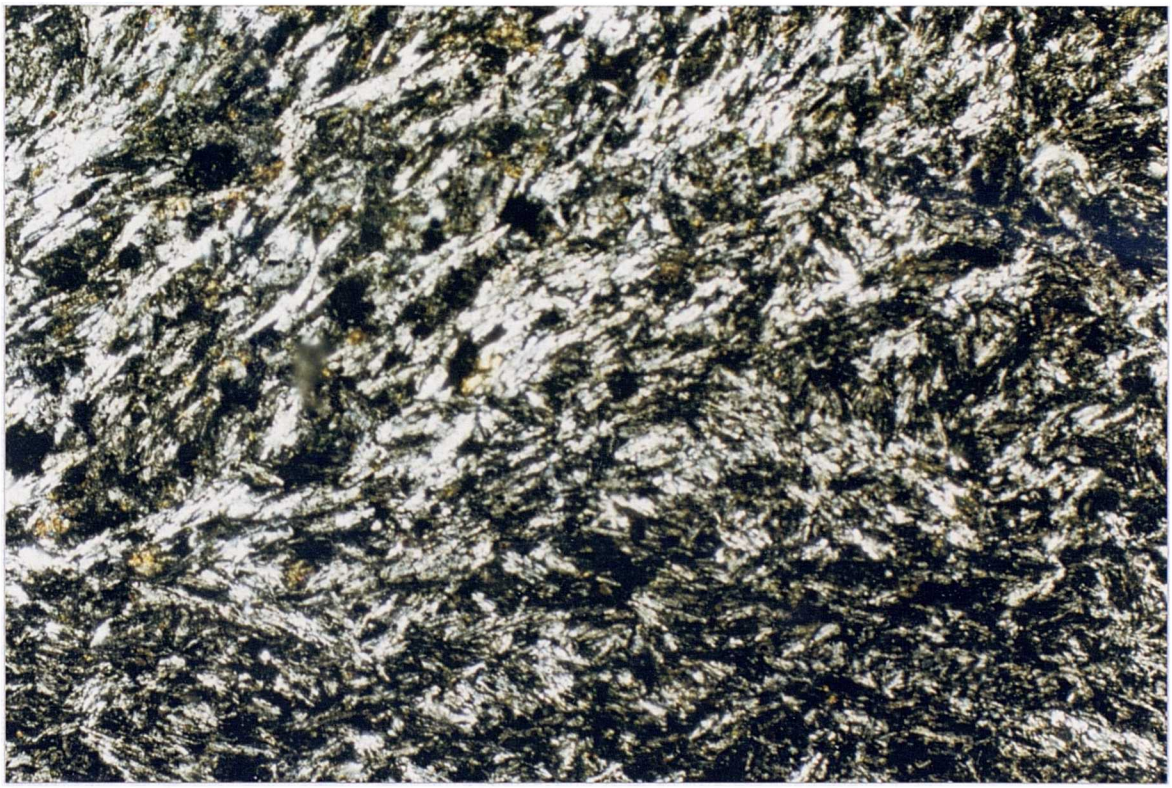


Plate 3.12 Photomicrograph of flow BM60, showing sub-aligned albite-oligoclase laths, with interstitial clinopyroxene and sodic alkali feldspar. Field of view - 3.5mm.

MPG mugearites. This fact combined with the presence of alkali feldspar and greenish pyroxene reflect the more evolved and more oxidised character of these lavas. Also in the trachytes, minute high relief, granular crystals can be found, and given the abundance of zirconium in these lavas (~1000ppm), the high relief crystals may well be zircons.

3.1.6 Coire Gorm magma type (CG)

The chemistry of this magma type will be described in detail in Chapter 6, at this stage it is sufficient to say that they lie stratigraphically above the evolved lavas, near the top of Ben More, and they are all of basaltic composition (7-12% MgO), with a trace element signature distinct from the MPG. All these lavas lie within the greenschist-facies zone of alteration (figure 1.1) and as a result they are quite badly oxidised and altered, to a variety of secondary mineral phases.

Their textures and mineralogies display many similarities to the MPG basalts (section 3.1.1). The main phenocryst phase in the more mafic lavas was once olivine, which now exists as mostly euhedral pseudomorphs, (plate 3.13) of chloritic material, serpentine and oxide, up to 2-3mm in diameter, which occasionally group together to form glomerocrysts. These olivine pseudomorphs can also contain deep red-brown Cr-spinel inclusions.

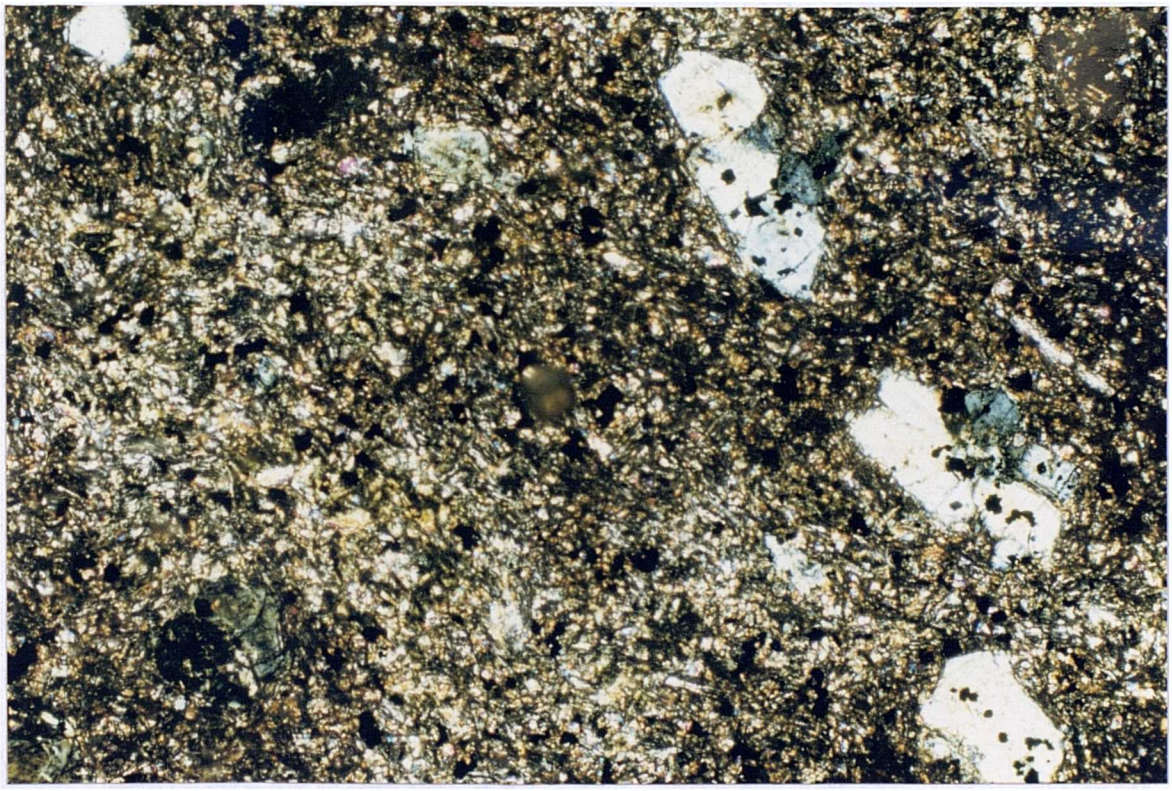


Plate 3.13 Chloritic pseudomorphs after olivine glomerocrysts and phenocrysts. The groundmass is composed of plagioclase laths and granular clinopyroxene. Field of view - 3.5mm.

With increasing degrees of evolution, partially altered labradorite phenocrysts (1-2mm in length) become more common. Sparse resorped, rounded phenocrysts of andesine-labradorite (up to 5mm in length) composition, perhaps with slight regrowth around the edges may also be found.

The groundmass of these lavas has quite a variable grainsize, from very fine (<0.2mm) to medium-grained (~1mm). Clinopyroxene has not been found in phenocryst form in any of these lavas, it is however an abundant groundmass phase. Like the MPG basalts it exists in several different forms; granular (plate 3.13) and subophitic crystals and oikocrysts, which give the rock an ophimottled texture. These pyroxenes have a tendency to be paler than those of the MPG basalts, they do however frequently become more purple coloured towards their margins and they enclose or partially enclose labradorite laths. In some of the lower MgO samples, have these have developed a distinct fluxion texture. Subophitic, anhedral oxides are also well represented within the groundmass mineralogy, although they are nowhere near as abundant as in the more evolved MPG lavas. Some small apatite needles have also been noted within the groundmass, along with rare biotites, although it is difficult to determine if the latter is of a primary igneous origin.

Epidote, chlorite, oxides and various clay-like minerals are the predominant secondary alteration minerals within these lavas. They can replace the groundmass and phenocryst minerals, fill in vesicles and/or form a network of veinlets penetrating through the rock.

3.1.7 Central Mull Tholeiites (CMT)

These lavas lie stratigraphically above the Coire Gorm magma type, and all the CMT lavas collected during the present study have come from within the central zone of alteration. These lavas display various textures and range from tholeiitic basalts to andesites. The groundmass varies from quite fine-grained (eg. CA12; <0.2mm) to medium-grained (eg. CA3B; ~1mm) and is chiefly composed of plagioclase needles, along with granular to subophitic pale brown clinopyroxene and interstitial to subhedral oxide phases. The plagioclase in the groundmass varies from labradorite in the basalts, to andesine in the more evolved lavas. Accompanying this change in feldspar compositions the magnetite crystals become more abundant and have a tendency to be more euhedral, while small, granular, olivine pseudomorphs become less abundant.

Several of these lavas are essentially aphyric (eg. CA15 and CA17), however most possess varying kinds of phenocrysts, and they can essentially be divided into two types;

a/ *Labradorite-bytownite phyric lavas (eg. CA3B, CA16, CA19 & 20).*

Some of the phenocrysts in several of these lavas have been analysed and their core compositions range from An_{87} to An_{74} with more sodium-rich rims. Labradorite phenocrysts have also been optically detected among these crystals, which may be up to 10mm long, although 3-4mm is a more common length. They can compose up to 30-40% of the lava, form euhedral to subhedral lath-shaped crystals, and often form glomeroporphyritic crystal clusters (plate 3.14). A couple of the 'lavas' (CA19 & 20) appear to be partially composed of more angular fragments of calcic plagioclase, sometimes with strained and kinked twinning (plate 3.15). As can be seen in plate 3.15 the groundmass of CA19 is quite altered and messy, with the only recognisable primary mineral being small plagioclase laths. The nature of the groundmass material combined with the fragmental plagioclase crystals, gives some clues as to how these highly plagioclase phyric magmas were able to erupt. Some of them at least seem to have been erupted with explosive force, possibly leading to the formation of ash-crystal tuffs (eg. CA19 &20).

Donaldson (1977) reported on the chemistry of gabroic dykes from Skye, which contain abundant megacrysts and xenoliths of anorthite/bytownite plagioclase. He proposed that these crystals concentrated in shallow chambers, through which fresh magma, containing calcic plagioclase phenocrysts was pulsing. These low-alkali, high CaO magma batches dumped their plagioclase phenocrysts in the chamber, before erupting as the sparsely porphyritic Preshal More magma type. Donaldson (op.cit) showed that although these phenocrysts had crystallised from low-alkali, high CaO magmas, the phenocrysts and the matrix in each dyke were not cognate.

The high abundance of plagioclase phenocrysts in some of these low-alkali, high CaO, CMT lavas from Mull, also suggests that they similarly did not crystallise from the groundmass in which they now reside. It is probable that these phenocrysts formed by concentration in a magma chamber, but unlike Skye where feldspar phyric tholeiitic (Preshal More) lavas did not reach the surface, eruptions from the chamber seem to have been more explosive. This extra pressure would have enabled more viscous plagioclase phyric magmas to be expelled from the chamber, with some forming lava flows and perhaps the more explosive eruptions forming ash-crystal tuffs.

b/ *Andesine-labradorite phyric lavas (eg. CA12 &CA18)*

These more evolved phyric lavas occur interleaved with the bytownite phenocryst lavas, suggesting that they have a similar origin. These phenocrysts have a predominantly andesitic composition and can be up to 5mm in length. In flow CA12 some crystals show evidence of resorption and slight regrowth around their margins.

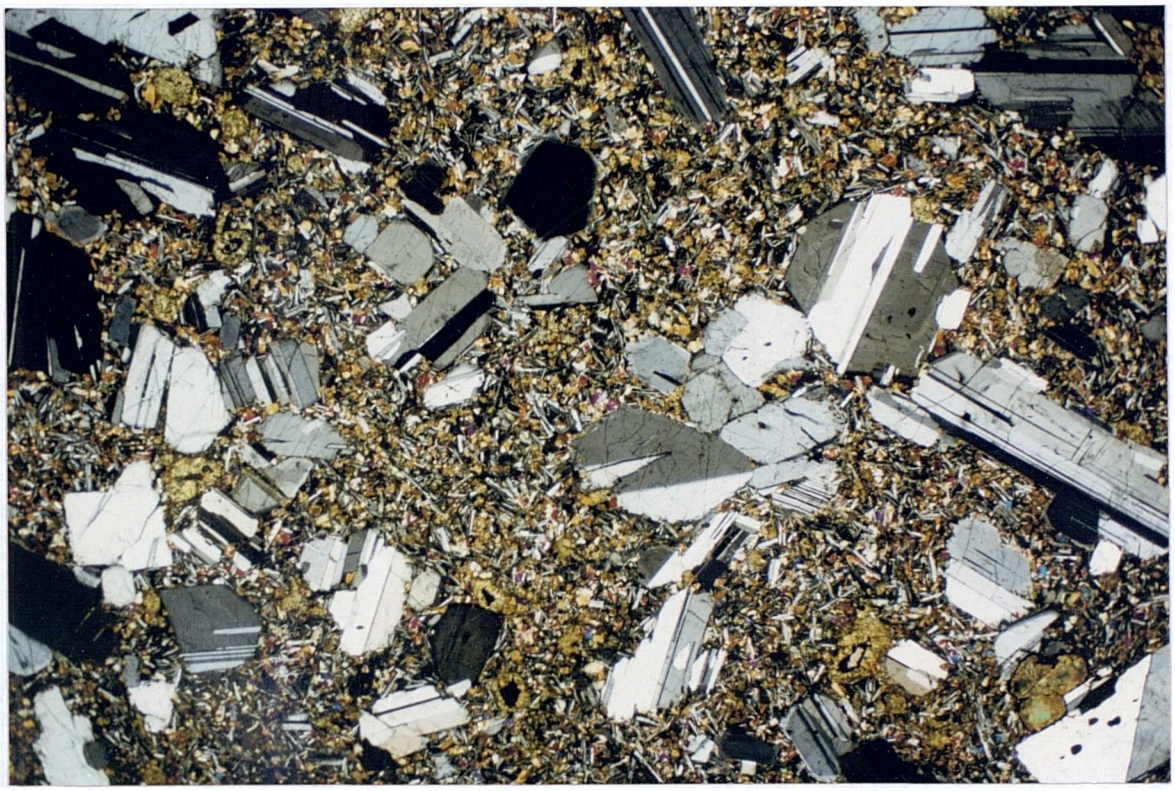


Plate 3.14 Bytownite glomerocrysts set in matrix of plagioclase laths and ophitic clinopyroxene [flow CA3B]. Field of view - 13.8mm.

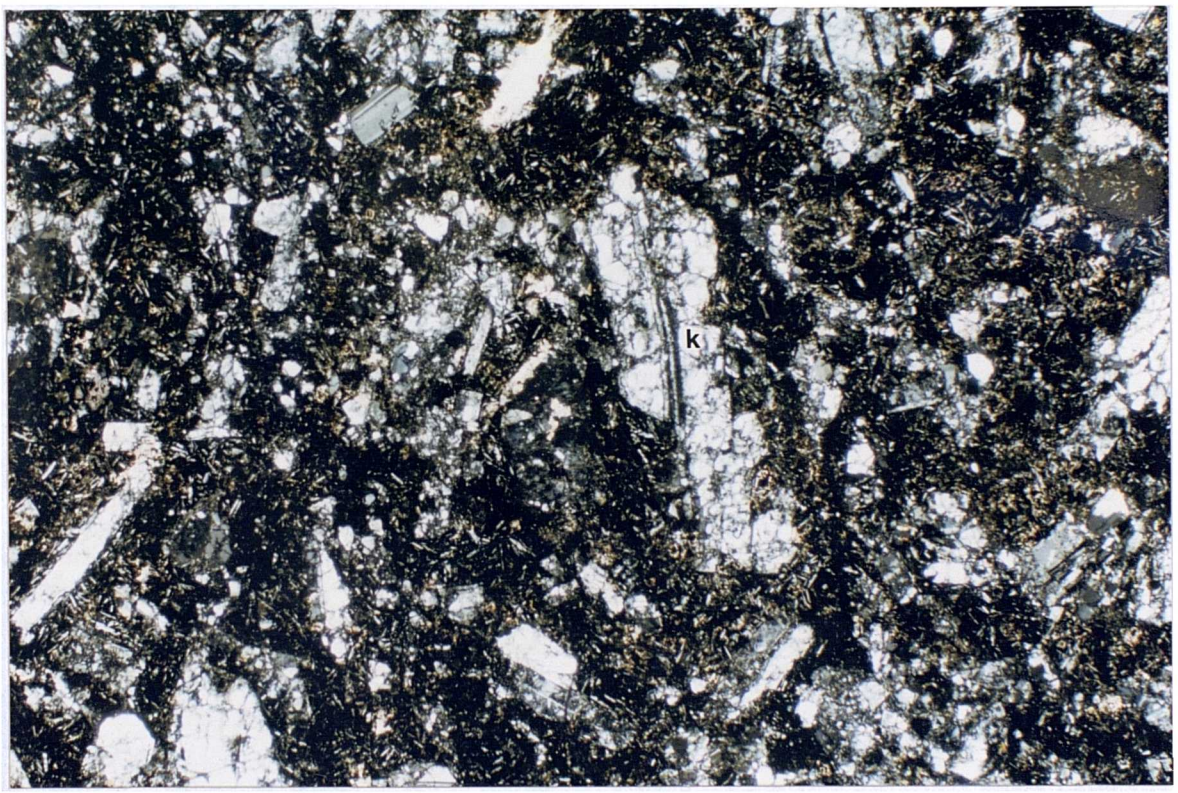


Plate 3.15 Photomicrograph of 'flow' CA19 showing laths and angular fragments of plagioclase phenocrysts, set in an altered, oxidised matrix. One of the crystals shown in this plate displays 'kinked' twinning (k). Field of view - 7mm.

Subhedral to skeletal phenocrysts of Fe-Ti oxides are also an important feature of this evolved CMT rock type.

3.1.8 The Staffa Magma sub-Type (SMT)

In the field these lavas are all distinctly columnar (Chapter 2), and occur very near the base of the succession. They are quite fine-grained (<0.3mm) and are only very sparsely porphyritic. Plagioclase is the most common phenocryst (up to ~1mm in length) and occurs as laths and angular fragments which may be grouped together to form glomerocrysts, occasionally along with pyroxene phenocrysts. The fragmental nature of some of the plagioclase phenocrysts suggests that they may have been torn off the walls of a magma chamber, or conduit, during eruption.

Microprobe analysis of these plagioclases in sample W4 has revealed that they are of bytownite compositions (An_{88-84}). These phenocrysts are not in equilibrium with their host rock which contains 6.6% MgO and has a chemical composition which the TRACE program of Neilsen (1988)[3] predicts would be in equilibrium with plagioclase of An_{69}. Analysis of the groundmass plagioclase in W4 reveals it to be composed of An_{69-70}. Clinopyroxene also forms reasonably common, euhedral to subhedral phenocrysts, up to 0.4mm in diameter, the larger of which occasionally display sector zoning. Small olivine phenocrysts can also occur within some of the more primitive lavas of the sub-type.

The fine-grained groundmass is composed of labradorite laths, granular to subophitic, pale brown clinopyroxene (less calcic than the MPG pyroxenes; section 3.2.2), interstitial Fe-Ti oxides and serpentine and/or iddingsite which is seen to be either wholly or partially replacing small granular olivines. Secondary alteration minerals, commonly serpentine, chlorite, oxide material and occasionally iddingsite are also abundant within the groundmass of these lavas.

3.2 Mineral Chemistry

The olivine, clinopyroxene, feldspar, and Fe-Ti oxides from the lavas of the Mull succession have been analysed by electron microprobe at the Universities of Durham and St. Andrews. Analytical procedures can be found in Appendix 2 and the results in Appendix 4d.

[3] The TRACE program will be described in more detail in section 4.3

3.2.1 Olivine

In section 3.1 it was noted that the most evolved rocks lie within the central zone of intense alteration, where no fresh olivine could be found. Consequently, most of the olivine analysed during the present study was from basaltic lavas. Figure 3.1 shows that the $Mg/(Mg+Fe^{2+})$ ratio (forsterite content - Fo) of the analysed samples ranges from Fo_{89}, in the most Mg-rich basalt, to Fo_{59} in the evolved basaltic-hawaiite. The MPG olivines are similar to those from the Skye Main Lava Series (SMLS), where Williamson (1979), reported basalts with up to Fo_{90} and hawaiites with Fo_{60}. Williamson (op.cit) was also able to analyse fresh olivines from the trachytes of the SMLS, with compositions of ~Fo_{20},

Where the margins of the olivines are not altered, zoning can often be observed (section 3.1). This usually only spans a few %Fo, sometimes however, olivines with quite marked compositional zoning can be found, eg. BM10. The extent of this olivine zonation is summarised in table 3.1

Sample	Core composition	Rim composition
BM10	Fo85	Fo78
BR5	Fo87	Fo85
MR9	Fo78	Fo73
BM8	Fo87	Fo84

Table 3.1 Summary of the compositional variation in some zoned olivine crystals from the MPG.

As would be expected the olivines become more Fe-rich towards their margins, reflecting the progressive degree of evolution of the residual magma.

Minor element variation in olivines

In figure 3.1a-d, Fo content has been used as a differentiation index, to assess how minor elements in olivines from the MPG vary, as the host magma becomes more evolved. Al_2O_3, K_2O, TiO_2 and Na_2O display no systematic variation with Fo content, in contrast to MnO, NiO, Cr_2O_3 and CaO;

MnO (figure 3.1a)

MnO shows a reasonable scattered negative correlation with Fo content, varying from ~0.1% in the most Mg-rich olivines, to 0.7% in the more Fe-rich olivines. Williamson (1979), in his study of the SMLS, noted a similar range in values, and a negative correlation between MnO and Fo content. Simkin & Smith (1970) examined the minor element variations shown by olivines which had crystallised in

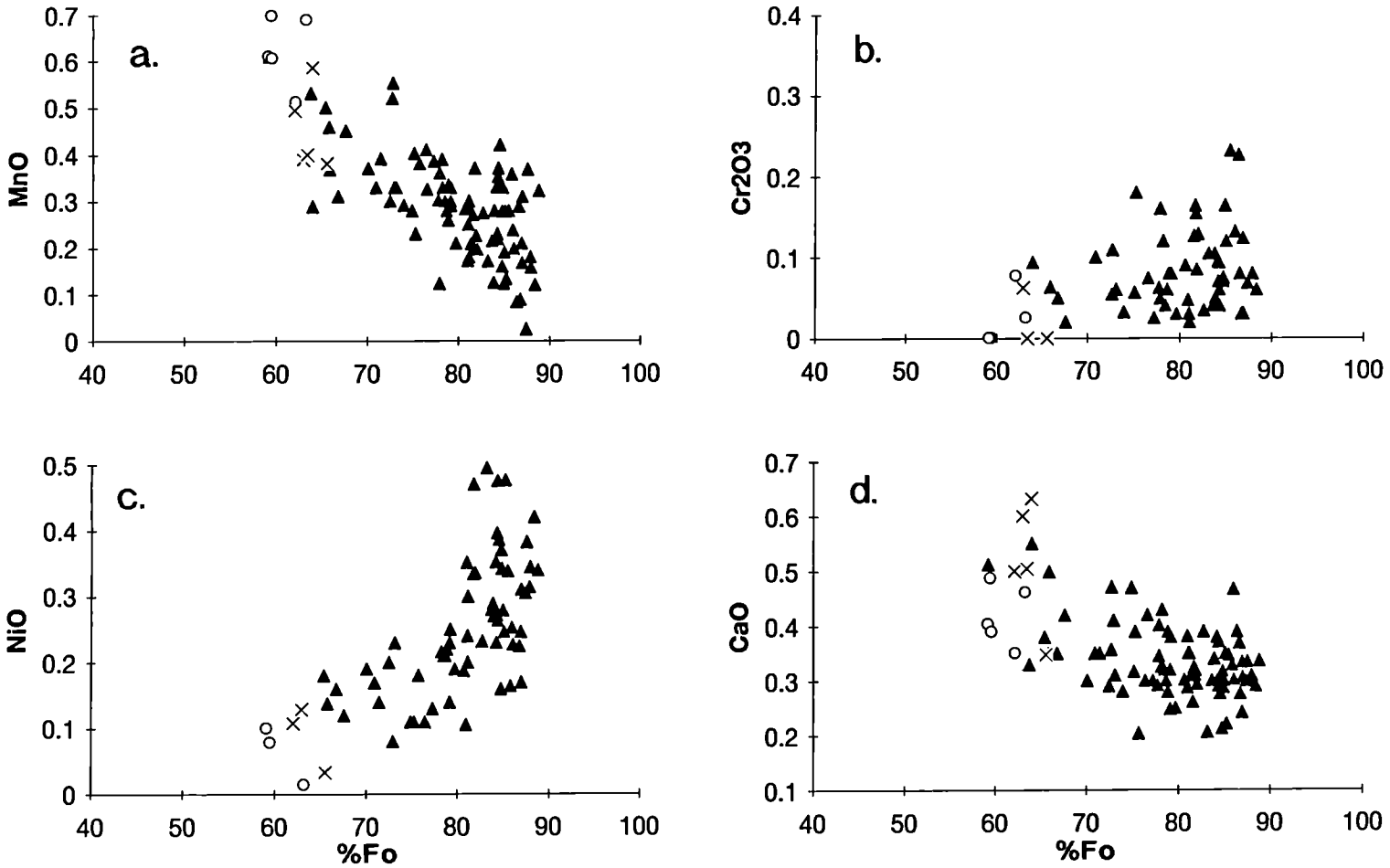


Figure 3.1 Minor element variations within the olivines of the MPG. [SYMBOLS; filled triangles - basalts; open circles - basaltic hawaiites; crosses - hawaiites].

different environments. They suggested that the distribution of Mn in olivine was dependant on the bulk composition of the magma, and whether or not Fe-Ti oxide was a co-precipitating phase. Mn^{2+} substitutes for Fe^{2+} and, since the contents of both these elements in the host magma increase with differentiation, this substitution becomes more favourable.

Cr_2O_3(figure 3.1b)

Cr_2O_3 exhibits quite a scattered pattern when plotted against Fo content, however a scattered positive correlation is still discernable. The highest Cr_2O_3 contents (0.25%) occur in some of the most forsteritic olivines, while the lowest values (<0.1%) can be found in the basaltic-hawaiites. Since the olivines from the most primitive basalts frequently contain included Cr-spinels, the higher Cr_2O_3 of the more forsteritic olivines may well be due to the electron beam striking a small Cr-spinel during analysis. Although Cr normally exists in the Cr^{3+} state it can, under reducing conditions, also exist as Cr^{2+}. In this 2+ state (atomic radius, 84pm)[4] it could conceivably substitute for Fe^{2+} (atomic radius, 76pm). Henderson (1982) reported an average partition coefficient for Cr in olivine of 2.1.

The chief control on the Cr content of olivine, whether as part of the structure or as minute included crystals, seems the abundance of Cr in the magma from which the olivine crystallises. Since Cr is compatible in both Cr-spinel and clinopyroxene, fractionation of these phases (section 4.3) will markedly reduce the Cr content of an evolving magma, and this is why olivines from the hawaiites contain less Cr_2O_3.

NiO (figure 3.1c)

NiO shows a reasonable positive correlation with Fo content, and varies from ~0.45% in high MgO basalts, to <0.1% in the hawaiites. Williamson (1979) noted a near identical range of NiO contents in olivines from the SMLS. The distribution of Ni, like Mn, is dependant upon the bulk composition of the melt (Simkin & Smith 1970). Ni is highly compatible in forsteritic olivine[5], substituting readily for the similarly sized Mg^{2+} cation.

CaO (figure 3.1d)

CaO displays a reasonable negative correlation with Fo content, i.e. the lowest CaO values (~0.2%) are generally found in the more forsteritic olivines, with higher values (~0.6%) in the Fe-rich olivines.

---

[4] Values of atomic radi in pico-meters (pm) from Mortimer (1984).

[5] Partition coefficient of Ni in forsteritic olivine = 14 (Henderson 1982).

Simkin & Smith (1970) proposed that the crystallisation environment played a major role in determining the Ca content of olivines, with deep crystallising plutonic rocks having lower CaO (<0.1%) in their olivines, than extrusive and shallow intrusive rocks (>0.1%). This therefore implied a pressure control on the CaO content of olivines, with the larger Ca cation finding it more difficult to substitute for the smaller Mg, Ni & Mn cations at higher pressures. *However,* more recent work by Jurewicz & Watson (1988) experimentally determined Ca partition coefficients of olivine in a melt, at varying temperatures, pressures and fO_2. They proposed that the Ca content of an *equilibrated* olivine is chiefly dependent on *both* the CaO and the FeO content of the melt. High FeO values result in olivines with higher CaO contents. It was also observed that fO_2 has no direct effect on CaO content, and although temperature does not greatly effect Ca partitioning, it does influence the CaO/MgO distribution.

The general increase in CaO in the less forsteritic olivines from the MPG, *may* reflect increasing CaO in the melt. However, the fractionation of clinopyroxene and plagioclase, with differentiation from a high-MgO basalt to an hawaiite (section 4.3), keeps the CaO content of the magma at a relatively constant level. Therefore, it is possible that the higher CaO contents of the more fayalytic MPG olivines, are more likely to be the result of the higher Fe contents of the host melts.

3.2.2 Clinopyroxene

The pyroxene quadrilaterals in figure 3.2a & b summarise the compositional ranges for the various types of Mull lavas outlined in section 3.1. The MPG pyroxenes range from $Ca_{46}Mg_{45}Fe_9$ in the most basaltic lavas, to $Ca_{46}Mg_{22}Fe_{32}$ in the trachytes. This falling MgO/FeO ratio with increasing degrees of evolution of the host magma, parallels the fall in MgO/FeO in the olivines and is probably caused by crystal fractionation processes (see section 4.3). Due to their relatively high Ca contents, the pyroxenes of the MPG straddle the boundary between diopside and augite (Morimoto 1988); i.e. they are diopsitic augites. The clinopyroxene of the MPG basalts spans quite a wide compositional range, and overlaps those of the more evolved lavas (figure 3.2a). A similar overlap in composition between basalts and hawaiites, was observed by Williamson (1979) within the SMLS.

The more Fe-rich basaltic pyroxenes presumably crystallised at a late stage from residual, more evolved magma. In order to test this proposal, the cores and rims of several pyroxene crystals have been analysed (these are noted in appendix 4d). The rims contain more FeO, TiO_2, Al_2O_3, MnO and Na_2O than the cores, along with less SiO_2, MgO and CaO. These *intra*-lava chemical trends reflect crystallisation from an

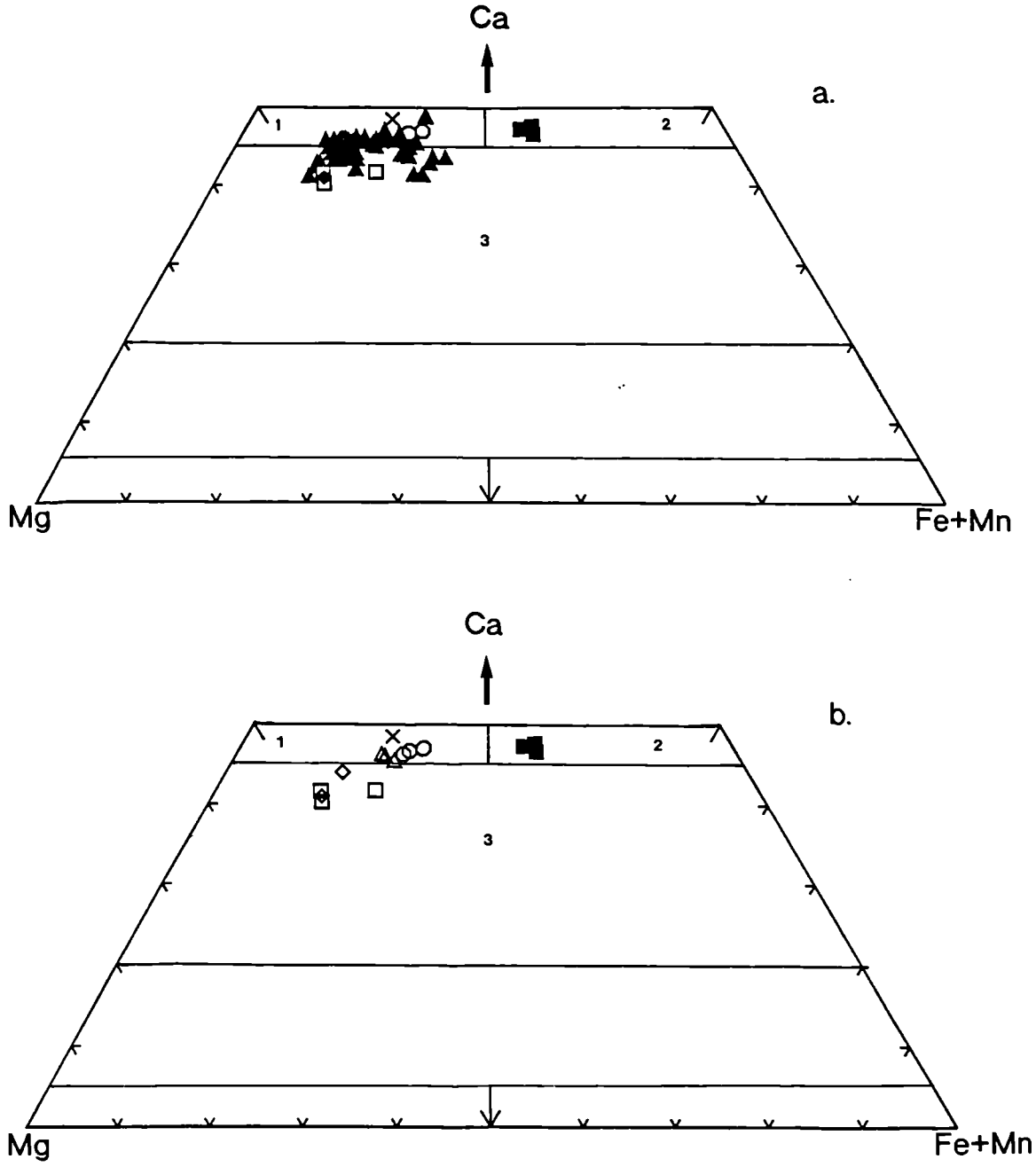


Figure 3.2 Clinopyroxene compositions plotted on pyroxene quadrilaterals. ***a.*** all the pyroxenes analysed during the present study, ***b.*** all pyroxenes except those from MPG basalts. [SYMBOLS; as in figure 3.1 plus, open triangles - mugearites; filled square - trachytes; open squares - SMT lavas; open diamonds - CMT lavas]. Numbered fields; 1 - diopside; 2 - hedenbergite; 3 - augite (from Morimoto 1988)

increasingly evolved magma. Similar *inter*-lava trends have also been found (see below)

In addition to the MPG analyses, pyroxenes from the Staffa Magma sub-Type (SMT), and the Central Mull Tholeiites (CMT) have also been analysed. Figure 3.2b shows that, for the most part, the pyroxenes of these tholeiites contain lower Ca than the MPG basalts. The pyroxenes in the SMT sample (W4) range from $Ca_{42}Mg_{47}Fe_{11}$ to $Ca_{42}Mg_{41}Fe_{17}$, while in the CMT (sample CA3A) the two analysed pyroxenes have an average composition of $Ca_{43}Mg_{45}Fe_{12}$.

Figure 3.3 compares the pyroxene compositions from the Mull lava succession with the Tertiary volcanics from the Skye lava succession (Williamson 1979; Thompson 1974). Also plotted on this diagram are the trends of pyroxene compositions from the Skaergaard intrusion Wager & Brown (1967), and the Shiant Isles Sill (Gibb 1973). The MPG pyroxenes most closely compare with those from the SMLS, however, the pyroxenes from the MPG trachytes are more calcic than those from the SMLS trachytes. This observation is simply a reflection of the more alkaline nature of the MPG trachytes (section 4.3).

Minor element variations in pyroxenes (figure 3.4)

Al_2O_3 and TiO_2

As figure 3.4a & b shows these two elements behave in a similar fashion, with increasing differentiation (lower Mg/Mg+Fe+Mn+Ca of the pyroxene), and figure 3.4f bears out this point. This covariance of Al and Ti in a suite of pyroxenes from genetically related rock types, is due to the coupled substitution;

$$(Mg, Fe)^{VI} + 2Si^{IV} \rightarrow Ti^{VI} + 2Al^{IV}$$

Other Tertiary Hebridean lavas (eg. the SMLS, Williamson 1979) and intrusive bodies (eg. the Shiant Isles sill, Gibb 1973 and the Trotternish sill, Skye, Gibson 1988) also display a similar positive correlations between Al and Ti. Figure 3.4f however, also reveals that there is *excess* Al available for other substitutions, and these probably include;

$$(Mg, Fe)^{VI} + Si^{IV} \rightarrow Al^{VI} + Al^{IV} \text{ and,}$$

$$(Mg, Fe)^{VI} + Si^{IV} \rightarrow (Fe3+, Cr)^{VI} + Al^{IV}$$ Larsen *et al.* (1989)

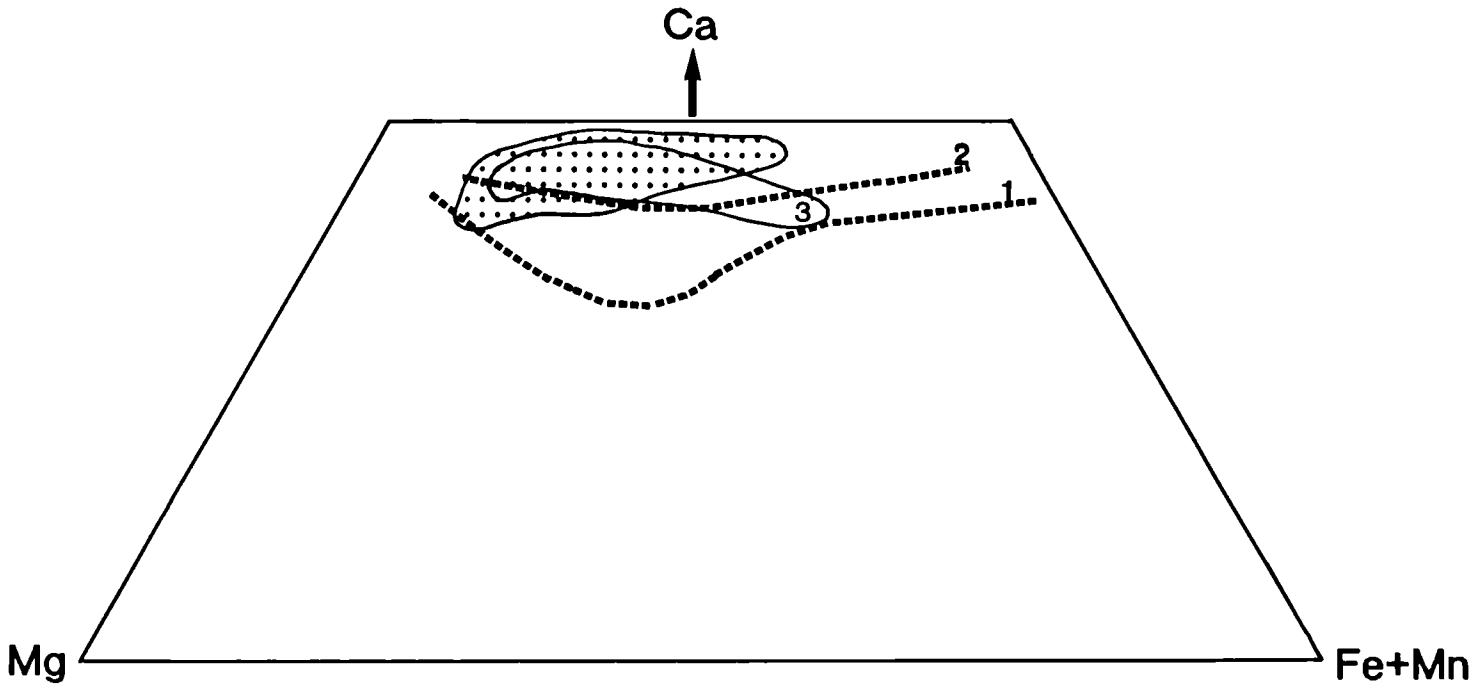


Figure 3.3 Comparative pyroxene quadrilateral showing, analyses from the present study (shaded area), trends for the Skaergaard intrusion (1), and the Shiant Isles sill (2), and the range of compositions for pyroxenes from the SMLS (3)

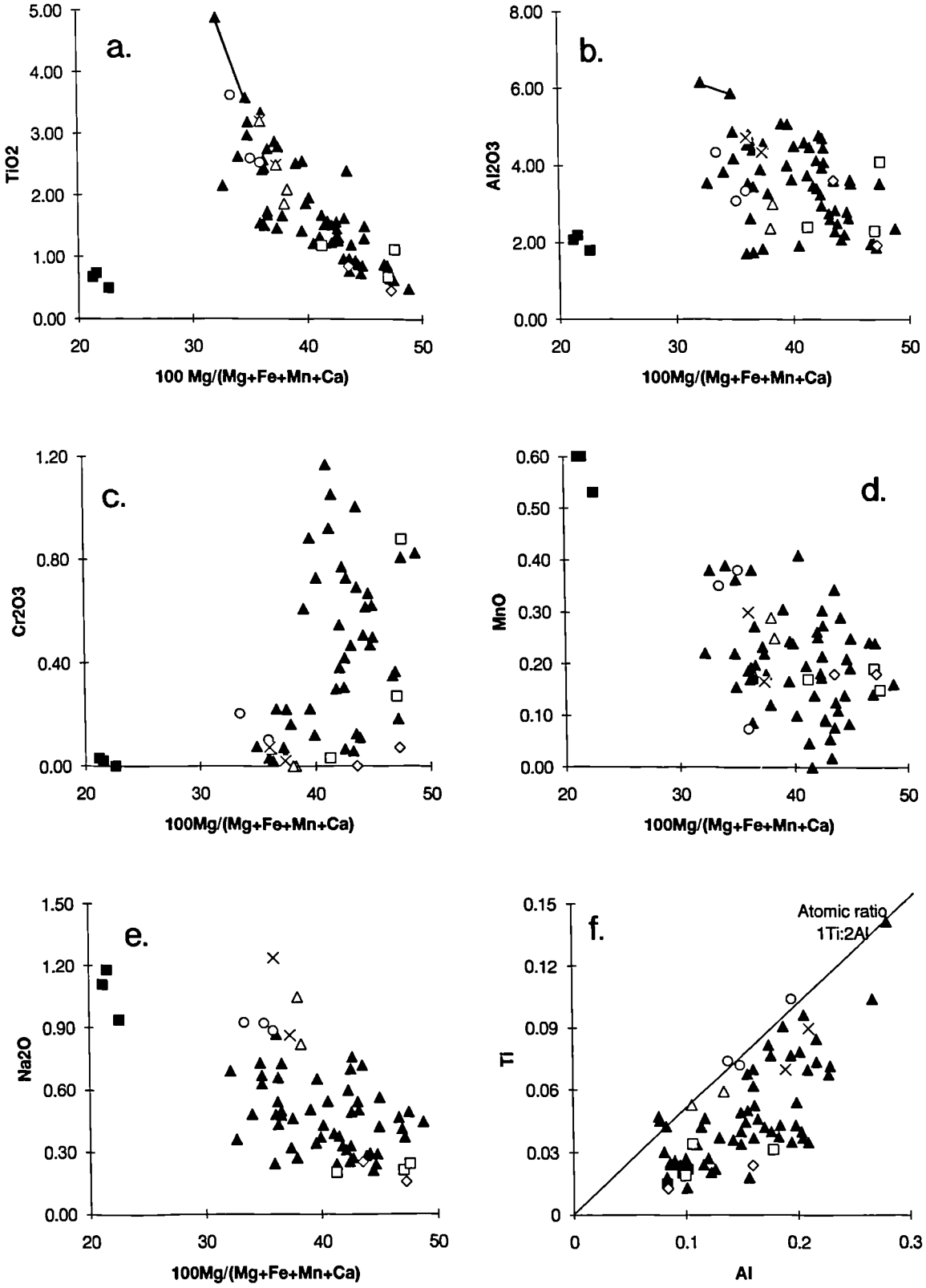


Figure 3.4 Minor element variations in pyroxenes. Symbols as for figures 3.1 and 3.2. The line connecting two of the analyses on figures a. and b. is explained in the text. (In figure 3.4f several analyses plot slightly above the Ti:2Al line and this presumably due to analytical error).

The products of these coupled substitutions are known as the "Tschermaks" pyroxene components, and can account for the larger scatter of Al contents, as opposed to Ti (figures 3.4b & a respectively). Hertzberg & Chapman (1976) showed that the "tschermakite" component in clinopyroxene (from a spinel lherzolite) increased with increasing temperature. The pyroxenes from the lower temperature evolved lavas of the MPG generally plot closer to the Ti:2Al line (figure 3.4f) than the higher temperature basalts. This observation supports the conclusions of Hertzberg & Chapman (op.cit). Larsen *et al.* (1989) in their study of the Tertiary basalts from the Scoresby Sund region in East Greenland, noted that the groundmass pyroxenes generally contained less tschermaks component than the pyroxene phenocrysts.

As pointed out by Gibb (1973) the fractionation of Fe-Ti oxide will remove Ti from the melt, while the fractionation of plagioclase will lower the Al content (Upton *et al.* 1984). As a result the pyroxenes crystallising from these liquids will contain less Ti and Al. Pyroxenes from one of the trachytic lava flows of the MPG contain significantly lower levels of Ti and Al than the hawaiites and mugearites. In section 4.3 it will be shown that plagioclase begins to fractionate from the MPG magmas at ~8-9% MgO, while Fe-Ti oxide will fractionate below ~5-6% MgO. Significant quantities of Al will therefore be removed from the magma before Ti. However, the basaltic pyroxenes have 2Al>Ti and, as has already been demonstrated, this excess Al which contributes to the tschermaks component of the pyroxenes, will be reduced *before* the Al involved in the couple substitution with Ti. Therefore the coupled substitution $(Mg, Fe)^{VI} + 2Si^{IV} = Ti^{VI} + 2Al^{IV}$ is dependant upon the quantity of Ti available. Fractional crystallisation of Fe-Ti oxides from the MPG trachytes will lower the concentration of Ti in the melt, and so will impair the couple substitution of Ti and Al.

Sample C4 (analyses connected by a line on figure 3.4a & b) contains pyroxenes with more Ti and Al than the rest of the MPG pyroxenes. As will be shown in section 4.5 this lava belongs to a sub-type of the MPG. These lavas have been contaminated with a small-fraction-melt from the lithospheric mantle and as a result they are enriched in the incompatible trace elements (including TiO_2). Therefore the higher concentrations of Ti and Al in the pyroxenes of this lava, simply reflects the more Ti rich nature of the original melt.

Cr_2O_3, MnO & Na_2O

Cr_2O_3, varies from over 1% in the pyroxenes of some of the least evolved samples, to virtually zero in the hawaiites, mugearites, and trachytes. Having said this, the pyroxenes from the basalts themselves also span a similar range of Cr_2O_3 contents.

Cr probably exists as a 3+ cation in these magmas and so it can, along with Al, substitute for Si and Fe (or Mg) to form a tschermacks molecule (see above).

From figure 3.4c it can be observed that the Cr content of the pyroxenes falls rapidly at <40% En, suggesting that the Cr content of the liquid has been rapidly depleted by the fractionation of Cr-spinel and clinopyroxene (section 4.3). A similar feature was noted by Gibson (1988) in the pyroxenes of the Trotternish sill, Skye.

MnO (figure 3.4d), displays quite a wide scatter, with values varying from 0.6% in the trachytes to <0.1% in some of the basalts. Like in the olivines Mn readily substitutes for Fe^{2+} within the pyroxene structure and, as a result, a negative correlation between Mn and Mg/(Mg+Fe+Mn+Ca) can be observed with increasing Mn and Fe in the melt. The scatter on this diagram may well be due to the fact that Mn can substitute for Fe^{2+}, not only in pyroxene, but also in olivine (section 3.2.1) and Fe-Ti oxides.

The Na_2O content of pyroxene (figure 3.4e) shows a broad tendency to increase with progressive differentiation of the host rock, from <0.3% in the most basaltic lavas, to 1.2% in the more evolved magmas. This may well reflect the coupled substitution,

$$(Mg^{2+})^{VI} + (Ca^{2+})^{M2} = (Al^{3+}, Fe^{3+})^{VI} + Na^{M2}$$

since Fe^{3+} and Na increase within the melt as differentiation proceeds.

The minor element variation in the SMT and the CMT covers the same compositional range as the more magnesian pyroxenes of the MPG. An exception to this seems to be Na, with the pyroxenes from the SMT and the CMT containing quite low levels (<0.3%) in comparison with the MPG. This fact reflects the more tholeiitic character of the magmas from which the pyroxenes crystallised.

3.2.3 Feldspar

Figure 3.5 summarises the compositional range exhibited by the feldspars of the Mull lava succession, in terms of the An, Ab and Or components. The MPG feldspars vary from $An_{74}\,Ab_{25}\,Or_{<1}$ (bytownite) in the most magnesian basalts (MR2 & BM8) to $An_{<1}\,Ab_{24}\,Or_{75}$ (sanidine) in the groundmass of the trachytes (BM61). Williamson (1979), reported that the plagioclases from the SMLS ranged in composition from $An_{73}\,Ab_{26}\,Or_{<1}$ in the basalts, to $An_2\,Ab_{67}\,Or_{31}$ in the trachytes.

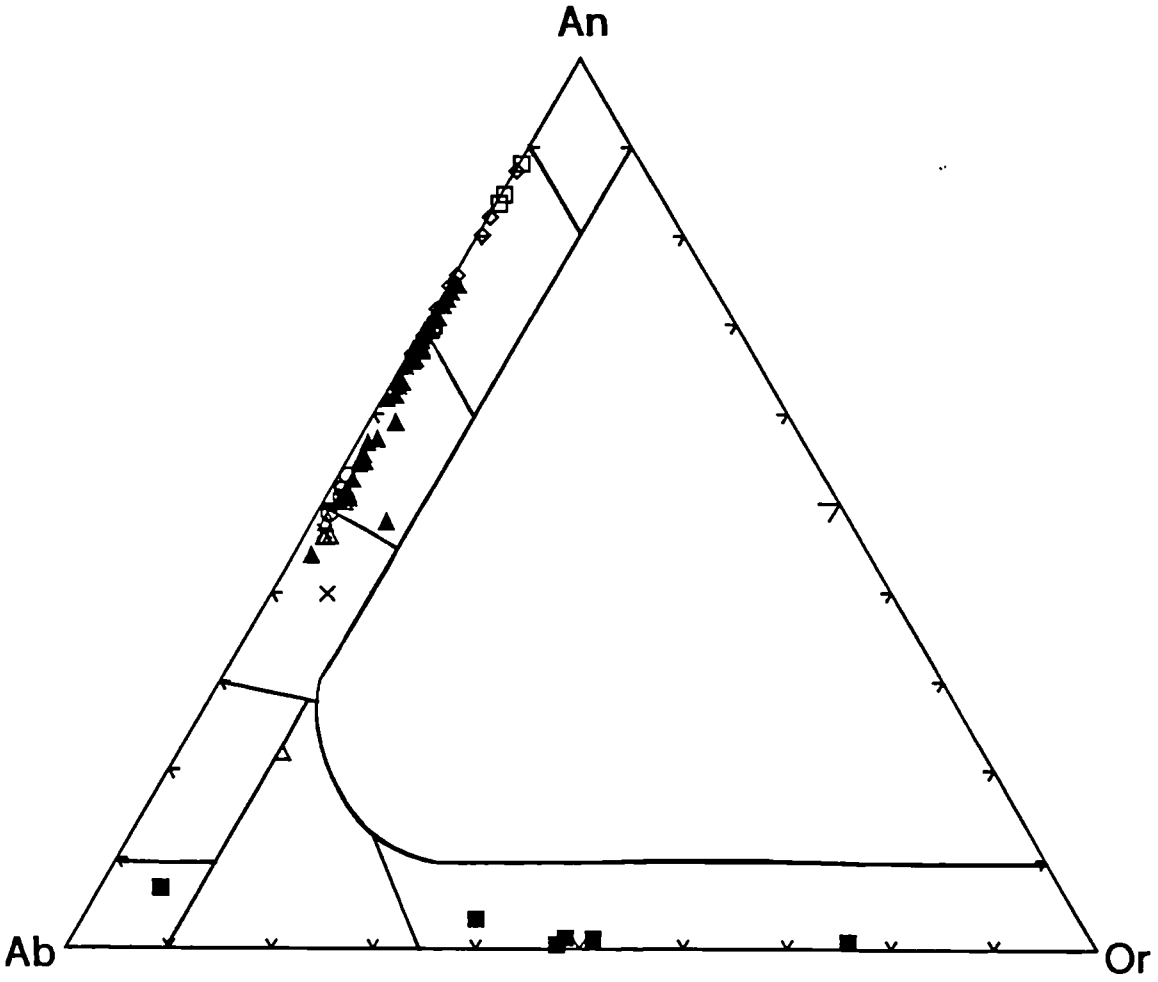


Figure 3.5 Feldspar compositions of the different rock types from the Mull lava succession. Symbols as for figures 3.1 and 3.2.

Analysis of the cores and rims of several plagioclase phenocrysts (table 3.2) reveals that, except where the crystals have

Sample	Core	Rim	Groundmass
BM51	An68	An55	An55
BR22*	An64	An71	An68
MR37	An50	An47	Not analysed

Table 3.2 Average compositions of the cores and rims of plagioclase phenocrysts from the MPG, along with the composition of coexisting groundmass plagioclase. (* BR22 the rim of the phenocryst analysed from this sample has been resorped and regrown. See section 3.1.*)

suffered resorption and regrowth of fresh material (section 3.1), they seem to show normal zoning.

Table 3.3 shows the range of plagioclase compositions shown by some MPG samples, along with the calculated[6] composition of the first plagioclase to crystallise.

Sample	Range of An content	Calculated An content
BR19	39-47	47
BR5	48-67	68
MR9	44-73	71
BM2	63-70	67
BR27	49-53	55
MR2	52-74	72

Table 3.3 The range of An content in some MPG plagioclases, compared with the calculated composition of the first formed plagioclase.

The table reveals that the plagioclases in samples BR19, BR5 and BR27 have calculated An contents similar to, or slightly less than, the most anorthitic plagioclase analysed from that lava. However, flows MR9, BM2, and MR2 contain plagioclase with maximum An values 2-3% *more* than the calculated composition. Some of these plagioclase crystals therefore, might be xenocrystic in origin. Since, however, they are only slightly more basic than the calculated equilibrium plagioclase, their disequilibrium compositions will only have a negligible effect on the whole rock composition.

[6]From the bulk rock analysis using the TRACE program of Nielsen (1988).

As was mentioned in section 3.1.7 & 8, the plagioclase phenocrysts in the SMT and the CMT are more calcic than those of the MPG. The SMT can contain up to An_{88}, while the plagioclase phenocrysts of the CMT range up to An_{87}, and are zoned to less calcic compositions at their margins. The groundmass plagioclase found in these lavas falls within the compositional range of the MPG plagioclases.

Minor element variation in feldspars

Figure 3.6a & b shows the variation of MgO and TiO_2 with decreasing An content. Within the feldspar structure, Mg can substitute for Ca, and Ti for Al (Deer *et al.* 1992). The abundance of each of these elements in the feldspars of the Mull lava succession seems to be broadly dependant on the TiO_2 and MgO content of the melt from which they crystallised. Consequently, Mg in the MPG plagioclases, shows a scattered tendency to decrease with increasing differentiation of the host rock (figure 3.6a). The CMT and the SMT lavas contain lower whole rock MgO contents, despite their high An plagioclase, and so the Mg content of the plagioclases is also low.

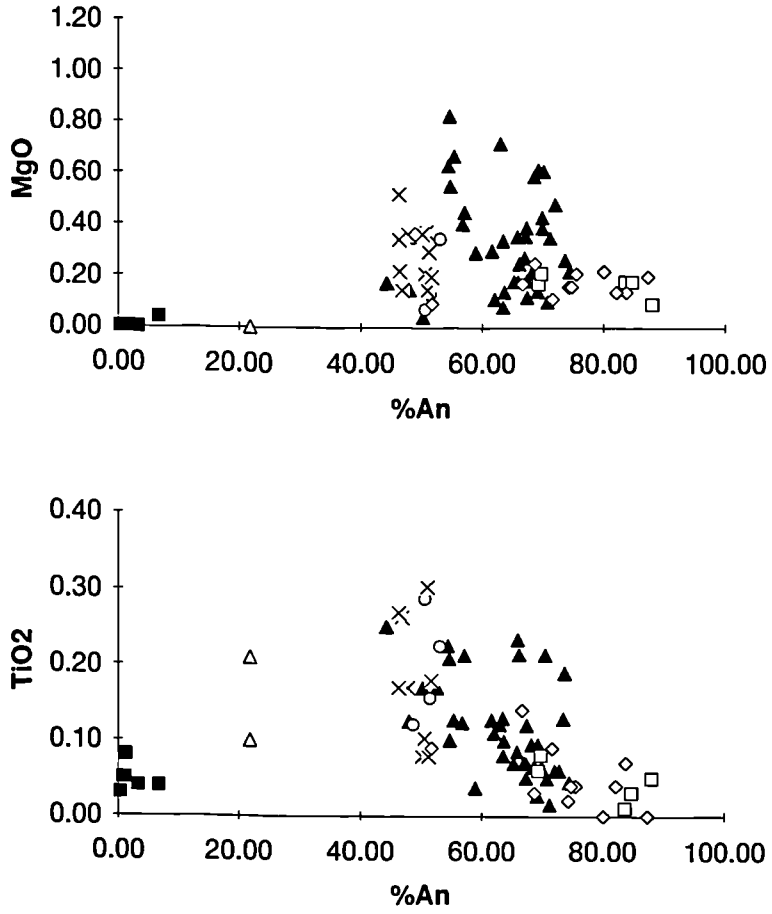


Figure 3.6 MgO and TiO_2 variation in the feldspars from the Mull lava succession. Symbols as for figures 3.1 and 3.2.

Ti in the MPG feldspars gradually increases reaching a maximum of 0.3% in the hawaiites. However, with increasing differentiation involving Fe-Ti oxides the Ti content of the melt starts to fall, and this is reflected in the lower Ti contents of feldspars from the mugearites and trachytes.

The K_2O content (figure 3.5) similarly displays a marked tendency to increase with increasing fractionation, and this parallels the increasing K content of the melt. Fe and Mn, two elements which can also substitute into the feldspar structure (Deer *et al.* 1992), display no systematic variation with falling An content.

3.2.4 Oxide minerals[7]

It is convenient to group the oxide minerals into two groups;

1/ octahedral crystals which are enclosed, or partially enclosed by euhedral to subhedral olivines, and

2/ irregular crystals within the groundmass of the basalts. They can also occur as subhedral to euhedral crystals in the more evolved lavas.

Oxide minerals enclosed in olivines.

As will be demonstrated in section 4.3, Cr-spinel was the first phase to crystallise

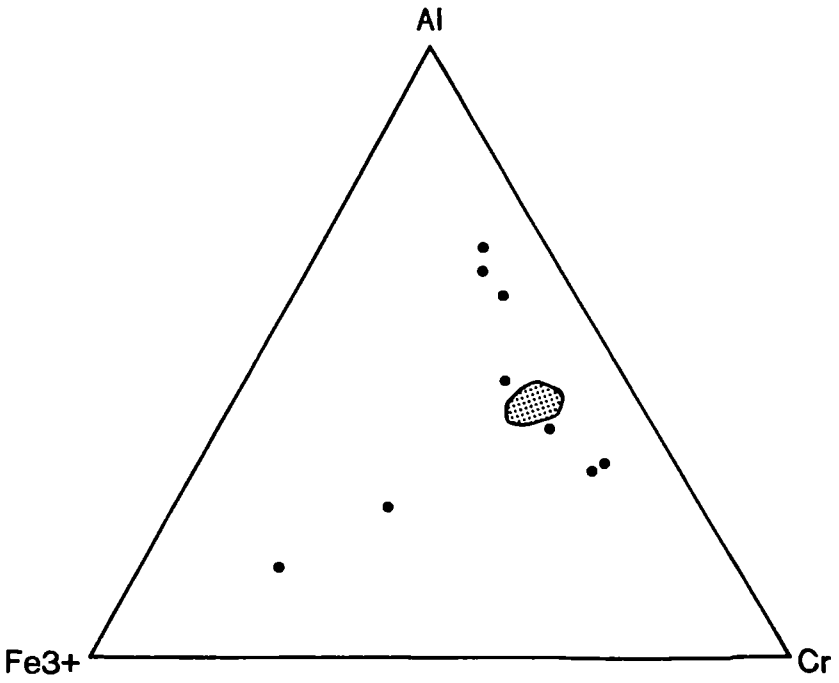


Figure 3.7 Variation of Fe^{3+}, Al and Cr in the Cr-spinels of the MPG basalts. The shaded area represents the compositional range of some Cr-spinels from the SMLS (Williamson 1979).

[7] Fe_2O_3 calculated using the method of Droop (1987)

from many of the more basaltic Cr-rich basalts and, it is probable that these crystals provided nucleation sites on which olivine crystallised.

However, if these spinels were only partially enclosed within olivines, reaction with more differentiated melts in the later stages of crystallisation, led to the formation of more Cr- and, in some cases, more Fe^{3+}-rich spinels (figure 3.7). i.e.

Al-rich chrome-spinel + melt → Cr-rich chrome spinel + plagioclase

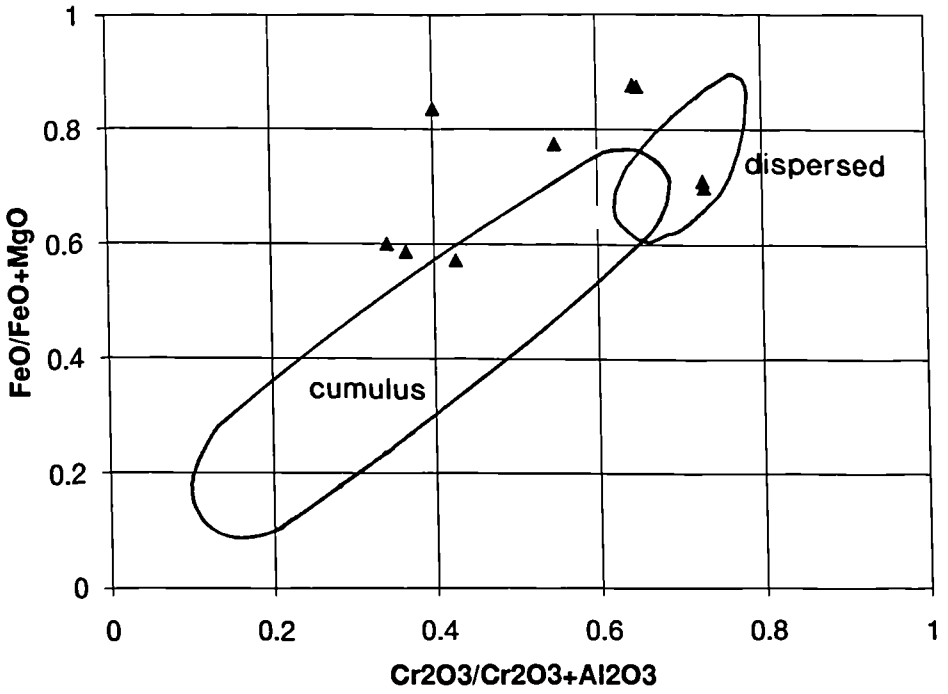


Figure 3.8 A plot of FeO/(FeO+MgO) against $Cr_2O_3/(Cr_2O_3+Al_2O_3)$ for the Cr-spinels of the MPG lavas. The fields for cumulus and dispersed spinels from the Cullin intrusion (Bell & Claydon 1992) are also shown.

Therefore the three MPG Cr-spinels which contain the most Al, may well represent the composition of the primary unaltered Cr-spinel, while those with more Cr than Al, have perhaps undergone reaction with more residual melts.

Bell & Claydon (1992) in a study of Cr-spinels in from the Tertiary Cullin intrusive complex, Skye, observed that the cumulus (seam) spinels were more enriched in Al than those dispersed throughout the rest of the intrusion. They, like Ridley (1977), proposed that the primary character of the spinels had been Al-rich, and they attributed the lower Al contents of the dispersed spinels, to a similar reaction with the residual melt. Figure 3.8 shows the fields for cumulus and dispersed spinels from Bell & Claydon (1992) in terms of FeO/(FeO+MgO) and $Cr_2O_3/(Cr_2O_3+Al_2O_3)$, along with Cr-spinels from the present study.

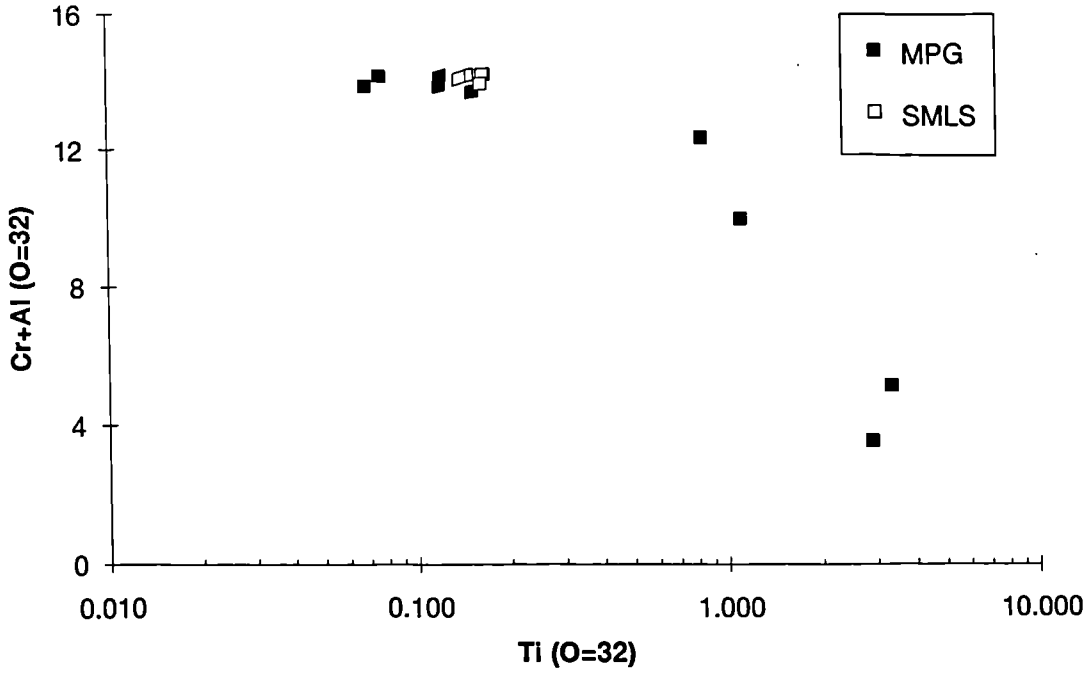


Figure 3.9 A plot of Cr+Al vs. Ti (O=32) for the MPG and SMLS Cr-spinels (Williamson 1979).

Pressure exerts a strong control on the relative distribution of Cr and Al in early crystallising spinels (Fisk & Bence 1980; Dick & Bullen 1984), with higher pressures favouring the formation of more Al-rich spinels. Dick & Bullen (op.cit) suggested that this may well be due to the variation of the partition coefficient of Cr. This varies from 1, at depths appropriate to melt segregation, in contrast to the higher values generally accepted at lower pressures. This implies that the Al-rich chrome-spinels, which have been found in the basalts the Small Isles, the SMLS, the Cullin intrusion, and now also in the basalts of the MPG, crystallised at quite considerable depths. As section 4.3 will demonstrate, this conclusion is entirely consistent with the major element data, which suggest that these basalts last equilibrated at pressures around 9kb.

Figures 3.7 & 3.8 also suggest that during the reaction, Al-rich chrome-spinel + melt $\rightarrow$ Cr-rich chrome spinel + plagioclase, other substitutions involving both Fe^{2+} and Fe^{3+} are important. A negative correlation between Cr+Al and Ti in the MPG spinels (figure 3.9) suggests that late stage exchange processes (possibly $Cr^{3+} + Al^{3+} \rightarrow Ti^{4+} + Fe^{2+}$; Haggerty 1976)), with melts enriched in Ti, have also played a role in modifying the composition of the primary igneous spinels. Corroded relics of Cr-spinel, showing progressive replacement by titaniferous magnetite, have been found in the least fractionated lava flows of the Lower Fionchra Formation, Isle of Rum (Emeleus 1985).

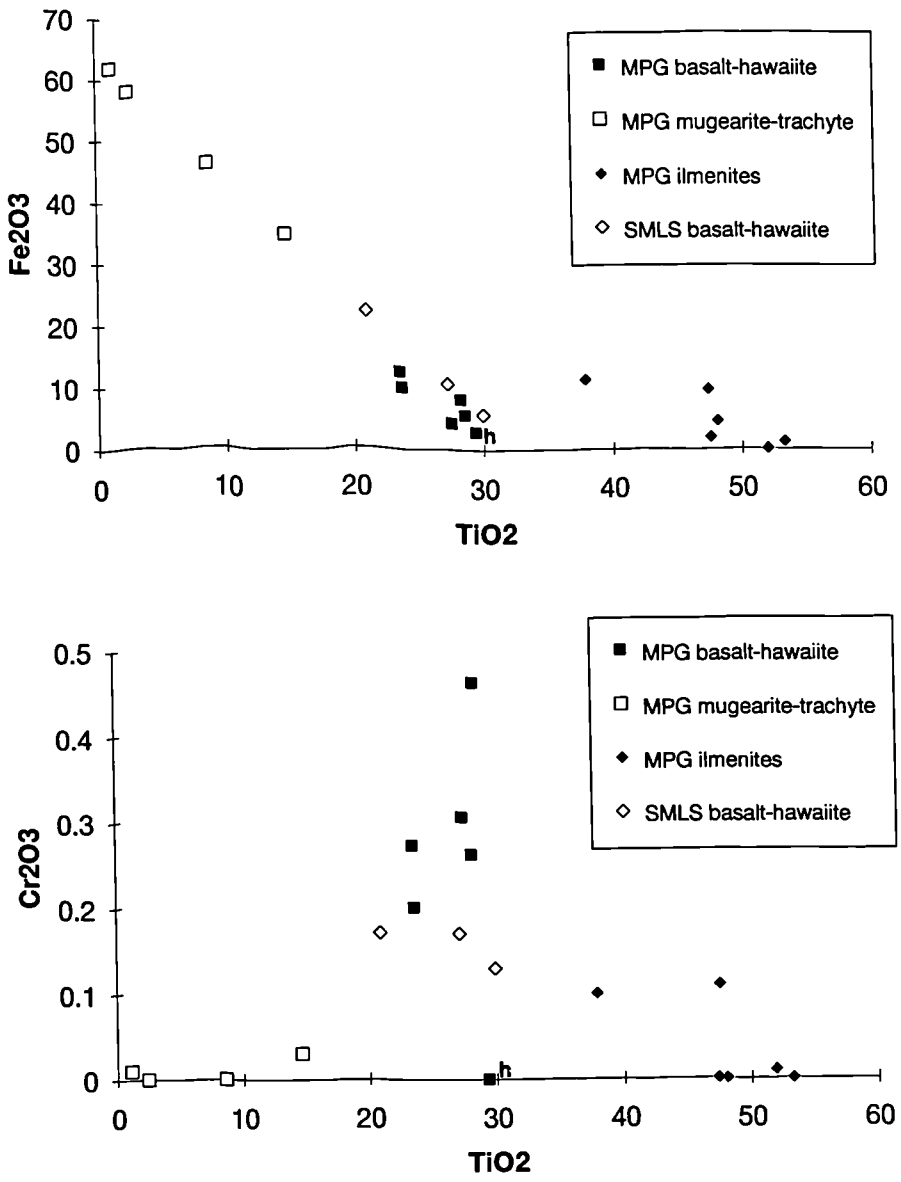


Figure 3.10 Variation of Fe_2O_3 and Cr_2O_3 with TiO_2 in the groundmass oxide minerals of both the MPG and the SMLS (from Williamson 1979). All the symbols except filled diamonds (ilmenites) represent magnetite or titano-magnetite. (Magnetites from hawaiites are denoted by an 'h' beside the sample point).

Oxide minerals within the groundmass

The compositional variation of these oxide minerals within the MPG is summarised in figure 3.10a & b, along with some oxides from SMLS basalts (Williamson 1979). Illmenites, which sometimes occur as exsolution lamellae, as expected contain abundant Ti and Fe^{2+} along with variable (0-10%) amounts of Fe^{3+}.

Opaque minerals of the magnetite series make up the rest of the groundmass oxides. In figure 3.10a &b it can be seen that these magnetites span quite a wide compositional range, and this range seems to be dependant on the bulk composition of the melt from which they crystallised. The highest Cr contents occur in magnetites from the MPG basalts (figure 3.10b >0.1% Cr_2O_3), while magnetites from more the evolved lavas contain virtually no Cr at all. These two observations tally with the whole rock geochemistry of the lavas, i.e. basalts frequently contain >500ppm Cr, and more evolved lavas usually have <100ppm.

The more basaltic MPG lavas contain magnetite with >20% TiO_2, while the one analysed magnetite from an hawaiite contains ~30% TiO2. As a result these oxides can be called "titano-magnetites". However, as figure 3.10a reveals, the magnetites from more evolved lavas (mugearites and trachytes) show a steadily declining Ti content with increasing differentiation. This fall in the Ti content of the magnetites, is explained by the fractionation of Fe-Ti oxides at lower whole rock MgO contents. It is interesting to note that this *decrease* in Ti in magnetite is matched by a concomitant *increase* in Fe^{3+}, leading to an excellent negative correlation between the two variables. This increase in Fe^{3+} with increasing differentiation, is presumably a reflection of the more oxidised state of the last dregs to crystallise from these more evolved magmas.

The petrographic observations and the mineral chemistry discussed in this Chapter, strongly suggest that the processes of fractional crystallisation have played an important role development of the Mull Plateau Group, the Coire Gorm magma type and the Central Mull Tholeiites. This evidence will be further substantiated in section 4.3, when whole rock chemical data will be used to demonstrate crystal fractionation.

Chapter 4

Petrogenetic processes - magmatic plumbing.

This chapter, as the title implies, is principally concerned with the nature of the processes that occur the *after* generation of magma by partial melting in the mantle source region, en route to the surface. It is vital that these processes be stripped away and accounted for, before *any* attempt is made to assess the nature of the mantle source region(s) and melting processes. Similarly, before an assessment of the igneous processes can be made, the effects of secondary, sub-solidus alteration must be considered.

4.1 Post-magmatic alteration effects and elemental mobility

A fundamental prerequisite of any study of igneous processes, in hydrothermally altered rocks, is an intimate knowledge of the relative mobility of the various elemental and isotopic species in the hydrothermal fluids. If the potential mobility of elements is not considered, then erroneous conclusions may well be reached about the nature of the primary igneous processes. All too often in the geochemical literature the possibility of sub-solidus elemental mobility is virtually ignored, and this despite the fact that some of the primary minerals and glass are often visibly broken down and replaced by secondary minerals.

The altered nature of the Hebridean Tertiary lavas has been recognised for quite some time. Bailey *et al.* (1924) noted that no fresh olivine could be found within a central region, close to the intrusive complexes, that they called "the zone of pneumatolysis". As was noted in Chapter 1, Walker (1970a) has since redefined this zone in terms of the nature of the secondary mineral assemblage, and found it to be composed of an inner epidote zone (greenschist facies), grading outwards to a narrow (~2km) prehnite zone (figure 1.2). Beyond this are flat-lying, lower grade, zeolite zones, where the least altered lavas can be found. These secondary minerals form chiefly in vesicles. Nevertheless, they also often replace primary minerals, most especially the groundmass, where they may in some instances replace small amounts of glass (Morrison 1979). It is therefore abundantly clear that some elements *must* have been mobile in these lava flows, and the extent of this mobility will be discussed below.

4.1.1 Factors governing elemental mobility.

The factors which govern elemental mobility during hydrothermal alteration are far from simple, and elemental mobility within every igneous formation/area must be individually assessed.

Among the controlling factors are;

1. The primary igneous mineralogy and chemistry of the rock; ie. if a mineral is relatively easily altered and it contains a significant amount of a particular trace element, then the potential mobility of that element increases.

2. The temperature, pressure and composition of the altering fluid. Associated with these is the permeability of the rock (i.e. is it vesicular or does it contain vugs or cracks and fractures?). These would assist fluids to penetrate the rock and so cause more alteration.

3. The compatibility of the mobilised elements in the secondary mineral phases. This of course will be dependant on what secondary mineral phases are forming.

4. The primary igneous crystallisation history of the rock (see below).

It is apparent from the above factors that no hard and fast ground rules can be laid down with respect to elemental mobility. At this juncture it should be stressed that the terms "mobile" and "immobile" are only relative terms, since no element can be classed as truly immobile. An element can, however, be said to be relatively immobile if, after break-down of a primary mineral phase, it readily finds a suitable lattice site in a nearby secondary mineral phase. On the other hand, some elements will be incompatible in the new secondary mineral phases and, as a result, they are much more susceptible to removal from the system (i.e. the igneous body under consideration).

4.1.2 Previous alteration studies

Various studies throughout the world have been undertaken to assess the alteration and elemental mobility in basalts and other basic rocks. The results of some of these studies are pertinent to elemental mobility in the Mull lava succession and are reviewed below;

Eastern Iceland

Wood *et al.* (1976) investigated elemental mobility in some zeolite-facies, metamorphosed basalts. They concluded that Ti, P, Zr, Nb, Ta, Hf and the heavy REE were for the most part immobile, because they showed a high degree of correlation with each other. In sharp contrast Rb, K_2O and Sr were poorly correlated

with elements such as Zr and Nb, and these were interpreted as being mobile in the hydrothermal fluids. The light REE were found to be mobile, since their principal repository was in the interstitial glass, which was relatively easily altered. The glass in these basalts was originally present in sufficient amounts for it to be an important residence site for some of these incompatible trace elements. (This point will be further discussed later.)

The study of Wood *et al.* (op.cit) was only concerned with lavas which had been metamorphosed to laumontite grade. However, a further assessment of elemental mobility in Tertiary volcanics from Eastern Iceland, was made by I.L.Gibson *et al.* (1982). This research focused attention on elemental mobility in basaltic flows from a 2km drill hole, in which the deeper flows had been metamorphosed to greenschist-facies grade. It was discovered that even when flows were extensively epidotized, Nb, Y, Zr, Ta and Hf, preserved good correlations with each other and so were relatively immobile. Rb, and to a lesser extent Sr, had been mobilised by the hydrothermal fluids. In marked contrast to Wood *et al.* (1976) it was concluded that, since the variation in Ce/Yb ratio could be explained in terms of *igneous* processes, that *all* the REE's were immobile, even during greenschist-facies metamorphism.

Archean metavolcanics, Abitibi Greenstone Belt, Quebec.

It seems reasonable to assume that, the older the rock, the greater the chance that it will have undergone some form of alteration. Therefore, if elemental immobility in older rocks can be demonstrated, then other younger igneous rocks should at least show similar immobility, and because they have been around for less time they may well display a lesser degree of elemental mobility. Archean metavolcanics are therefore, in effect, potentially the worst case scenario.

Ludden *et al.* (1982) studied elemental mobility in Archean metavolcanics, from the Abitibi Greenstone Belt, by comparing the less-altered cores (zeolite-facies) of pillow lavas with the with the extensively altered margins (lower amphibolite-facies). They concluded that, at low grades of alteration, Zr, Y, Ti, and the REE were immobile. However, where alteration was extreme, the REE had been leached and redeposited by carbonate- and potassium-rich fluids. Ba, K, Rb and, to a lesser extent Sr, were mobile at all levels of alteration.

Ordovician Cliefden volcanics, New South Wales, Australia.

These volcanics lie within a prehnite-pumpellyte zone of metamorphism. Smith & Smith (1976) assessed the mobility of various elements by plotting chemical data from the Cliefden volcanics on the (then recently proposed) tectonic discrimination diagrams of Pearce & Cann (1973) and Floyd & Winchester (1975). The scatter of

points on diagrams involving Sr and K, was attributed to mobility of these elements during hydrothermal alteration. In contrast plots only involving a combination of Ti, Zr, Y, P, and Nb displayed little scatter, and it was concluded that these elements were immobile.

Upper Carboniferous Basalts, New Brunswick, Canada.

As with the Cliefden volcanics, these basalts have also been metamorphosed to prehnite-pumpellyte grade, although some have, in addition, been subjected to extensive silicification. Dostal & Strong (1983) concluded that Y, Zr, Hf, Th, Sc, Nb, Ti and the REE were relatively immobile. Silicification had, however, led to a simple dilution of these elements. K, Rb, Sr and Ba abundances and ratios showed a wide scatter and probably had been modified by secondary processes.

Oceanic basalts

Humphris & Thompson (1978) analysed hydrothermally altered basalts from the Mid-Atlantic Ridge. Sr and Ca had been leached from the pillow margins and taken up in epidote rich assemblages. Cu, Zn and Mn had also been extensively mobilised by the hydrothermal fluids. Ba, Co and Ni showed only slight variation with increasing degree of hydrothermal alteration, whereas Ti, V, Y, Zr and Cr did not appear to have been affected by the alteration.

The influence of rock crystallisation history

Humphris *et al.* (1978) compared REE mobility in basalts from Eastern Iceland and the Mull Tertiary lava succession, in an attempt to assess the importance of rock crystallisation history, in determining REE mobility. In Eastern Iceland the flows analysed by Wood *et al.* (1976), in which the light REE had been mobilised, were reassessed; and in Mull a zeolitised Tertiary lava showing virtually no REE mobility from the centre to the margin, and a greenschist-facies lava displaying constant $(Ce/Yb)_n$ ratios, were chosen for study.

The difference in REE mobility between Iceland and Mull is clearly not related to the metamorphic grade, since in both instances alteration occurred under similar environmental conditions. The difference appears to be due to the crystallisation history of the rock. The Reydarfjordur flow, from Eastern Iceland, contains augite, olivine and plagioclase microphenocrysts in a groundmass of granular augite, plagioclase and Fe-Ti oxides. Abundant spaces between the groundmass grains were originally filled with pale brown glass. This has been dissolved away and replaced with secondary minerals. The Mull lavas studied by Humphris *et al.* (op.cit.) contain

virtually no interstitial glass and are composed of well-formed olivines and poikilitic augites enclosing plagioclase laths and Fe-Ti oxides.

In the Reydarfjordur flow the glass had a high LREE/HREE ratio, due to early crystallisation of augite, in which the HREE are mildly compatible (in contrast with olivine and plagioclase in which all the REE are strongly incompatible). As a result, the residual liquids were relatively enriched in the LREE and so the last-formed glass would have been similarly enriched. Since the phase most readily attacked by the hydrothermal fluids was this LREE enriched glass, the LREE would have been preferentially mobilised. In contrast the Mull lavas are almost entirely holocrystalline (<<1% glass, Morrison 1979). Added to this there was no early crystallisation of augite; it is all late interstitial augite. Therefore the residual liquids, and hence the small amounts of interstitial glass, did not become greatly relatively enriched in the LREE. The LREE are therefore relatively immobile in the studied Mull lava flow, and the chief reason for this is the *igneous* crystallisation history.

4.1.3 Trace element mobility within the Mull lava succession.

Having established the relative immobility of the REE in the Mull Tertiary basalts, it is also necessary to assess the potential mobility of the other trace elements and the major elements. In order to achieve this, the work of Morrison (1978;1979) on elemental mobility and alteration in the Mull Tertiary basalts, will be combined with observations and experiments from the present study.

Morrison (op.cit.) sampled vertically through several flows, both in the zeolite-facies and greenschist-facies zones of alteration. Several of these flows were sampled from a drill hole sunk in Pennygown quarry (NM487432), within the greenschist-facies zone of alteration.

Since the originally vesicular margins of the flows provided a porous region for migrating hydrothermal fluids to gain access to the lava pile, the most altered regions of the lava flows are the margins. Morrison (1979) established that leaching around these vesicles (now infilled with secondary minerals) led to a reduction in SiO_2, Al_2O_3, CaO, Na_2O and K_2O values. With the net loss of some of these major components, the REE show an apparent increase due to mass-balance effects.

Zeolites often form in the vesicular cavities and they can also sometimes be seen to replace groundmass minerals. The work of Morrison (1979) revealed that Sr was the only trace element present in any appreciable quantity in Mull zeolites. Lyle (1974) in a study of the Antrim Tertiary lavas, similarly discovered that their vesicular zeolites contained significant amounts of Sr (up to 1500ppm in chabazite) and Rb.

During the present study several large zeolites, and a greenschist-facies vesicle infill assemblage, were collected from Mull and analysed for major and trace elements.

The results of these analyses are presented in table 4.1, along with the analysis of a zeolitic pod collected from a Tertiary lava flow at Glenariff, Co.Antrim (GZ). This table shows the abundance of Sr and Rb in these infilling pods.

	BM55Z	BR2Z	GZ	AM14Z	BRZ1	BRZ4
SiO_2	82.18	51.50	35.69	54.60	53.03	53.94
Al_2O_3	5.83	21.54	26.46	27.33	24.61	22.83
Fe_2O_3	2.62	0.19	0.31	0.28	0.08	0.04
MgO	0.28	0.63	0.40	0.20	0.34	0.24
CaO	2.49	4.41	6.13	10.50	3.83	2.88
Na_2O	0.65	10.62	9.81	6.27	10.20	10.18
K_2O	0.07	0.17	0.00	0.00	0.00	0.00
TiO_2	0.01	0.03	0.01	0.01	0.02	0.01
MnO	0.05	0.00	0.00	0.00	0.00	0.00
P_2O_5	0.02	0.03	0.01	0.01	0.01	0.00
Total wet	94.20	89.12	96.80	99.17	92.12	90.12
Ba	44.0	1.1	0.0	0.0	1.0	0.0
Cr	0.0	0.0	3.2	0.4	0.0	0.0
Cu	34.0	nd	nd	nd	nd	nd
Ga	7.2	10.0	10.7	15.1	10.8	8.9
Nb	3.0	3.1	0.0	0.0	2.1	2.4
Ni	9.0	0.0	2.4	0.0	0.0	0.0
Rb	1.0	3.0	2.1	1.9	4.4	4.7
Sc	1.0	4.0	4.3	10.6	2.4	1.3
Sr	275.0	126.0	118.9	84.7	44.8	9.1
V	6.0	0.0	0.0	0.0	2.9	0.0
Y	0.3	0.0	0.0	0.0	1.1	1.1
Zr	1.0	12.0	9.2	9.2	11.3	12.7
La	1.0	0.0	0.0	0.0	0.2	0.0
Ce	0.0	0.0	0.0	2.4	1.1	0.0
Nd	1.0	0.0	0.0	0.0	0.5	0.0

Table 4.1 The bulk compositions of some zeolitic pods. All have been collected from lava flows of the MPG with the exception of GZ which is from a Tertiary lava flow exposed at Glenariff, Co. Antrim. (Locations; BM55Z - NM514318; BR2Z - NM363455; AM14Z - NM 461326; BRZ1, BRZ4 - NM354458).

The small amounts of Nb and Zr in the analyses (table 4.1) may well be caused by basalt contamination, as not all the surrounding host rock could always be totally removed in the preparation stage. The significant quantity of Cu, in the greenschist mineral assemblage supports Morrisons proposal that Cu and Zn were mobilised at higher temperatures of alteration. The relative abundance of Sr and Rb in zeolitic assemblages, strongly points to the mobility of these elements during zeolitisation of the Tertiary Mull basaltic lava flows. This is supported by plots of Rb vs. Zr and Sr vs. Zr (figure 4.1), from the present work. These display a great deal of scatter, presumably as a result of elemental mobility. This is in sharp contrast to plots of

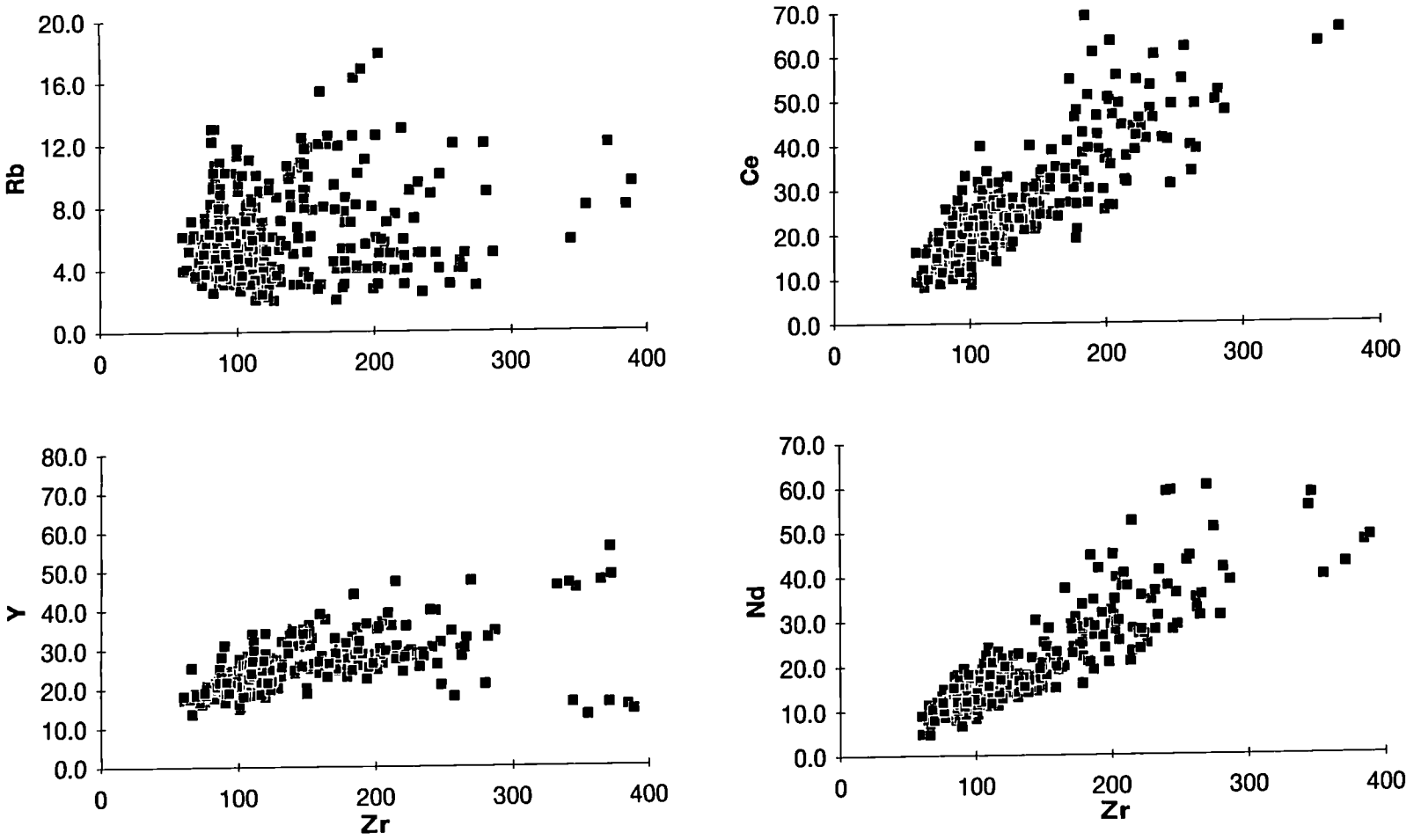


Figure 4.1 Plots of various incompatible elements against Zr, for the MPG lavas. Note the greater scatter on the Rb and Sr vs. Zr diagrams suggesting that these elements were relatively mobile.

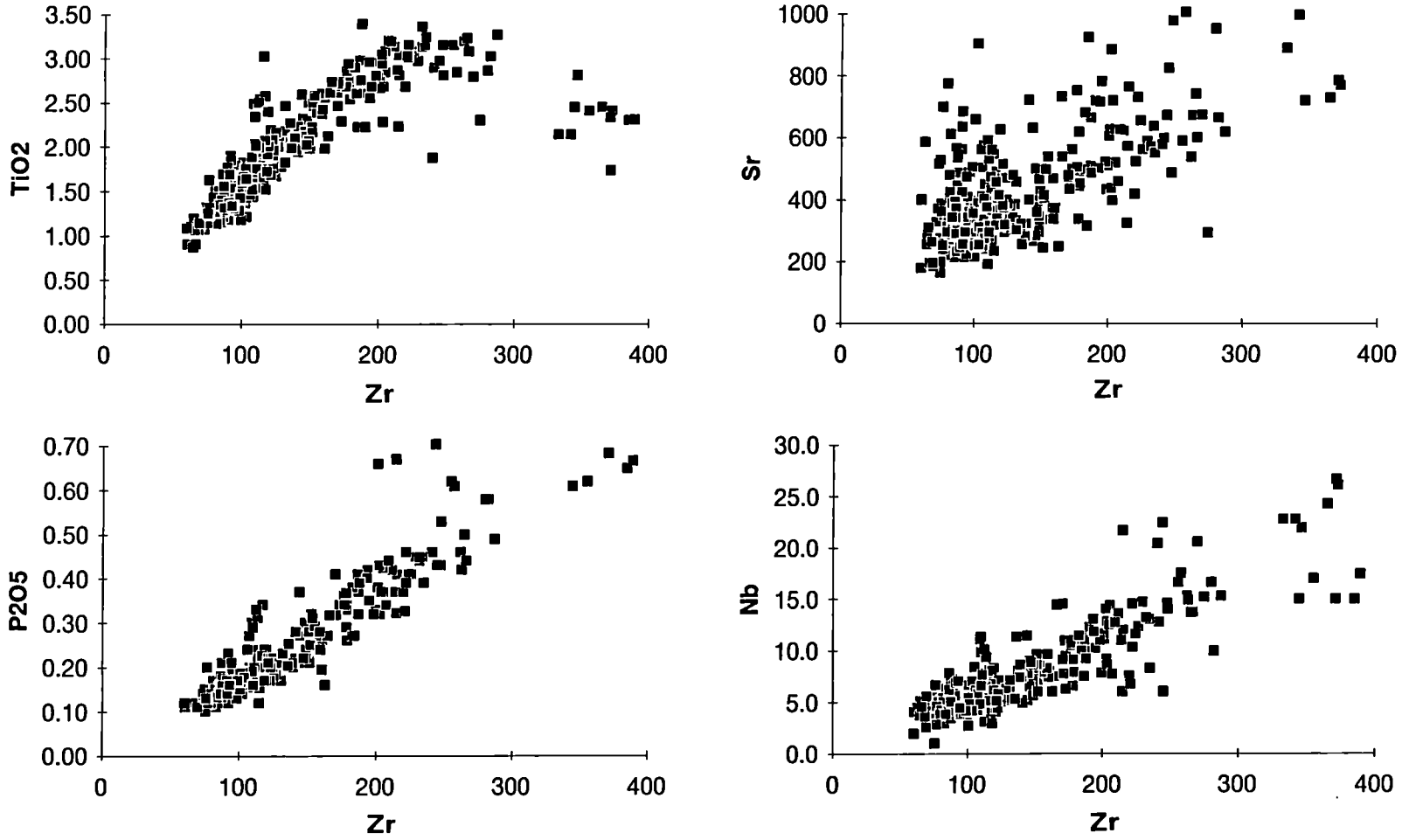


Figure 4.1 (continued)

TiO_2, Nb, P_2O_5, Y, Ce and Nd vs. Zr, which have much tighter linear arrays (figure 4.1). It is difficult to see how this could occur unless these elements were relatively immobile.

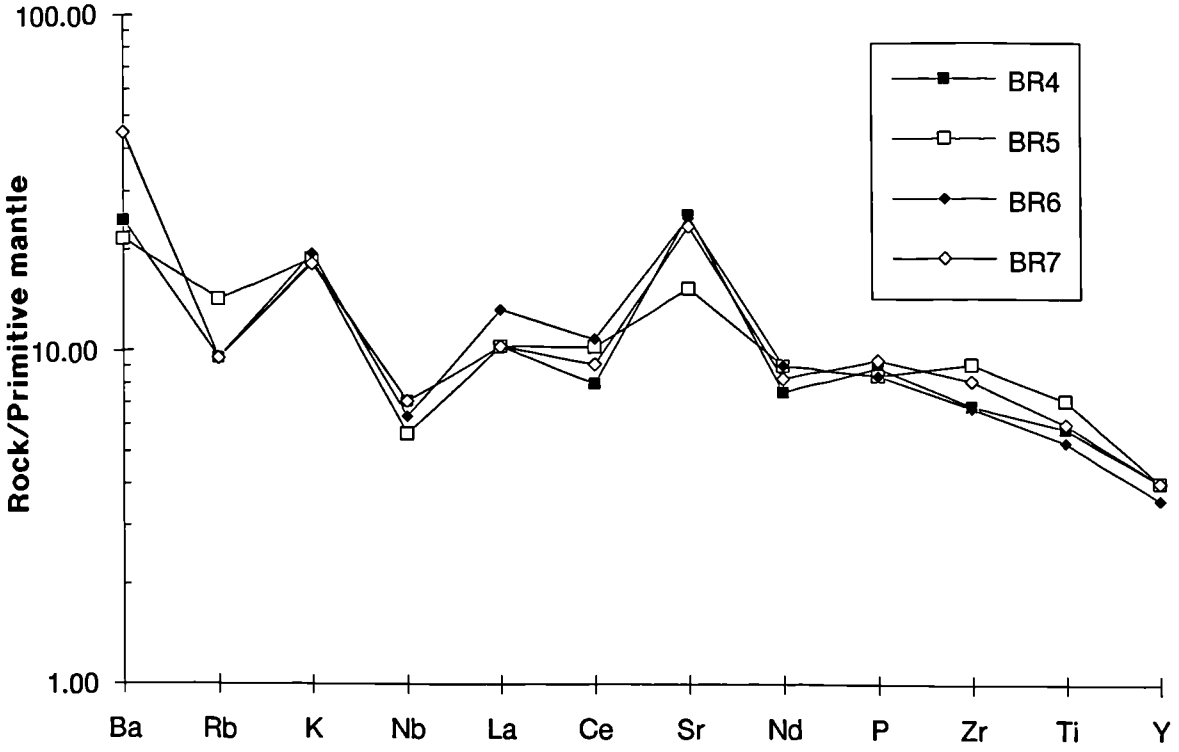


Figure 4.2 Spidergram of lavas BR4-7 showing Sr peaks as a result of net addition of Sr during hydrothermal alteration. Primitive mantle values from Sun & McDonough (1989).

The lavas in which Sr abundances are most enhanced by Sr introduced during the precipitation of in interstitial and amygdoidal zeolites, are those with the lowest initial Sr contents, ie. the most basic lavas. This net addition of Sr to the bulk composition of basic lavas is reflected in Sr peaks on Primitive Mantle normalised spidergrams (figure 4.2) . While every attempt has been made to remove all the *visible* zeolitic material at the crushing stage of sample preparation, Sr peaks still remain a feature of the spidergrams. Tarney & Jones (1993) have noted similar Sr peaks in other continental basaltic rocks and attribute this feature to some kind of mantle source heterogeneity. In order to test this proposal for the Mull lava succession, samples which had quite a large Sr peaks,were closely examined in thin section. More often than not, these high-Sr basalts contained significant amounts of interstitial zeolites, which would have been impossible to remove by hand picking.

One of these samples (BR7), with a Sr peak and interstitial zeolites, was leached in 35% HCl for 30 minutes, to remove any interstitial secondary material, and subsequently reanalysed for trace elements. As would be expected, most of the

elements vary to a slight extent (<10%). In contrast Sr drops by 46% from 471ppm to 286ppm on leaching. Such a drop obviously reflects the high content of Sr in the secondary minerals, most especially the zeolites. A 58% drop in Sr values after leaching (311ppm to 129ppm) has similarly been reported by Hawkesworth &Morrison (1978) from a Tertiary Mull lava, altered to greenschist-facies grade. Leaching therefore effectively removes the Sr peak. Therefore in the Mull lavas at least, the Sr peak is entirely due to secondary alteration effects and not as Tarney & Jones (op.cit) maintain, a mantle source feature.

Morrison (1978;1979) concluded that at zeolite-facies levels of alteration most elements, with the exception of Sr and Rb, appeared to be immobile. With greenschist-facies alteration, more elements are mobile, including Ba and the major elements, except of TiO_2 and possibly P_2O_5. Zr, Nb, Y, Ta, Hf, the REE and possibly Cr are relatively immobile, even with more intense greenschist-facies alteration. As previously mentioned, the scatter for Rb and Sr on figure 4.1 and the good correlations for TiO_2, P_2O_5, Nb, Y and the LREE vs. Sr obtained during the present study, support Morrison's conclusions.

A subsequent study of elemental mobility in Hebridean Tertiary rocks (Dickin and Jones 1983a) focused attention on a basic sill from Skye, cut by thin vertical veins, which were at one time conduits for hydrothermal fluids. Material was collected at regular intervals away from a 6mm wide vein, in order to assess elemental mobility during alteration.

In the severely altered zone (SAZ) (<20mm from the vein centre) K, Rb, Ba, and Cs are strongly leached from the wall rock. Si, Al, Pb and Sr have suffered slight depletion in the SAZ, and isotopic evidence suggests that some form of elemental exchange process, between the rock and the fluid, may have occurred. A slight enrichment of the REE, Mg, Sc, Co, Th, Ti, Fe, Sb, Ta, Hf and P is observed in the SAZ, and yet the evidence from Nd isotopes rules out any addition of Nd to the sill from hydrothermal fluids. This enrichment was therefore considered to be relative, caused by the leaching of major elements such as K, Si, and Al. Ca and Na markedly increase in the SAZ, and this can not be explained by relative addition alone, thus addition of Ca and Na from the hydrothermal fluids to the wall-rock must be invoked. Dickin and Jones (1983a), concluded that fluid composition played a subordinate role to the primary igneous mineralogy in determining the secondary mineral assemblage.

4.1.4 Sampling, sample preparation procedures and geochemical interpretation - - in light of the alteration studies.

From the work of Morrison (1978;1979), it is clear that the primary igneous chemistry is most likely to be preserved in the compact centres of the flows, and not in the more altered amygdoidal margins. With this in mind, an effort was made during the present study, to sample, were possible, from the massive less altered centres of the lava flows. Elemental mobility in the zeolite zone of alteration would seem to be restricted to Rb and Sr. Consequently therefore, little quantitative primary igneous petrogenetic information will - nor indeed I feel, can - be derived from the *elemental* abundances of these elements, as found in the Mull Tertiary lavas. It was not always possible to obtain a sample free from visible zeolites and in such instances every effort was made to pick out all noticeable zeolite-infilled vesicles at the coarse-crushing stage of sample preparation (See Appendix 2).

85% of the lava samples collected during the present study have been collected outwith the greenschist-facies zone of alteration. However, elemental mobility in the remaining samples, from inside this greenschist-facies zone, is much greater. As a result, only TiO_2, Zr, Nb, Y, Ta, Hf, the REE and possibly Cr and P_2O_5, are immobile at these intense levels of alteration. Consequently little reliable petrogenetic information can be derived from the elemental abundances of the Large Ion Lithophile elements (LIL), and most of the major elements in these greenschist-facies lavas.

4.1.5 Potential isotopic mobility

As with elemental and oxide abundances, various isotopic ratios - both radiogenic and stable - can also be modified by hydrothermal alteration. Forrester & Taylor (1976) noted a reduction in $\delta^{18}O$ from "normal" mantle-derived terrestrial magma values of +9.1, well outside the greenschist-facies alteration zone, to -6.5 inside. Forrester & Taylor (op.cit.) attributed this decrease in $\delta^{18}O$ - as the central complex is approached - to interaction of heated meteoric groundwater with $\delta^{18}O$ of -11 to -12. They proposed that this occurred in hydrothermal convective systems by a combination of isotope exchange and a growth of metasomatic minerals in equilibrium with the fluid. Such a dramatic change in $\delta^{18}O$ values begs the question *'Are Sr, Nd and Pb isotopic ratios subject to similar degrees of alteration?'*.

Hawkesworth & Morrison (1978) went a long way towards answering this question. They analysed various samples from a Mull Tertiary lava flow exposed in Pennygown Quarry, within the greenschist-facies zone of alteration. They reported a decrease in whole-rock, unleached, $^{87}Sr/^{86}Sr$ from near the base of the flow (0.70519) towards the top (0.70467). Fresh clinopyroxene separates from the same flow,

yielded a $^{87}Sr/^{86}Sr$ value of 0.70519, whereas a whole-rock sample, leached in 6M HCl, gave a value of 0.70516. These two values are within analytical error of each other and they strongly imply that leaching of whole rock samples is an efficient way of eliminating secondary $^{87}Sr/^{86}Sr$. In sharp contrast $^{143}Nd/^{144}Nd$ analysis produced constant values of (0.51265±3 -- 2σ), throughout the flow.

As mentioned above, Dickin and Jones (1983a) examined elemental mobility in a basic sill from Skye which was cut by thin vertical veins. However, they also studied isotopic mobility. They discovered that in the severely altered zone (<20mm from the vein centre) $^{206}Pb/^{204}Pb$ and $^{87}Sr/^{86}Sr$ ratios increased. This they proposed was due to interaction and isotopic exchange with fluids of Torridonian-type isotope systematics. Nevertheless, further away from the vein centre the $^{206}Pb/^{204}Pb$ and $^{87}Sr/^{86}Sr$ ratios level out and become more constant.

From the above studies it is apparent that, although sub-solidus, secondary alteration can modify Sr and Pb isotope compositions, leaching is a effective means of removing the secondary minerals and so eliminating secondary contamination. Having said this, it is interesting to note that samples analysed for isotopes from the Skye Main Lava Succession (Moorbath and Thompson 1980; Dickin 1981) were not leached before analysis. They, however, only studied some of the freshest lavas on Skye and there was therefore less need to leach their samples.

The samples selected for isotopic work have all been leached in 6M HCl and the leachate discarded prior to analysis. The methodology is further described in Appendix 2.

4.2 Classification of the Mull Plateau Group (MPG) lavas

Previous workers on the lavas of the British Tertiary Igneous Province have used a classification system based on the Thornton-Tuttle Differentiation Index and the normative anorthite content (Thompson *et al.* 1972 ; Beckinsale *et al.* 1978; Morrison 1979; Lyle & Thompson 1983). However, during the present study the recommendations of the IUGS Subcommission on the Systematics of Igneous Rocks (Le Bas & Streckeisen 1991) have been followed. Consequently the classification system employed is the total alkali vs. silica plot, (figure 4.3) with the fields as defined by Le Bas & Streckeisen (op. cit.)

The MPG lavas analysed during the present study are plotted on the alkali-silica diagram, figure 4.3. Several points may be noted from this diagram;

The vast majority of lavas are of relatively basic compositions, basalt to basaltic-hawaiite compositions (>5-6% MgO). These basic lavas, like the Skye Main Lava

Series (SMLS) (Thompson *et al.* 1972) plot on both sides of the tholeiitic-alkalic divide (taken from Miyashiro (1978) and shown on figure 4.3). This strongly implies that these lavas reached their present compositions at quite high pressures (~10kb; Thompson *et al.* op. cit.) where the low pressure silica saturation thermal barrier is not operational.

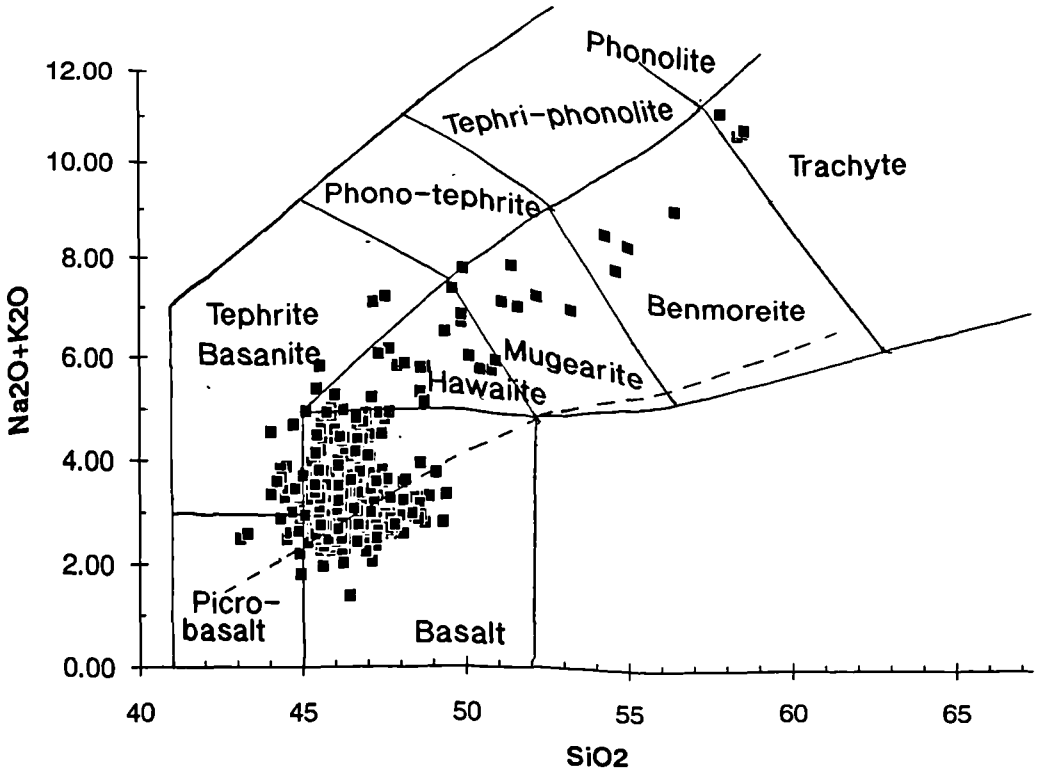


Figure 4.3 MPG lavas plotted on an alkali-silica diagram with the fields proposed by Le Bas & Streckeisen (1991). The dashed line represents the tholeiitic-alkalic divide (Miyashiro 1978)

The transitional nature of these basalts is further confirmed by normative calculations[1] (Appendix 3) which give both Ne and Hy normative basalts. The normative compositions of the MPG basalts and hawaiites are summarised on figure 4.4a, a normative Ne-Hy-Di-Q-Ol plot (Thompson 1982). It can be seen that the lavas plot around the 9kb (±1.5) olivine-plagioclase-clinopyroxene cotectic, on both sides of the 1 atm. critical plane of silica undersaturation. A similar result was obtained for the SMLS by Thompson (op. cit.) (Figure 4.4b).

Returning to the alkali-silica diagram, and focusing on the more evolved lavas (>6.5% total alkalis), it can be seen that they broadly define one fractionation trend. This is in marked contrast to the SMLS which Thompson *et al.* (1972) showed to be

[1] The norms have been calculated for the basalts and hawaiites assuming a $Fe_2O_3/(FeO+Fe_2O_3)$ ratio of 0.1. The scheme adopted by Thompson et al. (1972) for the calculation of Fe_2O_3 and FeO values for the SMLS has not been used, instead their values have been recalculated using the present scheme.

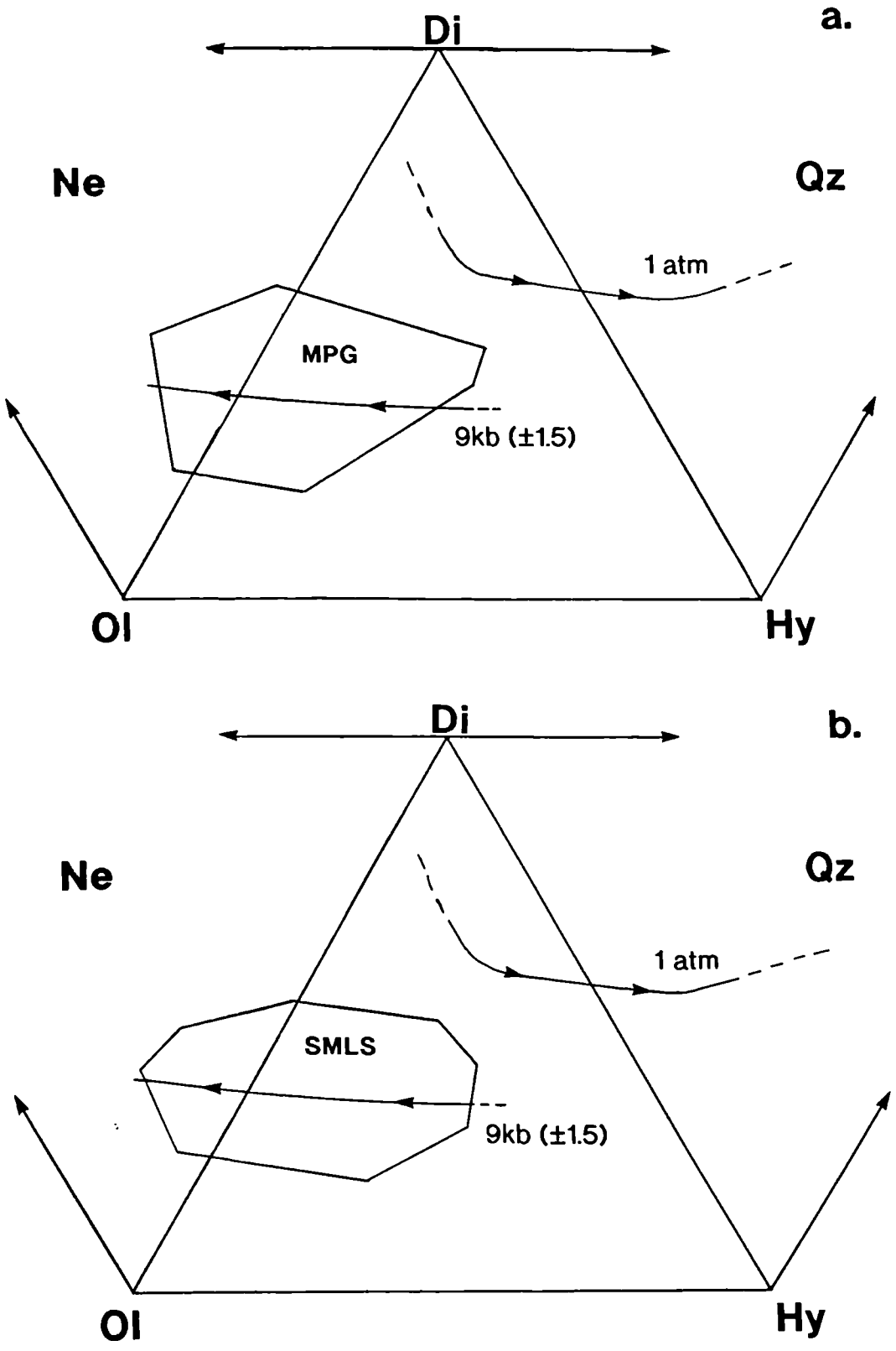


Figure 4.4 Normative Ne-Hy-Di-Q-Ol plots, showing the fields for the MPG and the SMLS. The 1atm. and 9kb cotectics shown are those from (Thompson 1982). *a.* MPG basalts and hawaiites from the present study, *b.* SMLS basalts and hawaiites from Thompson *et al.* (1972).

composed of two trends (figure 4.5) a basalt - hawaiite - benmoreite trend and a basalt - low iron intermediate - trachyte trend. The Mull data seems to conform better to the first of these trends and this is confirmed by the absence of low Fe intermediates within the MPG.

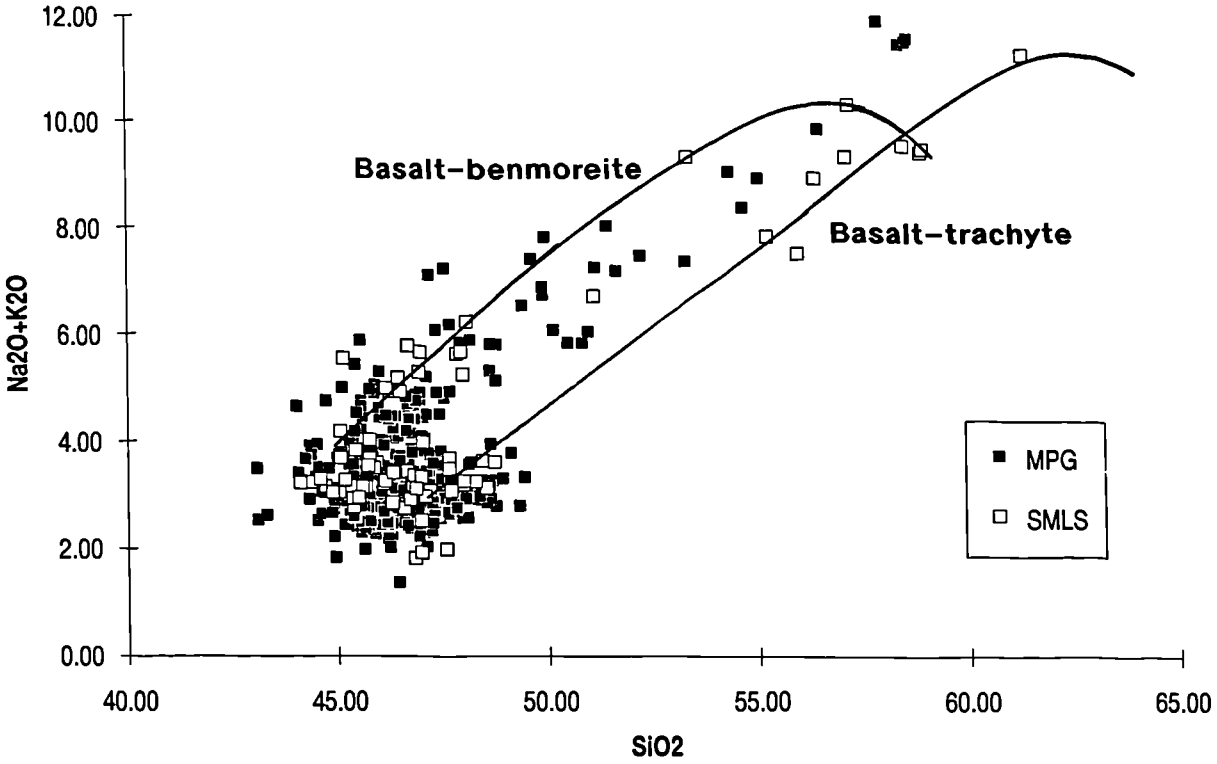


Figure 4.5 The SMLS and the MPG plotted on an alkali - silica diagram, with the basalt-benmoreite and the basalt-trachyte trends proposed by Thompson *et al.* (1972).

An interesting point, borne out by figure 4.5 is the presence of a "basaltic-hawaiite gap" in the SMLS data. Thompson *et al.* (1972) speculated as to whether this gap had a petrogenetic explanation, or whether it was due to insufficient sampling. Cattell (1989) subsequently proposed that the basaltic-hawaiite gap in the SMLS corresponded to a density maximum in the fractionation sequence, which would have meant that these basaltic-hawaiites were too dense to erupt. The new data for the MPG however, shows little evidence for a similar basaltic-hawaiite gap and while the gap may be real for the SMLS, the evidence from Mull suggests that the SMLS gap is more likely to be due to insufficient sampling.

Well over 90% of the MPG lavas collected during the present study are basalts or hawaiites, and the fractionation processes involved in their petrogenesis will be discussed in detail first, before moving on to a consideration of the more evolved lavas.

4.3 Fractional crystallisation

4.3.1 Basalt to hawaiite.

The last significant work on the petrogenesis of the MPG lavas by Beckinsale *et al.* (1978) concluded on the basis of analyses from 17 lava flows that "fractional crystallisation . . . . . has not been a major factor in the production of evolved magma compositions". Instead they concluded that differential partial melting of a "vertically heterogeneous mantle" could account for most of the observed chemical variation in the MPG lavas. The last chapter has clearly shown that a sequence of fractional crystallisation can explain the observed mineral compositions (a line of evidence ignored by Beckinsale *et al.* (op.cit.)) and the following discussion will demonstrate that the conclusions of Beckinsale *et al.* (op.cit) with regard to fractional crystallisation, were almost certainly incorrect.

The choice of a differentiation index is always important in a study such as this. Trace elements, provided they are incompatible over the observed range of compositions and are unaffected by crustal contamination, partial melting, or secondary alteration, can be good indicators of differentiation. Thompson *et al.* (1980) used the $(FeO+Fe_2O_3)/(FeO+Fe_2O_3+MgO)$ ratio (the iron ratio) as a differentiation index since they believed that all of the analysed trace elements had either been incorporated into at least one of the separating solid phases or their compositions were influenced by mantle processes. A slight modification of the above iron ratio has been used in the present study, namely $(total\text{-}Fe_2O_3)/(total\text{-}Fe_2O_3+MgO)$, hereafter abbreviated to F/F+M. A result of this modification is that the F/F+M values calculated during this study, are slightly higher (0.02-0.03), than if they had been calculated by the method of Thompson *et al.* (op.cit).

Major and trace elements analysed by X-ray fluorescence are plotted against F/F+M in figure 4.6. Inflections in differentiation trends usually imply the addition of a new mineral phase to the fractionating assemblage (Cox *et al.* 1979).

Some of the incompatible elements (LREE, Zr and Nb) show a significant range of values at a particular F/F+M ratio. Part of this scatter is due to contamination by an enriched small-fraction-melt from the lithospheric mantle (section 4.5), while the rest can be attributed to varying degrees of partial mantle melting (Chapter 6). These two processes, followed by fractionation, will create bundles of differentiation lineages, so leading to the observed scatter. In attempting to qualitatively model this fractionation, it is important to be able to identify primitive end-member compositions which approximate most closely to a primary mantle melt. Bearing in mind that Thompson (1974) and Cox (1979) proposed that basalts erupted in

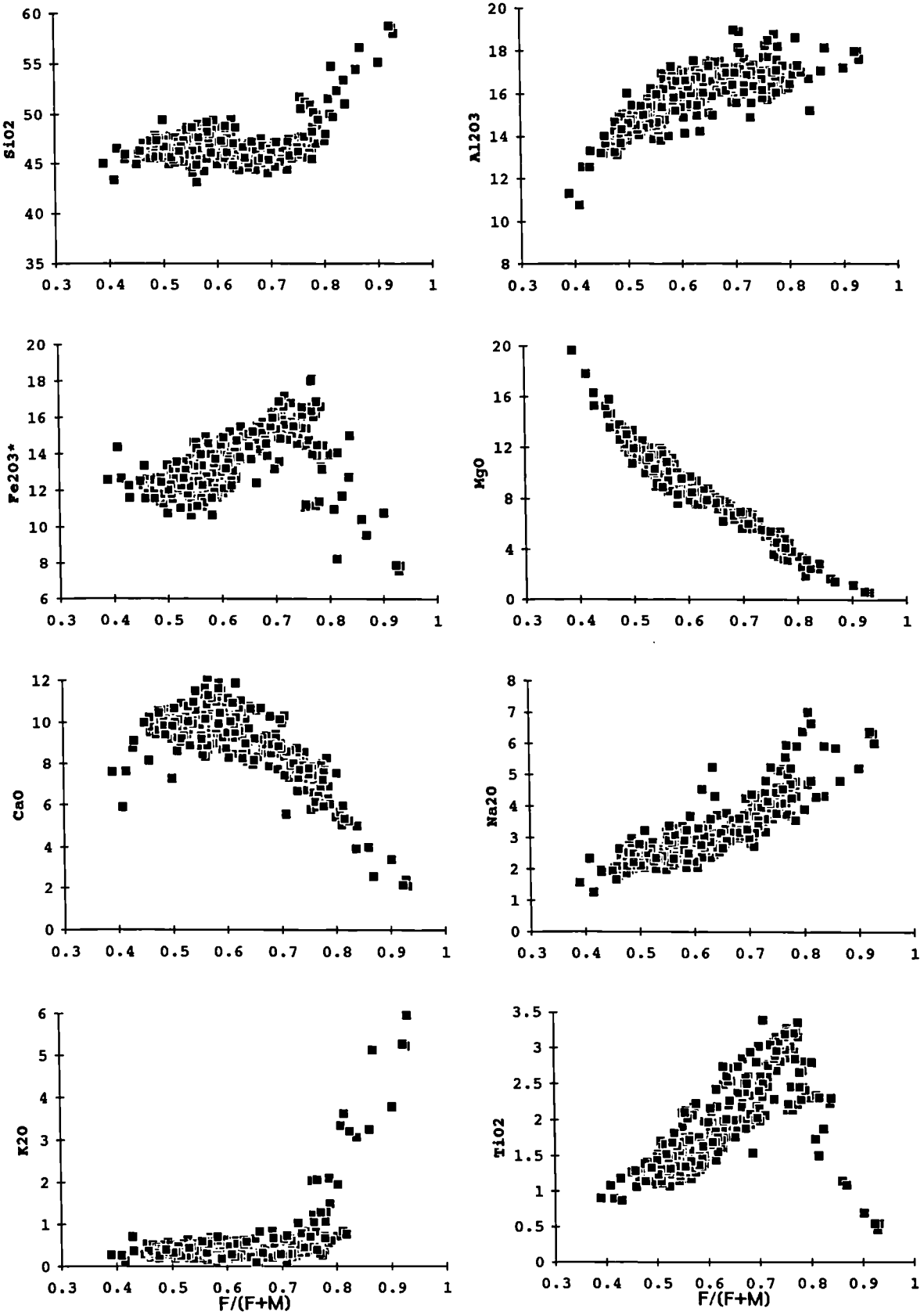


Figure 4.6 Plots of major and trace elements vs. F/(F+M) for the MPG lavas.

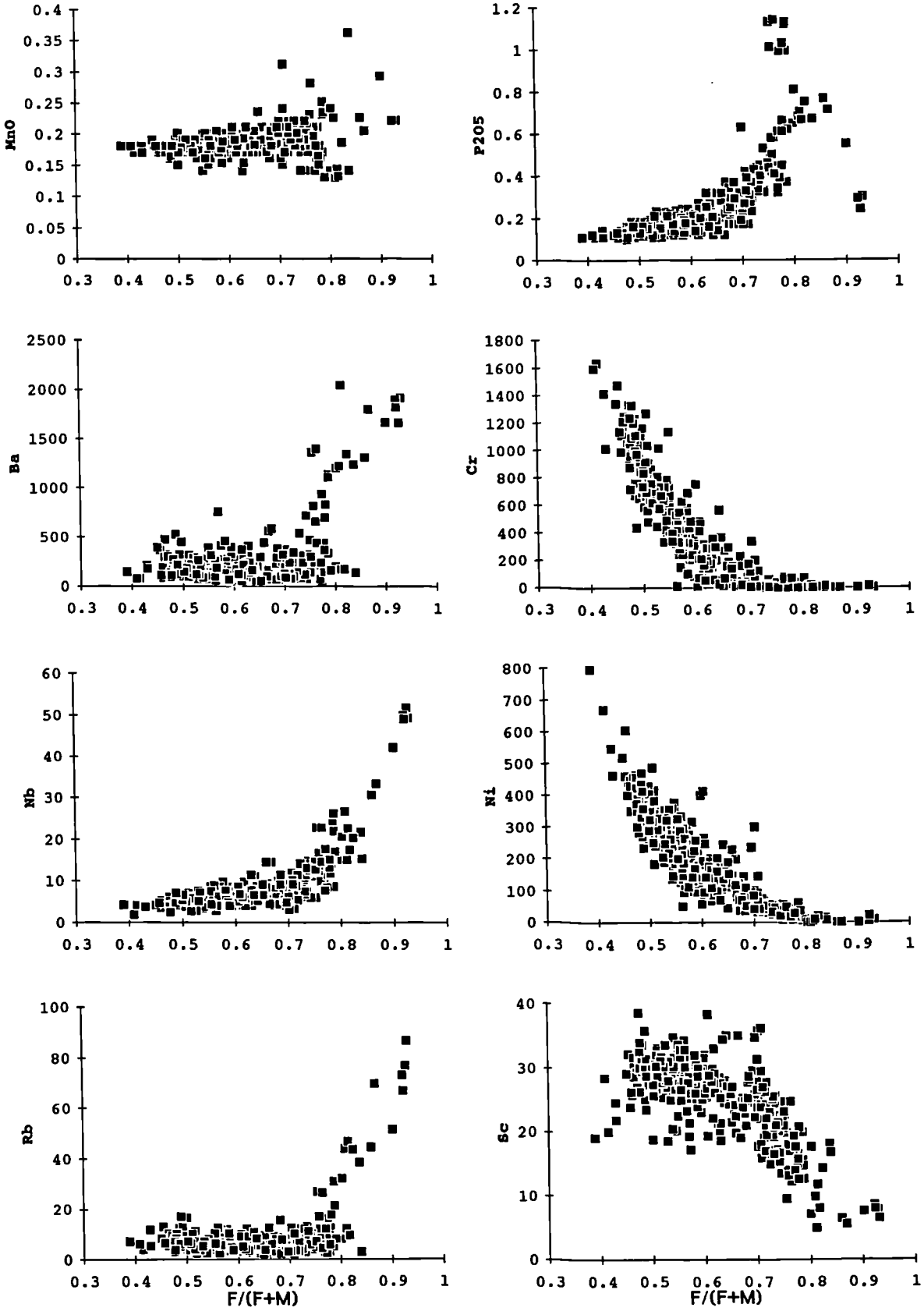


Figure 4.6 (continued)

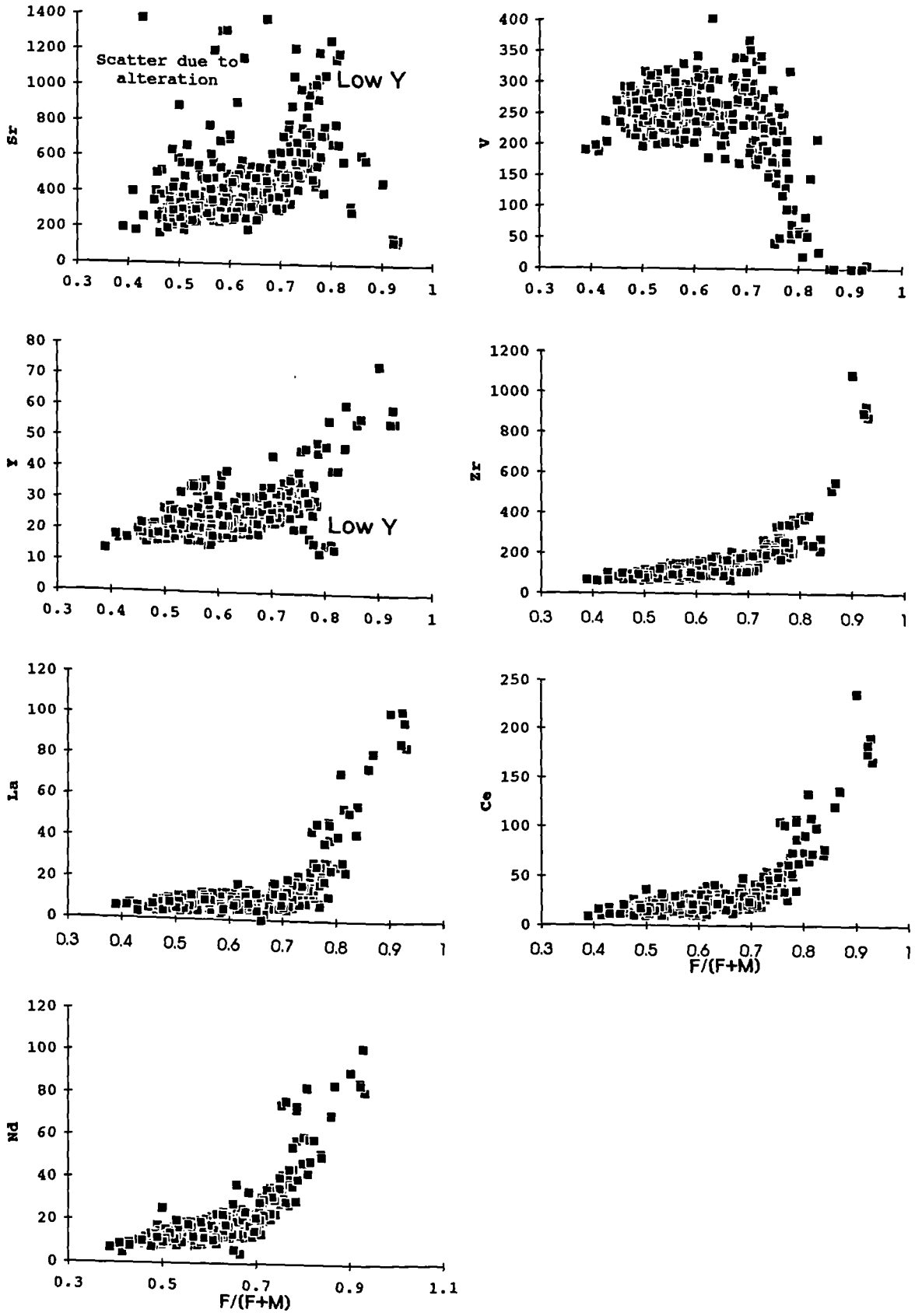


Figure 4.6 (continued)

continental settings may well have undergone some high-pressure fractionation at the MOHO, it is best to consider the most basic magmas as *primitive or parental magmas* and not *primary magmas* as such.

Selection of parental MPG magmas

The three most MgO-rich basalts contain 18-20% MgO and the compositions of their olivine phenocrysts reach a maximum of Fo_{87}. The calculated composition[2] of olivine in equilibrium with a magma containing 19% MgO is, however, Fo_{92} (table 4.2). Since the measured Fo values are significantly less than the calculated Fo content of olivine in equilibrium with a magma containing 19% MgO, these lavas *cannot* represent original liquid compositions and probably contain abundant cumulus olivine (~10-15%). The Fo_{87} olivines in these high-MgO lavas would have crystallised in equilibrium with a magma containing 12-13% MgO (Roeder & Emslie 1970).

Many of the sampled Mull basalts contain olivine microphenocrysts, or at least well-formed olivines slightly larger than the groundmass crystals. Figure 4.6 shows that the MgO-rich lavas are relatively abundant up to about 14% MgO. But do these bulk analyses represent compositions which were originally all liquid? That is to say, are the olivine phenocrysts in equilibrium with the groundmass, or have they accumulated olivine?

Several methods may be employed in order to address this problem;

1./ Electron microprobe analysis of the phenocrysts and the groundmass olivines to see if they are identical, and hence in equilibrium.

2./ Comparison of the Fo-content of the olivine phenocryst cores with calculated Fo values for the bulk composition of the lava. If these two values are in agreement then the bulk analysis probably represents an original liquid composition.

The first approach was largely impractical for two reasons; firstly the alteration of the lavas is such that the olivines are the first mineral phase to be altered, and more often than not the smaller groundmass olivines are virtually completely altered to chlorite, serpentine, iddingsite and oxide minerals. Secondly, since most of the mineral compositions were analysed using the electron microprobe at Durham, the resolution of the electron beam was not good enough to focus on, and analyse the small remnants of groundmass olivine. Instead the cores of olivine phenocrysts have been analysed in several samples with high MgO contents and compared with the compositions of the first-formed olivines calculated from the whole rock analysis,

[2] Using the computer program TRACE (Nielsen 1988), see later for an explanation of this program.

using the TRACE program of Nielsen (1988) The calculated and the observed Fo contents for some lavas are shown in table 4.2.

	Analysed Olivine core	Calculated Fo content
BM1 and 10*	Fo87-85	Fo91-92
BR5	Fo88	Fo87
BM2	Fo85	Fo85
BM5	Fo82	Fo86
BM8	Fo89	Fo87
MR2*	Fo83	Fo88

Table 4.2 Analysed olivine Fo content, compared to the Fo content as calculated by the TRACE program of Nielsen (1988) from the whole rock analysis. (* These samples contain cumulus olivine, and therefore do not represent original liquid compositions)

For samples BR5, BM2, BM5 & BM8 the two values are very similar, strongly suggesting that the phenocrysts are in equilibrium with the groundmass. Therefore the most primitive magmas found within the MPG contain 13-14% MgO with Fo_{88-89}. As was noted above some samples have higher calculated Fo contents than their observed phenocrysts and so these lava flows contain cumulus olivine. Upton *et al.* (1984) studied the North-East Greenland Tertiary tholeiites, which are a similar age to the MPG, and are likewise related to the North Atlantic plume. They found that some of the basalts from the Upper Series contained olivines with core compositions up to Fo_{90}.

In the Hebrides, previous to this study, Thompson *et al.* (1972) and Thompson (1974) used an average magnesian basalt containing 11.7% MgO as a parental liquid and only a few of their SMLS analyses ranged above 12% MgO. They however only selected the freshest lavas for analysis and, since the present study has shown that the olivine rich flows tend to be the most altered, it is conceivable that Thompson *et al.* (op. cit.) did not select the most primitive samples for study, because they were more altered. More recent work on the SMLS by Scarrow (1992) has revealed the presence of more MgO-rich flows than analysed by Thompson *et al.* (1972). As a result, Scarrow (pers comm 1992) has proposed that the most primitive magmas of the SMLS contain 13-14% MgO. R. Kent (pers comm.) has calculated a parental magma composition of 12-14% MgO for Hebridean basalts. The results from these two studies and this one are therefore in agreement, with regard to the MgO contents of primitive Hebridean magmas.

	BM2	BM4	BM5	MR2	B11	BB9	BHL15	AM9	T2	T4	ave
SiO2	46.67	47.03	46.22	45.65	46.30	45.78	47.13	45.18	45.79	45.73	46.15
Al2O3	15.24	14.15	14.69	13.91	15.46	15.39	14.26	15.35	14.48	14.76	14.77
FeO	11.01	9.83	9.98	10.19	9.33	10.89	9.70	10.84	10.82	10.64	10.56
Fe2O3	1.36	1.21	1.23	1.26	1.15	1.34	1.20	1.34	1.34	1.31	1.30
MgO	11.11	13.38	12.00	14.66	11.06	10.36	13.17	11.42	13.32	12.58	12.31
CaO	9.64	10.54	9.88	9.50	10.69	10.09	10.51	9.93	9.18	9.31	9.93
Na2O	2.41	2.34	2.67	1.76	2.05	2.26	1.86	2.26	2.22	2.50	2.23
K2O	0.18	0.21	0.25	0.22	0.21	0.16	0.20	0.18	0.28	0.24	0.21
TiO2	1.90	1.27	1.43	1.28	1.11	1.75	1.14	1.63	1.48	1.47	1.45
MnO	0.18	0.18	0.17	0.18	0.17	0.20	0.17	0.18	0.20	0.18	0.18
P2O5	0.17	0.13	0.14	0.11	0.11	0.16	0.10	0.17	0.17	0.17	0.14
Total	101.09	101.37	99.77	99.85	98.79	99.58	100.53	99.69	100.48	100.09	100.12
LOI	3.76	3.31	4.25	3.53	4.16	1.46	3.99	4.03	2.57	3.58	3.46
Ba	72	100	101	85	86	57	94	91	101	92	88
Cr	610	1017	794	1106	475	342	875	330	843	774	716
Ga	20.3	17.9	19.3	14.4	19.4	22.1	17.8	22.1	16.4	18.6	18.8
Nb	6.6	4.7	5.4	5.1	5.5	4.1	3.4	5.4	6.2	6.6	5.30
Ni	291	389	345	441	182	239	375	355	405	383	340
Rb	2.5	4.8	5.2	5.7	3.5	3.4	4.0	2.4	7.0	5.4	4.39
Sc	26	31	26	26	31	31	33	30	30	29	29
Sr	294	287	306	164	183	258	198	316	292	215	251
V	262	265	245	262	268	296	288	262	235	248	263
Y	22.0	18.0	17.5	17.3	19.0	25.6	18.4	22.6	26.6	27.5	21.5
Zr	123	83	96	75	70	103	76	116	100	101	94
La	6.0	6.4	7.0	5.8	4.0	7.3	5.3	8.5	6.6	6.7	6.4
Ce	18.0	16.4	18.0	12.0	16.8	22.8	13.2	25.7	20.3	20.0	18.3
Nd	16.0	13.0	12.0	9.0	10.5	16.6	8.9	16.5	11.8	12.1	12.6

Table 4.3 Compositions of primitive MPG basalts, which show little evidence of contamination with continental crust or lithospheric mantle.

Fe2O3/Fe2O3+FeO = 0.1

Modelling of fractional crystallisation

These primitive magma compositions should, for the purposes of modelling, be relatively free from any crustal contamination, as well as free from any incompatible element enriched small-fraction-melt from the lithospheric mantle. The selection of a MPG basaltic composition containing little in the way of lithospheric contaminants (<0.25% K_2O; Thompson *et al.* 1982 and the next section on crustal contamination) has not been easy. The reason for this, as the next section will demonstrate, is that as a general rule the most primitive lavas are the most contaminated with continental crust. However, a handful of the most basic lavas appear to have traversed the continental crust with minimal *elemental* contamination, even though isotopic ratios may have been disrupted. These basalt compositions are shown in table 4.3.

Fractional crystallisation was initially modelled using the TRACE program of Nielsen (1988). This program models 1 atmosphere differentiation processes, by combining trace element partitioning with a major element phase equilibrium model. The model also takes account of the temperature and compositional dependence of trace element partition coefficients. From a starting composition at a given fO_2, TRACE calculates successive liquid compositions and the proportions and compositions of the crystallising mineral assemblage.

Sample No.	Initial MgO spinel + olivine	Plagioclase	Clinopyroxene	Titanomagnetite
B11	11.06	8.86	7.21	5.18
BM4	13.38	8.47	7.39	5.37
MR2	14.66	8.85	6.88	5.16
BM5	12.00	8.56	6.70	5.35
T4	12.58	8.11	6.30	5.52

Table 4.4 MgO (wt %) contents at which phases begin to fractionate according to the TRACE program (fractional crystallisation only, with no recharge, assimilation or eruption factors included). Cr-spinel is always the initial phase and it is almost immediately joined by olivine.

The liquid compositions for several primitive compositions have been calculated using this program (with fO_2 set 1 log unit below the QFM buffer). These liquid compositions have been calculated as far as 70% crystallisation, about 4% MgO. To calculate liquid compositions below this MgO level is inadvisable since phases appear on the natural liquidus which TRACE does not model eg. apatite and alkali feldspar. All five compositions show the following appearance of minerals on the

liquidus; Cr-spinel, olivine, plagioclase, clinopyroxene, and titanomagnetite. The MgO contents (and by implication the temperatures; Thompson 1973) at which each of these phases joins the fractionating assemblage are summarised in table 4.4 and it can be seen that they are broadly similar.

Fractional crystallisation of an average parental magma composition (sample BM4) has been modelled using TRACE and the calculated liquid compositions (to 70% crystallisation) for some major and trace elements are plotted in figure 4.7, along with the MPG lavas from the present study.

It can be seen from the diagrams that, while the MPG data fit the modelled compositions reasonably well, the modelled and the actual values are different at several points and the following discussion suggests why. It has already been noted that the MPG magmas probably last equilibrated at pressures around 10kb (figure 4.4). TRACE, however, calculates fractionating crystal assemblage at 1 atmosphere and, as will be shown, most of the discrepancies can be explained by this fact.

The MPG data have relatively constant CaO, Sc and V in the range 0.45-0.6 F/F+M. Over this basaltic range TRACE predicts that olivine, along with minor amounts of Cr-spinel should be the only fractionating phases, and indeed the only phenocryst phase observed are olivines with inclusions of Cr-spinel. The modelled values for CaO, Sc and V (all incompatible in olivine) thereforeshow a progressive rise until plagioclase and clinopyroxene (Sc & V compatible) start to fractionate. In contrast the MPG data suggest that the CaO, Sc and V values are being suppressed in the melt, by removal of another phase not predicted by TRACE. A likely phase to account for this effect is clinopyroxene, in which CaO is a major constituent, and Sc and V are compatible (Ewart 1989) . However, very few clinopyroxene phenocrysts have been found in the MPG lavas, both in this study, and by Bailey *et al.* (1924).

This "invisible" fractionation of clinopyroxene is a common problem not only in continental basalts, but also in MORB (Larsen *et al.* (1989); Cox (1979) and references therein). It has been noted in the studies of Thompson *et al.* (1972) and Thompson (1974) from the SMLS. One atmosphere melting experiments on SMLS basalts Thompson (1972), revealed that clinopyroxene crystalises well below the liquidus, in other words, the magmas are undersaturated with respect to clinopyroxene *at 1 atmosphere.*

This was explained by postulating that the lava compositions were controlled by fractional crystallisation at high enough pressures for clinopyroxene to be a significant fractionating phase. Thompson (1974) carried out high-pressure melting experiments on some Skye basalts in order to further test this hypothesis. These experiments showed that, with increasing pressure, the field of clinopyroxene stability moved closer to the liquidus and so was probably a fractionating phase at

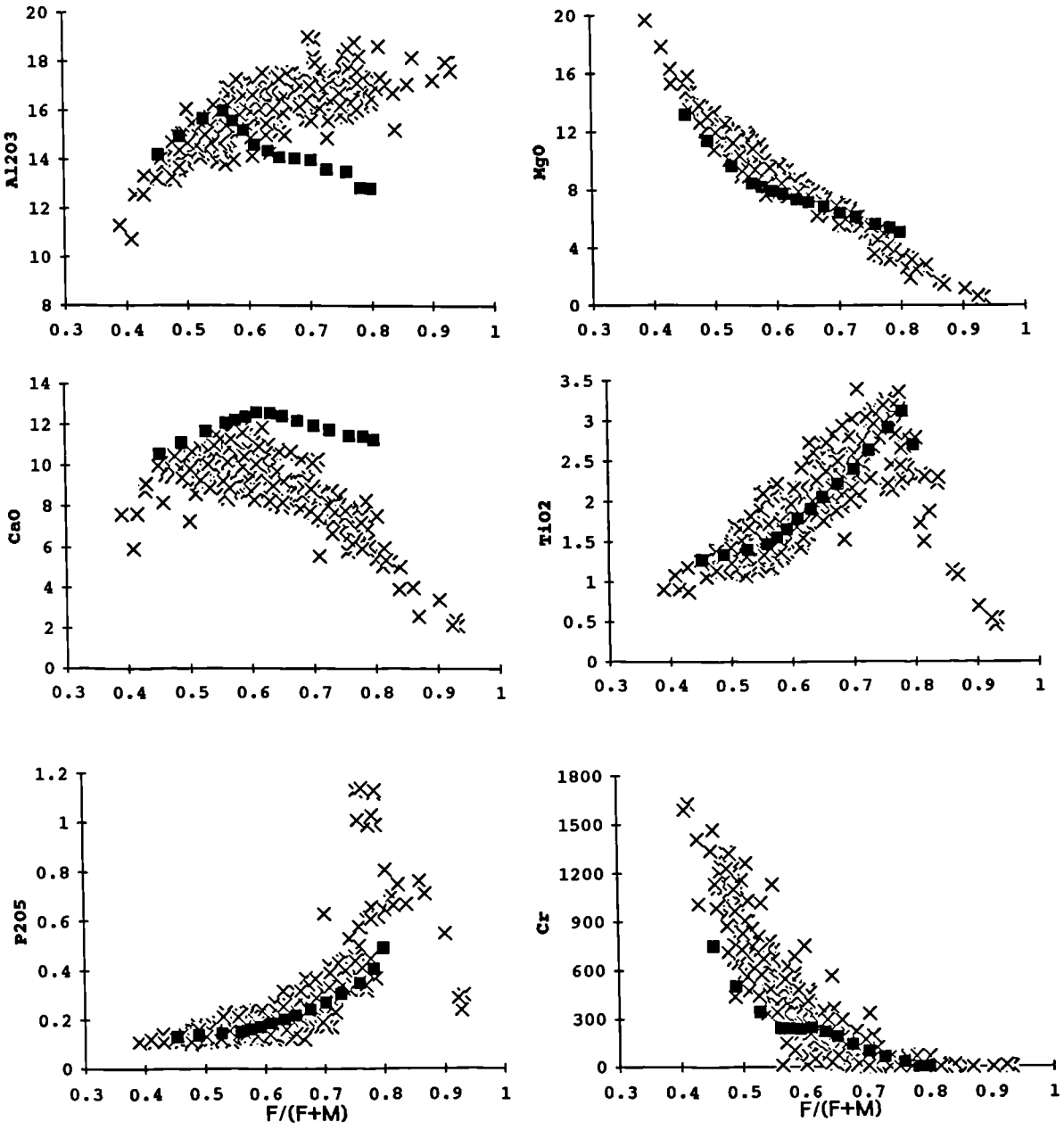


Figure 4.7 Selected major and trace elements vs. F/(F+M). The MPG are represented by crosses, and the solid squares mark the TRACE calculated fractionation path for BM4 [F/(F+M) = 0.44). Each square represents 4% crystallisation.

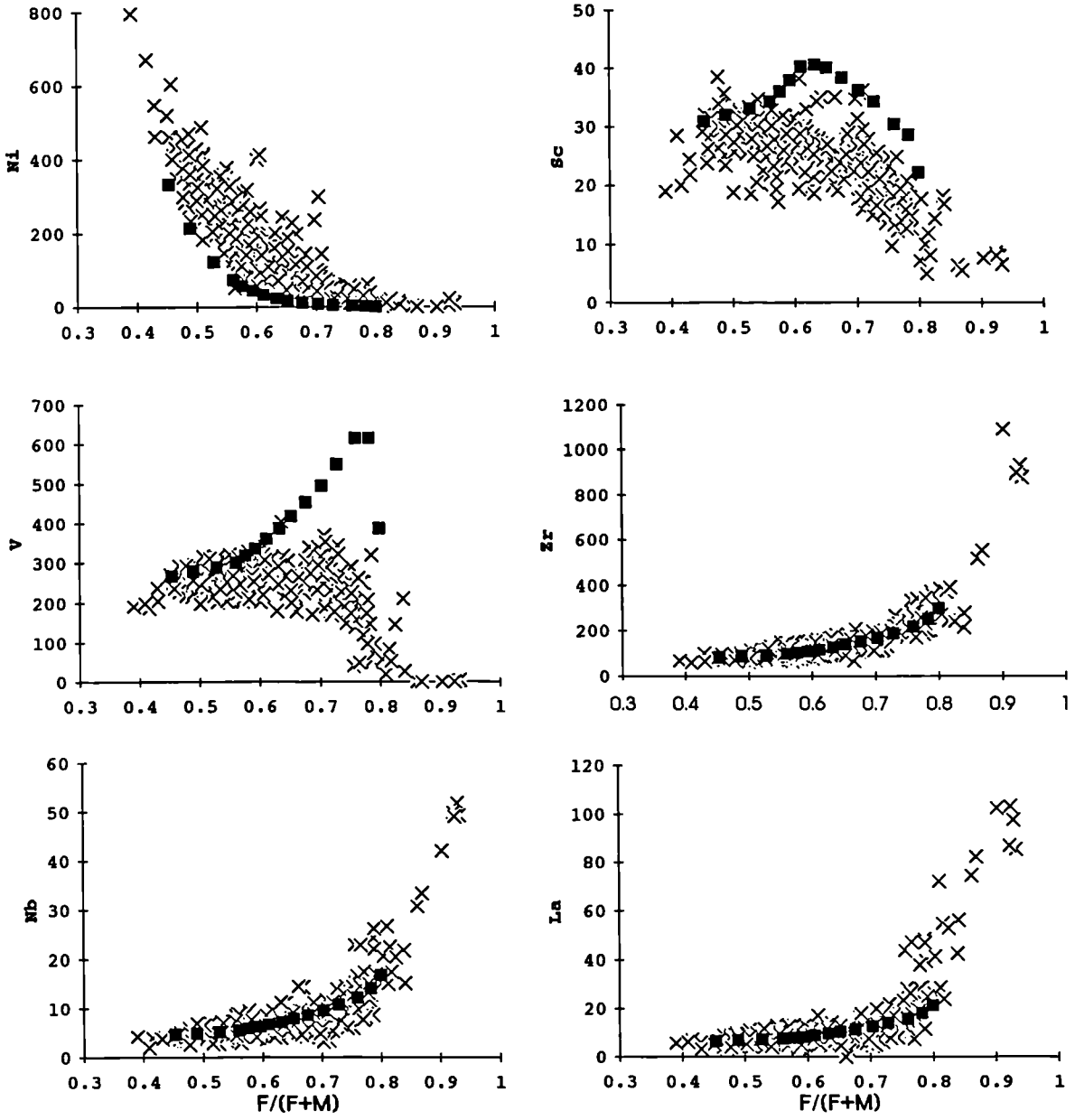


Figure 4.7 (continued)

higher pressures. These augites - crystallised at high pressures from SMLS basalts - have lower CaO and higher Al_2O_3 than clinopyroxene crystallised at 1 atm. (table 4.5).

	A	B	C
SiO_2	52.10	47.20	49.30
Al_2O_3	5.46	14.4	3.17
Cr_2O_3	0.48	0.04	--
FeO	9.35	9.82	8.79
MgO	24.30	11.4	14.00
CaO	7.14	13.8	21.90
Na_2O	0.54	1.78	--
K_2O	0.01	--	--
TiO_2	0.34	0.93	1.90

Table 4.5 **A** - pyroxene crystallised from a SMLS basalt (66018) at 17kb and 1340 °C. **B** - Pyroxene crystallised from a SMLS low-MgO basalt SK971 at 20kb and 1300 °C. **C** - Groundmass pyroxene in 66018 at 1 atm. (All analyses from Thompson 1974)

Thompson *et al.* (1980) proposed that the SMLS magmas had paused for long enough during their ascent from sub-crustal levels to dissolve their high pressure phenocryst assemblage and crystallise low pressure assemblage, without significant fractionation occurring. While this still remains a viable mechanism for explaining the absence of augite phenocrysts in the MPG, in-situ crystallisation could also explain this absence. In-situ, or side-wall crystallisation (Langmuir 1989) can produce a situation where the geochemistry of the erupted magmas cannot be completely explained by the removal of the observed phenocryst phases. One of the main reasons for this is because the invisible phases have crystallised on the walls of the chamber and so would not have been easily erupted. Such a situation can be envisaged for the MPG lavas *at high pressure,* and could explain the absence of augite phenocrysts.

It should be stressed however, that an acceptance of the in-situ model does not invalidate the high pressure fractionation of augite, rather it is an alternative explanation to account for the *nonexistence* of the phenocrysts at the surface. This removal of a small proportion of augite throughout the basalt fractionation range, has been successfully modelled by least squares, mass balance calculations (Bryan *et al.* 1969), (table 4.6) using a high pressure pyroxene (table 4.5 analysis A from Thompson 1974) and a magnesian olivine (Fo_{83}). Table 4.6 shows that to produce the

composition of a basalt containing 10-11% MgO from one containing 13-14% MgO, requires the removal of 5% olivine and 2% augite. The wide range in CaO, Sc and V at a given F/(F+M) may well reflect differing proportions of fractionating olivine and augite in different magma batches.

According to the least squares model, augite fractionation[3] becomes much more dominant below 7% MgO (table 4.8). TRACE, however, does not model this fractionation very well, predicting higher Ca contents, than are observed (figure 4.7). This can be explained by postulating fractionation of more augite, in relation to plagioclase, than is predicted by TRACE. Again no pyroxene phenocrysts have been observed but the decline of Sc and V contents with increasing fractionation, reveals that the process is likely to have occurred. Higher observed Al_2O_3 values than the values modelled by TRACE, similarly confirms that the augite to plagioclase fractionation ratio is probably higher than that predicted by TRACE.

Inspection of figure 4.7 reveals that TRACE does not model the composition of Cr particularly well. Again the early crystallisation of augite can explain this observation. The amount of crystallisation of Cr-spinel as predicted by TRACE is not sufficient to deplete Cr contents to the observed levels and so the fractionation of augite has to be invoked once again to explain the Cr depletion. As can be seen from table 4.5, the high pressure pyroxene crystallised from a Skye Mg-basalt contains 0.48% Cr_2O_3, so Cr would seem to have a high partition coefficient in high pressure pyroxenes. This is confirmed by Irving (1978). Interestingly, Upton *et al.* (1984) also attributed lower Ca, Sc and Cr contents in the Tertiary East Greenland lavas, to high pressure fractionation of clinopyroxene.

On the V vs. F/F+M plot the MPG data for V appears to behave in a similar manner to Sc, that is a relatively flat trend in the basaltic range which drops sharply once augite fractionation starts to become dominant. TRACE however predicts that V has a low partition coefficient in clinopyroxene and is not substantially removed from the magma until titanomagnetite fractionation. This is plainly not the case for the MPG lavas in which V appears to be compatible in clinopyroxene.

Vanadium exists in 3 oxidation states which show different geochemical properties (Shervais 1982). V^{4+} and V^{5+}, which exist under more oxidising conditions readily substitute for Ti^{4+}. V^{3+}, the more reduced ionic species, commonly substitutes for Fe^{3+} and Cr^{3+}. Consequently the partition coefficients of V in the pyroxene of magmatic rocks are strongly dependent on the oxidation state of the magma. For reduced magmas (log fO_2 = -12, at 1200 °C) V has an augite/liquid partition coefficient of 5, whereas for a more oxidised magma (log fO_2 = -10, at 1200 °C) the

[3] Using augite B in table 4.5; a sub-calcic aluminous augite crystallised from a less MgO-rich SMLS basalt at high pressures (Thompson 1974).

same partition coefficient has dropped to 1 (Shervais 1982). Consequently the difference between the observed and modelled trends for V can be explained by postulating that the MPG lavas were relatively reduced.

Least squares mass balance calculations

This method assumes that oxides vary linearly between the two liquid compositions being considered, this will, however only be true over relatively small compositional ranges. Because of this the calculations from high-MgO basalt to basaltic-hawaiite have been carried out in several small steps. The compositions of the fractionating mineral phases are assumed to remain constant over the crystallisation interval; this is another reason why a small compositional interval has been used.

High-MgO basalt (T4) to moderate MgO (10-11%) basalt (BB9), table 4.6

As has been previously discussed, this change in liquid composition can be modelled by 7% crystallisation, with the removal of 5% olivine (Fo_{83}) and 2% high pressure augite. (Table 4.5, analysis A)

Moderate MgO (10-11%) basalt (BB9) to low MgO basalt (BR17), table 4.7

The solution for this least squares calculation can best be achieved by the fractionation of 7% olivine (Fo_{77}) and 1-2% plagioclase (An_{67}) with perhaps minor amounts of clinopyroxene.

Low-MgO basalt (BR20) to basaltic-hawaiite (BR29), table 4.8

This requires 35% crystallisation of BR20 in order to produce the composition of BR29. According to the model this fractionation involves the crystallisation of 20.5% sub-calcic aluminous augite (Analysis B, table 4.5) 7.1% olivine (Fo_{63}) and 7.4% plagioclase (An_{52})

4.3.3 Fractionation of evolved lavas (>6.5% total alkalis)

Evolved compositions represent <5% (20 samples) of the lavas collected, (figure 4.8) and as can be seen from figure 4.9 they span the range of compositions from hawaiitic-mugearite through to trachyte. Also included on this diagram are several plugs (stars on figures 4.8 & 4.9) of evolved compositions which cut the Mull lava succession. For the purposes of this study the evolved lavas have been divided into two groups;

1. An early group of hawaiites and mugearites, which occur near the base of the lava succession. They plot in the circled field on figure 4.9.

Table 4.6

Least squares solution for high-Mg basalt (T4) to moderate-MgO basalt (BB9)						
	Parent T4	Daughter BB9	Augite17kb	Fo83	Calculated BB9	Residual
SiO2	45.73	45.78	52.10	39.65	46.72	0.06
TiO2	1.47	1.75	0.34	0.00	1.58	0.18
Al2O3	14.76	15.39	5.46	0.24	15.75	-0.34
FeO*	11.82	12.09	9.35	15.87	11.71	0.52
MnO	0.18	0.20	0.18	0.28	0.18	0.03
MgO	12.58	10.36	24.30	42.65	0.02	-0.18
CaO	9.31	10.09	7.14	0.39	10.36	0.27
Na2O	2.50	2.26	0.54	0.22	2.67	-0.41
K2O	0.24	0.16	0.01	0.02	0.26	-0.10
Mix		92.6	2	5.4		

Sum of squares of residuals = 0.701
Fo83 - From sample BR5 (present study)
Augite 17Kb - from Thompson (1974) (crystallised from a SMLS Basalt)

Table 4.7

Least squares solution for moderate-Mg basalt (BB9) to low-MgO basalt (BR17)						
	Parent BB9	Daughter BR17	Fo77	An67	Calculated BR17	Residual
SiO2	45.78	46.74	39.12	51.32	46.94	-0.20
TiO2	1.75	1.66	0.12	0.09	1.92	-0.26
Al2O3	15.39	16.63	0.06	28.73	16.51	0.12
FeO*	12.09	11.85	21.06	1.02	11.62	0.23
MnO	0.20	0.18	0.37	0.12	0.19	-0.01
MgO	10.36	8.12	39.60	0.36	8.28	-0.16
CaO	10.09	10.33	0.42	13.52	10.88	-0.55
Na2O	2.26	2.68	0.06	3.82	2.42	0.26
K2O	0.16	0.34	0.01	0.10	0.18	0.16
Mix		91.4	7.3	1.2		

Sum of squares of residuals = 0.590
Fo77 - from sample MR9 (present study)
An67 - from sample MR9 (present study)

Table 4.8

Least squares solution for low-Mg basalt (BR20) to Hawaiite (BR29)							
	Parent BR20	Daughter BR29	An52	Fo63	Aug 20kb	Calculated BR29	Residual
SiO2	46.35	46.25	53.45	37.04	47.20	46.30	-0.05
TiO2	2.21	3.08	0.16	0.00	10.93	3.09	-0.01
Al2O3	16.74	16.94	26.28	0.16	14.40	17.81	-0.87
FeO*	13.43	13.91	0.70	31.44	9.82	14.14	-0.23
MnO	0.18	0.19	0.00	0.29	0.20	0.18	0.01
MgO	8.36	5.42	0.13	31.38	11.40	5.93	-0.51
CaO	8.84	7.75	10.34	0.55	13.80	8.00	-0.25
Na2O	2.90	4.03	5.24	0.23	1.78	3.26	0.77
K2O	0.34	0.52	0.15	0.00	0.00	0.51	0.01
Mix		65.1	7.4	7.1	20.5		

Sum of squares of residuals = 1.72
An52 - from sample BR27 (present study)
Fo63 - from sample BR22 (present study)
Augite 20kb - from Thompson (1974) (crystallised from a SMLS low-Mg Basalt)

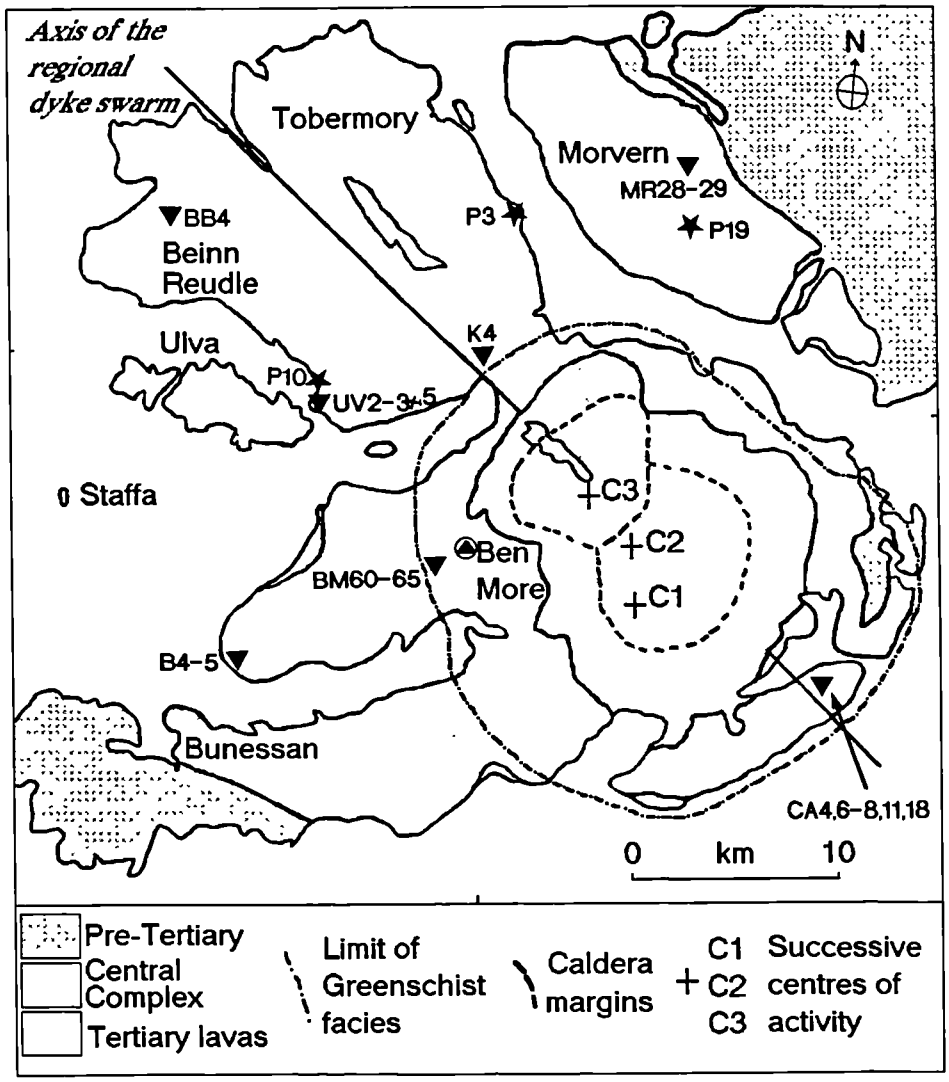


Figure 4.8 Map of the Mull and Morvern lava field showing the locations of evolved MPG lavas (inverted triangles) and plugs (stars). Sample numbers are shown beside the symbols.

2. A later group of mugearites, benmoreites and trachytes, which are found near the top of the succession.

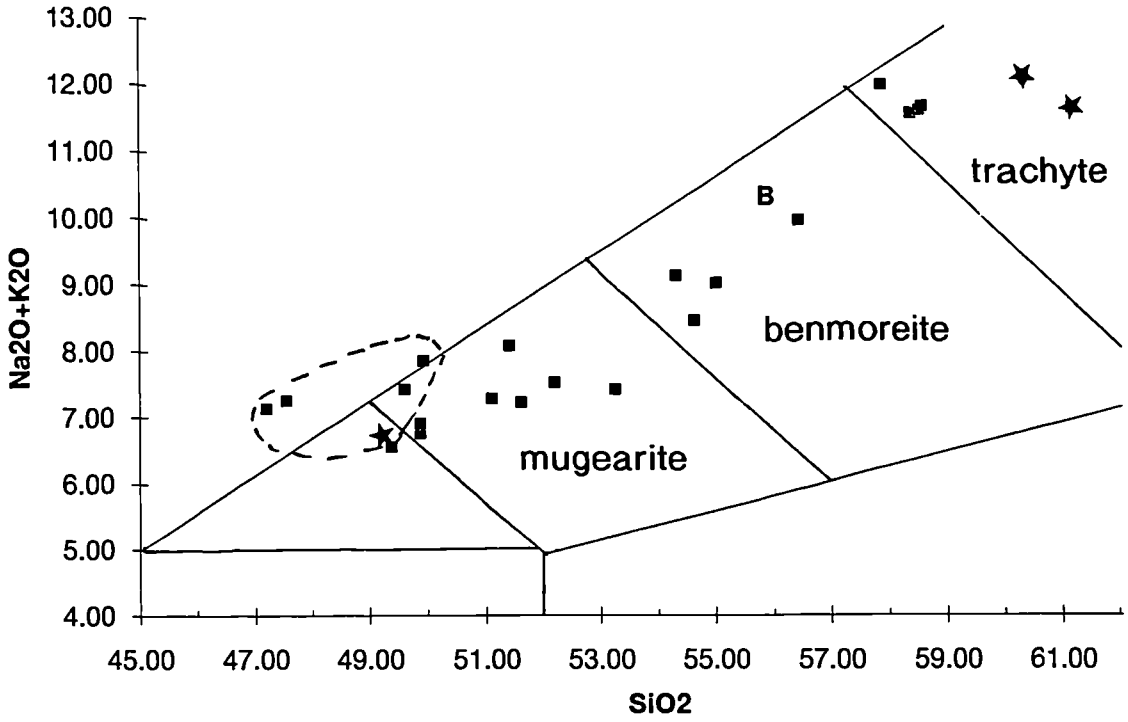


Figure 4.9 The evolved MPG lavas (squares) and plugs (stars) plotted on an alkali - silica diagram. 'B' represents benmoreite from the type locality (Tilley & Muir 1964). The Ulva Ferry mugearites (see later) fall with in the dashed field.

The late differentiates - fractionation processes.

As has already been mentioned - and demonstrated on figure 4.9 - the MPG lavas display a single trend to more evolved compositions. This contrasts with the SMLS, which shows both a basalt - benmoreite trend and a basalt - low-Fe intermediate - trachyte trend. The MPG lavas conform better to the more alkaline basalt - benmoreite SMLS sequence, however, the MPG trend continues to trachyte before falling to lower total alkali contents with increasing differentiation (figure 4.9).

The lack of two differentiation trends for the MPG lavas is again borne out by figure 4.10 which shows that the low-Fe trend evident for the SMLS is not observed on Mull. This low-Fe trend was attributed by Thompson *et al.* (1980); Moorbath and Thompson (1980), Dickin (1981), to more oxidising conditions in magma chambers at mid-crustal levels. The higher fO_2 oxidised Fe^{2+} to Fe^{3+} in the magma, which resulted in the suppression of olivine fractionation in favour of titanomagnetite. Since the MPG lavas follow the normal-Fe SMLS trend, it has been assumed that the evolved MPG magmas fractionated under relatively reducing conditions. This is

supported by the fact that - as was shown earlier - vanadium was probably also present in its reduced form, V^{3+}.

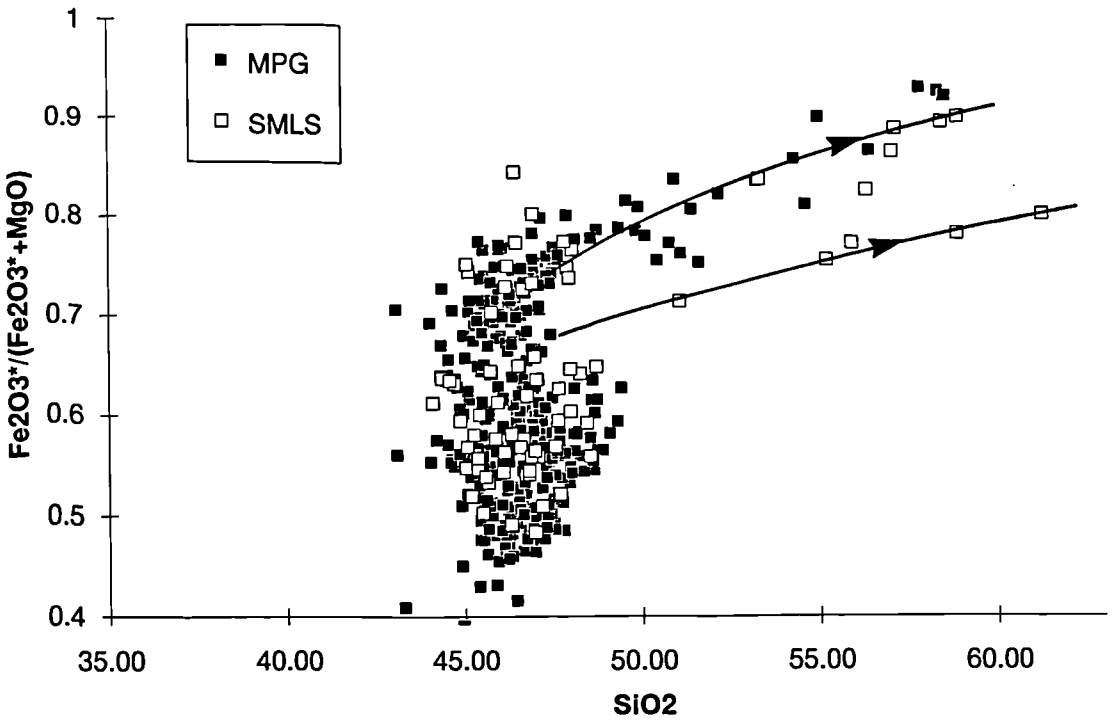


Figure 4.10 F/(F+M) vs. SiO_2 for the MPG and the SMLS. Above 50% SiO_2 the SMLS display two trends, a low Fe trend, and a higher Fe trend. However, the MPG lavas do not show the low Fe trend (basalt-benmoreite trend, see figure 4.5).

The alkali-silica diagram (figure 4.9) shows that the Mull evolved rocks have some peralkaline tendencies, and this seems to be confirmed by the high Zr contents (~1000ppm) of the Mull trachytes (BM60-63); this is in contrast to the most evolved Skye lavas, which are less alkaline and contain 350-400ppm Zr. Zr saturation in felsic melts is critically dependent on the Na_2O+K_2O/Al_2O_3 ratio (a measure of peralkalinity) (Watson 1979). The higher this ratio, the more Zr can concentrate in the melt before zircon begins to fractionate, this is probably due to Zr complexing with the abundant alkalis to form alkali zircono-silicate complexes, which keeps Zr in the melt phase (Watson op.cit.).

An interesting point which should be noted here is that the four most evolved lavas from the Pale Group (Bailey *et al.* 1924), two-thirds of the way up Ben More - the type locality for benmoreites - are trachytes! The evolved lava from Mull reported by Tilley & Muir (1964), which they used along with two Skye samples to define the new rock type "benmoreite", does not actually come from Ben More. It was collected east of Kinloch Hotel (NM535283) by Bailey *et al.* (op.cit.) who proposed that these lavas, and the evolved lavas on Ben More (BM60-63 - this study), were part of the

same series of evolved flows. The difference in stratigraphic height of approximately 600m and chemical differences between the Kinloch flow (labelled B on figure 4.9) and the Ben More flows, makes this quite unlikely.

On Ben More these highly fractionated flows obviously represent a period of low magma supply from the mantle, perhaps due to a temporary cessation of mantle melting. These trachytes and mugearites are overlain by a more basaltic sequence and, as will be shown in Chapter 6, they are of a different magma type to the MPG and, as such represent the onset of a new phase of mantle melting.

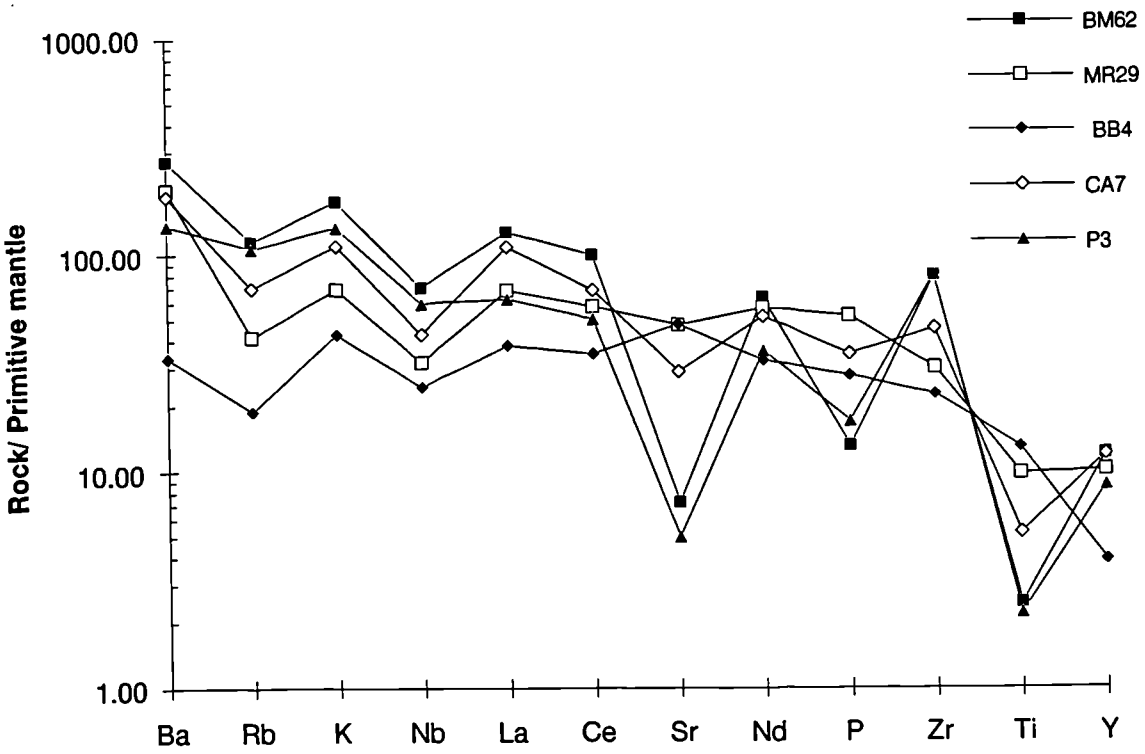


Figure 4.11 Primitive Mantle normalised variation diagram showing representative samples of evolved lavas and plugs from the MPG. BM62 - trachyte; MR29 - mugearite; BB4 - less evolved mugearite; CA7 - benmoreite; P3 - trachytic plug.

Unlike the earlier modelling of the fractionation of basalt to hawaiite, quantitative modelling to more evolved residua has not been attempted, since most of the evolved rocks lie within the greenschist facies zone of alteration (figure 4.8). A qualitative assessment of the nature of the fractionating phases can, however, be made. This is most easily achieved with the use of a Primitive Mantle Normalised spidergram (figure 4.11). On this diagram a selection of the most evolved rocks has been plotted, from mugearite (BB4 & MR29), to benmoreite (CA7), through to trachyte (BM62) and to a yet more evolved plug (P3).

Certain troughs on this diagram can reveal the nature and relative extent of fractionating phases as differentiation proceeds. Of the two mugearites, MR29 is more evolved (higher LREE, & Zr) than BB4 (which verges on hawaiite compositions). Unlike the rest of the samples on the diagram, it has no P and Ti troughs reflecting little apatite and titanomagnetite fractionation respectively. Falling Sc, V and Ni contents, along with observed plagioclase phenocrysts, suggest that olivine, plagioclase and clinopyroxene continued to be major fractionating phases. This observation is in accord with the conclusions of Thompson *et al.* (1980) for the SMLS.

The more evolved mugearite had, however, begun to fractionate titanomagnetite, as is evidenced by a Ti trough on figure 4.11. The trough at Nb may also be in part due to the fractionation of titanomagnetite, since Nb^{5+} can substitute for Ti^{4+} (Thompson *et al.* 1980), however the bulk partition coefficients as calculated by TRACE (Nielsen 1988) for Nb, only increase from 0.03 to 0.08 with the onset of titanomagnetite fractionation. TRACE therefore predicts that relatively little Nb is substituted for Ti in the titanomagnetite lattice. The data for the evolved rocks from Mull would seem to confirm this in that the lowest Ti values do not correspond to the lowest Nb values, indeed Nb increases with fractionation. Thus, while the sizes of the Ti^{4+} and Nb^{5+} ions are similar (~70pm) the 5+ charge on Nb would seem to render it more incompatible than was supposed by Thompson *et al.* (op.cit.). An additional explanation of Nb troughs in evolved rocks is therefore required. This involves the addition of crust, and this will be discussed in the next section.

Returning to the consideration of figure 4.11, the benmoreite (CA7) has a more pronounced trough at Ti than the mugearite, as well as a P trough. These factors indicate continued fractionation of titanomagnetite and the commencement of apatite fractionation and indeed small quantities of apatite crystals have been found in the more evolved lavas (Chapter 3). CA7 also shows a Sr trough suggesting the fractionation of plagioclase. Although plagioclase had already been fractionating as the magma evolved from basaltic-hawaiite to mugearite, Sr has only now started to drop significantly. This is because the partition coefficient of Sr in plagioclase ranges from 1.8 in basaltic magmas to 6.0 in trachytes (Henderson 1982). So plagioclase fractionation, although operative over quite a wide composition range only efficiently removes Sr from the magma at more evolved compositions.

The trachyte, BM62, has fractionated plagioclase, titanomagnetite and apatite (deep Sr, Ti, & P troughs; figure 4.11) and, by this stage of evolution of the magma, olivine and clinopyroxene are probably only minor fractionating phases. It has already been noted that the trachytic plug, P3, is probably more evolved than BM62 and reference to figure 4.11 shows that it too, has fractionated plagioclase,

titanomagnetite and apatite. However, the lower values of Ba, Rb and K (in comparison with BM62) and lower total alkalis (figure 4.9) probably reflect some fractionation of alkali feldspar. The presence of abundant biotite crystals in the extreme differentiates suggests that mica, may also have been a fractionating phase at evolved compositions.

In order to produce the trachytes (<1% MgO) from basaltic magmas (13-14% MgO) requires major crystal fractionation. The magmatic differentiation program TRACE, has been used to fractionate a basalt to 12% of its original volume (88% crystals removed). This, however, only lowers the MgO content of the residual magma to ~3%, yet the most evolved magma compositions of the MPG contain <1% MgO. Therefore the degree of fractionation required to produce the trachytes from the basalts is at least 90% and perhaps even over 95%. High degrees of fractionation to produce evolved magmas from basic compositions, have also been reported by Thompson *et al.* (1980) from the SMLS and by Wood (1978) from Iceland.

The late differentiates - possible crustal contamination processes

It has so far been assumed that the most evolved rocks, the trachytes and benmoreites are fractionated products of the basalts, however, another alternative should be considered, namely the possibility that these evolved rocks are melts of Lewisian upper and/or lower crust. A simple way to test this is by a comparison of the REE patterns of Lewisian crustal material (which is considered to represent most of the crustal basement below Mull, (Bamford *et al.* 1977)) with the patterns of evolved MPG rocks. The REE patterns of some amphibolite and granulite facies Lewisian crust from Weaver & Tarney (1980) (samples 18Z, 20F, 16Y & 7H), some Lewisian crust from the Isle of Tiree (30km west of Mull) (samples P40, P43 & P50) are shown in figure 4.12 along with two evolved lavas. Clearly the evolved lavas have REE levels which are too high to be near crustal melts. All but one of the Lewisian samples in figure 4.12 has a positive Eu anomaly, whereas the evolved lavas do not have a Eu peak. This observation does not, however preclude the possibility that these lavas are mildly contaminated with crust.

Earlier it was suggested that a crustal input into the most evolved magmas was required in order to explain the Nb trough. Thompson *et al.* (1982) reported spidergram patterns with similar Nb troughs, for the low-Fe intermediate rocks of the SMLS, the main causative factor of which was believed to be a significant crustal input; this was confirmed by high $^{87}Sr/^{86}Sr$ ratios of 0.7047-0.7057. No isotope values have been determined for the more evolved lavas (mugearites to benmoreites) during the present study. One benmoreite from the MPG was, however, analysed for $^{87}Sr/^{86}Sr$ by Beckinsale *et al.* (1978) and yielded a value of 0.70616, significantly

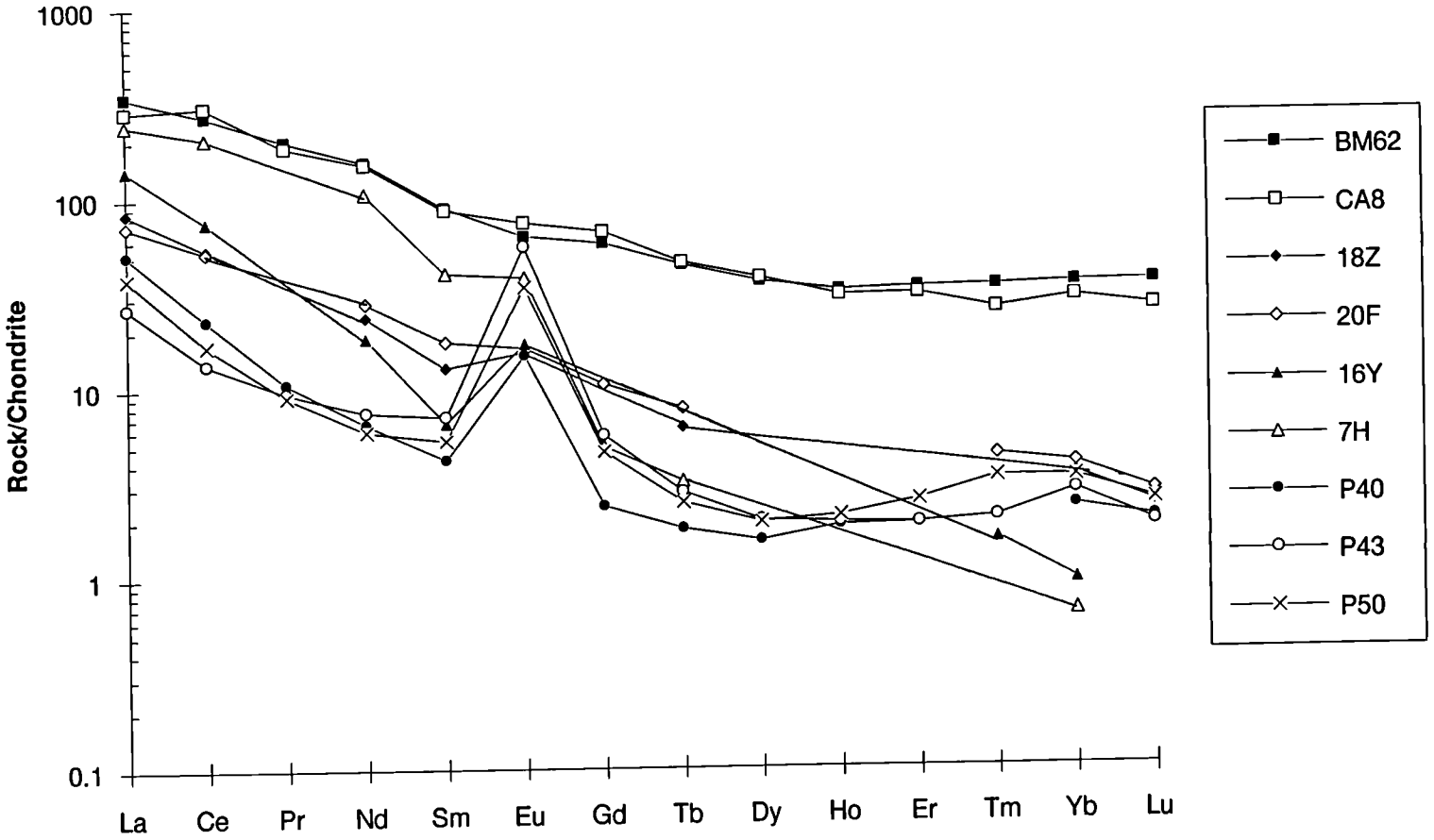


Figure 4.12 Chondrite normalised REE plot of evolved lavas (BM62 & CA8) and some Lewisian crust (18Z, 20F, 16Y & 7H from Weaver & Tarney 1980; P40, P43 & P50 from the present study.)

greater than the value for sub-Hebridean mantle of 0.7028 proposed by Dickin & Jones (1983)b, which strongly suggests that it has been significantly contaminated with crustal material. Figure 4.11 shows that most of the evolved MPG lavas have Nb dips. This fact, combined with the above isotopic evidence from Beckinsale *et al.* (op.cit), implies that MPG evolved rocks have assimilated significant quantities of Lewisian crust *during* their fractionation.

All these facts suggest that the evolved magmas (<3% MgO) may well have fractionated within the continental crust. Section 4.4 will show that the early magma chambers were probably thin dyke-and sill-like bodies, which enabled the most basic magmas to assimilate fusible crustal material. While the evolved magmas may have assimilated some crust by this mechanism, it seems highly probable that, since these magmas had to fractionate to <10% of their original mass within the crust, the latent heat provided by this crystallisation would have promoted crustal melting and assimilation, i.e. the AFC process of De Paolo (1981). Such a situation could eventually lead to the coalescence of the small, thin magma chambers. Thus it is a distinct possibility that prolonged differentiation could lead to the formation of larger, sub-spherical magma chambers.

Figure 4.12 shows that the evolved magmas (BM62 and CA8) do not have REE patterns with a Eu trough, despite the fact that the evidence already discussed for Fe and V strongly supports the view that these evolved MPG magmas are quite reduced. In these magmas, therefore, the Eu^{2+} state should predominate over the Eu^{3+} state, and since Eu^{2+} is compatible in plagioclase, the obvious removal of plagioclase crystals from these evolved MPG should lead to Eu troughs in the REE patterns. Thompson *et al.* (1980) in their study of the SMLS noted a similar lack of a Eu troughs for reduced magmas which had obviously fractionated plagioclase and they suggested that this was due to some bulk compositional effect on Eu reduction or partitioning. It has already been shown that these evolved MPG rocks probably contain significant proportions of Lewisian crust. Figure 4.12 shows that for the most part acidic Lewisian crust has quite pronounced Eu spikes. One can thus envisage a situation where Eu was being removed from the magma by fractionation of plagioclase, and at the same time was being replenished in the magma by assimilation of Lewisian crust. This would effectively buffer the Eu contents of the more evolved magmas, so masking the removal of Eu during plagioclase fractionation.

Fractionation of the early differentiates

These flows occur almost at the base of the succession in several parts of the island (figure 4.8)[4] They are for the most part mugearites (ringed on figure 4.9), although

[4] The samples BR18-19, BB4, UV2-3, B4-5.

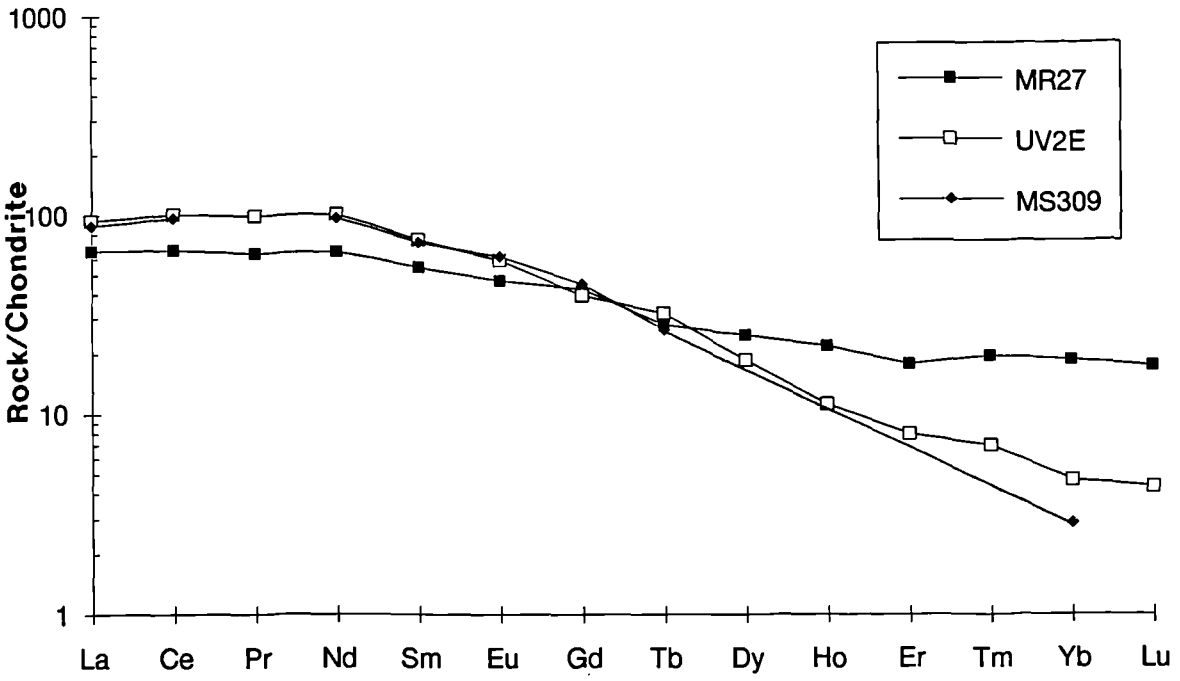


Figure 4.13 Chondrite-normalised REE plot of some MPG mugearites. UV2E and MS309 (Thompson 1982) - Ulva Ferry mugearites; MR27 - 'normal' MPG mugearite.

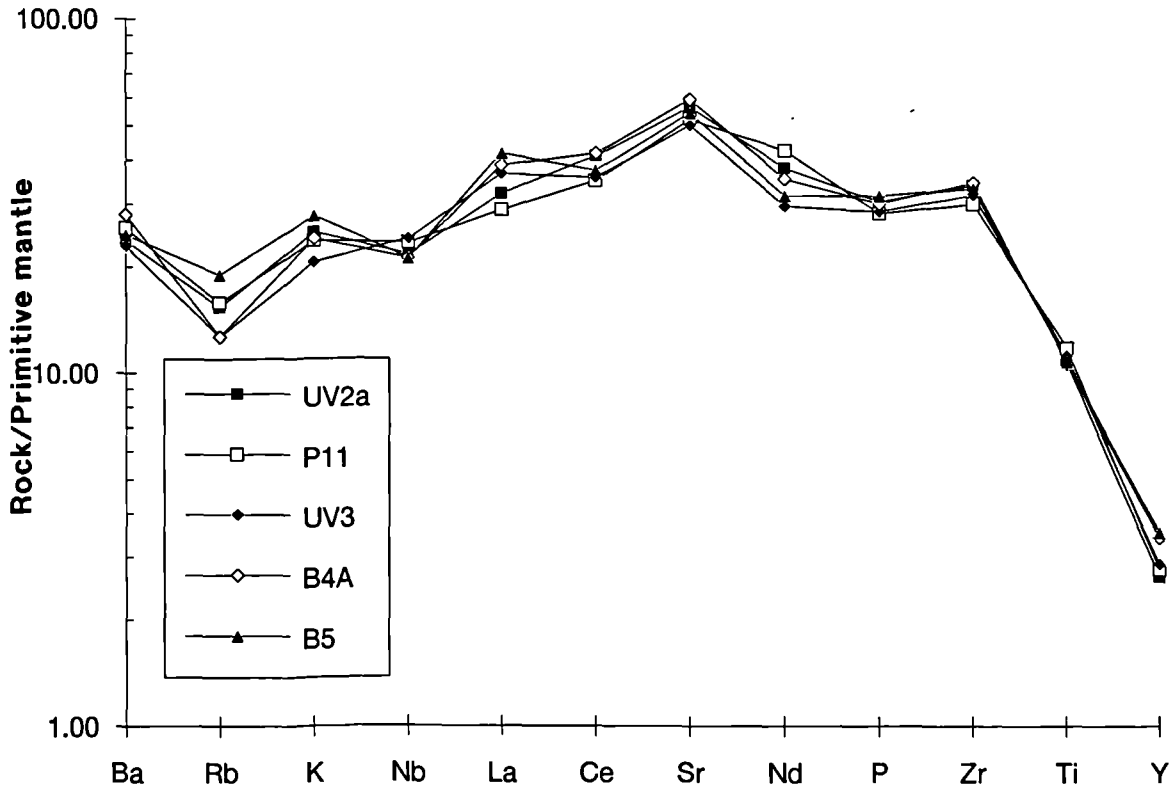


Figure 4.14 Primitive Mantle normalised diagram showing the characteristic Y-depletion of the Ulva Ferry mugearites.

less evolved hawaiites with the distinctive geochemical characteristics of this group -- termed Ulva Ferry mugearites, after the location [NM453402] where they were first noted as distinctly different by Beckinsale *et al.* (1978) -- have also been found, again quite near the base of the succession (samples BR18 & 19 and BB4). The most distinctive geochemical feature of these lavas is the very depleted HREE patterns (figure 4.13) and very low Y (figure 4.14), in comparison with "normal" MPG mugearites.

Beckinsale *et al.* (op.cit) proposed that these lavas were direct mantle melts of garnet peridotite and had not undergone any subsequent fractionation. Thompson (1982) challenged this interpretation and proposed that, since the Ulva Ferry mugearites had much higher Sr, as well as lower Y than normal mugearites, they had been formed by fractionation of an assemblage including garnet at pressures below the field of plagioclase stability. These higher values therefore imply that Sr was behaving as an incompatible element.

The present study has located another Ulva Ferry type mugearite, again at the base of the succession, three flows above the columnar flow which encloses MacCulloch's fossilised tree (samples B4a & B5; NM404276). This flow, along with the several low-Y hawaiites and three low-Y mugearites and the nearby plug at Ulva Ferry (samples; P10-11), which is assumed to be the eruptive vent for the nearby mugearites, define a sub-trend on the Y vs. F/(F+M) plot (figure 4.6). Figure 4.15 shows a plot of Sr vs. F/(F+M) for the *all* the Mull mugearites (both low Y and "normal" types. It can be seen that the two types define two very distinct trends. Hence this new data would seem to confirm the conclusions of Thompson (1982), that fractionation occurred too deep for plagioclase to crystallise.

An interesting feature not noted by Thompson (op.cit.) is the fact that the Ulva ferry mugearites, in comparison with the other mugearites, also have low P contents (figure 4.16). As was demonstrated earlier, apatite does not begin to fractionate until benmoreite compositions are reached (>8% total alkalis), yet some of these low-P, low-Y lavas are hawaiites. In melting experiments Thompson (1975) crystallised sodic garnets containing up to 0.6% P_2O_5 and 0.4% Na_2O from a Snake River Plain olivine tholeiite at pressures from 18kb to 36kb. It appeared that Na and P were involved in a coupled substitution for Ca and Si in the garnet structure. Thus the high-pressure fractionation of garnet can again be appealed to, in order to explain this P depletion in the low-Y, Ulva Ferry type mugearites.

Since plagioclase crystallising from a basic magma can contain well over 10 times more sodium than garnet, one would expect that significant fractionation of garnet would raise the Na_2O content of the melt, in comparison with a magma which had fractionated plagioclase. This is indeed what is observed for the Ulva Ferry

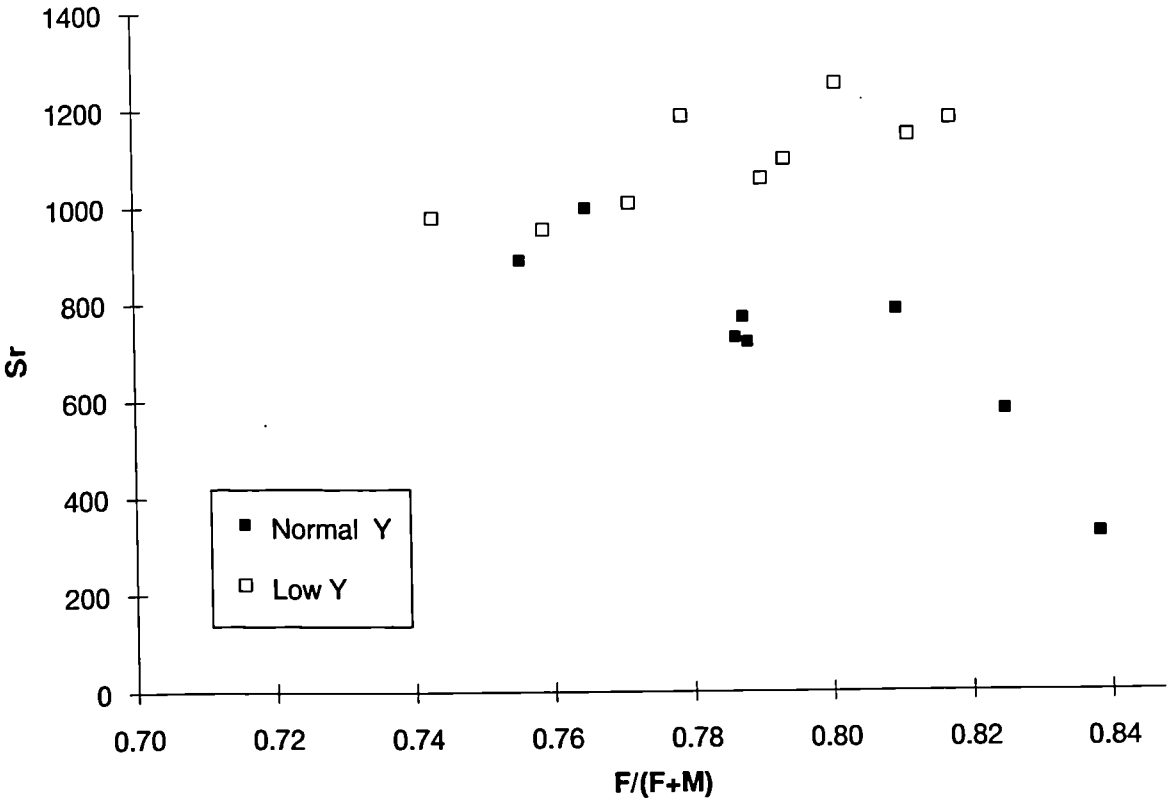


Figure 4.15 A Sr vs. F/(F+M) comparing 'normal' and low-Y mugearites.

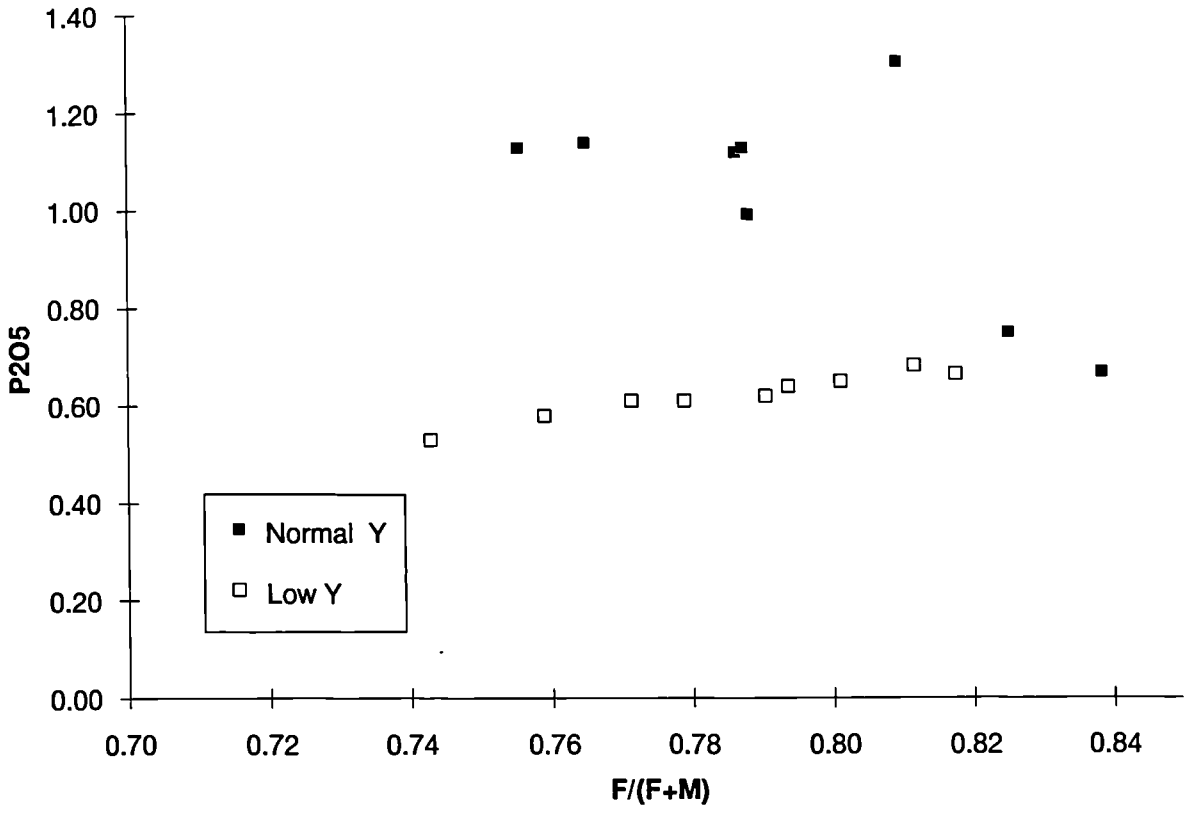


Figure 4.16 A P_2O_5 vs. F/(F+M) comparing 'normal' and low-Y mugearites.

mugearites, which contain more Na_2O than the other MPG mugearites and, as a result are displaced towards higher total alkali contents, off the main mugearite trend. This point is clearly demonstrated on figure 4.9.

The high-pressure experimental work of Thompson (1974; 1975) has clearly shown that garnet *can* crystallise from basaltic magmas at pressures above 18kb (approximately equivalent to mid-to lower lithospheric mantle depths). However, phases other than garnet also seem to have fractionated from the Ulva Ferry mugearites. Significant olivine fractionation is strongly suggested by Ni contents of <40ppm, combined with the presence of olivine microphenocrysts. Like the "normal" MPG mugearites, fractionation of titanomagnetite is important, as testified to by lower Ti contents (figure 4.14). Similarly, the low V contents of the Ulva Ferry mugearites point to the fractionation of clinopyroxene. The Ulva Ferry mugearites lie on the main fractionation trends for Ni, Sc, V, and TiO_2, which argues strongly against any origin by direct melting of the mantle.

The extreme unlikelihood of mugearites being direct mantle melts, as proposed by Beckinsale *et al.* (1978) is further confirmed by experimental petrology (Wyllie 1984). This work demonstrated that, with several rare exceptions, magmas from the mantle are essentially limited to compositions less evolved than basaltic andesite.

Low-Y hawaiites and mugearites have also been discovered in several other places. Holm (pers. comm.) and Holm *et al.* (1992) noted several low-Y hawaiites low in the Tertiary lava succession of East Greenland. However no explanation was offered as to their petrogenesis. Low-Y mugearite lava flows have also been reported from the Small Isles of Invernesshire (Ann Morrison pers. comm) and from Arran (M. Norry pers.comm).

It is interesting to note that the East Greenland low-Y lavas, like the Ulva ferry mugearites, also occur near the base of the lava succession, and this perhaps provides a clue to their petrogenesis. In the early stages of the evolution of a magmatic plumbing system in the continental environment, it is likely that magma batches find it relatively difficult to penetrate through the lithosphere and so tend to pond and fractionate. These lower lithospheric mantle fractionates, seem to only rarely ascend to the surface. However, in places where they do, extension and sudden fracturing of the lithosphere may permit the rapid ascent and eruption of these low-Y, high-pressure fractionates. Irving & Price (1981) reported the occurrence of spinel lherzolite xenoliths in phonolitic lavas from various localities, and proposed that these magmas had fractionated at upper mantle pressures (10-15kb).

It is interesting to note that the three Ulva Ferry mugearites analysed by Beckinsale *et al.* (1978) have some of the lowest ($^{87}Sr/^{86}Sr$)i values yet reported from the BTIP (~0.7028) and so are essentially uncontaminated with continental crust (section 4.4).

These magmas must therefore have fractionated at sub-crustal levels, and as a result when they passed through the crust they were too cool to assimilate very much material.

It is acknowledged that deep garnet fractionation is not a commonly invoked process in igneous petrogenesis, nevertheless, it should also be remembered that low-Y mugearites are similarly not a common phenomenon, therefore an explanation slightly out of the ordinary is *necessary* to explain their petrogenesis.

4.3.4 Fractional crystallisation - conclusions

Table 4.9 summarises the petrogenetic relationships proposed in this section for the MPG lavas, (excluding the low-Y, Ulva Ferry mugearites and hawaiites). Also shown on this diagram is the petrogenetic scheme for the SMLS basalt to benmoreite trend (Moorbath & Thompson 1980). It can be seen that the two proposed fractionation sequences are very similar, and only differ in the percentages of fractionating minerals.

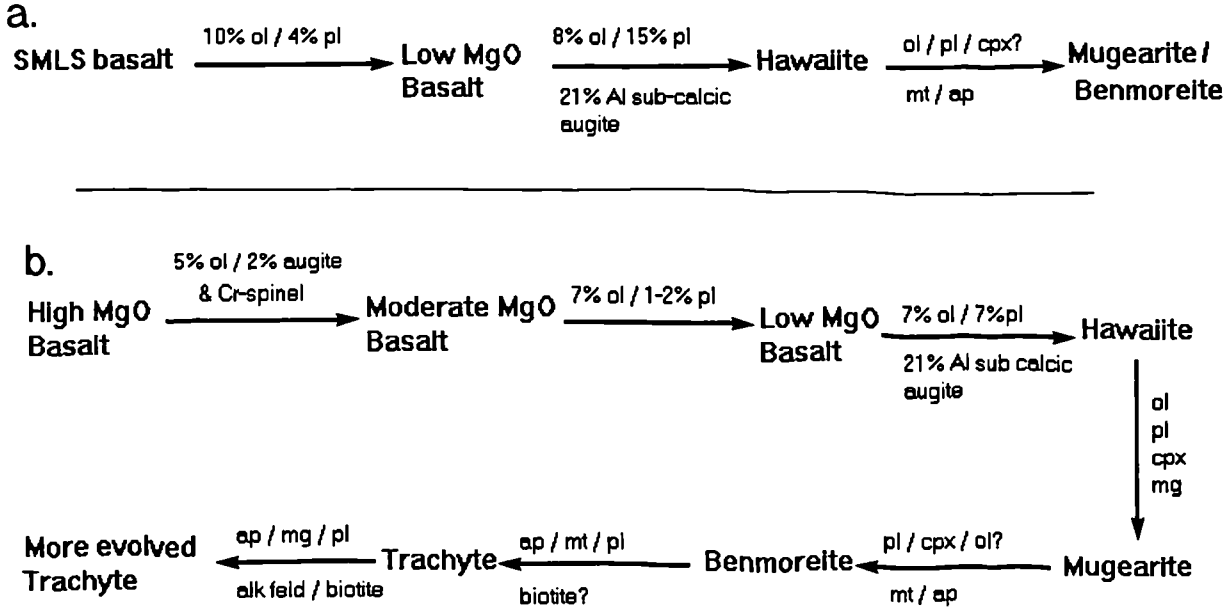


Table 4.9 The petrogenetic relationships proposed for the SMLS (Moorbath & Thompson 1980) and the MPG (this study). [Abbreviations, ol = olivine, pl = plagioclase, cpx = clinopyroxene, mt = titanomagnetite, ap = apatite, alk feld = alkali feldspar.

The above discussion has clearly demonstrated that fractional crystallisation, has played an important role in the petrogenesis of the evolved MPG lavas from the most

basic ones. Thus the conclusions of Beckinsale *et al.* (1978) -- that fractional crystallisation was not important in the development of the MPG lavas -- are rejected.

4.4 Crustal contamination processes and their contribution to the petrogenesis of basic to intermediate MPG lavas.

Crustal contamination of hot basaltic magmas erupted through thick continental crust, whether by partial or bulk assimilation, is an intuitively reasonable and thermodynamically possible process, which has been geochemically demonstrated time and time again in many different igneous provinces (eg. Deccan Traps - Cox & Hawkesworth 1985, Devey & Cox 1987; Karoo - De Paolo and Wasserburg 1977; Parana - Mantovani *et al.* 1985; British Tertiary Igneous Province (BTIP) - Thompson 1982, Dickin *et al.* 1984, Thompson *et al.* 1986; East Greenland - Larsen *et al.* 1989, Blichert-Toft *et al.* 1992. Furthermore, field evidence in support of crustal melting caused by the heat of minor intrusions is also widespread eg. East Greenland, (Blichert-Toft *et al.* op.cit) and the BTIP (Kille *et al.* 1986; Wyllie 1961).

4.4.1 Introduction

A crustal input into the magmas of the BTIP has long been speculated upon. Bailey *et al.* (1924) suggested that assimilation of acidic crust by the "Hebridean Plateau Magma Type" generated the tholeiitic (NPC) magma type with its tendency towards silica oversaturation. The question of whether the rocks of the BTIP contained crust or not, remained in doubt until the 1960's, when pioneering Sr and Pb isotope studies on Skye by Moorbath & Bell (1965) and Moorbath & Welke (1969), identified a significant Lewisian crustal component in many Hebridean magmas.

In the intervening years, the Hebrides (and particularly Skye) have become a testing ground for new isotopic techniques. Carter *et al.* (1978), showed that the variation in $^{143}Nd/^{144}Nd$ ratios of Hebridean lavas could be explained by contamination with variable amounts of Lewisian crust. Dickin *et al.* (1987) analysed $^{138}Ce/^{136}Ce$ ratios in twelve Skye lavas and found that these values, like other isotopic studies, strongly supported crustal contamination. Despite the massive weight of evidence for crustal contamination in Hebridean magmas, Beckinsale *et al.* (1978) proposed that partial melting of a vertically heterogeneous mantle, leading to pseudoisochrons on isotope variation diagrams, could explain the geochemistry of the MPG lavas. Pseudoisochrons were believed to date a mantle differentiation event, and Beckinsale *et al.* (1978) noted a Rb-Sr whole rock isochron age for the MPG lavas (17 samples)

of 128±15 Ma, which they interpreted as "a younger limit for an isotopic homogenisation event in the plagioclase lherzolite source region".

Moorbath & Thompson (1980) studied the Sr isotope systematics of the SMLS and pointed out that, since Sr is more compatible than Rb in plagioclase, if magmas which had fractionated feldspar, were excluded from consideration, then no correlation was observed between $^{87}Sr/^{86}Sr$ and Rb/Sr. "Figure 8" of Beckinsale *et al.* (1978) shows that their construction of the 128±15 Ma isochron was exceedingly tenuous, even before two evolved samples (which have obviously fractionated plagioclase) are excluded.

As Thompson (1982) pointed out the conclusions of Beckinsale *et al.* (op.cit) cannot be totally disproved. This is because the approach of Beckinsale *et al.* will always give the "right answer", since it assumes no post-melt-generation processes. Therefore, the nature the mantle source region for each individual lava is "tailor made" to fit the observed composition of each flow. Certainly no published literature on Hebridean magma petrogenesis over the last fifteen years has attempted to totally rule out crustal contamination and fractional crystallisation in the same way as Beckinsale *et al.* (op.cit.).

4.4.2 Possible mechanisms of contamination

There are two main ways in which crust can become incorporated into a magma:

1. Bulk Assimilation with concomitant Fractional Crystallisation (AFC - Bowen 1928; De Paolo 1981)
2. Assimilation of a fusible acidic fraction of crust by the most-basic magmas during their Turbulent Ascent. (Patchett 1980; Huppert & Sparks 1985).

The AFC process was outlined and modelled by De Paolo (1981). It depends on the existence of a sub-spherical magma chamber with a low surface-to-volume ratio. Fractionation in the magma chamber leads to the release of latent heat of crystallisation into the surrounding wall rocks. This can lead to wholesale melting of the country rocks, which can subsequently be incorporated and mixed into the magma in the chamber. Such assimilation will itself tend to cool the magma, leading to yet more crystallisation, and so more melting of country rock. AFC processes lead to positive correlations between fractionation indices and indices of crustal contamination (eg. $^{87}Sr/^{86}Sr$ or Ba/Nb), with the result that the most evolved rocks become the most contaminated.

The Assimilation during Turbulent Ascent (ATA) process (Patchett 1980; Watson 1982; Huppert & Sparks 1985) demands the existence of magma chambers with high

surface-to-volume ratios. These chambers allow a larger surface area of magma to come into contact with the country rock, and so permit partial fusion of the more acidic or volatile rich portion of the crust over relatively short time scales. This process is, however, critically dependant not only upon the temperature of the magma, but on the type of flow in the magma conduit. Under laminar flow conditions most heat transfer will be by conduction, this will tend to result in the formation of a chilled margin around the conduit. Without prolonged magma flow through the conduit, this chilled margin is not easily eroded and so it can insulate the later magmas from possible contamination effects (Campbell 1985).

Huppert & Sparks (1985) and Campbell (op.cit.) have however shown that basaltic magma can ascend turbulently, if the flow rate is sufficiently high and the conduit width greater than ~3m. Under such circumstances a chilled margin is much more likely to be eroded away. This brings turbulently ascending hot basaltic magma into continual contact with surrounding country rock and so the most fusible wall rock components can be melted and incorporated into the magma. Calculations by Huppert & Sparks (op.cit) suggest that maximum contamination will occur in dykes which are barely wide enough for fully turbulent flow.

Such a process will lead to the most primitive (ie. the hottest magmas) becoming the most contaminated. The more evolved magmas will not only be "too cool" to assimilate very much crust, but they will also be less likely to ascend turbulently due to their more viscous nature. This should theoretically lead to a negative correlation between contamination and degree of evolution.

The chemical effects - of crustal melting processes involved in ATA - on basaltic magma compositions have been discussed by various authors (Thompson *et al. 1982*; Watson 1982; Huppert & Sparks 1985; Campbell 1985). Thompson (1981) carried out a series of melting experiments at 1kb P_{H_2O}, on Lewisian crustal rocks from NW Scotland and showed that alkali feldspar was one of the first minerals to be melted in a leucogneiss. Melting commenced at temperatures slightly above 700 °C and at 780 °C all the alkali feldspar had been digested, along with some quartz and biotite. Clearly, since the temperature of hot basaltic magmas is of the order of 1300 °C - ie 600 °C hotter than the minimum fusion temperature of acidic Lewisian crust - partial assimilation during turbulent magma ascent, involving the more felsic crustal components (particularly alkali feldspar) is a very realistic possibility.

The quenched glass - the composition of the liquid - formed during the melting experiments of Thompson (op.cit.) contained significant quantities of K_2O (>4.00% - op.cit., table 4), as would be expected from the breakdown of alkali feldspar. Although not mentioned by Thompson (op.cit), alkali feldspars can contain

significant quantities of Ba (Smith 1983, and P43, a pegmatite from Tiree containing over 60% alkali feldspar with a whole-rock Ba concentration of over 6000ppm, Appendix 4a.vii). It is thus obvious that the melting and breakdown of alkali feldspar by the turbulent ascent of hot basic magma, will also add substantial amounts of Ba to the melt.

These observations are confirmed by the experimental work of Watson (1982) who demonstrated that, while quartz and alkali feldspar were easily melted by basaltic magmas, the resulting component introduced into the basalt does not have to have exactly the same composition as the melting felsic material. He proposed that diffusivity was an important controlling factor in determining the composition of the crustal contaminant. Of these elements, K_2O and the alkalis (particularly Ba and Rb) have the highest diffusivities. This, combined with a high initial felsic-melt/basalt K_2O and Ba activity gradient, would lead to *selective* contamination of the magma with K_2O and Ba. Watson also found that the LREE similarly had high diffusivities, and concluded that basaltic magma rising through continental crust could experience contamination with both the LREE and alkalis. This would not be reflected by an increase in SiO_2 concentration because of low diffusivity values for SiO_2 between a felsic melt and a basaltic liquid.

The selection of suitable crustal samples for the modelling of both ATA and AFC processes is fundamentally important. Since AFC processes involve bulk assimilation of crust, the use of samples of intermediate composition for modelling would seem to be entirely reasonable. However, as should be apparent from the above discussion, whole-rock crustal material available at the surface may not necessarily represent the compositions of the partial melts or selective partial melts which acted as potential contaminants. Therefore, crustal rock compositions which are used to model ATA processes should, as far as possible, meet the criteria outlined above; that is, a high modal proportion of alkali feldspar, resulting in a contaminant relatively enriched in Ba and K_2O. Ideal rocks to sample are veins of felsic material which have themselves formed by previous partial melting of the basement rocks. As will be discussed later, the Lewisian basement material collected during the present study contains such felsic veins.

4.4.3 The nature of the crust beneath Mull

As has previously been mentioned, the crust underlying the Mull igneous centre is assumed to be predominantly Lewisian in age, with amphibolite facies rocks overlying lower crustal granulites (Bamford *et al.* 1977). The uppermost crust is composed of Moine schists, in turn overlain by younger sediments (Thompson *et al.*

1986). A similar basement also seems to exist under Skye (Bamford *et al.* op.cit.). Nevertheless the Great Glen Fault cuts the SE corner of Mull and, as a result, the area south of the fault is probably underlain by basement of Proterozoic age (Dickin & Bowes 1991). Thus it is possible that the potential crustal contaminant of the Mull lavas is Proterozoic rather than Lewisian. Isotopic evidence points to a Proterozoic crustal input into Tertiary magmas from Arran (Dickin *et al.* 1981) and Antrim (Wallace *et al.* 1993).

For this study the lavas analysed for isotopes were collected from well north of the inferred surface trace of the Great Glen Fault and, as will be shown later, show strong evidence for a contaminant of Lewisian age. Lavas south of the divide between the two contrasting basements may well be contaminated with Proterozoic crust but, since this region lies within the greenschist facies zone of alteration, only a few samples have been collected from this area and none have been analysed for isotopes.

Workers on the Skye Tertiary lava succession, (Moorbath & Bell 1965; Moorbath & Welke 1969; Moorbath & Thompson 1980; Thompson *et al.* 1982) have made extensive use of Lewisian material collected from NW Scotland (eg. Weaver & Tarney 1980;1981), in order to model crustal contamination. Nevertheless, although the basement below Mull is for the most part Lewisian, it was considered unwise to use Lewisian crustal material from NW Scotland to model crustal contamination in the MPG lavas (over 100 km to the south), in case fundamental differences existed between the nature of the Lewisian crust under the two regions. As a result, local surface exposures of Lewisian basement (the Islands of Tiree - 30km west of Mull - and Iona) were visited and twenty samples collected during the present study.

While representative samples of all the major Lewisian rock types have been collected, sample collection has been biased towards the more fusible acidic rocks. These acidic rocks are mostly in the form of thin (<30cm) concordant and discordant veins, often rich in microcline. However one sample (P43) was collected from a granitic/pegmatitic body (30-40m across) on the southern coast of Tiree (NL936424) This rock contains 6900ppm Ba and 5.40% K_2O and, as such, is one of the most Ba and K_2O enriched Lewisian samples analysed to date. It will be used to model crustal contamination later in this section. Several of these acidic samples (including P43) have also been analysed for isotopes and the REE.

4.4.4 Contamination of the MPG lavas

As will be demonstrated in Chapter 7, the lower half of the Mull lava succession is composed of units of chemically distinctive flows (figure 4.17) which are occasionally interleaved. These units are predominantly of two types; a high-MgO basalt (>8% MgO) type, relatively enriched in Ba and K, and a low-Mg basalt-

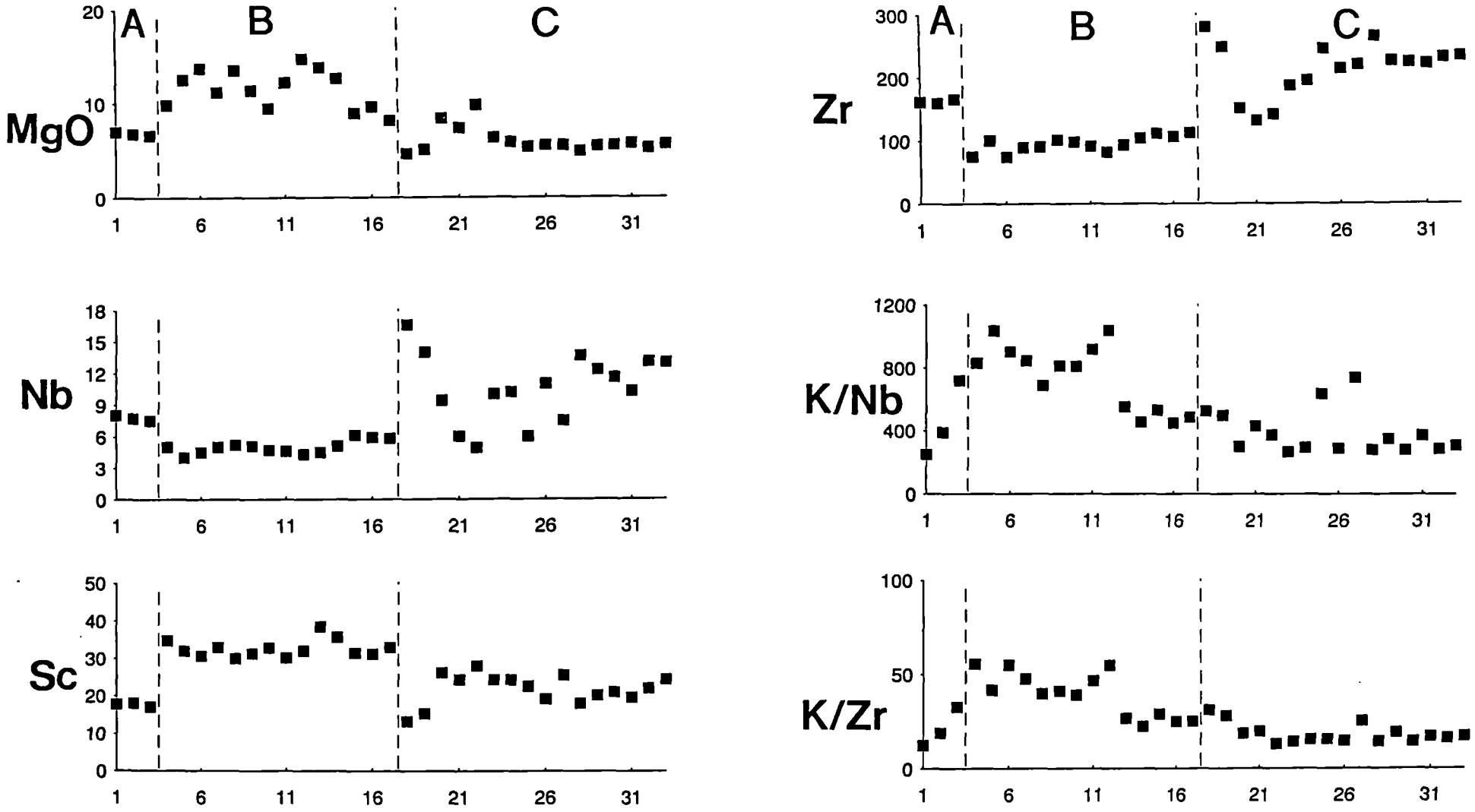


Fig. 4.17 Variation of MgO, trace elements and incompatible element ratios within the BR lava section. The horizontal axes represent flow numbers with (BR) 1 at the base and 33 at the top. A, B and C are chemically distinctive flow units referred to in the text.

hawaiite type, with lower values of Ba and K. These differences can be seen on a Primitive Mantle normalised diagram showing representative samples of the two different types (figure 4.18).

In the west of the island, the Beinn Reudle (BR) section (figures 2.2 & 4.17) is composed of approximately 33 flows and may be taken as typical of many of the other sections collected (see Chapter 7 and figure 7.1), in that it contains distinctive units of flows, of the two types outlined above (figure 4.18). The first three flows (unit BR-A) are of the low-MgO type (figure 4.17), on top of these lie a series of approximately 15 flows of high-MgO basalts (unit BR-B). The rest of the section marks a return to low-MgO flows (unit BR-C) which are very similar in composition to the BR-A flows.

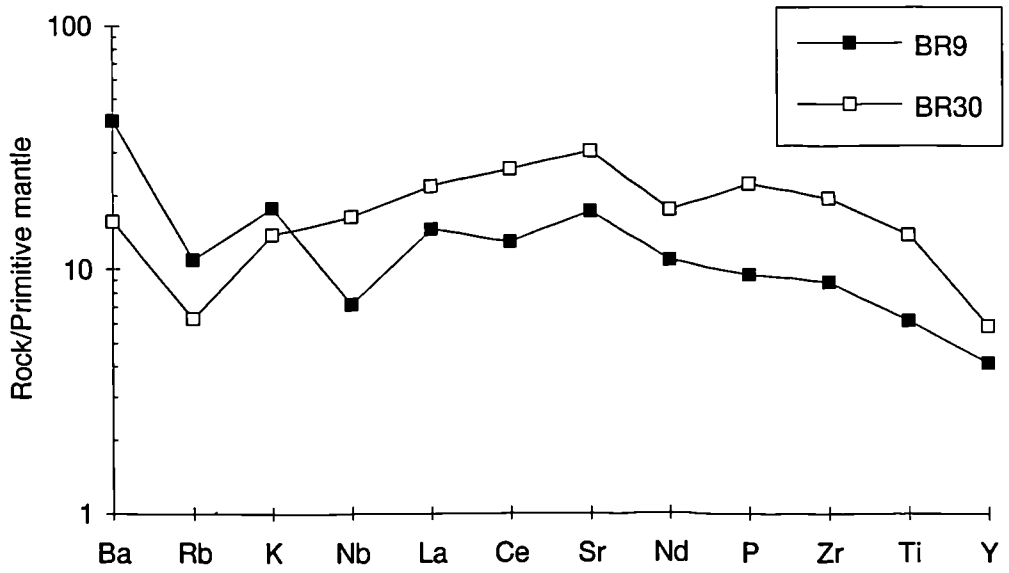


Figure 4.18 Primitive Mantle normalised diagram showing typical analyses of the two chemically distinctive types found in the BR section. BR9 represents the high-MgO BR-A lava unit, and BR30 represents the more evolved BR-A & -C units.

It will be shown in Chapter 7 that it is possible to correlate these lava units (BR-A, BR-B & BR-C) between sections. Figure 4.19 shows that the high-MgO basalt type, with enriched Ba and K, can be found in the lower half of the lava succession all over the island (figure 7.1). Similarly, figure 4.20 shows that the low-MgO basalt type found at Beinn Reudle, also occurs throughout the lava field. It is for this reason, and because the Beinn Reudle flows are significantly less altered than many others on Mull, (they are on the coast far away from the central complex and its associated alteration effects) that the lavas from this section are assumed to be representative of the lower half of the succession. As a result, most of the lavas from this section have been analysed for the REE and several for radiogenic isotopes.

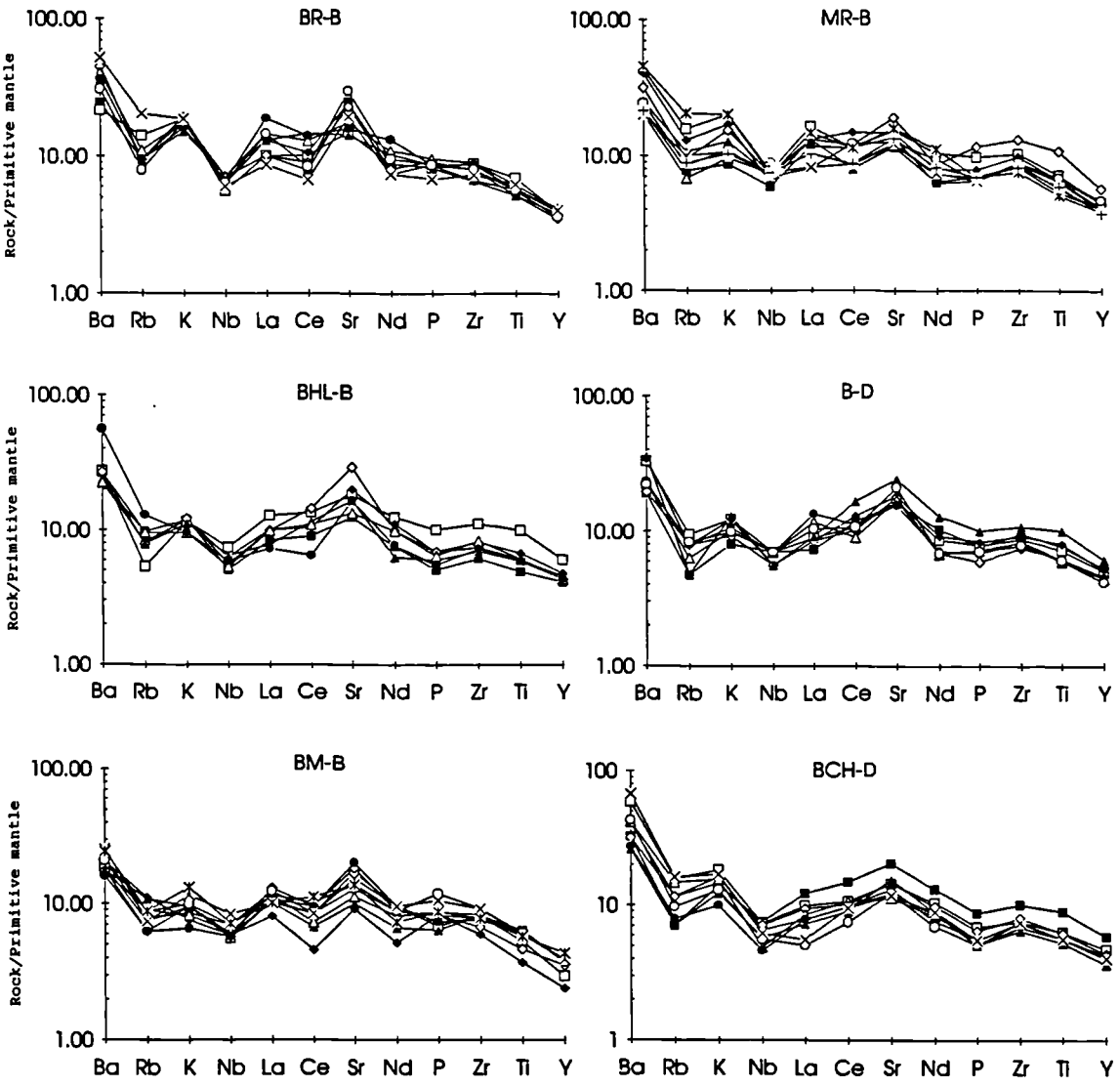


Figure 4.19 Primitive Mantle normalised diagrams showing lava units of high-MgO basalt with enriched Ba and K, found near the base of the succession throughout lava field. Figure 7.1 shows the locations of, and proposed correlations between, these units.

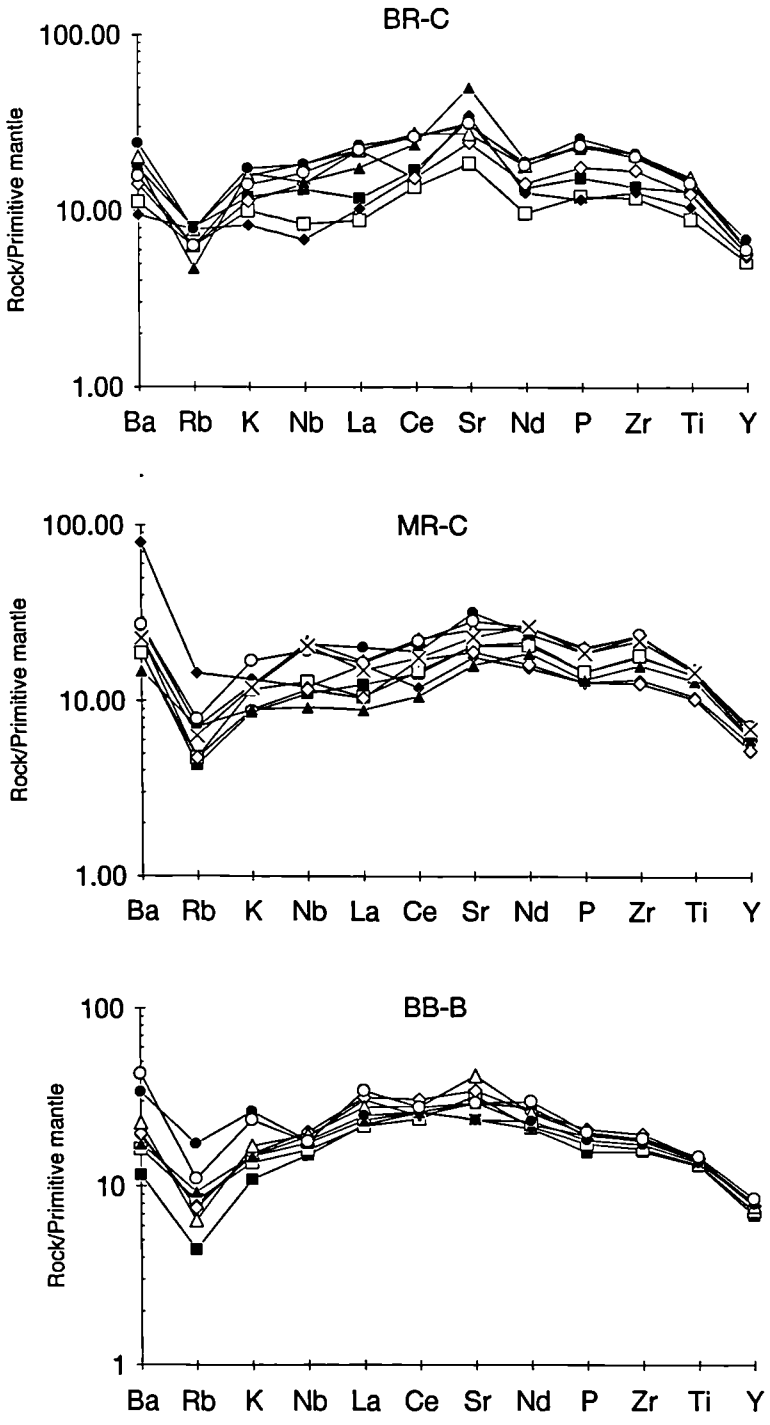


Figure 4.20 Primitive Mantle normalised diagrams showing lava units composed of more evolved (<8% MgO) basalt, which can be found throughout lava field. Figure 7.1 shows the locations of, and proposed correlations between, these units.

Crustal contamination - elemental evidence

In the following section an attempt will be made to model and explain the distinctive trace element and isotopic ratios of the most-basic magmas of the Mull lava succession. Reasons why the more-evolved magmas often no not show these enrichments will also be discussed. The elemental evidence will be discussed first, before returning to a fuller discussion of the isotope results.

Huppert & Sparks (1985) suggested that a plot of Ni vs. K_2O (figure 4.21), could be used to assess the nature of crustal contamination. They argued that the interaction of a basaltic magma with acidic crust would lead to mixing trends away from the main fractionation trend and produce a scatter of data points, such as are observed on figure 4.21.

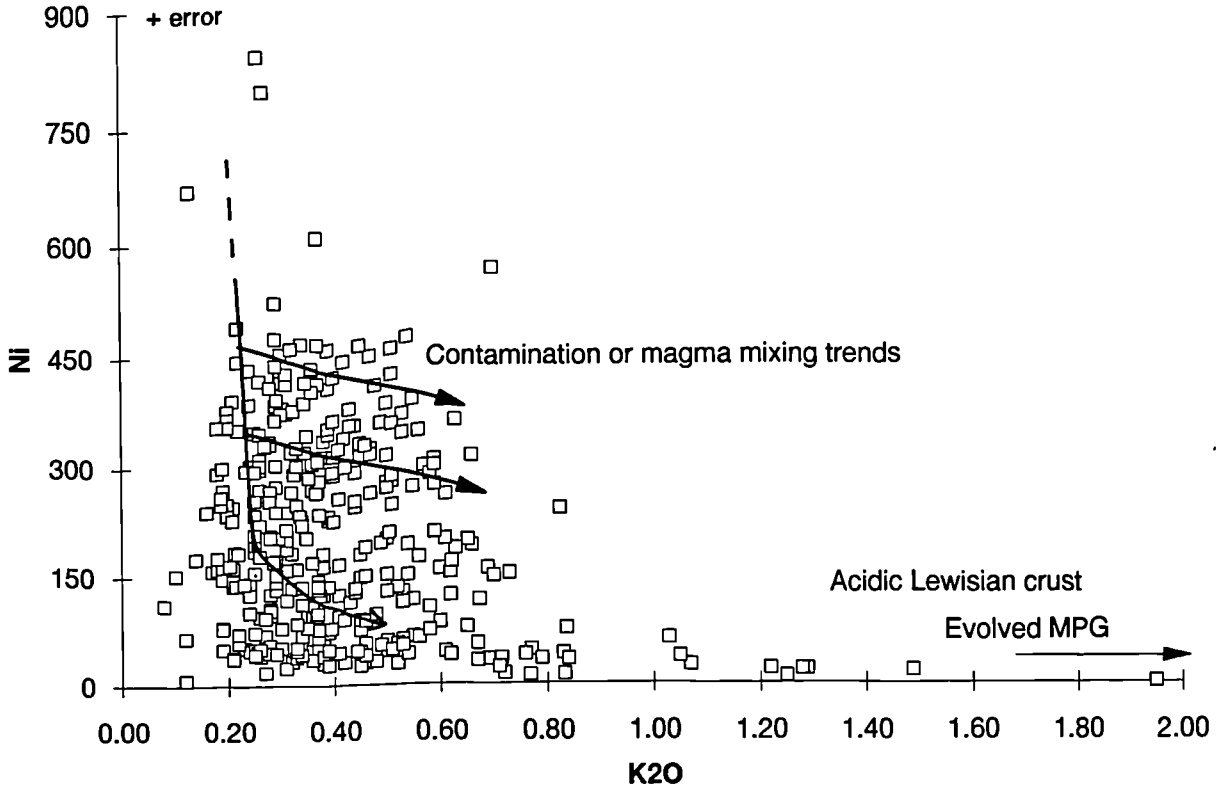


Figure 4.21 Plot of Ni vs. K_2O for the MPG lavas. Possible contamination and/or magma mixing trends, and a hypothetical (using TRACE) fractionation curve are also shown.

However, from inspection of this diagram it is obvious that mixing of basic magma with evolved magmas could conceivably produce a similar scatter of data, without the need to invoke crust.

The use of a Ni vs. Zr plot (figure 4.22) should, since neither element is present in large quantities in acidic Lewisian crust (ALC), eliminate the effects of crustal

contamination. This diagram shows that a significant amount of the scatter on (figure 4.21) has been eliminated. This suggests that the scatter on figure 4.21 is caused by contamination of basic magmas with K_2O-rich acidic Lewisian crust.

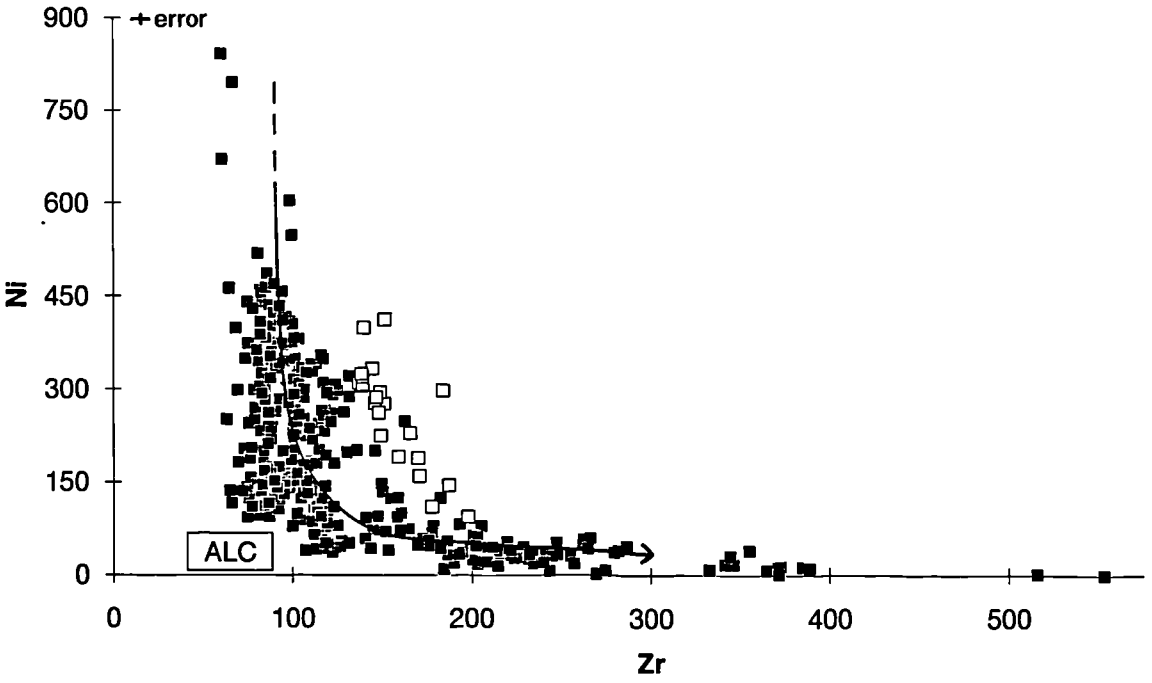


Figure 4.22 Plot of Ni vs. Zr for the MPG lavas (solid squares), and MPG lavas which have been contaminated with lithospheric mantle (open squares). Also shown is a possible fractionation trend, and the compositional range of acidic Lewisian Crust (ALC).

Some of the scatter which remains may well be due to magma mixing (for which there is also petrographic evidence - as demonstrated in Chapter 3). However, some of the scatter is also due to contamination of a few early magma batches with a small-fraction-melt from the lithospheric mantle (see section 4.5); these samples are marked on the diagram. As will be demonstrated in section 4.5, this lithospheric contaminant contains much higher quantities of the incompatible trace elements (including Zr) and is, along with magma mixing, responsible for the scatter on figure 4.22.

Primitive Mantle normalised diagrams for various basic lavas are plotted in figure 4.23. This figure shows that these lavas all have Ba and K peaks and a resultant Nb trough. The lavas plotted on this diagram come from throughout the succession, (figure 2.2, table 2.3 and Appendix 1) and they have been chosen because they represent the range in compositions shown by this distinctive lava type. Table 4.3 shows analyses of ten relatively basic samples (>11% MgO), which have lower Ba and K and no Nb trough, unlike like the vast majority of more basic samples. One of

these low Ba and K samples (BM2) has been used as the starting composition in modelling the elemental signature of the basic magmas with higher K and Ba.

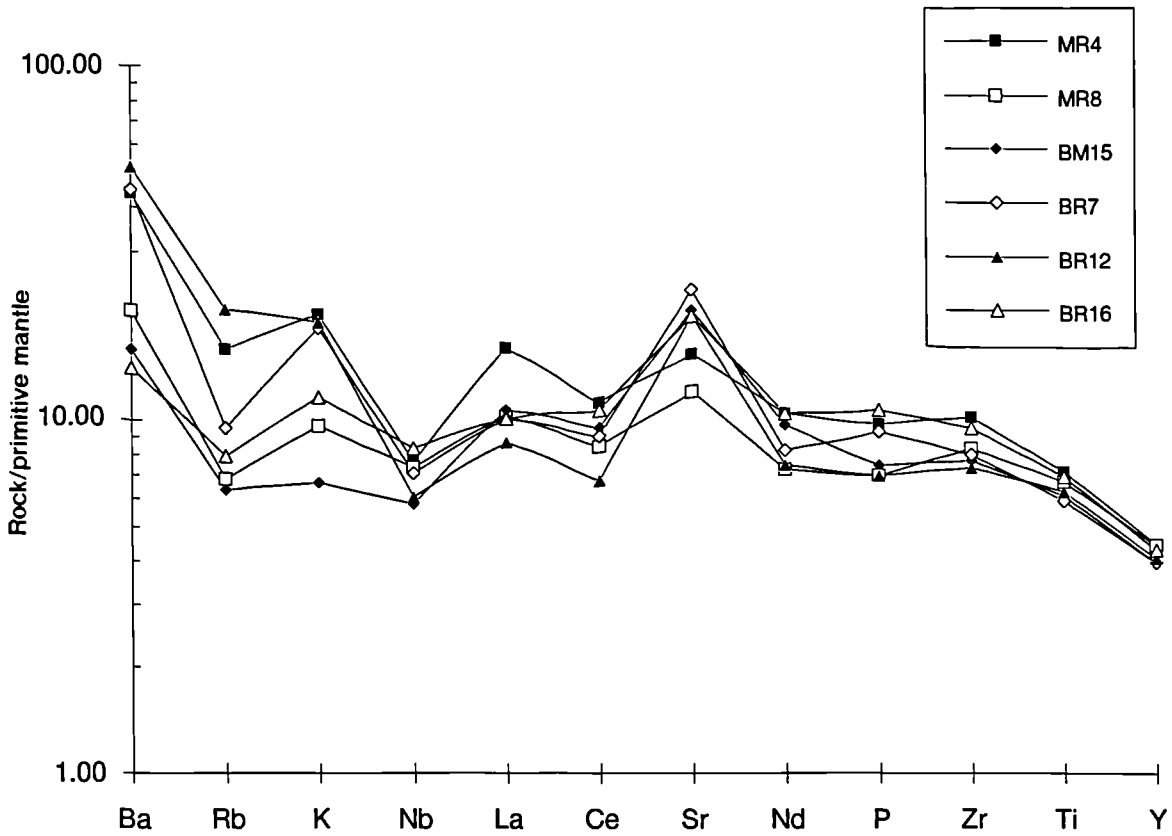


Figure 4.23 Primitive Mantle normalised diagram showing lavas from throughout the Mull lava field. See figure 2.2 and Appendix 1 for sample locations.

Figure 4.24 shows that addition of variable small amounts (<3%) of the acidic Lewisian crustal sample (P43, discussed above) is capable of reproducing most of the chemical features shown on figures 4.19 and 4.23. The use of P43 as a contaminant does not significantly raise the La content of the magma; La enrichment relative to Nb is, however, observed in figure 4.23. The explanation for this, lies in the fact that P43 does not contain enough La (6ppm) to significantly alter the composition of La in the magma. However, as will be discussed in more detail below, Lewisian felsic rocks have quite variable La contents. In figure 4.25 an acidic Lewisian sample containing 24ppm La (P37) has been used to model the composition of the lavas in figure 4.23. As can be seen, the use of this contaminant can produce a $(La/Nb)_{pmn}$[5] value of >1, similar to those observed. This contaminant is less enriched in Ba and contains more Rb than P43, and so the modelled pattern is slightly different. Nevertheless, it would seem that addition of <5% acidic Lewisian contaminant can

[5] Primitive mantle normalised (Sun & McDonough 1989)

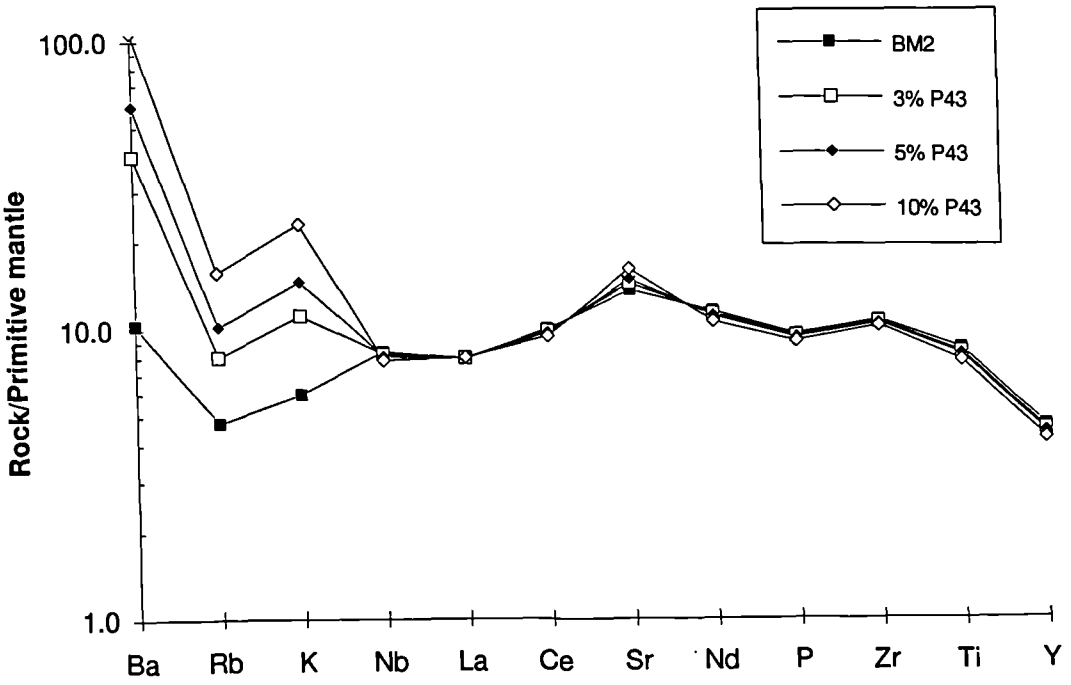


Figure 4.24 Primitive Mantle normalised diagram showing the effects of adding 3, 5 and 10% acidic Lewisian crust (P43) to an uncontaminated primitive MPG basalt (BM2).

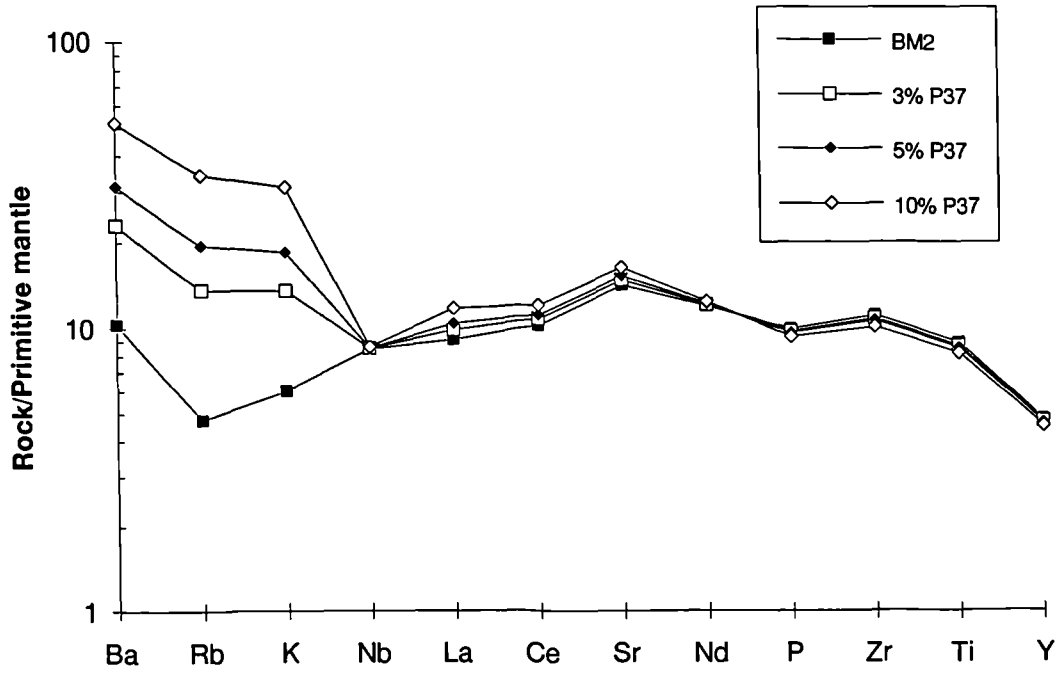


Figure 4.25 Primitive Mantle normalised diagram showing the effects of adding 3, 5 and 10% acidic Lewisian crust (P37) to an uncontaminated primitive MPG basalt (BM2).

explain the enrichments in the Large Ion Lithophile (LIL) elements, with minimal influence on silica saturation or on major element composition.

As previously discussed, Watson (1982) proposed that basalts could be selectively contaminated with Ba & K from acidic partial melts of continental crust. The modelling and observations discussed above would tend to support this theory for the MPG basalts.

Previous work on crustal contamination processes in the SMLS (Thompson *et al.* 1982) showed that major element compositions, between contaminated and uncontaminated lavas, were not significantly different, except for K_2O. It was noted that addition of more than 5% acidic Lewisian crust to an uncontaminated basalt would significantly alter the major element chemistry of the lava. Thus the major elements suggested that the amount of acidic Lewisian contaminant required was not more than 5%. In marked contrast, trace element compositions required the quantity of contaminant to be of the order of 20%. The acidic Lewisian sample (7H) used chiefly for modelling by Thompson *et al.* (1982) contains 1800ppm Ba and 2.34% K_2O. In contrast, P43 and P37 (used in this study) contain an average of 6.5% K_2O and 5000ppm Ba. Therefore, if contaminants containing much more Ba and K_2O are invoked, the need for the addition of 20% acidic Lewisian crust to explain the LIL element enrichment in the SMLS basalts, is removed.

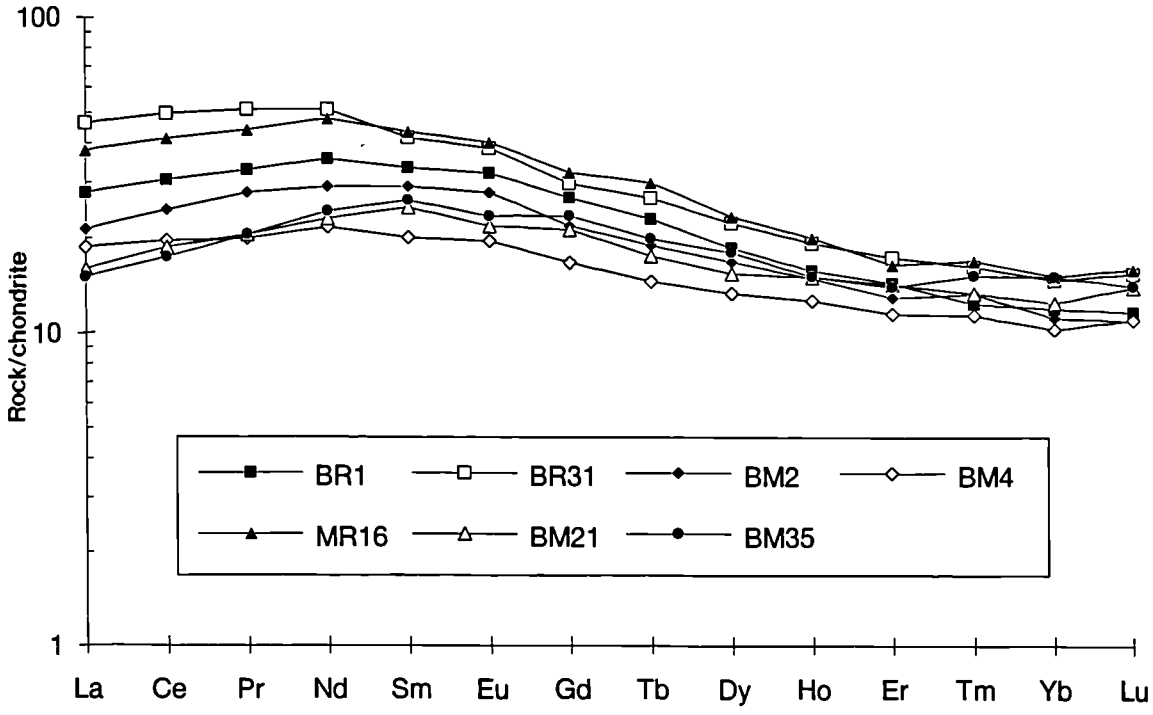


Figure 4.26 Chondrite-normalised REE plots of some MPG lavas (basalts and hawaiites) that are free from a significant crustal input. (For sample locations see Appendix 1 and figure 2.2)

The REE can also be used to demonstrate crustal contamination. Watson (1982) observed that the LREE had high diffusivities and so had the potential to selectively contaminate a magma. Campbell (1985) similarly proposed that the LREE enriched nature of continental basaltic rocks could be explained by crustal contamination processes. Figure 4.26 shows chondrite-normalised REE patterns for seven lavas (basalts to basaltic-hawaiites) from the MPG which, from the criteria discussed above, contain little crust $[(Ba/Nb)_{pmn} < 2]$. All these lavas have slightly down-turned LREE patterns $[(La/Nd)_{cn} < 1)$[6] and this feature is probably caused by mantle processes (see Chapter 6).

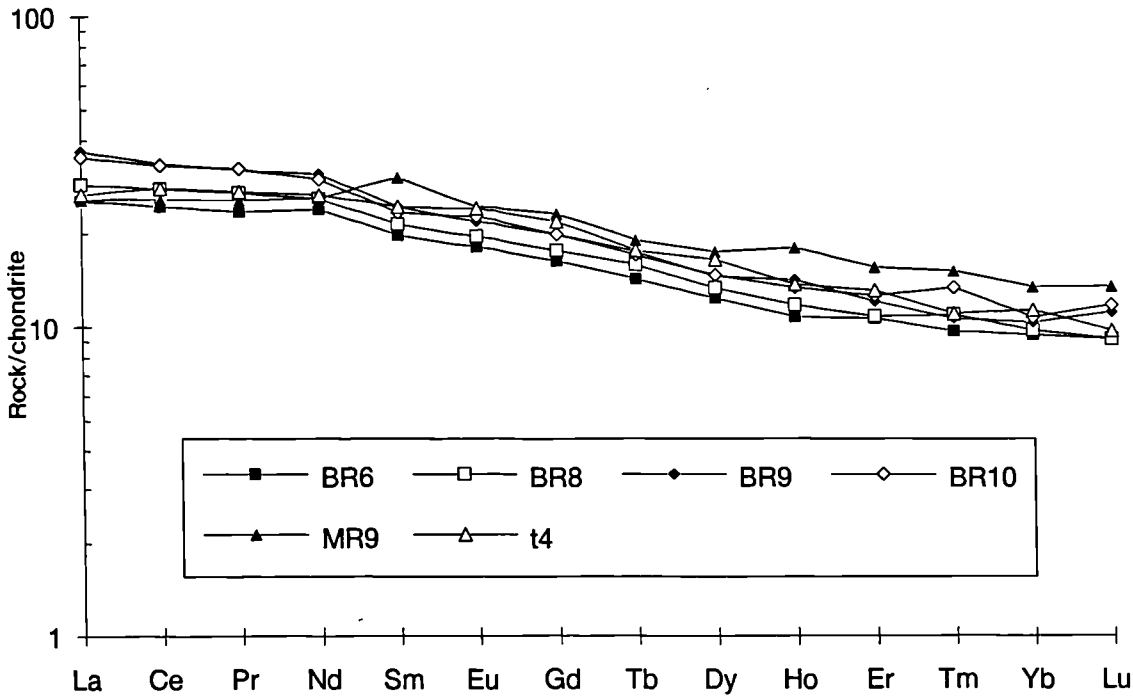


Figure 4.27 Chondrite-normalised REE plots of some MPG basalts which, based on the criteria discussed above, contain a significant crustal input. (For sample locations see Appendix 1 and figure 2.2)

Displayed on figure 4.27 are the chondrite-normalised REE patterns of six basaltic lavas which, from the criteria discussed above, have been contaminated with continental crust $[(Ba/Nb)_{pmn} > 2]$. In contrast with the uncontaminated lavas, they have $[(La/Nd)_{cn} > 1)$. Therefore crustal contamination has increased the LREE contents of the magmas, as proposed by Watson (1982) and Campbell (1985).

Lewisian upper amphibolite facies crust contains significantly more Th than granulite facies lower crust (table 4.4). This large difference in Th content should make the detection of an upper crustal amphibolite facies contaminant in the MPG

[6] Chondrite-normalised (Sun & McDonough 1989)

lavas relatively easy. Figure 4.28 is a plot of Ba/Th vs. La/Nb. On this diagram it is relatively easy to distinguish between upper and lower crust (upper crust has lower Ba/Th). Consequently, it should likewise be a relatively simple matter to distinguish between upper and lower crustal contamination.

	Th content (ppm)
Mean of 254 granulite facies gneisses	0.42
Mean of 39 amphibolite facies gneisses	8.4

Table 4.4 Showing the differing Th contents of Lewisian granulite and amphibolite facies rocks, (After Weaver & Tarney 1981)

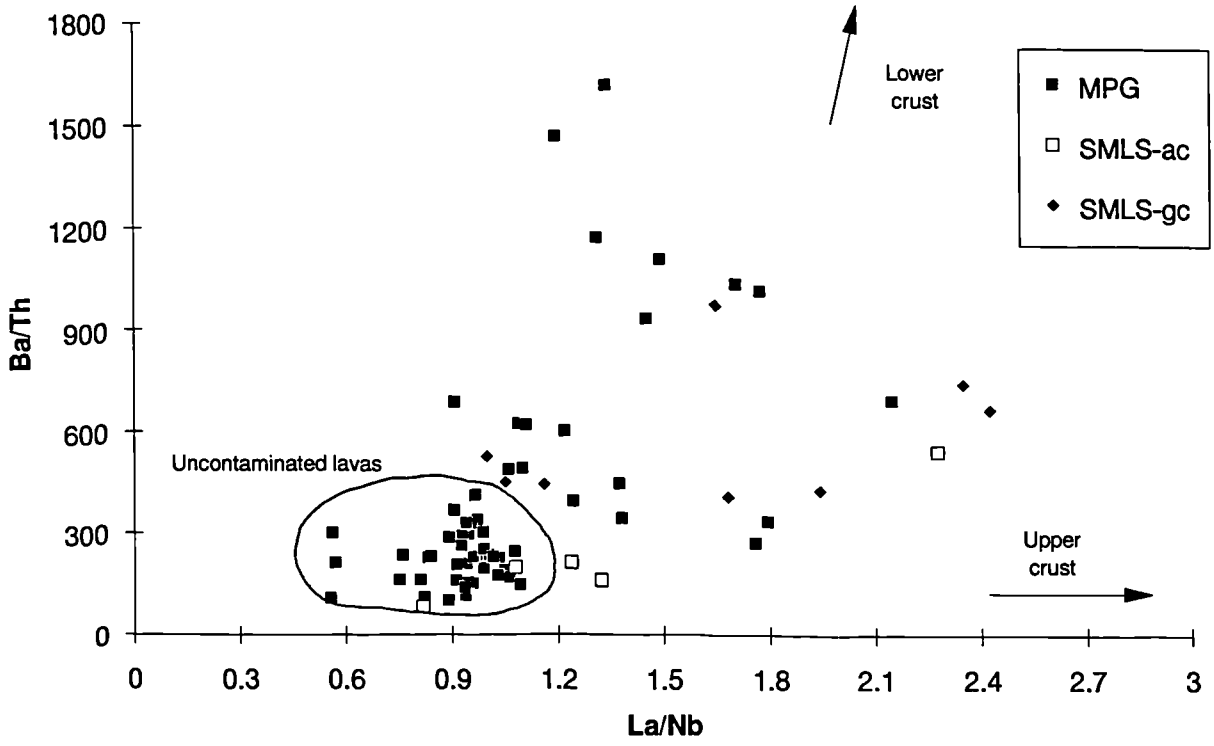


Figure 4.28 Plot of Ba/Th vs. La/Nb for the MPG, SMLS-ac - Skye lavas contaminated with amphibolite and granulite facies Lewisian crust, and SMLS-gc - Skye lavas contaminated with granulite facies crust. Arrows pointing towards average Lewisian lower crust (granulite facies) and upper crust (amphibolite facies) are also shown (from Weaver & Tarney 1980; 1981)

The diagram shows MPG samples analysed for Th, along with SMLS samples which appear to have been contaminated with granulite facies Lewisian crust and/or amphibolite facies crust (Thompson *et al.* 1982; Dickin 1981). Also marked on the diagram is a field of relatively uncontaminated lavas (low La/Nb and Ba/Th) from the present study. This data would seem to suggest that most of the crustal input into the

MPG lavas was granulite facies lower crust. Isotopic evidence, as will be shown later, supports this interpretation. It is, however, worth noting that, like the SMLS, there seems to be a slight upper crustal component in several of the lavas.

Comparison of the spidergram of a basic lava containing little crust with that of a more evolved lava (figure 4.29) shows that, with the exception of Sr (which has been shown to be mobile; section 4.1), two patterns are remarkably parallel. This is entirely consistent with an origin for these basaltic-hawaiites by fractional crystallisation (see section 4.3) with very little Lewisian crustal contamination.

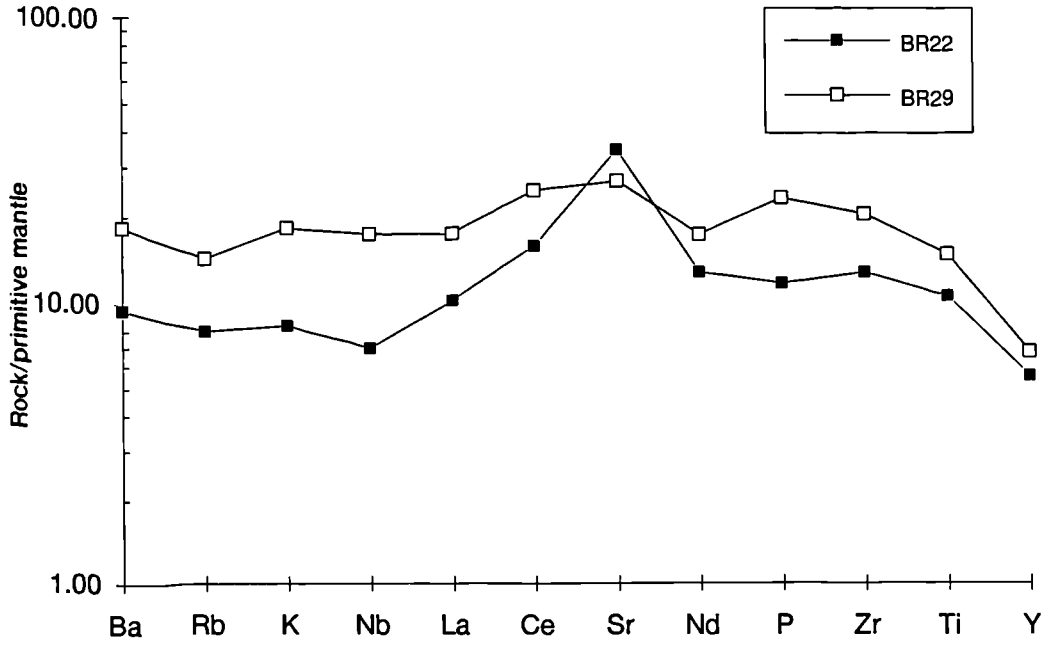


Figure 4.29 Primitive mantle normalised spidergrams showing two uncontaminated MPG lavas.

Isotopic evidence for crustal contamination.

Radiogenic isotope diagrams (eg. figure 4.30) clearly show that the most basic MPG magmas are the most contaminated with acidic Lewisian crust. In contrast most of the more evolved (basaltic-hawaiite to hawaiite) lavas contain virtually no Lewisian crust. Moorbath & Thompson (1980); Thompson *et al.* (1982) reported very similar results for the SMLS. This provides very strong evidence for Assimilation of acidic crust during Turbulent magma Ascent (ATA). Furthermore, the lavas show little sign of having undergone AFC processes. This evidence is in marked contrast to the Tertiary Trotternish sills on Skye (Gibson 1990) and the cone sheets cutting the Cullin Intrusion, Skye (Bell *et al.* 1993) which have assimilated crust *during* fractionation.

Figure 4.31 shows a $(^{207}Pb/^{204}Pb)i$ vs. $(^{206}Pb/^{204}Pb)i$ plot for the MPG samples from the present study, along with the SMLS Pb isotope values as reported by Dickin (1981). On this diagram the MPG and the SMLS samples lie on an identical trend,

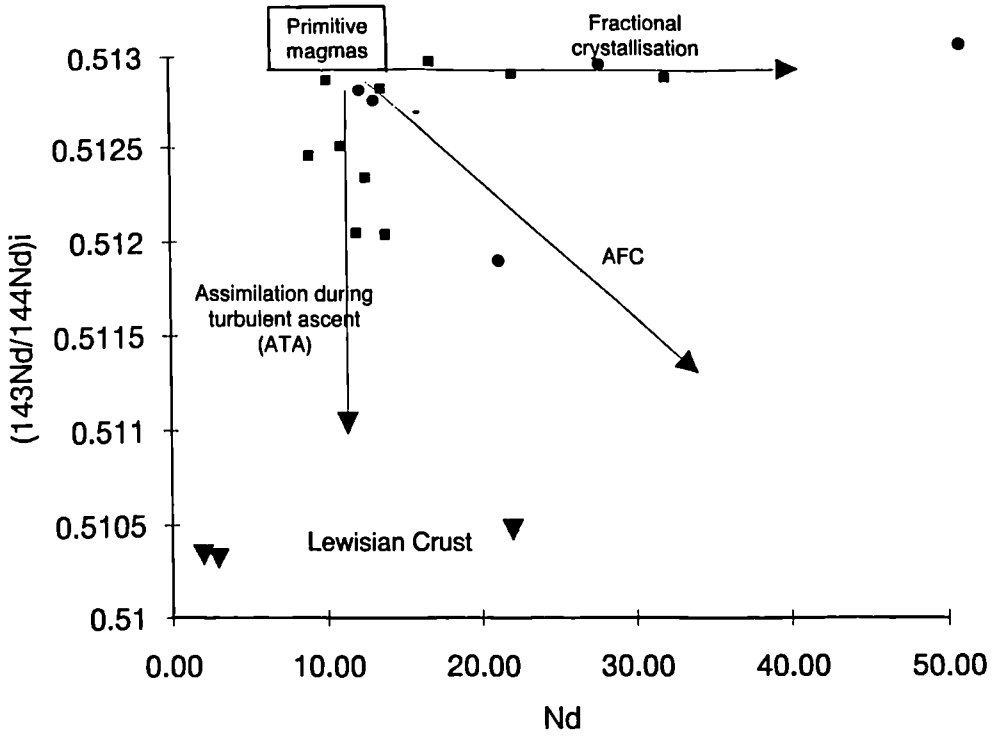


Figure 4.30 Plot of ($^{143}Nd/^{144}Nd$)i* vs. Nd, showing trends for fractional crystallisation, AFC, and assimilation during turbulent ascent. **Symbols;** solid squares - MPG lavas this study; filled circles - MPG lavas from Carter *et al.* (1978); inverted triangles - Lewisian crust from Tiree (this study). (*All isotopic ratios plotted on this and subsequent diagrams are age corrected to 60 Ma (i), using the same decay constants as Dickin & Jones 1983b).

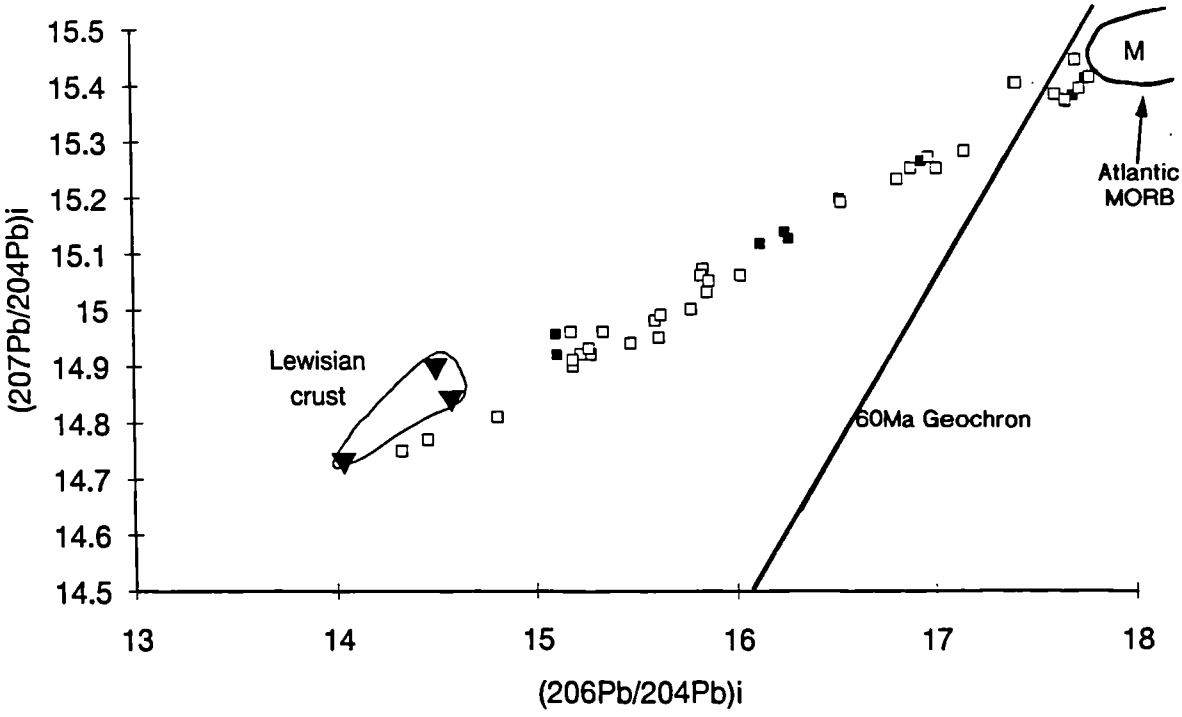


Figure 4.31 Plot of ($^{207}Pb/^{204}Pb$)i vs. ($^{206}Pb/^{204}Pb$)i for the MPG lavas (filled squares) along with SMLS data from Dickin (1981) (hollow squares) and Lewisian crust (inverted triangles). Also shown is the Geochron calculated from the growth curve of Stacey & Kramers (1975), the field of Atlantic MORB (Holm *et al.* 1988), and the proposed composition of sub-Hebridean mantle (Dickin 1981).

that is, on a direct mixing line between the proposed values for Tertiary Hebridean mantle (M) (Dickin 1981) and Lewisian crust (amphibolite and granulite).

Decreasing $(^{206}Pb/^{204}Pb)i$ with increasing $(Ba/Nb)_{pmn}$ may be used to test if this ratio is in fact a good elemental yardstick with which to assess the degree of crustal contamination. A plot of $(^{206}Pb/^{204}Pb)i$ vs. $(Ba/Nb)_{pmn}$ (figure 4.32) has a negative correlation, proving that increasing $(Ba/Nb)_{pmn}$ ratios do indeed indicate more extensive crustal contamination.

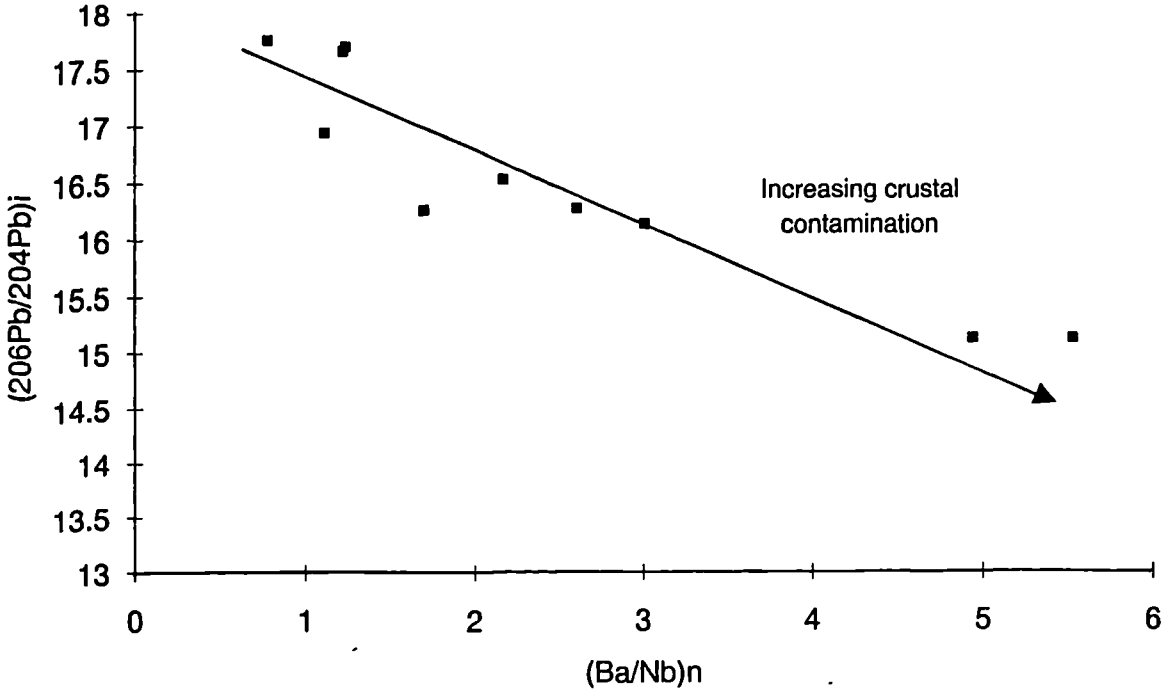


Figure 4.32 A plot of $(^{206}Pb/^{204}Pb)i$ vs. $(Ba/Nb)_{pmn}$ for the MPG lavas.

Inspection of figure 4.31 reveals that several of the MPG lavas and quite a few of the SMLS samples contain over 60% crustal Pb. The major and trace element data do not support such a massive crustal input to these magmas. This observation led Dickin (1981) to propose a process of selective Pb contamination, to explain the high crustal Pb components in these magmas. Acidic Lewisian crustal rocks usually contain over 10ppm Pb (Appendix 4a.vii and Weaver & Tarney 1980;1981). In contrast, uncontaminated basalts from the MPG contain less than 1ppm Pb. Addition, therefore, of ~5% of acidic Lewisian crust (containing 10-15ppm Pb) to an uncontaminated lava containing (<1ppm Pb), will result in a contaminated magma containing significant amounts (>50%) of crustal Pb. Therefore, although selective contamination *may* have played a role, the main reason for the high crustal Pb component in contaminated MPG lavas is simply due to swamping of the small amount mantle derived Pb, by <5% acidic Lewisian crustal melt containing up to twenty times more Pb.

This interpretation is supported by the negative correlation between ($^{206}Pb/^{204}Pb$)i and Pb (figure 4.33). It is obvious from this diagram and the foregoing discussion that Pb isotope systematics of "clean" Hebridean magmas will be easily modified by even the smallest input (~0.2%) of Lewisian crust. Therefore it is extremely unlikely that the three more evolved (basaltic-hawaiite) lavas (BR1, 18 & 24; figure 4.32), which are relatively uncontaminated [>17.5 ($^{206}Pb/^{204}Pb$)i], fractionated within the crust. A much more likely place for these magmas to fractionate would have been within the refractory upper lithospheric mantle, perhaps at the density discontinuity represented by the MOHO (~30km). (As was borne out earlier in figure 4.4 major element data *also* suggest that the MPG lavas last equilibrated at ~9kb). Consequently, when these magmas eventually passed through the crust, they would have been cooler than the basaltic magmas, and so much less likely to fuse and incorporate acidic Lewisian crust.

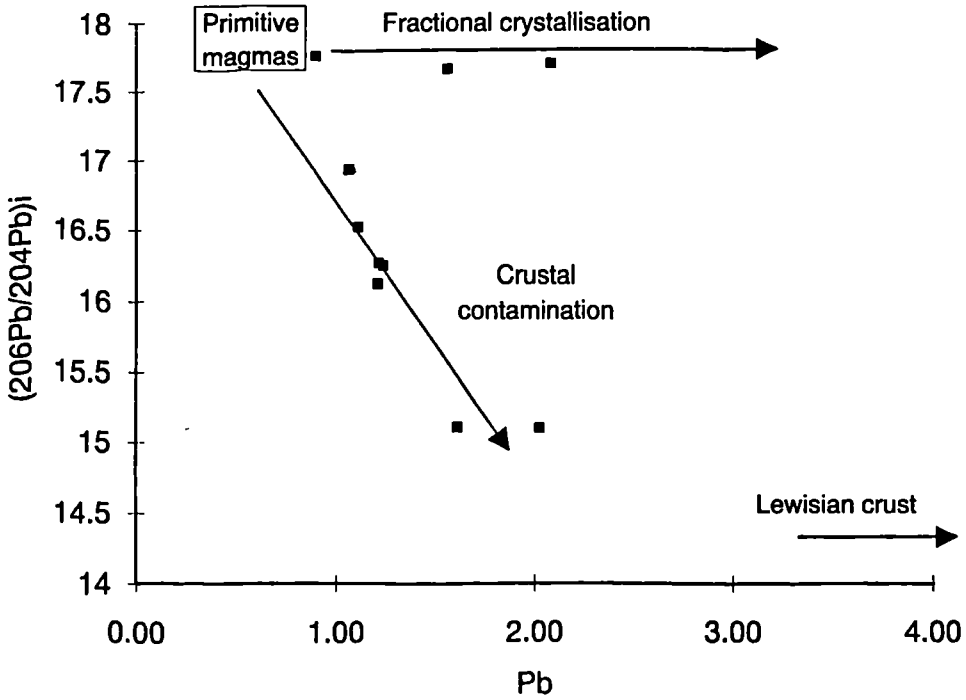


Figure 4.33 Plot of ($^{206}Pb/^{204}Pb$)i vs. Pb for the MPG lavas.

Figure 4.34, again shows that the MPG and the SMLS (Moorbath & Thompson 1980; Dickin *et al.* 1987) form very similar arrays, between Tertiary Hebridean mantle and acidic granulite facies Lewisian crust. As would be expected, a plot of ($^{208}Pb/^{204}Pb$)i vs. ($^{206}Pb/^{204}Pb$)i (figure 4.35) supports crustal contamination and, like figure 4.34 it is able to distinguish between granulite and amphibolite crustal contamination (ie. lower and upper crust respectively). This is because amphibolite facies Lewisian crust has higher values of ($^{208}Pb/^{204}Pb$)i than granulite facies Lewisian crust (Dickin 1981). The diagram shows that, while a few of the Skye lavas

appear to be contaminated with upper crust, the MPG lavas as a whole contain little upper crust. This conclusion confirms the evidence for a predominantly lower crustal contaminant, within the MPG lavas, which was previously gleaned from the Ba/Th vs. La/Nb plot (figure 4.28).

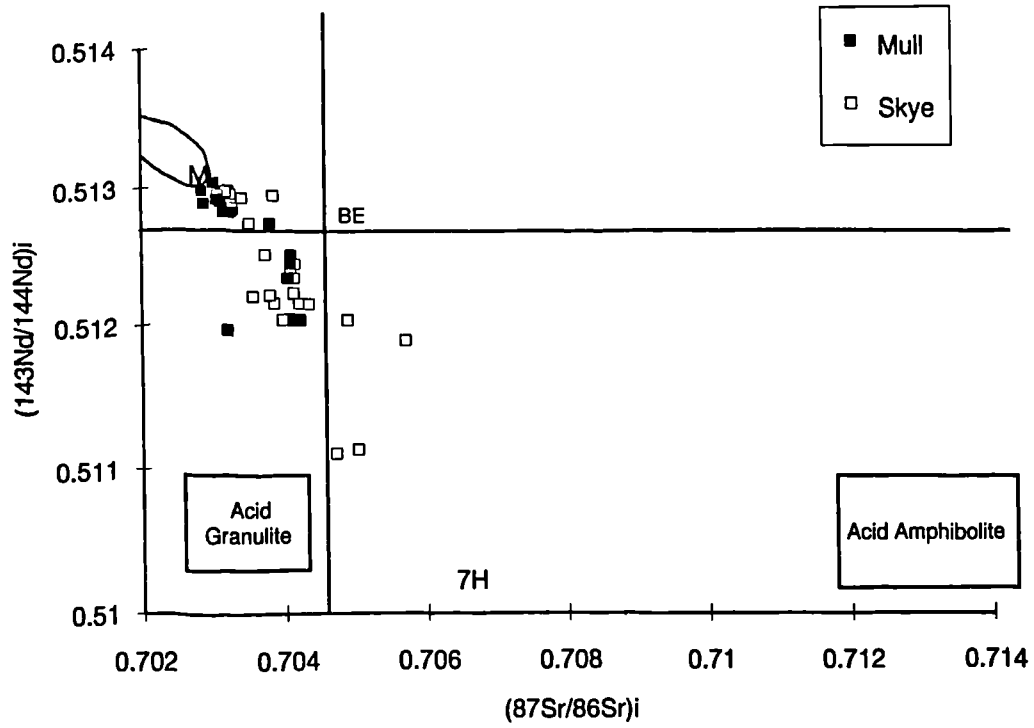


Figure 4.34 Plot of ($^{143}Nd/^{144}Nd$)i vs. ($^{87}Sr/^{86}Sr$)i for the MPG and the SMLS, M and MORB field as for figure 4.31. 7H - Acidic Lewisian crust (Thompson *et al.* 1982), BE - Bulk Earth, Fields for Acid Granulite and Amphibolite facies Lewisian crust from Thompson (1982).

Thompson *et al.* (1985; 1986) made a detailed study of the chemistry of the "Staffa Magma Type" (SMT); the series of columnar, tholeiitic flows which occur near the base of the Mull lava succession in several parts of the island (see Chapters 2 and 5). They established that the SMT lavas - in contrast to the overlying MPG lavas - fractionated and equilibrated in the upper third of the crust while assimilating significant quantities of Moine schist. Obviously, therefore, it is important to assess whether the MPG lavas are also contaminated with Moine schist. Figure 4.36 clearly shows that, while the SMT are significantly contaminated with Moine Schist (and some granulite facies Lewisian crust), the MPG lavas display no similar deviation to higher $^{87}Sr/^{86}Sr$ which would be indicative of Moine contamination.

As was pointed out by Thompson *et al.* (1982), the upper crust contains more water-bearing minerals than the lower crust, and as a result will be relatively more fusible. Why then, if this is the case, is most of the contamination in the both the SMLS and the MPG from the lower crust? Huppert & Sparks (1985) suggested that

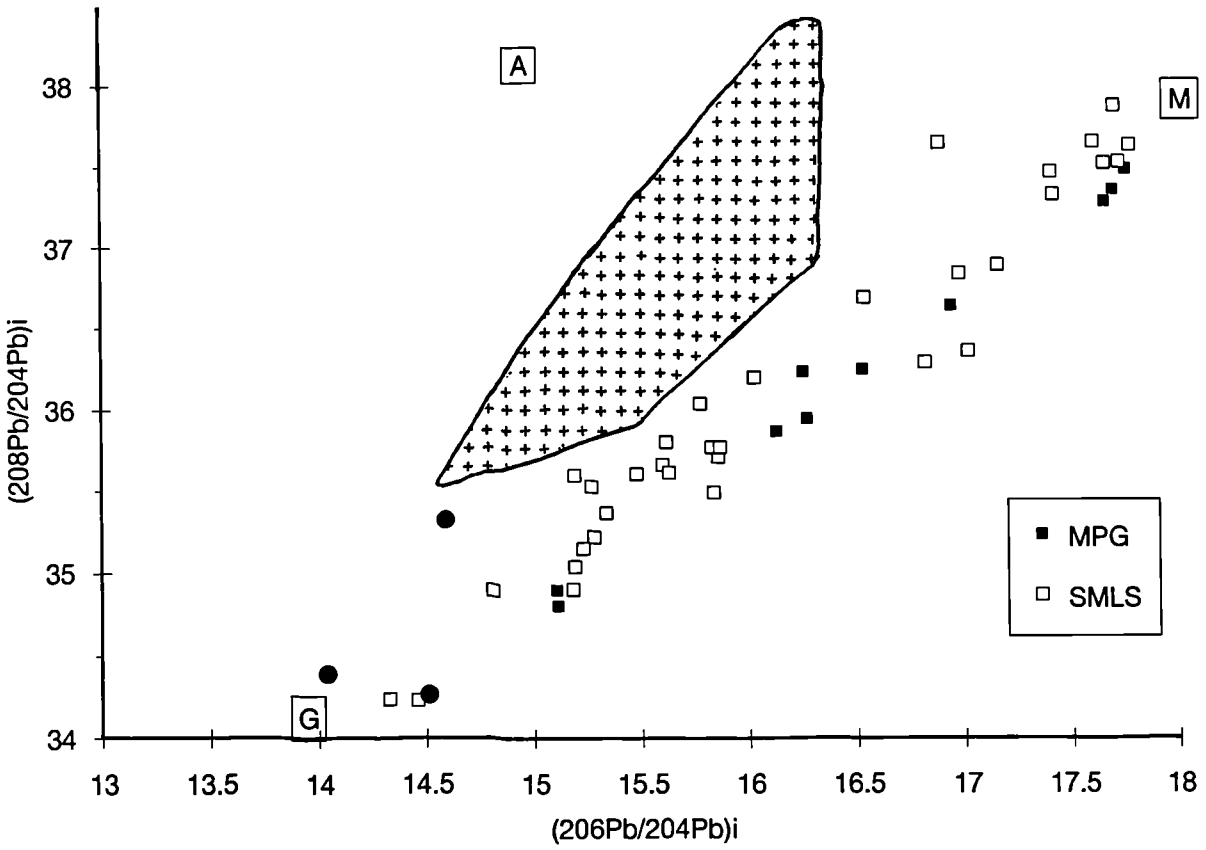


Figure 4.35 Plot of ($^{208}Pb/^{204}Pb$)i vs. ($^{206}Pb/^{204}Pb$)i for the MPG and the SMLS. Circles represent acidic Lewisian crust and 'M' as in figure 4.31. 'G' and 'A' are average Lewisian granulite and amphibolite facies crust (Dickin 1981). Also shown on this diagram (shaded field) is the compositional range for the Skye granites (Dickin & Jones 1983).

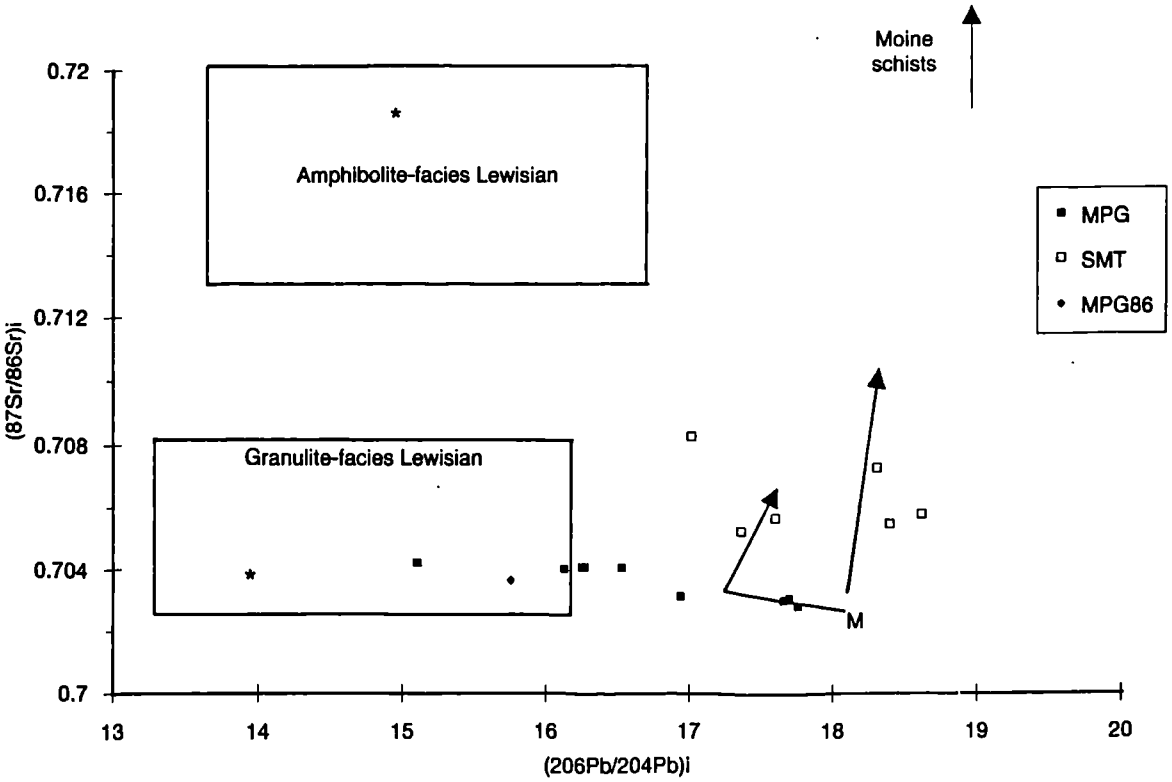


Figure 4.36 (After Thompson *et al.* 1986) plot of ($^{87}Sr/^{86}Sr$)i vs. ($^{206}Pb/^{204}Pb$)i for the MPG and the SMT. MPG86 - MPG lava analysed by Thompson *et al.* (op.cit); stars - weighted means of amphibolite and granulite facies Lewisian crust; M - as in figure 4.31.

the explanation lay in the fact that the ascending magma is hotter and more fluid at depth, and so will tend to selectively assimilate lower crustal material. The net result of this was calculated by Huppert & Sparks (op.cit.) to be a steady *decrease* in crustal melting rate with height, because the magmas were cooler and more viscous than at lower crustal depths. The lack of upper crustal contamination in the MPG and the SMLS magmas could also be because the magmas briefly ponded in the lower crust assimilating some material, before being erupted rapidly through though the upper crust (Thompson *et al.* 1986).

4.3.5 Implications for magmatic plumbing systems

As was discussed earlier, crustal assimilation during turbulent ascent of the hottest, most basic magmas, requires the contamination to occur in thin dyke- and sill-like magma chambers, with a high surface-to-volume ratio. Such long and narrow magma chambers have been proposed as feeders of the SMLS (Thompson *et al.*, 1972,1982), and the available evidence from the contamination mechanisms of MPG lavas suggests that they also developed in similar elongated, thin magma chambers.

Although units of flows with very similar compositions occur up succession, individual flows of differing compositions do sometimes interleave (eg. BM44-53, BHL11-18 and BCH5-13). This observation implies that distinctive magmas were erupted at approximately the same time and so also supports the idea of thin, poorly connected magma chambers, with separate eruption vents.

It has been shown that the more evolved and less contaminated low-MgO basalts and basaltic-hawaiites probably ponded and fractionated at sub-crustal levels (eg flows BR18-33 - "BR-C"). Thus, when these magmas eventually passed through the crust they were relatively cool and, unlike their more basic counterparts, were unable to fuse much Lewisian crust.

Some of these more evolved magmas display petrographic evidence for magma mixing (Chapter 3). This evidence takes the form of partially resorped and regrown plagioclase phenocrysts, suggesting that a fractionating magma chamber was being recharged with more primitive magma. This petrographic evidence raises the question "Does the geochemical evidence support the idea of a 'periodically **R**efilled, periodically **T**apped, continuously **F**ractionating magma chamber' (**RTF** -magma chamber) as envisaged by O'Hara and Mathews (1981)"? One of the geochemical signatures of such a process, in a sequence of lavas, is a *progressive* enrichment in the incompatible elements at *approximately constant* MgO contents. O'Hara (in discussion of Dickin *et al.* 1984) has argued for such a process in the SMLS. Recent geochemical work has, however found little evidence for such a process in the SMLS, (K. Cox, pers. comm 1993).

If long lived RTF-magma chambers - as envisaged by O'Hara and Mathews (1981) - did supply the Mull lava succession, then a sequence of lavas such as BR-C, should show progressive enrichment in such elements as Nb at constant MgO contents. Figure 4.37 shows that this is *not* the case, and no enrichment in Nb is observed up this sequence. Therefore, although some magma mixing did occur, the existence of an RTF-magma chamber is inconsistent with the geochemical data.

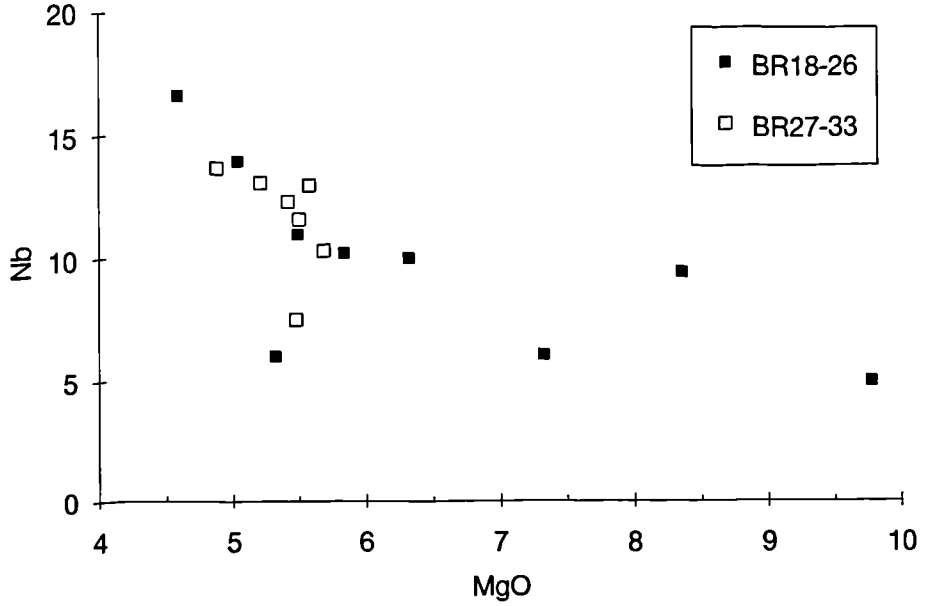


Figure 4.37 Plot of Nb vs. MgO for the BR-C lava unit, BR18-26 are the earlier flows in the unit and BR27-33 the later ones.

The idea of basic continental magmas ponding and fractionating at the crust-mantle boundary, because they were too dense to pass upwards into the crust, was proposed by Thompson (1974) and Cox (1979). Some of the more basic magmas from the MPG obviously failed to pond for long periods and therefore to fractionate significantly at MOHO depths. Why should this be? One possibility is that the volume of magma supply from the mantle was at times too much for it all to pond at the MOHO. The density constraints imposed at low magma supply rates therefore broke down at high magma supply rates. This, in combination with active lithospheric extension and the resultant fracturing, could well have led to the eruption of more basic magmas. The discovery of ash deposits between MPG flows (Chapter 2) provides evidence for the explosive nature of at least some of the MPG eruptive events. Build-up of gas could also have provided a means of forcing the more basic magmas to the surface.

If the ATA model is correct, it might be expected that the more-basic magmas further up the succession should contain less crust, since the earliest magmas would

have 'sweated out' the most fusible crustal components. There seems, however, to be little evidence for this process, in that the lavas BM37-42 (half way up Ben More) have similar values of Ba and K_2O to BM8-18, suggesting that they contain similar amounts of crust. The reason for this probably lies in the fact that the most favourable situation for contamination to occur is where magma batches follow each other at regular intervals through the same zone of crust (Patchett 1980). In such a situation, some of the earliest magmas would melt and incorporate the most-fusible portion of crust and in doing so they would heat up the surrounding crust. The later magma batches would have greater potential to melt some of this less-fusible but warmed crust, which was not quite melted by the earlier magma batches.

The lavas from the BR section show an interesting phenomenon. Figure 4.38 shows a plot of $(K/Zr)_{pmn}$ vs. $(Ba/Nb)_{pmn}$ with crustally contaminated lavas plotting at higher values of $(K/Zr)_{pmn}$ and $(Ba/Nb)_{pmn}$. The BR-B lavas are given their flow/sample numbers on figure 4.38, with flow 4 at the bottom of the group and 17 at the top.

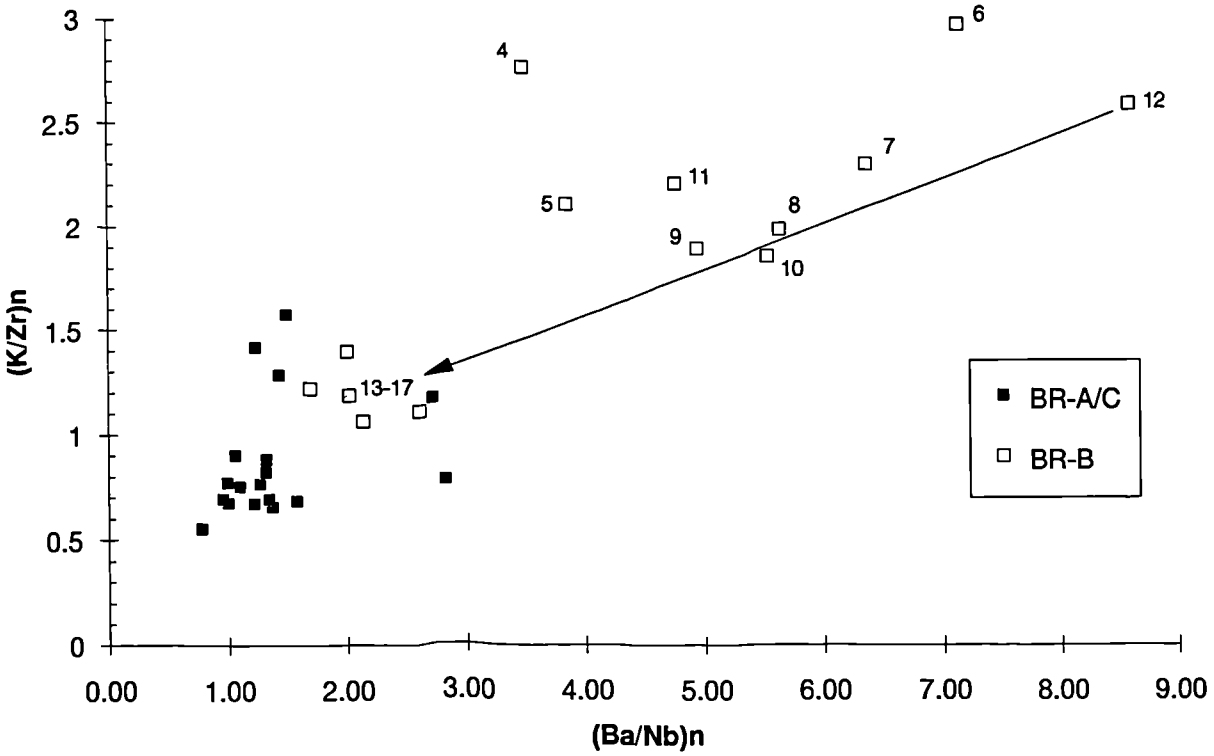


Figure 4.38 Plot of $(K/Zr)_{pmn}$ vs. $(Ba/Nb)_{pmn}$ for lavas from the BR section (figure 2.2). Numbers beside data points refer to flow/sample numbers for each lava in this crustally contaminated BR-B unit (eg. 4 = BR4 lowest flow in the unit, and 17 = BR17 the top-most flow).

It can be seen that flows BR4-11 contain significant amounts of crust. BR12, however, is quite enriched in Ba and K, and probably therefore contains more crust than the preceding flows. In sharp contrast, flows BR13-17 contain significantly less crust. BR12 has the highest MgO content, and it would therefore appear that this

magma stripped a lot of the acidic fusible material from its adjacent wall rocks; thus, there was less acidic crust available to contaminate the next few magma batches (BR13-17). A similar situation has also been observed in the early flows of the Morvern section (MR, this study). Dickin *et al.* (1984) in a study of the Storr lava section (12 flows collected) on Skye, similarly found that the degree of contamination decreased with time, up this short section.

The contamination model outlined above holds true for most of the lavas analysed from the MPG. However, as figure 4.39 reveals some lavas do not fit this general model and these can be sub-divided into two groups;

a/ basic magmas which contain little crust (eg. MR2, BM2-5, B11, & BHL15).

These lavas predominantly occur low in the succession, and obviously they passed quickly through the crust while it was still relatively cold, in the early stages of magmatism, and as a result they are essentially free from crustal input.

b/ contaminated basaltic-hawaiites (eg. MR6, MR4, BM53, BCH13 & BHL23)

These magmas may have assimilated Lewisian material while fractionating within the crust (AFC). Alternatively, they may have interacted with partially molten crust, which had been warmed up and melted by the previous passage of a hotter basaltic magma.

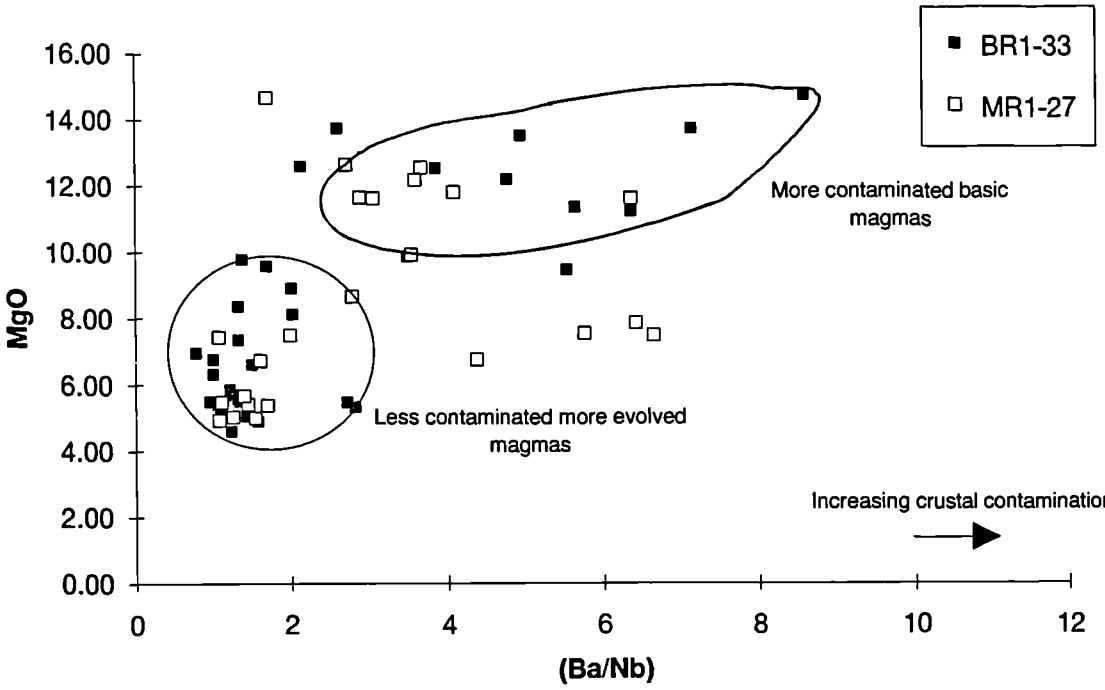


Figure 4.39 Plot of MgO vs. $(Ba/Nb)_{pmn}$ for lavas from the MR and BR sections (figure 2.2), showing the field of less contaminated, more evolved lavas, and a field representing more crustally contaminated basic magmas.

The waning of magmatic activity, and the ultimate development of trachytes on Ben More, has been extensively dealt with in the previous section. Only the main conclusions will be summarised here for the sake of completeness. The mugearites, benmoreites, and trachytes at the top of the MPG seem to contain significant amounts of crustal material. They probably fractionated in the mid-to-lower crust, and the resultant latent heat of crystallisation led to crustal fusion, and contamination of the magmas (AFC). This prolonged fractionation and likely crustal melting, probably led to the coalescence of the thin dyke-and sill-like magma bodies to form larger chambers.

In conclusion, this comprehensive geochemical study on the MPG lavas has demonstrated that crustal contamination is indeed a viable and an important process. The lavas which Beckinsale *et al.* (1978) classed as 'Group 1', which had low $(^{87}Sr/^{86}Sr)i$, are those basalts to basaltic-hawaiites which are essentially free from a crustal input. 'Group 3' of Beckinsale (op.cit.) are essentially crustally contaminated basalts, and 'Group 2' are contaminated tholeiites (Chapter 5) plus evolved magmas, Therefore, none of these groups identified by Beckinsale *et al.* (op.cit) owe their distinctive chemistry to any mantle source characteristics.

4.5 Contamination by an enriched small-fraction-melt from the lithospheric mantle.

4.5.1 Introduction

Several recent studies on continental mafic magma genesis have focused on the importance of small degree, low-temperature, melt fractions that are relatively enriched in incompatible trace elements. These are thought, through time, to have migrated from the convecting asthenosphere into the cold rigid continental lithosphere and solidified there (Frey & Green 1974; McKenzie 1989). Subsequent extension of the lithosphere, with some extra heating, may cause asthenospheric upwelling and decompression melting. This leads to the generation of basaltic magma in the asthenosphere, which migrates upwards through the lithosphere to the surface. In several parts of the world these magmas have been shown to pick up some of this enriched small-fraction-melt from the lithospheric mantle, thus modifying their asthenospheric compositions (e.g. Gibson *et al.* 1991; Ellam & Cox 1991).

The basalts of the British Tertiary Igneous Province (BTIP) display a wide variation in the concentrations and ratios of incompatible trace elements and Sr, Nd, Ce and Pb isotopes (eg. Thompson *et al.* 1982; 1986). This range has previously been attributed to a combination of varying degrees of mantle fusion and varying amounts of crustal contamination. As has been seen in section 4.4, those basalts of the BTIP which show little geochemical evidence of crustal assimilation are relatively depleted in incompatible trace elements, when compared to other basalts erupted in continental settings, eg. the Snake River Plain, western USA (figure 4.40).

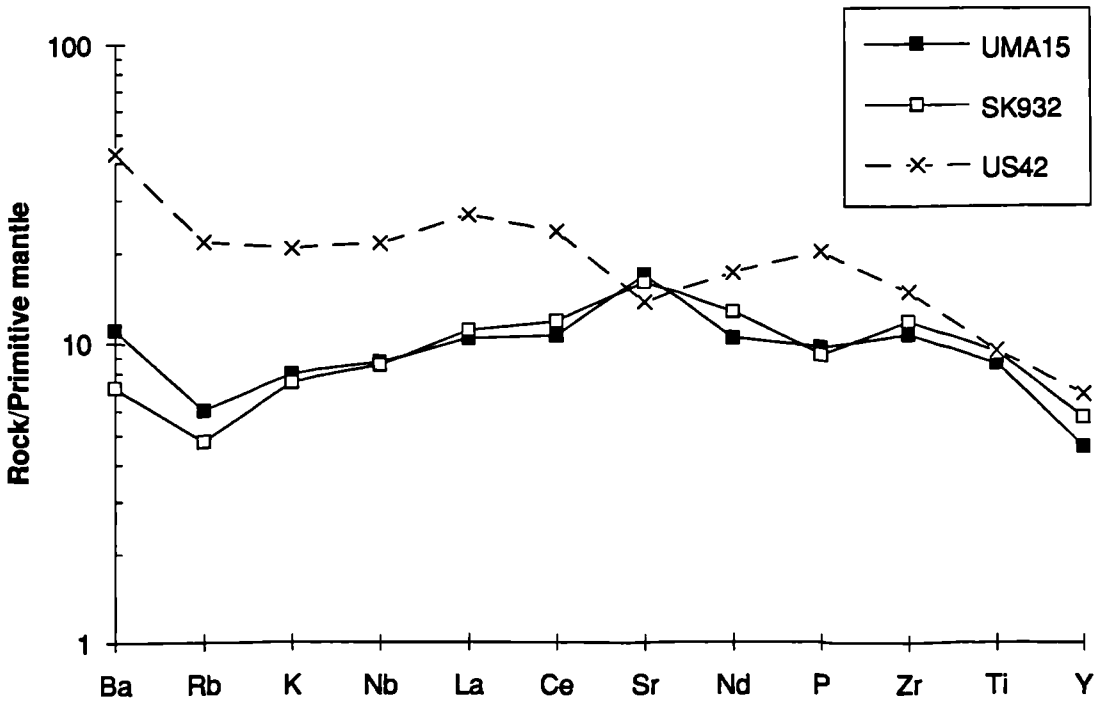


Figure 4.40 Primitive mantle normalised diagram, for UMA15, an average of 15 Mull basalts, which lack geochemical evidence for crustal contamination. SK932, an uncontaminated basalt from Skye (Thompson *et al.* 1982). US42, basalt from the Snake River Plain, western USA (Thompson *et al.* 1983).

The explanation given by Morrison *et al.* (1980); Thompson & Morrison (1988) for this depletion was that most of the enriched small-fraction-melt had already been extracted by magmatism associated with minor extension during the Permian and Carboniferous. It was not therefore widely available as a potential input to the BTIP magmas; unlike many of the basalts in the western USA, which have a geochemical signature of an enriched lithospheric component (Fitton *et al.* 1991; Gibson *et al.* 1991) (figure 4.40).

In the Hebrides, the youngest pre-Tertiary, low-temperature, small-volume, melts are preserved as a series of Permo-Carboniferous, lamprophyric dykes (mostly camptonites and monchiquites) in western Scotland (Morrison *et al.* 1987; Baxter

1987). These dykes are relatively enriched in incompatible trace elements, such as Ba, Rb, K, Nb and the LREE, when compared to Tertiary lavas (eg. figure 4.49).

4.5.2 The enriched MPG flows

Figure 4.40 shows the average normalised incompatible element abundances for 15 MPG basalts -- which seem to contain little crust -- along with the same data for SK932, a SMLS basalt which has been shown to be elementally and isotopically uncontaminated with continental crust or lithospheric mantle (Thompson *et al.* 1982). In section 4.4 it was demonstrated that MPG basalts with low levels of Ba & K are relatively free from a crustal input. Such a sequence of incompatible-element-depleted, uncontaminated basalts has been found on the slopes of Ben More (BM2-7), within the lower third of the lava pile (figure 4.41). BM6, which occurs among these depleted and uncontaminated flows is, nevertheless, relatively enriched in *all* the incompatible trace elements (figure 4.41).

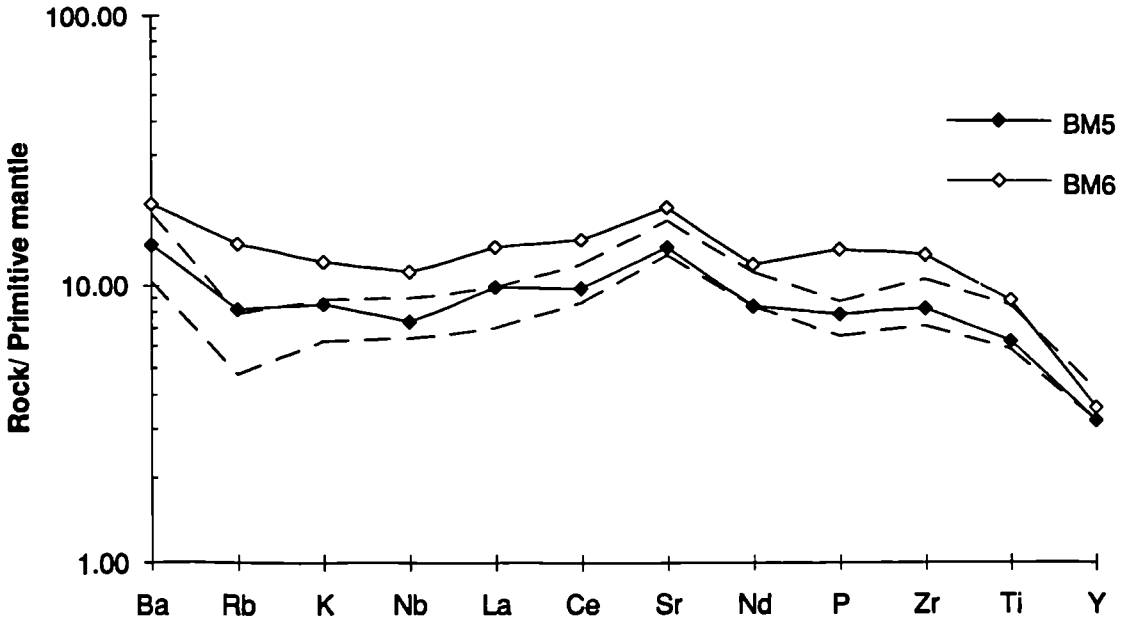


Figure 4.41 Primitive Mantle normalised diagram showing incompatible element enrichment of flow BM6 compared to BM5. The area between the dotted lines represents the compositional range of BM2-5 & 7.

At Gribun, at the base of the succession, 2km north of the BM2-7 section, a series of eight flows exist which are all, like BM6, relatively enriched in the incompatible trace elements. Five similarly enriched flows also occur, again at the base of the succession at Carsaig[7].

[7] The enriched flows found during this study are located; near Gribun [NM3245], AM1-5 & BHL1-10 on both sides of the valley; Allt Chreaga Dubha [NM486317] BM6; Malcolms Point [NM501487] C1-5; Bearraig [NM415265] B15.

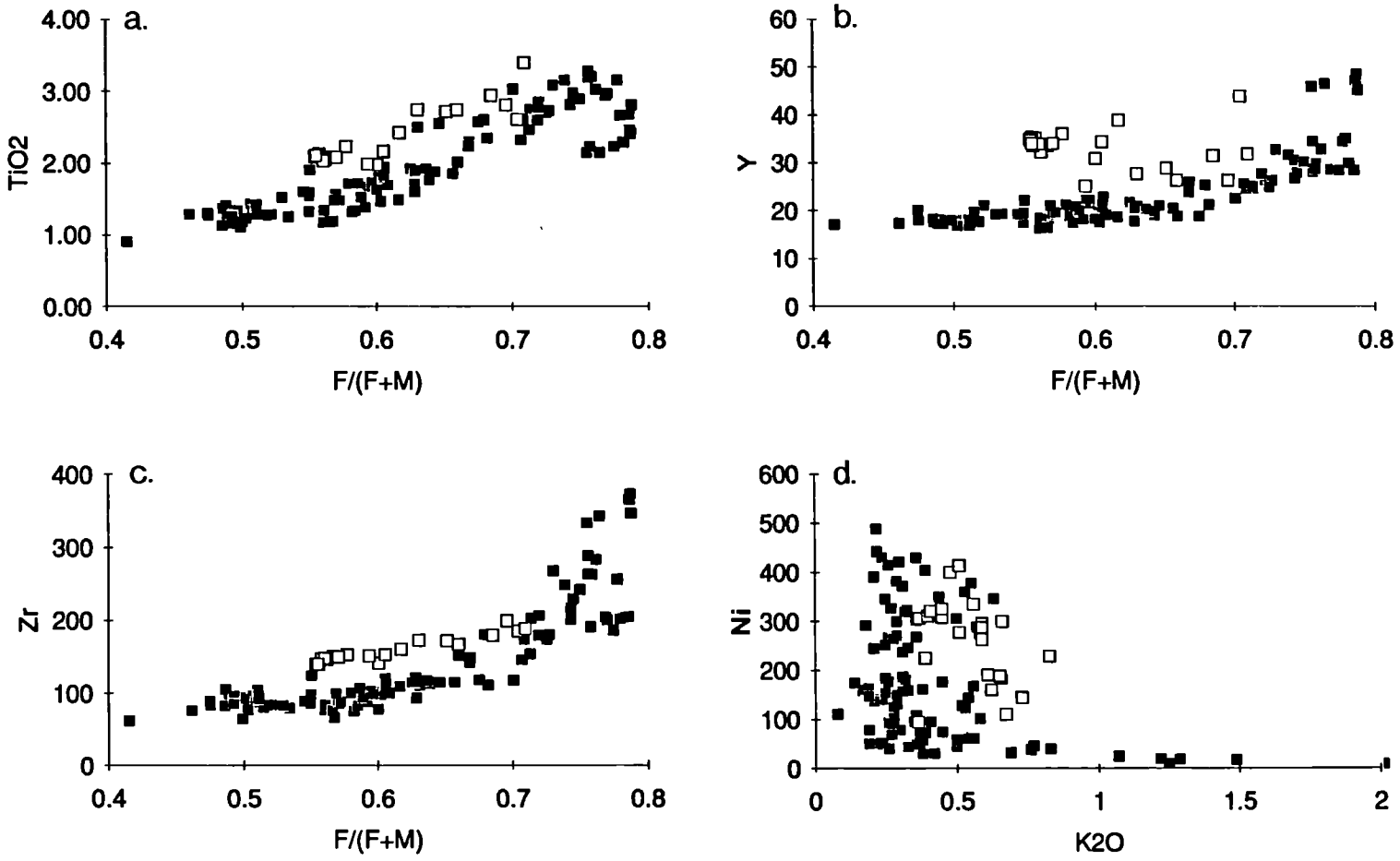


Figure 4.42a-c Plots of TiO_2 Y and Zr vs. F/(F+M). Figure 4.42d plot of Ni vs. K_2O. Hollow squares - enriched MPG lavas, solid squares - 'normal' more-depleted MPG lavas.

This relative enrichment in the incompatible trace elements is illustrated in figures 4.42a-d. It can be seen that at a given F/(F+M) value the enriched flows contain higher levels of TiO_2, Zr & Y (figure 4.42a-c), therefore, some of the scatter observed on figure 4.6 is caused by the inclusion of these enriched flows. In section 4.4 and figure 4.22 it was noted that, while some of the scatter on a plot of Zr vs. K_2O was due to magma mixing, some scatter was also caused by some incompatible element enriched flows. Figure 4.42d (cf. figure 4.21) shows that when these samples are excluded from consideration, the array is, for the most part, confined to a simple fractionation trend, with perhaps some elements of mixing. Figure 4.43 shows primitive mantle normalised spidergrams for four enriched MPG lavas (EMPG); BM6, BHL7, AM1 & C2, along with two crustally uncontaminated and more depleted MPG lavas (UMPG); BM5 & MR2.

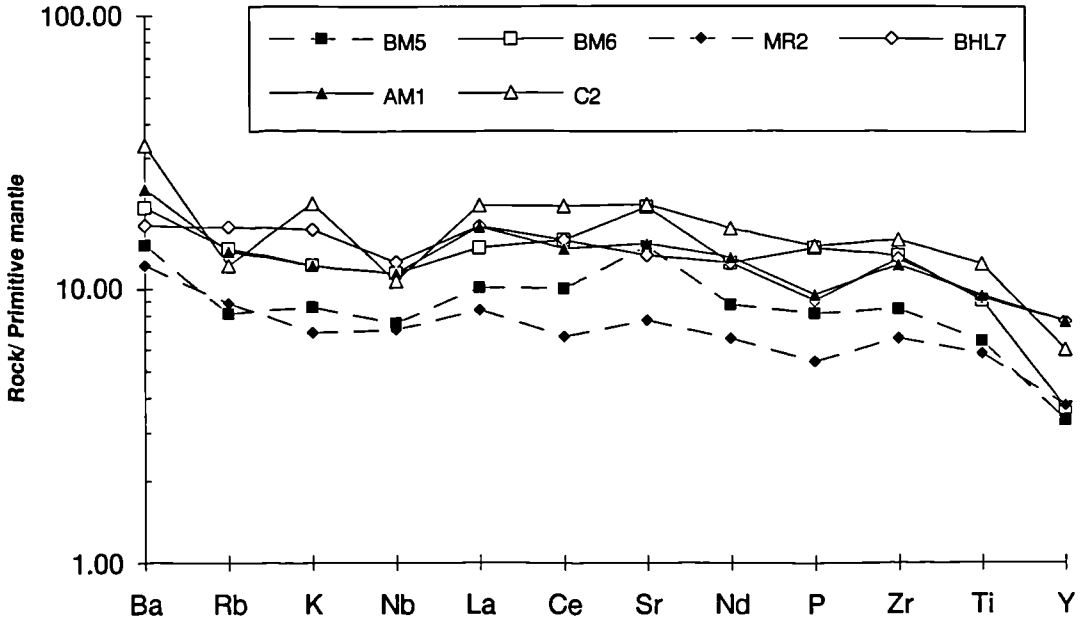


Figure 4.43 Comparative Primitive Mantle normalised diagram for the EMPG (symbols connected by solid lines) and the UMPG (dashed lines).

Nevertheless, this enrichment of the basal flows is by no means a universal feature of the Mull lava succession and in Morvern and north of Tobermory -- two other places where the base of the succession is definitely exposed -- no incompatible element enriched flows have been found. BM2-7 lie stratigraphically immediately above the enriched flows at Gribun and because BM6 is directly underlain by a primitive flow BM5, which shows little evidence of crustal contamination, the latter has been chosen as a starting point for modelling the composition of BM6.

BM6 and the other enriched flows are not significantly petrographically different from BM2-7; most are fine-to-medium grained with variable quantities of well formed olivine microphenocrysts. The groundmass consists principally of plagioclase

and interstitial pale brown/lilac clinopyroxene, with smaller amounts of Fe/Ti oxides, olivine and secondary alteration products including zeolites and chlorite. The enriched flows show a tendency towards more lilac coloured clinopyroxene, which is undoubtedly a reflection of the higher bulk Ti content in these lavas.

Chemically these basalts are much more distinctive and, as has been noted above, contain higher levels of the incompatible trace elements (figure 4.43). The major element compositions of the lava flows strongly suggest that the magmas last equilibrated at quite high pressures, and indeed the lavas plot close to the 9kb cotectic on the normative Ne, Hy, Di, Ol and Q diagram (figure 4.4).

4.5.3 Possible mechanisms of enrichment

Several possible explanations may be advanced in attempting to explain the relative incompatible element enrichment in flow BM6 and the other enriched flows;

a/ Fractional crystallisation

BM5, the flow below BM6, is slightly more primitive and obviously fractional crystallisation must therefore be regarded as a contender to explain the relative enrichment of the latter. However, this process is rejected for two reasons, 1) two other flows in the same succession, (BM3 & 7) are more evolved than BM6 and yet they contain lower levels of incompatible elements (figure 4.41). 2) Modelling with the TRACE program (Nielsen 1988), using MR2 as a starting composition, clearly demonstrates that, although fractionation will raise the Nb content of the residual liquid, it will also significantly lower its Ni content (figure 4.44). Fractional crystallisation cannot be the cause of the observed enrichment.

b/ Crustal contamination

As was discussed in the last section, crustal contamination has played an important role in the petrogenesis of the MPG lavas and therefore it is important to assess if the observed enrichments could be explained by contamination with Lewisian crust. Simple mixing of variable amounts of average acidic Lewisian crust (T-ave) with BM5, produces spidergram patterns (figure 4.45) which although they are enriched in Ba, Rb & K do not -- like the EMPG lavas -- have higher Ti and Zr . Addition of a Moine schist to BM5 has much the same effect as adding Lewisian crust.

Several of the EMPG flows shown on figure 4.43 have higher Ba and K than the rest of the EMPG resulting in a Nb trough. This suggests that some of the EMPG lavas have been contaminated with crustal material, however it is highly improbable that the addition of crustal material is responsible for the relative enrichment in all the incompatible elements.

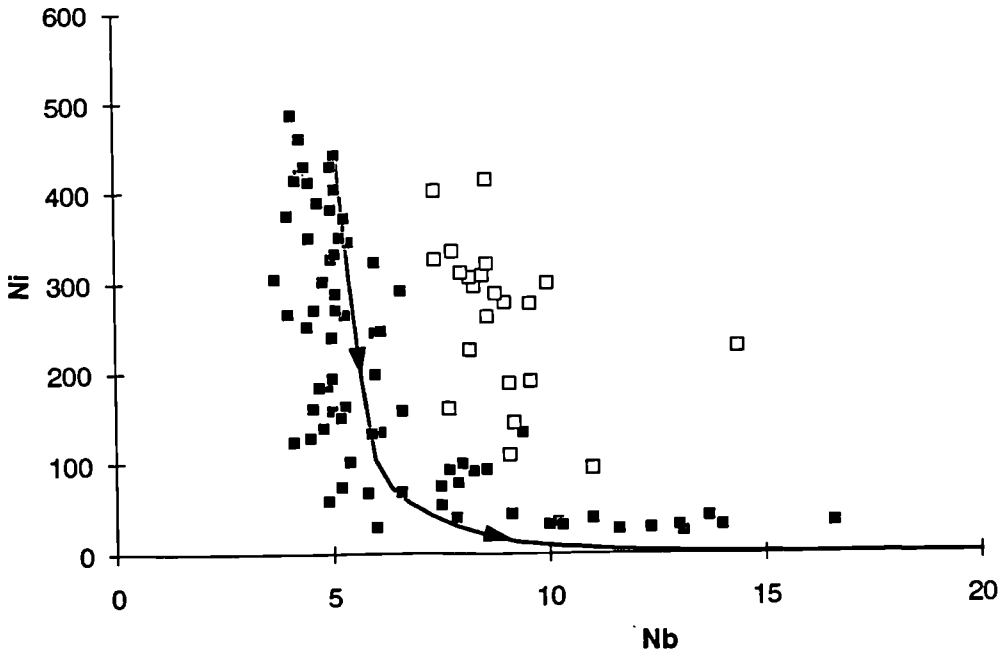


Figure 4.44 Plot of Ni vs. Nb for the some MPG lavas, along with a hypothetical fractionation trend. Symbols as for figure 4.42.

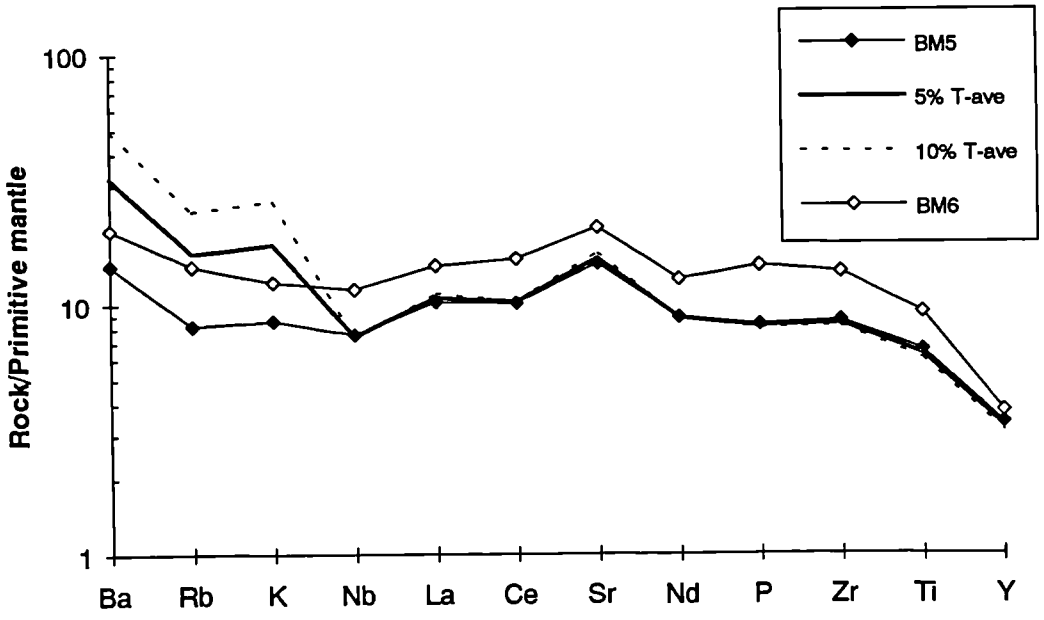


Figure 4.45 Primitive Mantle normalised diagram showing the chemical effect of adding 5 & 10% lower crustal material (T-ave)*, to an uncontaminated lava, BM5. An enriched flow BM6 is shown for comparison. * T-ave is an average of all the acidic Lewisian samples collected from Tiree (Appendix 4a.vii)

c/ Asthenospheric, OIB (Ocean Island Basalt) like source

Thompson & Morrison (1988) reported that the youngest Tertiary dykes on Skye, the Beinn Dearg Mhor (BDM) swarm, were enriched in the incompatible trace elements. The concentrations and ratios of incompatible elements in these dykes were found to be very similar to typical North Atlantic OIB compositions. They postulated that the Tertiary BDM dykes were derived chiefly from an asthenospheric OIB-like source, after extensive melting had stripped away a significant amount of the lithosphere during the earlier Tertiary magmatism.

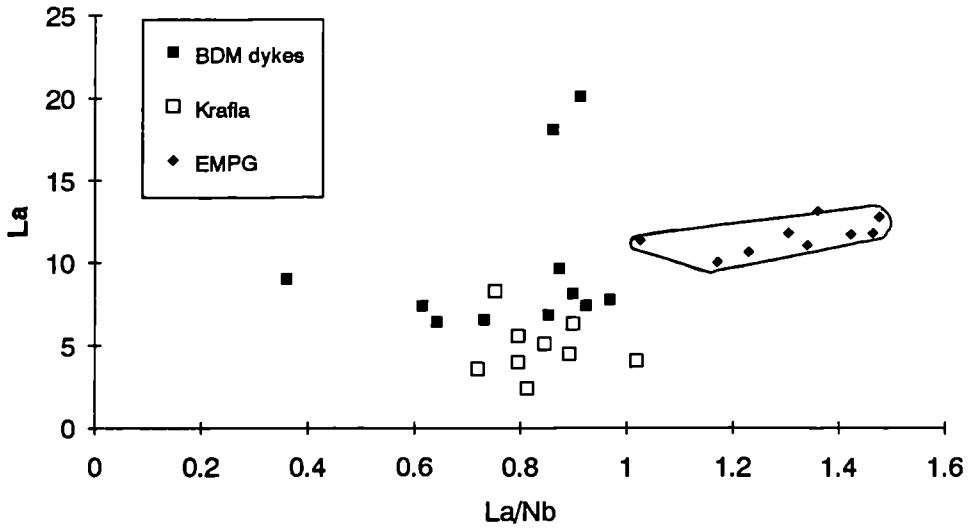


Figure 4.46 Plot of La vs. La/Nb for the EMPG, the BDM dykes and lavas from Krafla,* Iceland (Nicholson & Latin 1992). (* Representing "North Atlantic OIB")

It is therefore possible that the enrichment of the Tertiary lava flows at the base of the Mull lava succession could be explained by invoking an asthenospheric source region for the magmas, similar to the postulated source for the BDM dykes. Figure 4.46 shows that North Atlantic OIB and the BDM dykes, have quite distinctive La/Nb ratios of <1.00, and one would therefore expect that if the enriched Mull basalts had been derived from an enriched OIB-like source, then they should have similar low La/Nb ratios. This is, however, not the case and figure 4.46 shows that those EMPG lavas which contain little crust, have La/Nb >1.0. It would therefore seem highly unlikely that an enriched, asthenospheric, OIB-like source could have been the cause of the enriched flows at the base of the MPG.

d/ Variable mantle partial melting

In an attempt to explain the variation of incompatible element abundances and ratios in primitive, uncontaminated Hebridean lavas, Morrison *et al.* (1980) proposed a model which involved varying degrees of mantle fusion. Thus, the possibility that the enrichment in EMPG is simply due to a smaller degree of partial mantle melting than UMPG should also be considered, and in this respect it is useful to look at $(La/Ce)_{pmn}$ ratios. The $(La/Ce)_{pmn}$ values for these two groups are displayed on figure 4.47. Those EMPG lavas which contain little crust have higher, (>1) $(La/Ce)_{pmn}$ than the UMPG lavas [$(La/Ce)_{pmn} \leq 1$].

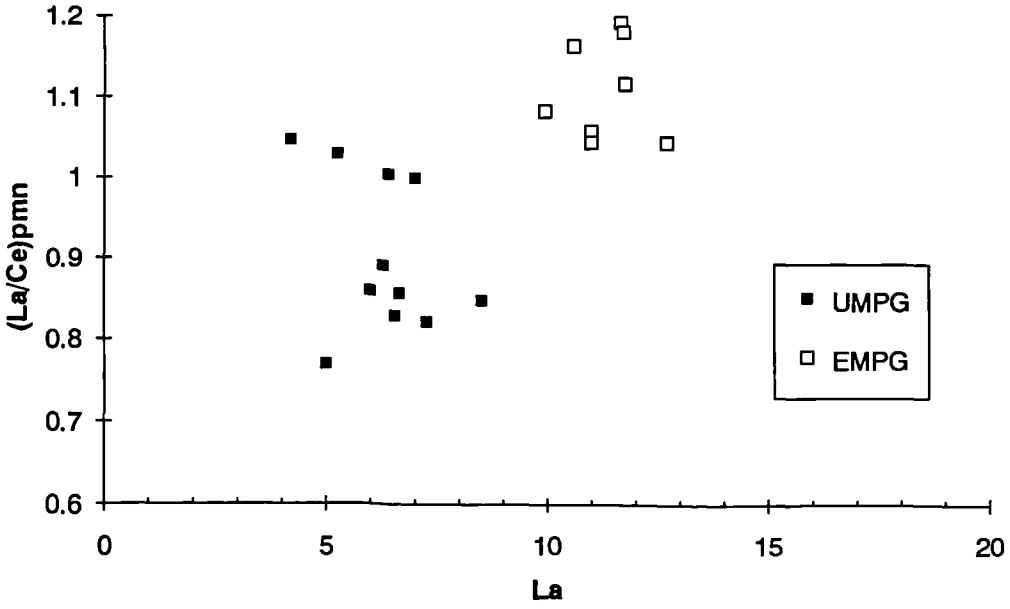


Figure 4.47 A plot of $(La/Ce)_{pmn}$ vs. La for the UMPG and the EMPG (all samples relatively free from crustal contamination.

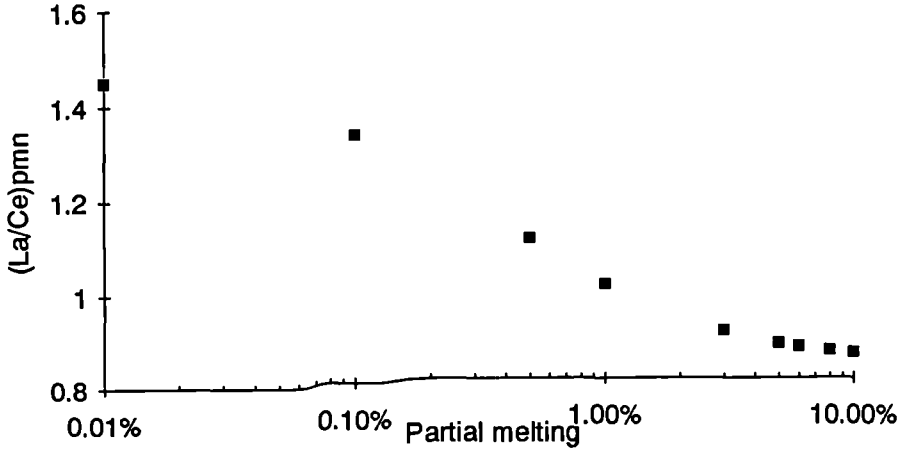


Figure 4.48 Modelled $(La/Ce)_{pmn}$ values at varying degrees of non-modal batch melting of depleted spinel lherzolite. Spinel lherzolite phase compositions, elemental abundances, melting proportions and partition coefficients used in the calculations are taken from Kostopoulos & James (1992).

Modelling of mantle melting (figure 4.48) shows that, in the calculated liquids, the $(La/Ce)_{pmn}$ ratio hardly changes above 1-2% partial melting of a spinel lherzolite. Nevertheless, below 1-2% partial melting $(La/Ce)_{pmn}$ increases dramatically. Therefore, such a change in the ratios of two highly incompatible elements, such as La and Ce, such as is observed between UMPG lavas and EMPG lavas, cannot be produced by a slight variation in the amount of melting, with moderate degrees (2-5%) of mantle fusion. But a possible way to explain this increase in $(La/Ce)_{pmn}$, is to invoke the addition of a small-fraction-melt (<2% melting), to a lava such as BM5 (an UMPG lava).

e. Contamination by an enriched small-degree-melt fraction

Much of the small-degree, low-temperature melt fraction, had probably been extracted from the lower lithosphere or uppermost asthenosphere beneath Mull, in the Permo-Carboniferous. But a small proportion of the enriched Permo-Carboniferous melt probably remained, frozen within the upper lithospheric mantle; perhaps in localised, disseminated pockets. Support for this contention is provided by the work of Morrison *et al.* (1987) who suggested that few of the Permo-Carboniferous dykes fed surface lava fields, and that significant volumes may have been frozen within the lower crust and upper lithospheric mantle.

The massive influx of Tertiary magmas into the upper lithosphere could have remobilised this enriched material and led to its incorporation into some of the Tertiary magmas. One would predict that such occurrences would be quite rare and restricted to some of the earliest lava flows, due to the extraction of most of the enriched melt in the Permo-Carboniferous.

A Permo-Carboniferous camptonite dyke (L1) from Morvern has been analysed (Appendix 4a.vii) and its chemical composition compares favourably with an average of previously analysed Permo-Carboniferous dykes, (Morrison *et al.* 1987; Baxter 1987). These dykes represent the closest approximation to the small-melt fraction [$(La/Ce)_{pmn}$ = 1.34 for L1] sparsely available within the Tertiary lithospheric mantle below the Hebrides. When 5-10% of L1 are added to BM5 (UMPG) the Primitive Mantle normalised pattern of BM6 (EMPG) can be reproduced for most of the elements (figure 4.49).

The disagreement between the observed and modelled values for Ti, Zr and P may cause slight concern, but elsewhere in the world these elements are highly variable in rocks of lamprophyric composition (Rock 1991). Baxter (1987) has shown that the Permo-Carboniferous lamprophyre dykes of Scotland are no exception and have incompatible element values which are extremely erratic. This he attributed to a

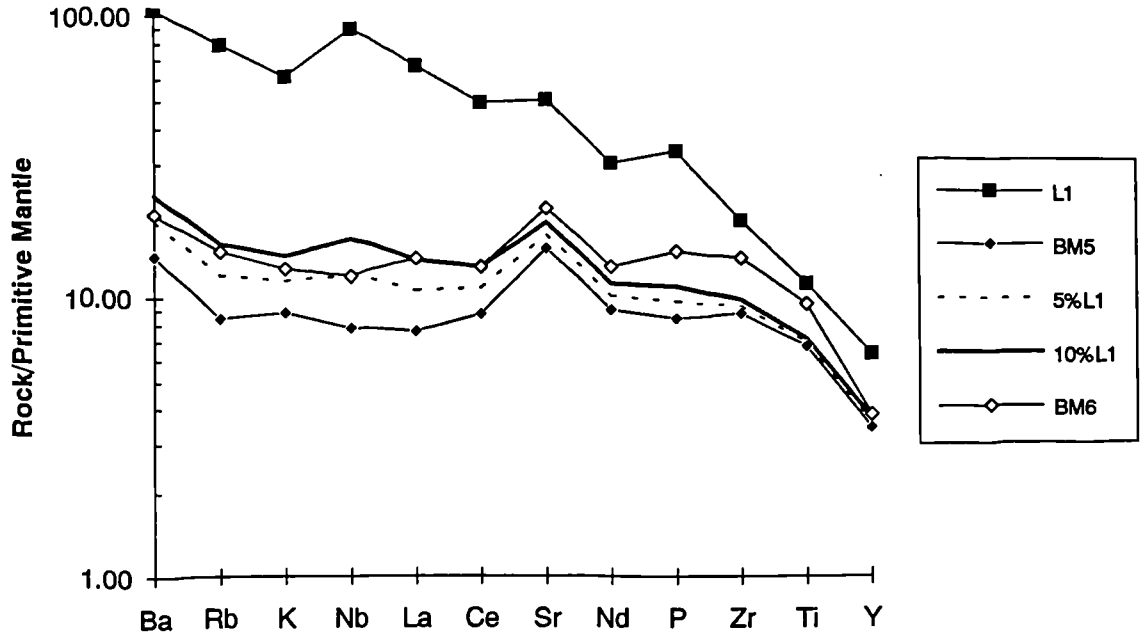


Figure 4.49 Primitive mantle normalised diagram showing how the addition of 5-10% of an enriched component, L1, to BM5 can reproduce the pattern of the BM6 (EMPG). The mismatch for P, Ti and Zr is discussed in the text.

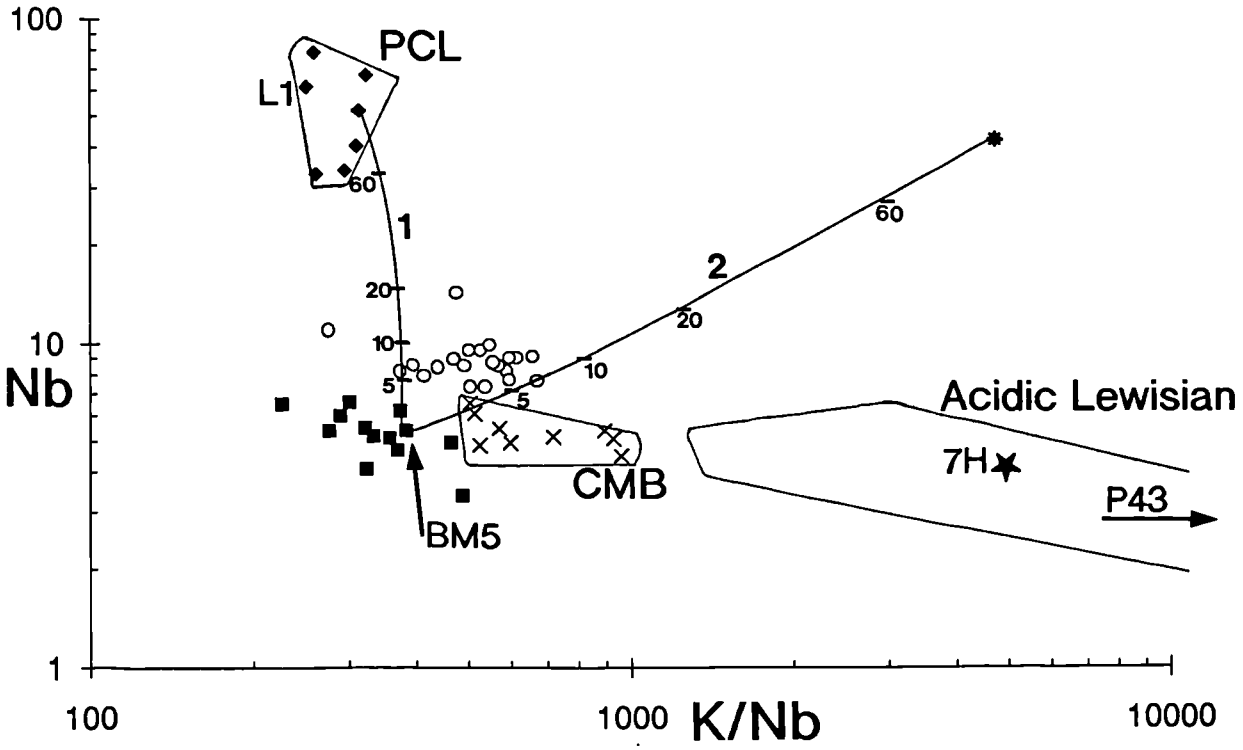


Figure 4.50 Plot of Nb vs. K/Nb, showing two mixing lines; **1** and **2** (see text). The ticks on the mixing lines represent the addition of 5, 10, 20, and 60% contaminant. Also shown are PCL - Permo-Carboniferous lamprophyres, (Morrison *et al.* 1987; Baxter 1987); Acidic Lewisian crust, (Weaver & Tarney 1980; 1981); CMB - crustally contaminated Mull basalts (crosses); UMPG - crosses and EMPG - circles. L1 and P43 are discussed in the text, 7H from Thompson *et al.* (1982).

localised heterogeneity of the Permo-Carboniferous mantle. Thus the mismatch between modelled and observed values probably reflects some local heterogeneity. This clearly demonstrated in figure 4.50, which shows a wide range of compositions for Permo-Carboniferous dykes from NW Scotland. Therefore, the enriched material available for sampling at the surface may not necessarily be an exact representation of the enriched melt fraction available either, a) at depth and/or b) in the Tertiary period. The variability of the small-fraction-melt contaminant is borne out by the variations in Ti, Zr & Y of the four enriched lavas in figure 4.43, which come from several different localities 20km apart.

Mixing line 1 on figure 4.50 clearly shows that the addition of 5-10% variably enriched Permo-Carboniferous melt to flow BM5 can produce the observed Nb enrichment of the EMPG flows. Mixing trend 2 on figure 4.50 -- between BM5 and a composite contaminant (asterisk on figure 4.50) made up of 25% acidic Lewisian crust (P43) and 75% Permo-Carboniferous lamprophyre (L1) -- supports the earlier proposal that some of the EMPG have also been contaminated with a small amount of crust (<2%).

It is envisaged that small localised concentrations of highly fusible, enriched melt material existed within the lithospheric mantle below Mull prior to the onset of Tertiary magmatism. These small-scale concentrations may have been a remnant of the Permo-Carboniferous magmatic event, or they may have accumulated subsequent to it; bleeding from the underlying asthenosphere. These frozen, enriched melt fractions would have been relatively easy to re-mobilise because a) they probably took the form of thin dykes and veins which would require minimal heat to melt them and, b) they contained a reasonably high volatile content, as is evidenced by the presence of abundant kaerusitic amphibole and biotite in the Permo-Carboniferous dykes. This would have lowered their solidus temperature, so making them much more fusible than the anhydrous parts of the lithospheric mantle.

4.5.3 Wider implications

The fact that an enriched lithospheric input to BTIP lavas has hitherto been unreported in the published literature, is testament in itself to the scarcity of an enriched lithosphere beneath western Scotland during the Tertiary. Menzies *et al.* (1986, 1987) noted the occurrence of a Tertiary monchiquite dyke containing enriched mantle xenoliths at Loch Roag, on the Isle of Lewis, over 150km north-west of Mull. This isolated dyke cannot, however, be interpreted as evidence for the *widespread* existence of an enriched lithospheric mantle below western Scotland. The great weight of evidence from the BTIP as a whole, with its incompatible-element-depleted basic igneous rocks, argues very strongly against the presence of

such an enriched mantle. Rather, the Loch Roag dyke probably represents the refusion of a small pocket of an enriched, low-temperature, small-fraction melt, similar to the proposed pockets of enriched material which contaminated the lower Mull basalts.

With the exception of one study (Baxter & Mitchell 1984), the Permo-Carboniferous dykes of western Scotland have mostly been "dated" by their directional trends and distinctive lamprophyric geochemistry, with the Loch Roag dyke being the only noted example of a BTIP lamprophyre. Yet, in the western USA, where a small-melt input into basaltic magma has been proposed, the enriched lithospheric contaminants are associated with the same magmatic event as the lavas (Gibson *et al.* 1991). No Tertiary lamprophyre dykes have been found which cut the Mull lavas. This is hardly surprising, since the enriched small-melt component would have been mobilised early in the magmatic event, when the lava field would not have been very thick or extensive. But the experience of other lava fields suggests that Tertiary lamprophyre dykes should exist and further extensive dating of the assumed Permo-Carboniferous dykes of western Scotland may well reveal that some of them are of Tertiary age.

It is also worth noting that the proposed lithospheric contaminant of the Mull lavas is of a sodic-alkaline composition, whereas the enriched lithospheric contaminants invoked by Gibson *et al.* (1991) and Ellam & Cox (1991) are of an ultra-potassic nature. The exact reason for this difference is not clear but it may well reflect something of the past tectonic and magmatic history of western Scotland. The magmatism in the western USA has been strongly influenced by a relatively recent subduction event, but in western Scotland the most recent subduction appears to have been associated with the closure of the Iapetus ocean in the Silurian/Ordovician. The chemical difference, therefore, would seem to be dependant on whether the small-fraction melt, migrating into the lithosphere from below, contained a subduction related component or not. Rogers (1992) in a study of the potassic magmatism in Italy and the Virunga province in East Africa, similarly proposed that the absence of a subduction related component in the mantle source region, would result in the formation of more sodic-alkaline magmas.

The ten or so enriched basaltic flows discovered on Mull can be classified as belonging to a sub-type of the Mull Plateau Group and this chapter has identified three sub-types of the MPG; 1) basalts which have not been contaminated with either crust or a small-fraction, lithospheric melt; 2) basalts contaminated with partial melts of Lewisian crust (≤5%); and 3) basalts which have been contaminated with 5-10 %

of an enriched small-fraction-lithospheric melt, with or without some crustal contamination.

Chapter 5

The Petrogenesis of the Staffa Magma sub-Type

The tholeiitic Staffa Magma sub-Type (SMT) occurs mostly as columnar flows, (Chapter 2) near the base of the lava succession, in several parts of the island. These flows were first identified as chemically distinctive by Bailey *et al.* (1924), who recognised that they were more silicious than the overlying lavas. Bailey *et al.* (op.cit.) grouped these lavas into the NON-PORPHYRITIC CENTRAL (NPC) magma type along with other lavas of tholeiitic affinity, which occurred near the top of the lava succession in central Mull. On the basis of major element chemistry and petrology they assumed that the both the early Staffa type and the much later Central Mull Tholeiites (CMT), had a similar petrogenetic history. As a result they attempted to explain the origin of the NPC (tholeiitic) magma type *as a whole*, by assimilation of siliceous crust by basic magmas. As will be shown, this is probably the case for the SMT, but the CMT have an entirely different trace element chemistry, and Chapter 6 will establish that different mantle melting processes can account for the geochemical signature of the CMT.

In line with Bailey *et al.* (1924), Thompson *et al.* (1986) called these columnar tholeiitic lavas the "Staffa Magma Type". However, as this chapter will show, these lavas are derived from similar parental magmas as the MPG and so the Staffa lavas are best defined as a magma *sub*-type, rather than a true magma type.

The SMT has recently been the subject of a detailed geochemical study (Morrison *et al.* 1985; Thompson *et al.* 1986), and so this chapter is, for the most part, a review of that work. Having said this, SMT lavas from several localities[1] not studied by Thompson *et al.* (op.cit) have been analysed. Samples have also been collected from most of the same flows as Thompson *et al.* (op.cit.), and all the analyses from the present study will be compared with the published data.

The alkali-silica diagram (figure 5.1) confirms the tholeiitic nature of the SMT basalts, and indeed one of the samples collected during the present study (C6) has evolved along a silica-enriched, tholeiitic fractionation trend, to a basaltic-andesite. These tholeiitic tendencies are also apparent on a CIPW normative Ne-Hy-Di-Q-Ol plot (figure 5.2). In contrast to the MPG lavas, which plot around the 9kb cotectic, the SMT lavas predominantly plot slightly below the 1 atmosphere cotectic with its

[1] Five flows at Aird na h-Iolaire (NM404484), samples W1-5; several columar flows on Ulva, around Caisteal Mor (NM410380), samples BCH1, 7, 7A & 7B; a flow at Ulva Ferry (NM446398), sample UV1; a columnar flow near Bloody Bay, north of Tobermory (NM493574), sample T1.

trend towards more quartz-normative residua. This would seem to indicate that most of the SMT magmas have equilibrated in the uppermost crust.

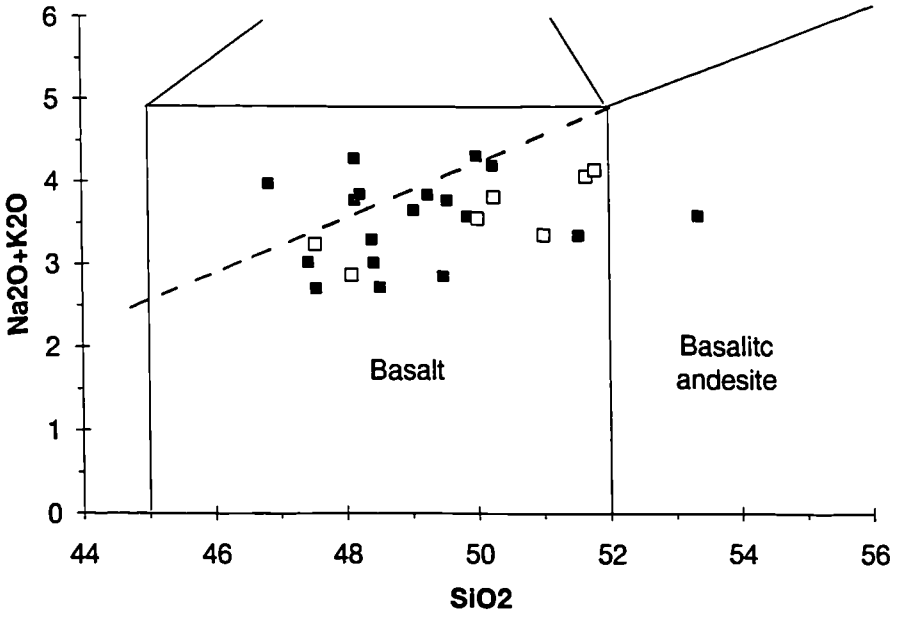


Figure 5.1 Alkali vs. silica diagram for the Staffa Magma sub-Type (SMT). Filled squares - lavas collected during the present study, open squares - lavas from Thompson *et al.* (1986), dotted line - tholeiitic-alkalic divide (Miyashiro 1978).

Morrison *et al.* (1985) and Thompson *et al.* (1986) used major and trace element chemistry in conjunction with Sr, Pb and O isotope data, to show that the most evolved SMT lavas could not have been derived from the more basic SMT magmas *solely* by closed system fractionation of the observed phenocryst phases (olivine, augite and plagioclase). However, a weak positive correlation for the SMT lavas on a plot of $(^{87}Sr/^{86}Sr)i$ vs. $^{87}Rb/^{86}Sr$ (Thompson *et al.* 1986; figure 5), was interpreted by Thompson *et al.* (op.cit) as evidence of AFC (assimilation with concomitant fractional crystallisation; De Paolo 1981) type processes.

It was mentioned earlier (Chapter 4) and shown on figure 4.36, that the SMT lavas are significantly contaminated with Moine schist, as well as variable amounts of Lewisian lower crust. This, combined with the fact that Moine schist makes up a significant part of the upper crust below Mull (Thompson *et al.* 1986), and that the normative compositions of the SMT lavas indicate that they equilibrated at relatively low pressures (figure 5.2), strongly suggest that AFC took place in the upper region of the crust which was composed of Moine schist.

In Chapter 4, Th values were used to assess the relative contamination input, from the upper and lower crust, into MPG basalts. Because amphibolite facies Lewisian

upper crust contains appreciably more Th than granulite facies crust (table 4.4), upper crustal contamination will consequently lead to magmas with higher Th values. Th contents of the MPG lavas and the SMLS have been shown (figure 4.28) to support the isotopic evidence for predominantly lower crustal granulite facies contamination.

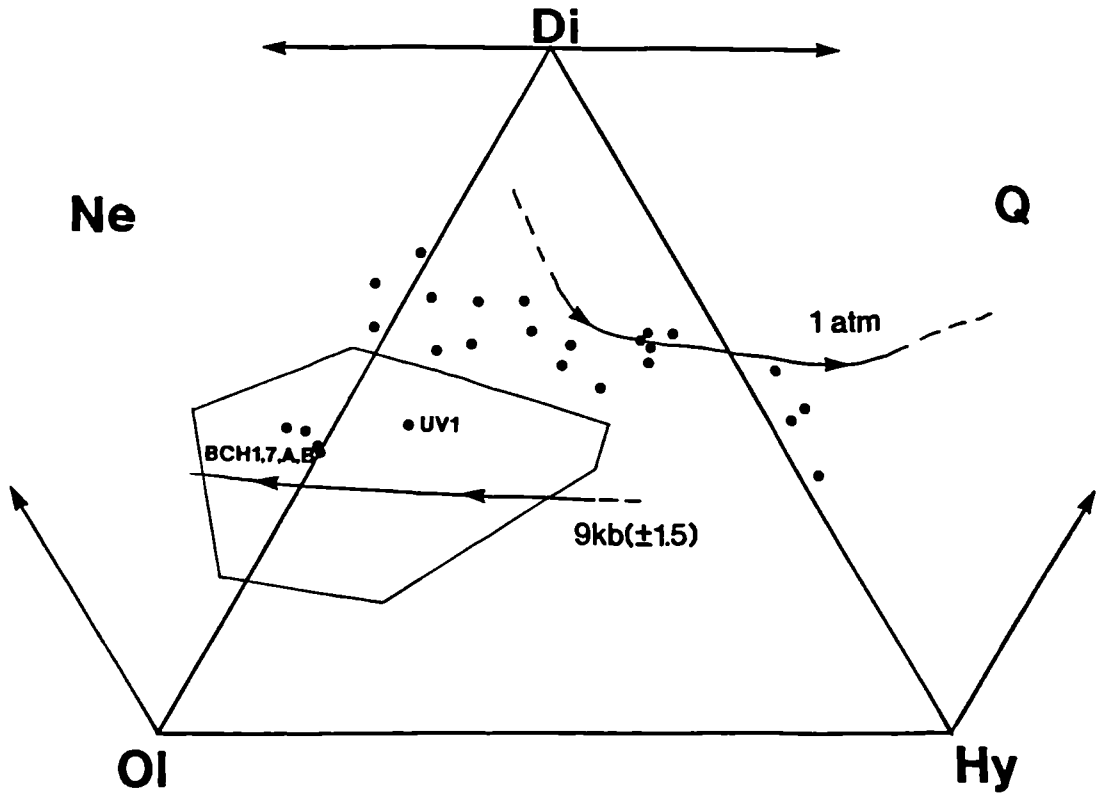


Figure 5.2 Normative Ne-Hy-Di-Q-Ol plots, showing the SMT lavas (filled circles) and the field for the MPG. The 1atm. and 9kb cotectics are those from (Thompson 1982). The labelled samples plotting within the MPG field will be discussed below.

Thompson *et al.* (1986) reported a Th content of 21ppm in a pelitic schist (MS324) from the Ross of Mull. Therefore contamination of the SMT by partial melting of Moine schist, (as supported by Sr, Pb and O isotopes) has the potential to significantly raise the Th content of a basic magma, and in figure 5.3 this is indeed shown to be case. On this spidergram it is apparent that the four SMT lavas, (W4, MS193, MS313 & MS314[2]) contain significantly more Th than the three MPG lavas (BR4, 5 & 6), which have undergone predominantly lower crustal contamination. Figure 5.4 also confirms that, at a given F/(F+M), the SMT have generally much higher Th than the MPG. These observations support the proposed contamination of the SMT lavas by Moine schist as envisaged by Thompson *et al.* (1986).

[2] Samples MS192, MS193, MS194, MS313, MS314, M61 & M92 from Thompson et al. (1986)

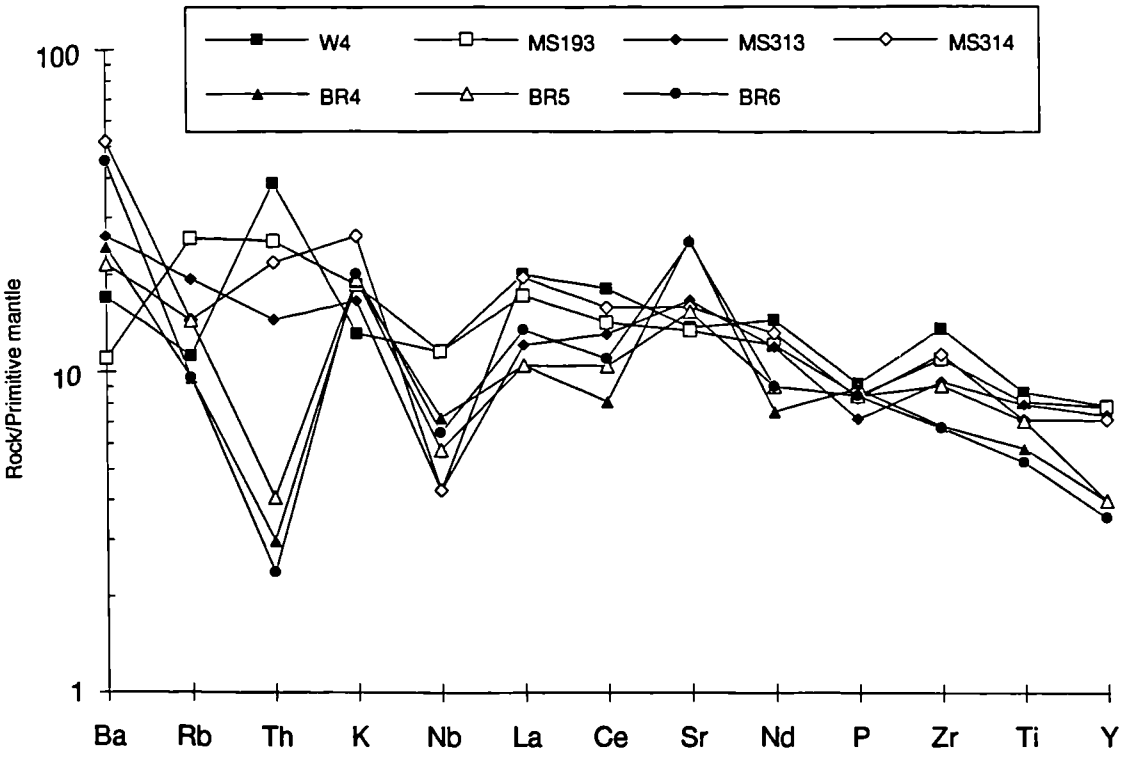


Figure 5.3 Primitive Mantle normalised spidergram comparing the incompatible element compositions of the MPG (BR4, BR5 & BR6) with the SMT (W4), and (MS193, MS313 & MS314; from Thompson *et al.* 1986)

Figure 5.4 reveals more chemical differences, between the MPG and the SMT;

The slightly higher K_2O contents for some of the SMT may well reflect the fact that they are contaminated with K_2O-rich Moine schist.[3] The SMT also have higher CaO, Sc (and to a lesser extent) V and Y, at a given F/(F+M), value than their MPG counterparts. These observations strongly suggest that no clinopyroxene has fractionated from the more basic SMT lavas [<0.65 F/(F+M)]. This contrasts sharply with the more MgO-rich lavas of the MPG which were shown in section 4.3 to have fractionated clinopyroxene at high pressures (>9kb). This high-pressure fractionation has suppressed the build-up, in the residual magma, of the elements (CaO, Sc and V) compatible in clinopyroxene.

Reference to figure 4.7 reveals that the 'TRACE' predicted fractionation trends of an MPG magma, *at 1 atmosphere,* have higher CaO, Sc and V, than the actual MPG lavas. These higher values for the predicted MPG trends are, in fact, much closer to

[3] A pelitic schist (MS324) analysed by Thompson et al. (1986) contains 5.70 % K_2O.

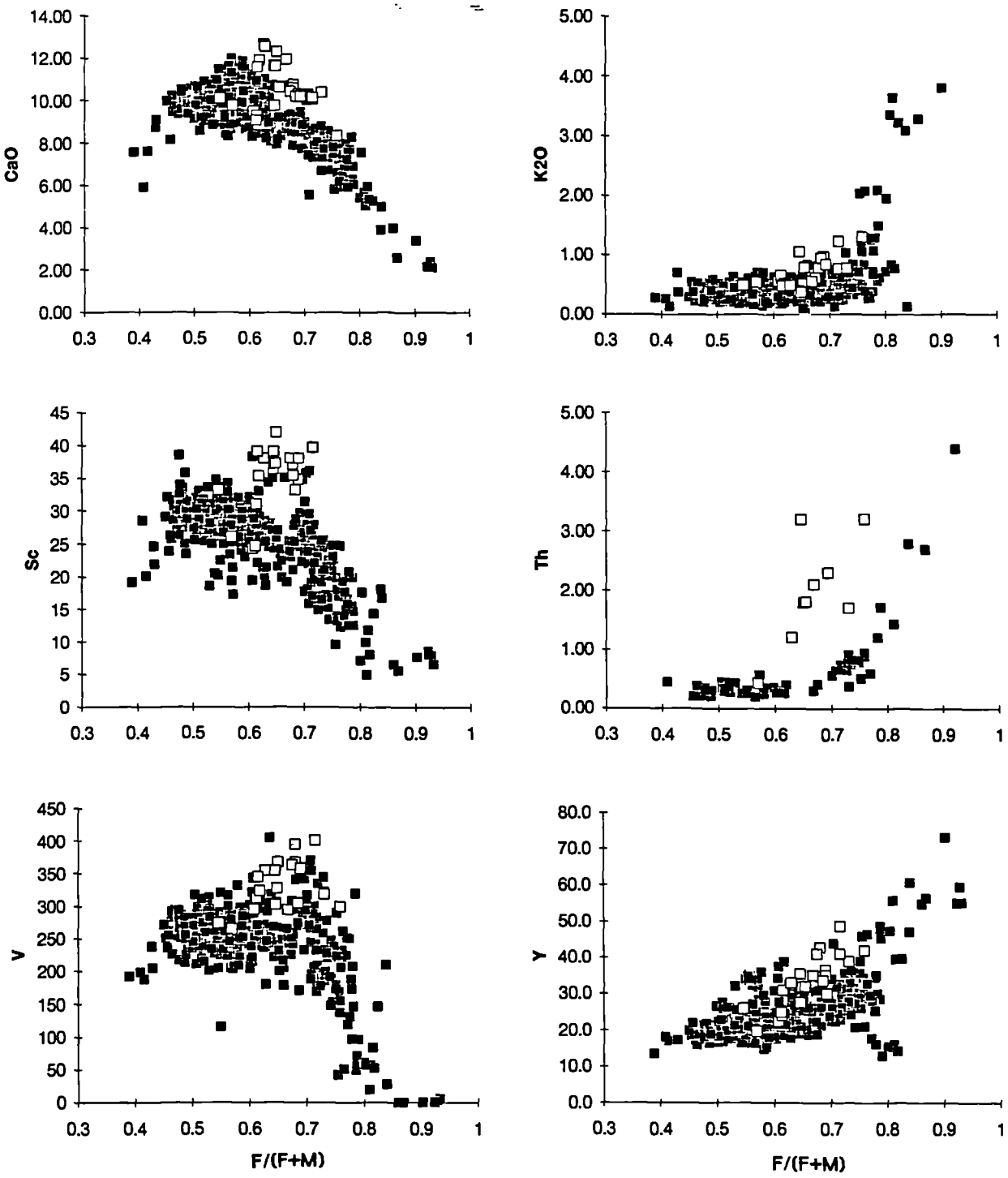


Figure 5.4 Selected major and trace elements plotted against F/(F+M), for the MPG (solid squares) and the SMT (open squares).

the SMT fractionation trends. This is hardly surprising when one considers the other evidence for low pressure equilibration of the SMT which has already been presented. Thus it would appear that the SMT lavas did not significantly pond and fractionate at high pressures, but rather they seem to have ascended with minimal delay from their mantle source regions and ponded in upper crustal magma chambers.

Another important feature of the SMT lavas is that they all have LREE enriched rare-earth patterns. This is borne out on figure 5.5, where the SMT lavas (W3, W4, MS192 and M92) have $(La/Nd)_{cn}$ >1. This contrasts with some uncontaminated basaltic-hawaiites (BR30-33) in which the $(La/Nd)_{cn}$ <1. As was demonstrated in Chapter 4, crustal contamination of a basaltic magma, by granulite facies lower crust, can increase LREE content of a basaltic MPG magma. A Moine schist (P58B) collected during the present study from the Ross of Mull contains 60ppm La and has a $(La/Nd)_{cn}$ ratio of 2.3. Therefore, contamination with Moine schist has increased the LREE content of the SMT lavas.

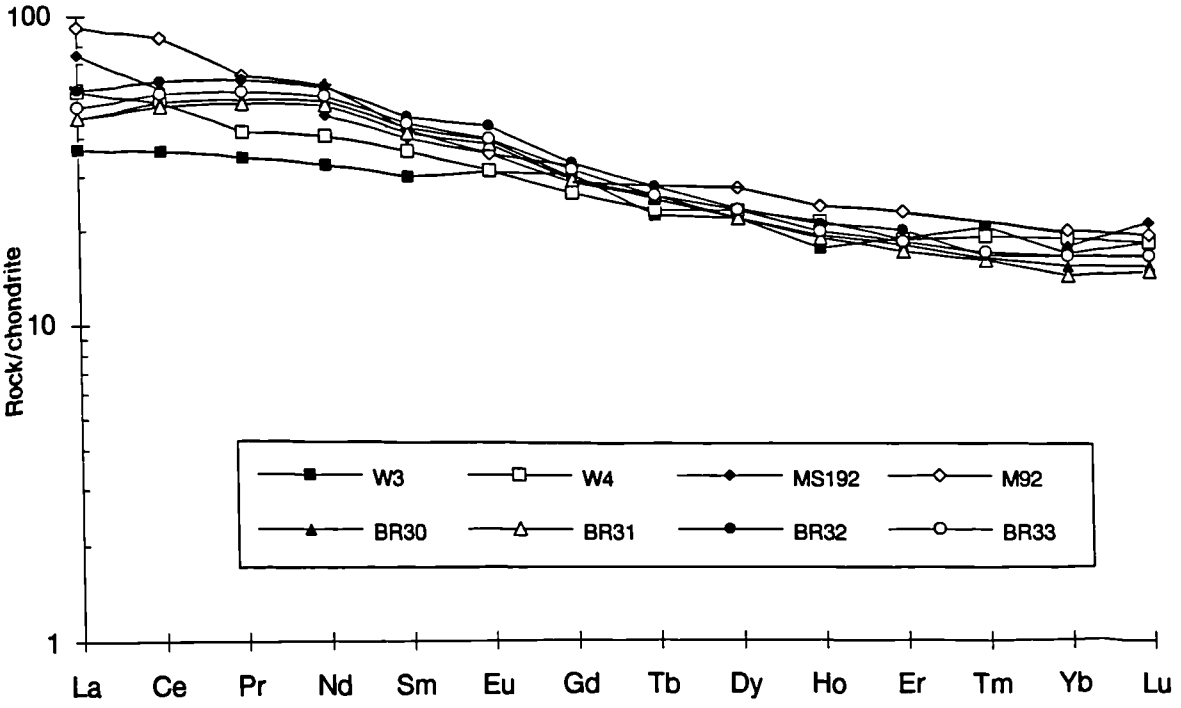


Figure 5.5 Comparative chondrite-normalised REE of MPG basalts (BR30-33) and SMT lavas (W3, W4, MS192 & M92). MS192 and M92 are from Thompson *et al.* (1986)

Fawcett (1961) and Thompson (1982) pointed out that, although the MPG and the SMT showed the familiar tholeiitic/alkalic contrast at more evolved compositions (<7%), at higher MgO contents this contrast all but disappeared. This observation is borne out by several samples collected during the present study. Samples BCH1, BCH7, 7A & 7B, are quite basic (>8% MgO) and, as figure 5.2 shows, they plot close to the 9kb cotectic. They also fall mostly within the compositional range of trace

elements in the MPG (figure 5.4). Nevertheless, these basalts all have well developed columnar jointing, and look little different in the field from the more evolved SMT lavas. A closer inspection of the geochemistry of these four samples reveals that they possess some features of the SMT lavas (slightly higher SiO_2, and V) as well as some MPG characteristics.

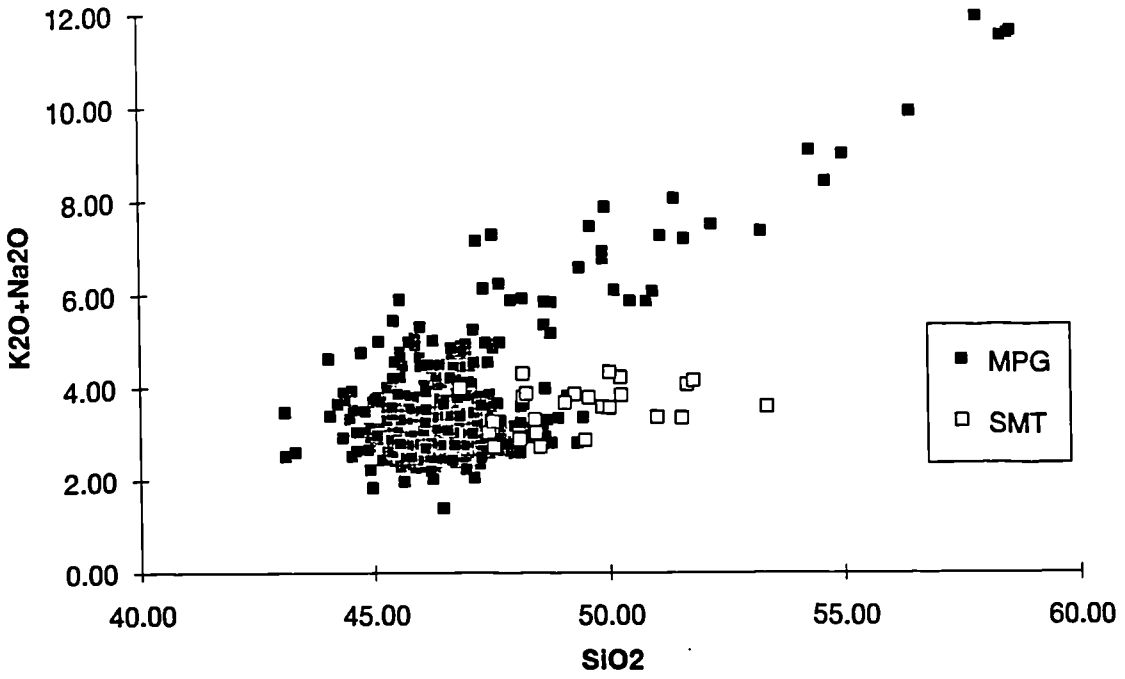


Figure 5.6 Comparative alkali vs. silica plot of the MPG and the SMT lavas

If the MPG and SMT lavas are plotted together on an alkali/silica diagram, it can be seen that there is significant overlap between the two types (figure 5.6). Some of the basic lavas identified earlier as MPG type have higher SiO_2 values, similar to the SMT. This suggests that a few of the MPG lavas higher up succession may have ponded in the upper crust, or they may simply be fractionates of higher degree primary mantle melts, which would also make them more tholeiitic. The fact that some of the more-tholeiitic MPG lavas do not have significantly higher Th than their alkalic counterparts, suggests that the latter explanation may be nearer the truth.

The foregoing discussion tends to lead one to the conclusion that the SMT and the MPG lavas were derived from very similar parental magmas, and that their differing chemistry can be explained in terms of post mantle-melting process within the crust and lithospheric mantle. Obviously those incompatible element ratios which are relatively unaffected by crustal contamination can be used to assess the viability of this hypothesis, ie. 'Are the SMT and the MPG derived from similar parental magmas?'. Figures 4.26 & 4.27 show that while the LREE patterns for the MPG and the SMT may be disturbed by crustal contamination, the middle to heavy REE are relatively

unaffected. On a plot of Eu/Yb vs. Ti/Zr (figure 5.7), the field for the SMT and the MPG substantially overlap, strongly supporting the idea that they are derived from similar primitive mantle melts. Some samples from the Coire Gorm magma type, are also plotted on figure 5.7. This magma type has incompatible element ratios which are distinct from both the MPG and the SMT, and as will be shown in Chapter 6, this chemical difference stems from the mantle.

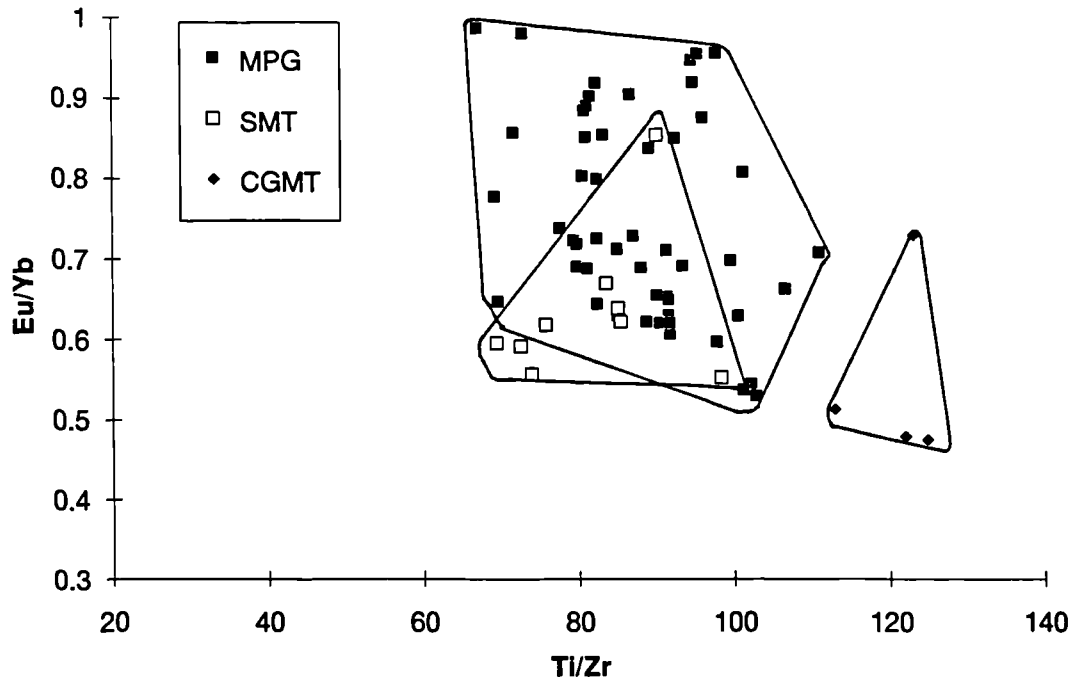


Figure 5.7 A plot of Eu/Yb vs. Ti/Zr for the MPG, the Staffa Magma sub-Type (SMT) and the Coire Gorm magma type (CG).

In conclusion, it would therefore appear that the Staffa Magma sub-Type and the Mull Plateau Group are derived from mantle melts which have very similar compositions. Some of the early magma batches did not pond for long periods of time at MOHO depths, rather they rose to the upper crust (assimilating variable amounts of granulite facies lower crust *en route*) where they underwent concomitant fractional crystallisation and assimilation of Moine schist. Thompson *et al.* (1986) suggested that the Moine thrust, which passes through the area, may well have played a part in providing a zone of crustal weakness by which these early magma batches reached the surface.

Most of the later MPG magma batches appear to have last equilibrated at pressures around 9kb and some have fractionated at these MOHO depths. The magmas then traversed the crust with little fractionation, during which the hottest magmas assimilated some acidic lower crust, while the more evolved (cooler) magmas remained essentially uncontaminated.

Chapter 6

Mantle melting, and possible mantle sources.

6.1 Introduction

Much of the pioneering work on the nature and processes of mantle melting centred on the evidence derived from experimental petrology, eg. Yoder & Tilley (1962), Green & Ringwood (1967), Ito & Kennedy (1967), O'Hara (1968), Mysen & Kushiro (1977), Jaques & Green (1980). Within the last fifteen years however, numerous workers have built upon this experimental framework and have attempted to constrain more rigourously, the physical and chemical processes involved in the melting of the mantle, and the segregation and ascent of the melt from the residue. Contrasting sources are thought to be the lithospheric (eg. Hawkesworth *et al.* 1992) and/or the asthenospheric mantle (eg. Gibson *et al.* 1991; 1992 and Ellam & Cox 1991)

It is important at this stage to establish what we mean by the term "lithosphere". McKenzie & Bickle (1988) have defined the crust and the rigid non-convecting upper part of the mantle - where heat transfer occurs by conduction - as the "mechanical boundary layer" (MBL). Between this and the convecting adiabatic upper mantle is what McKenzie & Bickle (op. cit.) defined as the "thermal boundary layer" (TBL). This layer may be seen as a transitional zone between conducting and convecting mantle, with conductive processes dominant near the top, and convective processes more important at its base. The lithosphere may therefore be defined as the MBL and the conducting upper part of the TBL. This latter layer episodically becomes unstable and is replaced by hotter mantle material. According to McKenzie & Bickle (op.cit) most mantle melting occurs within or just above the TBL.

A magma generated near the base of a lithosphere 80km thick may cool by as much as 80 °C as it travels to the surface, *even though it looses no heat.* This process is called adiabatic decompression, and it also affects the solid upwelling region of the mantle. However, as McKenzie & Bickle (1988) point out, it is often necessary to compare the heat content of material at different pressures. To overcome this problem McKenzie & Bickle (op.cit) calculated potential temperatures (T_p). This is defined as the temperature that a mass of material would have, if it were compressed or expanded to a constant reference pressure[1]. McKenzie & Bickle (op.cit) calculated that the normal T_p of the mantle is 1280 °C, but the T_p of a hot rising jet or plume could be as much as 1480 °C.

[1]The expression for the calculation of T_p is given by McKenzie & Bickle (1988) equation 5.

For mantle peridotite to begin to melt it must intersect its solidus. This may be achieved by decompression melting during adiabatic upwelling of mantle, in response to a thinning of the lithosphere, or in places where this thinning has previously occurred. This process does not require elevated mantle potential temperatures (>1280 °C) and is widely regarded as the mechanism by which Mid-Ocean Ridge Basalts (MORB) are generated (McKenzie & Bickle 1988; Plank & Langmuir 1992). As has been noted, elevated mantle potential temperatures (~1480 °C) are caused by hot mantle plumes that are thought to rise from the core-mantle boundary and eventually impinge on the base of the lithosphere, where melting can occur if the lithosphere is thin enough. Below thick (>150km) continental lithosphere little melt will be produced, even if mantle potential temperatures are in the region of 1480 °C. Nevertheless, if a region of continental lithosphere has undergone a period of extension and resultant thinning, the hot (>1480 °C) rising mantle will be able to upwell further, so leading to the production of extensive volumes of melt. The volume of melt generated, is therefore dependant on the T_p of the upper mantle and the thickness and amount of extension of the lithosphere.

One of the most important findings of these later studies is that melt extraction is exceedingly efficient even at small (<1-2%) degrees of melting (Ahern & Turcotte 1979, McKenzie 1984; 1989, Ribe 1985, Falloon & Green 1988, McKenzie & Bickle 1988). An important implication of this is that melting can occur in a vertical section of mantle, and that melts from throughout the vertical height of the column can be simultaneously extracted and mixed. Magmas erupted at the surface therefore represent pooled partial melts from separate mantle sources. McKenzie & Bickle (1988) defined the 'point average composition' as the instantaneous melt composition at a constant pressure, while the 'point & depth average' composition was defined as the weighted average of melt generated over the entire melting interval.

Kostopoulos & James (1992) pointed out that this tapping and mixing of melt from different depths within a single column could result in the interdigitation of lavas showing the effects of low degrees of melting at high pressures, with those showing high degrees of melting at low pressures. Isobaric equilibrium melting therefore only represents a simplified analogue of the natural melting processes.

Klein & Langmuir (1987) and McKenzie & Bickle (1988) have used the results of experimental petrology to establish the melting systematics of major elements in response to changes in pressure, and these are summarised in table 6.1. It can be seen from this table that the major element compositions of a suite of basaltic magmas may potentially be used to assess the pressure and extent of mantle melting. (Provided that they have not undergone significant subsequent fractional crystallisation involving minerals that contain the elements under consideration). If the concept of a melting

column is valid, then one would expect to see a positive correlation between Na_2O and FeO* at a constant MgO; this is an intra-column 'local' trend (Klein & Langmuir 1989). Relatively low Na_2O combined with low FeO* is indicates the predominance of extensive melting at relatively low pressures; i.e. more of the pooled melt has come from the top of the melting column. In contrast relatively high Na_2O and high FeO* suggest predominance of less extensive melting at higher pressures; i.e. the pooled melt represented by these compositions has a deeper 'point & depth average'. Higher rates of extension and greater degrees of melting will lead to more tholeiitic magmas being produced, whereas an increase in pressure and deeper melting will lead to more alkalic magmas.

Major element melting systematics.	
SiO_2	- at constant MgO, increases with X and decreases with increasing pressure.
Al_2O_3	- decreases with X, perhaps decreases with increasing pressure.
FeO*	- constant or decreases slightly with X at constant pressure, increases with increasing pressure.
MgO	- increases with X at constant pressure, increases with increasing pressure.
Na_2O	- decreases with X, not pressure dependant.
CaO	- increases with X, decreases with increasing pressure.
TiO_2	- decreases with X, incompatible in mantle phases.
K_2O	- decreases with X, incompatible in mantle phases.

Table 6.1 Major element melting systematics for anhydrous peridotites (Klein & Langmuir 1987; McKenzie & Bickle 1988). X is the melt fraction, and clinopyroxene is taken to be a residual phase (true up to 22% melting).

Although the extent and pressure of melting are important influences in controlling the chemical composition of the magma produced, other factors also play a significant role. One of the most important of these is the metamorphic facies of the source material. This is generally regarded to be predominantly plagioclase, spinel or garnet lherzolite. The stability of each of these aluminous index minerals is critically dependant on pressure and hence depth. Plagioclase lherzolite transforms to spinel bearing lherzolite at pressures greater than 10kb (~30km; Wyllie 1988). Thus, below continental regions, with thick refractory lithosphere (>50km) there will be little or no

melt generation in the plagioclase stability field. Of much more importance for magma generation below continents is melting within the spinel stability field. This transforms gradually into garnet bearing lherzolite between 60-80 km depth - the 'spinel-garnet transition zone' (Ellam 1992).

The heavy rare earth elements (HREE) are much more compatible in garnet than in spinel[2]. Therefore any fusion in the garnet stability field, or even the spinel-garnet transition zone, (leaving behind residual garnet), will cause the resultant melt to be relatively depleted in the HREE [$(Sm/Yb)_{cn}$ >>1]. In sharp contrast, shallower melting which occurs entirely within the spinel stability field will produce magmas with relatively flat chondrite normalised REE patterns [$(Sm/Yb)_{cn}$ ~1]. McKenzie & O'Nions (1991) used this difference to calculate, from REE data, the relationship between melt fraction and depth in an upwelling mantle column. A similar approach will be adopted later in this chapter in order to make some assessment of the depth of melting involved in the genesis of the Mull lavas.

6.1.1 Types of mantle melting processes

(i) Equilibrium or batch melting; this process produces a given proportion of melt in one melting event and the melt produced is removed in one batch. This melt is in equilibrium with its source region. All experimental studies on magma genesis produce melts which approximate to batch melts.

(ii) Fractional melting; this process produces melts which are instantaneously removed from the source region. Therefore with this type of melting most of the incompatible trace elements will be will be removed in the first melts to be produced.

(iii) Dynamic melting (Langmuir et al. 1977); this process involves the production of a small volume of melt in an ascending mantle column. This is followed by the extraction of some of the magma, leaving the rest of the melt within the mantle residue. The extracted melts pool and migrate upwards, while the residual melt is left with the source and becomes incorporated into the next extracted magma batch. Such a process prevents the highly incompatible elements from becoming too depleted in the source region.

The batch melting model has been criticised by various authors (eg. Wood 1979, Johnson *et al.* 1990) as being a physically unrealistic process. However, Plank & Langmuir (1992) stressed that, although melting occurs in a column over a wide range of depths, the pooled magma produced is virtually indistinguishable from a magma which has been batch melted from a point & depth average. Eggins (1992) concluded

[2] Partition coefficient for Lu in garnet 5.5; for Lu in spinel 0.01 (McKenzie & O'Nions 1991).

that at moderate to large (5-25%) degrees of melting, dynamic melt segregation produced similar incompatible trace element abundances and ratios to batch melting.

Thus it would appear that, although melting *processes* probably involve the pooling of different melts from throughout a melting column (ie. dynamic melting), the melt *compositions* erupted at the surface approximate to magmas modelled by batch melting of the point & depth average mantle compositions.

6.1.2 Previous work on mantle melting processes in the BTIP

Thompson (1974) reported the results of a series of high pressure melting experiments on a SMLS basalt, containing 11% MgO. He concluded that the SMLS basalts were the products of partial melting of spinel lherzolite upper mantle at about 60km depth, followed by variable amounts of fractionation en route to the surface. Thompson (op.cit) proposed that the Palaeocene upper mantle beneath Skye contained phlogopite, and that the variable break-down of this phase could explain the range of silica-saturation observed in the SMLS basalts (but see below).

Beckinsale *et al.* (1978), in their study of the Mull lava succession, proposed that "Group 1" lavas (crustally uncontaminated hawaiites and mugearites) were derived from mantle melting deep in the garnet stability field (>30kb), whilst "Group 2" lavas (Staffa type lavas combined with contaminated and evolved MPG lavas) were proposed to have been derived from partial melting of a plagioclase lherzolite source region (~10 kb). As has been mentioned before, these authors ascribed *all* the geochemical variation in the Mull lava succession to variable degrees of partial mantle melting of a vertically heterogeneous mantle and *did not* consider the processes of crustal contamination and fractional crystallisation.

Mattey (1979) proposed that the three magma types[3] which could be found as lavas and dykes in Skye could all be derived through dynamic partial melting of the same mantle source region composed of spinel lherzolite with phlogopite.

Morrison *et al.* (1980) observed a slight LREE depletion (relative to the MREE) in some lavas from the MPG and the SMLS. In Chapter 4 it was shown that lavas with these distinctive sigmoidal REE patterns have been discovered in the present study, and they are therefore not due to analytical error. Morrison *et al.* (op.cit) recognised that these lavas had to be derived from a source that had been depleted in the highly incompatible trace elements. This depletion was attributed to the removal of ~1% enriched melt from the source mantle in the Permo-Carboniferous.

Thompson *et al.* (1980) observed that increasing silica saturation correlated with lower levels of incompatible trace elements, such as Nb, Ta, Ti, Zr and P. This was

[3] 1/ SMLS, 2/ Fairy Bridge magma type, 3/ Preshal More magma type (Thompson *et al.*1972; 1980 Esson *et al.* 1975; Mattey *et al.* 1977)

interpreted to be the result of variable degrees of mantle fusion at approximately constant depth. The ne-normative, more incompatible element enriched flows were considered to represent smaller degrees of mantle fusion, than the hy-normative, incompatible element poor flows. These hy-normative flows were interpreted to be more extensive melts of spinel lherzolite, resulting in more dilution of incompatible elements. They proposed that the observed variation could be accounted for by varying the degree of spinel lherzolite melting from 3-6%, and did not require the involvement of mantle phlogopite. The tholeiitic, more incompatible element depleted Preshal More magma type, was proposed to be formed at the climax of crustal extension, by more extensive dynamic melting of the same volume of upper mantle as that which produced the SMLS magmas.

Thompson & Morrison (1988) noted that radiogenic isotope ratios, major elements and compatible trace elements in those BTIP magmas containing little crustal input encompassed the same range as other magmas from the North Atlantic region. They proposed that the BTIP magmas were ultimately derived from the same asthenospheric source as Iceland. However, the lower levels of highly incompatible trace elements (ie. Ba, Th, Nb & Ta) required the previous extraction of a small melt fraction from their source. Thompson & Morrison (1988) proposed that this was caused by the Permo-Carboniferous magmatic event and that this depleted asthenosphere subsequently accreted to the base of the thinned lithosphere (see section 4.4). It was suggested that, during the early stages of Tertiary magmatism, the melts derived from upwelling asthenosphere, became substantially contaminated with this depleted lithospheric material, leading to the incompatible element depleted signature of the SMLS magmas. The more enriched nature of the late stage Beinn Dearg dykes and some hawaiites near the top of the SMLS was interpreted as evidence for the involvement an OIB-like asthenospheric source region.

Ellam (1992) noted the distinct change in the REE patterns between the SMLS (HREE depleted) and the Preshal More basalts (a much flatter HREE pattern). He proposed that this chemical change was caused by melting in the asthenosphere at progressively shallower depths, as the lithosphere thinned in response to extensional tectonics.

6.2 The magma types of the Mull lava succession

For the purposes of this study magma types are defined as those groups of flows with chemical differences between them which cannot be explained in terms of contamination, fractionation or magma mixing processes. Rather, an origin for their

distinctive chemical signatures must be looked for in terms of mantle processes. In addition to the MPG magma type (Morrison *et al.* 1980), two further magma types have been identified within the Mull lava succession; the Coire Gorm (CG)[4] magma type and the Central Mull Tholeiite (CMT) type.

These two magma types lie stratigraphically above the MPG, with the CMT lavas overlying the CG lavas. These lavas, however, all lie within the central greenschist zone of alteration and, as a result, most of their major elements and large ion lithophile (LIL) elements, have probably been mobilised. This mobility effectively precludes any attempt to assess crustal contamination using elemental constraints, as well as preventing all but a qualitative appraisal of fractional crystallisation processes. Consequently, norms have not been calculated, and the major element data will only be used to a small extent. Although the most immobile elements in these lavas (REE, Nb, Ti, P, Zr, & Y) reveal little about contamination and fractionation processes, they do provide important information about mantle source regions.

The three recognised Mull magma types have distinctly different REE patterns. A similar three-fold division of the Skye lava succession and dyke swarm has been noted (Esson *et al.* 1975; Mattey *et al.* 1977; Mattey 1979; Williamson 1979; Thompson *et al.* 1980). Figure 6.1 compares the REE patterns of representative samples of the three types from Skye and Mull. It can be seen that the latter are broadly similar to the three magma types previously reported from Skye. Mattey *et al.* (1977) showed that the SMLS and the Fairy Bridge (FB) magma type could not have been derived from the Preshal More (PM) type by crystal/liquid processes involving olivine and plagioclase. Ti/Zr and Gd/Yb ratios are virtually unaffected by fractional crystallisation of olivine, clinopyroxene, and plagioclase over the basalt-hawaiite compositional range. Figure 6.2 shows a plot of these two ratios for samples from the Mull and Skye lava successions and dyke swarms (Lamacraft 1978; Mattey 1979). The diagram clearly shows that the Fairy Bridge / Coire Gorm magma types and the Preshal More / Central Mull Tholeiite types are distinct from MPG / SMLS types and so they cannot be related by fractional crystallisation. As was demonstrated in Chapter 4 the HREE are virtually unaffected by the addition of crust, and so it is highly unlikely that crustal contamination can account for the observed differences in HREE content.

[4] Since this magma type predominantly occurs near the top of Ben More, the magma type has been named after the corrie on the western face of Ben More - Coire Gorm (NM520327).

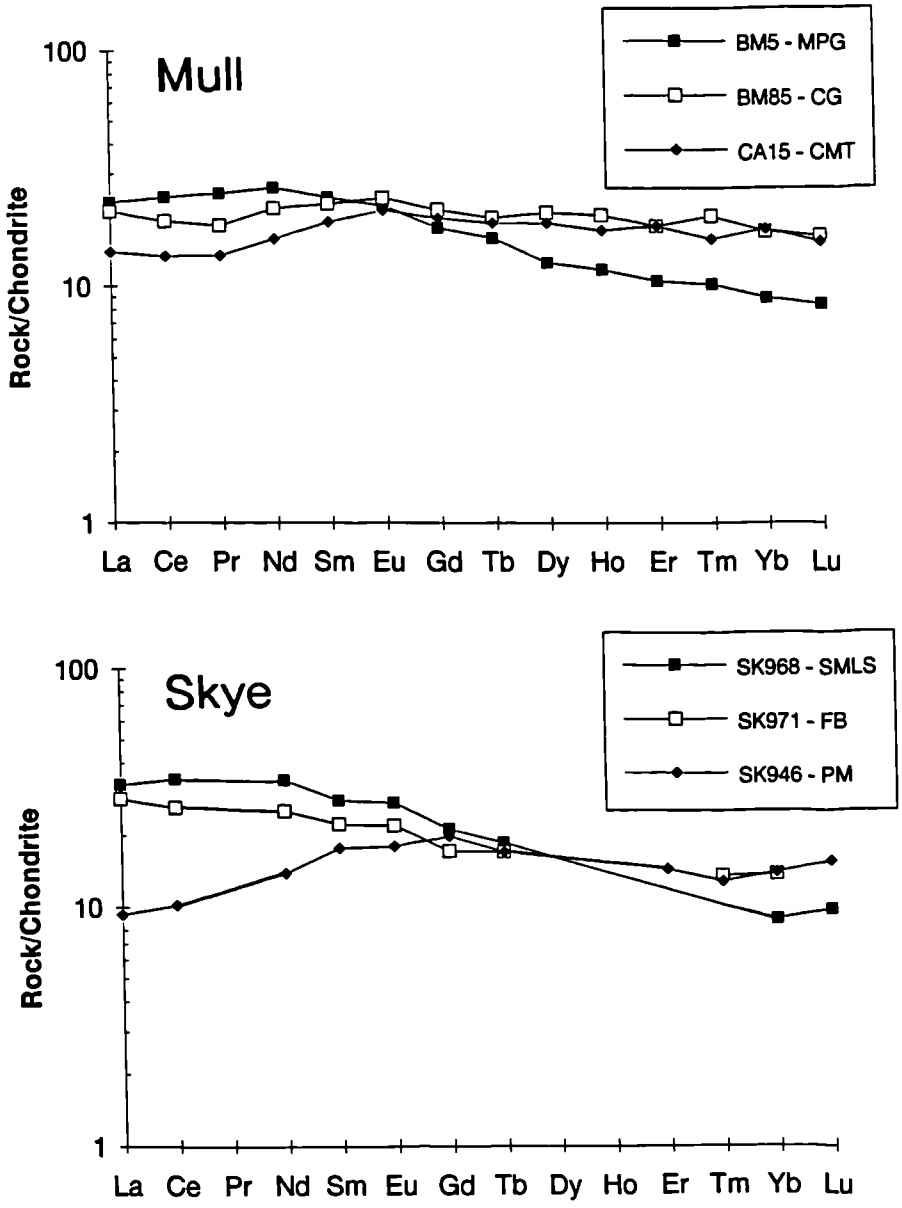


Figure 6.1 Comparative chondrite normalised REE plots of the magma types of Mull and Skye (data from Thompson *et al.* 1980; 1982). [Abbreviations: MPG - Mull Plateau Group; CG - Coire Gorm magma type; CMT - Central Mull Tholeiites; SMLS - Skye Main Lava Series; FB - Fairy Bridge magma type; PM - Preshal More magma type].

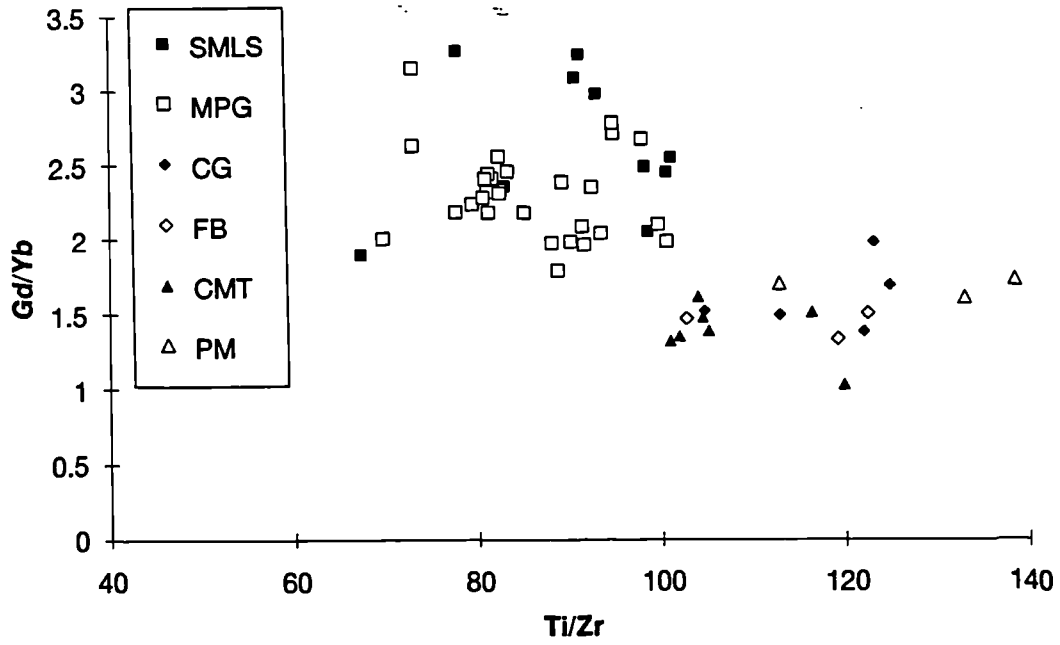


Figure 6.2 Plot of Gd/Yb vs. Ti/Zr for the three Mull magma types identified in this study (MPG, CG, and CMT), along with the three magma types previously identified on Skye (SMLS, FB and PM).

6.2.1 The Central Mull Tholeiites

The CMT lie near the top of the exposed lava section on Mull and they are well represented within the late-stage calderas of central Mull. Most of the samples of this type were however, collected from the Croggan Peninsula[5] (figure 2.2), where they are interdigitated with evolved MPG lavas. Based mostly on field and petrographic observations, Bailey *et al.* (1924) subdivided these tholeiites into the Non-Porphyritic Central type and the Porphyritic Central magma type. As has previously been noted Bailey *et al.* (op.cit) classified all the feldspar-phyric basalts as "Central" magma types, but during this study feldspar-phyric mugearites and hawaiites of MPG type have been found in the Croggan section (eg. CA4-5, 10 & 18). Some of the CMT are also highly feldspar-phyric and, as was noted in Chapter 3, they can be divided into two types:

a/ basalts containing labradorite/bytownite phenocrysts[6], (CA3b, 16, 19-20 & EX17) and

b/ basaltic andesites containing andesine phenocrysts (CA12-14). Several of the CMT are aphyric (CA15, 17 & MS184), like the Preshal More lavas.

---

[5] The CMT samples studied are CA3b, 12-17 & 19-20, EX 7-8, 17, K2, and MS184 & MS185 from Thompson (1982).

[6] These samples are similar to the high-Ca, low-alkali anorthosite phenocryst bearing dykes from Skye analysed by Donaldson (1977). Two of Donaldsons powders (144 & 44) have been analysed for REE during the present study, and they have REE patterns similar to the CMT.

Thompson (1982) reported the analysis of a Preshal More type 'flow' from Mull (sample MS133). The locality in question (NM451242) was visited during the present study and further field and geochemical work has shown that this is probably is an intrusive tholeiitic sheet (samples EX13 and 15). CMT type minor intrusions are common throughout the Mull lava succession, and are particularly abundant on the Ross of Mull (Kille *et al.* 1986).

Several of the distinctive chemical features of these magmas have been noted earlier, however there are more notable differences between the CMT and the CG and MPG lavas;

Despite their altered nature, the SiO_2 and alkali contents of the CMT suggest that they are of a tholeiitic affinity, as opposed to the transitional nature of the MPG and the CG magma type (figure 6.3).

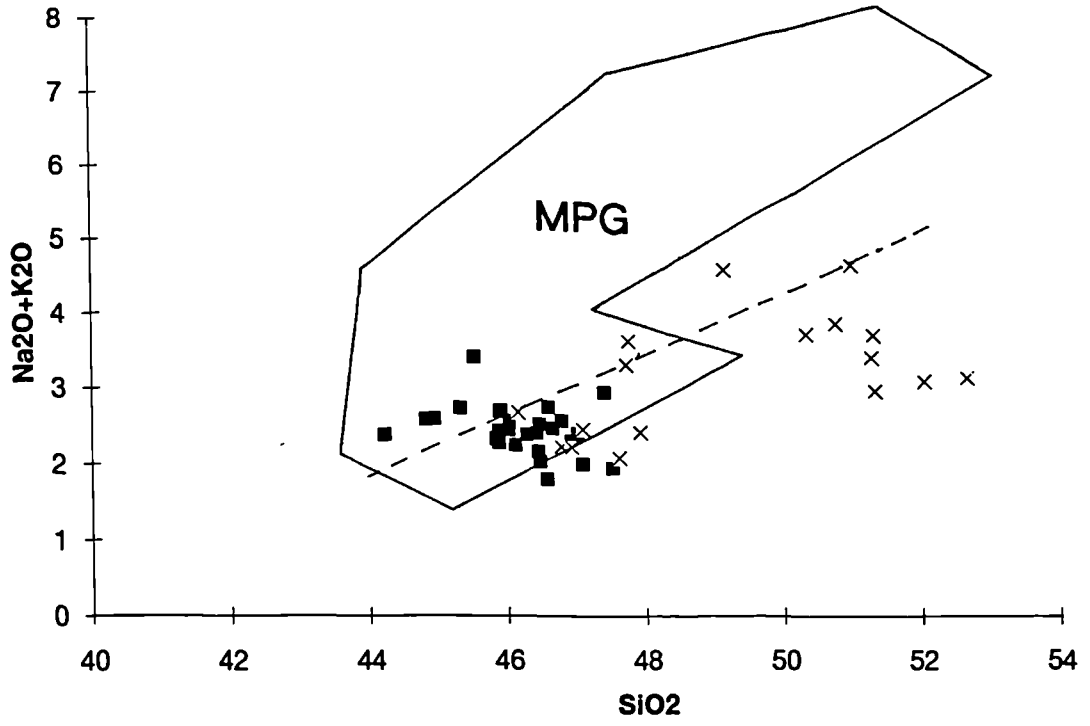


Figure 6.3 Comparative alkali vs. silica diagram of the Mull magma types. MPG lavas are enclosed by the irregular field (see figure 4.3), CG magma type represented by solid squares, and the CMT by crosses. Also shown (dashed line) is the tholeiitic-alkalic divide (Miyashiro 1978).

Relatively unaltered tholeiitic Tertiary dykes from the Mull swarm have very similar "immobile" trace element geochemistry to the CMT type (Lamacraft 1978). This strongly suggests that the lower alkali contents of the CMT type (figure 6.3) are not primarily the result of alteration processes.

The CMT lavas (for a given F/F+M value) also have higher values of CaO than the other two types, as figure 6.4 shows. This may be due in part to the high (~10-20%)

modal abundance of labradorite/bytownite in several of the samples. However, the fact that the aphyric CMT samples and the aphyric Preshal More lavas from Skye also have higher CaO values, strongly suggests that it is a real feature of this magma type.

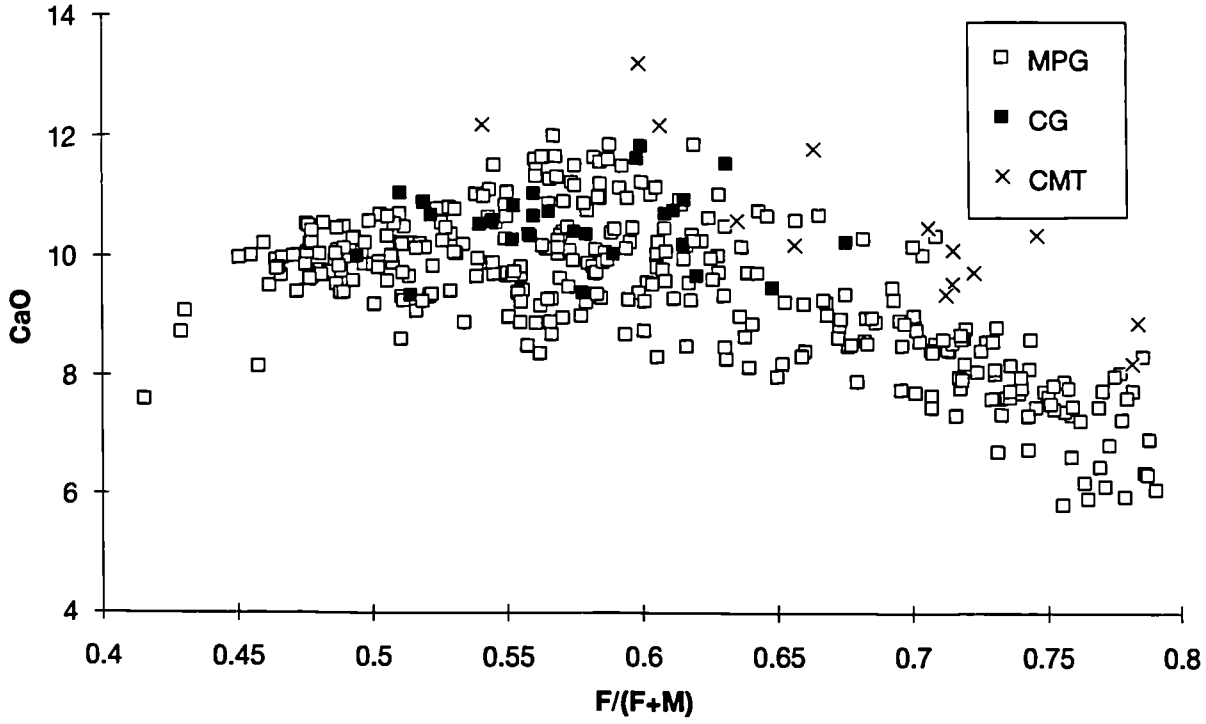


Figure 6.4 Plot of CaO vs. F/(F+M) for the three Mull magma types.

The CMT lavas - as has previously been mentioned - are generally relatively depleted in the LREE. This point is borne out by figure 6.5 which shows chondrite normalised REE patterns for two lavas from the present study (CA3b & 15), a Mull dyke of similar composition (25; Lamacraft 1978), a Preshal More flow from the type locality, Skye (SK 983; Thompson *et al.* 1980), and the marginal facies of an anorthosite-bearing dyke from near Bracadale, Skye (sample 44; collected by Donaldson, 1977).

However, as figure 6.6 shows, not all of central lavas of tholeiitic affinities have LREE depleted patterns. Samples CA16 & 19 have all the characteristics of the CMT lavas except that they have $(La/Nd)_{cn} > 1$. This REE signature is similar to the pattern of the Coire Gorm magma type (figure 6.1) and could be caused by crustal contamination (section 4.4). Alternatively the relatively LREE enriched patterns could be the result of mantle processes. Bell (1984) analysed some lavas from the Eastern Red Hills, Skye and found that they had relatively flat REE patterns, while at the same time having an overall tholeiitic composition. In the light of this new data he proposed that a continuum of compositions existed between the Fairy Bridge and the Preshal More magma types.

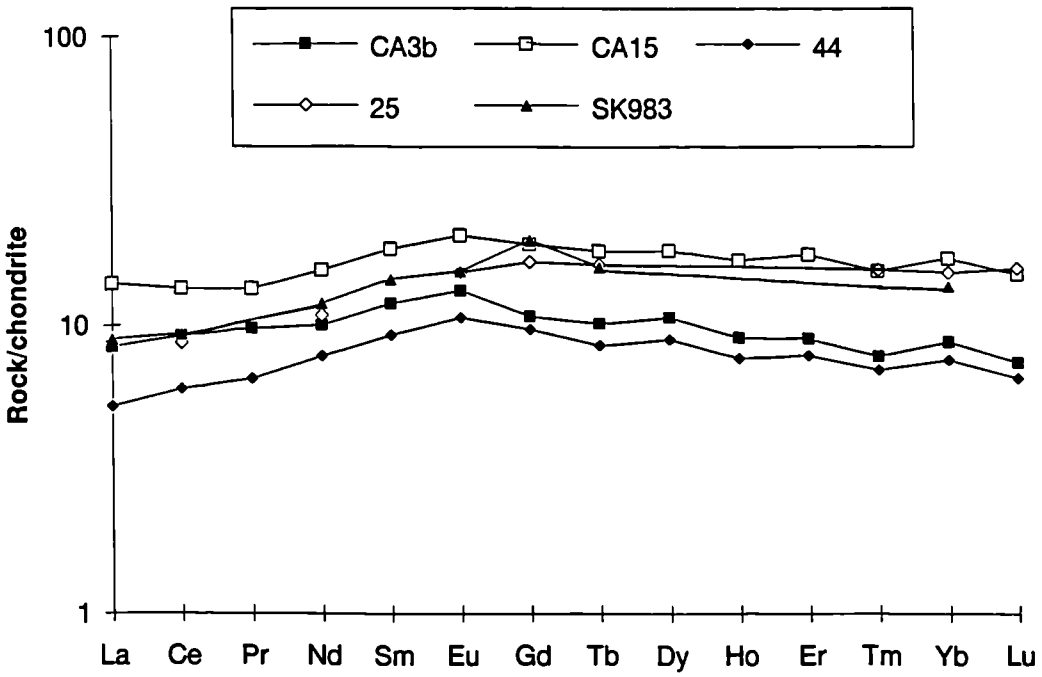


Figure 6.5 Comparative chondrite normalised REE plot showing the CMT type (CA3b, CA15 & 25) and the Preshal More type (25 & SK983). See text for data sources.

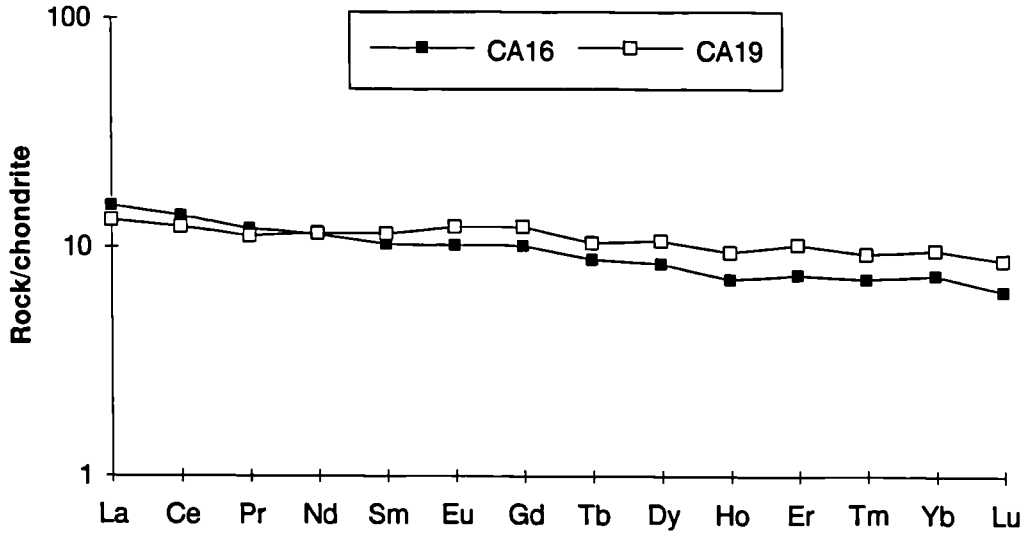


Figure 6.6 Chondrite normalised REE plot of several CMT lavas which are not LREE depleted.

Figure 6.7 reveals another important feature of the CMT lavas, namely their lower levels of incompatible trace elements, than those of the MPG lavas (at similar MgO content). Thompson *et al.* (1980) similarly noted that the Preshal More lavas from Skye had relatively depleted trace element signatures. As will be shown in section 6.3 this feature reveals important information about the nature of, and the melting processes in, the mantle source region.

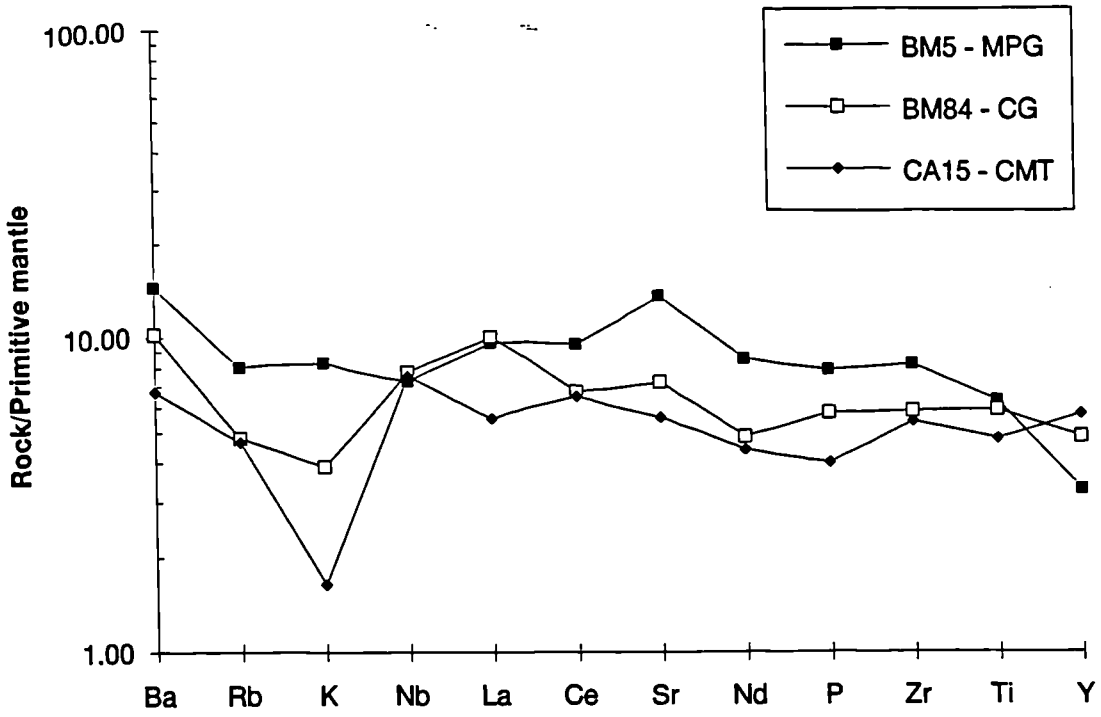


Figure 6.7 Spidergram showing representative samples of the three Mull magma types identified in this study.

6.2.2 The Coire Gorm magma type.

The lava flows which comprise this magma type can be found mostly at the top of Ben More (samples BM 73-99) although one flow has been found in the lower part of the Croggan section (CA2). No lavas of the CMT type have been found at the top of Ben More, but the existence in the Croggan section of a CG type flow *below* the CMT flows, helps to establish the relative chronology of the three types. The MPG are obviously the earliest flows, and these are overlain by the CG type, followed by the CMT lavas. A similar age progression from SMLS type through the Fairy Bridge type to the Preshal More type was observed by Thompson *et al.* (1980) within the Skye lavas. Close inspection of the chemical data from the Mull dyke swarm (Lamacraft 1978) reveals that some of the dykes have chemical characteristics of the CG type (Ti/Zr >110, with transitional major element chemistry).

The major element chemistry of the CG magma type is more closely aligned to that of the MPG than the CMT type and figures 6.3 and 6.4 bear this out. Figure 6.3 demonstrates that the CG samples are all basaltic, and the range of MgO (7-12%) also confirms this. Fractionation of olivine and plagioclase from these magmas is evidenced by the presence of pseudomorphs after olivine, and some plagioclase phenocrysts (Chapter 3).

The CG type have relatively flat REE patterns (figure 6.8a) that are similar to the Skye Fairy Bridge type-locality flow (SK971; Thompson *et al.* 1980) and also a Skye Fairy Bridge dyke (H060; Mattey 1979) figure 6.8b. It can be seen from figure 6.1 that the CG and the CMT magma types, like the Fairy Bridge and the Preshal More types, have quite flat middle-to-heavy REE (M-to-HREE) patterns, which are in sharp contrast to the HREE depleted patterns of the MPG and the SMLS. Figure 6.7 shows that the CG magma type, like the CMT, is more depleted in the incompatible trace elements than the MPG lavas. At constant MgO the CG lavas contain slightly higher levels of the moderately incompatible elements (P, Zr, Ti & Y), than the CMT.

To summarise, it would thus appear that the Coire Gorm magma type possesses some characteristics of the MPG lavas (transitional, tholeiitic to alkalic major element compositions), and some features of the CMT type (relatively depleted incompatible trace element signatures, and flat M-to-HREE patterns).

6.3 Modelling of mantle melting processes

6.3.1 The Mull Plateau Group

As was mentioned at the beginning of Chapter 4 it is important that the effects of lithospheric contamination (from both crust and mantle), fractional crystallisation, and alteration be taken into account, *before* any attempt is made to assess mantle source regions and melting processes. Those magmas that have interacted with little crust, and are also relatively primitive, have the potential to reveal most about the mantle melting processes. In section 4.3, a series of primitive, uncontaminated basalts have been identified (table 4.3) within the MPG. Crustally contaminated basalts can also be used to elucidate mantle processes, but those elements which are affected by contamination processes (Ba, K, Rb, La, Ce & Nd - section 4.4) ***must first be excluded.*** Other incompatible elements, such as the M-to-HREE, Ti, P, Y and Zr, can yield important mantle petrogenetic information even in crustally contaminated basalts, as can most of the major elements if they are used with extreme caution.

Evidence for a melting column beneath Mull

a/ *Major elements*

The effects of pressure and extent of melting on the major element concentrations have already been discussed in section 6.1. Klein & Langmuir (1987; 1989), in a global study of basalts from mid-ocean ridges, made extensive use of major element compositional trends to assess the relative pressures and extents of mantle melting. In order to do this, they first eliminated the effects of fractional crystallisation. This was

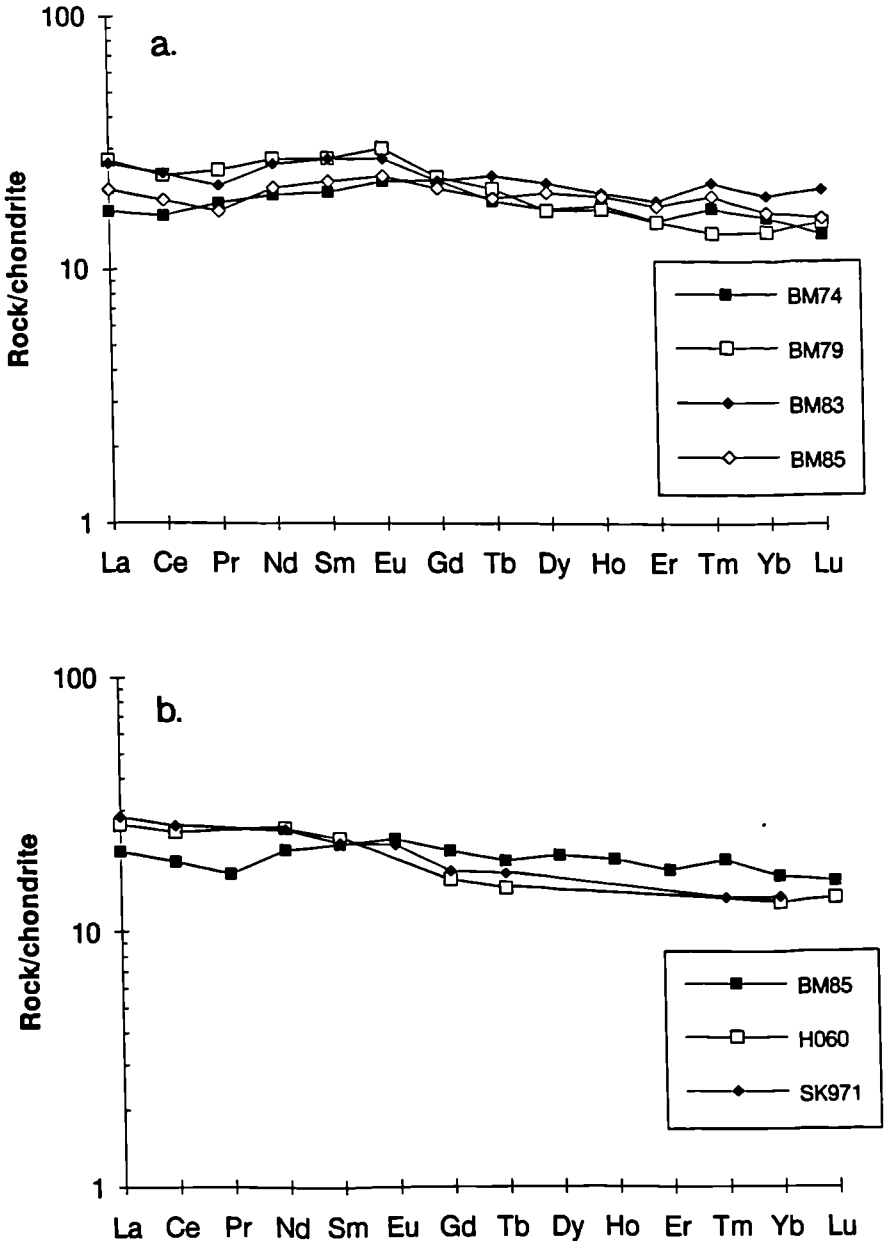


Figure 6.8 Chondrite normalised REE plots of *a.* the Coire Gorm magma type and *b.* a comparison of the Coire Gorm magma type and the Fairy Bridge magma type (H060 & SK971).

achieved by re-calculating FeO, SiO_2 and Na_2O values after the MgO content of each basalt was set at 8% (these are the so-called $Fe_{8.0}$ $Si_{8.0}$ & $Na_{8.0}$ values)[7].

$Fe_{8.0}$ $Si_{8.0}$ & $Na_{8.0}$ values have been calculated for the MPG lavas which contain between 6 and 8.5% MgO. However, following the discussion in Chapter 4 it should be obvious that, before proceeding any further, the effects of crustal contamination on the major elements should be considered. Table 6.2 shows that contamination with between 3 and 5% acidic Lewisian crust has negligible effects on Al_2O_3, Na_2O, TiO_2, MnO and P_2O_5. Fe_2O_3*, MgO, CaO, and SiO_2 seem to be affected to a small extent.

	BB9	P43	+3% crust	+5% crust
SiO_2	45.78	72.07	46.57	47.09
Al_2O_3	15.39	14.25	15.36	15.33
Fe_2O_3*	13.42	1.70	13.07	12.83
MgO	10.36	0.59	10.07	9.87
CaO	10.09	0.86	9.81	9.63
Na_2O	2.26	3.21	2.29	2.31
K_2O	0.16	5.40	0.32	0.42
TiO_2	1.75	0.18	1.70	1.67
MnO	0.20	0.00	0.19	0.19
P_2O_5	0.16	0.09	0.16	0.16

Table 6.2 Showing the effects of 3 and 5% contamination with acidic Lewisian crust (P43), on the major element concentrations of an uncontaminated basalt BB9.

As was demonstrated in section 4.4, the low MgO basalts (<8%) and basaltic hawaiites are less contaminated with continental crust than the more basic lavas. Since the calculation of $Fe_{8.0}$ $Si_{8.0}$ & $Na_{8.0}$ only involves basalts with 6 - 8.5% MgO, it is effectively the less contaminated MPG lavas which have been used to calculate these values.

The results of the calculations are graphically displayed in figures 6.9a & 6.9b and, while the diagrams show a considerable amount of scatter, overall trends may still be observed. The trends on both diagrams approximate to the intra-column (local) trends of Klein & Langmuir (1989) with higher pressures of melting corresponding to lesser extents of melting, and lower pressures to greater extents of melting. Some of the scatter on these diagrams is probably caused by crustal contamination, which on both

[7] These values are calculated using basalts with 6-8.5 wt % MgO. The equations for calculating $Na_{8.0}$ and $Fe_{8.0}$ are given in figure 2 of Klein & Langmuir (1987) and the equation for $Si_{8.0}$ is given in figure 1 of Klein & Langmuir (1989).

diagrams will produce contamination vectors at approximately right angles to the "local" trends. When one considers that these basalts have been erupted through thick (>50km) continental lithosphere (Ellam 1992) the preservation of these trends is remarkable.

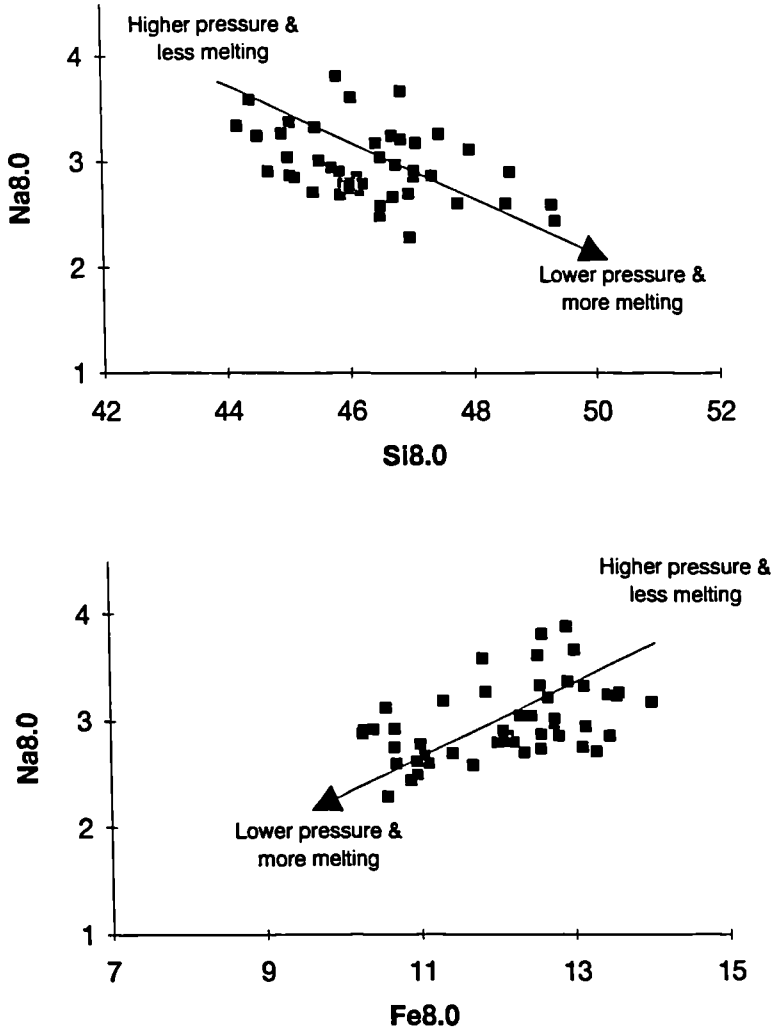


Figure 6.9 Plots of *a.* $Na_{8.0}$ vs. $Si_{8.0}$ and *b.* $Na_{8.0}$ vs. $Fe_{8.0}$ for MPG lavas containing between 6 and 8.5% MgO. Both diagrams display intracolumn or local trends (Klein & Langmuir 1989), with higher pressures of melting corresponding to lesser extents of melting, and lower pressures to greater extents of melting. [See text and footnote 7 for more details].

The evidence therefore from the major element systematics strongly suggests that the mantle melting which produced the MPG basalts occurred over a range of depths, within a melting column. As was noted above, in such a situation the magmas erupted at the surface represent pooled melts (point & depth average compositions) from different parts of the melting column. It is intuitively obvious that the lavas with a signature of deeper melting are made up of a greater proportion of deeper melts and vice versa.

As pointed out by Gill *et al.* (1992) the minimum depth of melting beneath a continent - unlike a mid-ocean ridge - is restricted by the presence of a thick mechanical boundary layer. A natural consequence of such a restriction on the minimum melting depth below continental regions will be that, for a given value of T_P, melting will probably occur over a shorter depth range than below a mid-ocean ridge. Ellam (1992) has suggested that the thickness of the continental lithosphere exerts an important control on the trace element geochemistry of the magmas produced.

b/ *Trace elements*

Thompson *et al.* (1980) during their study of the SMLS noted that, at any particular F/(F+M), a range of values could be observed for some incompatible elements. For TiO_2, P_2O_5, Zr, Hf, Nb, Ta and the MREE this variation could be correlated with the degree of silica saturation - expressed as percentage normative ne or hy - in the basalts. The more ne-normative basalts tended to have higher levels of incompatible elements than their hy-normative counterparts. Thompson *et al.* (op.cit) interpreted this in terms of 'variable degrees of partial fusion at approximately constant depth', with Ti, P, Zr, Hf, Nb, Ta & the MREE partitioning strongly into the first formed ne-normative melt. With increasing degrees of melting these elements would become more diluted and the magma more hy-normative.

It was observed in Chapter 4 that, at a given value of F/(F+M), there was a significant range of incompatible element values within the MPG lavas. Like the SMLS, crude negative correlations exist between silica saturation and Na_2O, TiO_2 & Zr at approximately constant F/(F+M) [0.48-0.52] figure 6.10a-d. As in the SMLS, Y, a more compatible element, preserves approximately constant values with increasing silica saturation, since it does not partition as strongly into the first formed melt. This evidence from the trace elements in MPG supports the major element evidence for a melting column, in that the more incompatible element enriched basalts are more ne-normative. These magmas therefore represent pooled liquids which contain proportionately more high-pressure, low-degree melts, than the more incompatible element depleted hy-normative basalts.

Since the work of Thompson *et al.* (1980) the concepts of a melting column, and of erupted basalts representing pooled melts from throughout the column, have become ingrained in the literature. These concepts therefore can provide an *explanation* for the observation of Thompson *et al.* (op.cit) that SMLS magmas erupted at the surface represent different degrees of melting in the mantle source region.

McKenzie & Bickle (1988) calculated that little basaltic magma will be produced in continental regions without either some extension (expressed in terms of the β factor) and/or mantle potential temperatures which are well in excess of 1280 °C. The

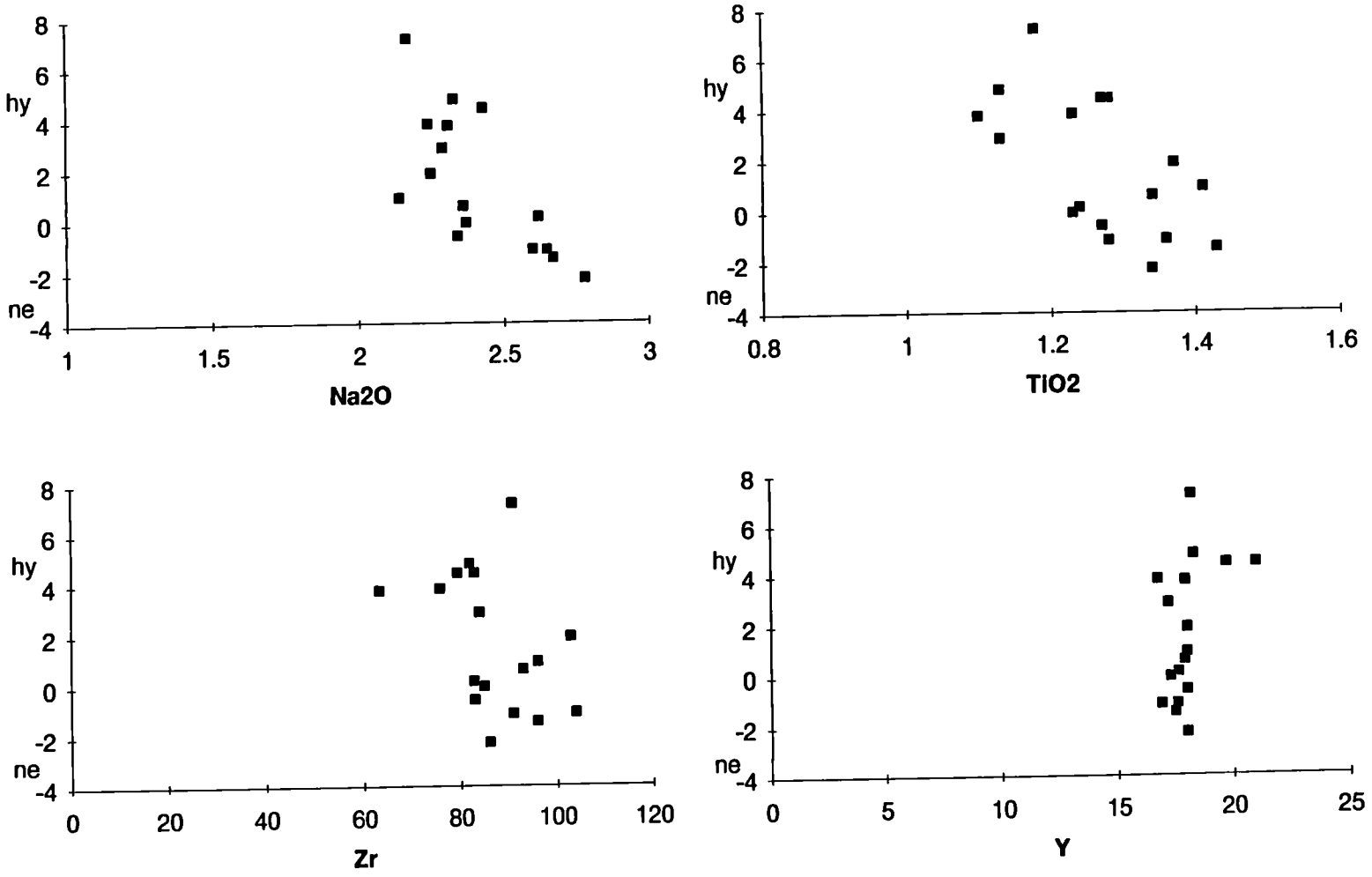


Figure 6.10 Plots of silica saturation (hy or ne CIPW normative) vs. Na_2O, TiO_2 (wt%), Zr and Y (ppm), for MPG lavas with F/(F+M) between 0.48-0.52.

intensity of Tertiary dyke swarms can give an approximation of the amount of local extension during the Tertiary magmatic event. Away from the central complexes this extension rarely exceeds 10% (β =1.1) and, more often than not is closer to 5% (Speight *et al.* 1982). However, Thompson & Gibson (1991) suggested that Palaeocene extension in the Hebridean region, superimposed on the previous Mesozoic sedimentary basins, may have resulted in lithospheric "thin-spots" below which more decompression melt generation could have occurred locally.

Using the equations and diagrams from McKenzie & Bickle (1988) it is possible to estimate a range of T_p and extent of melting for a suite of magmas, and such an approach has been used by Gill *et al.* (1992) for the West Greenland picrites. An average composition of the most basic MPG magmas from table 4.3[8] has been used to estimate T_p, and the average extent and pressure of melting.

For the parental MPG magmas with an MgO content of 13.5 %, T_p is estimated to be between 1420 and 1460 °C, depending on whether the entropy of melting (ΔS) is taken to be 250 J K^{-1} kg^{-1} (McKenzie & Bickle op.cit), or 400 J K^{-1} kg^{-1} (Watson & McKenzie 1991). The calculations also suggest that the mean extent of melting is of the order of 7-11% at pressures in the range of 20-25 kb. These estimates of course represent 'point average' melt compositions.

The nature of the mantle source region.

Thompson (1974) and Thompson *et al.* (1980) proposed that the SMLS magmas had been derived from a spinel lherzolite mantle source region. This deduction was chiefly based on the experimental melting behaviour of a SMLS basalt. Other workers on the BTIP have also noted the most of the Tertiary lavas must have had a depleted mantle source region (Beckinsale *et al.* 1978; Morrison *et al.* 1980; Lyle 1985; Thompson & Morrison 1988).

In order to assess the nature of the source region, non-modal, equilibrium (batch) melting equations (taken from Kostopoulos & James 1992) have been used to calculate trace element contents of the liquids produced during partial melting of various mantle sources. As was noted earlier, batch melting, while not being an accurate representation of the melting *processes,* seems to give a reasonable approximation to the composition of the liquids produced from a particular mantle source at moderate degrees (>5%) of melting.

Modelling with fifteen different mantle compositions has been attempted, these are summarised in table 6.3. As can be seen, these are composed of 5 different bulk

[8] Average composition of the most basic, uncontaminated magmas; MgO = 13.42%, SiO_2 = 46.27, Al_2O_3 = 14.31, CaO = 9.81, Na_2O = 2.14.

chemical compositions, which span a wide range of mantle compositions from quite enriched to relatively depleted.

Number (Fig. 6.11)	Source composition	Previous melt extraction	Modal mineralogy
1	Depleted Mantle	1%	gnt lherzolite
2	Depleted Mantle	1%	sp/gnt lherzolite
3	Depleted Mantle	1%	sp lherzolite
4	Enriched Mantle	1%	gnt lherzolite
5	Enriched Mantle	1%	sp/gnt lherzolite
6	Enriched Mantle	1%	sp lherzolite
7	Depleted Mantle	--	gnt lherzolite
8	Depleted Mantle	--	sp/gnt lherzolite
9	Depleted Mantle	--	sp lherzolite
10	Enriched Mantle	0.1%	gnt lherzolite
11	Enriched Mantle	0.1%	sp/gnt lherzolite
12	Enriched Mantle	0.1%	sp lherzolite
13	Enriched Mantle	--	gnt lherzolite
14	Enriched Mantle	--	sp/gnt lherzolite
15	Enriched Mantle	--	sp lherzolite

Table 6.3 Mantle compositions and modal mineralogies used in the non-modal, batch melt modelling. The rest of the table is discussed in the text. (gnt = garnet; sp = spinel; sp/gnt = a 50/50 mixture of spinel and a garnet lherzolite)

For each of these chemical compositions, three different mantle mineral assemblages have been modelled; garnet lherzolite, spinel lherzolite and a 50/50 mixture of both spinel and garnet lherzolite. This latter composition was chosen in order to simulate melting in the garnet-spinel transition zone. The modal mineralogy and the melting proportions of each of these sources, the partition coefficients and the source compositions are from Kostopoulos & James (1992). They called their enriched source "Bulk Silicate Earth" and their depleted source "Depleted MORB Mantle" but, for the purposes of this study, these compositions will be known as Enriched Mantle and Depleted Mantle respectively.

Morrison *et al.* (1980) and Thompson & Morrison (1988) proposed that part of the mantle source region of the BTIP had been depleted by the extraction of a small degree melt in the Permo-Carboniferous. Thus, in order that this possibility might be reassessed, initial melt modelling was used to extract some small degree (0.1 and 1%)

partial melts from several of the mantle compositions used, prior to the main melt modelling. The mantle compositions for which a previous melting event has been modelled, and the melt extracted, are noted in table 6.3.

Earlier it was calculated, on the basis of major element constraints, that the average amount of melting was approximately between 7 and 11%. Therefore the compositions of calculated melts at 8.5% partial fusion have been used, so that some information on possible and impossible mantle sources can be obtained. This information has been summarised on figure 6.11, along with data for some of the most primitive, uncontaminated MPG samples. The $(La/Nd)_{cn}$ ratio may be used to assess the amount of depletion in the source, and the $(Sm/Yb)_{cn}$ ratio gives a guide to the modal mineralogy of the source.

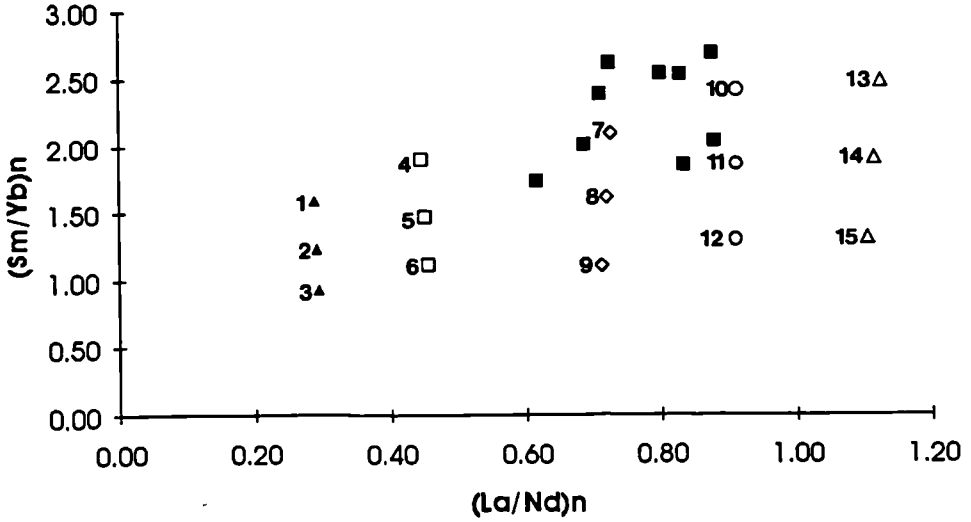


Figure 6.11 $(Sm/Yb)_n$ vs. $(La/Nd)_n$ (both chondrite normalised) showing the compositions of melts produced by 8.5% partial fusion of various source regions, (**filled triangles** - depleted mantle, 1% previous melt extraction; **hollow squares** - enriched mantle, 1% previous melt extraction, **hollow diamonds** - depleted mantle, hollow circles - enriched mantle, 0.1% previous melt extraction, hollow triangles - enriched mantle). The numbers beside each melt composition are the same as those numbers in table 6.3, which summarises the chemical composition and modal mineralogy of 15 possible mantle sources. Primitive uncontaminated MPG basalts (solid squares) are also shown on the diagram.

This diagram enables some of the mantle sources from table 6.3, to be effectively excluded from further consideration. It is obvious that the source region of the MPG magmas *must* contain some garnet, since melting of a spinel lherzolite (compositions 3, 6, 9, 12 & 15; table 6.3) *cannot* produce the higher $(Sm/Yb)_{cn}$ ratios of the MPG lavas.

In section 4.4 the LREE depleted nature of uncontaminated MPG basalts has been noted (figure 4.26) and, as figure 6.11 shows, they have $(La/Nd)_{cn}$ ratios of between

0.6 an 0.9. This means that either a depleted or an enriched mantle source, with 1% previous melt extraction (compositions 1-6), will produce liquids which are too depleted in the LREE to be appropriate sources for the MPG lavas. Melting of Enriched Mantle (compositions 13-15 in table 6.3 and on figure 6.11) will produce magmas which are too LREE enriched to represent the MPG compositions. It would therefore appear that the MPG lavas were the result of melting in the spinel-garnet transition zone of a depleted mantle, or an enriched mantle which had a very small-degree melt previously removed from it.

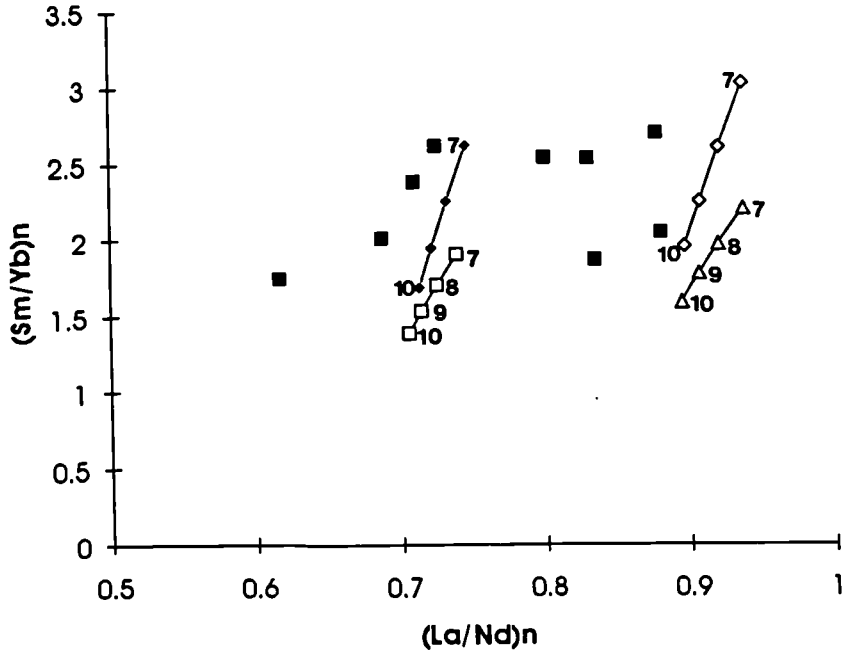


Figure 6.12 $(Sm/Yb)_n$ vs. $(La/Nd)_n$ (both chondrite normalised) showing the modelled compositions of melts generated by 7-10% batch melting of possible mantle sources. The degree of fusion (in %) is given by numbered points on each melt curve. [SYMBOLS; **solid diamonds** - melts of depleted garnet lherzolite, (composition 7, table 6.3); **hollow squares** - melts of depleted spinel/garnet lherzolite, (composition 8, table 6.3); **hollow diamonds** - melts of enriched garnet lherzolite, with previous 0.1% melt extraction (composition 10, table 6.3); **hollow triangles** - melts of enriched spinel/garnet lherzolite, with previous 0.1% melt extraction (composition 11, table 6.3), **solid squares** - primitive uncontaminated MPG basalts.

This is further confirmed by figure 6.12 which shows the liquid compositions that will be generated by 7-10% partial melting of compositions 7-8 & 10-11 (table 6.3). The MPG lavas which have higher $(Sm/Yb)_{cn}$ ratios, seem to be smaller degree melts from sources that contain more garnet than spinel. This is confirmed by the norms of these lavas which, are on the whole, more ne-normative than the norms of those lavas with lower $(Sm/Yb)_{cn}$ ratios.

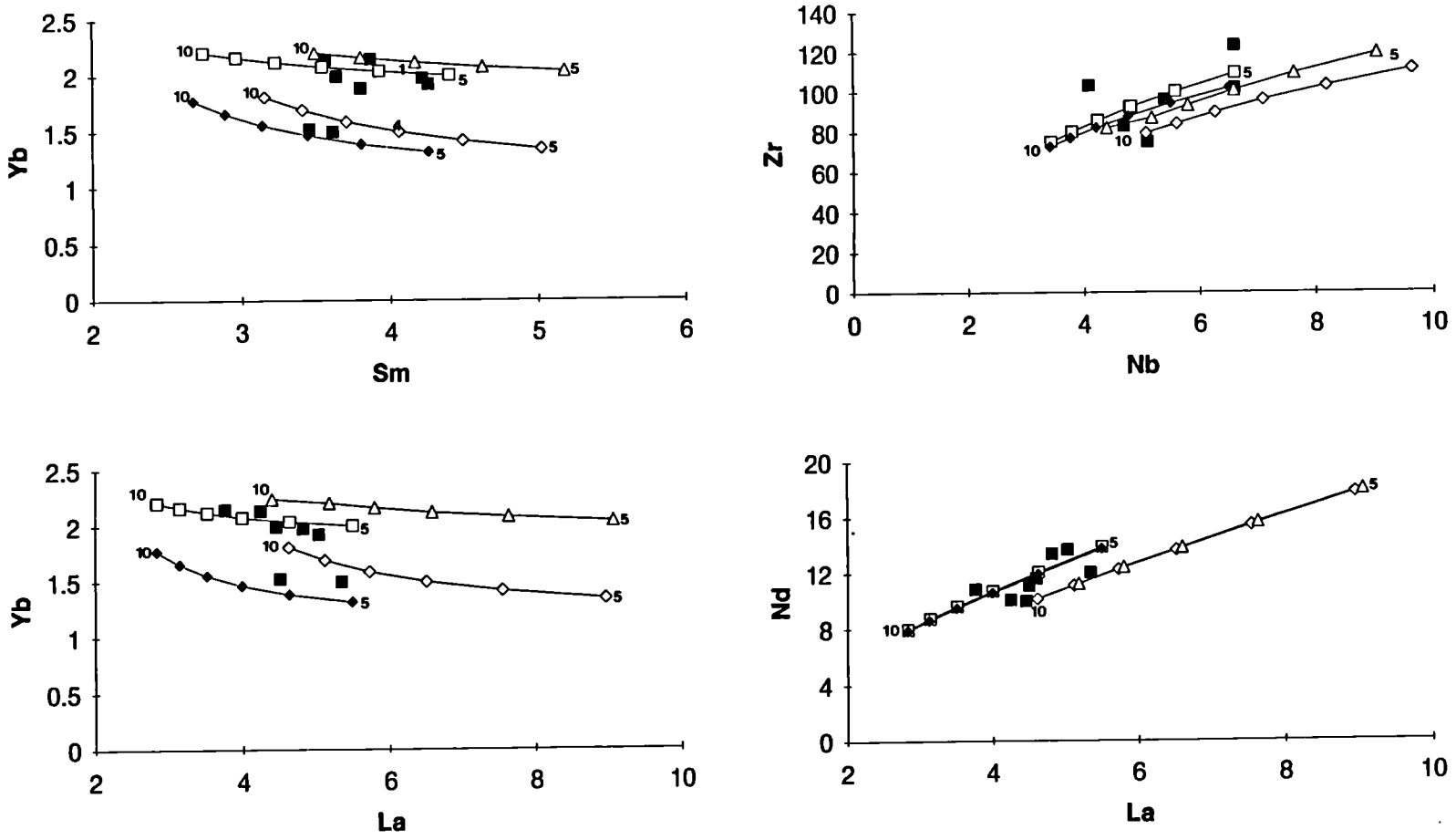


Figure 6.13 Incompatible trace element variation diagrams, showing melting curves for partial fusion of four possible mantle sources. Symbols as for figure 6.12, except that the melting curves represent 5-10% fusion (symbols every 1%).

So far, only elemental *ratios* have been used to assess the nature of the source region and the degree of mantle melting, nevertheless elemental *abundances* should also be considered, and figure 6.13 takes these into account. Although figure 6.12 suggests that it is possible to generate the observed ratio of $(Sm/Yb)_{cn}$ in MPG lavas by melting of a garnet lherzolite, this set of diagrams (figure 6.13) reveals that elemental abundances do not support this idea. Most of the magmas seem to have been generated within the spinel/garnet transition zone. However, several of the lavas perhaps represent pooled melts with a greater contribution from deeper melting in a more garnet-rich source region. From these diagrams the extent of melting, which produced the MPG magmas, within this spinel/garnet transition zone can be estimated. This approximates to 5.5-8% for depleted mantle, and 7-11% for enriched mantle (with previous fusion and removal of 0.1% melt). These estimates are close to values derived from the major elements (7-11%) and trace element ratios (6-10%; figure 6.12).

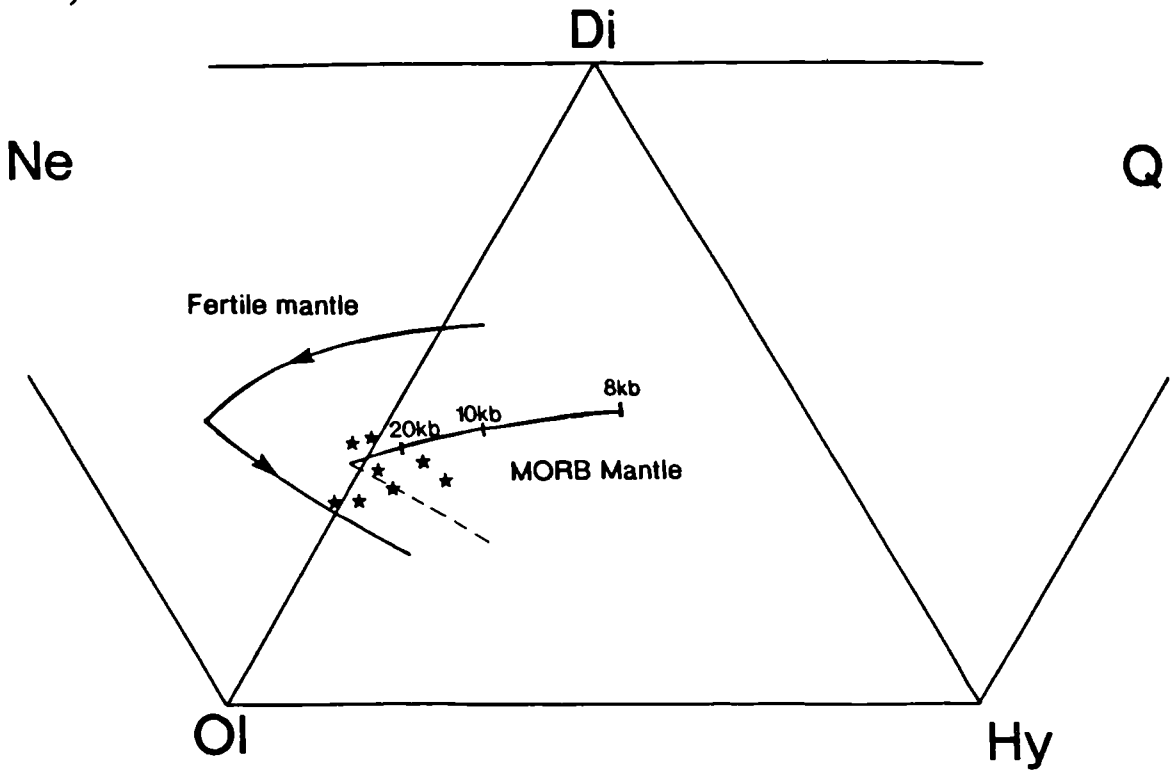


Figure 6.14 Normative Ne-Ol-Di-Hy-Q-Di plot, showing the loci of initial melts of MORB source mantle and fertile mantle (Thompson 1987). Primitive uncontaminated MPG basalts are represented by stars.

The least contaminated, most primitive lavas (from table 4.3) plot close to the loci of the initial melts from a depleted MORB source mantle (figure 6.14). This diagram, taken from Thompson (1987), also shows that most of the samples plot around and above the 20kb region on the loci of initial melts. This major element evidence

therefore supports the previous conclusions that the MPG magmas were derived from a depleted source region at 60-80km depth.

The least contaminated MPG samples have quite low ($^{87}Sr/^{86}Sr$)i <0.7032 and relatively high ($^{143}Nd/^{144}Nd$)i, (figure 6.15). Uncontaminated basalts from the rest of the NATIP similarly have low values of ($^{87}Sr/^{86}Sr$)i. These have been noted by Carter *et al.* (1979) in the region as a whole, Moorbath & Thompson (1980) in Skye, Gariepy *et al.* (1983) in the Faeroes, Upton *et al.* (1984) in East Greenland, Holm *et al.* (1993) in West Greenland, and Wallace *et al.* (1993) in Ulster. (See section 6.4).

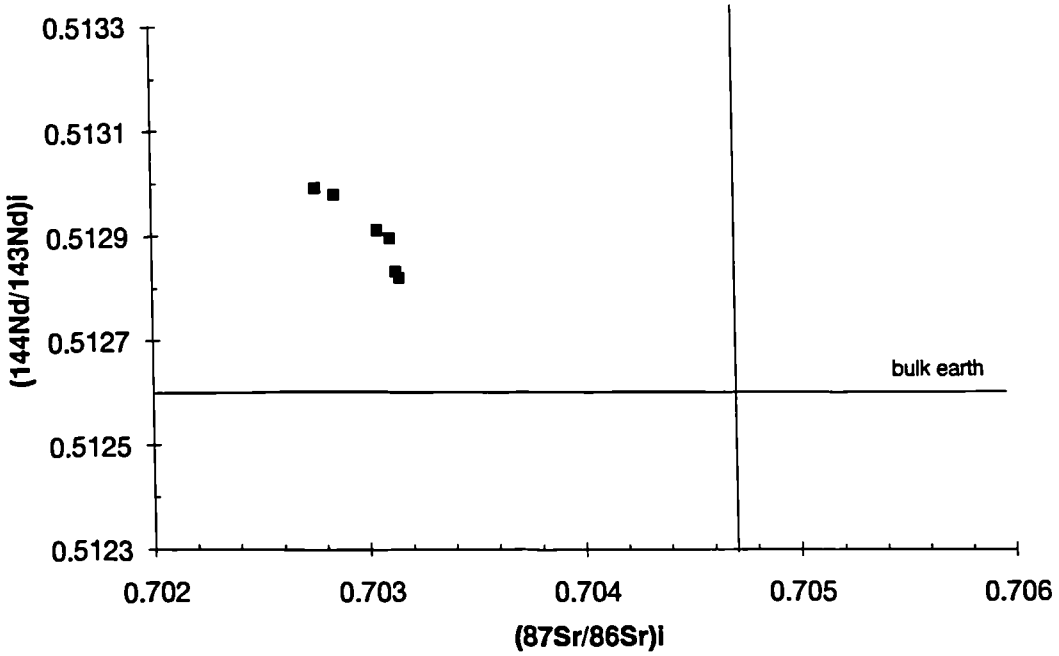


Figure 6.15 Plot of ($^{87}Sr/^{86}Sr$)i vs. ($^{143}Nd/^{144}Nd$)i, for the least contaminated MPG lavas.

Conclusions from this section;

1. The mantle source region of the MPG magmas must be depleted, relative to Bulk Earth.

2. Varying extents of melting occurred over a range of depths, mostly within the spinel/garnet transition zone. Nevertheless there was probably also a contribution to the pooled magmas from the deeper parts of the melting column; i.e. within the garnet stability field.

3. The average extent of melting, as expressed by the pooled magmas, seems to be between 6 and 11%. These figures are, however, essentially based on point-and-depth average compositions and it is likely that, at the top and bottom of the melting column, the extent of fusion will be respectively greater or less than this range.

6.3.2 The Coire Gorm magma type.

As has previously been noted, the CG magma type occurs at the top of Ben More. These lavas overlie some of the most evolved rocks within the MPG (BM60-66; section 4.3, appendix 4a.i). These facts, combined with their distinctive chemistry and more basic nature, strongly suggests a decline in magma production in the mantle at the end of the MPG phase of magmatism. This gave time for these later MPG magma batches to fractionate, before the onset of a new phase of mantle melting as represented by the CG magma type.

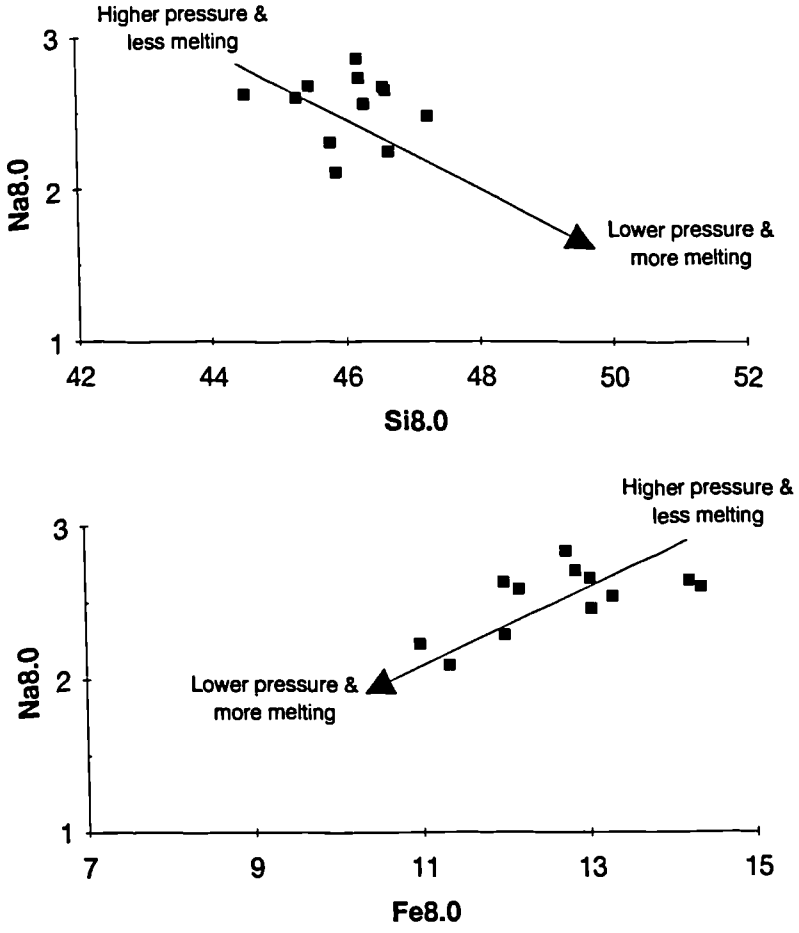


Figure 6.16 Plots of *a.* $Na_{8.0}$ vs. $Si_{8.0}$ and *b.* $Na_{8.0}$ vs. $Fe_{8.0}$ for CG lavas containing between 6 and 8.5% MgO. The $Na_{8.0}$ vs. $Fe_{8.0}$ diagram displays an intracolumn or local trend (see caption to figure 6.9 and footnote 7 for more details). The poor correlation in the $Na_{8.0}$ vs. $Si_{8.0}$ is discussed below

Major elements

Figure 6.16b shows a good positive correlation between $Na_{8.0}$ and $Fe_{8.0}$[9], suggesting that these magmas, like the MPG, are a result of the pooling of melts from different

[9] $Na_{8.0}$, $Fe_{8.0}$ & $Si_{8.0}$ have been calculated using the same equations and range of MgO contents, as in section 6.3.1.

depths within a column. Figure 6.16a shows a very poor correlation between $Na_{8.0}$ and $Si_{8.0}$ which may well be due to post-magmatic processes, since all these flows lie within the central greenschist-facies zone of alteration (figure 1.2). The CG magmas have on the whole higher CaO and lower $Na_{8.0}$ values than the MPG lavas (figure 6.17). The major element melting systematics in table 6.1 therefore suggest that the CG magmas represent more extensive degrees of melting than the MPG. Although CaO and Na_2O may have been affected by alteration, "immobile" trace elements (see below) *also* suggest that the CG magmas are the result of more extensive degrees of partial mantle melting.

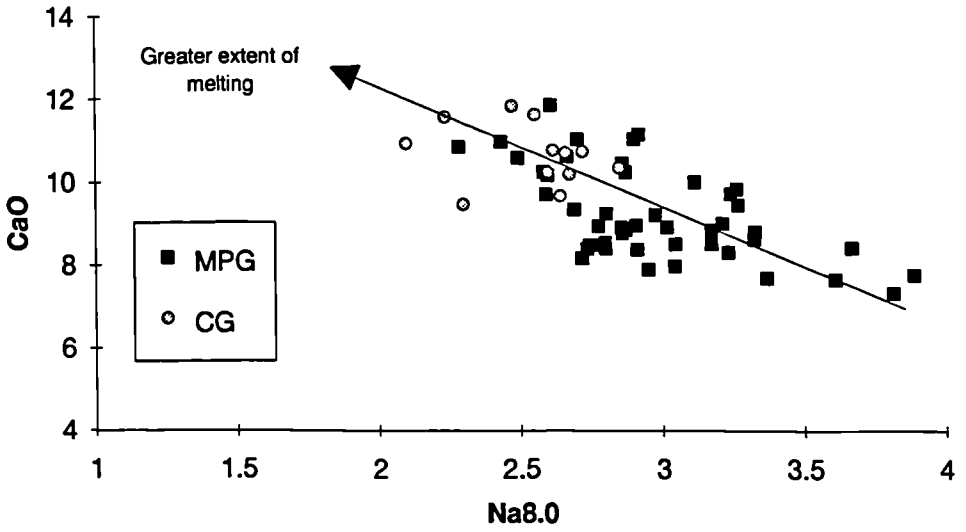


Figure 6.17 CaO vs. $Na_{8.0}$ for the MPG and the CG lavas, suggesting that the CG lavas are the result of more extensive degrees of mantle melting.

Trace elements

In section 6.2.2 it was clearly shown that the CG magma type had much flatter M-to-HREE patterns, ie. $(Sm/Yb)_n$ ratios <1.4 and, as was demonstrated in the last section, this has important implications for the nature of the mantle source region. Lavas such as the CG magma type, with low values of $(Sm/Yb)_n$, can only be produced when melting occurs predominantly within a spinel lherzolite source mantle (figure 6.11). This is verified by figure 6.18 which shows the melting (4-10% fusion) trends for five spinel lherzolites of widely differing bulk chemistry (numbers 3, 6, 9, 12 & 15 in table 6.3). This diagram suggests that, like the MPG, the REE patterns of the CG magmas can be explained by moderate degrees of melting of a depleted mantle source. Some of these lavas have slightly higher $(Sm/Yb)_n$ ratios than others and, as a result, the predicted extents of melting from this diagram are about the same as that for the MPG. However, figure 6.17 suggests that the CG magmas are the result of more extensive melting than the MPG. These two apparently contradictory lines of evidence can be

reconciled by suggesting that a slight amount (~1%) of melting occurred within the spinel/garnet transition zone. This can raise the $(Sm/Yb)_n$ ratio by 0.1.

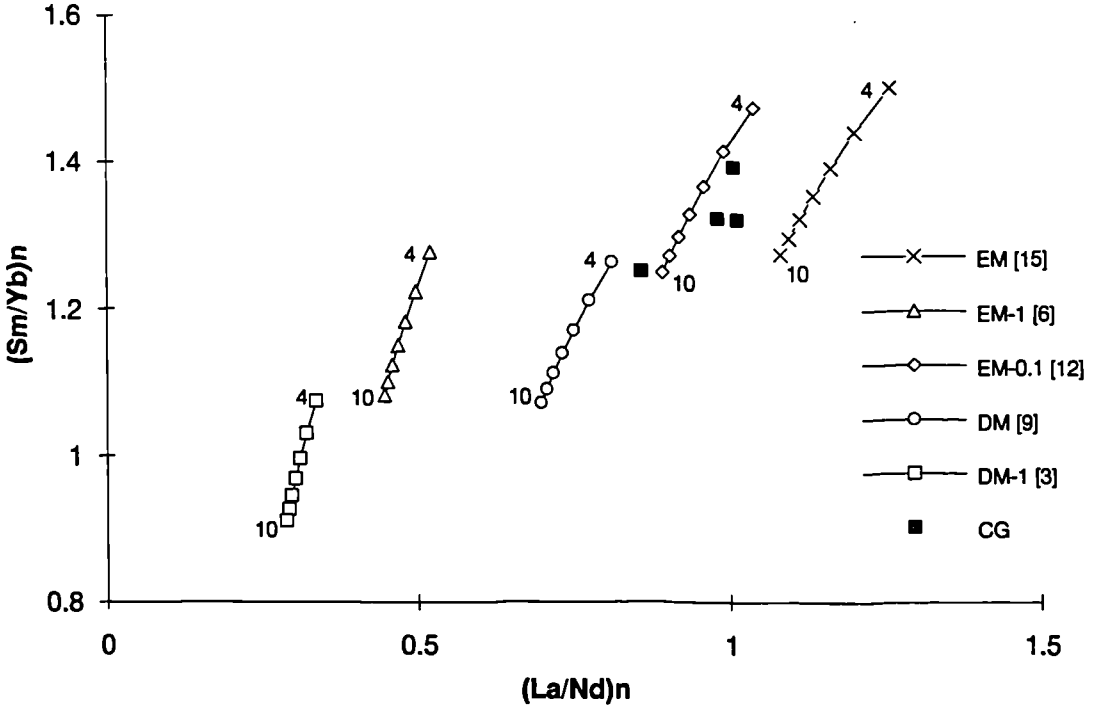


Figure 6.18 Plot of $(Sm/Yb)_n$ vs. $La/Nd)_n$ showing some CG lavas (filled squares) along with calculated batch melting curves (4-10% fusion) for some spinel lherzolites. [KEY; **EM** - enriched mantle; **DM** - depleted mantle, **EM-1** and **EM-0.1** - enriched mantle, previous 1% and 0.1% melt extraction, respectively, **DM-1** - depleted mantle previous 1% melt extraction. Numbers in square brackets refer to table 6.3].

The calculated REE compositions of the magmas with varying degrees (4-10%) of partial melting of a depleted mantle, and an enriched mantle (with previous small degree melt extraction 0.1%) are shown in figure 6.19a & b. Also displayed on this diagram is one of the more basic CG lavas, BM85 (MgO = 11%). For both these mantle sources 10-12% melting is required in order to produce the concentrations of the M-to-HREE in CG. A few of the CG lavas have MgO contents of over 11.5% (eg. BM88) and, although none of these most mafic CG lavas have been analysed for all the REE, they have lower La and Y than BM85. It can therefore be predicted that these most basic CG lavas would have lower REE abundances, and therefore to produce them more mantle melting (~13-14%) would be required.

In figure 6.19 the LREE contents of the CG magma type are best modelled using the composition of the enriched mantle (with a previous 0.1% melt extraction) ie. the less depleted of the two sources in figure 6.18. However, it is important to realise that crustal contamination may well have played a role in modifying the LREE contents of

the CG magma type and, if this has been the case, then the depleted mantle (figure 6.19a) would also be a reasonable source region.

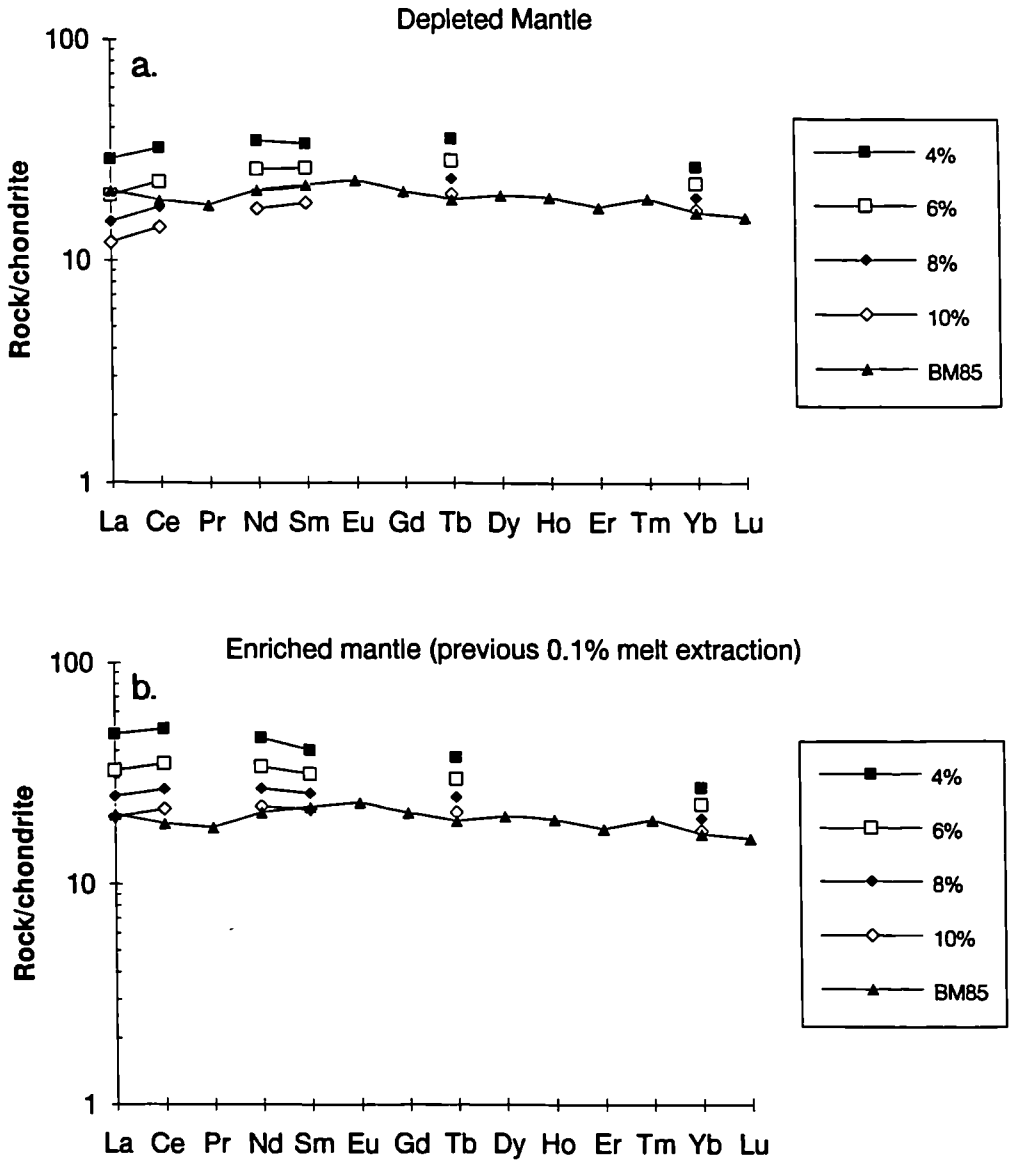


Figure 6.19 Chondrite normalised REE patterns showing the compositions of modelled batch melts (4-10% in legend) of *a.* depleted spinel lherzolite (composition 3; table 6.3) and *b.* enriched spinel lherzolite, previous 0.1% melt extraction (composition 12; table 6.3). A typical CG basalt (BM85) is also plotted on both diagrams.

Conclusions from this section;

1. The mantle source region of the CG magmas must, like the source of the MPG be depleted, relative to Bulk Earth. However there is some evidence to suggest that the source of the CG magmas *may* be slightly more enriched, than that of the MPG.

2. Varying extents of melting occurred over a range of depths, mostly within spinel lherzolite mantle. Nevertheless, there may well have been a small (~1%) contribution to the pooled magmas from the deeper spinel/garnet transition zone.
3. The average extent of melting which produced the pooled CG magmas, was of the order of 10-14%

6.3.3 The Central Mull Tholeiites.

When the highly porphyritic samples are excluded from consideration only a few of the CMT lava samples are left. As a result non-porphyritic CMT type dykes from Mull (Lamacraft 1978) have been used to supplement the CMT lava samples.

Major elements

As was noted in section 6.2.1, the CMT are more silica saturated than both the MPG and the CG, This implies that the CMT are the result of more extensive melting, and the depleted incompatible trace element signature (figure 6.7) also points to the same conclusion. Figure 6.20 shows that the CMT have higher CaO and lower $Na_{8.0}$ than the MPG and the CG type, this is again consistent with a higher degree of melting for the CMT. Although hydrothermal alteration may have modified the compositions of these oxides, relatively immobile trace elements *also* suggest that the CMT are the result of more extensive degrees of mantle melting (see below).

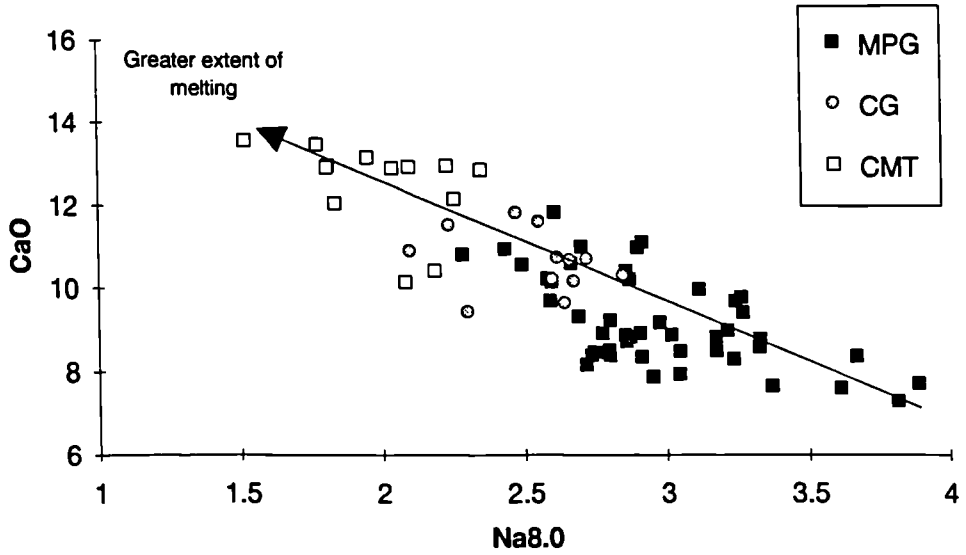


Figure 6.20 CaO vs. $Na_{8.0}$ for the MPG the CG and the CMT lavas, suggesting that the CMT lavas are the result of more extensive degrees of mantle melting than the MPG and the CG lavas.

Trace elements

The CMT have very similar M-to-HREE patterns to the CG type, with $(Sm/Yb)_n$ ratios of <1.4. Therefore the CMT were also probably derived from a spinel lherzolite

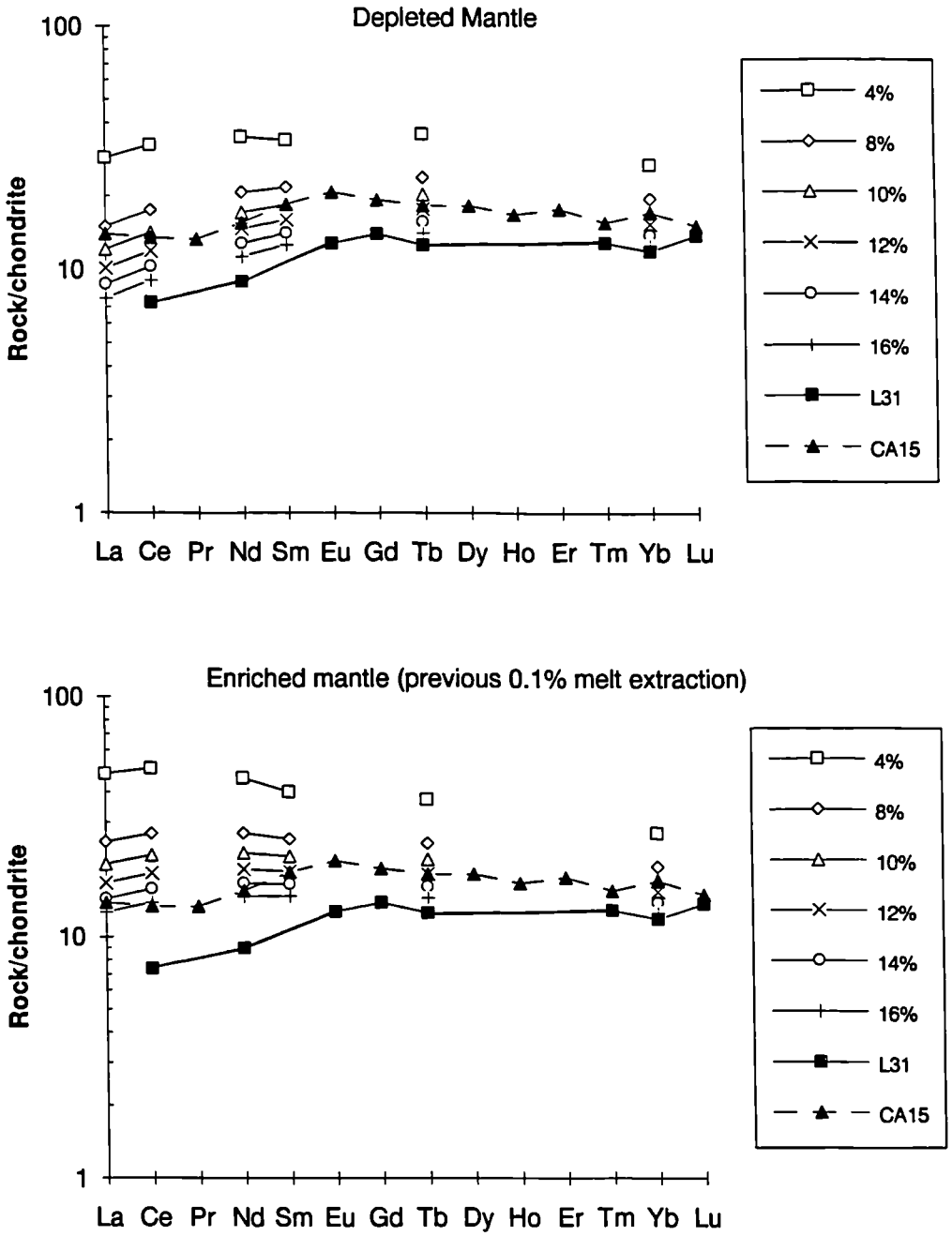


Figure 6.21 Chondrite normalised REE patterns showing the compositions of modelled batch melts (4-16% in legend) of *a.* depleted spinel lherzolite (composition 3; table 6.3) and *b.* enriched spinel lherzolite, previous 0.1% melt extraction (composition 12; table 6.3). A CMT lava (CA15) and a CMT dyke (L3) are also plotted on both diagrams.

source and figure 6.21 confirms this. CA15, the most-basic, non-porphyritic CMT lava has been plotted on this diagram. It however only contains 8% MgO and has probably fractionated from its original primary magma composition, which would have had lower REE contents. In addition to this sample, the most-basic CMT dyke (sample (L)3; MgO = 9.3) from Lamacraft (1978) is also shown on figure 6.21. From this diagram it can be estimated that the extent of melting required to produce the REE contents of the CMT is of the order of 13-17% of a depleted mantle source. The source region appears to be slightly relatively more depleted in LREE & MREE than that of the CG type. This perhaps suggests that the source region of the CMT may have been *residual* from the melting event which produced the CG type. The fact that the compositions of the two types also tend to overlap (figures 6.2, 6.3 & 6.20), combined with the fact that the lavas of the more enriched CG type are earlier than those of the more depleted CMT type, also supports this contention.

Conclusions from this section;

1. The mantle source region of the CMT magmas seems to be more depleted than that of the CG magma type, and it may well be that they represent second-stage melts from a mantle which had already produced the earlier CG magmas. Chemical similarities between the CG and the CMT magma types, seem to support this idea. This is line with the proposal of Bell (1984) that the similar (to the CG and CMT) magma types from Skye, the Fairy Bridge and the Preshal More lavas, represented the end members of a compositional spectrum.
2. The average extent of melting of a depleted spinel lherzolite source required to produce the pooled CMT magmas *appears to be* 13-17%, although the actual amount of melting may well have been less than this, *if the mantle source region had already produced the CG magmas.*

6.3.4 Modelling conclusions

1. The MPG magmas are derived from a relatively depleted source region. However the source of the CG and CMT magmas may have been slightly more enriched, but higher degrees of melting mean that these later magma types have lower levels of incompatible elements.

2. The magmas represent pooled partial melts, from various depths (and hence pressures) within a melting column. Smaller extents of melting occur at deeper levels, with more extensive melting at shallower depths.

3. The declining influence, with time, of melts from a source region containing garnet strongly suggests that, as the magmatic system developed, melting occurred at progressively shallower depths in response to lithospheric thinning. This thinning was chiefly caused by regional extension (as evidenced by dense Hebridean dyke swarms; Speight *et al.* 1982), probably with some lower lithospheric erosion. This postulate is in accord with the suggestion of Ellam (1992) that lithospheric thinning acts as an important control on basalt chemistry.

4. The potential temperature T_p of the upwelling mantle which underwent decompression melting to produce the MPG basalts, was of the order of 1420-1460 °C. Such asthenospheric temperatures are well above the ambient mantle potential temperature of 1280 °C and support the presence of a mantle plume beneath Mull in the Palaeocene.

5. Lithospheric thinning would enable the hot (~1440 °C) upwelling asthenospheric mantle to decompress further and so melt even more. Consequently, one would expect the later melts, to be the products of greater degrees of mantle fusion. This is exactly what is observed within the Mull lava succession and is summarised in figure 6.22.

6.4 Comparison with the rest of the NATIP

6.4.1 Skye

The chemistry of lava succession on Skye has been extensively reviewed earlier in the chapter and only the main features will be summarised here. Mattey *et al.* (1977) and Thompson *et al.* (1980) recognised three magma types within the lava succession: 1/ the earliest SMLS flows are transitional alkali basalts that had $(Ce/Yb)_{cn}$ >2.5 and flat to slightly depleted LREE patterns; 2/ the Fairy Bridge magma type has essentially flat REE patterns; 3/ the later Preshal More magma type is distinctly tholeiitic in nature, and has a flat M-to-HREE chondrite normalised pattern with a depleted LREE signature and low abundances of other incompatible trace elements. Moorbath & Thompson (1980) suggested that, since the least contaminated of the SMLS and Preshal More magmas had similar $(^{87}Sr/^{86}Sr)i$ ~0.7030, they had been derived from the same volume of spinel lherzolite upper mantle. The last phase of magmatism on Skye, represented by the more alkaline Beinn Dearg dyke swarm has elemental concentrations similar to present-day North Atlantic OIB (Thompson & Morrison 1988). These basalts have $(Sm/Yb)_{cn}$ >2 and, although some of them are LREE enriched, a few samples have $(La/Ce)_{cn}$ <1.

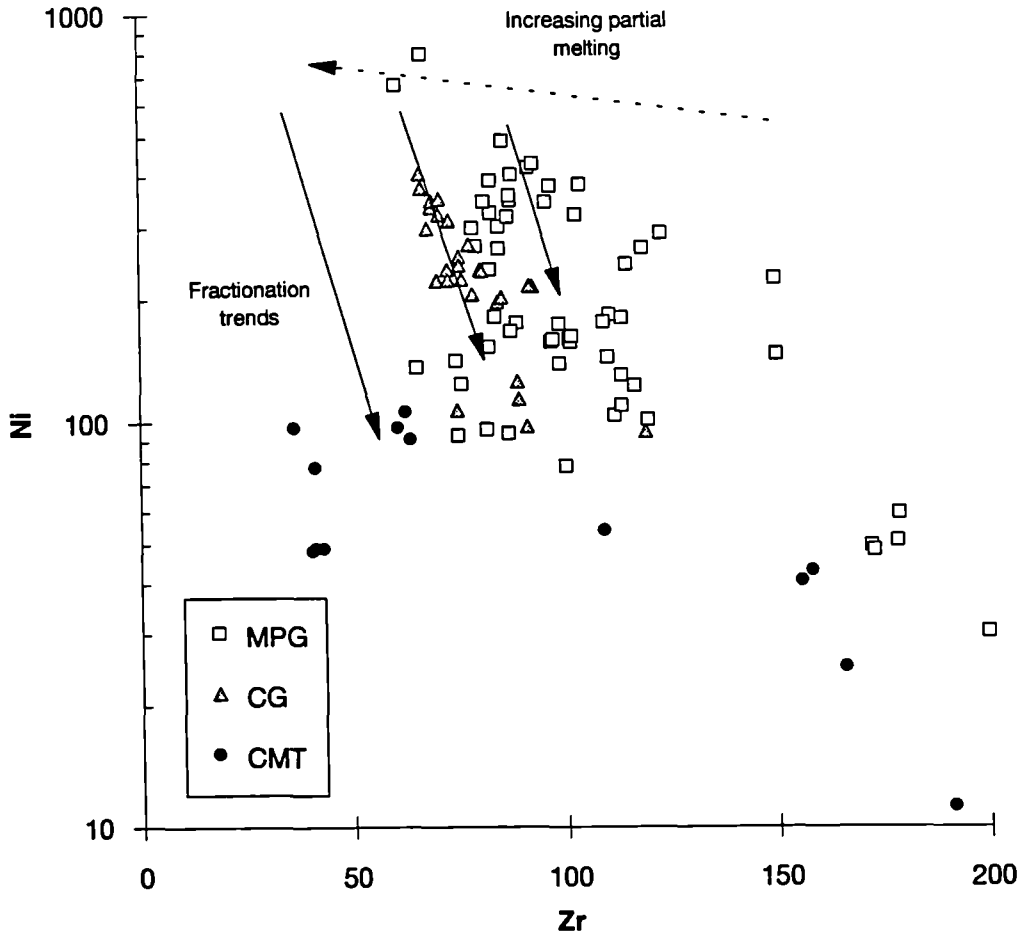


Figure 6.22 Ni vs. Zr for the three magma types of the Mull lava succession. Also shown are possible fractionation and partial melting trends. The lower Zr contents of the CMT are consistant with increased mantle melting.

6.4.2 Ulster

The Tertiary lavas cover an area of 3500 km^2 and are essentially tholeiitic in nature. Their chemistry has been investigated by Lyle (1974, 1980, 1985) and Wallace *et al.* (1993). The succession consists of a Lower Basalt Formation (LBF) with intermediate tholeiites near the top (the Causeway Tholeiite Member), overlain by the Upper Basalt Formation (UBF). The LBF have HREE depleted patterns $(Sm/Yb)_{cn}$ >2 with down-turned LREE signatures $[(La/Nd)_{cn}$ <1]. In contrast the UBF have much flatter REE patterns $(Sm/Yb)_{cn}$ <1.4 and lower levels of incompatible elements. Lyle (1985) proposed that the LBF, like the SMLS and the MPG (Morrison *et al.* 1980) had been derived from a spinel lherzolite source region which had a small-fraction melt fraction extracted from it in the Permo-Carboniferous. The more depleted UBF were interpreted to be second-stage melts from the same mantle which produced the LBF. Low ($^{87}Sr/^{86}Sr$) have been interpreted by Wallace *et al.* (1993) as evidence for a predominantly asthenospheric source region.

6.4.3 Faeroe Islands

The Faeroes lava succession, which is over 5 km thick, can be divided into a Lower, Middle and Upper Series (Schilling & Noe-Nygaard 1974), that are all of tholeiitic composition. The Lower and Middle Series have essentially a very similar chemistry with $(Sm/Yb)_{cn}$ ratios >2 (Gariepy *et al.* 1983). Although crustal contamination has influenced the LREE contents of the Faeroe basalts, those samples with the lowest $(^{87}Sr/^{86}Sr)i$ have sigmoidal REE patterns like the MPG. The Upper Series is composed of two contrasting types of basalts (Gariepy *et al.* 1983): Firstly there are LREE depleted flows with flat M-to-HREE patterns and lower levels of incompatible elements and they seem to be the result of more extensive degrees of melting. Secondly, there are some LREE enriched flows with $(La/Yb)_{cn}$ >2 which Gariepy *et al.* (op. cit.) grouped with the basalts from the Lower and Middle Series. However closer inspection of the geochemical data reveals them to be subtly different from the Lower basalts, in that they have higher levels of incompatible trace elements and even the least contaminated basalt has a $(La/Nd)_{cn}$ >1

Gariepy *et al.* (op.cit.) proposed that the basalts of the Lower and Middle Series were the result of partial melting of either sub-continental lithosphere or deep mantle blobs. The LREE depleted basalts were interpreted as partial melts of the sub-oceanic asthenosphere. A similar model invoking two distinctive sources has been proposed by Schilling & Noe-Nygaard (1974). However, Wood (1979) has put forward a dynamic partial melting model, involving only one mantle source region, to explain the geochemical variations within the Faeroes lava pile.

6.4.4 Voring Plateau

The DSDP (Leg 38) core samples of the lavas from the Voring Plateau (50-60 Ma - Kharin 1976) have been quite extensively altered, however it is still possible to determine that overall they have relatively high alkali contents and so are more similar to the plateau basalts of the Faeroes and the Hebridean region (Kharin op.cit.), than to MORB. This is especially true of lavas from site 342, which also have flat to slightly depleted LREE signatures. These observations, combined with a depletion in the HREE, confirm the similarities between these basalts and those of the Hebrides and the lower Faeroes basalts. At site 338 more tholeiitic lavas have been found which contain lower levels of incompatible elements and have flat REE patterns (Schilling 1976; Kharin 1976). Schilling (op.cit.) attributed the more LREE enriched basalts to the involvement of a plume source region.

6.4.5 East Greenland

This region represents the largest sub-aerial lava field of the NATIP, covering an area of at least 80 000 km^2. For the purposes of this discussion this predominantly tholeiitic lava field will be divided (from north to south) into three regions; 1/ Wollaston Forland and Hold with Hope; 2/ Scoresby Sund and 3/ Blosseville Kyst.

1. Wollaston Foreland / Hold with Hope

The geochemistry of the lavas from this region has been studied in detail by Upton *et al.* (1984). The Lower Plateau Lava Series (LPLS) are relatively depleted in the incompatible trace elements, and have $(La/Nd)_{cn}$ <1 combined with slightly HREE depleted signatures. In contrast the Upper Plateau Lava Series (UPLS) are much more enriched in the incompatible trace elements and have $(La/Y)_{cn}$ >3. They mostly range from olivine tholeiites to quartz tholeiites, but several more anomalous flows range from olivine tholeiites to alkali olivine basalts and even to basanites. Upton *et al.* (1984) proposed that the depleted lower basalts were formed by large-scale melting at shallow depths within the asthenospheric mantle. It was speculated that the later enriched basalts were the products of deeper off-axis melting of a relatively unthinned lithosphere.

2. Scoresby Sund

Larsen *et al.* (1989) have made an extensive study of these basalts. Most of the succession consists of olivine to quartz tholeiites which could be explained in terms of variable degrees of partial melting of a 'moderately depleted mantle'. These basalts are quite depleted in the incompatible trace elements and have $(La/Y)_{cn}$ ratios ~2. Near

the top of the succession several lavas of MORB type compositions have been erupted and, as would be expected, they have even more depleted trace element signatures and flatter chondrite normalised patterns than the main basalts. In the top-most Igtertiva Formation several of the basalts have a more trace element enriched composition than the main basalts, which Larsen *et al.* (1989) tentatively attributed to an input from recycled basalt or another mantle source.

3. Blosseville Kyst

This sequence basically consists of enriched early picrite flows with steep REE patterns [$(Ce/Yb)_{cn}$ >7] which are overlain by more depleted tholeiites with lower $(Ce/Yb)_{cn}$ = 3-7 (Brooks *et al.* 1976; Brooks & Nielsen 1982; Gill *et al.* 1988). Gill *et al.* (op.cit) noted the occurrence of later tholeiitic dykes which were more depleted than the upper lavas and had lower $(Ce/Yb)_{cn}$ <3.

Gill *et al.* (op.cit) proposed that these lavas were ultimately derived from an asthenospheric source, with the earliest magma batches scavenging incompatible elements from the lithospheric mantle. They suggested that this contamination decreased with time as the fusible lithospheric contaminant was gradually stripped away. The later magmas were therefore interpreted in terms of a decreasing contribution of highly incompatible elements from a progressively thinning lithosphere.

6.4.6 West Greenland / Baffin Island

These lavas cover an area of 55, 000 km^2 and lie on either side of the Baffin Bay/ Davis Straight spreading centre. The sequences basically consist of picrites and tholeiitic picrites which are overlain by more evolved tholeiitic lavas, with a tendency to become more alkaline and more incompatible trace element enriched near the top of the sequence (Clarke 1970; O'Nions & Clarke 1972; Holm *et al.* 1992, 1993; Gill *et al.* 1992).

Holm *et al.* (1993) divided the picrite lavas into three sub-groups; 1/ the earliest picrite lavas on Disco Island have depleted levels of incompatible trace elements, with $(La/Nd)_{cn}$ <1 and $(Sm/Yb)_{cn}$ >1.5. O'Nions & Clarke (1972) also noted the occurrence of LREE depleted picrites in Baffin bay. These magmas were interpreted by Holm *et al.* (op.cit) as being derived from mixtures of MORB and plume source mantle; 2/ the lavas overlying this lowest sequence on Disco are slightly more enriched in the incompatible trace elements and have similar chondrite normalised REE patterns to the lower lavas. Holm *et al.* (op.cit) proposed that these magmas had been generated by melting of the North Atlantic plume; 3/ further north, some of the basal picrites contain levels of incompatible trace elements which are higher than those of the second group (see above). These lavas have steep, LREE enriched chondrite normalised patterns,

and Holm *et al.* postulated that they had been variably contaminated with enriched melts from the lithospheric mantle.

6.5 Concluding remarks

From the above discussion it is apparent that, despite the wide area over which early Tertiary volcanism occurred in the North Atlantic region, similarities exist in the chemistry of the erupted magmas and also in the order which the different types were erupted.

The earliest magmas erupted throughout the whole province appear to have been derived from a mantle source depleted in incompatible trace elements. This depletion is therefore not a feature peculiar to the BTIP but rather appears to be a source characteristic of the NATIP *as a whole.* Figure 6.23 shows chondrite normalised REE patterns of representative samples (all relatively free from crustal and lithospheric contamination) from each of the main lava fields of the North Atlantic early Tertiary Province. The similarity of patterns throughout the region is quite striking, not least the persistent LREE depleted signatures.

If samples with $^{87}Sr/^{86}Sr$ <0.7032 are considered (i.e. those which are relatively uncontaminated) then radiogenic isotopes also point to a *similar* mantle source region throughout the North Atlantic, during the early Tertiary (figure 6.24). Some of the scatter may well be due to contamination by high $^{87}Sr/^{86}Sr$, low $^{143}Nd/^{144}Nd$ basement material. It is, however, also possible that some scatter stems from heterogeneity within the mantle source region. Carter *et al.* (1979), on the basis of Sr and Nd isotopes, concluded that the mantle which supplied the early Tertiary North Atlantic magmas was isotopically similar to the present-day oceanic mantle, and that there was "no evidence for an undepleted source region beneath the continent at this time".

It is also noticeable that, towards the top of the lava succession in Mull, Skye, Ulster, the Faeroes and the Scoresby Sund, the lavas have a tendency to become more MORB-like with respect to their elemental chemistry. This suggests that these magmas formed by shallow and extensive mantle melting at the climax of local lithospheric extension.

The latest magmas in several of these regions, in contrast to the earlier depleted MORB-like lavas, are relatively enriched in the incompatible trace elements. They also have predominantly LREE enriched chondrite patterns with $(La/Yb)_{cn}$ >2. Thus the youngest magmas in Skye (the Beinn Dearg dyke swarm), some of the lavas of the UPLS at Hold with Hope, and the top-most lavas of the Igtertiva Formation, at

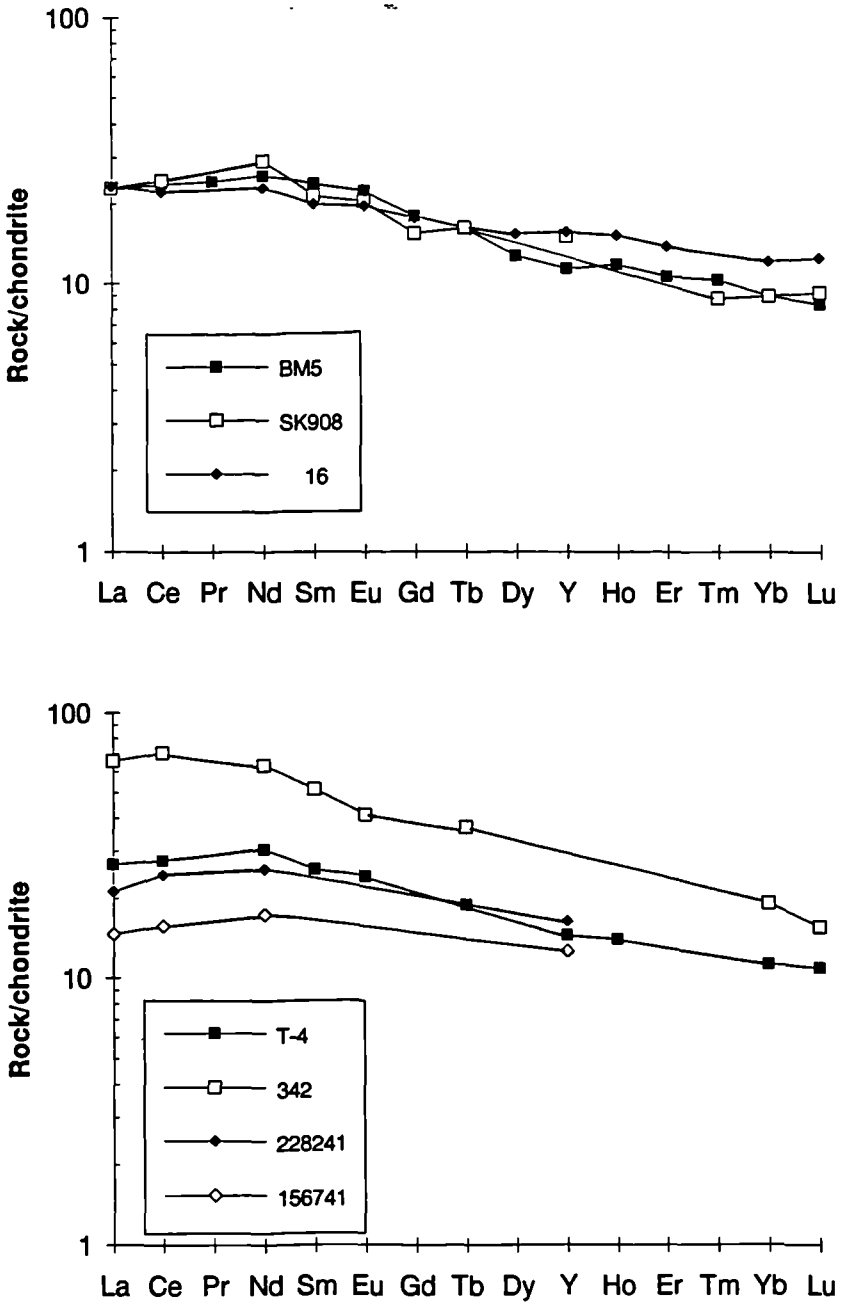


Figure 6.23 Comparative chondrite normalised REE plots (with Y) of early lavas from throughout the NATIP. [BM5 - MPG (this study); SK908 - SMLS (Thompson *et al.* 1982); 16 - LBF, Ulster (Lyle 1985); T-4 - Middle series, Faeroe Islands (Gariepy *et al.* 1983), 342 - Voring Plateau (Schilling 1976); 228241 - Wollaston Forland basalt, East Greenland (Upton *et al.* 1984); 156741 - Ordlingassoq Member, West Greenland].

Scoresby Sund, all have enriched levels of incompatible trace elements, in comparison with the earlier magmas from their respective regions.

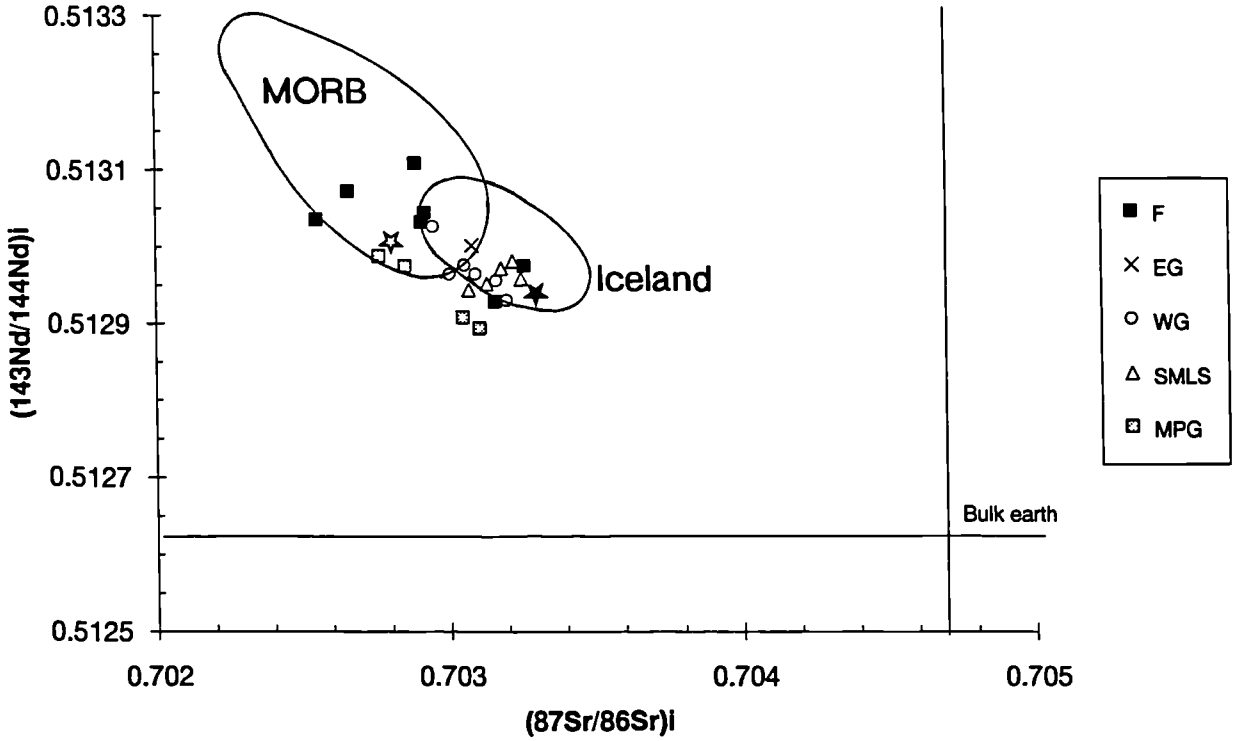


Figure 6.24 Plot of ($^{87}Sr/^{86}Sr$)i vs. ($^{143}Nd/^{144}Nd$)i, for the least contaminated early NATIP lavas. **Key; F** - Faeroe Islands (Gariepy *et al.* 1983); **EG** - East Greenland (Holm 1988); **WG** - West Greenland (Holm *et al.* 1993); **SMLS** (Moorbath & Thompson 1980; Dickin *et al.* 1987); **MPG** (this study), **hollow star** - "sub-Hebridean mantle" Dickin (1981), filled star - composition of the Iceland plume (Holm *et al.* 1993). The fields for MORB (Cohen & O'Nions 1982) and Icelandic basalts (Condomines *et al.* 1983) are also shown.

In conclusion therefore it appears that, when the effects of contamination from both the crust and the lithospheric mantle are excluded, similar patterns in the chemistry of the early Tertiary magmas can be identified from throughout the North Atlantic region. This observation has important implications for the nature of the early North Atlantic Plume (ca >50 Ma) and these will be discussed in the closing chapter.

Chapter 7

Lava sequences and geochemical correlations.

As was noted in Chapter 2 the lava field has not been mapped. Nevertheless, chemically distinctive units of flows have been found (section 4.4), and an attempt has been made to correlate these across the succession. This chapter also discusses the geochemical variation exhibited by the lava succession, from the coast to the top of Ben More (970m asl). Finally, the nature of the vents from which the lavas erupted will be briefly considered.

7.1 Geochemical correlations

The Mull lava succession today covers an on-land area of 840km^2, and the curved line along which the correlation has been attempted is approximately 60km in length. This line of section stretches from Morvern (MR) in the east, to Beinn Reudle (BR) in the west, terminating at Carsaig (C) in the south (figure 7.1; in the back pocket of the thesis). It is, however, important to note that all but three of the lava sequences under consideration (MR, T and C) are in western Mull, along a 30km line of section. Therefore, the most *dependable* correlations are likely to be between these more westerly sections. The Croggan peninsula (CA section) has not been included in the correlation diagram (figure 7.1), due to the fact that it lies ~25km away from the next nearest section (figure 2.2). The short section collected at A'Mhaol (AM) on the lower slopes of Ben More (NM458327) has also not been included. This is because this shorter section was collected from the opposite side of the valley to the BHL sequence, and displays very similar geochemical variation up sequence.

Lyle (1988) has used field, petrographic and geochemical criteria from the Tertiary Upper Basalt Formation in Northern Ireland to correlate groups of flows. This was over 30-40km, i.e. a similar distance to the correlation attempted in this study. However, Myers *et al.* (1990) in South Africa, and Larsen *et al.* (1989) in East Greenland, have correlated geochemically distinctive lava units over hundreds of kilometres.

With the exceptions noted above, figure 7.1 shows the geochemical variation with stratigraphic height of the lava sections collected. The lavas have been subdivided on a *geochemical* basis (Chapters 4 & 5) and each geochemically distinctive unit of flows has been assigned a letter, with 'A' representing the lowest unit, 'B' the next unit

and so on. From figure 7.1 it can be seen that the most common lava sub-type of the MPG, are those basic flows which have been contaminated with continental crust *en route* to the surface (section 4.4). The lower parts of the sequences from all over the lava field appear to be composed of this type of flow. Bearing in mind that only a few minor faults cut the lava field, and that the lavas generally preserve shallow dips (<5°; figure 1.1) a tentative correlation across the succession has been attempted (figure 7.1).

Correlation between the primitive crustally contaminated flows

The sections BHL, B, UV[1] and BCH and the lower part of BM lie within an area of 15km diameter and this obviously is a good place to start to correlate the successions. Figure 4.19 shows that the units **BR**-B, **BHL**-B, **BM**-B & D, **B**-D and **BCH**-D, all have a similar incompatible trace element geochemistry. In figure 7.2 the F/F+M ratio in the BM-B/D, BR-B, BCH-D and B-D sections is plotted against height (as represented by increasing sample numbers). From these four diagrams two interesting points may be noted: firstly, the base of each of these units seems to be marked by flows with F/F+M >0.5, which gives way up the succession to more primitive flows (F/F+M ≤0.5); secondly, near the top of these units the flows have a tendency to become more evolved once again. These common features between the different units, combined with both their relatively uniform incompatible element signatures and the similar stratigraphic height of each section, strongly suggest that, at least in western Mull, this unit can be correlated over quite a wide area.

The correlation of these units with the MR and T sections is more tentative. These sections have units (T-C and MR-B) low in their sequences with similar geochemical signatures to BR-B etc. in western Mull. However, as figure 7.2 reveals, these units do not become more evolved up sequence. Nevertheless, such evidence as there is at present tends to support the existence of a 1-200m thick sequence of Mg-rich crustally contaminated basalts at a low stratigraphic level throughout the Mull lava succession. This is not to say that all the lavas forming this sequence were erupted from the same fissure or vent. Indeed the presence of units in the eastern portion of the lava field with slightly different patterns of geochemical evolution towards the top, points to the existence of several or more eruptive vents for this unit. This sequence of crustally contaminated basalts seems to be thicker on the peninsula to the east of Ben More where it attains a thickness of over 150-200m, a feature which points to the close proximity of the eruptive vent.

[1]Although only 11 samples were collected from this section, Fawcett (1961) analysed some samples from further up Beinn na Drise (NM475427) and these appear to be crustally contaminated basalts, similar to UV5-11 (present study).

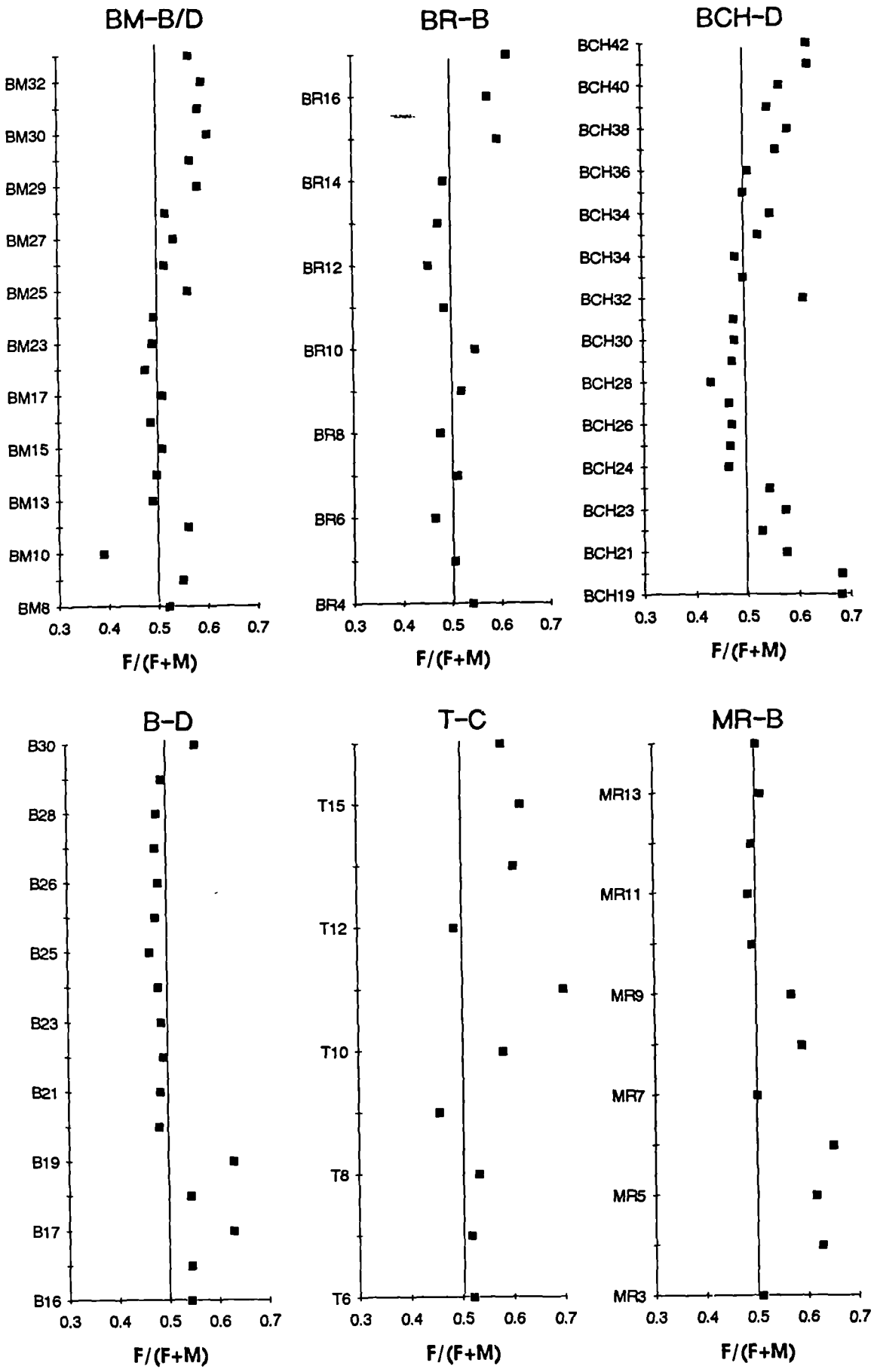


Figure 7.2 Variation of F/(F+M) with height (increasing sample no.) for crustally contaminated lava units, occurring near the base of the succession. See text and figure 7.1 for further details.

Correlations between more evolved (~5-8% MgO) uncontaminated flows.

These flows also form distinct units within the stratigraphic successions. However, unlike the more basaltic units, with which they are interbedded, they frequently have quite a localised occurrence and even some relatively thick units seem to die out laterally quite rapidly. In figure 7.1, it can be seen that unit B-C (here over 100m thick) seems to completely die out in a northerly direction, and it cannot be found at all in the BHL section, which is only 6-7km away. Likewise, a geochemically equivalent unit to BM-C cannot be found in the BHL section, and this despite the fact that the two sections were collected on either side of a valley, less than 2km apart. This lack of lateral continuity is probably due to these more-evolved magmas having higher viscosities and less-voluminous eruptions than their more basaltic counterparts.

As was noted in section 4.4, these different lava units, and flows of geochemically distinct types, are often interleaved. This phenomenon is particularly common at the base of the lava succession, especially in the UV, BCH, BHL and B sections (figure 7.1), but it can occur anywhere within the stratigraphic sequence. This feature suggests that these chemically distinctive flows issued from separate eruption vents, at approximately the same time. It has been argued in section 4.4 that this characteristic of the lava succession militates *against* the presence of one large magma chamber beneath Mull.

Correlation of individual flows

Only where individual sections are in close proximity to each other can individual flows be correlated. When sections from the same general area are examined only a few flow can be matched up with any degree of certainty.[2] Between the BB and the BR section BR18 and BB4 are quite chemically similar and perhaps represent the same flow. The same is true of pairs of flows from the BHL and AM sections (which have been collected up either side of a valley) and flows BHL16 and AM9 are chemically similar, as are BHL14A and AM6.

7.2 Temporal geochemical variation during the development of the lava succession

Figure 7.3 shows composite geochemical sections (Ti/Zr, MgO & $(Ba/Nb)_{pmn}$) of the lava succession, as exposed from the base of the pile at Gribun to the top of Ben

[2] A similar situation has been found within the Parana flood basalt province in South America, i.e poor correlations of distinctive flows between sections, but good correlations between geochemically distinctive flow units (D. Peate pers.comm).

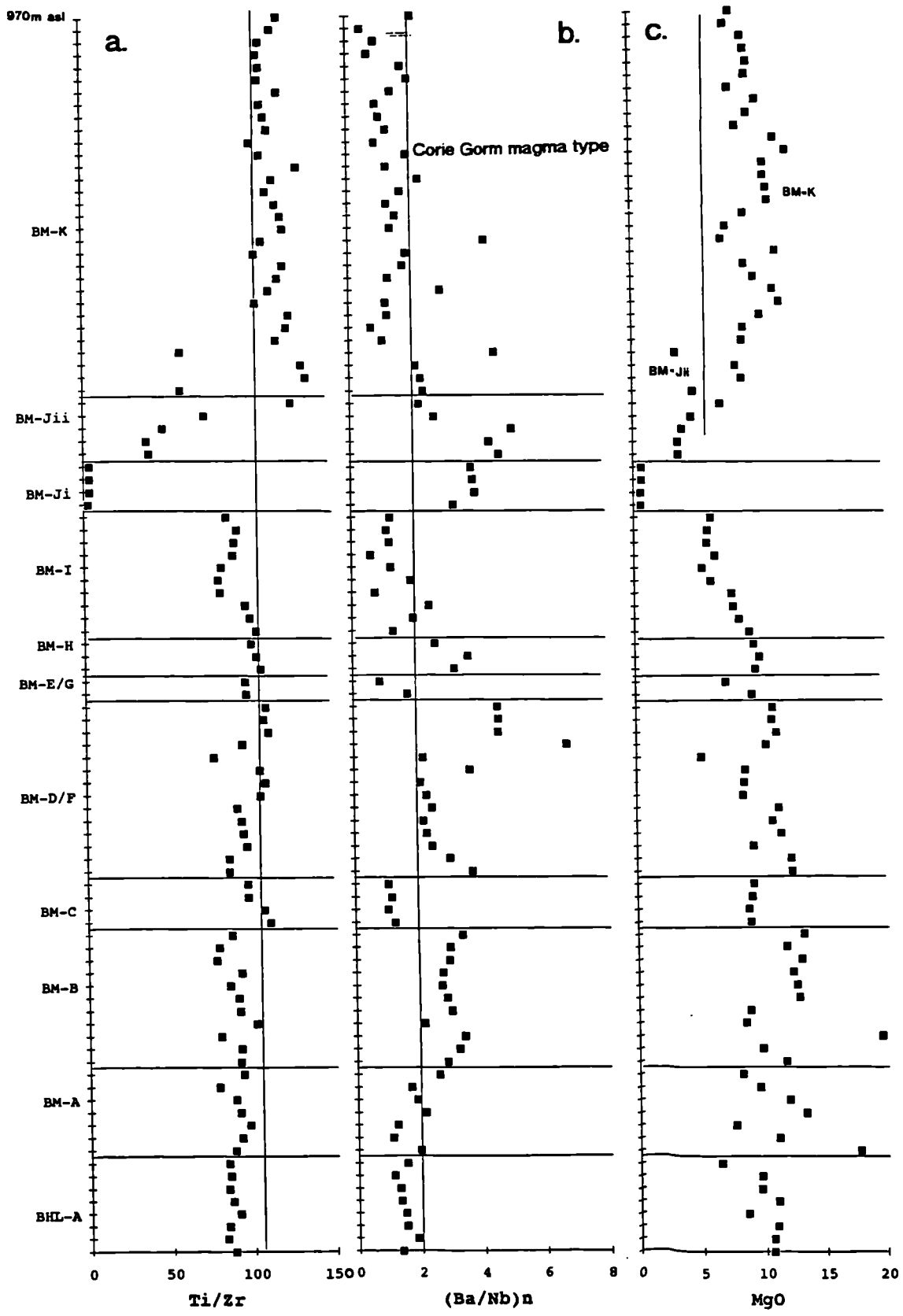


Figure 7.3 Composite geochemical sections [Ti/Zr, MgO & $(Ba/Nb)_{pmn}$] of the lava succession from Gribun to the top of Ben More. Each point marks the composition of an individual flow and horizontal lines indicate junctions between flow units (figure 7.1).

More. The geochemical data used in figure 7.3 have been compiled using the BHL section (unit BHL-A) and the two Ben More sections (figure 7.1).

However, before these geochemical sections are considered in detail, it is important to note that the Staffa and Ulva Ferry sub-types[3] of the MPG are not to be found in the Gribun to Ben More summit section. As has already been noted, these two sub-types occur near the base of the succession, like the Enriched MPG (EMPG; section 4.5). Table 7.1 summarises the occurrence of these types throughout the succession.

Section	SMT	UFM	EMPG	Stratigraphic order
MR, BR	-	-	-	-
T, A, BCH	present	-	-	-
UV	present	present	-	SMT overlain by UFM
BHL	-	-	present	-
BM	-	-	present	-
B	present	present	present	SMT overlain by UFM, 1 EMPG flow well up succession
C	present	-	present	EMPG overlain by SMT

Table 7.1 The occurrences and stratigraphic order of the magma sub-types; SMT, UFM and EMPG.

From this table it can be seen that, where the SMT and the UFM occur in association (i.e. the B and UV sections) the UFM always overlies the SMT. The relationship between the EMPG and the SMT is, however, more enigmatic. In the Carsaig (C) section the EMPG flows quite clearly lie below the SMT (figure 7.1). However, in the Bearraich (B) section, the one EMPG flow lies well above the SMT flows. It therefore appears that, in the initial stages of the development of the Mull lava succession, some magma batches were contaminated with sub-continental lithospheric mantle (EMPG) and, as proposed by Thompson *et al.* 1986, some ascended along lines of crustal weakness and ponded and fractionated at shallow depths (SMT). Other magma batches found it difficult to penetrate the cold lithosphere and so ponded and fractionated deep within the lithospheric mantle (UFM).

Returning to consideration of figure 7.3, another compositional feature of the early stages of volcano development is the eruption of basic magmas relatively uncontaminated [$(Ba/Nb)_{pmn}$ <2] with continental crust, eg. BM-A. Similar primitive

[3]See Chapter 5 for the geochemistry of the Staffa Magma sub-Type, and section 4.3 for a geochemical account of the Ulva Ferry mugearites.

uncontaminated lavas can be found near the base of the MR, T, BHL and B sections (see Chapter 4).

In Chapter 6 it was demonstrated that the lavas which occur near the top of Ben More are probably the result of more extensive melting, of a different mantle source region, than that which produced the earlier MPG. As figure 7.3a shows one of the most striking geochemical features of this Coire Gorm (CG) magma type is its elevated (>105) Ti/Zr ratios, in contrast to the lower values (<105) of the earlier MPG.

Figure 7.3b shows how $(Ba/Nb)_{pmn}$ varies with stratigraphic height. As was shown in section 4.4, in the absence of isotopic data this ratio provides an accurate assessment of the extent of crustal contamination (figure 4.32). Turning first to consider the MPG, it is obvious that contaminated and uncontaminated units alternate up the succession (figure 7.1 also establishes this point). The most basic magmas (figure 7.3c) tend to be the most contaminated. However, a notable exception is the group of trachytes and mugearites two-thirds of the way up the succession, which appear to be quite contaminated. In section 4.3 it has been proposed that these magmas, unlike the more basic magmas, have assimilated crustal material *during* fractional crystallisation i.e. AFC. On first sight it appears that the CG magma type are relatively uncontaminated with continental crust, however, it should be remembered that these lavas are quite extensively altered and therefore Ba may have been leached from the rock, so lowering the Ba/Nb ratio. Nevertheless, one *would* expect the CG magmas to show less crustal contamination, simply because the earlier MPG magmas would have scavenged most of the more-fusible crustal material. This remains uncertain, and possibly the only way the problem can be resolved is by a study of the Nd isotopes.

Figure 7.3c reveals the way in which MgO content varies up succession. For the most part, up to unit BM-B, the MgO content lies between 8 and 13%. Above this unit, however, the MgO content gradually falls, culminating in trachytes and mugearites (unit BM-J), presumably as the magma supply from the mantle diminishes. The CG magma type (unit BM-K) marks a return to more basic compositions (8-12% MgO) and, as has been proposed in Chapter 6, represents the onset of a new phase of mantle melting.

7.3 Eruptive vents

The nature of the vents from which these lavas erupted has, in the past, been quite a 'bone of contention'. As was pointed out in section 1.1, in the late 18th century two

rival theories grew up in an attempt to explain the eruptive mode of the lavas. Judd (1874 & 1889) proposed that these Hebridean lavas had mostly been erupted from one large central vent, with a few parasitic side vents. Gekie (1867 & 1888) held that the MPG magmas chiefly erupted through numerous fissures, now represented by the extensive Mull dyke swarm. He also proposed that preferential eruption along a localised portion of a fissure could lead to the formation of a near-circular vent.

Delaney & Pollard (1982) and Bruce & Huppert (1990) in several general studies of the flow of basaltic magma through conduits, proposed that magma flowing through a narrow (<1-2m) fissure will loose heat, by conduction to the surrounding country rock. As a result, magma solidifies on the walls. Soon the flow of magma will becomes constricted and, in a matter of days (Bruce & Huppert 1990), the fissure becomes completely blocked. In fissures with wider initial widths the supply of heat from the flowing magma can, after a while, exceed the heat that is lost by conduction. In such a situation the magma which has initially solidified on the walls of the conduit will be progressively melted away.

The calculations of Delaney & Pollard (1982) and Bruce & Huppert (1990), suggest that the critical fissure width, determining which of these two flow regimes will operate, is of the order of 1-2m. Bruce & Huppert (op.cit) additionally proposed that, close to this critical value, fissures may become only partially blocked, resulting in the formation of one or more isolated eruptive vents.

Although no dykes have been discovered on Mull which are seen to directly feed a lava flow (Bailey *et al.* 1924) over half of the dykes from the Mull swarm, are in excess of 2m in width (Lamacraft 1978). This fact strongly suggests that many of these dykes did in fact act as feeders of the lava pile. The presence of a few basaltic plugs throughout the lava field, especially in northern Mull and Morvern, points to initial eruptions along fissures. Solidification along most of the length of such a fissure would have led, in time, to localised eruptions from a near-circular vent, as envisaged by Gekie (1888). Cann (1965) studied the thermal metamorphism around one of the largest of these; the 'S Airde Beinn plug (NM472540). He showed that the plug had extensively thermally metamorphosed the surrounding basalts, an observation consistent with the 'S Airde Beinn plug having acted as a substantial feeder to the lava pile.

7.4 Conclusions

In conclusion this chapter has shown that many of the lava sections collected during the present study have chemically distinct units, which can be correlated across the succession. Vertical chemical variations within the section from Gribun to the top of Ben More demonstrate that the MPG lavas become more evolved nearer the top of the

succession. They are followed by a chemically different magma type (CG), which may well represent the onset of a new phase of mantle melting.

Chapter 8

Concluding discussion

8.1 Summary

This thesis has attempted to assess how two main petrogenetic spheres, namely magmatic plumbing processes and mantle sources, changed and evolved as the Mull volcano developed.

Field investigations (Chapter 2) during the course of this study have chiefly been concerned with the collection of ~500 lava samples, on a flow-by-flow basis, from sixteen different sections throughout the lava field. Some of the red interlava horizons, which most previous workers in the Hebridean region had ascribed to in-situ weathering of flow tops, have been reinterpreted as being of a pyroclastic origin. The average thickness of lava flows from the Mull Tertiary succession is of the order of 5-7m.

Petrographic observations and mineral chemistry are discussed in Chapter 3. The progressive appearance of (micro)phenocrysts of olivine (with included Cr-spinel), olivine (without Cr-spinel), plagioclase, Fe-Ti oxides, apatite and sodic alkali feldspar phenocrysts, with falling MgO content, are consistent with an origin by fractional crystallisation.

The effects of post-magmatic, hydrothermal alteration on the primary mineral phases are an obvious feature of the lavas throughout the succession. This alteration grades from greenschist facies near the central complex, to less intense zeolite facies alteration (mesolite) near the periphery of the island. The effects of this alteration on the whole rock geochemistry are investigated in detail in section 4.1. The elevated Sr values of some of the MPG basalts appear to be caused by the high Sr contents of interstitial secondary zeolites, and leaching experiments, in order to extract the secondary minerals, have proved this point. The work of Morrison (1979) has shown that, under conditions of zeolite facies alteration, only Rb and Sr appear to be mobile. However, with more intense alteration, more elements are mobile. Potential sub-solidus elemental mobility has, therefore, been taken into account during the petrogenetic studies.

The lavas of the MPG are mostly transitional tholeiitic-alkalic basalts (section 4.2), implying that they last equilibrated at ~10kb, i.e. at pressures too high for the low pressure silica saturation thermal barrier to exist. MPG lavas with 13-14% MgO have been found, and these contain olivine phenocrysts with up to Fo_{89}. These olivine

phenocrysts are, for the most part, in equilibrium with their host lava, suggesting that the parental magmas of the MPG lavas contained at least 13-14% MgO.

Modelling of differentiation processes (section 4.3) shows that the fractionation of Cr-spinel (<0.5%), olivine (~5%) and high-pressure augite (~2%) from one of these parental magmas is required, in order to produce the composition of an MPG magma containing 10-11% MgO. Chemical constraints (*both* major and trace elements) appear to demand the high-pressure fractionation of augite from these magmas, despite the fact that it is rarely found as a phenocryst phase. This can be explained by proposing that, either these high-pressure phenocrysts dissolved on their way to the surface (Thompson 1974), or that pyroxene crystallised *in-situ* on the walls of the chamber and so was not easily erupted. Differentiation of moderate-MgO magmas to low-MgO magmas and hawaiites requires the removal of olivine (~13%), plagioclase (~8%) and aluminous sub-calcic augite (~18%).

With increasing differentiation to trachytic residua (with peralkaline tendencies), titanomagnetite, apatite, biotite and alkali feldspar progressively become liquidus phases. It is proposed that most of these evolved magmas (which occur near the top of the succession) have undergone AFC-type process within the crust. Near the base of the succession, several mugearites with depleted Y and HREE contents are found. It is likely that these magmas fractionated an assemblage of minerals including garnet, deep within the lithospheric mantle (>55km), at an early stage in the evolution of the volcano.

In section 4.4 elemental **and** isotopic evidence have been presented which strongly favour contamination of the most MPG basic magmas with acidic partial melts of Lewisian lower crust. In all probability this contaminant was quite enriched in Ba and K_2O. Lewisian pegmatite veins, with a high modal proportion of alkali feldspar, most closely approximate to the chemical composition of the proposed assimilant. This assimilation occurred with little concomitant fractional crystallisation, and appears to have been facilitated by the turbulent ascent of magma through thin dyke- and sill-like magma chambers (Assimilation during Turbulent magma Ascent - ATA). These chambers had high surface-to-volume ratios. Contamination with (<5%) acidic partial melt of Lewisian crust has caused these basalts to have higher Ba, K_2O, LREE and $^{87}Sr/^{86}Sr$, and lower $^{144}Nd/^{143}Nd$, than some less-contaminated basalts.

The more evolved MPG basalts (<8% MgO) and basaltic-hawaiites have, on the whole, lower levels of Ba, K_2O and $^{87}Sr/^{86}Sr$, and higher $^{144}Nd/^{143}Nd$, than the more basic lavas. These factors strongly imply that the more evolved lavas are less contaminated with continental crust. Therefore, these basalts probably reached their evolved compositions within the lithospheric mantle rather than the crust, possibly ponding and fractionating at the density discontinuity represented by the MOHO.

When they eventually passed through the crust they appear to have been too cool to assimilate much material.

Although most of the basalts and hawaiites of the MPG fall into one of the two groups outlined above, several exceptions do occur:

1. Some of the more mafic MPG lavas (>10% MgO) near the base of the succession display little geochemical signature of crustal contamination, and probably passed through the crust in the early stages of volcano growth, while the it was still relatively cold.
2. Several basaltic-hawaiites appear to have assimilated some crustal material, suggesting that they have perhaps undergone AFC type processes, within the crust.

In section 4.5 it has been demonstrated that contamination of some of the earliest MPG magmas with a small-fraction-melt from the lithospheric mantle, has led to an enrichment of their incompatible trace element contents. This enriched contaminant may well be residual from the Permo-Carboniferous magmatic event, since the use of a Permo-Carboniferous lamprophyre to model the observed enrichment works rather well.

Therefore, in Chapter 4, three sub-types of the MPG are identified;

1. Magmas which have been contaminated with Lewisian crust,
2. Magmas contaminated with an enriched small-fraction-melt from the lithospheric mantle.
3. Those magmas which are uncontaminated with either crust or lithospheric mantle.

Chapter 5 investigates the geochemistry of the tholeiitic Staffa Magma sub-Type (SMT). It has been shown that the SMT probably represents some batches of MPG magma which ascended along a zone of crustal weakness to a high-level magma chamber (within Moinian crust), where they underwent AFC-type processes.

In addition to the MPG, two other magma types with more depleted trace element signatures have been identified (Chapter 6). The first, the Coire Gorm (CG) magma type, lies stratigraphically above the trachytes on Ben More, and is characterised by higher (>105) Ti/Zr ratios and flatter REE patterns than the MPG. Also lying stratigraphically above the MPG, and the CG type, are flows of the Central Mull Tholeiite type (CMT). The CMT have similar middle-to-heavy REE contents to the CG type, they have, however, more depleted LREE and other incompatible element contents.

It has been concluded that the MPG magmas were ultimately derived by decompression melting of an upwelling, relatively depleted, spinel-garnet lherzolite source region, with a potential temperature of 1420-1460 °C. The compositions of the erupted magmas represent pooled melts, from throughout the vertical height of a melting column. The later CG and the CMT magma types may have been derived from more extensive melting of slightly enriched mantle, with most melting occurring in the spinel lherzolite stability field. Lithospheric thinning has therefore resulted in melting at increasingly shallower depths, as the magmatic system developed. Mantle potential temperatures of 1420-1460 °C, are entirely consistent with the presence of a plume beneath Mull at ~60Ma.

Units of flows of distinctive chemistry interdigitate up sequence, as do individual flows (Chapters 4 & 7). This feature of the lava succession implies that the Mull lava field was not fed by one large magma chamber. Instead it suggests the existence of a poorly connected network of thin dyke-and sill-like magma chambers, feeding each chemically distinctive lava unit. Some of the lava units with higher MgO contents (>8%) can be correlated across the succession. However, units of lower-MgO basalts and basaltic-hawaiites, are not easily correlated between sections, suggesting that these flows were less voluminous and more viscous, than their more basaltic counterparts.

8.2 The initial composition of proto-North Atlantic plume.. depleted or what?

In section 4.5 it was observed that, after those lavas which are contaminated with crust or lithospheric mantle have been *excluded* from consideration, similar patterns could be observed in the chemistry of the early Tertiary lavas from all over the North Atlantic region.

One of the most noticeable features of the earliest *uncontaminated* lavas throughout the area is, as figure 6.23 demonstrates, the fact that they have relatively depleted levels of incompatible elements.. The depleted nature of the early Tertiary Hebridean lavas has long been recognised, eg. Ridley (1971), Morrison (1979) and Morrison *et al.* (1980). Morrison *et al.* (op.cit) and Thompson & Morrison (1988) have proposed that this depletion was due to the extraction of an incompatible element enriched small-fraction-melt from the source region during the Permo-Carboniferous (see section 6.1.3 for a fuller review of Morrison *et al.* 1980 and Thompson & Morrison, 1988). However, the recognition of such a signature in the early lavas *throughout* the proto-North Atlantic region, would seem to require a wider explanation than depletion of the source region in the Permo-Carboniferous, and suggests that it may be a feature of the

plume source. Elementally depleted plume signatures have also been reported from Gorgona (Aitken & Echeverria 1984), related to the Galapagos plume, and from Mauna Kea, Lanai and Koolau on Hawaii (Leeman *et al.* 1980, Budhan & Schmitt 1985).

Recent modelling and observations of plume behaviour (eg. Davies 1990; Campbell & Griffiths 1990, 1992; Griffiths & Campbell 1990, 1991; Loper 1991) highlight important factors which can influence the composition of plume related magmas. It now seems to be widely agreed that plumes ascend from the Core-Mantle Boundary (CMB)[1] (see above references and R.A. Kerr 1991). Loper & Stacey (1983) state the case very succinctly: *'D" and core heat provide the only plausible driving forces for plumes, and the plumes provide the only satisfactory mechanism for the removal of core-heated material from D".'*

If this is so, why do the earliest melts from the proto-North Atlantic plume, as represented Tertiary lavas, have a depleted geochemical signature?

1. A contribution from depleted lithospheric mantle?

The cold, rigid lithosphere can only be heated by conduction, or by infiltration of plume derived melts. Therefore, it is unlikely to contribute significantly to continental flood volcanism (Campbell & Griffiths 1990, 1992 and White & McKenzie 1989), unless more-fusible, enriched, small-melt-fractions are present (eg. A.C. Kerr 1993; Thompson *et al.* 1993). In the light of subsequent studies, is doubtful therefore, whether the depleted signature of the Hebridean basalts can be the result of substantial contamination of enriched plume melts, by depleted lithospheric mantle, as proposed by Thompson & Morrison (1988).

2. Interaction with MORB-source upper mantle?

The depleted LREE patterns and $^{87}Sr/^{86}Sr$ and $^{144}Nd/^{143}Nd$ ratios (figure 6.24) of these uncontaminated early Tertiary basalts, bear compositional similarities to MORB. It is therefore possible that these basalts represent melting of a mixture of upwelling OIB mantle and an upper mantle MORB source region. However, Loper & Stacey (1983) and Griffiths & Campbell (1990) have proposed that the material entrained into a plume head - from which the earliest decompression melts are derived - is predominantly from the *lower* mantle. This means that the upper mantle contribution to plume related volcanism will be relatively insignificant.

[1] The D" layer.

3. A depleted plume from the lower mantle?

The upwelling mantle material in the plume head, which undergoes decompression melting, will be a mixture of material from just above the CMB and entrained lower mantle. Two possibilities therefore exist; either the compositional characteristics of the initial melts from the proto-North Atlantic plume are due to entrained, depleted lower mantle material, or the depletion stems directly from the plume source region (i.e. the CMB).

The source material of plumes, at the CMB, is believed to represent subducted lithosphere that descends to the lowermost mantle (Hill 1990). Hill (op.cit) also proposed that significant amounts of this subducted material becomes partially mixed into the lower mantle. The enriched trace element and isotopic composition of most OIB lavas, strongly suggests that the material available for sampling by plumes at the CMB is, of an "enriched" composition (Campbell & Griffiths 1992). Nevertheless, the presence of depleted mantle plumes is consistent with the idea that some of the material at the CMB, and within the lower mantle, may be depleted. The depleted nature of the source region of early Tertiary lavas, during the opening of the North Atlantic, has been recognised by Carter *et al.* (1979). In study of the W Greenland picrites Holm *et al.* (1993) proposed that the proto-North Atlantic plume had a "depleted signature".

The reason why the Hebridean lavas are depleted, would seem not to be the result of an enriched melt being extracted from their *source region* in the Permo-Carboniferous. Rather, the asthenospherically derived Permo-Carboniferous magmas (Smedley 1988) appear to have stripped out the enriched, most and fusible parts of the lithospheric mantle, so leaving little to contaminate the depleted melts from the proto-North Atlantic plume. Therefore, this study proposes that the Permo-Carboniferous magmatic event, although playing a different role from that envisaged by Morrison *et al.* 1980, can nonetheless explain why depleted magmas are more common in the BTIP than the rest of the North Atlantic region.

In concluding this section it appears that the initial nature of the proto-North Atlantic plume, was either caused by a depleted source region above the CMB, or by entrainment of depleted material from the lower mantle, by the head of the starting plume.

8.2.1 Compositional variation of the North Atlantic plume, with time.

The descent of a range of subducted lithospheric material into the lower mantle means that a potentially diverse plume source exists, in both the lower mantle and at the CMB. Because of this it is highly unlikely that plumes retain the same geochemical

signature over their entire lifetime (eg. R.A. Kerr 1991; Davies 1990). In this regard, White & Cheatham 1990) have discovered that epsilon Nd values change from +7 at the Deccan end of the Chagos-Laccadive Ridge to +4 at Reunion, suggesting that the geochemistry of the Reunion plume has changed with time. Similarly the presence of both LREE depleted and enriched basalts on the Hawaiian Islands (Leeman *et al.* 1980, Budhan & Schmitt 1985) supports the concept of variable plume compositions with time.

Holm *et al.* (1993) seem to suggest that the composition of the Icelandic (proto-North Atlantic) plume has remained essentially constant over the last 60Ma. However, the recognition in the North Atlantic Tertiary Igneous Province of depleted early plume melts, and later enriched plume melts (section 6.5) suggests that the composition of the plume has changed with time. Likewise, isotopic and trace element variations among the Icelandic basalts (Hemond *et al.* 1993, Condomines *et al.* 1983), are consistent with a secular variation in the composition of the plume source (Hemond *et al.* 1993, Campbell & Griffiths 1992)

8.3 Possible future work

Aspects of the Tertiary igneous geology of the Isle of Mull, especially parts of the Central intrusive complex, have received little attention since the study of Bailey et al. (1924) and obviously significant scope exists to elucidate the geochemical nature of these high-level magma chambers.

This thesis has chiefly been concerned with the geochemistry of the lavas outside the central complexes. Nevertheless, the brief study made of some of the central lavas has shown that, despite their altered nature, some useful petrogenetic information can be derived from them. Detailed mapping and geochemical analysis (perhaps with the use of Nd isotopes) of the lavas within the central complex, should help to further constrain the temporal variation of the three Mull lava types identified in this study.

Further work in attempting to relate the geochemical characteristics of the Hebridean lavas to the magmatism in the rest of the North Atlantic Igneous Province is possible *if* lavas with suspected lithospheric contamination are firmly *excluded* from consideration. These 'clean' lavas (and dykes) can provide an invaluable geochemical window into the composition of the plume source and how it varies with time.

References cited in the text

ALLWRIGHT, E.A., 1980. The structure and petrology of the volcanic rocks of Eigg, Muck and Canna, N.W. Scotland. Unpublished M.Sc. Thesis, University of Durham.

AHERN, J.L. & TURCOTTE, D.L. 1979. Magma migration beneath an ocean ridge. *Earth and Planetary Science Letters,* **45,** 115-122.

AITKEN, B.G. & ECHEVERRIA, L.M. 1984. Petrology and geochemistry of komatiites and tholeiites from Gorgona Island, Colombia. *Contributions to Mineralogy and Petrology,* **86,** 94-105.

ANDERSON, F.W. & DUNHAM, K.C. 1966. The geology of northern Skye. *Mem. Geol. Surv. G.B., Scotland.*

ARGYLL, DUKE OF 1851. On Tertiary leaf beds in the Isle of Mull. *Quarterly Journal of the Geological Society, London,* **7,** 89--103.

BAILEY E.B., CLOUGH, C.T., WRIGHT, W.B. RICHEY, J.E. & WILSON, G.V. 1924. Tertiary and post-Tertiary geology of Mull, Loch Aline and Oban. *Mem. Geol. Surv. G.B., Scotland.*

BAMFORD, D., NUNN, K., PRODEHL, C. & JACOB, B. 1977. LISPB-III. Upper crustal structure of Northern Britain. *Journal of the Geological Society, London,* **133,** 481-8

BAXTER, A. N. 1987. Petrochemistry of late Palaeozoic alkali lamprophyre dykes from N Scotland. *Transactions of the Royal Society of Edinburgh: Earth Sciences,* **77**(for1986), 267-277.

BAXTER, A. N. & MITCHELL, J.G. 1984. Camptonite-Monchiquite dyke swarms of Northern Scotland; age relationships and their implications. *Scottish Journal of Geology,* **20,** 297-308.

BECKINSALE, R.D., PANKHURST, R.J., SKELHORN, R.R. & WALSH, J.N. 1978. Geochemistry and petrogenesis of the Early Tertiary lava pile of the Isle of Mull, Scotland. *Contributions to Mineralogy and Petrology,* **66,** 415-427.

BELL, B.R. 1984. The basic lavas of the Eastern Red Hills district, Isle of Skye. *Scottish Journal of Geology,* **20,** 73-86.

BELL, B.R. & HARRIS, J.W. 1986. An excursion guide to the Geology of the Isle of Skye. Geological Society of Glasgow. p317.

BELL, B.R. & CLAYDON, R.V. 1992. The cumulus and post-cumulus evolution of the chrome-spinels in ultrabasic layered intrusions: evidence from the Cullin Igneous Complex, Isle of Skye, Scotland. *Contributions to Mineralogy and Petrology,* **112,** 242-253.

BELL, B.R., CLAYDON, R.V. & ROGERS,G. 1993. The petrology and geochemistry of cone-sheets from the Cuillin Igneous Complex, Isle of Skye: Evidence for combined assimilation and fractional crystallisation during lithospheric extension. Submitted to *Journal of Petrology.*

BLICHERT-TOFT, J., LESHER, C.E. & ROSING, M.T. 1992. Selectively contaminated magmas of the Tertiary East Greenland macrodyke complex. *Contributions to Mineralogy and Petrology,* **110,** 154-172.

BOTT, M.H.P. 1988. A new look at the causes and consequences of the Icelandic hot-spot. In: *Early Tertiary Volcanism and the Opening of the NE Atlantic.* Morton, A. C. and Parson, L. M. eds. Geological Society Special Publication, no. **39,** 15-23.

BOWEN, N.L. 1928. *The evolution of the igneous rocks,* Princeton University Press.

BROOKS, C.K., NIELSEN T.D.F. & PETERSEN, T.S. 1976. The Blosseville Coast basalts of E Greenland: Their occurrence, composition and temporal variations. *Contributions to Mineralogy and Petrology,* **58,** 279-292.

BROOKS, C.K. & NIELSEN T.D.F. 1982. The East Greenland continental margin: a transition between oceanic and continental magmatism. *Journal of the Geological Society, London,* **139,** 265-275.

BRUCE, P.M. & HUPPERT, H.E. 1990. Solidification and melting along dykes by the laminar flow of basaltic magma. In: *Magma Storage and Transport;* Ed. M.P. Ryan. Published by J. Wylie and Sons. p87-101.

BRYAN, W.B. 1983. Systematics of modal phenocryst assemblages in submarine basalts: Petrologic Implications. *Contributions to Mineralogy and Petrology,* **83,** 62-74.

BRYAN, W.B., FINGER, L.W. & CHAYES, F. 1969. Estimating proportions in petrographic mixing calculations by least squares approximation. *Science,* **163,** 926-927.

BUDAHN, J.R. & SCHMITT, R.A. 1985. Petrogenetic modelling of Hawaiian tholeiitic basalts: a geochemical approach. *Geochimica et Cosmochimica Acta,* **49,** 67-87.

CAMPBELL, I.H. 1985. The difference between oceanic and continental tholeiites: a fluid dynamic explanation. *Contributions to Mineralogy and Petrology,* **91,** 37-43.

CAMPBELL, I.H. & GRIFFITHS, R.W. 1990. Implications of mantle plume structure for the evolution of flood basalts. *Earth and Planetary Science Letters,* **99,** 79-93.

CAMPBELL, I.H. & GRIFFITHS, R.W. 1992. The changing nature of mantle hot-spots through time: Implications for the chemical evolution of the mantle. *Journal of Geology,* **92,** 497-523.

CANN, J.R. 1965. The metamorphism of amygdales at 'S Airde Beinn, northern Mull. *Mineralogical Magazine,* **33,** 533-562.

CARTER, S.R., EVENSEN, N.M., HAMILTON, P.J. & O'NIONS, R.K. 1978. Neodynium and strontium isotope evidence for crustal contamination of continental volcanics. *Science,* **202,** 743-747.

CARTER, S.R., EVENSEN, N.M., HAMILTON, P.J. & O'NIONS, R.K. 1979. Basalt magma sources during the opening of the North Atlantic. *Nature,* **281,** 28-31.

CAS, R.A.F. AND WRIGHT, J.V. 1987. Volcanic Successions. Unwin Hyman, London.

CATTELL, A.C. 1989. The Skye Main Lava Series: liquid density and the absence of basaltic hawaiites. *Geological Magazine,* **126,** 681-684.

CLARKE, D.B. 1970. Tertiary basalts of Baffin Bay: Possible primary magma from the mantle. *Contributions to Mineralogy and Petrology,* **25,** 203-224.

COHEN, R.S. & O'NIONS, R.K. 1982. The lead, neodynium and strontium isotopic signature of ocean ridge basalts. *Journal of Petrology,* **23,** 299-324.

CONDOMINES, M., GRONVOLD, K., HOOKER, P.J., MUEHLENBACHS, K, O'NIONS, R.K., OSKARSSON, N. & OXBURGH, E.R. 1983. Helium, oxygen, Strontium and neodymium isotopic relationships in Iceland volcanics. *Earth and Planetary Science Letters,* **66,** 125-136.

COX, K.G., 1979. A model for flood basalt vulcanism. *Journal of Petrology,* **21,** 629-50.

COX, K.G., BELL, J.D. & PANKHURST, R.J. 1979. The interpretation of igneous rocks. London. Allen and Unwin, 450 pages.

COX, K.G. & HAWKESWORTH, C.J. 1985. Geochemical stratigraphy of the Deccan traps, at Mahabaleshwar, Western Ghats, India, with implications for open system magmatic processes. *Journal of Petrology.* **26,** 355-77.

COX, K.G. & MITCHELL, C. 1988. Estimating proportions in petrographic mixing calculations by least squares approximation. *Nature,* **333,** 447-449.

DAVIES, G.F. 1990. Mantle plumes, mantle stirring and hot-spot geochemistry. *Earth and Planetary Science Letters,* **99,** 94-109.

DE GRAFF, J.M. & AYDIN, A. 1987. Surface morphology of columnar joints and its significance to mechanics and direction of joint growth. *Geological Society of America Bulletin,* **99,** 605-617.

DE PAOLO, D.J. 1981. Trace element and isotope effects of combined wall rock assimilation. *Earth and Planetary Science Letters,* **53,** 189-202.

DE PAOLO, D.J. & WASSERBURG, G.J. 1977. The source of island arcs as indicated by Nd and Sr isotopic studies. *Geophysical Research Letters.* **4,** 465-468.

DEER, W.A., HOWIE, R.A. & ZUSSMAN, J. 1966. An introduction to the rock-forming minerals. Longman, 528pp.

DEER, W.A., HOWIE, R.A. & ZUSSMAN, J. 1992. An introduction to the rock-forming minerals; Second edition. Longman, 696pp.

DELANEY, P.T. & POLLARD, D.D. 1982. Solidification of basaltic magma during flow in a dyke. *American Journal of Science,* **282,** 856-885.

DEVEY, C.W. & COX, K.G. 1987. Relationships between crustal contamination and crystallisation in continental flood basalt magmas with special reference to the Deccan Traps of the Western Ghats, India. *Earth and Planetary Science Letters,* **84,** 59-68.

DICK, H.J.B. & BULLEN, T. 1984. Chromian spinel as a petrogenetic indicator in abyssal and alpine-type peridotites and spatially associated lavas. *Contributions to Mineralogy and Petrology.* **86,** 54-76.

DICKIN, A.P. 1981. Isotope geochemistry of Tertiary igneous rocks from the Isle of Skye. *Journal of Petrology,* **22,** 155-190.

DICKIN, A. P., MOORBATH, S., & WELKE, H. 1981. Isotope, trace element and major geochemistry of Tertiary igneous rocks, Isle of Arran, Scotland. *Transactions of the Royal Society of Edinburgh; Earth Sciences,* 72, 159-170.

DICKIN, A.P. & JONES, N.W. 1983a. Relative elemental mobility during hydrothermal alteration of a basic sill, Isle of Skye, NW Scotland. *Contributions to Mineralogy and Petrology,* **82,** 147-153.

DICKIN, A.P. & JONES, N.W. 1983b. Isotopic evidence for the age and origin of pitchstones and felsites, Isle of Eigg, NW Scotland. *Journal of the Geological Society, London,* **140,** 691-700.

DICKIN, A. P., BROWN, J. L., THOMPSON, R. N., HALLIDAY, A. N. & MORRISON, M. A. 1984. Crustal contamination and the granite problem in the British Tertiary Volcanic Province. *Philosophical Transactions of the Royal Society; London,* **A310,** 755-780.

DICKIN, A.P., JONES, N.W., THIRLWALL, M.F. & THOMPSON, R.N. 1987 A Ce/Nd isotope study of crustal contamination processes affecting Palaeocene magmas in Skye, Northwest Scotland. *Contributions to Mineralogy and Petrology.* **96,** 455 464.

DICKIN, A.P. & BOWES, D.R. 1991. Isotopic evidence for the extent of early Proterozoic basement in Scotland and northwest Ireland. *Geological Magazine,* **128,** 385-388.

DONALDSON, C.H. 1977. Petrology of anorthite-bearing gabbroic anorthosite dykes in NW Skye. *Journal of Petrology,* **18,** 595-620.

DOSTAL, J. & STRONG, D.F. 1983. Trace-element mobility during low grade metamorphism and silicification of basaltic rocks from St. John, New Brunswick. *Canadian Journal of Earth Sciences,* **20,** 431-435.

DROOP, G.T.R. 1987. A general equation for estimating Fe3+ concentrations in ferromagnesian silicates and oxides from microprobe analyses using stoichiometeric criteria. *Mineralogical Magazine,* **51,** 431-435.

EGGINS, S.M. 1992. Petrogenesis of Hawaiian tholeiites: 2, aspects of dynamic melt segregation. *Contributions to Mineralogy and Petrology.* **110,** 398-410.

ELLAM, R.M. 1992. Lithospheric thickness as a control on basalt geochemistry. *Geology,* **20,** 153-156.

ELLAM, R. M. & COX, K. G. 1991. An interpretation of Karoo picrite basalts in terms of interaction between asthenospheric magmas and mantle lithosphere. *Earth and Planetary Science Letters,* **105,** 330-342.

EMELEUS, C.H. 1973. Granophyre pebbles in Tertiary conglomerates on the Isle of Canna, Inverness-shire. *Scottish Journal of Geology,* **9,** 157-159.

EMELEUS, C.H. 1985. Tertiary lavas and sediments of Northwest Rhum, Inner Hebrides. *Geological Magazine,* **122,** 419-437.

EMELEUS, C.H. 1991. Tertiary igneous activity. In: *Geology of Scotland,* Ed Craig, G.Y. Published by Geol. Soc. London, 455-502.

ESSON, J., DUNHAM, A.C. & THOMPSON, R.N. 1975. Low-alkali, high-calcium olivine tholeiite lavas from the Isle of Skye, Scotland. *Journal of Petrology,* **16,** 488-497.

EWART, A. 1989. East Australian petrology and geochemistry. In, *Intraplate volcanism in Eastern Australia and New Zealand.* Ed. R.W. Johnson, Cambridge University Press, 189-256.

FALLOON, T.J. & GREEN, D.H. 1988. Anhydrous partial melting of peridotite from 8-35kb and the petrogenesis of MORB. *Journal of Petrology special Lithosphere Issue,* 379-414.

FAWCETT, J.J. 1961. The petrology of the flood basalts of the Isle of Mull, Argyllshire. Unpublished Ph.D. Thesis, Univ. Manchester.

FISK, M.R. & BENCE, A.E. 1980. Experimental crystallisation of Cr-spinel in FAMOUS basalt 527-1-1. *Earth and Planetary Science Letters,* **48,** 111-123.

FITTON, J. G. , JAMES, D. & LEEMAN, W.P. 1991. Basic magmatism associated with late Cenozoic extension in the western United States: compositional variations in space and time. *Journal of Geophysical Research,* **96, B8,** 13693-13711.

FLOYD, P.A. & WINCHESTER, J.A. 1975. Magma type and tectonic setting discrimination using immobile elements. *Earth and Planetary Science Letters,* **27,** 211-218.

FORESTER, R.W. AND TAYLOR, H.P. Jr. 1976. 18O-depleted igneous rocks from the Tertiary complex of the Isle of Mull, Scotland. *Earth and Planetary Science Letters,* **32,** 11-17.

FREY, F.A. & GREEN, D.H. 1974. The mineralogy, geochemistry and origin of lherzolite inclusions in Victorian basanites. *Geochimica et Cosmochimica Acta,* **38,** 1023-1059.

GARDINER, J.S. 1887. On the leaf beds and gravels of Ardtun, Carsaig etc. in Mull. *Quarterly Journal of the Geological Society, London,* **43,** 270-300.

GARIEPY, C., LUDDEN, J. & BROOKS, C. 1983. Isotopic and trace element constraints on the genesis of the Faeroe lava pile. *Earth and Planetary Science Letters,* **63,** 257-272.

GEKIE, A. 1867. On the tertiary volcanic rocks of the British Islands. *Geological Magazine,* **4,** 316-319.

GEKIE, A. 1888. The history of volcanic action during the Tertiary period in the British Isles. *Transactions of the Royal Society of Edinburgh; Earth Sciences,* **35,** 21-184.

GIBB, F.G.F. 1973. The zoned clinopyroxenes of the Shiant Isles Sill, Scotland. *Journal of Petrology,* **14,** 203-230.

GIBSON, I.L., KIRKPATRICK, R.J., EMMERMAN, R., SCHMINCKE, H-U., PRITCHARD, G., OAKLEY, P.J., THORPE, R.S. & MARRINER, G.F. 1982. The trace element composition of the lavas and dykes from a 3km vertical section through the lava pile of Eastern Iceland. *Journal of Geophysical Research,* **87-B8,** 6532-6546.

GIBSON, S.A. 1988. The geochemistry, mineralogy and petrology of the Trotternish sill complex, N Skye, Scotland. Unpublished PhD. University of Kingston.

GIBSON, S.A. 1990. The geochemistry of the Trotternish sills, Isle of Skye: crustal contamination in the British Tertiary Volcanic Province. *Journal of the Geological Society, London,* **147,** 1071-1081.

GIBSON, S. A., THOMPSON, R.N., LEAT, P. T., MORRISON, M. A., HENDRY, G. L. & DICKIN, A. P. 1991. The Flat Tops Volcanic field 1. Lower Miocene open-system, multisource magmatism at Flander, Trappers Lake. *Journal of Geophysical Research,* **96, B8,** 13609-13623.

GIBSON, S. A., THOMPSON, R.N., LEAT, P. T., DICKIN, A. P. MORRISON, M. A., HENDRY, G. L. & MITCHELL, J.G. 1992. Asthenosphere-derived magmatism in the Rio Grande rift, western USA: Implications for continental break-up. In: *Magmatism and the Causes of continental Break-up;* Eds. Storey, B.C., Alabaster, T. & Pankhurst, R.J. Geol. Society Special Publication **68,** 61-89.

GILL, R.C.O., PEDERSEN, A.K. & LARSEN, J.G. 1992. Tertiary picrites in West Greenland: melting at the periphery of a plume? In: *Magmatism and the Causes of continental Break-up;* Eds. Storey, B.C., Alabaster, T. & Pankhurst, R.J. Geol. Society Special Publication **68,** 335-348.

GILL, R.C.O., NIELSEN, T.D.F., BROOKS, C.K. & INGRAM, G.A. 1988. Tertiary volcanism in the Kangerlugssuaq region, East Greenland: trace element geochemistry of the Lower Basalts and tholeiitic dyke swarms. In: *Early Tertiary Volcanism and the Opening of the NE Atlantic.* Morton, A. C. and Parson, L. M. eds. Geological Society Special Publication, no. **39**, 161-179.

GOVINDARAJU, K. 1989. Special issue of the Geostandards Newsletter. Volume 8.

GREEN, D.H. & RINGWOOD, A.E. 1967. The genesis of basaltic magmas. *Contributions to Mineralogy and Petrology.* **15,** 103-190.

GRIFFITHS, R.W. & CAMPBELL, I.H. 1990. Stirring and structure in mantle starting plumes. *Earth and Planetary Science Letters,* **99,** 66-78.

GRIFFITHS, R.W. & CAMPBELL, I.H. 1991. On the dynamics of long-lived plume conduits in the convecting mantle. *Earth and Planetary Science Letters,* **103,** 214-227.

HAGGERTY, S.E. 1976. Opaque mineral oxides in terrestrial igneous rocks. In: Oxide Minerals. Ed. D. Rumble. Mineralogical Society of America, Reviews in Mineralogy, Vol. 3.

HARKER,. 1904. The Tertiary igneous rocks of Skye. *Memoirs of the Geological Survey G.B., Scotland.*

HAWKESWORTH, C.J. & MORRISON, M.A. 1978. A reduction in 87Sr/86Sr during basalt alteration. *Nature.* **276,** 381-383.

HAWKESWORTH, C.J., GALLAGHER, K., KELLEY, S., MANTOVANI, D.W., PEATE, D.W., REGELOUS, M. & ROGERS 1992. Parana magmatism and the opening of the South Atlantic. In: *Magmatism and the Causes of continental Break-up;* Eds. Storey, B.C., Alabaster, T. & Pankhurst, R.J. Geol. Society Special Publication **68,** 221-240.

HEMOND, C., ARNDT, N.T., LICHTENSTEIN, U., HOFFMANN, A.W. OSKARSSON, N. & STEINTHORSSON, S. 1993. Icelandic hot-spot: New Nd-Sr-O isotopes and trace element constraints. *Journal of Geophysical Research,* In press.

HENDERSON, P. 1982. Inorganic geochemistry. Pergamon. 353 p.

HERZBERG, C.T. & CHAPMAN, N.A. 1976. Clinopyroxene geothermometry of spinel lherzolite. *American Mineralogist,* **61,** 626-637.

HILL, R.I. 1991. Starting plumes and continental break-up. *Earth and Planetary Science Letters,* **104,** 398-416.

HOLM, P. 1988. Nd, Sr and Pb isotope geochemistry of the Lower Lavas, E Greenland Tertiary Igneous Province. In: *Early Tertiary Volcanism and the Opening of the NE Atlantic.* Morton, A. C. and Parson, L. M. eds. Geological Society Special Publication, no. **39,** 181-195.

HOLM, P., HALD, N. & NIELSEN, T.D.F. 1992. Contrasts in composition and evolution of tertiary CFBs between West and East Greenland and their relationships to the establishment of the Icelandic mantle plume. In: *Magmatism and the Causes of continental Break-up;* Eds. Storey, B.C., Alabaster, T. & Pankhurst, R.J. Geol. Society Special Publication **68,** 349-362.

HOLM, P., GILL, R.C.O., PEDERSEN, A.K., LARSEN, J.G., HALD, N. & NIELSEN, T.D.F. & THIRLWALL, M.F. 1993. Tertiary picrites from West Greenland: contributions from 'Icelandic' and other sources. *Earth and Planetary Science Letters,* **115,** 227-244.

HUMPHRIS, S.E., MORRISON, M.A. & THOMPSON, R.N. 1978. Influence of rock crystallisation history upon subsequent lanthanide mobility during hydrothermal alteration of basalts. *Chemical Geology,* **23,** 125-137.

HUMPHRIS, S.E. & THOMPSON, G. 1978. Trace element mobility during hydrothermal alteration of oceanic basalts. *Geochimica et Cosmochimica Acta,* **42,** 127-136.

HUPPERT, H.E. & SPARKS, R.S.J. 1985. Cooling and contamination of mafic and ultramafic magmas during ascent through continental crust. *Earth and Planetary Science Letters,* **74,** 371-386.

IRVING, A.J. 1978. A review of experimental studies of crystal/liquid trace element partitioning. *Geochimica et Cosmochimica Acta,* **42,** 743-770.

IRVING, A.J. & PRICE, R.C. 1981. Geochemistry and evolution of lherzolite-bearing phonolitic lavas from Nigeria, Australia, East Germany and New Zealand. *Geochimica et Cosmochimica Acta,* **45,** 1309-1320.

ITO, K. & KENNEDY, G.C. 1967. Melting and phase relations in a natural peridotite to 40kb. *American Journal of Science.* **265,** 519-88.

JAQUES, A.L. & GREEN, D.H. 1980. Anhydrous melting of peridotite at 0-15kb pressure and the genesis of tholeiitic basalts. *Contributions to Mineralogy and Petrology,* **73,** 287-310.

JOHNSON, K.T.M., DICK, H.J.B. & SHIMIZU, N. 1990. Melting in the oceanic upper mantle: an ion microprobe study of diopsides in abyssal peridotites. *Journal of Geophysical Research,* **B95,** 2661-2678.

JUDD, J.W. 1874. The secondary rocks of Scotland. Second paper. On the ancient volcanoes of the Highlands and the relations of their products to the Mesozoic strata. *Quarterly Journal of the Geological Society, London,* **30,** 220-302.

JUDD, J.W. 1889. The Tertiary volcanoes of the Western Isles of Scotland. *Quarterly Journal of the Geological Society, London,* **45,** 187-218.

JUREWICZ, A.J.G. & WATSON, E.B. 1988. Cations in olivine, Part 1: Calcium partitioning and Ca-Mg distribution between olivines and coexisting melts, with petrologic applications. *Contributions to Mineralogy and Petrology,* **99,** 176-185.

KERR, A.C. 1993. Elemental evidence for an enriched small-fraction melt input into Tertiary Mull basalts, Western Scotland. *Journal of the Geological Society, London,* **150,** 763-769.

KERR, A.C. & HARDY, R. 1993. Sodiun contamination of fused X-ray fluorescence discs. *Journal of the Arthur Holmes Society,* **7 (New series),** 38.

KERR, R.A. 1981. Do plumes stir the earths entire mantle?. *Science,* **252,** 1068-1069.

KHARIN, G.N. 1976. The petrology of magmatic rocks, DSDP Leg 38. Initial Reports of the DSDP, **38,** 685-715.

KENNEDY, W.Q. 1933. Trends of differentiation in basaltic magmas. *American Journal of Science,* **25,** 239-256.

KILLE, I.C., THOMPSON, R.N., MORRISON, M.A. & THOMPSON, R.F. 1986. Field evidence for turbulence during flow of basalt magma through conduits from southwest Mull. *Geological Magazine,* **123,** 693-697.

KLEIN, E.M. & LANGMUIR, C.H. 1987. Global correlations of ocean ridge basalt chemistry with axial depth and crustal thickness. *Journal of Geophysical Research,* **B92,** 8089-8115.

KLEIN, E.M. & LANGMUIR, C.H. 1989. Local versus global in ocean ridge basalt composition: a reply. *Journal of Geophysical Research,* **B94,** 4241-4252.

KOSTOPOULOS, D. K. & JAMES, S. D. 1992. Paramertarization of the melting regime of the shallow upper mantle and the effects of variable lithospheric stretching on mantle modal stratification and trace-element concentrations in magmas. *Journal of Petrology,* **33,** 665-691.

LAMACRAFT, H.M. 1978. The geochemistry of the Mull, Islay and Jura dyke swarms. Unpublished M.Phil. Thesis, University of London.

LANGMUIR, C.H. 1989. Geochemical consequences of in situ crystallisation. *Nature,* **340,** 199-205.

LANGMUIR, C.H., BENDER, J.F., BENCE, A.E. & HANSON, G.N. 1977. Petrogenesis of basalts from the Famous area: Mid-Atlantic Ridge. *Earth and Planetary Science Letters,* **36,** 133-156.

LARSEN, L.M., WATT,W. S. & WATT, M. 1989. Geology and petrology of the lower Tertiary plateau basalts of the Scoresby Sund region, East Greenland. *Bulletin 157. Greenland Geological Survey.* 162 p.

LE BAS, M.J. & STRECKEISEN, A.L. 1991. The IUGS systematics of igneous rocks. *Journal of the Geological Society, London,* **148,** 825-833.

LEEMAN, W.P, BUDAHN, J.R., GERLACH, D.C. & POWELL, B.N. 1980. Origin of Hawaiian tholeiites: trace element constraints. *American Journal of Science,* **280A,** 794-819.

LOPER, D. E.. 1991. Mantle plumes. *Tectonophysics,* **187,** 373-384.

LOPER, D. E. & Stacey, F.D. 1983. The dynamical and thermal structure of deep mantle plumes. *Physics of the Earth and Planetary Interiors,* **33,** 304-317.

LUDDEN, J., GELINAS, L. & TRUDEL, P. 1982. Archean metavolcanics from the Rouyn-Noranda, district, Abitibi Greenstone Belt, Quebec. Mobility of trace elements and petrogenetic constraints. *Canadian Journal of Earth Sciences,* **19,** 2276-2287.

LYLE, P., 1974. The petrology and petrochemistry of Tertiary basaltic rocks of NE Ireland and NW Iceland. Unpublished PhD Thesis, Queen's University of Belfast.

LYLE, P., 1980. A petrological and geochemical study of the Tertiary Basaltic rocks of NE Ireland. *Journal of Earth Sciences of the Royal Dublin Society,* **2,** 137-152.

LYLE, P., 1985. The petrogenesis of Tertiary basaltic and intermediate lavas of NE Ireland. *Scottish Journal of Geology,* **21,** 71-84.

LYLE, P. 1988. The geochemistry, petrology and volcanology of the Tertiary lava succession of the Binevenagh-Benbraddagh area of County Londonderry. *Irish Journal of Earth Sciences,* **9,** 141-152.

LYLE, P. & THOMPSON, S.J. 1983. The classification and chemistry of the Tertiary intermediate lavas of NE Ireland. *Scottish Journal of Geology,* **19,** 17-27.

LYLE, P. & PATTON, D.J.S. 1989. The petrography and geochemistry of the Upper Basalt Formation of the Antrim lava group in NE Ireland. *Irish Journal of Earth Sciences,* **10,** 33-41.

MANTOVANI, M.S.M., MARQUES, L.S., DE SOUSA, M.A., CIVETTA, L., ATALLA, L. & INNOCENTI, F. 1985. Trace element and Sr isotope constraints on the origin and evolution of Parana continental flood basalts of Santa Catarina State (Southern Brazil). *Journal of Petrology,* **26,** 187-209.

MATTEY, D.P. 1979. The petrology of high-calcium, low-alkali tholeiite dykes from the Isle of Skye regional swarm. Unpublished PhD thesis, University of London.

MATTEY, D.P., GIBSON, I.L., MARRINER, G.F. & THOMPSON, R.N. 1977. The diagnostic geochemistry, relative abundance, and spatial distribution of high-calcium, low-alkali olivine tholeiitic dykes in the lower tertiary regional swarm of the Isle of Skye, NE Scotland. *Mineralogical Magazine,* **41,** 273-285.

MACKENZIE, W.S., DONALDSON, C.H. & GUILFORD, C. 1982. Atlas of igneous rocks and their textures. Longman, London. 148pp.

MCKENZIE, D. P. 1984. The generation and compaction of partially molten rock. *Journal of Petrology,* **25,** 713-765.

MCKENZIE, D. P. 1989. Some remarks on the movement of small melt fractions in the mantle. *Earth and Planetary Science Letters,* **95,** 53-72.

MCKENZIE, D. P. & BICKLE, M.J. 1988. Partial melt distributions from inversion of rare earth element concentrations. *Journal of Petrology,* **32,** 1021-1091.

MCKENZIE, D. P. & O'NIONS, R.K. 1991. The volume and composition of melt generated by extension of the lithosphere. *Journal of Petrology,* **29,** 625-679.

MEIGHAN, I.G., HUTCHINSON, R., WILLIAMSON, I.T. & MACINTYRE, R.M. 1982. Geological evidence for the different relative ages of the Rhum and Skye Tertiary central complexes. *Journal of the Geological Society, London,* **139,** 659.

MENZIES, M. A., HALLIDAY, A. N., HUNTER, R.H., MACINTYRE, R. M. & UPTON, B.G.J. 1986. The age composition and significance of a xenolith-bearing monchiquite dyke, Lewis, Scotland. Proceedings of the 4th International Kimberlite Conference, Vol. 2. *Geological Society of Australia, Special Publication,* **14,** 843-852.

MENZIES, M. A., HALLIDAY, A. N., PALACZ, Z., HUNTER, R.H., UPTON, B.G.J., ASPEN, P. & HAWKESWORTH, C. J. 1987. Evidence from mantle xenoliths for an enriched lithospheric keel under the outer Hebrides. *Nature,* **325,** 44-47.

MIYASHIRO, A. 1978. Nature of alkalic volcanic rock series. *Contributions to Mineralogy and Petrology,* **66,** 91-104.

MOORBATH, S. AND BELL, J.D. 1965. Strontium isotope abundance studies and rubidium-strontium age determinations on Tertiary igneous rocks from the Isle of Skye, north-west Scotland. *Journal of Petrology,* **6,** 37-66.

MOORBATH, S., & WELKE, H. 1969. Lead isotope studies on igneous rocks from the Isle of Skye, northwest Scotland. *Earth and Planetary Science Letters,* **5,** 217-30.

MOORBATH, S. & THOMPSON, R.N. 1980. Strontium isotope geochemistry and petrogenesis of the Early Tertiary lava pile of the Isle of Skye, Scotland, and other basic rocks of the British Tertiary Province: an example of magma-crust interaction. *Journal of Petrology,* **21,**295-321.

MORIMOTO, N. 1988. The nomenclature of pyroxenes. *Mineralogical Magazine,* **52,** 535-550.

MORRISON, M.A. 1978. The use of immobile trace elements to distinguish Palaeotectonic affinities of metabasalts: applications to the Palaeocene basalts of Mull and Skye, NW Scotland. *Earth and Planetary Science Letters,* **39,** 407-16.

MORRISON, M.A. 1979. Igneous and metamorphic geochemistry of Mull lavas. Univ. London, unpublished Ph.D. thesis.

MORRISON, M.A., THOMPSON, R.N., GIBSON, I.L. AND MARRINER, G.F. 1980. Lateral chemical heterogeneity in the Palaeocene upper mantle beneath the Scottish Hebrides. *Philosophical Transactions of the Royal Society; London,* **A297,** 229 -244.

MORRISON, M.A, THOMPSON, R.N. & DICKIN, A.P. 1985. Geochemical evidence for complex magmatic plumbing during development of a continental volcanic centre. *Geology,* **13,** 581-584.

MORRISON, M.A, HENDRY, G. L. & LEAT, P. T. 1987. Regional and tectonic implications of parallel Caledonian and Permo-Carboniferous lamprophyre dyke swarms from Lismore, Ardgour. *Transactions of the Royal Society of Edinburgh: Earth Sciences,* **77** (for1986), 279-288.

MORTIMER, C.E. 1984. Chemistry; fifth edition. Wadsworth, 760p.

MUSSETT, A.E. 1986. ^{40}Ar ^{39}Ar step-heating ages of the Tertiary igneous rocks of Mull, Scotland. *Journal of the Geological Society, London,* **143,** 887-896.

MYERS, R.E., MCCARTHY, T.S., BUNYARD, M., CAWTHORN, R.G., FALATSA, T.M, HEWITT, T., LINTON, P., MYERS, J.M., PALMER, K.J. & SPENCER, R. 1990. Geochemical stratigraphy of the Klipriviersberg Group volcanic rocks. *South African Journal of Geology,* **93,** 224-238.

MYSEN, B.O. & KUSHIRO, I. 1977. Compositional variations of co-existing phases with degree of melting of peridotite in the upper mantle. *American Mineralogist,* **62,** 843-865.

NICHOLSON, H & LATIN, D 1992. Olivine tholeiites from Krafla Iceland: Evidence for variations in melt fraction within a plume. *Journal of Petrology,* **33,** 1105-1124.

NIELSEN, R.L. 1988. A model for the simulation of combined major and trace element liquid lines of descent. *Geochimica et Cosmochimica Acta,* **52,** 27-38.

O'HARA, M.J. 1968. The bearing of phase equlibria studies on the origin and evolution of basic and ultrabasic rocks. *Earth Science Reviews,* **4,** 69-133.

O'HARA, M.J. & MATTHEWS, R.E. 1981. Geochemical evolution in an advancing, periodically replenished, periodically tapped, continuously fractionated magma chamber. *Journal of the Geological Society, London,* **143,** 887-896.

O'NIONS, R.K. & CLARKE, D.B. 1972. Comparative trace element geochemistry of Tertiary basalts from Baffin Bay. *Earth and Planetary Science Letters,* **15,** 436-446.

PATCHETT, P. 1980. Thermal effects of basalt of continental crust and crustal contamination of magmas. *Nature,* **283,** 559-61.

PEARCE, J.A. & CANN, J.R. 1973. Tectonic setting of basic rocks determined using trace element analysis. *Earth and Planetary Science Letters,* **19,** 290-300.

PLANK, T. & LANGMUIR, C.H. 1992. Effects of the melting regime on the compositions of the oceanic crust. *Journal of Geophysical Research,* **B97,** 19749-19770.

PRESTON, J. 1982. Eruptive volcanism. In Sutherland, D. (Ed.) Igneous rocks of the British Isles. Wylie, Chichester.

RIBE, N.M. 1985. The generation and composition of partial melts in the earths mantle. *Earth and Planetary Science Letters,* **73**, 361-376.

RIDLEY, W.I. 1977. The crystallisation trends of Spinels in Tertiary basalts from Rhum and Muck and their petrogenetic significance. *Contributions to Mineralogy and Petrology,* **64**, 243-255.

ROCK, N.M.S. 1991. *Lamprophyres.* Blackie, Glasgow.

ROEDER, P.L. & EMSLIE, R.F. 1970. Olivine-liquid equilibrium. *Contributions to Mineralogy and Petrology,* **29**, 275-289.

ROGERS, N.W. 1992. Potassic magmatism as the key to trace-element enrichment processes in the upper mantle. *Journal of Volcanology and Geothermal Research,* **50**, 85-99

SCARROW, J. 1992. The geochemistry of the Skye lava succession. Unpublished Ph.D. thesis, University of Oxford.

SCHILLING, J.G. 1973. Iceland mantle plume: geochemical evidence along Reykjanes Ridge. *Nature,* **242**, 565-571.

SCHILLING, J.G. 1976. Rare earth, Sc, Cr, Fe, Co and Na abundances in DSDP Leg 38 basement basalt: some additional evidence on the evolution of the Thulean volcanic province. *Initial reports of the DSDP,* 38, 741-753.

SCHILLING, J.G AND NOE-NYGAARD, A. 1974. Faeroe-Iceland plume: rare earth evidence. *Earth and Planetary Science Letters,* **24**, 1-14.

SHERVAIS, J.W. 1982. Ti-V plots and the petrogenesis of modern and ophiolitic lavas. *Earth and Planetary Science Letters,* **59**, 101-118.

SIMKIN, T. & SMITH, J.V. 1970. Minor element distribution in olivine. *Journal of Geology,* **78**, 304-325.

SKELHORN, R.R. 1969. The Tertiary igneous geology of the Isle of Mull. *Geol. Assoc. Guides,* **No. 20.**

SMEDLEY, P.L. 1988. The geochemistry of Dinantian volcanism in South Kintyre and the evidence for provincialism in the southern Scottish mantle. *Contributions to Mineralogy and Petrology,* **99,** 374-384.

SMITH, J.V. 1983. Some chemical properties of feldspars. In: *Feldspar Mineralogy* (second edition), P.H. Ribbe ed. Mineralogical Society of America, Reviews in Mineralogy, **2,** 281-296.

SMITH, R.E. & SMITH, S.E. 1976. Comments on the use of Ti, Zr, Y Sr, K, P, and Nb in classification of basaltic magmas. *Earth and Planetary Science Letters,* **32,** 114-120.

SPARKS, R.S.J. & HUPPERT, H. 1984. Density changes during fractional crystallisation of basaltic magmas: fluid dynamic implications. *Contributions to Mineralogy and Petrology,* **85,** 300-309.

SPEIGHT, J.M., SKELHORN, R.R., SLOAN, T. & KNAPP, R.J. 1982. The dyke swarms of Scotland. In: *Igneous Rocks of the British Isles.* Sutherland, D.S., ed. Wiley pp. 449-459.

STACEY, J.S. & KRAMERS, J.D. 1975. Approximation of terrestrial lead isotope evolution by a two-stage model. *Earth and Planetary Science Letters,* **26,** 207-221.

SUN, S.-S & MCDONOUGH, W.F. 1989. Chemical and isotopic systematics of oceanic basalts: implications for mantle compositions and processes. In: *Magmatism in the Ocean Basins,* A.D. Saunders & M.J. Norry, eds. Geological Society Special Publication, **42,** 313-345.

TARNEY, J. & JONES, C.E. 1993. Trace element geochemistry of orogenic igneous rocks and crustal growth models. Unpublished abstract Volcanic Studies Group conference, Milton Keynes.

THOMPSON, R.N. 1972. The one - atmosphere melting patterns of some basaltic volcanic series. *American Journal of Science,* **272,** 901-932.

THOMPSON, R.N. 1973. One-atmosphere melting behaviour and nomenclature of basaltic lavas. *Contributions to Mineralogy and Petrology,* **41,** 197-204.

THOMPSON, R.N. 1974. Primary basalts and magma genesis. *Contributions to Mineralogy and Petrology,* **45,** 317-341.

THOMPSON, R.N. 1975. Is upper mantle phosphorus contained in sodic garnet? *Journal of Petrology,* **26,** 417-424.

THOMPSON, R.N. 1981. Thermal aspects of the origin of Hebridean Tertiary acid magmas. I. An experimental study of partial fusion of Lewisian gneisses and Torridonian sediments. *Mineralogical Magazine,* **44,** 161-70.

THOMPSON, R.N. 1982. Magmatism of the British Tertiary Volcanic Province. *Scottish Journal of Geology,* **18,** 49-107.

THOMPSON, R.N. 1987. Phase equlibria constraints on the genesis and magmatic evolution of oceanic basalts. *Earth Science Reviews.* **24,** 161-210.

THOMPSON, R.N., ESSON, J. & DUNHAM, A.C. 1972. Major element chemical variation in the Eocene lavas of the Isle of Skye. Scotland. *Journal of Petrology,* **13,** 219 253.

THOMPSON, R.N., GIBSON, I.L., MARRINER, G.F., MATTEY, D.P. & MORRISON. M.A. 1980. Trace-element evidence of multistage mantle fusion and polybaric fractional crystallisation in the Palaeocene lavas of Skye, NW Scotland. *Journal of Petrology,* **21,** 265-93

THOMPSON, R.N., DICKIN, A.P., GIBSON, I.L. & MORRISON, M.A. 1982. Elemental fingerprints of isotopic contamination of Hebridean Palaeocene mantle derived magmas by Archean sial. *Contributions to Mineralogy and Petrology,* **79,** 159-168.

THOMPSON, R.N., MORRISON, M. A., DICKIN, A. P. & HENDRY, G. L. 1983. Continental flood basalts ... Arachnids rule OK? In: *Continental Basalts and Mantle Xenoliths,* Hawkesworth, C. J. & Norry, M. J. eds. Shiva Publishing, pp. 158-185.

THOMPSON, R.N., MORRISON, M.A, DICKIN, A.P., GIBSON, I.L. & HARMON, R.S. 1986. Two contrasted styles of interaction between basic magmas continental crust in

the British Tertiary Volcanic Province. *Journal of Geophysical Research,* **91,** 5985-5997.

THOMPSON, R.N. & MORRISON, M. A. 1988. Asthenospheric and lower-lithospheric mantle contributions to continental extensional magmatism: an example from the British Tertiary Province. *Chemical Geology,* **68,** 1-15.

THOMPSON, R.N. & GIBSON, S.A. 1991. Subcontinental mantle plumes, hotspots and pre-existing thinspots. *Journal of the Geological Society, London,* **148,** 973-979.

THOMPSON, R.N., GIBSON, S. A., LEAT, P. T., MITCHELL, J.G., MORRISON, M. A., HENDRY, G. L. & DICKIN, A. P. 1993. Early Miocene continental extention-related basaltic magmatism at Walton Peak, northwest Colorado: further evidence on continental basalt genesis. *Journal of the Geological Society, London,* **150,** 277-292.

TILLEY, C.E. 1950. Some aspects of magmatic evolution, *Quarterly Journal of the Geological Society, London,* **106,** 37-61.

TILLEY, C.E. & MUIR, I.D. 1962. The Hebridean Plateau Magma Type. *Transactions of the Edinburgh Geological Society,* **19,** *208-215.*

TILLEY, C.E. & MUIR, I.D. 1964. Intermediate members of the oceanic basalt-trachyte association. *Geolgiska Foreningens i Stockholm Forhandlingar.* 85, 434-443.

TODT, W., CLIFF, R.A., HANSER, A., & HOFMANN, A.W., 1984, ^{202}Pb and ^{205}Pb double spike for lead isotopic analyses, *Terra Cog.,* **4,** 209.

UPTON, B.G.J., EMELEUS, C.H. & BECKINSALE, R.D. 1984. Petrology of the Northern East Greenland Tertiary flood basalts: evidence from Hold with Hope and Wollaston Forland. *Journal of Petrology,* **25,** 151-184.

WAGER, L.R. 1956. A chemical definition of fractionation stages as a basis for comparison of Hawaiian, Hebridean and other basic lavas. *Geochimica et Cosmochimica Acta,* **9,** 217-48.

WAGER, L.R. & BROWN, G.M. 1967. Layered Igneous Rocks. Oliver and Boyd, Edinburgh.

WALKER. G.P.L. 1970a. The distribution of amygdale minerals in Mull and Morvern (Western Scotland). In Murty, T. V. V. G. R. K. and Rao, S. S. (Eds.) Studies in Earth Sciences, West Commemoration Volume. 181-194.

WALKER. G.P.L. 1970b. Compound and simple lava flows and flood basalts. *Bulletin of Volcanology,* **35,** 579-90.

WALLACE, J.M., ELLAM, R.M., MEIGHAN, I.G., LYLE, P. & ROGERS, N.W. 1993. Sr isotope data for the Tertiary lavas of N. Ireland: Evidence for open system processes. *Journal of the Geological Society, London,* In press.

WATSON, E.B. 1979. Zircon saturation in felsic liquids: experimental results and applications to trace element geochemistry. *Contributions to Mineralogy and Petrology,* **70,** 407-419.

WATSON, E.B. 1982. Basalt contamination by continental crust: Some experiments and models. *Contributions to Mineralogy and Petrology,* **80,** 73-87.

WATSON, S & MCKENZIE, D. 1991. Melt generation by plumes a study of Hawaiian volcanism. *Journal of Petrology,* **32,** 501-537.

WEAVER, B.L. & TARNEY, J. 1980. Rare earth geochemistry of Lewisian granulite facies gneisses, NW Scotland: Implications for the petrogenesis of Archean lower continental crust. *Earth and Planetary Science Letters,* **51,** 279-286.

WEAVER, B.L. & TARNEY, J. 1981. Lewisian gneiss geochemistry and Archean crustal development models. *Earth and Planetary Science Letters,* **55,** 171-180

WHITE, R.S. 1988. A hot-spot model for early Tertiary volcanism in the North Atlantic. In: *Early Tertiary Volcanism and the Opening of the NE Atlantic.* Morton, A. C. and Parson, L. M. eds. Geological Society Special Publication, no. **39,** 3-13.

WHITE, R.S. 1992a. Crustal structure and magmatism of the North Atlantic continental margins. *Journal of the Geological Society, London,* **149,** 841-854.

WHITE, R.S. 1992b. Magmatism during and after continental break-up. In: *Magmatism and the Causes of continental Break-up;* Eds. Storey, B.C., Alabaster, T. & Pankhurst, R.J. Geol. Society Special Publication **68,** 1-16.

WHITE, R.S. & MCKENZIE, D.P. 1989. Magmatism at rift zones: The generation of volcanic continental margins. *Journal of Geophysical Research,* **94,** 7685-7729.

WHITE, W.M. & CHEATHAM, M. 1990. Mantle plumes, hot-spots and flood basalts: Inferences from isotopic studies from leg 115 basalts. *EOS Transactions, American Geophysical Union.***71,** 1387.

WILLIAMSON, I.T. 1976. On the occurrence of ponded and valley-infilling lavas from west-central Skye NW Scotland. *Arthur Holmes Society Journal.* **5,** 54-60.

WILLIAMSON, I.T. 1979. The petrology and structure of the Tertiary volcanic rocks of West-Central Skye, NW Scotland. Unpublished PhD thesis, University of Durham.

WOOD, D.A. 1978. Major and trace element variations in the Tertiary lavas of Eastern Iceland and their significance with respect to the Iceland geochemical anomaly. *Journal of Petrology,* **19,** 393-436.

WOOD, D.A. 1979. Dynamic partial melting: its application to the petrogenesis of basalts erupted in Iceland, the Faeroe Islands, the Isle of Skye (Scotland) and the Troodos Massif (Cyprus). *Geochimica et Cosmochimica Acta,* **43,** 1031-1046.

WOOD, D.A., GIBSON, I. L. & THOMPSON, R. N. 1976. Elemental mobility during zeolite-facies metamorphism of the tertiary basalts of Eastern Iceland. *Contributions to Mineralogy and Petrology,* **55,** 241-253.

WYLLIE, P.J. 1961. Fusion of Torridonian sandstone by a picrite sill in Soay (Hebrides). *Journal of Petrology,* **2,** 1-37.

WYLLIE, P.J. 1984. Constraints imposed by experimental petrology on possible and impossible mantle sources and products. *Philosophical Transactions of the Royal Society; London,* **A310,** 439-456.

WYLLIE, P.J. 1988. Solidus curves mantle plumes and magma generation beneath Hawaii. *Journal of Geophysical Research,* **B93,** 4171-4181.

YODER, H.S. & TILLEY, C.E. 1962. Origin of basalt magmas: an experimental study of natural and synthetic systems. *Journal of Petrology,* **3**, 342-532.

Appendix 1

FIELD AND PETROGRAPHIC NOTES.

1. The lavas of Mull and Morvern.

Ardtun, Port umah na Gaibhre (NM381249)

A1 Columnar basalt, below the Ardtun leaf beds, very fine grained (<1mm) at least 5m thick. A nearby sill has glassy tachylite margins.

A2 Columnar basalt, above the Ardtun leaf beds, fine grained (<1mm) greater than 10m thick.

A3 and A4 Upper and lower flows from the Torr Mor outlier (NM384244) Values taken from Thompson et al. 1986; samples MS194, 195.

A5 South of the Ardtun road (NM386233). Quite a fresh flow, fine-medium grained, with noticeable olivine phenocrysts. 3-4m thick

3-4m rise before the next flow.

A6 Platy, fine grained flow at least 3-4m thick. (NM386232) With olivine phenocrysts.
NB - Trees grow around the base of A6 . . . . they also grow around the base of Torr Mor.

A Mholl (NM4532)

AM1 Basal flow with red/brown mudstone/ash below, blocky spheroidally weathered flow, quite olivine rich, 5-8m thick. (NM454328) T/S- clustered, skeletal zoned phenocrysts of olivine, fine-medium grained
There may be a fault up the stream Allt na Teangaidh down-throw several meters to the east.

AM2 Olivine rich, blocky-spheriodally weathered flow, well over 5m thick, fine-medium grain size, 1mm, similar to the previous flow.
2A, B and collected at the bottom, middle and top.

AM3 Next flow collected at the top of the gully, about 50m further south. It is very spheroidally weathered, with an irregular red bole at the base, it has a thick slaggy base and is 2-3m thick. T/S- Fine-medium grain size, with a patch of pegmatite material that has more sodic plagioclase and more lilac coloured pyroxene.

AM4 20-30m further south, 4-5m thick, spheroidally weathered, olivine rich, quite altered. Thin 4-5cm red bole at its base.

Cross over the road, 100m further south, small roadside exposure.

AM5 Spheroidally weathered, poorly exposed, at least 2m thick with indistinct pipe infills at the base. T/S- very badly altered, no fresh olivine, it has gone completely to oxide and iddingsite.

50m further south, 8-10m grassy slope, no exposure.

AM6 At least 3-4m thick, spheroidally weathered, fine-medium grained. T/S- contains less olivine and it contains a few plagioclase phenocrysts. (NM456327)

50m further south.

AM7A Blocky flow, at least 2-3m thick. T/S- contains numerous olivine phenocrysts, fine-medium grained.

AM7B Probably the same flow as 7A, blocky weathering, fine-medium (1mm) grained.

AM8 The escarpment is composed of two flows, the lower one is 6-8m thick, is slightly feldspar phyric, and fine grained and has a thin 5-7 cm red horizon below.

AM9 Fine grained, with olivine phenocrysts, 5m thick, red and vesicular base.

AM10 At least 3-4 m thick, fine grained, feldspar pyhric, with platy-blocky weathering. Not very laterally continuous.

5-8 m grassy slope before the next flow.

AM11 Blocky flow 4-5m thick, fine (1mm) grain size, quite altered.

AM12 Vesicular flow, very spheroidally weathered, undulating top to the previous flow, 5m thick, T/S- fine-medium grained quite badly altered to oxide, chlorite and sericite.

AM13 Above this is a series of thin, reddened and altered, vesicular olivine rich flows, 30-60cm

AM14 thick, with thin red bands in between, fine-medium grained. AM15 is slightly more evolved

AM15 (NM461326) and contains some plagioclase phenocrysts.

Bearraig (NM417275)

B1 Columnar flow enclosing Maculloch's tree. At least 10m thick, very fine grained (<<1mm) with plagioclase phenocrysts, contains agates. (NM404276)

B2 Second columnar flow in the sea cliff 1-200m east of B1, very fine grained (<<1mm), three tiered structure well over 10m.

B3 Rubbly, vesicular flow in the cliff above B2, over 20m thick, Fine-medium grained (1-2mm) the flow has a similar texture to W6 (it might well be the same flow).

B4A Valley fill flow, rubbly, over 20m thick at its thickest point. Sample collected below the waterfall. Thin bole below this flow. T/S- fine grained (<1mm) with aligned plagioclase crystals.

B4B Approx 1km east of B4A, possibly the same flow is exposed, however, in thin section it is very similar to B3 (the chemistry confirms this). Again it has rubbly weathering and here it is 5m thick. (NM413264)

B5 100m further east, 6-8m thick flow with a crude columnar jointing. Very fine grained (<1mm) with aligned plagioclase, very similar to B4B. (NM414264)

B6 100m further east, poorly exposed platy flow, at least 4m thick, fine-medium grained (1-2mm) with olivine and plagioclase phenocrysts. There could however be other flows above and below, since there is a 5m grassy rise both above and below it.

B7 Fine grained (<1mm) quite evolved, massive flow, at least 7-8 m thick and the base is obscured.

B8 Fine grained (<1mm) flow, with spheroidal weathering, very similar to the previous flow. It has a thin bole below and a slaggy top and bottom. 5m thick.

B9 10cm bole between B8 and B9. The flow is shperoidally weathered and poorly exposed, fine/medium grained, at least 5m thick.

B10 The flow is about 5m thick and is badly weathered, fine-medium grained (1mm) very similar to the previous couple of flows. 130m asl.

B11 A badly weathered flow, quite red in places, fine grained (<1mm) olivine phyric. 3-4m thick. (NM415265)

B12 Blocky spheroidally weathered fine grained (<1mm) flow, with a rubbly bottom, olivine phyric, at least 4-5m thick.

B13 Massive flow, well over 10m thick. Blocky appearance with, a distinct platyness on the surface, fine grained (<1mm) again with olivine phenocrysts.

B14 A platy flow with crude columnar jointing, which can be well over 1m in diameter, 10-15m thick. Fine grained, contains much fewer olivine phenocrysts than the previous couple of flows (NM415265)

B15 Top-most flow that can be seen from the Maculloch's tree path, pinches in from the west, platy and columnar, fine grained (<1mm), with aligned plagioclase. about 10m thick. The sample was taken quite near the top of the flow, 170-180m asl.

3-4m grassy rise before the next flow.

B16A Crudely columnar, platy, fine-medium grained, olivine phyric, with a few vesicles. 8-10m thick. (NM413267)

There is possibly a fault between here and the next flow, the displacement is 1-2m at most. Flow B16B collected to check this.

B17 Possibly another flow, fine-medium grained (1mm) the feldspars display a crude alignment, poorly exposed, columnar. At least 4-5 m thick. 200m asl, (NM215267)

4-5 m grassy rise before the next flow.

B18 A rubbly, spheroidal, badly weathered flow with, altered red patches. Medium grained (1-2mm), it almost contains good shaped pyroxenes, at least 5 m thick.

B19 A platy, crudely columnar flow, with some big feldspars. Fine grained (<1mm), well over 7m thick.

Above this there is a fault trending approx. E-W, with a 2 m down-throw towards the south. 250m asl. (NM415268)

B20 4-5m grassy slope before the next flow. Blocky spheroidally weathered flow. Fine-medium grained (1mm). It is quite olivine rich and some of this olivine is zoned. 5m thick.

B21 4m grassy rise before the next flow. Which is at least 10 m thick, a rubbly flow with spheroidal weathering. Fine-medium grained very similar to the flow below. Underlain by a 4-5cm red bole 290m asl. (NM416271)

8-10m grassy rise before the next flow

B22 Poorly exposed flow in a stream section, quite altered and packed with zeolites. Fine grained (<1mm) olivine phyric, 10m thick.

B23 A rampart forming, platy flow, yet quite olivine rich. Very similar to the flow below, except it contains plagioclase phenocrysts as well as olivine. At least 10m thick.

B24 A well jointed, olivine rich flow, at least 5 m thick, but quite poorly exposed, petrographically very similar to B22. 330m asl.

3-4 m grassy rise then a small fault may be seen trending NE-SW with a down throw of 2m towards the SW. A sample was collected from both sides of the fault in order to check this down throw

B25A A blocky olivine rich flow, fine-medium grained (1mm). 3-4m thick. Contains interstitial zeolites.

B25B A fresher flow, but still olivine rich T/S- finer grained (<1mm) but it contains olivine phenocrysts some of which form clusters. 5m thick.

B26 Blocky, spheroidal weathering, with a nobbly, pitted surface. Very olivine rich, similar to the previous flow. 5-7m thick, 350m asl, (NM427272)

B27 Again an olivine rich flow, very similar to the flow below with a pitted surface. Fine grained (<1mm). Well over 5m thick.

B28 Thick rampart flow, quite olivine rich and badly weathered, similar to the flow below, at least 15m thick. 380m asl.

B29 Similar to the previous flow, olivine rich, nobbly surface, fine grained (<1mm). At least 10m thick.

B30 Top most flow, with less olivine, it has quite a columnar appearance. T/S- does not contain phenocrysts of olivine, fine-medium grained (<1mm) at least 15m thick.

Beinn Bhuidhe (NM3749)

BB1 Spheriodally weathered flow, with a red slaggy base, fine-medium grained (1mm). 3-4m thick. (NM362483) T/S- very altered with numerous interstitial zeolites.

BB2 Blocky weathering, fine-medium grained (1mm), at least 5m thick. T/S- zoned olivine phenocrysts.

BB3 Nobbly weathering, at least 4m thick, similar to the flow below. (NM363484). T/S- groundmass olivine can be seen.

BB4 Platy flow, with elongated vesicle infills, very fine grained (<<1mm), at least 3-4m thick. T/S- aligned plagioclase.

BB5 Poorly exposed flow to the north of a stream gully, several meters thick, very similar to the previous flow. T/S- contains some skeletal and angular crystals of olivine

BB6 Escarpment flow, with blocky weathering, fine (<1mm) grained, 4-5m thick.

BB7 Still on the north side of the stream, a 5m thick flow is exposed, fine/medium grained. T/S- aligned plagioclase crystals.

BB8 The flow on the opposite side of the stream is more platy than BB7, and so there may be a minor fault in here (down-throw to the north, 2-4m ??). It is fine grained (<1mm) and is 4-5m thick. T/S- contains aligned plagioclase and olivine phenocrysts.

BB9 The flow above BB8 is 3m thick and is fine (<1mm) grained and it is quite vesicular with fibrous infilling zeolites. (NM367488)

BB10A Fine grained platy flow, with fibrous zeolites, 3-4m thick. T/S- phenocrysts of olivine and plagioclase. The groundmass plagioclase is aligned.

100m WSW of this over a scrubby, poorly exposed flat area, before what is possibly the same flow.

BB10B Platy, very fine grained (<<1mm) flow, with elongated vesicle infills, 4-5m thick.

BB11 Fine grained (<1mm), platy with a convoluted flow banded texture in places, 6-8m thick. (NM372488). Aligned plagioclase.

BB12 Very similar to the previous flow, very platy, fine grained, with feldspar phenocrysts (up to 5mm), 6-8m thick.

BB13 Fine grained (<1mm), platy flow, with zeolites and some feldspar phenocrysts, 6-8m thick. Very similar to the flow below.

BB14 4-5m thick, fine grained (<1mm) with a convoluted flow banded texture, contains more plagioclase phenocrysts (up to 1.5cm long). T/S- the plagioclase phenocrysts show some evidence of resorption and regrowth, also contains a few olivine phenocrysts.

BB15 Very similar to the flow below but with fewer feldspar phenocrysts, 4-5m thick. T/S- olivine (needle-like) and plagioclase phenocrysts.

BB16 3-4m thick, fine grained, platy flow, no plagioclase phenocrysts, but the flow contains numerous zeolites.

BB17 4-5m thick, platy flow, similar to the flow below. but it is quite altered along the plates. T/S- plagioclase and olivine phenocrysts.

BB18 3-4m thick, with numerous zeolites, very platy and fine (<1mm) grained.

BB19 Very similar to the flow below, but it contains some plagioclase phenocrysts (up to 0.75cm), which are zoned and resorped.

3-4m grassy rise before the next exposure.

BB20 Poorly exposed flow, at least 2m thick (may be the same as flow 21) blocky weathering. T/S- fine-medium grained, contains olivine phenocrysts.

5-6m grassy rise before the next flow

BB21 Fine-medium grained (1mm), with blocky/platy weathering, at least 3m thick. T/S- contains more zoned olivine phenocrysts than the flow below

BB22 Fine-medium grained (1mm) with a lot of olivine, (in clusters) the flow has a reddened base and is 1-2m thick.

BB23 Very similar to the previous flow, nobbly/blocky weathering, 1-2m thick.

BB24 Platy flow, fine grained (<1mm) 1-2m thick, with quite a lot of vesicle infills. (NM375493). T/S- plagioclase phenocrysts.

Beinn Chreagach, Ulva (NM404402)

BCH1 Columnar flow at the base (?) of the Ulva lava pile. This flow is well in excess of 20 m thick and it possesses the characteristic three tier jointing. Forms the headland, Carraig Chorach (NM412378). The small islands out to the west form the slaggy top of the flow. T/S- fine grained (<1mm) with clusters of olivine phenocrysts.

BCH2 Thin bole between BCH1 and 2 and good pipe vesicles form above this. They are inclined eastwards thus implying an eastward direction of flow for the lava. This flow is quite olivine rich, altered, fine-medium grained (1mm) and looks distinctly alkalic. 5 m thick. Sampled from the next headland west of BCH1, (NM408379).

Above this there are a series of thin, vesicular, olivine rich flows, some of which seem to die out quite rapidly.

BCH3 This flow is olivine rich and has a reddened base, fine-medium grained (1mm). It dies out seawards quite rapidly, but at its maximum it is 2 m thick.

BCH4 Very similar to the flow below with a reddened base and a lot of olivine, fine grained (<1mm). It is more laterally continuous and is about 4 m thick.

BCH5 The flow is quite fresh and the top of it is weathered to a 20 cm red bole, fine-medium grained (1mm). 5 m thick. Red horizon before the next flow.

BCH6 This flow is the one immediately below the columnar flow at the top of the cliff, fine grained (<1mm). The flow is 10 m thick, has a slaggy vesicular top and it is quite olivine rich.

BCH7 Columnar flow forming the cliff top. It contains agates and is very fine grained (<<1mm). At least 5-7 m thick.

BCH7A 200 m farther inland, flow 7 is possibly picked up again, a fault cuts the lavas between here and the coast, so the is some doubt as to it being the same flow. The flow is platy and

columnar, fine grained (<1mm). It is well over 10 m thick and contains agates. (NM412383)

BCH2X-4X These were collected on the northerly side of the fault, from beach level up to BCH7A.

BCH2X Olivine rich flow several meters thick, at beach level. T/S- the sample appears to be a mix of two magma types intermingled, one is fine grained with olivine phenocrysts, the other is coarser and is more evolved.

BCH3X 5 m thick, fine-medium grained (1mm) with blocky platy weathering.

BCH4X 5 m thick, fine-medium grained, quite altered,with a rubbly base.

There may be a fault between 7A and 7B they seem to be the same flow (check) down-throw of several meters to the SW.

BCH7B Platy, crudely columnar flow, fine grained (<1mm) at least 4-5m thick. T/S- olivine and plagioclase phenocrysts.

BCH8 Head northwards over a ruined wall, the flow is fine grained (<1mm) and is 5m thick. It contains a few feldspar phenocrysts as well as some olivine phenocrysts .

200m north of BCH7

BCH9 Fine grained <1mm, 4-5m thick, blocky weathering. This may be the same flow as 8, since there is a dip in the topography before this flow. (NM413386)

BCH10a The next flow is 5-8m thick, and is underlain by a 20-30cm red horizon and has a rubbly vesicular base. The main body of the flow has a platy texture and it contains elongated vesicles. T/S- fine grained (<1mm), quite altered in places.

BCH10b Fine grained and with platy weathering. This is the last flow before the road. (NM413388) T/S- contains aligned plagioclase.

BCH11 The first flow N of the road, opposite a gate with wooden slats. 5-8m thick, very similar to BCH10b.

BCH12 5-8m thick, fine grained (<1mm), very platy appearance. Some of the plates appear to be convoluted and bent. Contains rounded feldspar phenocrysts (up to 0.75cm)

BCH13 The next flow is 6-8m thick, fine-medium grained (1mm), with some small aligned plagioclase needles (larger feldspars are less numerous than in the previous flow) and platy weathering, (NM413390).

BCH14 The fourth flow up from the lane, the third rampart flow. The flow is 4-5m thick, less platy than BCH13, fine grained (<1mm). It contains olivine phenocrysts.

BCH15 At least 6m thick, fine grained (1mm) and more platy than the previous flow, laterally continuous for 20-30m. T/S- contains clusters of zoned olivine phenocrysts.

BCH16 Poorly exposed flow in the middle of a low boggy hollow between BCH15 & 17. Fine-medium grained (1mm), with noticeable plagioclase and olivine, blocky weathering.

BCH17 The flow is 2-3m thick and is of medium (1-2mm) grain size, rubbly/nobbly weathering, quite a fresh flow. T/S- contains olivine phenocrysts, the rock is quite altered.

2-3m grassy rise before the next flow.

BCH18 Very fresh flow, forms a prominent scarp to the west of a stream with perhaps a minor N-S trending fault in its valley (down-throw 1-2m to the W). At least 5m thick, fine grained and platy, with crude columns (NM414393). T/S- aligned plagioclase.

BCH19 4-5m thick, platy weathering, (slightly convoluted in places). Fine grained (<1mm), altered and vesicular, with elongated vesicles (in the direction of the plates). 20-30cm slaggy base.

BCH20 The flow is at least 4-5m thick, with a slightly convoluted platy texture. Fresher flow, fine grained (<1mm) with some rounded feldspar phenocrysts.

5m grassy rise before the next flow.

BCH21 Escarpment flow, at least 10m thick, crudely columnar, 1mm grain size with a few feldspar phenocrysts. T/S- fine grained groundmass, contains numerous phenocrysts of plagioclase and olivine, which form glomeroporphyitic clusters.

BCH22 Blocky weathered flow, 2-3m thick, fine-medium grain size, looks to contain more olivine phenocrysts (NM414394).

BCH23 Flow 3-4m thick, with blocky/nobbly weathering, fine grained (<1mm). The flow contains zeolite rich bands between more blocky bands, yet there is no reddening between any of these, which suggests that it is a compound? flow. Two samples collected, A at the bottom and B at the top. T/S- the two samples are similar (olivine phyric) except that A contains coarser, more evolved pegmatite patches.

BCH24 Flow 4-5m thick, fine grain size, with reddened olivine phenocrysts and a blocky/platy texture.

BCH25 The flow is at least 2m thick, has blocky/nobbly weathering, fine-medium grained (1-2mm), with a reasonable amount of olivine.

2-3m grassy rise before the next flow.

BCH26 Very similar to the flow below, it is quite badly altered and contains a lot of olivine phenocrysts.

BCH27 Poorly exposed blocky flow, at least 2m thick, fine grained (NM415397). Contains clusters of olivine phenocrysts.

3m rise before the next rampart flow.

BCH28 Over 5m thick, medium grained, with a lot of brown altered olivine phenocrysts and blocky weathering. T/S- quite a lot of interstitial zeolites.

BCH29 The top-most flow on the hill to the east of Glen Glass (200m asl). BCH29 is seen to flow over the nose of BCH28, 3-4m thick, with blocky/nobbly weathering, 3-4m thick, fine grained (<1mm). T/S- olivine phenocrysts and lath shaped opaques.

NW for 3-400m, across Glen Glass and started to collect up Beinn Chreagach (Westwards) from near the water-shed of three streams at the head of Glen Glass (NM411401). Collection was started at a lower stratigraphic level than BCH29 so the first few flows above BCH29 may be identical to BCH27-28.

BCH30 3-4m thick, fine grained (<1mm) blocky weathering. T/S- olivine phenocrysts, very similar to BCH29.

BCH31 Poorly exposed, blocky flow, 4-5m thick, fine, with a reasonable amount of olivine (some needle-like crystals). Quite a fresh flow. T/S- contains coarser pegmatite patches.

2-3m rise before the next flow

BCH32 Rampart flow, 4-5m thick with blocky weathering, fine-medium grain size, quite fresh. T/S- with zoned olivine phenocrysts.

2-3m grassy rise before the next flow.

BCH33 Poorly exposed flow, with blocky/nobbly weathering, 1-2m thick, fine-medium grained (1-2mm) quite vesicular. T/S- olivine phenocrysts (some needle-like) patchy alteration.

BCH34 The flow has a blocky texture in places and in other places it has a convoluted flow-banded texture, these two types seem to form indistinct bands, no separating boles seen. Fine-medium grained three samples collected A & B collected from the convoluted parts and C collected from the blocky part. T/S- A & B very similar with olivine phenocrysts, C contains coarser more evolved pegmatite patches.

BCH35 1-2m thick, fine-medium grained, with a lot of olivine phenocrysts. The flow is quite vesicular, with the infills being fibrous zeolites.

2-3m rise before the next flow.

BCH36 At least 2m thick, with crude platy weathering, fine grained (<1mm) with brown altered olivine.

2-3m rise before the next flow.

BCH37 Blocky/nobbly weathering, at least 2-3m thick, fine-medium grained (1mm). T/S- crudely aligned plagioclases.

BCH38 At least 2-3m thick, fine grained, very similar to the flow below. It is in a depression so it might be the same flow. (NM407403)

BCH39 Very similar to BCH37 with a lot of zeolite infills, at least 1-2m thick. T/S- more altered.

3-4m grassy rise before the next flow.

BCH40 Medium grained (1-2mm) with visible plagioclase and olivine, a blocky flow, 2-3m thick. T/S- contains some zoned and twinned phenocrysts of pyroxene.

5m grassy rise before the next flow.

BCH41 The flow is 5-6m thick, with blocky columnar weathering, fine-medium grain size, with a few conspicuous plagioclase laths.

BCH42 Poorly exposed flow, at least 3m thick, very similar to the flow below. T/S- contains some zoned plagioclase phenocrysts.

3-4m rise with no exposure.

BCH43 Fine grained, rampart flow, 6-8m thick, a platy flow with vesicle infills streaked out in the direction of the plates. T/S- aligned plagioclase crystals.

BCH44 Fine grained (<1mm), less platy flow, 6-8m thick, E of a small lochan. West of this flow there is a minor fault trending approx. N-S, with a down-throw to the E of 3-4m.

BCH45 Fine grained (<<1mm), platy flow, 6-7m thick, with a rubbly more platy top.

3-4 m rise before the next flow.

BCH46 Fine grained (<1mm) platy flow, 4-5m thick. (NM404403).

Beinn Ghormaig, (NM658574)

These lava flows were collected as a supplement to the Morvern (MR) samples, since the base of the Morvern succession was poorly exposed.

BG1 No exposed contact of the underlying Mesozoic sediments with the basal lava flow was observed here and BG1 may not be the basal flow. A fine-medium grained, spheriodally weathered flow, 4-5m thick. 300m asl. (NM656569)

5m grassy rise before the next flow.

BG2 Very rubbly, poorly exposed flow, very similar to the flow below. At least 2-3m thick.

7-8m grassy rise before the next flow.

BG3 Medium grained (1-2mm), spheroidally weathered flow, with a vesicular top and base. 2-3m thick.

BG4 Rampart flow, 6-8m thick, with blocky weathering and crude columnar jointing. Underlain by a 3-4cm BOLE!. T/S- fine grained (<1mm) groundmass with olivine and plagioclase phenocrysts with a few zeolites.

BG5 Spheroidally weathered flow, with a thin red bole below and a rubbly top and bottom. 3-4m thick. T/S- fine grained groundmass, with phenocrysts of PYROXENE! and plagioclase.

BG6 Similar to the flow below, quite weathered, dies out eastwards. 3-4m thick.

BG7 A rampart forming flow, with fine grain size (<1mm), a few zeolites and platy weathering. 3-4m thick. 360m asl. T/S- aligned plagioclase crystals.

5m grassy rise before the next flow.

BG8 Platy weathered, fine grained (<1mm), contains crystals with a shiny lustre. At least 1-2 m thick.

Beinn na h-Iolaire (NM4531)

BHL1 This is the same sample as AM1.

BHL2 Probably very similar to AM2, the flow is 6-8 m thick, with blocky platy weathering fine-medium grained. There is a minor fault in the stream gully with a down throw of about 3-4m to the west. T/S- contains olivine phenocrysts.

BHL3 The flow has a reddened vesicular top, with spheroidal weathering, 2m thick (NM454328) olivine rich, fine-medium grained (1mm), quite reddened and altered. T/S- olivine phyric.

BHL4 2-3m thick, with a similar texture to the previous flow, except it is a lot fresher. This flow is level with the road. T/S- the texture is very un-lava like, with ophitic pyroxene crystals enclosing plagioclase crystals. Because of its tholeiitic chemistry it is probably a sheet.

BHL5 Very similar to the two previous flows, olivine rich, fine-medium grained, but not as altered, 3-4m thick.

BHL6 Further up the hill on the southern side of an old rusty fence, there is a flow with a rubbly top and base, it is quite altered but it is very similar to the flow below, contains olivine phenocrysts, fine grained. 1-2m thick.

BHL7 On a little knoll which is visible from the road, the flow has a vesicular base and is about 2m thick. It is less spheroidally weathered and is of fine-medium grain size (1mm). T/S- contains phenocrysts of olivine and plagioclase.

Above this is an area of poorly exposed ground, that on both sides of the valley at this height. The reason for this can be found in the cliff section, which exposes this area of poor exposure. It is composed of highly vesicular, slaggy lava flows, with bands of less vesicular rock making up the flow centres. These flows have red bands between them and so they are not part of a pahoehoe flow. There

are about 4-5 flows with each being about 1-2 m thick. The more compact centres of the flows can be any thing up to 40-50cm thick. Three of these flows were collected (BHL8, 9 & 10)

BHL8&9 These two flows are medium grained (1-2mm), they contain a lot of olivine phenocrysts, and are very altered.

BHL10 This flow appears fresher, it seems to contain less olivine. T/S- contains olivine and plagioclase phenocrysts in a fine grained groundmass.

BHL11 The flow above this is 4-5m thick, fine (<1mm) grained, it contains quite a lot of red altered olivine. T/S- phenocrysts of plagioclase and olivine.

BHL12 1-2m thick, medium grained (1mm) olivine rich, quite altered flow. T/S- phenocrysts of plagioclase and olivine.

BHL13 Similar texture to the previous flow, 1-2m thick. T/S- 2-3mm olivine phenocrysts set in a fine grained groundmass.

BHL14 The next flow forms a headland along the Gribun ridge, the feature is clearly visible from the road, heading towards Iona. Blocky/spheroidal weathering, the flow looks to be 12-15m thick. It has a fine grained (<1mm) compact texture and contains less olivine. T/S- contains plagioclase phenocrysts.

BHL15 At least 5m thick, with blocky/spheroidal weathering, quite fresh, fine grained (<1mm). T/S- large olivine crystals, not quite phenocrysts.

BHL16 Platy weathering, quite plagioclase rich, fine-medium grained (1mm). A quite evolved flow, at least 3-4m thick. T/S- plagioclase and olivine phenocrysts.

BHL17 5m thick, not as platy the flow below, fine grained (<1mm) (NM353324) T/S- olivine phenocrysts with some sign of aligned plagioclases.

2m grassy rise before the next flow.

BHL18 At least 4m thick, fine-medium grained, platy flow. T/S- contains plagioclase and olivine phenocrysts.

BHL19 4-5m thick, fine-medium grained (1mm), blocky weathering, with quite a few ill formed olivines.

BHL20 Poorly exposed flow, at least 2-3m thick, with blocky weathering, medium grained (1-2mm). T/S- very altered with a lot of fibrous zeolites.

BHL21 Rampart flow, with blocky weathering, medium grained with a vesicular base, at least 5m thick. T/S- a few larger crystals of plagioclase and olivine, quite altered.

BHL22 Poorly exposed flow, at least 2m thick, spheroidal weathering. T/S- fine-medium grained with plagioclase

BHL23 Rampart flow, fine grained, platy, 4-5m thick. T/S- contains a few phenocrysts of plagioclase and olivine.

2-3m grassy rise before the next flow.

BHL24 4m thick, vesicular flow, fine-medium grained (1mm) quite altered, spheriodally weathered. T/S- aphyric.

BHL25 Very similar to the previous flow, 1-2m thick. T/S- fine-medium grained (1mm) with olivine and plagioclase phenocrysts.

BHL26 Again similar a texture, poorly exposed flow, at least 2m thick. T/S- plagioclase and olivine phenocrysts.

BHL27 Platy top, olivine rich flow, like the ones below, with blocky/nobbly weathering, 3-4m thick, fine-medium grain size. T/S- plagioclase and olivine phenocrysts.

Poorly exposed rise of 5m.

BHL28 Fine-medium grained, blocky weathering, 3-4m thick. T/S- aphyric.

BHL29 Platy rampart flow, fine grained (<1mm), 6-8m thick.

BHL30 Olivine rich flow, at least 2-3m thick, fine-medium grained (1mm) with a red slaggy base and top.

4m grassy rise before the next flow.

BHL31 2-3m thick, fine-medium grained (1mm). T/S- contains olivine phenocrysts.

BHL32 3-4m thick, fine-medium grained, blocky flow. T/S- quite altered with olivine phenocrysts.

3-4m grassy/scree rise before the next flow. (NM451320)

BHL33 5m thick, platy crudely columnar flow, with convoluted flow banding in places, fine-medium grained. T/S- olivine phenocrysts, and coarse pegmatitic segregations.

BHL34 3-4m thick, with nobbly spheroidal weathering, quite altered, with a lot of olivine fine-medium grained (1mm). T/S- olivine phenocrysts

BHL35 The flow is at least 2-3m thick, medium grained, with platy weathering. It looks to contain olivine phenocrysts. T/S- contains coarse segregations, with olivine and plagioclase phenocrysts.

7-8m of grass and scree before the next flow.

BHL36 This is a rampart forming flow, over 10m thick, fine grained, with a red ash/bole below. The red material contains pieces of basalt up to 5-10cm across, it might also contain crystals.

Ben More

BM1- 12 Stream section up Allt Chreaga Dubah.

BM1 Poorly exposed lava at the bridge over Allt Chreaga Dubah on the B8035. Quite badly weathered, medium-coarse grained (3mm) at least 1-2m thick. (NM468317)

BM2 Reasonably fresh lava, fine-medium grained (1mm), 5m thick.

BM3 A red bole separates this lava from the underlying one, the flow itself is bright red in colour and is therefore very altered, plagioclase pseudomorph needles recognisable, fine-medium grained (1mm). It is about 3m thick.

BM4 Fresher than the previous lava, but it has a curious red-yellow weathered surface, fine-medium grained (1mm), 3m thick.

BM5 Thick flow, fine grained with olivine phenocrysts (2-3mm), 8-10m thick.

BM6 5m thick flow, fine grained (<1mm) there is possibly a thin flow between BM5 & 6.

BM7 Fresh flow, medium grained (1-2mm), 1-2m thick. T/S- looks to have a glomeroporphyric texture in places.

BM8 Three inch red bole underlies this flow, which contains large (1cm) amygdales, infilled with zeolites and a green micaceous mineral, fine grained (<1mm) groundmass with olivine phenocrysts (1-2mm), 5m thick.

BM9 3m thick flow, with a spheroidally weathered surface, it looks to contain a lot of red, altered olivine, fine-medium grained (1mm).

BM10 Olivine & clinopyroxene rich flow, medium grained (1-2mm) 3m thick. Three further samples collected, from the top, middle and base of the flow, BM10A, B, & C.

BM11 Rubbly, spheroidal weathering, medium grained (1-2mm), 5m thick.

BM12 5 m thick, with spheroidal weathering, the rock is quite altered and it is medium grained (1-2mm).

BM13 Lava, forming a rampart flow, fine grained (<1mm) with olivine phenocrysts (2-3mm) several feldspar phenocrysts were also noted. 10m thick. (NM469319)

BM14 In a small stream bed to the south-west of Allt Chreaga Dubah, at least 2m thick, fine-medium grained (1mm), quite altered. (NM472318)

BM15 Small rusty red outcrop, poorly exposed. The red alteration appears to be patchily developed and red veins may also be seen. The lava is at least 2m thick and is medium grained (2mm).

BM16 A fine grained (<1mm) flow with a few feldspar phenocrysts and green infilled vesicles, forms the next rampart. It looks to have a platy weathering texture, 3-4m thick.

BM17 Reasonably fresh lava, very similar to BR16, contains some zeolites, 3m thick.

Between this flow and BMS1 there is a grassy area with no exposure, this represents 10m in height and may hide another flow. (NM474318)

BMS1 This forms a rampart about 10m thick. In the field this 'flow' was strongly suspected to be a sill. Upon subsequent examination the lack of vesicles, the anomalously fresh nature of the rock and its markedly different chemical composition confirmed this suspicion.

BM18 The lava has a blocky appearance, fine-medium grained (1mm) with well formed olivine crystals 4m thick.

BM19 The flow contains large green vesicular infillings, very fine grained (<<1mm) 2m thick.

BM20 Platy/blocky weathering, green infillings, very fine grained (<<1mm), 2-3m thick. 335m asl. (NM477320)

BM21 Five meter grassy rise before the next flow, which is platy weathered and contains flow banding, 2-3m thick. T/S- fine grained (<1mm), with slight alignment of plagioclase.

BM22 Poor exposure possibly a separate flow, slightly platy weathered again with green infillings, fine grained (1mm), 2-3m thick.

BM23 Less platy with fewer amygdales, patchy outcrop, 3-4m thick. T/S- fine grained (<1mm) with olivine phenocrysts (up to 2mm), which show slight evidence of resorption.

BM24 More massive blocky flow, dies out southwards, it contains small feldspar phenocrysts and elongated amygdales, fine-medium grained (1mm), 5-6m thick.

BM25 Similar to the flow below, it contains cracks infilled with secondary minerals, fine-medium grained (1mm), 6-7m thick.

BM26 Southward along 350m contour for 400m, very little exposure. The next flow encountered has a blocky appearance and has a nobbly surface, 10m thick, T/S- fine-medium grained with quite a lot of poikilitic clinopyroxene. Sample collected from near the top of the flow.

3m grassy rise before the next flow.

BM27 Possibly 2-3m thick but very poorly exposed and badly altered. Significant quantities of zeolitic material and red altered olivine can be seen, medium grained (1mm). 3m grassy rise before the next flow.

BM28 The flow seems to dip in towards Ben More (3-4°). It has a red patchy surface and has a blocky appearance. At least 3-4m thick, fine-medium grained (1mm) with well formed olivines. 370m asl (NM487316).

6-7m grassy rise before the next flow.

BM29 Vesicular, zeolite packed base with slight development of pipe amygdales. The flow is 7-8m thick and is spheroidally weathered, fine-medium grained (1mm), quite altered. It contains a few veins of zeolitic material along joints. BM29A collected near the bottom of the flow, BM29B collected near the top.

Poorly exposed flow between BM29 & 30 which was not sampled. 3m grassy rise before the next flow.

BM30 Poorly exposed blocky flow, at least 3m thick. Approx. 400m asl. T/S- Quite fresh, it contains numerous plagioclase phenocrysts, they show some evidence of resorption, and are slightly glomeroporphyritic medium grained (1-2mm).

BM31 4m grassy rise then a 5-6m flow, with blocky, spheroidal weathering, quite badly weathered, medium grained (1-2mm).

BM32 Badly weathered, both spheroidally and along cracks and joints, medium grained (1-2mm). 3m thick.

BM33 Next flow collected up the first tributary of Allt a' Mhuchaidh (NM488320) Very poorly exposed, spheroidally weathered, very similar to BM32 fine-medium grained (1mm).

BM34 Quite fine grained (<1mm), fresh flow, patchy outcrop, 4-5m thick.

BM35 At least 5m thick, with excellent flow textures, some infillings seem to align along flow bands. T/S- contains plagioclase and olivine phenocrysts (1-2mm with a fine grained groundmass.

BM36 Blocky, spheroidal weathering, 5m thick, medium grained (1-2mm). 445m asl.

Head between the two hills (keeping approximately to the 420m contour line) to the north face of Maol Mheadhonach where samples BM37 & 38 were collected (NM501325). Since the lavas seem to dip gently westwards in this region and since 25m in altitude has been lost since the last outcrop. BM37 is stratigraphically lower in the succession than BM36. these two lavas were collected to help in geochemical correlation between BM1-36 and the remainder of the Ben More section.

BM37 Very altered, blocky flow, contains some large green vesicle infillings. 3-4m thick. T/S- contains a lot of clinopyroxene, medium grained (1-2mm).

BM38 Quite fine grained (<1mm), blocky appearance, with large (1-2cm) green and white infillings.

The next sample was collected from the highest point of the valley between the main slope of Ben More and Maol Mheadhonach (NM508324) 400m asl.

BM39 Poorly exposed outcrop, blocky weathering, very altered (reddish colour), fine grained?, alteration makes it difficult to tell. Contains many infillings (some epidote), at least 2-3m thick. 5m grassy rise before the next flow.

BM40 Poorly exposed, less altered flow, fine-medium grained (1mm), at least 2m thick.

Before the next definite flow there is a 12m rise littered with large scree blocks it is therefore difficult to work out what might be a flow and what is a block. As a result no samples were collected here.

BM41 Poorly exposed, blocky flow. Quite badly altered to a greenish/red colour, fine-medium grained (1mm). At least 2m thick, 420m asl.

5m grassy rise before the next flow.

BM42 Blocky weathering with dark green amygdale infillings (up to 1cm in diameter) 2m thick.

15-20m of grass and scree before the next positively identifiable flow. (NM510322)

BM43 Greenish, fine grained, slightly platy weathered, 5m thick. 460m asl.

BM44 Platy pale weathered flow with blocky joints, 8-10m thick. Contains a small vein (5-15cm) of basaltic material.

15-20m of scree to the base of the next flow.

BM45 Very similar to BM44 but much more vesicular. 5-7 m thick. 485m asl.

BM46 Flow at least 4m thick. Platy weathered at the base and top but with a massive compact interior. Vesicular bands run through the flow.

BM47 Very similar to the previous flow, but contains feldspar phenocrysts. Flow at least 2m thick. (NM512323)

BM48 Massive interior, platy margins, contains feldspar phenocrysts. Quite badly weathered. 2-3m thick.

BM49 Rubbly, platy flow, very altered with numerous green infillings. 2m thick. Approx. 510m asl.

BM50 Platy flow, feldspar phyric and very altered. 3m thick.

BM51 Blocky weathering with a slight platyness, weak flow textures can be seen. Contains vertical vesicle bands, up to 5cm across and a few thin (1-5mm) green veins. 3m thick.

5-7 m grassy stony, grassy rise before the next flow

BM52 Poorly exposed flow, probably 2-3m thick. Fine grained, badly weathered along plates. 530m asl. T/S- very altered, with many serpentinous infillings, a few plagioclase laths may be seen and perhaps some pyroxene, fine grained.

BM53 Platy flow, contains a few vesicles which seem to line up along the direction of the plates, very fine grained (<1mm). 4-5m thick.

BM54 A very platy flow, with a few large green vesicle infillings, composed of chloritic material, epidote and a clay mineral. 4m thick. T/S- fine grained (<1mm) flow banded with more Fe/Ti oxide rich bands in places, a few resorped plagioclase phenocrysts may be seen in places.

4m grassy rise before the next flow.

BM55 Platy flow, with large (1-5cm) infillings, some of which are lensoid in the direction of the plates, appears to contain flow textures, fine grained (<1mm), with a few altered plagioclase phenocrysts, quite evolved. Contains a few veins. At least 3-4m thick.

BM56 Less platy, with fewer infillings, fine grained (<1mm). More platy towards the top and base. This flow can be traced along the hill side for at least 200m. 5-6m thick. (NM514318). T/S- contains quite a lot of plagioclase, some of which is glomeroporphyritic.

BM57 Poor exposure, vertically jointed with a platyness in places. 3m thick. T/S- fine grained with some alignment of plagioclase crystals, quite evolved.

5m grassy slope before the next flow.

BM58 Quite vesicular, some are 2-4cm in diameter. the infillings appear to be zoned with green and white bands near the margin, with a central portion of fibrous needles. A platy, fine grained (<1mm) rock, feldspar phyric. At least 4m thick.

5m grassy slope before the next flow.

BM59 Weak platy weathering, with some large zoned infillings. 3-4m thick. The lavas seem to dip towards Ben More, very fine grained (<1mm). Approx 600m asl (NM516319).

5m scree rise before the next flow.

BM60 Very fine grained (<<1mm), very pale flow with platy weathering and few vesicle infillings. 3m thick. T/S- contains aligned plagioclases.

BM61 Flow seems to dip ESE 15-20°. Very platy and fine grained (<<1mm). 5-6 m thick. T/S- the pyroxene, which is interstitial has a greenish tinge in places.

BM62 Less platy, very fine grained (<<1mm). It appears to have a convoluted flow texture in several places, aligned plagioclase. 5m thick. 630m asl.

BM63 Poorly exposed platy flow beside two small lochans. 2-3m thick. T/S- fine grained (<1mm), with aligned plagioclase.

BM64 Very platy flow, some flowage textures, with infillings aligned along the plates, very fine grained (<<1mm) seems to dip in a NNE direction. 2m thick.

BM65 Very similar to the last flow. 2m thick. T/S- very fine grained (<<1mm), with a flow banded texture. The infillings have a tendency to be aligned and contain epidote, chlorite and clays.

BM66 Platy flow with some flowage textures, few infillings. 5-7m thick. 670m asl. (NM522322). T/S- very fine grained (<<1mm) with aligned plagioclase crystals.

BM67 Less platy, more infillings, seems to dip NNE. Contains big feldspars (up to 4cm long) with rounded corners. 3-4m thick. T/S- fine grained (<1mm), with zoned and resorped plagioclase phenocrysts.

BM68 Platy, fine grained flow, poorly exposed. Shows flowage textures. 4-5 m thick. 685m asl. T/S- plagioclase and olivine phenocryst pseudomorphs (1mm) set in a very fine grained (<<1mm) groundmass.

BM69 Again it shows a flowage texture and is fine-medium (1mm) grained but it is less platy. 3m thick.

BM70 Similar to the flow below. At least 4m thick. T/S- fine grained (<1mm), with poikilitic clinopyroxene.

5-7m grassy/scree rise before the next flow.

BM71 Riddled with infillings and veins, which seem to feed some pods (some up to 10cm long) of infill material, fine-medium grained (1mm) with pseudomorphs of olivine phenocrysts. Platy flow, 4m thick.

3-4m grassy rise before the next flow.

BM72 Platy flow with fewer infillings. Badly weathered along the plates 4m thick. T/S- fine grained (<1mm) with corroded plagioclase phenocrysts one clinopyroxene phenocryst noted.

10m grassy rise before the base of the next flow.

BM73 Blocky, platy flow, with large elongated infillings (5cm) 7m thick, fine grained (1mm) with well formed olivine phenocrysts and a few corroded plagioclase crystals.. 740m asl. (M523323)

BM74 Very similar to the flow below but feldspar phyric (corroded), fine-medium grained (1-2mm) with poikilitic pyroxene crystals. 4m thick.

The next flow was not sampled, because it was stuffed with infillings, 5m thick.

BM75 Platy vesicular flow, with green and white infillings and dark green, black alteration patches, opaques (secondary alteration), fine-medium grained (1mm), with well formed olivine phenocrysts. 5m thick.

BM76 Vesicular, platy flow, with the vesicle infillings aligned along the plates. T/S- fine-medium grained (1mm), with disseminated granular pyroxene and olivine phenocryst pseudomorphs. The flow seems to dip in a northerly direction. 7m thick.

BM77 Platy flow with some large (10cm) vesicle infillings and numerous smaller ones, very similar to the previous flow. 6m thick. 780m asl. (NM524324)

BM78 Fine grained (<1mm) with remnants of well formed olivine phenocrysts, platy flow with green/white infillings. A few feldspar phenocrysts can be seen. 3-4m thick.

BM79 Platy, flow banded structure, quite vesicular, fine grained (<1mm), with green/black patches. 2-3m thick.

BM80 A sheet cuts across the lavas at this point, it is 1-2m thick and dips steeply in towards Ben More. Platy flow, quite vesicular, with infillings aligned along plates. 4-5m thick. T/S- fine-medium grained (1mm), once was olivine phyric, very altered.

The next flow is 4-5m thick, but is very vesicular and so was not sampled. 820m asl.

BM81 Very vesicular very altered and oxidised fine-medium grained (1-2mm), platy flow with plagioclase phenocrysts, 4-5m thick.

BM82 Thin vesicular, platy flow, very similar to the previous flow, except it is fresher, 2-3m thick.

BM83 Platy flow, fine grained (1mm) with poikilitic pyroxenes, with infillings aligned along the plates. Some infillings are up to 5cm long and 2-3cm wide. The flow is also shot through with pale green veins. 5m thick.

3m scree rise before the next flow.

BM84 Weak indistinct, platy weathering, with quite a few infillings 3-4m thick. T/S- fine grained (<1mm), with olivine phyric pseudomorphs, and poikilitic pyroxene.

BM85 Very vesicular and quite platy with feldspar phenocrysts. 3-4m thick. T/S- very similar to the previous flow, but slightly coarser.

7-8m scree slope before the next flow. A poorly exposed green bole (5-7cm thick) was found half way up this slope. Quite a few dykes and sheets cut the lavas here. 870m asl.

BM86 Platy flow with green infillings (serpentine), fine grained (<1mm). 3-4m thick. (NM526325)

3-4 m sheet before the next flow.

BM87 Less platy but still vesicular and badly altered, very fine grained <<1mm). It contains some deep red patches, in thin section these look to be oxidised and altered patches. 3-4m thick.

BM88 Platy flow, fine grained <1mm) with some vesicle infillings up to 5cm across. 3-4m thick. 3-4m to the top of the ridge (NM527326) 900m asl.

BM89 Between the cairn and the first ridge (NM526327), green, altered, vesicular flow. It is not easy to see individual flows. T/S- Was once olivine phyric, now psuedomorphs.

BM90 3m rise, sample again, fine grained, less green. T/S - Plagioclase and olivine phyric.

BM91 Similar to BM90, but fresher, well formed olivine pseudomorphs, fine-medium grained.

BM92 Slaggy slightly reddened base to the flow, which is 3-4m thick. T/S - olivine and plagioclase phenocrysts, fine grained.

BM93 Feldspar phyric flow , the plagioclase is labradorite and it has a fragmental habit. (NM525328)

BM94 A 3-4m thick flow. Now individual flows can be identified. Fine grained.

BM95 3-4m thick flow, with a platy top and bottom, fine-medium grained and a hard solid interior, epidote seen.

BM96 The flow is at least 4-5m thick, it is fine grained and has a platy top and bottom. T/S - aphyric with well formed olivines.

BM97 Contains patches and streaks of green vesicle infills areas, fine grained (1mm). T/S- olivine phyric.

BM98 1-2m flow, platy, fine grained. T/S- with plagioclase phenocrysts, which seem quite calcic.

BM99 The top-most flow on Ben More (NM526330/1) at least 2-3m thick, green and altered, fine grained (<1mm).

Beinn Reudle Section, Western Mull. (NM363464)

BR 1 Massive lava, beside sheep shelter, base obscured by the beach, at least 2-3m thick. (NM363455). T/S- Fine grained, contains some, aligned and zoned plagioclase phenocrysts.

BR2 Similar to previous lava but very difficult to get a zeolite free sample, 3-4m thick. T/S- fine grained (<1mm).

BR3 Again similar, 5m thick. T/S- fine grained (<1mm) quite fresh, well formed olivines.

BR4 Very difficult to get a fresh, unzeolitised sample, 3m thick. T/S- Fine-medium grained (1-2mm) interstitial zeolites.

BR5 Fresh lava with olivine phenocrysts, very fine grained (<<1mm) 4m thick, (NM363455).

BR6 Massive flow, crudely with trees at the base, medium grained (1-2mm) 15 - 20m thick. (NM364457). T/S- contains interstitial zeolites.

BR7 - 13 These represent a series of thin olivine rich flows, separated by several centimetres of red bole, only the larger flows within this group were able to be sampled.

BR7 Contains pipe vesicles at the base (Westwards flow direction) medium grained (1-2mm), 2m thick. T/S- contains interstitial zeolites.

BR8 Similar to previous lava, medium grained (1-2mm), 3m thick.

BR9 0.5m thick, thins out rapidly, very altered, medium grained (1-2mm). T/S- some of the olivine crystals are embayed.

BR10 0.5m thick, thins out rapidly, very altered, fine-medium grained (1mm). Pipe vesicles at the base - flow direction eastwards.

BR11 Quite badly weathered, blocky appearance, 4m thick. T/S- Medium grained (1-2mm), some well formed olivines, but some are embayed.

BR12 Fine grained (<1mm) olivine lava, 2m thick. T/S- well formed olivines show slight evidence of zoning.

BR13 Quite fresh with red weathered olivine, 0.5 m thick, fine grained (<1mm). T/S- coarser stringy patch within the section .

BR14 Fresh, fine grained (<1mm), massive lava, 3m thick. (NM363458)

BR15 Rubbly, massive flow, badly weathered, 4m thick, medium grained (1-2mm), underlain by a thick bole, 15-20cm thick.

BR16 Fresh, medium grained (2-3mm) lava, few zeolites, 2m thick.

BR17 Quite an altered flow, 4-5m thick. T/S- medium grained (2-3mm) with poikilitic clinopyroxenes.

BR18 Poorly exposed blocky flow with numerous zeolites, very fine grained (<1mm) at least 3m thick. T/S- aligned plagioclase crystals.

BR19 Very similar to BR18, fine grained (<1mm) at least 2m thick. T/S- aligned plagioclase.

BR20 Very fine grained (<<1mm), massive flow with fewer zeolites, 4m thick.

BR21 Contains a lot of olivine, fine grained (<1mm), quite poorly exposed, at least 4m thick.

BR22 Quite fine-medium grained (1mm), with a few large zeolites, 3-4m thick.

BR23 Platy weathering with flow textures, fine grained (<1mm) 5m thick. Situated 20m north of a tiny lochan at a sharp bend in a fence.

BR24 Again this lava has a platy weathering texture, the outcrop is small but judging by the topography the flow is at least 4m thick. (NM364462) Approx. 160m a.s.l. T/S- very fine grained (<<1mm), with orientated plagioclase crystals.

BR25 This lava is more massive, however, it still retains a platy texture, fine grained (1mm) contains feldspar phenocrysts 1-2cm in length. 3m thick at its maximum but the flow thins rapidly to the west.

BR26 A platy, fine grained (<1mm) flow showing marked flow textures, appears to be quite badly weathered, 4m thick.

BR27 A platy weathered big feldspar lava with really curious curved flow textures (see chapter on field observations) fine grained (<1mm). 5m thick. T/S- zoned and resorped plagioclase phenocrysts.

BR28 Big feldspar (zoned), platy lava, fine grained (<1mm), fresh fine grained basalt, 5m thick.

BR29 More massive lava, fine-medium grained (1mm) with numerous zeolites and feldspar phenocrysts. T/S- contains feldspar phenocrysts which are zoned and show evidence of resorption and regrowth.

BR30 Platy weathering, forms a large ridge near the top of the hillside, 5m thick. T/S- fine-medium grained (1mm) with zoned, aligned plagioclase crystals.

BR31 Poorly exposed massive flow, at least 3m thick. T/S- very fine grained (<1mm), with aligned plagioclase.

BR32 Not a very fresh lava, fine grained (<1mm), 3m thick.

BR33 Forms the top of Beinn Reudle, shows blocky weathering, fine grained (1mm), aligned plagioclase, at least 2m thick.

Carsaig, Malcolms Point (NM501187)

C1 Vesicular flow on the sea shore, 2-3m thick, fine-medium grained (1mm). T/S- interstitial deep lilac-pink clinopyroxene, quite altered.

C2 Poorly exposed flow, 1-2m thick, with plagioclase phenocrysts (small) it has a frothy slightly reddened top. T/S- fine-medium grained, with no fresh olivine, pyroxene the same colour.

C3 The flow is 2m thick including 1m of slag on the top, fine-medium grained (1mm) with a reddened top above the slag. The flow is quite altered and it once contained olivine phenocrysts.

C4 Flow 2-3m thick, with a 1m slaggy top and a massive interior, fine-medium grained. T/S- very similar to the previous flow, more altered.

Above this there is a thin coaly mudstone 40-50cm thick, which is overlain by a conglomerate with blocks of basalt and flint up to 20-50cm across. Basalt and flint sampled C5. The flinty conglomerate fines towards the top (up to 4-5cm in diameter). This horizon grades upwards into a darker shaley horizon of about 0.5m, thickness. The basalt is very altered and fine grained with pseudomorphs after olivine.

C6 1-2m thick flow above this, crudely columnar, the upper contact is uneven. T/S- fine grained, with clear granular clinopyroxene.

C7 Fine grained (<1mm) distinctly columnar flow, over 10m thick. T/S- contains discrete phenocrysts of clinopyroxene with included plagioclase, also fragments of plagioclase. Carsaig Arches (NM495185)

C8 Columnar flow above the arches, 10m thick, possibly the same flow as C7. Very similar to the previous flow.

C9 Fine flinty bed below the Carsaig Arches sill. T/S- contains pieces of rounded strained quartz and fragments of feldspar rich basalt as well as fragments of plagioclase crystals.

C10 Breccia/agglomerate underlying the flinty bed. T/S- flinty tuff grades upwards into a more volcanic tuff.

Croghan Peninsula

20-30m south of the road (NM699273).

CA1 Fine grained flow (<1mm) at least 3-4m thick, it is very altered and is cut by white veinlets, CA1-Fi. T/S- plagioclase and perhaps some olivine phenocrysts portion of the flow is made up of a coarser, rock, which may be a pegmatite segregation, sampled as well, CA1-Co.

Heading in a SW direction, 3-4m grassy rise before the next flow.

CA2 Again very altered with white veins, the vesicle infills contain a whitish green material, The flow is medium grained (1-2mm) and at least 3m thick. T/s- Plagioclase phenocrysts, the flow is quite evolved.

CA3A The next flow has a platy texture, is fine grained and is at least 4-5m thick. Very altered with numerous veinlets which form a net-like pattern. T/S- Very altered, could well be some form of ash since there are no crystals in the groundmass. The rock contains plagioclase phenocrysts, some of which appear fragmental.

CA3B The next flow contains numerous labradorite-bytownite phenocrysts (3-4mm), as well as a few olivine phenocrysts. The groundmass is quite fine grained and the rock is reasonably fresh.

8-10m rise before the next flow.

CA4 Similar to the flow below with some small andesine phenocrysts, again it is very altered with little greenish veins, poorly exposed flow, South of CA1, 50-70m asl, fine-medium grained. T/S- Plagioclase needles up to 5mm long.

"Inclined basic sheet" above CA4 .

CA5 Above the sheet in a SW direction, the flow is very altered with green and white vesicle infills, contains a few rounded plagioclase phenocrysts (up to 1cm long) at least 1-2m thick. T/S- fine grained, quite evolved - the feldspars have a low extinction angle.

CA6 The next flow is immediately to the south of a ruined farmstead, (NM698268) Blocky-platy flow, fine grained (<1mm) and compact, with alteration veinlets, 3-4m thick. The flows dip gently to the SE. T/S- flow banded, aligned feldspar.

6-8m vertical rise before the next flow

CA7 Poorly exposed flow but can be traced laterally, similar to the flow below, 4-5m thick., fine grained.

CA8 Fine grained, very badly altered, probably 5m thick. T/S- platy with aligned feldspar phenocrysts.

CA9 Fine grained (<1mm) very similar to the flow below, 3-4m thick, very altered with green epidote and a few red patches. T/S- May well be an ash fall deposit composed of the same material as CA8 since the chemistry is identical. The rock contains aggregates of plagioclase crystals, with a fragmentary shape. The finer grained "groundmass" looks also to contain fragments of plagioclase and clinopyroxene.

CA10 On the other side of a stream gully trending approx. E-W, with a solitary tree growing on the southern side. It might be the same flow, it is similarly fine grained but contains feldspar phenocrysts, 3-4m thick. T/S- similar in texture and chemistry to CA2. The plagioclases look to be labradorite.

3-4m gap before the next flow.

CA11 Flow about 5m thick, fine grained, blocky weathering, contains disseminated sulphide minerals. Similar to CA8 and 9.

Head south-west. 5m rise before the next flow.

CA12 Rampart flow, (NM697263) feldspar phyric (up to 0.75cm), groundmass is fine grained. Massive blocky flow 5m thick. T/S- the feldspar is andesine and seems to occur in irregular fragments.

CA13 The next flow is fine grained, it has blocky weathering and contains disseminated sulphides. 1-2m thick. T/S- Andesine phenocrysts, needle-like 1-2mm long.

5m grassy rise before the next flow.

CA14 The flow is at least 3-4m thick and is feldspar phyric. T/S- fine-medium grained, with needle like pyroxene and plagioclase crystals occurring in star-like clusters.

3-4m rise before the next flow.

CA15 Fine grained, aphyric, poorly exposed flow, at least 1-2m thick. May be the equivalent of the Skye Preshal Mhor type.

Head westwards over flat lying boggy ground for 2-300m, no exposure. Started collecting at a lower altitude than CA15.

CA16 Altered feldspar phyric lava, poorly exposed at least 1-2m thick. T/S- the plagioclase is labradorite, the rock seems also to contain clots of labradorite (cf. Donaldson 1977).

CA17 Flow at least 3m thick, fine grained <1mm and platy.

CA18 Flow over 5m thick, with obvious plagioclase needles, some of which appear fragmental.

Across a boggy valley, westwards for 1-200m.

CA19 Probably the same flow as CA18, over 5m thick, feldspar phyric. There may be a bole between this and the overlying flow. T/S- the feldspars are labradorite, and they appear quite fragmental and in several instances slightly bent. It may well be an ash/crystal tuff.

CA20 Top-most flow, at least 5m thick, medium grained with feldspar phenocrysts (up to a 1cm in length) T/S- very similar to the "flow" below, (NM696254).

Killiechronan (NM542243)

K1 Close to a forest track junction (NM545420), fine grained (<1mm) flow, 4-5m thick. It is quite vesicular and has a patchily reddened top. T/S- aligned plagioclase, with plagioclase phenocrysts.

K2 Fine-medium grained (1mm), fresher flow, at least 5m thick but could be as much as 8m.

K3 Fine grained, compact flow, at least 4m thick. T/S- with aligned plagioclase phenocrysts.

K4 Pale, platy flow, fine grained (<1mm), well over 10m thick. (NM542413) T/S- flow banded, perhaps contains some amphibole.

Morvern (Sidhean na Raplaich)

MR1 Quite a fresh, fine grained (<1mm) poorly exposed lava, overlying Jurassic/Triassic sediments, at least 3m thick. (NM644548) Approx. 100m asl.

MR2 Coarse-medium (2-3mm) grained, olivine rich flow, with crude columnar jointing, 15m thick.

MR3 This flow thins out rapidly on both sides, it has a slight layered appearance and at its maximum is 8m thick, fine-medium grained (1mm) with well formed olivine crystals.

MR4-7 Four, thin, quite badly weathered flows each about 2-3m thick. MR6 contains feldspar phenocrysts and it is fine grained (<1mm), unlike MR4,5 & 7 which are medium grained (2mm). MR6&7 have a pink material associated with the zeolites.

MR8 Badly altered flow, in a gully at the edge of the forest, 8m thick, medium grained (1-2mm).

Below this flow is a thin (0.5m) altered flow, which was not collected.

MR9 Fine-medium grained flow (1mm), olivine rich flow with spheroidal weathering, 10m thick. T/S- Well formed olivine crystals, which have a tendency to aggregate together.

MR10 Similar to the previous flow, fine grained, 4m thick. (NM642547) Approx. 250m asl.

MR11 Opposite a small fenced off area, contains numerous zeolites, 3m thick, fine-medium grained (1mm) with well formed olivine crystals, which have a tendency to form aggregates.

MR12 To the west of the previous outcrop, the flow has green grass around the base, at least 3m thick. T/S- medium grained (1-2mm) with olivine aggregates and poikilocrysts of clinopyroxene.

MR13 The top-most plateau flow, at least 2m thick. T/S- fine grained, contains a few large zeolites, next to one of these fresh olivine may be found.

The plateau continues for 1.5km in a south easterly direction before the slopes of Sidhean na Raplaich are reached.

MR14 SE of MR13 for 3-400m there is no exposure over low peaty ground. Blocky flow, with a few white vesicle infillings and some small feldspar phenocrysts and well formed olivines, fine-medium grained (1mm). 2-3m thick. (NM641538)

MR15 ESE of MR14 for 5-600m over low peaty ground (10m rise). Blocky flow, slightly platy, fine grained (<1mm). 2-3m thick. 290-300m asl. (NM643532)

MR16 Very fine grained (<<1mm), blocky/platy appearance, poor scrubby exposure 3-4m thick. T/S- contains corroded phenocrysts of plagioclase.

MR17 50-100 m ESE of the last flow, forms a ridge. Platy, with quite a few vesicle infillings and some small feldspar phenocrysts, fine grained (<1mm). 3-4m thick. 310 m asl.

MR18 Red, vesicular platy weathered bottom, very fine grained (<1mm) with aligned plagioclase, blocky appearance. It contains a few 1cm infillings. 4-5m thick.

MR19 Quite platy, especially near the base of the flow, fine grained with some plagioclase phenocrysts. The plates show some evidence of flowage textures. A pale flow, with few zeolites. 4-5m thick.

MR20 3-4m thick, similar to the flow below, but fine-medium grained (1mm), more olivine rich and more weathered.

MR21 A fine grained (<1mm) blocky/platy flow, but with large feldspar phenocrysts. T/S- quite evolved, with a lot of aligned plagioclase. 4-5m thick. 330m asl.

MR22 Platy, fine grained (<1mm), feldspar phyric rock, quite altered. 4-5m thick.

MR23 Fine grained (<<1mm) and very platy with plagioclase phenocrysts, forming the top of a knoll before a plateau. 5 m thick. 355m asl. (NM643529)

MR24 150m SW of MR23, low peaty ground in between the two flows, a poorly exposed flow, which looks superficially blocky, but inside it is quite platy, very badly weathered, with a few vesicular infillings, fine grained (<1mm). At least 2m thick.

MR25 100m further south at 375m asl, to the south side of a small stream valley, where a platy flow with feldspar phenocrysts is exposed. T/S- fine grained (<1mm) with rounded plagioclase phenocrysts.

MR26 Flow 4-5m thick, with a blocky/platy appearance. Contains a few vesicles and feldspar phenocrysts can be seen on weathered surfaces, very fine grained (<<1mm). The flow rapidly dies out westwards, were another (MR27) appears to flow over the top of it.

MR27 Very similar to the one below, fine grained (<1mm) plagioclase phenocrysts have been resorption and regrowth, quite altered. 3-4m thick.

Grassy, peaty rise (5-7m) before the next flow.

MR28 A platy, fine grained (<<1mm) highly feldspar phyric flow. The feldspars are up to 3cm long and have rounded corners ie. they appear to have suffered resorption.

MR29 A very platy, pale, fine grained (<1mm) flow, highly feldspar phyric (up to 2cm in length). 3-4m thick. 415m asl.

7-10m vertical rise with no exposure.

MR30 Spheriodally weathered flow, fine-medium grained (1mm) with a vesicular base and small feldspar phenocrysts. 4-5m thick. (NM523639)

MR31 Blocky flow, fine-medium grained (1mm) with a few fibrous zeolite infilled vesicles. 2m thick.

MR32 Badly weathered, rubbly flow, with a zeolite packed base, looks quite olivine rich, fine-medium grained (1mm). 3m thick.

5 m grassy rise with no exposure.

MR33 Very poorly exposed flow, looks to be platy. Very fine grained (<1mm) with a few plagioclase phenocrysts and some zeolites. At least 2m thick. 460m asl.

MR34 The flow shows spheroidal weathering, fine grained (1mm) with a rubbly base, rounded feldspar phenocrysts (2-3cm long) and aligned vesicles. Despite superficial weathering inside the flow, fresh samples can be obtained. 5m thick. T/S- aligned plagioclase and poikilitic pyroxene.

MR35 Very fine grained, poorly exposed flow, with a platy appearance. T/S- patchy chloritic alteration. Labradorite phenocrysts, groundmass andesine. At least 2m thick.

10-15m vertical rise with no exposure and I had to veer 2-300m to the west in order to get the next exposed flow.

The next four flows appear quite pale in the field.

MR36 Blocky, highly feldspar phyric flow, the feldspars are rounded and are set in a fine grained (<1mm) groundmass. The feldspar laths seem to be less rounded than previous flows. Rampart flow 8-10m thick. Top of the flow 500m asl. (NM635520)

MR37 Rampart flow, with a blocky, platy appearance, fine grained groundmass (<1mm). Again highly feldspar phyric. 7-10m thick.

MR38 Platy at the bottom and crudely columnar further up. Less feldspar phyric than the previous flow. T/S- fine grained groundmass, the plagioclase phenocrysts are highly resorped. 8-10m thick. (NM638517)

MR39 Poorly exposed badly weathered flow, with a large number of feldspar phenocrysts, similar grain size to the flow below. At least 2m thick.

MR40 4m grassy rise before the next flow which is 5m thick. This blocky flow is more basaltic and contains no feldspar phenocrysts or zeolites. Fine grained (<1mm), with glomeroporphyritic plagioclase phenocrysts.

MR41 Blocky, basaltic, slightly feldspar phyric flow, fine grained with a few zeolites. T/S- very similar to the previous flow. Seems to curve gently over the top of the hill. 550m asl (NM636527)

Tobermory - Bloody Bay (NM493574)

T1 Columnar flow 10-15m thick, with the characteristic three tier structure. The thickness of the basal columns can be up to 0.75m. Fine grained (<1mm) with plagioclase phenocrysts and fragments of clinopyroxene

T2 Crudely columnar, fine-medium grained (1mm) the flow is about 5m thick. T/S- olivine phenocrysts.

T3 Fine-medium grain size, a few small olivine phenocrysts can be seen, at least 10m thick.

T4 Possibly a separate flow, texture similar to T3. T/S- fine-medium grained, with well formed olivines and lath shaped Fe-Ti oxides.

T5 Blocky flow with a slaggy base and a thin bole below, 5-8m thick, fine grained, olivine phenocrysts.

T6 Possibly a separate flow. It has blocky weathering and contains a reasonable amount of olivine. 3-4m thick. T/S- fine grained.

T7 Similar to the flow below but more altered and vesicular, 3-4m thick.

3-4m grassy rise between this and the next flow.

T8 Flow 3-4m thick, quite fresh, with less vesicles, medium-fine grained. T/S- variable colour of clinopyroxene, olivine phenocrysts altered.

Walked 3-400m westwards over some gently undulating ground, dissected by a few streams, (Glac Mhor) to the foot of An Speireachan (NM487565)

T9 A flow from this intervening "flat" ground was collected. A poorly exposed flow. T/S- quite altered, contains a lot of olivine phenocrysts.

T10 Below a deer fence. The flow is not very well exposed, it is at least 3-4m thick, blocky flow, with plagioclase and sparse olivine phenocrysts.

T11 The first flow west of the deer fence, a poorly exposed flow but at least 3-4m thick, with blocky weathering. Very altered, with chlorite and palagonite?. T/S- medium grain size, quite altered.

5m grassy rise before the next flow.

T12 The flow has blocky-platy weathering, and is about 5m thick, contains visible altered olivine, quite altered, reasonably laterally persistent. T/S- clustered olivine (2-3mm) in a fine grained groundmass.

4-5m grassy rise before the next flow.

T14 Blocky weathering, fine grained, at least 5m thick, feldspar phyric. T/S- also contains olivine phenocrysts, the plagioclases are crudely aligned.

T15 Very similar to the flow below, 3-4m thick, not noticeably feldspar phyric, but in thin section plagioclase phenocrysts can be seen.

T16 Top-most flow on the hillside, An Speireachan (NM484564) Very fine grained, with blocky weathering and fine grain-size. T/S- phenocrysts of plagioclase.

Lagganulva (NM452454)

UV1 A columnar flow, with a tendency towards platy weathering. The flow is well over 10m thick. Some of the columns are up to 1m wide at their base. T/S- fine grained (<1mm)

UV2A-F These of pale mugearitic lava samples come from opposite Ulva Ferry School, fine grained (<1mm), with a lot of Fe/Ti oxide and aligned plagioclase. (NM453402) They were

collected along the flow at 100m intervals to test intra-flow variation. The flow is well over 10m thick and is exposed for 0.75km.

UV3 Fine grained (<1mm) with blocky, platy weathering. Similar to the flow below, 5-7m thick.

Sample collection above this point is difficult because a valley dissects the landscape.

UV4 The sample was collected half way up the next hill, it may well be the same as UV3 since it is platy, fine grained and contains a few plagioclase phenocrysts. The flow is well over 5m thick and has a red base. (NM456407).

Again a valley cuts the succession, UV5 -11 were collected from the base of the valley up the next hill.

UV5 This flow may well be stratigraphically lower than UV4. It is very altered, fine grained, platy and contains some plagioclase phenocrysts. 3-4m thick. (NM458408)

UV6 3-4m thick, with a platy and very altered top and bottom, fine grained with phenocrysts of plagioclase.

UV7 Quite fresh fine-medium grained, olivine phyric flow, about 5m thick.

UV8 Poorly exposed flow, fine-medium grained, with weathered olivines on the surface. The flow is at least 1m thick. (Sample lost)

UV9 Fine grained with spheroidal weathering, 3-4m thick.

UV10 Platy flow, quite altered, fine grained. 1m thick. (NM459409)

UV11 Quite a continuous, flow, fine-medium grained with a lot of olivine.

Wilderness (NM404485)

W1 Very fine grained (<<1mm), basalt block in the basal volcanic breccia, with phenocrysts of olivine and pyroxene. (NM404284)

W2 The same flow as B1, ie the flow containing MacCulloch's tree, very fine grained (<<1mm), with a few phenocrysts of plagioclase and pyroxene. (Locally 20-30m thick)

W2A Could well be the top to the tree lava, only the frothy vesicular (agate infilled) top 5m of the flow is exposed, 30-40m asl. The flow is fine grained. (NM204235)

W3 Flow possesses the characteristic three tiered columnar structure, it is fine grained (<1mm) contains agates and has an irregular slightly reddened top. 5m thick. T/S- contains clusters of plagioclase enclosing pyroxenes.

W4 The base of the flow is distinctly columnar, with 1-2m of straight columnar jointing, again it has the three tiered structure, fine grained (<1mm) with the same plagioclase clusters as the previous flow. It contains agates and is well over 10m thick.

W5 Less distinctly columnar, with a slightly reddened top, no sign of any infilled vesicles, fine grained (<1mm). 15m thick.

W6 Similar to the flow below, except it contains small agates?, perhaps contains more olivine. The texture in thin section is markedly different from W5, in that it contains olivine phenocrysts and is fine-medium grained. 8m thick.

W7 Crude columnar bottom underlain by a red bole. T/S- similar to W6. No agates found, flow 5-8m thick.

Other lava samples.

P35 Lava flow close to the 'S Airde Beinn plug (NM472538) fine grained (<1mm).

P12 Lava flow sample collected from the carbonate zone of Walker (1970). It has a few vesicle infillings and it appears quite fresh, fine grained (<1mm). 1-2m thick. (NM553557)

EX1-3 Collected from a road cutting on the (A849). This lava occurs within the Epidote zone of Walker (1970). (NM620432) T/S- fine grained (<1mm), quite altered with poikilitic pyroxene.

EX6 This lava occurs within the central complex and lies above the Beinn a Ghraig Granophyre, it is quite altered, fine grained (<1mm). (NM545373). Three small chips were analysed separately.

EBM13A-G These samples were collected from flow BM13, at 100m intervals along its 0.75km outcrop.

EX7 Central group lava, collected at the road junction (NM547292). Green altered, with black and white infillings. T/S- fine grained groundmass, with pyroxene poikilocrysts and (1mm) and plagioclase phenocrysts.

EX8 Further east along the road, about 0.75km, a very vesicular altered rock, with numerous infillings, which are green and white, fine grained (<1mm). (NM549297)

EX9 Again eastwards along the road (NM552304). Green and fine grained, a possible green bole was noted below EX9 close to here by the road side.

EX10 0.75km further east along the road. The lava is green and has a 'fresh' appearance in the hand specimen, but in thin section it is very altered with aligned plagioclases. It is fine grained and contains white, green and dark grey infillings. (NM559306)

EX14 Crudely columnar flow which contains a significant proportion of olivine phenocrysts (1-2mm) the groundmass is fine grained.

EX17 Lava next to the Glen More ring dyke. Sample donated by J. Seedhouse, St. Andrews University. T/S- the rock is quite altered, with plagioclase phenocrysts (too altered to distinguish extinction angle)

EX19 Coastal flow, 5m thick columnar, Ulva (NM448393) T/S- fine grained (<1mm), with a few olivine phenocrysts (2-3mm).

EX20 Next flow up from EX19, platy, fine (<1mm) grained, 3-4m thick. T/S- aligned feldspar phenocrysts.

EX24 Altered basalt from near the base of the succession. Collected from a road cut along the A849, west of Loch Don (NM710314).

STA2 Flow overlying the Fingals cave lava, Staffa. Probably the same as sample MS314 of Thompson et al. (1986) (NM327358)

STA3 Flow above STA2, poorly exposed, olivine rich.

2. Plugs and minor intrusions

Ardnacross plug (NM547497)

P3 150m in from the margin of the plug (NM552494). Pale, platy rock with biotite flakes and feldspar phenocrysts. T/S- carbonate has in places replaced alkali feldspar, amphibole has been altered to serpentine.

Na Torranan plug, Ulva Ferry (NM451416)

P10 Sample collected from the eastern margin of the plug. Pale, fine grained (<1mm) with some evidence of flow banding. T/S- aligned plagioclase.

P11 Fine grained (1mm) rock from nearer the interior of the plug. T/S- aligned plagioclase with a few olivine micro phenocrysts.

Cnoc Carach plug (NM660478)

A trachytic plug with pale, platy weathering and some evidence of flow banding.

P18 Centre of the plug; medium grained (1-2mm), feldspar phenocrysts (aligned) along with biotite flakes may be seen.

P19 Closer to the margin the rock is finer grained (1mm) harder and more flinty. A few biotite flakes can still be seen. T/S- perhaps some zircon.?

P20 The margins of the plug are very platy, with the plates dipping steeply inwards. A few badly weathered fragments were collected here. T/S- contains less plagioclase microphenocrysts.

Minor intrusions

EX13 Sill, with a lower chilled margin intruded into the middle of a lava flow on the coast (NM449244) it has a close spaced blocky jointing, and fine grain size, which is very similar to the "Preshal Mhor flow" on the road SE of here (MS133).

EX15 MS133 of Thompson (1982) by the side of the road (NM451242), fine grained <1mm. This sill contains pegmatite segregations.

EX16 An "inclined basic sheet" dipping in a northerly direction, medium-coarse grained (2-3mm) with noticeable plag needles, 8-10m thick. Croghan (NM699271)

3. Skye lavas and dykes.

JE208 Trachyte, roadside below Ros a'Mheallain on B885. (NG367404)

SK906 Basalt, on the roadside on B885, 0.5km SW of the River Snizort (NG417438)

SK940 Basalt, cliff beside Arnisort Church (NG348532)

SK971 Basalt, roadside on A850 0.9km S of Fairy Bridge (NG277505)

SK974 Basalt, quarry beside Loch Dunvegan, on the NW slope of Beinn Mhic Uillein. (NG233531)

Samples JE208-SK974 originally analysed by Thompson et al. 1972;1980 and 1982

MS184 Lava, Glen More, Mull, Non-porphyritic type. (Morrison 1978)

(CD)17 Chilled marginal facies of a gabroic anorthosite dyke (E3), nr. Bracadale.

(CD)44 Chilled marginal facies of a gabroic anorthosite dyke (E2), nr. Bracadale.

(CD)123 Chilled marginal facies of a gabroic anorthosite dyke (E9), nr. Bracadale.

(CD)124 Centre of a plagioclase phyric, gabroic anorthosite dyke (E9), nr. Bracadale.

(Samples (CD)17- (CD)124 donated by Dr. C.H. Donaldson, St. Andrews University, initially analysed by Donaldson (1977))

4. Vesicle infills

BM55z Vesicle infill from flow BM55, it contains some epidote.

BR2z Vesicle zeolite infilling from flow BR2. It contains analcite, mesolite and thompsonite (XRD)

G-Z Vesicle infill from Glenariff, Co. Antrim.

AM14Z Vesicle infill from flow AM14.

5. Other rocks and potential contaminants.

Inter-lava Tertiary ash etc.

EX21 "Fissile black shale " of Bailey et al. (1924) It contains pale and dark clasts up to 6-7cm in diameter. The outcrop is very poor but finer and fissile areas noted as well. (NM520338) T/S- composed of dark oxidised patches and clasts of plagioclase rich rock (2-3 different types). It also contains some feldspar fragments, some are fragmental, some are also bent and have strained extinction.

Moine and Caledonian

P32 Vein in Moine schist, composed largely of quartz and K feldspar, with some biotite. Coarse grained (3-4mm) in places but in other places the interlocking quartz crystals are under 1mm. (NM667548)

P57 Caledonian granite, Ross of Mull (NM330231) T/S- quite altered with microcline biotite and strained quartz.

P58 Moine schist, 2 samples, collected along the A849. (NM337222) T/S- Well foliated rocks with biotite and garnet (most of which seems to be pre-tectonic) as well as localised occurrences of muscovite.

Iona Lewisian

P60 Granitic gneiss, occurs in irregularly developed bands within more mafic material. It contains quartz and a lot of microcline. (NM267239)

P61 2-300m further south there seems to be a vein which brecciates and breaks up the surrounding rock, quite felsic.

P62 More mafic material which P61 cuts. It seems to contain horneblende with some microcline.

Tiree Lewisian

P36 Metasediment from Hynish, coarsely banded, contains garnets. Medium-coarse grained (3mm) (NL989387)

P37 Vein cutting the metasediments, contains quartz, biotite, sulphide and alkali feldspar similar locality to P36. Coarse grained (>5mm).

P38 Granulite facies pyroxene gneiss with felsic bands/concordant veins. The sample is of this granitic component, contains microcline. Coarse grained (3-4mm), the quartz is highly strained, and the microcline very altered. (NL969387)

P39 Mafic portion of the pyroxene gneiss, contains pyroxene, amphibole, quartz and microcline. Medium grained (2mm) P39A is more granitic and contains garnet. From the same locality as P38.

P40 Granitic vein from the "well foliated pyroxene gneiss" of Durry 1973 although it did not appear to be well foliated. Contains quartz, altered microcline, sulphides and strained, kink banded biotite, coarse grained (<5mm). (NL400986)

P41 Mafic band from, banded gneiss on the southern shore of the island contains horneblende, pyroxene, feldspar and quartz. Medium grained (2mm) (NL936427)

P42 Felsic band from the same banded gneiss as P41, contains pyroxene, horneblende, microcline and quartz. Fine-medium grained (1mm)

P43 Granitic/pegmatitic body, 30-40m across, enclosed within the banded gneiss of P41. Contains strained quartz, exsolved and altered alkali feldspar. Not chilled against the pyroxene gneiss, it is in fact coarser towards the margins. Contains biotite, microcline and quartz. (NL936424)

P44 Mafic granofels, with a coarse granoblastic texture, contains some altered pyroxene, horneblende, quartz and feldspar. Collected from the western side of Beinn Hough. (NL945457)

P45 A selection of pegmatitic material from over Beinn Hough. Some veins are quite microcline rich whereas others are virtually devoid of microcline, coarse grained (4-5mm). Quite brecciated and altered in places.

P46 Pink Tiree marble, with dark green pyroxene crystals. Beach at Balephetrish. (NM012475)

P47 Pink "granite", quite coarse-medium grained (3mm) with a crude NE-SW lineation. T/S- quite sheared and deformed. Headland east of Balephetrish beach. (NM014478)

P48 Mafic resistate, from amphibolite facies migmatite. From an old quarry at Baugh. T/S- fine grained (1mm) and altered. (NM023437).

P49 Felsic mobilisate from the same locality, with quartz and alkali feldspar. The rock has been altered and sheared, with mortar textures. Mostly coarse grained (>5mm) but mortar areas are <1mm.

P50 Pegmatite from the rocky promontory 200m of the church at Baugh. T/S- contains microcline, orthoclase, quartz and biotite. Coarse grained (5mm).

P51 Felsic dyke at Vaul, predominantly a fine grained felsic rock with mafic patches. Fine grained and altered with remnants of feldspar phenocrysts. (NM051487).

Permo-Carboniferous dykes

L1 Thin camptonite dyke, cutting the Strontian granite, from a road cut in Morvern (NM782595)

L2 Thin, 0.5m dyke cutting the Torridonian on Iona. The dyke trends ESE and thickens in this direction. T/S- clinopyroxene phenocrysts, sit in a fine grained matrix.

Appendix 2

Analytical methods and data accuracy

A2.1 Sample preparation

All of the samples have been prepared for analysis at Durham University. Initially all the weathered surfaces were removed from the samples with the aid of a rock splitter and a clipper saw. After washing to remove any surface contamination, a substantial portion of the sample was coarsely (~1cm diameter) crushed, using a *Fritsch Pulverisette* jaw crusher. At this stage the crushed rock was inspected and any visible zeolites, or altered material was removed, before final crushing to fine (<0.5cm) material. The plates of the jaw crusher were cleaned between preparation of each sample, with a wire brush and absolute alcohol. Approximately 150g of each sample was then reduced to a fine powder, using an agate ball mill.

A2.2 X-Ray Fluorescence (XRF)

All of the samples listed in Appendix 4a have been analysed by XRF at the University of Durham, using fusion discs and pressed powder pellets.

Fusion disc preparation

4-5g of rock powder were accurately weighed out, and heated in porcelain crucibles at 900 °C for 2 hours. The ignited powders were then allowed to cool in a dessicator, and re-weighed to determine the loss on ignition (LOI). Approximately 0.45g of ignited rock powder was accurately weighed out, along with exactly five times (i.e ~2.25g) the amount of dried lithium metaborate and lithium tetraborate flux (Johnson Matthey "Spectroflux 100B"). After thorough mixing, this 1:5 rock-to-flux mixture was placed in a platinum crucible (with lid) in a furnace at 1050 °C for 15-20 minutes. The molten mixture was then removed from the furnace, swirled briefly in the Pt crucible to ensure complete mixing, poured into graphite moulds on a hot-plate set at 250 °C, and a disc formed using a stainless steel plunger. Following slow cooling for 20 minutes the disc was labelled, bagged and stored in a dessicator. During this latter procedure, great care was taken to ensure that the analytical surface of the disc did not come into contact with the surface of the skin. Touching the surfaces of these fusion discs causes considerable contamination with Na_2O, P_2O_5 and K_2O (Kerr & Hardy 1993).

Pressed powder pellet preparation.

Approximately 8g of rock powder was added with ~10 drops of PVA "Mowiol" organic binding solution, to a small beaker and mixed thoroughly. The mixture was then subjected to ~10 tonnes of pressure for half a minute, within a mould. The pellets were dried in an oven at 100 °C overnight, labelled and bagged.

XRF analysis

During this study the elements have been analysed using a Philips PW 1400, fitted with a PW1500/10 automatic sample changer. A Rh tube was used to provide the X-ray source (accelerating potential = 80kV, 35mA or, = 55kV, 50mA when analysing REEs). Philips X40 software has been used to process the raw count rates of the peaks and backgrounds.

The machine was calibrated by analysing the elemental count rates on various international standards, of 'known' composition (Govindaraju 1989). For each element being analysed the X40 program (after correction for interelement effects and possible line overlaps) generates a plot of count rates vs. known concentration of the standards, and calculates a best-fit straight line through the data. The operator can delete those standards which plot far from the regression line in order to optimise the calibration.

Data accuracy and precision

In order to ensure precision virtually all the samples were analysed twice, each time on a different calibration, and the results for the two runs have been averaged. If any samples or elements were radically different between the two runs then the sample was analysed again, this however, was quite a rare occurrence.

To further assess the reproducibility of the chemical data throughout the tenure of the PhD, six basalts were chosen, and have been analysed using each of the calibration programs used at Durham over the last 2-3years. The range of values obtained during the present study, for three of these samples are shown in table A2.1.

To assess the accuracy of the each calibration it is important to analyse standards which have not been used in the calibration (BOB-1, QUB-S3 & NBS 688 are the chief ones used in this study). The average composition of QUB-S3 (a basaltic dyke from the BTVP), as analysed by 17 British and Australian universities[1], can be seen in table A2.2a,b (UK-Ave). QUB-S3 has been analysed, over the past two years, utilising the same calibrations, used to analyse the Mull samples. These repeated analyses have been averaged, and the results are presented in table A2.2 along with

[1] Compiled by Dr I. Meighan, Queens University, Belfast.

the UK-Average. These analyses, and those presented in table A2.1, confirm the stability and accuracy of Durham XRF over the period in question.

	BR1	BR2	BR6
SiO2	45.18 - 46.12	46.04 - 46.68	46.48 - 46.92
Al2O3	15.50 - 15.93	15.51 - 15.92	13.31 - 13.75
Fe2O3*	16.01 - 16.39	16.28 - 16.54	11.68 - 11.90
MgO	6.92 - 7.05	6.78 - 6.86	13.42 - 13.91
CaO	7.69 - 7.80	7.58 - 7.74	9.45 - 9.70
Na2O	3.67 - 3.80	3.91 - 4.13	2.23 - 2.31
K2O	0.22 - 0.23	0.37 - 0.39	0.49 - 0.52
TiO2	2.56 - 2.59	2.59 - 2.73	1.13 - 1.15
MnO	0.19 - 0.20	0.19 - 0.19	0.17 - 0.17
P2O5	0.26 - 0.28	0.27 - 0.28	0.14 - 0.15
Ba	54 - 67	56 - 71	310 - 326
Cr	124 - 137	125 - 144	983 - 1002
Nb	7.0 - 8.8	7.3 - 9.8	4.0 - 5.1
Ni	101 - 116	99 - 114	329 - 352
Rb	2.0 - 4.0	1.9 - 3.1	5.5 - 8.0
Sc	18 - 23	18 - 23	24 - 28.5
Sr	373 - 389	374 - 383	498 - 520
V	230 - 257	229 - 245	221 - 240
Y	27 - 30	25 - 29	15.7 - 19
Zr	160 - 172	159 - 172	74 - 87
La	6.10 -10.2	7.0 - 10	6.7 - 10.0
Ce	23 - 28	22 - 27	16 - 19
Nd	17 - 22	16 - 20	9.0 - 13.7

Table A2.1 The range of values obtained by XRF during the present study on samples BR1, BR2 and BR6 (trace elements in ppm, major elements in weight %).

	SiO2	Al2O3	Fe2O3	MgO	CaO	Na2O	K2O	TiO2	MnO	P2O5
UK-Ave	45.07	14.41	13.99	11.44	9.82	2.54	0.35	2.11	0.19	0.24
Durham	45.09	14.57	13.95	11.33	9.80	2.53	0.36	2.10	0.19	0.25

Table A2.2a Major element values for QUB-S3, UK-Average compared with the average from the present study (Durham).

	Ba	Cr	Ga	Nb	Ni	Rb	Sc	Sr	V	Y	Zr	La	Ce	Nd
UK-Ave	140	516	20	4.0	310	5.0	30.0	430	302	23.0	160	9.3	26.1	19.5
Durham	149	540	21	5.0	303	5.0	30.1	425	293	22.9	157	9.3	26.8	20.7

Table A2.2b Trace element values for QUB-S3, UK-Average compared with the average from the present study (Durham).

A2.3 Inductively Coupled Plasma - Mass Spectrometry (ICP-MS)

The samples listed in Appendix 4b have been analysed for the REE, Th, Pb & U by ICP-MS at Royal Holloway and Bedford New College.

Sample preparation

0.1±0.001g of powdered sample was dried at 110 °C overnight. Each sample was then digested with 4ml of 48% HF and 1ml HNO_3 (analytical grade reagents) in a Savillex bomb, on a hot plate at 175 °C overnight. After evaporation to dryness, 1ml of HNO_3 was added and the sample evaporated to dryness again. A further 1ml of HNO_3 was added and the product evaporated to dryness, to ensure complete removal of HF, and formation of nitrate salts. The samples were redisolved in 25ml of deionised water and 2.5ml of nitric acid, sealed in the Savillex bomb and boiled for 1 hour on the hot-plate. The cooled solutions were made up to 50ml in a volumetric flask, and stored in plastic bottles before analysis. A reagent blank was prepared with each batch of samples. Three visits were made to the ICP-MS at Royal Holloway, and each time the samples were prepared no more than a month before hand.

Analysis

On the first two visits the machine used was a FI Elemental PlasmaQuad PQ2, and on the third and final visit, a FI Elemental PlasmaQuad PQ2 STE was used. Both of these machines were calibrated using solutions of known elemental concentrations. Correction for drift throughout the course of each run was achieved by analysing a drift monitor every six samples. The raw count rates were corrected for drift, and the ppm values calculated using "within-house" software at Royal Holloway. The values for the preparation blank were then subtracted from the measured values.

Data accuracy

In order to assess the accuracy of the data generated by ICP-MS, the International reference materials, MRG-1, W-2 & NIM-N, have been analysed in each of the three

analytical runs. In table A2.3 the averaged values for these standards over the three runs are compared with the values given by Govindaraju (1989).

	MRG-1 ICP	MRG-1 Standard	W-2 ICP	W-2 Standard	NIM-N ICP	NIM-N Standard
La	9.03	9.80	10.50	11.40	2.61	3.00
Ce	25.44	26.00	22.80	24.00	5.40	6.00
Pr	3.48	3.40	2.97	3.20	0.77	na
Nd	18.77	19.20	12.50	14.00	3.53	3.00
Sm	4.33	4.50	3.31	3.25	1.53	0.80
Eu	1.39	1.39	1.15	1.10	0.74	0.63
Gd	4.11	4.00	3.77	3.60	1.56	na
Tb	0.54	0.50	0.55	0.60	0.27	na
Dy	2.88	2.90	3.57	3.80	1.53	na
Ho	0.49	0.49	0.69	0.76	0.37	na
Er	1.30	1.12	2.17	2.00	1.26	na
Tm	0.17	0.11	0.34	0.40	0.24	na
Yb	0.98	0.60	2.11	2.05	1.20	0.70
Lu	0.15	0.12	0.31	0.30	0.22	0.20
Pb	8.90	10.00	7.64	9.30	5.60	7.00
Th	0.69	0.90	1.96	2.20	0.45	0.60
U	0.30	na	0.53	na	0.42	na

Table A2.3 Average values obtained by ICP-MS during this study for MRG-1, W-2 & NIM-N compared with standard values.

This table shows that, on the whole the results obtained on these standards, during the present study compare well with the internationally accepted values.

Comparison with XRF

La, Ce and Nd have been analysed by both ICP-MS and XRF, and so a comparison can be made between the two analytical methods. In figure A2.1 the ICP-MS values are plotted against the XRF and, on the whole, the results compare reasonably well. The Ce comparison diagram shows significantly more scatter than the other two, which may be due to the fact that Ce is relatively difficult element to analyse by XRF.

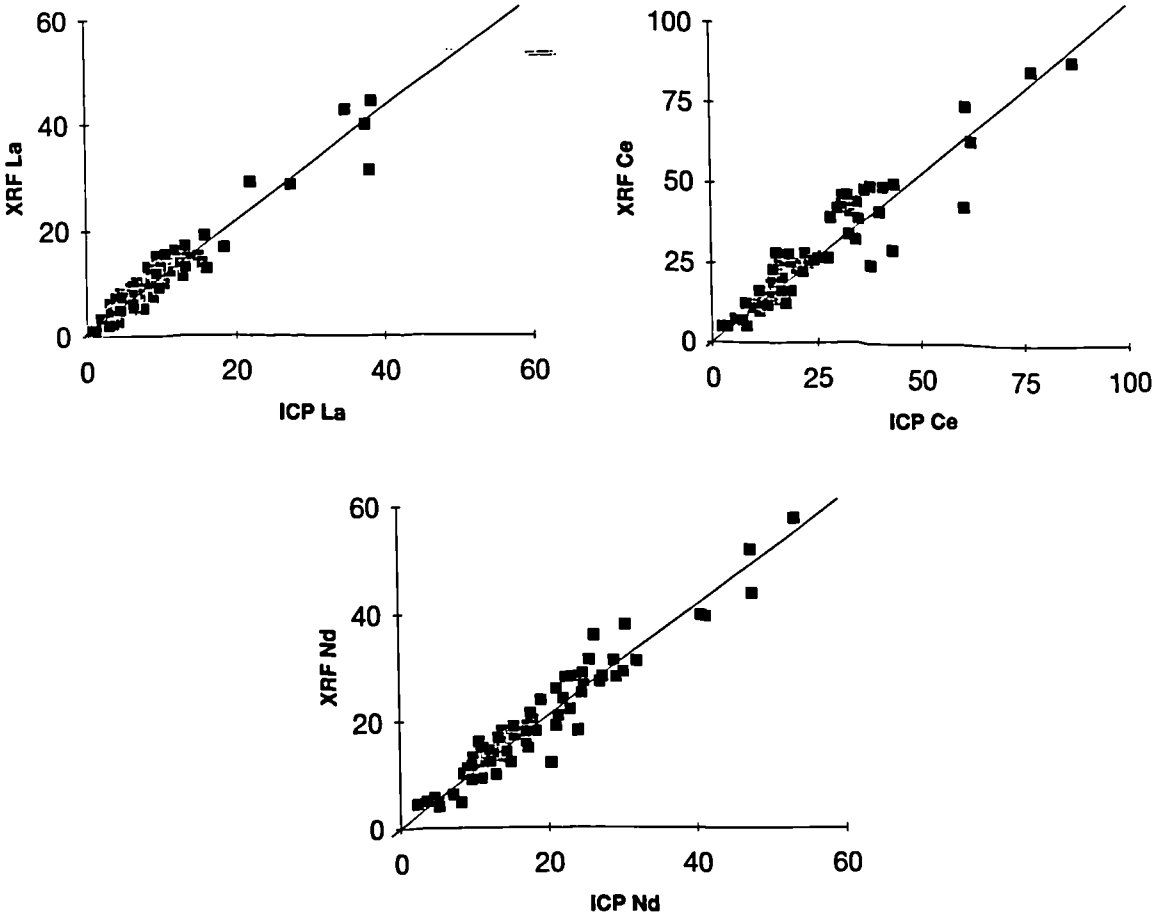


Figure A2.1 Comparison of XRF analyses with those of ICP-MS.

A2.4 Electron microprobe analysis

Mineral analyses have been carried out using two machines;

1. Cambridge Instruments Geoscan Mark 2 (University of Durham), using energy dispersive spectrometry (EDS). The electron beam diameter was 5-10μm, and the beam current was 5nA at 15kV.
2. JEOL 733 Superprobe (University of St. Andrews), using wavelength dispersive spectrometry (WDS). The beam diameter was 1μm, and the beam current was 20nA at 15kV.

The calibration of both these machines was checked by analysing minerals of known composition at the beginning of each day. Minerals from several of the samples were analysed on both machines and very similar results have been obtained in all cases.

A2.5 Analysis of radiogenic isotopes

Pb, Sr and Nd were extracted on the same dissolution using approximately 200 mg of powder. After dissolution using approximately 1ml of HNO3 combined with 3 to 5mls of HF, residues were converted to nitrate and finally chloride; 1ml of 1M HBr was then added to the residue. Pb was separated by passing the sample through columns prepared from PVC disposable pipette tips fitted with a 2mm diameter polyethylene frit and containing Dowex 1 x 8, 200-400 mesh resin; completely new columns were prepared for each sample to minimize the Pb blank.

The Sr and Nd fractions were collected in 2mls of 1M HBr and Pb collected in 1ml of 6M HCl. Sr and Nd were purified using standard one and two-column cation exchange techniques, respectively. Sr and Pb were run as the metal species on single Ta and single Re filaments, respectively, using a Finnegan MAT 262 multicollector mass spectrometer at the NERC Isotope Geosciences Laboratory (NIGL); Nd was run as the metal species on triple Re-Ta filament assemblies using a VG354 multicollector mass spectrometer, also located at NIGL. Blanks for Sr, Nd and Pb were less than 2.2ng, 200pg, and 365pg respectively.

Reference standards throughout the course of analysis averaged values of $^{87}Sr/^{86}Sr = 0.710226 \pm 38$ (2σ) for the NBS987 standard, $^{143}Nd/^{144}Nd = 0.511108 \pm 24$ (2σ) for the Johnson Matthey Nd standard. $^{87}Sr/^{86}Sr$ was normalized to $^{86}Sr/^{88}Sr = 0.1194$; $^{143}Nd/^{144}Nd$ was normalized to a value of $^{146}Nd/^{144}Nd = 0.7219$. Pb mass fractionation was 0.104% per a.m.u. Based on repeated runs of NBS981 common Pb standard, the reproducibility is better than 10.1%. Pb isotopic ratios were corrected relative to the average standard Pb isotopic compositions of Todt *et al.* (1984). Internal errors on individual isotope measurements were always much smaller than the standard reproducibility reported here, and therefore the ability to reproduce the standards should be taken as the limiting factor in interpreting the uncertainty of any given analysis.

Appendix 3

CIPW Normative values for the MPG lavas

The CIPW norms in the following tables have been calculated assuming a Fe2O3/(FeO+Fe2O3) ratio of 0.1, using the "Igpet III" © computer program of M.J. Carr.

Appendix 3 CIPW norms

Sample	A1	A2	A5	A6	AM1	AM2A	AM2B	AM2C
%AN	43.93	57.56	62.25	62.82	60.74	59.12	59.78	60.77
or	5.73	2.84	1.48	1.54	2.19	2.36	2.66	2.42
ab	28.26	21.41	18.95	17.69	17.11	18.56	18.30	18.31
an	22.15	29.03	31.26	29.88	26.47	26.83	27.19	28.36
ne	0.00	0.00	0.00	0.00	3.02	1.77	1.23	0.26
di	22.45	22.46	15.24	17.05	15.29	14.97	14.56	13.52
hy	3.54	4.85	3.38	5.81	0.00	0.00	0.00	0.00
ol	10.55	13.44	23.25	23.19	28.37	28.22	28.82	29.19
mt	1.81	1.80	1.78	1.67	2.12	2.10	2.12	2.12
il	3.34	3.21	2.49	2.17	3.99	3.97	3.97	3.95
ap	0.65	0.37	0.28	0.25	0.49	0.46	0.46	0.46

Sample	AM3	AM4	AM5	AM6	AM7A	AM7B	AM8	AM9
%AN	55.78	55.56	54.10	49.64	60.11	59.24	55.76	62.01
or	3.49	3.49	2.66	1.24	2.07	2.30	1.54	1.06
ab	21.00	20.62	21.68	30.52	17.73	18.54	24.89	19.12
an	26.49	25.79	25.56	30.08	26.71	26.94	31.37	31.21
ne	0.96	1.85	1.59	0.02	1.72	0.87	0.45	0.00
di	13.35	13.55	13.82	9.13	16.54	16.96	11.05	13.78
hy	0.00	0.00	0.00	0.00	0.00	0.00	0.00	0.44
ol	25.93	26.72	28.26	22.19	27.19	27.07	22.49	27.43
mt	2.00	2.00	2.07	2.13	1.84	1.78	2.25	1.94
il	3.93	3.84	3.99	3.95	3.08	2.89	3.80	3.10
ap	0.51	0.51	0.49	0.39	0.37	0.42	0.39	0.39

Sample	AM10	AM11	AM12	AM13	AM14	AM15	B1	B2
%AN	60.07	63.58	58.62	60.75	61.16	61.49	46.81	52.00
or	1.89	1.18	1.71	2.19	1.83	1.71	5.44	4.73
ab	19.64	18.76	20.99	18.06	20.56	17.08	27.67	23.52
an	29.55	32.74	29.73	27.96	32.38	27.28	24.35	25.49
ne	1.05	2.17	0.00	1.26	0.00	5.60	0.00	0.00
di	15.69	20.66	22.06	20.74	18.54	24.07	20.58	21.54
hy	0.00	0.00	2.86	0.00	3.61	0.00	6.45	13.08
ol	24.54	17.86	16.69	22.49	16.65	17.33	8.69	4.09
mt	1.94	1.81	1.67	1.77	1.64	1.73	1.78	1.83
il	3.36	2.94	2.66	2.56	2.53	2.56	3.32	4.10
ap	0.49	0.30	0.32	0.35	0.32	0.30	0.58	0.60

Sample	B3	B4A	B4B	B5	B6	B7	B8	B9
%AN	61.08	26.72	59.85	23.82	60.32	43.39	41.74	55.05
or	2.36	4.26	2.48	4.91	1.12	1.95	2.01	1.54
ab	17.15	37.07	18.87	41.36	19.63	31.31	34.89	26.57
an	26.90	13.51	28.13	12.93	29.85	23.99	25.00	32.54
ne	0.43	9.25	0.00	9.73	0.00	2.80	1.36	0.00
di	13.81	7.75	12.03	6.50	16.62	8.41	4.99	4.72
hy	0.00	0.00	1.22	0.00	2.01	0.00	0.00	6.68
ol	28.55	15.51	29.18	15.80	24.69	19.72	21.70	20.16
mt	2.13	2.03	2.12	2.04	1.87	2.28	2.28	2.09
il	4.03	4.37	3.97	4.44	3.17	5.75	5.75	3.80
ap	0.51	1.51	0.51	1.58	0.35	0.74	0.76	0.42

Appendix 3 CIPW norms

Sample	B10	B11	B12	B13	B14	B15	B16A	B16B
%AN	54.07	65.10	63.49	58.96	57.85	48.80	60.41	57.49
or	1.65	1.24	1.65	2.19	1.77	2.19	1.42	2.19
ab	27.08	17.35	17.69	19.13	21.54	23.55	18.70	20.12
an	31.88	32.36	30.75	27.49	29.56	22.44	28.52	27.20
ne	0.00	0.00	0.00	3.11	1.21	6.68	1.15	1.11
di	7.42	16.18	16.75	15.49	12.14	11.45	15.68	16.76
hy	4.27	5.64	6.20	0.00	0.00	0.00	0.00	0.00
ol	19.02	20.84	21.13	25.99	26.01	22.31	27.68	26.01
mt	2.04	1.67	1.71	1.93	2.20	2.33	2.00	1.91
il	3.76	2.11	2.17	3.19	4.14	5.32	3.19	2.96
ap	0.42	0.25	0.28	0.53	0.51	0.74	0.39	0.39

Sample	B17	B18	B19	B20	B21	B22	B23	B24
%AN	55.34	60.24	53.04	56.41	57.16	57.35	57.03	56.20
or	2.19	1.65	2.36	1.77	1.89	1.77	1.71	2.36
ab	25.13	19.23	24.66	18.82	18.43	18.97	20.03	18.34
an	31.14	29.14	27.86	24.35	24.59	25.51	26.58	23.53
ne	0.23	0.72	2.18	2.32	2.12	1.00	1.34	1.39
di	11.41	18.47	12.29	18.29	18.35	18.63	18.18	19.05
ol	23.69	22.74	22.60	28.76	29.01	27.72	28.58	29.32
mt	2.04	1.75	2.32	1.78	1.81	1.78	1.81	1.83
il	3.30	2.56	4.16	2.47	2.53	2.51	2.56	2.66
ap	0.42	0.30	0.51	0.37	0.35	0.35	0.37	0.32

Sample	B25A	B25B	B26	B27	B28	B29	B30	W1
%AN	55.41	61.89	61.43	58.93	55.63	60.43	55.64	56.29
or	2.13	1.83	2.01	1.71	2.07	2.19	2.07	3.07
ab	19.37	16.81	16.97	19.03	20.90	18.61	22.20	21.74
an	24.06	27.30	27.02	27.31	26.21	28.42	27.85	28.00
ne	1.61	0.47	1.03	0.05	0.23	1.33	1.59	0.92
di	19.11	17.99	19.62	18.26	18.30	16.93	18.26	27.55
ol	28.70	29.00	27.78	28.76	27.14	27.04	22.77	12.49
mt	1.71	1.77	1.77	1.77	1.70	1.71	1.81	1.62
il	2.18	2.49	2.49	2.20	2.22	2.15	2.68	3.10
ap	0.28	0.35	0.37	0.30	0.32	0.32	0.37	0.44

Sample	W2	W3	W4	W5	W6	W7
%AN	50.34	59.47	58.38	53.34	54.55	62.17
Q	0.00	0.00	0.00	1.87	0.00	0.00
or	4.61	1.95	2.30	3.60	2.25	1.95
ab	25.30	20.14	19.72	23.10	22.34	18.53
an	25.64	29.55	27.66	26.41	26.81	30.45
ne	0.00	0.00	0.00	0.00	0.00	0.00
di	20.62	24.99	23.74	19.49	13.81	12.17
hy	8.89	6.04	15.22	18.69	0.23	0.82
ol	7.48	9.37	2.71	0.00	28.52	28.17
mt	1.78	1.78	1.74	1.74	1.87	2.16
il	3.38	3.36	3.51	3.93	2.73	4.14
ap	0.67	0.39	0.46	0.60	0.39	0.53

Appendix 3 CIPW norms

Sample	BB1	BB2	BB3	BB4	BB5	BB6	BB7A	BB7B
%AN	60.92	56.81	57.97	33.64	46.83	59.84	53.13	60.01
or	2.42	2.25	2.19	7.56	3.55	1.30	1.48	1.48
ab	20.22	20.82	19.58	31.22	26.78	20.32	25.84	20.35
an	31.53	27.39	27.00	15.83	23.59	30.28	29.29	30.54
ne	0.00	0.82	4.98	10.41	5.57	2.24	2.32	1.81
di	17.52	16.30	15.91	8.76	8.74	12.88	9.80	12.52
hy	6.95	0.00	0.00	0.00	0.00	0.00	0.00	0.00
ol	13.83	26.66	22.27	15.76	20.66	25.24	22.81	25.77
mt	1.78	1.84	2.04	2.03	2.16	2.12	2.19	2.12
il	2.72	2.94	3.27	5.39	4.84	3.72	4.75	3.63
ap	0.32	0.44	0.42	1.41	0.97	0.51	0.56	0.46

Sample	BB8	BB9	BB10A	BB10B	BB11	BB12	BB13	BB14
%AN	53.06	62.13	52.17	48.26	42.27	44.02	43.85	46.42
or	1.30	0.95	3.07	1.95	2.42	2.66	2.72	2.60
ab	26.69	19.12	24.38	29.75	32.33	32.10	31.08	29.11
an	30.17	31.38	26.59	27.75	23.67	25.23	24.27	25.22
ne	0.85	0.00	1.46	2.59	4.54	2.69	3.47	2.93
di	8.53	14.38	11.83	8.26	8.43	8.12	8.21	9.45
hy	0.00	4.81	0.00	0.00	0.00	0.00	0.00	0.00
ol	22.98	22.11	21.13	20.40	19.44	19.00	18.83	19.27
mt	2.19	1.94	2.44	2.25	2.19	2.23	2.23	2.26
il	4.75	3.32	5.66	5.41	5.49	5.94	5.98	5.85
ap	0.58	0.37	0.95	0.79	0.88	0.97	1.07	0.97

Sample	BB15	BB16	BB17	BB18	BB19	BB20	BB21	BB22
%AN	46.81	46.33	45.83	51.54	51.54	54.87	56.55	59.61
or	3.01	4.67	4.20	3.19	3.60	2.95	3.25	3.13
ab	30.45	27.30	29.67	25.27	25.34	22.17	19.12	18.55
an	26.80	23.56	25.10	26.87	26.95	26.96	24.88	27.38
ne	1.61	4.33	1.21	3.14	2.64	0.00	3.12	0.26
di	8.46	10.02	8.88	11.04	10.94	14.27	15.93	14.44
hy	0.00	0.00	0.00	0.00	0.00	0.39	0.00	0.00
ol	19.14	19.33	20.42	21.20	20.52	26.19	25.90	28.96
mt	2.15	2.25	2.41	2.31	2.26	2.02	2.00	1.93
il	5.77	5.62	6.06	4.90	4.92	3.38	3.23	2.87
ap	1.00	0.93	1.02	0.72	0.86	0.51	0.49	0.39

Sample	BB23	BB24	BHL2	BHL3	BHL5	BHL6	BHL7
%AN	59.36	52.06	57.12	55.25	55.33	54.48	54.87
or	2.78	1.77	3.43	3.49	3.31	3.60	3.01
ab	17.81	25.58	17.04	21.84	21.83	21.40	21.32
an	26.01	27.78	22.70	26.96	27.04	25.61	25.92
ne	2.23	1.68	4.79	0.41	0.00	3.58	0.23
di	16.81	11.31	16.67	11.83	10.52	16.47	11.94
hy	0.00	0.00	0.00	0.00	1.35	0.00	0.00
ol	26.24	22.34	25.93	27.28	27.44	21.23	27.76
mt	2.00	2.41	2.12	2.03	2.04	2.00	2.02
il	3.32	4.67	4.22	3.93	3.87	4.60	4.03
ap	0.42	0.53	0.49	0.51	0.49	0.56	0.49

Appendix 3 CIPW norms

Sample	BCH1	BCH2	BCH3	BCH4	BCH5	BCH6	BCH7	BCH7A
%AN	57.95	53.57	53.77	55.39	51.58	56.15	51.38	50.04
or	2.84	2.78	1.83	2.01	2.54	2.95	3.31	3.55
ab	19.82	23.70	20.01	22.73	20.71	22.22	26.48	27.31
an	27.32	27.34	23.28	28.22	22.06	28.45	27.98	27.34
ne	1.27	2.38	3.96	2.81	8.54	0.84	0.37	0.06
di	17.68	14.58	14.98	16.60	13.50	10.31	14.70	14.54
ol	24.92	23.31	29.50	22.00	23.67	25.33	21.34	20.96
mt	1.88	1.88	1.91	1.78	2.20	2.25	1.87	1.87
il	2.92	2.92	2.64	2.91	4.82	4.96	3.17	3.17
ap	0.39	0.39	0.32	0.37	0.60	0.63	0.42	0.35

Sample	BCH2X	BCH3X	BCH4X	BCH7B	BCH8	BCH9	BCH10A	BCH10B
%AN	50.46	56.22	54.57	49.30	49.48	43.54	54.35	38.87
or	3.60	2.60	2.07	3.84	3.72	3.55	1.65	1.60
ab	23.50	23.10	22.12	26.58	26.40	28.88	22.68	33.51
an	23.94	29.67	26.57	25.85	25.86	22.27	26.99	21.31
ne	0.33	0.00	3.47	2.20	0.00	5.17	0.83	4.86
di	19.20	15.77	17.42	14.43	15.12	14.72	20.84	8.24
hy	0.00	0.30	0.00	0.00	0.16	0.00	0.00	0.00
ol	22.01	22.84	21.18	21.07	20.12	19.31	20.96	18.64
mt	2.06	1.86	1.80	1.87	1.74	1.75	1.59	2.32
il	4.03	2.94	2.98	3.15	2.83	2.91	2.03	6.15
ap	0.37	0.35	0.35	0.56	0.56	0.63	0.28	0.90

Sample	BCH11	BCH12	BCH13	BCH14	BCH15	BCH16	BCH17	BCH18
%AN	37.67	46.75	56.80	61.14	58.96	57.59	60.54	42.06
or	1.83	6.09	1.65	1.30	1.48	4.08	4.14	4.20
ab	30.97	24.43	21.74	18.45	21.12	21.23	15.30	28.24
an	18.71	21.45	28.58	29.02	30.34	28.83	23.47	20.50
ne	8.71	3.22	5.23	0.00	0.94	0.55	0.60	6.29
di	9.19	15.52	13.91	14.45	14.38	19.61	15.26	10.35
hy	0.00	0.00	0.00	3.11	0.00	0.00	0.00	0.00
ol	19.10	18.87	21.09	27.27	24.98	19.29	35.19	18.78
mt	2.38	2.28	2.23	1.93	1.96	1.70	1.78	2.45
il	6.08	4.35	4.03	2.94	3.29	3.00	2.24	6.38
ap	0.79	0.79	0.51	0.35	0.39	0.39	0.32	1.04

Sample	BCH19	BCH20	BCH21	BCH22	BCH23A	BCH23B	BCH24	BCH25
%AN	52.04	55.53	62.11	63.18	57.58	58.84	62.78	61.93
or	4.96	2.48	3.25	2.90	2.60	2.19	2.78	1.77
ab	24.93	22.99	18.87	17.60	21.75	21.75	16.16	16.75
an	27.05	28.71	30.93	30.20	29.51	31.09	27.26	27.26
ne	1.90	2.49	0.00	0.00	0.00	0.00	0.00	0.00
di	11.81	11.93	20.46	18.37	20.57	18.86	17.12	17.29
hy	0.00	0.00	3.16	5.28	0.92	3.91	3.82	3.65
ol	21.55	22.22	16.97	19.99	18.22	16.35	27.02	27.15
mt	2.19	2.20	1.71	1.74	1.68	1.54	1.74	1.75
il	3.76	3.68	2.58	2.34	2.54	2.17	2.32	2.32
ap	0.44	0.44	0.35	0.25	0.32	0.25	0.28	0.28

Appendix 3 CIPW norms

Sample	BCH26	BCH27	BCH28	BCH29	BCH30	BCH31	BCH32	BCH33
%AN	60.03	59.81	62.39	57.44	59.40	59.44	56.24	61.47
or	2.30	3.01	2.19	2.66	2.01	2.48	2.66	2.54
ab	18.11	17.85	16.08	18.04	18.62	18.53	23.17	16.01
an	27.20	26.57	26.67	24.35	27.24	27.16	29.77	25.54
ne	0.00	0.00	0.00	2.24	0.00	0.00	1.25	3.02
di	17.52	17.20	14.25	17.37	15.84	16.05	12.50	18.90
hy	0.32	1.64	4.75	0.00	3.93	3.81	0.00	0.00
ol	28.80	28.23	30.03	29.36	26.92	26.24	23.97	27.41
mt	1.74	1.73	1.68	1.75	1.77	1.74	2.02	1.80
il	2.30	2.32	1.65	2.17	2.18	2.30	3.40	2.49
ap	0.25	0.28	0.25	0.28	0.28	0.30	0.35	0.35

Sample	BCH34A	BCH34B	BCH34C	BCH35	BCH36	BCH37	BCH38	BCH39
%AN	63.70	58.10	55.84	61.80	60.65	60.25	55.53	61.34
or	2.19	2.36	2.42	3.01	2.48	2.95	2.60	2.72
ab	16.67	19.08	19.42	17.52	18.77	20.82	22.08	18.76
an	29.25	26.45	24.56	28.33	28.93	31.55	27.57	29.77
ne	0.00	0.99	1.81	0.00	0.10	0.00	1.74	1.02
di	14.87	20.18	21.99	17.37	17.31	19.19	20.90	21.34
hy	3.51	0.00	0.00	0.99	0.00	1.23	0.00	0.00
ol	27.34	24.62	23.23	26.92	26.87	18.79	18.72	19.71
mt	1.77	1.83	1.90	1.80	1.78	1.65	1.73	1.64
il	2.24	2.81	3.11	2.53	2.49	2.39	2.68	2.30
ap	0.28	0.35	0.39	0.32	0.32	0.35	0.44	0.35

Sample	BCH40	BCH41	BCH42	BCH43	BCH44	BCH45	BCH46
%AN	61.07	58.58	59.52	55.32	47.89	52.55	47.14
or	3.66	2.66	2.72	2.19	2.72	1.42	2.90
ab	18.59	22.49	22.00	21.78	27.14	25.26	28.51
an	29.16	31.81	32.35	26.97	24.94	27.97	25.42
ne	0.75	0.51	0.00	4.25	4.92	1.31	2.71
di	22.37	16.10	14.04	12.19	10.02	9.38	9.40
hy	0.00	0.00	2.31	0.00	0.00	0.00	0.00
ol	18.32	19.79	19.33	22.72	20.13	24.19	20.20
mt	1.67	1.86	1.90	2.25	2.20	2.22	2.20
il	2.49	3.06	3.34	4.52	5.09	4.50	5.22
ap	0.42	0.44	0.46	0.67	0.83	0.65	0.86

Sample	BG1	BG2	BG3	BG4	BG5	BG6	BG7	BG8
%AN	61.45	65.42	61.75	56.52	60.12	60.63	53.34	54.69
or	2.19	2.30	2.36	2.25	2.25	2.42	1.42	1.48
ab	20.56	18.28	19.46	21.66	21.07	20.22	27.67	26.15
an	32.78	34.59	31.42	28.15	31.77	31.15	31.63	31.56
di	9.52	9.75	12.34	18.63	17.05	18.06	7.97	7.77
hy	10.46	6.39	11.66	6.73	8.87	14.52	1.86	3.66
ol	18.20	22.36	16.89	17.49	13.66	8.24	22.44	22.11
mt	1.94	1.96	1.77	1.77	1.73	1.73	2.31	2.36
il	3.23	3.36	2.85	3.08	3.10	3.04	3.84	3.97
ap	0.56	0.37	0.42	0.42	0.42	0.39	0.39	0.39

Appendix 3 CIPW norms

Sample	BHL2	BHL3	BHL5	BHL6	BHL7	BHL8	BHL9	BHL10
%AN	57.12	55.25	55.33	54.48	54.87	61.61	51.62	54.32
or	3.43	3.49	3.31	3.60	3.01	2.84	3.01	3.90
ab	17.04	21.84	21.83	21.40	21.32	18.95	24.11	23.42
an	22.70	26.96	27.04	25.61	25.92	30.41	25.72	27.85
ne	4.79	0.41	0.00	3.58	0.23	0.00	0.60	0.24
di	16.67	11.83	10.52	16.47	11.94	9.44	11.50	16.51
hy	0.00	0.00	1.35	0.00	0.00	7.52	0.00	0.00
ol	25.93	27.28	27.44	21.23	27.76	21.43	26.49	18.76
mt	2.12	2.03	2.04	2.00	2.02	2.10	2.16	2.23
il	4.22	3.93	3.87	4.60	4.03	3.74	4.10	4.94
ap	0.49	0.51	0.49	0.56	0.49	0.49	0.49	0.63

Sample	BHL11	BHL12	BHL13	BHL14a	BHL14b	BHL15	BHL16	BHL17
%AN	52.15	59.47	64.08	54.96	61.77	65.57	61.90	58.71
or	3.66	2.60	2.01	1.24	2.30	1.18	1.12	1.54
ab	26.82	21.49	19.72	26.91	17.68	15.74	15.93	19.22
an	29.24	31.53	35.17	32.83	28.57	29.97	25.89	27.33
ne	0.00	0.00	0.00	0.00	0.78	0.00	5.99	3.48
di	16.22	16.16	15.69	8.53	16.14	17.39	17.48	15.59
hy	2.14	6.80	7.48	1.72	0.00	8.46	0.00	0.00
ol	16.07	16.06	14.31	21.02	28.01	22.56	25.17	26.13
mt	1.54	1.61	1.67	2.07	1.86	1.74	1.94	1.94
il	2.47	2.41	2.49	3.57	3.23	2.17	3.17	3.25
ap	0.35	0.37	0.39	0.39	0.39	0.23	0.42	0.46

Sample	BHL18	BHL19	BHL20	BHL21	BHL22	BHL23	BHL24	BHL25
%AN	57.79	60.43	60.48	61.85	60.84	53.57	59.15	59.20
or	1.54	2.13	1.36	1.24	1.24	2.07	2.13	2.01
ab	21.07	17.60	19.37	20.15	21.40	25.32	21.32	20.05
an	28.84	26.87	29.64	32.67	33.25	29.21	30.88	29.10
ne	1.38	0.00	0.23	0.73	0.05	0.91	0.00	0.00
di	14.64	18.65	19.08	19.50	18.75	11.51	21.99	19.92
hy	0.00	1.15	0.00	0.00	0.00	0.00	0.75	3.15
ol	26.19	27.75	24.59	19.06	19.33	22.68	17.08	19.64
mt	1.93	1.67	1.75	1.73	1.77	2.32	1.71	1.71
il	3.21	2.01	2.45	2.68	2.89	4.10	2.77	2.58
ap	0.46	0.25	0.28	0.28	0.30	0.51	0.35	0.35

Sample	BHL26	BHL27	BHL28	BHL29	BHL30	BHL31	BHL32	BHL33
%AN	61.89	54.82	57.07	59.36	60.80	60.47	61.40	65.26
or	2.19	1.71	2.01	1.89	1.54	1.71	1.71	1.71
ab	19.63	24.06	21.89	17.69	18.62	18.19	17.69	14.12
an	31.88	29.20	29.09	25.83	28.87	27.83	28.13	26.53
ne	0.00	0.44	1.57	0.00	0.00	0.00	0.00	1.20
di	20.22	19.37	20.74	16.96	17.91	17.03	16.01	17.89
hy	3.98	0.00	0.00	1.26	3.68	1.31	2.13	0.00
ol	16.34	19.93	19.34	29.35	23.09	27.74	27.62	32.59
mt	1.67	1.70	1.71	1.83	1.86	1.78	1.80	1.81
il	2.49	2.49	2.41	2.62	2.91	2.51	2.45	2.39
ap	0.35	0.30	0.30	0.30	0.32	0.32	0.30	0.28

Appendix 3 CIPW norms

Sample	BHL34	BHL35	BHL36	BM1	BM2	BM3	BM4	BM5
%AN	61.88	64.98	59.02	72.76	59.72	64.52	59.42	57.87
or	1.18	1.18	1.06	0.77	1.06	1.24	1.24	1.48
ab	17.14	16.84	21.85	10.58	20.39	15.34	18.77	19.92
an	27.82	31.24	31.48	28.25	30.24	27.89	27.49	27.36
ne	1.21	0.00	1.45	0.00	0.00	8.70	0.56	1.45
di	19.52	17.31	13.91	7.02	13.41	20.27	19.35	16.80
hy	0.00	5.15	0.00	23.67	5.77	0.00	0.00	0.00
ol	26.55	22.19	22.59	24.39	23.03	18.85	28.40	26.83
mt	1.81	1.86	1.99	1.84	1.97	2.00	1.75	1.78
il	2.72	2.83	3.49	1.71	3.61	3.55	2.41	2.72
ap	0.32	0.28	0.28	0.25	0.39	0.28	0.30	0.32

Sample	BM6	BM7	BM8	BM9	BM10	BM11	BM12	BM13
%AN	49.74	52.62	59.37	58.12	63.57	60.06	58.66	61.36
or	2.30	1.65	1.60	1.54	1.60	1.42	1.65	1.77
ab	24.90	24.25	20.56	21.92	13.20	22.51	22.25	17.01
an	24.64	26.93	30.04	30.42	23.03	33.85	31.57	27.01
ne	3.33	1.35	0.00	0.00	0.00	0.00	0.00	0.00
di	13.74	16.54	12.38	18.30	11.06	14.02	20.47	16.49
hy	0.00	0.00	4.44	0.69	7.26	1.11	0.98	10.59
ol	24.79	22.17	25.39	21.65	37.97	21.57	18.52	20.74
mt	2.03	2.12	1.86	1.74	1.83	1.93	1.64	1.78
il	3.76	3.34	2.43	2.51	1.71	3.21	2.22	2.68
ap	0.56	0.39	0.30	0.28	0.25	0.30	0.28	0.32

Sample	BM14	BM15	BM16	BM17	BM18	BM19	BM20	BM21
%AN	57.83	58.96	56.63	59.88	57.82	57.42	56.60	59.95
or	1.42	1.30	1.71	1.95	2.30	1.00	1.06	1.12
ab	19.97	19.31	19.96	19.04	19.58	24.10	24.96	22.48
an	27.39	27.75	26.06	28.41	26.85	32.50	32.56	33.65
ne	0.00	2.28	1.11	0.00	0.12	0.56	0.00	0.20
di	16.69	16.51	17.41	18.66	17.10	11.40	12.36	13.21
hy	0.61	0.00	0.00	1.89	0.00	0.00	0.38	0.00
ol	27.96	28.15	28.66	24.60	28.85	24.34	23.37	23.84
mt	1.81	1.86	1.80	1.78	1.74	1.97	1.97	1.94
il	2.54	2.54	2.58	2.60	2.45	3.42	3.46	3.15
ap	0.32	0.30	0.42	0.39	0.30	0.32	0.35	0.32

Sample	BM22	BM23	BM24	BM25	BM26	BM27	BM28	BM29A
%AN	60.39	58.04	58.97	61.91	58.70	61.27	56.08	62.63
or	1.12	2.13	1.89	1.48	1.71	1.71	1.83	1.24
ab	22.08	19.97	19.55	20.14	20.56	19.29	22.17	20.14
an	33.66	27.62	28.09	32.73	29.22	30.52	28.31	33.75
ne	0.69	0.05	0.00	0.00	0.00	0.00	0.00	0.00
di	12.71	18.97	17.78	18.67	16.66	15.47	17.26	18.84
hy	0.00	0.00	1.57	4.12	4.45	9.75	0.15	6.51
ol	24.48	26.46	25.71	17.90	22.74	18.32	25.39	14.64
mt	1.97	1.73	1.74	1.71	1.77	1.80	1.77	1.71
il	3.15	2.34	2.39	2.54	2.41	2.36	2.41	2.51
ap	0.35	0.35	0.37	0.35	0.30	0.32	0.35	0.32

Appendix 3 CIPW norms

Sample	BM29B	BM30	BM31	BM32	BM33	BM34	BM35	BM36
%AN	59.81	55.00	57.64	56.43	56.26	49.04	61.59	53.27
or	1.24	1.77	1.65	2.07	1.54	1.12	0.83	1.65
ab	21.92	25.22	23.95	24.49	24.62	28.82	20.56	27.58
an	32.61	30.82	32.59	31.71	31.67	27.73	32.97	31.43
ne	0.00	0.00	0.00	0.17	0.69	1.67	0.00	0.19
di	21.26	18.50	16.93	18.34	18.96	9.87	15.81	13.58
hy	2.84	1.76	1.63	0.00	0.00	0.00	2.76	0.00
ol	16.21	16.90	18.42	18.50	18.80	23.84	21.44	20.05
mt	1.62	1.71	1.70	1.68	1.61	2.17	1.91	1.84
il	2.26	2.77	2.54	2.62	2.24	3.82	3.23	3.23
ap	0.28	0.44	0.37	0.37	0.32	0.67	0.32	0.56

Sample	BM37	BM38	BM39	BM40	BM41	BM42	BM44	BM45
%AN	59.17	44.27	54.75	60.51	65.46	61.57	62.67	59.63
or	1.95	4.55	3.25	3.72	2.60	3.13	2.13	0.47
ab	22.48	32.95	21.43	19.55	16.75	18.87	19.38	23.69
an	32.58	26.18	25.93	29.96	31.75	30.23	32.54	35.00
ne	0.70	1.08	2.97	0.00	0.00	0.00	0.00	0.00
di	14.91	6.47	17.04	12.64	14.63	13.28	12.95	13.35
hy	0.00	0.00	0.00	3.48	8.15	5.69	7.13	2.64
ol	21.68	19.44	23.99	24.40	20.24	22.48	19.47	18.51
mt	1.86	2.19	1.83	1.81	1.91	1.88	2.06	1.99
il	3.27	5.64	2.92	2.87	3.00	3.04	3.68	3.51
ap	0.37	1.04	0.32	0.39	0.42	0.49	0.49	0.46

Sample	BM46	BM47	BM48	BM49	BM50	BM51	BM52	BM53
%AN	64.75	66.19	62.80	67.12	63.52	61.65	54.56	49.94
or	3.90	2.66	3.31	1.48	1.71	3.13	1.12	3.25
ab	18.02	18.02	19.46	17.35	20.65	20.90	25.13	28.73
an	33.10	35.28	32.85	35.41	35.94	33.60	30.18	28.66
ne	0.00	0.00	0.00	0.00	0.00	0.00	0.00	1.08
di	14.11	12.05	14.60	11.51	9.82	12.63	8.92	8.62
hy	5.62	4.23	5.22	8.25	7.41	6.13	7.48	0.00
ol	19.70	22.37	19.56	18.74	18.37	17.33	18.19	20.60
mt	1.84	1.90	1.84	2.03	2.02	1.99	2.25	2.19
il	2.85	2.94	2.81	3.67	3.63	3.63	5.39	5.20
ap	0.39	0.39	0.39	0.44	0.49	0.46	0.86	0.88

Sample	BM54	BM55	BM56	BM57	BM58	BM59	BM60	BM61
%AN	48.91	53.07	50.89	49.82	54.14	68.02	10.75	8.00
or	2.48	1.12	3.13	1.42	1.36	0.53	30.85	35.22
ab	30.55	27.50	28.53	30.63	27.67	15.99	42.54	38.14
an	29.24	31.10	29.57	30.41	32.67	34.01	5.12	3.32
ne	0.00	0.00	0.68	0.00	0.00	0.00	5.97	6.93
di	9.24	7.42	8.73	7.40	6.49	25.12	4.52	4.54
hy	0.46	9.08	0.00	1.61	4.90	11.45	0.00	0.00
ol	19.30	15.49	20.33	19.80	18.57	8.80	7.16	7.32
mt	2.28	2.25	2.23	2.23	2.26	1.84	1.10	1.13
il	5.30	4.96	5.18	5.11	4.92	1.88	0.87	1.03
ap	0.76	0.74	0.79	0.79	0.76	0.19	0.56	0.70

Appendix 3 CIPW norms

Sample	BM62	BM63	BM64	BM65	BM66	BM67	BM68	BM70
%AN	10.08	9.77	33.46	32.37	35.77	46.74	57.52	60.12
or	31.03	31.14	12.23	12.35	8.81	2.25	3.19	1.54
ab	43.39	43.22	37.05	36.84	36.56	31.39	21.60	20.05
an	4.86	4.68	18.63	17.63	20.36	27.55	29.24	30.23
ne	5.60	5.88	1.34	2.05	0.00	0.00	2.01	0.00
di	3.41	3.57	4.59	5.26	6.19	6.71	16.71	16.21
hy	0.00	0.00	0.00	0.00	0.78	5.45	0.00	5.27
ol	7.97	7.90	16.20	15.78	16.33	15.35	19.37	18.55
mt	1.15	1.15	1.93	1.91	2.10	2.35	2.16	2.15
il	1.03	1.03	4.65	4.58	5.34	5.98	4.44	4.73
ap	0.67	0.67	2.59	2.62	2.29	1.44	0.56	0.70

Sample	BR1	BR2	BR3	BR4	BR5	BR6	BR7	BR8
%AN	47.23	44.85	44.77	58.83	58.31	56.48	56.06	55.63
or	1.42	2.13	3.84	2.95	2.95	2.90	3.01	2.54
ab	28.61	29.59	27.26	20.76	18.92	19.35	20.20	19.68
an	25.61	24.06	22.09	29.66	26.46	25.12	25.78	24.68
ne	1.74	2.67	5.13	0.40	1.48	0.20	1.29	0.43
di	8.92	9.95	10.28	19.43	16.23	17.75	20.37	17.86
ol	23.60	22.73	22.69	21.56	28.46	29.50	23.75	29.37
mt	2.36	2.36	2.41	1.68	1.86	1.74	1.71	1.78
il	4.84	4.94	4.96	2.39	2.70	2.15	2.41	2.32
ap	0.60	0.63	0.63	0.35	0.35	0.32	0.37	0.37

Sample	BR9	BR10	BR11	BR12	BR13	BR14	BR15	BR16
%AN	53.65	56.07	58.89	62.40	59.31	52.91	57.34	55.04
or	2.95	2.72	3.01	3.19	1.77	1.65	2.30	1.89
ab	21.82	22.32	18.83	15.21	18.19	22.28	22.10	23.32
an	25.26	28.49	26.98	25.25	26.52	25.03	29.71	28.54
ne	0.56	0.29	1.17	1.02	0.00	1.55	1.60	2.68
di	19.33	20.46	19.30	19.05	18.11	17.21	12.74	12.97
hy	0.00	0.00	0.00	0.00	2.41	0.00	0.00	0.00
ol	24.79	20.35	25.80	30.88	27.91	27.60	23.63	24.65
mt	1.78	1.68	1.68	1.78	1.81	1.73	1.93	1.91
il	2.64	2.47	2.24	2.43	2.66	2.30	3.04	2.96
ap	0.42	0.39	0.37	0.28	0.32	0.35	0.42	0.42

Sample	BR17	BR18	BR19	BR20	BR21	BR22	BR23	BR24
%AN	58.04	38.46	39.09	54.67	55.83	58.26	49.28	47.15
or	2.01	6.21	4.96	2.01	1.83	1.30	1.89	2.13
ab	23.19	32.91	31.95	25.72	25.81	22.77	29.63	31.65
an	32.08	20.57	20.51	31.03	32.63	31.78	28.80	28.24
ne	0.00	5.73	6.76	0.00	0.00	0.14	1.50	0.64
di	14.78	6.97	7.82	9.05	9.69	10.26	8.71	6.59
hy	0.37	0.00	0.00	0.56	0.00	0.00	0.00	0.00
ol	21.01	17.65	18.32	24.54	22.68	27.19	21.37	20.72
mt	1.91	2.10	2.12	2.16	2.13	2.13	2.22	2.16
il	3.15	5.43	5.34	4.20	4.14	3.68	4.94	5.09
ap	0.42	1.34	1.23	0.65	0.51	0.51	0.74	0.81

Appendix 3 CIPW norms

Sample	BR25	BR26	BR27	BR28	BR29	BR30	BR31	BR32
%AN	41.04	44.69	44.37	42.77	44.77	46.22	45.45	45.65
or	2.72	2.25	3.96	2.72	3.07	2.30	2.72	2.66
ab	30.31	32.80	32.58	33.86	31.04	31.55	31.50	32.26
an	21.10	26.50	25.98	25.30	25.16	27.12	26.24	27.10
ne	4.62	1.12	0.00	2.06	3.13	1.38	2.37	0.95
di	10.67	7.20	7.72	6.98	8.85	8.78	7.25	6.79
hy	0.00	0.00	0.92	0.00	0.00	0.00	0.00	0.00
ol	19.35	19.81	19.34	18.77	19.30	19.44	20.33	19.72
mt	2.35	2.17	2.20	2.23	2.25	2.23	2.22	2.25
il	5.64	5.45	5.09	6.13	5.85	5.75	5.72	5.94
ap	1.00	0.86	0.86	1.16	0.95	0.95	0.90	1.02

Sample	BR33	K1	K3	K4	C1	C2	C3	C4
%AN	46.44	59.74	52.28	21.81	52.46	52.21	53.65	54.66
or	2.84	1.24	3.13	22.46	3.96	3.66	3.84	4.91
ab	32.51	20.96	27.50	44.09	25.24	23.95	23.27	21.01
an	28.19	31.10	30.13	12.30	27.86	26.16	26.94	25.34
ne	0.45	0.98	0.00	0.00	0.86	0.18	0.00	1.96
di	5.44	12.89	9.95	0.85	11.67	11.21	9.47	14.89
hy		0.00	1.10	1.59	0.00	0.00	6.18	0.00
ol	20.87	23.45	19.97	11.70	19.75	23.72	19.31	21.68
mt	2.26	2.17	2.02	1.57	2.12	2.13	2.19	2.20
il	5.98	4.29	2.91	1.31	5.58	5.18	5.15	5.18
ap	1.04	0.46	0.67	1.27	0.86	0.74	0.74	0.74

Sample	C6	C7	C8	MR1	MR2	MR3	MR4	MR5
%AN	54.28	56.49	56.03	53.50	66.38	60.97	54.84	56.00
Q	2.26	0.00	0.00	0.00	0.00	0.00	0.00	0.00
or	6.15	2.13	3.01	1.12	1.30	1.54	3.43	3.07
ab	21.66	21.07	21.24	26.82	14.89	18.11	23.35	22.42
an	25.71	27.35	27.07	30.86	29.41	28.29	28.36	28.54
di	18.09	24.22	25.39	5.24	13.72	17.38	15.07	16.85
hy	22.05	14.03	1.29	6.51	6.54	0.92	14.33	10.52
ol	0.00	4.67	14.08	20.23	28.35	27.74	9.21	12.00
mt	1.70	1.83	1.74	2.28	1.83	1.90	1.86	1.83
il	1.94	3.06	3.04	4.92	2.43	2.68	3.04	2.83
ap	0.30	0.35	0.37	0.67	0.25	0.35	0.51	0.46

Sample	MR6	MR7	MR8	MR9	MR10	MR11	MR12	MR13
%AN	50.81	59.36	63.14	57.28	61.81	59.39	60.03	57.19
or	2.66	2.13	1.71	1.83	1.83	2.95	3.37	1.65
ab	27.08	18.36	20.31	22.09	18.28	19.72	19.38	20.34
an	27.97	26.83	34.79	29.61	29.58	28.83	29.10	27.17
ne	0.00	0.00	0.00	0.00	0.00	0.00	0.00	1.13
di	9.85	17.06	12.84	16.46	13.78	15.83	16.97	18.23
hy	3.26	7.21	9.29	0.09	5.44	4.80	2.88	0.00
ol	20.75	21.97	15.51	23.92	25.24	23.05	23.20	25.68
mt	2.36	1.77	1.80	1.90	1.78	1.65	1.64	1.77
il	4.41	2.24	2.89	2.81	2.37	2.15	2.18	2.43
ap	0.63	0.35	0.32	0.35	0.32	0.32	0.35	0.30

Appendix 3 CIPW norms

Sample	MR14	MR15	MR16	MR17	MR18	MR19	MR20	MR21
%AN	61.09	45.14	43.74	50.48	52.10	52.01	60.56	41.91
or	1.95	1.54	1.95	2.42	1.60	1.60	1.48	2.13
ab	18.95	31.68	30.85	27.11	26.74	27.08	19.55	35.89
an	29.77	26.07	23.99	27.63	29.09	29.34	30.01	25.90
ne	0.00	0.07	2.13	0.94	0.00	0.00	0.00	0.95
di	18.07	8.43	9.05	12.40	12.13	7.70	17.59	6.12
hy	3.82	0.00	0.00	0.00	1.99	3.77	2.66	0.00
ol	22.58	22.38	22.15	22.26	21.05	21.49	24.11	19.40
mt	1.71	2.62	2.61	2.19	2.19	2.49	1.71	2.25
il	2.34	5.62	5.58	4.35	4.24	5.26	2.09	6.08
ap	0.32	0.74	0.74	0.70	0.65	0.67	0.25	1.07

Sample	MR22	MR23	MR24	MR25	MR26	MR27	MR28	MR29
%AN	43.47	45.30	44.50	44.58	46.97	45.00	31.04	31.67
or	2.25	2.95	2.19	2.95	4.08	4.49	12.00	12.17
ab	35.06	31.11	33.72	33.66	29.76	30.80	42.25	40.71
an	26.96	25.76	27.04	27.08	26.36	25.20	19.01	18.87
ne	0.12	2.17	0.43	0.15	1.02	1.74	0.81	1.78
di	5.65	9.07	6.80	7.20	9.14	8.15	1.99	2.47
ol	19.81	19.45	20.13	18.93	20.32	20.32	15.08	14.67
mt	2.26	2.22	2.25	2.25	2.32	2.32	1.61	1.61
il	6.06	5.85	5.98	6.21	5.34	5.49	4.06	4.06
ap	0.97	1.02	1.00	1.14	0.95	1.07	2.62	2.64

Sample	MR30	MR31	MR32	MR33	MR34	MR35	MR36	MR37
%AN	62.00	58.18	61.98	39.61	49.55	50.85	40.75	39.34
or	2.25	2.13	1.83	4.91	3.31	2.30	7.39	7.21
ab	20.31	22.11	19.38	33.61	30.21	28.43	38.92	39.09
an	33.13	30.76	31.59	22.04	29.66	29.42	26.77	25.35
ne	0.00	0.31	0.00	0.59	0.00	0.00	0.00	0.00
di	12.68	18.38	18.65	8.29	7.50	8.46	5.12	5.40
hy	7.18	0.00	5.17	0.00	2.46	0.77	2.08	1.52
ol	18.69	20.06	16.91	20.40	18.06	22.32	11.66	12.70
mt	1.90	1.97	1.88	2.41	2.41	2.33	1.62	1.62
il	3.25	3.59	3.08	5.74	5.09	4.67	4.22	4.22
ap	0.42	0.53	0.46	1.34	0.86	0.74	2.29	2.34

Sample	MR38	MR39	MR40	MR41	T1	T2	T3	T4
%AN	38.33	41.93	50.90	52.85	47.21	60.46	60.29	58.54
or	7.62	6.32	2.19	2.19	4.49	1.65	1.65	1.42
ab	39.13	35.49	27.48	24.55	25.13	18.79	18.55	20.07
an	24.31	25.63	28.48	27.52	22.48	28.72	28.16	28.35
ne	0.71	0.30	0.33	3.94	1.10	0.00	0.45	0.59
di	5.93	6.40	9.54	13.67	21.30	12.72	16.44	13.56
hy	0.00	0.00	0.00	0.00	0.00	2.12	0.00	0.00
ol	12.98	16.44	21.90	20.03	15.39	30.13	27.87	29.82
mt	1.65	2.02	2.29	2.12	2.12	1.94	1.97	1.90
il	4.33	5.05	5.74	4.88	4.46	2.81	3.25	2.79
ap	2.39	1.53	1.46	0.79	0.65	0.39	0.46	0.39

Appendix 3 CIPW norms

Sample	T5	T6	T7	T8	T9	T10	T11	T12
%AN	56.72	57.71	58.50	60.16	67.88	59.54	58.90	60.17
or	2.78	1.95	1.60	2.72	2.19	1.54	1.95	2.07
ab	20.28	18.69	19.72	19.46	14.05	20.67	25.09	17.77
an	26.58	25.51	27.79	29.38	29.69	30.41	35.95	26.84
ne	0.89	1.97	0.00	0.00	0.00	0.77	1.54	0.00
di	14.70	16.00	13.72	10.65	7.98	13.77	10.78	15.14
hy	0.00	0.00	0.54	9.23	12.72	0.00	0.00	7.96
ol	28.08	28.09	29.65	21.64	28.65	25.78	17.39	24.46
mt	1.84	1.91	1.96	1.90	1.93	2.03	1.91	1.84
il	2.70	2.77	2.89	3.46	2.43	3.32	4.56	2.49
ap	0.42	0.39	0.37	0.53	0.30	0.46	0.46	0.35

Sample	T14	T15	T16	A1	A2	A5	A6	STA2
%AN	57.66	53.17	56.35	43.93	57.56	62.25	62.82	49.79
or	2.84	3.13	4.14	5.73	2.84	1.48	1.54	5.56
ab	21.14	25.13	24.71	28.26	21.41	18.95	17.69	24.45
an	28.79	28.53	31.90	22.15	29.03	31.26	29.88	24.25
ne	2.12	0.32	0.00	0.00	0.00	0.00	0.00	0.00
di	20.74	17.17	12.28	22.45	22.46	15.24	17.05	20.69
hy	0.00	0.00	1.61	3.54	4.85	3.38	5.81	11.78
ol	17.59	18.32	19.97	10.55	13.44	23.25	23.19	3.96
mt	1.75	1.78	1.68	1.81	1.80	1.78	1.67	1.68
il	3.13	3.32	2.60	3.34	3.21	2.49	2.17	2.92
ap	0.39	0.46	0.39	0.65	0.37	0.28	0.25	0.44

Sample	STA3	UV1	UV2a	UV3	UV4	UV5	UV6	UV7
%AN	54.44	51.89	26.67	31.70	59.68	34.95	55.83	59.39
or	1.54	3.13	4.55	3.66	1.48	3.96	1.71	2.60
ab	15.09	26.40	41.33	40.34	18.67	39.51	26.74	19.89
an	18.03	28.47	15.03	18.72	27.63	21.22	33.80	29.08
ne	2.55	0.00	8.10	5.28	1.44	2.53	0.00	0.00
di	8.39	15.07	6.09	6.11	17.51	3.54	6.33	15.71
hy	0.00	2.75	0.00	0.00	0.00	0.00	7.88	0.69
ol	47.69	19.14	15.64	17.15	26.32	18.65	16.01	25.36
mt	2.09	1.70	2.04	2.10	1.83	2.10	2.15	1.84
il	2.05	2.58	4.39	4.58	3.15	4.65	3.93	3.19
ap	0.28	0.51	1.55	1.44	0.35	1.41	0.39	0.49

Sample	UV9	UV10	UV11	EX14	EX19	EX20
%AN	55.94	63.84	54.01	58.26	50.16	48.72
or	1.48	1.95	1.71	2.07	3.19	3.49
ab	25.30	17.24	24.85	19.36	26.23	28.08
an	32.12	30.43	29.19	27.02	26.40	26.68
ne	0.00	1.34	1.53	2.07	0.00	0.24
di	8.38	15.30	11.15	17.42	13.42	14.29
hy	4.17	0.00	0.00	0.00	1.14	0.00
ol	20.81	26.70	23.01	26.64	22.57	21.07
mt	2.32	2.03	2.32	1.78	1.78	1.61
il	3.78	3.27	3.86	2.49	2.70	2.54
ap	0.39	0.39	0.44	0.37	0.39	0.49

Appendix 4a - XRF data

4a.i	-	Mull Plateau Group (MPG)
4a.ii	-	Staffa Magma sub-Type (SMT)
4a.iii	-	Coire Gorm Magma Type (CGMT)
4a.iv	-	Central Mull Tholeiites (CMT)
4a.v	-	Plugs and minor intrusions
4a.vi	-	Skye lavas and dykes
4a.vii	-	Other rocks (mostly Lewisian gneiss, Moine schist and Permo-Carboniferous lamprophyres

In the following tables all iron is reported as Fe_2O_3* Major element values are given in wt%, and have been recalculated on a volatile free basis. Trace element values are given in ppm.

For sample localities see Appendix 1.

	A5	A6	AM1	AM2A	AM2B	AM2C	AM3	AM4	AM5	AM6	AM7A	AM7B	AM8	AM9	AM10	AM11	AM12
SiO2	46.20	47.25	44.63	45.14	45.09	44.63	45.28	45.53	46.26	47.46	44.92	45.58	45.57	45.18	45.38	46.10	47.83
Al2O3	15.41	14.67	14.51	14.51	14.45	14.49	14.77	14.76	14.64	17.19	14.23	14.21	16.78	15.35	15.37	16.64	15.29
Fe2O3*	12.25	11.54	14.58	14.49	14.61	14.62	13.78	13.80	14.31	14.74	12.65	12.34	15.50	13.38	13.35	12.53	11.54
MgO	11.02	12.63	11.67	11.57	11.76	11.75	10.37	10.81	11.47	6.83	12.08	12.21	6.86	11.42	10.11	7.69	8.95
CaO	10.24	10.42	9.40	9.38	9.35	9.33	8.93	8.84	8.85	8.51	9.71	9.89	9.23	9.93	10.11	11.84	11.63
Na2O	2.24	2.09	2.68	2.58	2.43	2.22	2.69	2.84	2.91	3.61	2.47	2.38	3.04	2.26	2.55	2.69	2.48
K2O	0.25	0.26	0.37	0.40	0.45	0.41	0.59	0.59	0.45	0.21	0.35	0.39	0.26	0.18	0.32	0.20	0.29
TiO2	1.31	1.14	2.10	2.09	2.09	2.08	2.07	2.02	2.10	2.08	1.62	1.52	2.00	1.63	1.77	1.55	1.40
MnO	0.18	0.18	0.20	0.19	0.19	0.19	0.19	0.18	0.20	0.19	0.18	0.18	0.21	0.18	0.18	0.18	0.18
P2O5	0.12	0.11	0.21	0.20	0.20	0.20	0.22	0.22	0.21	0.17	0.16	0.18	0.17	0.17	0.21	0.13	0.14
Total	99.22	100.29	100.37	100.55	100.63	99.94	98.89	99.61	101.39	100.98	98.37	98.87	99.63	99.69	99.36	99.56	99.73
LOI	2.36	2.4	2.14	2.21	1.53	2.1	3.49	3.26	5.32	3.59	2.9	2.86	2.04	4.03	0.82	3.2	4.04
Ba	118	107	161	152	133	111	141	137	102	68	149	176	98	91	197	103	256
Cr	441	712	357	353	346	344	323	358	391	11	708	724	27	330	330	286	526
Ga	22	18	20	18	17	21	19	18	17	20	19	21	26	22	23	20	17
Nb	2.8	2.5	8.2	8.0	8.5	8.6	8.6	8.8	7.4	4.4	5.7	5.0	5.4	5.4	6.3	4.1	4.0
Ni	205	299	306	311	308	320	262	288	325	36	340	349	49	355	263	164	170
Rb	3.7	3.6	8.8	9.8	10.1	8.0	10.7	12.4	10.3	2.2	6.2	6.1	5.3	2.4	3.6	3.5	5.0
Sc	34	34	30	27	32	33	29	28	25	25	30	26	30	30	28	29	30
Sr	239	195	313	316	322	288	346	359	281	372	317	338	313	316	478	338	393
V	292	293	260	276	265	263	239	241	233	269	282	270	286	262	287	314	300
Y	20	18	35	34	35	35	34	34	34	26	23	22	29	23	25	21	22
Zr	77	70	139	138	140	140	149	147	139	123	111	118	120	116	129	88	86
La	6.1	3.9	11.7	11.7	10.0	10.6	12.7	10.5	10.5	5.3	8.8	7.3	5.6	8.5	7.8	5.0	6.7
Ce	18.5	10.0	25.2	25.5	23.6	23.4	31.2	30.4	23.3	19.5	15.5	17.4	20.6	25.7	23.6	21.8	19.9
Nd	11.2	7.8	17.9	17.9	17.5	16.8	19.9	19.4	14.0	14.1	13.0	12.5	12.7	16.5	17.4	11.6	12.9

Appendix 4a.i MPG lavas

	AM13	AM14	AM15	B3	B4A	B4B	B5	B6	B7	B8	B9	B10	B11	B12	B13	B14	B15
SiO2	45.88	47.26	46.11	43.11	47.20	44.73	49.94	46.37	45.58	46.87	46.62	46.38	46.30	46.83	45.71	45.15	44.04
Al2O3	14.61	16.20	15.64	13.78	16.26	14.43	17.17	14.96	16.24	16.80	17.37	17.25	15.46	15.01	15.31	15.78	15.60
Fe2O3*	12.22	11.34	11.89	14.69	13.95	14.63	14.13	12.85	15.65	15.73	14.35	14.14	11.52	11.80	13.28	15.21	16.13
MgO	10.34	8.60	8.34	11.42	3.46	11.94	3.28	11.42	5.42	5.77	7.73	6.77	11.06	11.41	10.86	9.40	7.05
CaO	10.97	11.29	11.60	9.13	5.43	8.94	5.05	10.34	7.29	6.68	7.95	8.47	10.69	10.52	9.68	9.23	7.73
Na2O	2.41	2.43	3.24	2.12	6.40	2.23	7.01	2.32	4.31	4.42	3.14	3.20	2.05	2.09	2.94	2.81	4.24
K2O	0.37	0.31	0.29	0.40	0.72	0.42	0.83	0.19	0.33	0.34	0.26	0.28	0.21	0.28	0.37	0.30	0.37
TiO2	1.35	1.33	1.35	2.12	2.30	2.09	2.34	1.67	3.03	3.03	2.00	1.98	1.11	1.14	1.68	2.18	2.80
MnO	0.17	0.18	0.15	0.20	0.14	0.20	0.13	0.19	0.18	0.19	0.19	0.17	0.17	0.18	0.18	0.17	0.18
P2O5	0.15	0.14	0.13	0.22	0.65	0.22	0.68	0.15	0.32	0.33	0.18	0.18	0.11	0.12	0.23	0.22	0.32
Total	98.46	99.06	98.76	97.29	102.52	99.93	100.57	100.58	98.39	100.19	99.84	98.86	98.79	99.48	100.33	100.51	98.52
LOI	4.6	6.23	5.87	2.54	2.41	2.48	2.58	1.87	2.53	3.46	3.76	1.16	4.16	2.35	1.83	2.62	2.76
Ba	275	168	117	123	196	121	172	75	76	198	75	79	86	114	173	125	114
Cr	732	545	427	378	66	352	13	612	15	9	15	22	475	561	377	245	75
Ga	16	17	18	19	26	21	27	19	23	17	22	22	19	22	22	19	21
Nb	3.8	4.1	3.8	8.0	15.0	7.0	15.0	5.0	6.0	6.7	6.0	5.0	5.5	5.0	6.0	6.5	11.0
Ni	262	212	168	289	13	295	11	267	38	41	46	44	182	250	265	201	94
Rb	7.9	4.3	4.7	7.9	8.0	8.5	12.0	4.0	3.9	5.9	2.0	3.0	3.5	5.5	7.0	3.0	8.0
Sc	30	28	29	34	7	34	5	30	17	17	26	23	31	32	29	27	22
Sr	372	341	342	309	1249	294	1145	256	572	522	331	350	183	219	467	498	520
V	273	279	284	265	61	246	57	313	189	188	266	241	268	287	268	248	232
Y	20	20	20	34	15	34	16	21	27	28	25	26	19	21	19	26	26
Zr	87	87	84	149	385	149	371	102	215	221	127	124	70	79	117	147	198
La	4.2	4.6	6.0	7.7	26.4	10.3	28.6	5.7	8.1	7.8	6.1	6.3	4.0	5.4	6.4	6.6	10.2
Ce	16.8	15.5	15.8	26.4	74.0	22.1	66.0	11.6	37.4	38.9	23.4	20.7	16.8	16.0	18.0	25.1	30.0
Nd	10.0	10.6	15.1	15.8	47.7	15.0	42.8	9.1	23.2	23.7	13.9	15.2	10.5	11.0	11.2	15.4	20.8

Appendix 4a.i MPG lavas

	B16A	B16B	B17	B18	B19	B20	B21	B22	B23	B24	B25A	B25B	B26	B27	B28	B29	B30
SiO2	45.29	46.11	46.84	45.51	45.85	46.34	46.29	46.13	47.54	46.28	47.00	45.45	46.17	46.76	47.27	46.38	47.47
Al2O3	14.76	14.68	16.78	14.98	16.22	13.74	13.70	13.72	14.43	13.12	13.55	13.78	13.94	14.04	14.13	14.91	15.47
Fe2O3*	13.76	13.24	14.11	12.05	16.01	12.34	12.51	12.33	12.46	12.64	11.81	12.23	12.17	12.15	11.70	11.77	12.49
MgO	11.56	11.06	8.27	10.13	7.01	13.27	13.35	12.77	13.12	13.63	13.61	13.42	13.09	13.29	12.66	12.27	9.89
CaO	9.86	9.86	9.31	10.62	8.89	9.68	9.73	9.98	10.10	9.68	9.78	10.19	10.55	10.23	10.03	10.13	10.34
Na2O	2.46	2.62	3.02	2.43	3.39	2.73	2.64	2.46	2.66	2.47	2.64	2.09	2.23	2.26	2.52	2.49	2.97
K2O	0.24	0.37	0.37	0.28	0.40	0.30	0.32	0.30	0.29	0.40	0.36	0.31	0.34	0.29	0.35	0.37	0.35
TiO2	1.68	1.56	1.74	1.35	2.19	1.30	1.33	1.32	1.35	1.40	1.15	1.31	1.31	1.16	1.17	1.13	1.41
MnO	0.19	0.19	0.20	0.18	0.21	0.18	0.18	0.18	0.18	0.18	0.18	0.18	0.18	0.18	0.17	0.17	0.17
P2O5	0.17	0.17	0.18	0.13	0.22	0.16	0.15	0.15	0.16	0.14	0.12	0.15	0.16	0.13	0.14	0.14	0.16
Total	100.06	99.98	100.89	97.76	100.43	100.23	100.39	99.49	102.46	100.15	100.40	100.25	100.32	100.66	100.32	99.92	100.82
LOI	2.35	2.26	2.33	4.16	1.88	1.9	2.22	2.14	3.36	2.34	3.25	1.85	1.96	1.87	1.89	2.81	3.3
Ba	133	229	240	136	247	158	160	154	156	269	132	174	194	168	157	187	149
Cr	501	544	55	526	39	1185	1196	1036	1076	1325	1208	1049	1098	957	1087	757	477
Ga	18	21	24	20	21	15	19	19	18	17	17	18	15	16	18	17	21
Nb	5.0	5.0	4.0	4.0	4.0	5.0	5.0	5.0	4.5	5.0	4.0	6.0	5.0	5.0	4.0	5.0	5.0
Ni	300	278	97	201	77	377	374	370	361	417	431	424	384	389	283	233	201
Rb	3.0	6.0	5.0	5.0	3.0	4.0	5.0	5.3	4.7	10.2	5.5	3.0	5.5	4.6	8.2	5.0	5.0
Sc	29	27	28	32	26	30	32	31	31	29	32	32	34	31	31	31	29
Sr	335	353	388	378	513	363	330	445	343	361	380	284	401	288	281	423	280
V	271	253	305	249	289	260	262	267	260	287	253	265	265	265	251	225	245
Y	24	23	24	21	28	20	21	19	19	20	18	20	22	20	20	19	24
Zr	107	98	103	84	122	92	94	88	89	97	78	90	86	82	85	83	101
La	4.0	6.1	5.8	5.8	6.3	8.0	9.2	7.1	7.6	6.9	5.3	8.2	4.3	7.5	8.1	7.4	8.2
Ce	21.0	19.0	23.0	18.0	29.4	16.0	20.0	19.0	21.0	17.0	12.0	14.3	15.0	12.0	11.0	14.0	20.0
Nd	14.0	11.6	12.5	9.2	17.6	9.2	9.6	9.2	10.5	9.8	9.6	12.2	7.9	9.1	10.5	11.4	11.6

Appendix 4a.i MPG lavas

	BB1	BB2	BB3	BB4	BB5	BB6	BB7A	BB7B	BB8	BB9	BB10A	BB10B	BB11	BB12	BB13	BB14	BB15	BB16
SiO2	47.08	46.69	45.11	47.55	45.12	44.89	45.67	44.98	45.28	45.78	44.39	46.24	47.13	46.65	45.89	45.47	46.30	45.77
Al2O3	15.93	14.79	15.89	16.99	16.50	16.09	16.86	16.07	16.79	15.39	15.57	17.24	17.03	16.94	16.68	16.43	16.87	16.35
Fe2O3*	12.30	12.74	14.08	14.01	14.89	14.55	15.14	14.55	15.14	13.44	16.79	15.51	15.10	15.44	15.41	15.56	14.78	15.51
MgO	7.71	11.63	8.40	4.15	6.16	9.35	7.37	9.54	7.21	10.36	6.17	5.72	5.50	5.14	5.10	5.46	5.63	5.56
CaO	10.84	9.82	9.58	6.10	7.43	9.56	8.61	9.50	8.49	10.09	8.76	8.04	7.31	7.60	7.48	7.92	8.02	7.70
Na2O	2.39	2.64	3.40	5.96	4.38	2.89	3.56	2.80	3.34	2.26	3.20	4.08	4.81	4.38	4.43	4.08	3.95	4.17
K2O	0.41	0.38	0.37	1.28	0.60	0.22	0.25	0.25	0.22	0.16	0.52	0.33	0.41	0.45	0.46	0.44	0.51	0.79
TiO2	1.43	1.55	1.72	2.84	2.55	1.96	2.50	1.91	2.50	1.75	2.98	2.85	2.89	3.13	3.15	3.08	3.04	2.96
MnO	0.18	0.18	0.19	0.14	0.15	0.18	0.19	0.18	0.19	0.20	0.22	0.19	0.18	0.19	0.19	0.19	0.19	0.20
P2O5	0.14	0.19	0.18	0.61	0.42	0.22	0.24	0.20	0.25	0.16	0.41	0.34	0.38	0.42	0.46	0.42	0.43	0.40
Total	98.42	100.61	98.91	99.63	98.20	99.91	100.41	99.99	99.41	99.58	99.01	100.56	100.74	100.32	99.26	99.08	99.73	99.41
LOI	5.28	2.13	3.01	2.09	3.69	1.62	1.58	1.9	2.29	1.46	2.7	2.75	1.69	2.07	2.48	2.02	2.32	1.96
Ba	177	137	89	233	178	81	61	84	63	57	305	81	112	134	138	121	159	236
Cr	317	678	172	0	5	72	0	71	0	342	6	3	18	33	0	8	0	3
Ga	20	20	20	24	21	22	20	20	21	22	24	19	17	21	22	19	20	24
Nb	4.2	5.2	5.1	17.5	11.8	7.1	5.6	6.1	6.0	4.1	7.5	10.7	11.4	13.6	14.5	12.5	14.0	13.0
Ni	163	311	131	18	81	180	72	192	70	239	54	47	43	44	39	45	46	32
Rb	2.6	6.6	5.5	12.0	5.6	3.0	3.8	4.1	3.5	3.4	8.1	2.8	5.3	5.0	4.8	5.9	4.1	11.0
Sc	29	30	26	14	24	29	25	30	25	31	26	21	21	21	23	22	23	21
Sr	904	327	372	1006	717	470	466	359	414	258	1203	505	681	623	731	628	885	501
V	273	288	271	119	187	251	263	238	255	296	322	185	199	179	173	191	177	227
Y	25	22	23	18	22	28	31	25	31	26	35	32	33	36	36	37	36	36
Zr	103	117	109	257	194	124	149	119	152	103	187	177	183	212	222	205	202	193
La	6.2	9.3	6.6	26.3	16.5	10.0	8.8	7.8	10.8	7.3	15.1	15.3	14.9	20.9	21.7	16.2	19.1	17.1
Ce	22.3	20.6	22.1	62.0	42.3	27.8	24.1	27.6	33.7	22.8	51.2	46.2	42.7	44.4	54.7	46.7	50.0	46.5
Nd	12.4	15.5	13.6	44.5	26.7	19.9	20.6	14.1	24.3	16.6	34.6	28.7	29.4	37.7	35.6	30.0	34.9	31.7

Appendix 4a.i MPG lavas

	BB17	BB18	BB19	BB20	BB21	BB22	BB23	BB24	BCH2	BCH3	BCH4	BCH5	BCH6	BCH2X	BCH3X	BCH4X	BCH8
SiO2	46.16	45.58	45.42	46.32	45.40	45.34	44.94	45.16	47.23	45.82	47.28	44.74	44.49	47.19	47.36	46.54	47.20
Al2O3	16.17	16.47	16.41	14.73	14.55	14.31	14.30	16.08	15.99	14.18	16.14	15.64	15.59	14.12	15.84	15.66	15.29
Fe2O3*	16.55	15.87	15.58	13.87	13.79	13.30	13.76	16.58	12.97	13.17	12.31	15.24	15.48	14.16	12.76	12.41	12.01
MgO	5.45	6.33	6.11	10.61	10.61	12.20	11.02	6.51	9.26	12.61	9.32	8.59	8.78	9.14	9.49	8.98	8.17
CaO	7.78	8.50	8.57	9.25	9.23	9.33	9.64	8.64	9.33	8.60	10.00	8.10	8.62	9.76	10.07	9.85	9.25
Na2O	3.77	3.67	3.57	2.62	2.94	2.25	2.59	3.39	3.32	3.23	3.30	4.31	2.81	2.85	2.73	3.37	3.12
K2O	0.71	0.54	0.61	0.50	0.55	0.53	0.47	0.30	0.47	0.31	0.34	0.43	0.50	0.61	0.44	0.35	0.63
TiO2	3.19	2.58	2.59	1.78	1.70	1.51	1.75	2.46	1.54	1.39	1.53	2.54	2.61	2.12	1.55	1.57	1.49
MnO	0.22	0.21	0.20	0.18	0.18	0.18	0.19	0.21	0.17	0.17	0.17	0.18	0.18	0.20	0.17	0.18	0.18
P2O5	0.44	0.31	0.37	0.22	0.21	0.17	0.18	0.23	0.17	0.14	0.16	0.26	0.27	0.16	0.15	0.15	0.24
Total	100.43	100.07	99.42	100.10	99.17	99.11	98.84	99.54	100.58	99.79	100.65	100.38	100.95	100.49	100.67	99.16	97.58
LOI	2.35	2.47	2.5	2.46	2.27	4.05	2.38	1.13	6.78?	4.7	4.56	2.98	4.14	2.38	5.8	3.92	1.69
Ba	299	234	336	129	115	190	149	99	128	92	107	165	220	201	118	113	395
Cr	0	0	2	486	525	785	547	12	579	858	415	51	52	459	625	394	302
Ga	23	25	21	21	22	23	23	21	19	18	21	20	22	18	23	15	22
Nb	12.7	8.8	11.4	5.2	4.7	5.4	6.7	5.4	5.5	5.0	4.0	11.0	11.0	6.0	4.5	5.0	5.2
Ni	22	40	42	262	261	334	257	51	316	410	224	111	124	248	286	202	177
Rb	7.0	6.1	6.7	8.6	9.5	7.4	6.4	3.2	9.0	6.0	8.1	8.6	7.0	8.0	8.0	5.3	5.5
Sc	25	26	22	25	26	25	29	28	28	33	30	26	28	38	28	30	25
Sr	625	497	631	342	384	561	354	456	256	229	239	492	497	248	251	233	502
V	223	268	264	272	256	214	275	283	221	233	252	255	258	343	239	252	280
Y	39	33	32	20	20	18	22	26	25	25	25	23	25	38	28	27	24
Zr	209	154	144	129	124	106	118	132	101	99	107	179	183	163	107	115	106
La	23.6	15.2	17.5	10.7	9.0	8.8	10.2	10.6	9.7	8.9	6.3	12.8	14.4	13.1	7.6	7.4	13.2
Ce	49.3	34.3	39.9	21.6	24.2	25.9	27.6	26.0	23.0	14.0	30.3	32.0	38.3	35.0	15.0	21.4	31.8
Nd	40.6	28.4	30.1	14.2	13.7	14.8	14.8	22.7	14.4	11.1	14.7	22.0	21.0	19.6	11.3	12.1	20.6

Appendix 4a.i MPG lavas

	BCH9	BCH10A	BCH10B	BCH11	BCH12	BCH13	BCH14	BCH15	BCH16	BCH17	BCH18	BCH19	BCH20	BCH21	BCH22	BCH23A	BCH23B	BCH24
SiO2	48.76	47.64	46.00	45.57	45.99	45.30	45.79	45.86	47.48	45.43	45.43	46.63	45.00	47.25	47.19	47.51	48.05	46.34
Al2O3	16.28	14.90	16.36	16.34	14.88	16.88	14.46	15.83	15.64	12.55	16.03	16.35	16.34	15.60	15.02	15.52	16.02	13.64
Fe2O3*	12.12	11.04	16.03	16.38	15.73	15.38	13.28	13.48	11.70	12.26	16.88	14.45	15.19	11.82	11.99	11.62	10.63	11.96
MgO	7.54	10.01	4.70	4.90	5.82	6.82	12.56	9.98	8.78	16.29	4.81	6.72	7.05	8.73	10.68	8.62	8.92	13.80
CaO	8.46	10.77	6.79	6.43	8.52	9.43	9.64	9.89	10.88	8.74	7.21	8.57	8.94	11.48	10.79	11.21	11.08	9.93
Na2O	4.54	2.86	5.02	5.56	3.59	3.71	2.18	2.70	2.63	1.94	4.71	3.36	3.26	2.23	2.08	2.57	2.57	1.91
K2O	0.60	0.28	0.27	0.31	1.03	0.28	0.22	0.25	0.69	0.70	0.71	0.84	0.42	0.55	0.49	0.44	0.37	0.47
TiO2	1.53	1.07	3.24	3.20	2.29	2.12	1.55	1.73	1.58	1.18	3.36	1.98	1.94	1.36	1.23	1.34	1.14	1.22
MnO	0.17	0.17	0.18	0.20	0.22	0.21	0.18	0.19	0.18	0.18	0.16	0.20	0.20	0.17	0.17	0.20	0.16	0.17
P2O5	0.27	0.12	0.39	0.34	0.34	0.22	0.15	0.17	0.17	0.14	0.45	0.19	0.19	0.15	0.11	0.14	0.11	0.12
Total	100.28	98.86	98.98	99.22	98.42	100.33	100.01	100.09	99.72	99.40	99.78	99.95	98.54	99.35	99.75	99.17	99.05	99.56
LOI	3.15	3.97	2.52	2.55	2.41	2.18	2.88	2.13	4.36	3.56	2.45	2.7	2.03	3.02	3.93	1.08	2.01	3.04
Ba	369	201	60	75	534	132	107	106	212	205	147	216	226	410	284	223	182	291
Cr	165	556	0	0	12	3	639	239	479	1413	6	22	16	297	564	391	416	1206
Ga	18	17	20	21	24	25	17	21	20	20	20	25	25	19	15	22	19	17
Nb	5.1	3.6	8.3	7.7	6.3	5.1	4.1	4.2	4.3	3.8	13.2	7.4	5.4	5.2	4.7	5.1	4.1	3.5
Ni	151	204	17	23	59	54	349	232	151	548	33	72	88	111	188	124	135	441
Rb	6.1	4.9	2.5	5.7	11.9	3.2	4.1	3.5	9.5	11.7	9.5	15.4	4.5	9.9	7.3	7.3	4.5	9.3
Sc	22	29	18	19	25	28	31	30	27	25	16	25	28	31	27	30	29	29
Sr	450	371	550	457	561	378	276	333	1192	1374	1037	359	431	303	257	308	327	238
V	314	278	250	251	344	282	256	293	290	237	173	294	296	293	262	282	282	282
Y	22	18	28	29	30	27	23	24	23	17	25	28	27	21	18	20	17	19
Zr	108	73	235	208	173	128	102	118	101	100	232	161	113	84	77	90	72	83
La	17.2	6.2	20.2	17.5	21.8	12.4	4.9	6.3	7.9	5.9	19.4	16.6	8.4	6.8	5.4	6.5	5.0	5.8
Ce	39.8	18.4	60.3	55.7	54.7	32.8	18.7	19.3	19.6	16.9	53.3	38.8	26.3	18.9	17.1	18.1	15.8	19.0
Nd	22.3	11.8	41.3	37.6	30.8	22.2	11.4	13.4	14.5	9.3	36.7	21.8	17.8	14.1	11.6	13.2	11.9	11.3

Appendix 4a.I MPG lavas

	BCH25	BCH26	BCH27	BCH28	BCH29	BCH30	BCH31	BCH32	BCH33	BCH34A	BCH34B	BCH34C	BCH35	BCH36	BCH37	BCH38	BCH39	BCH40
SiO2	46.13	46.27	46.65	45.90	46.11	46.79	46.80	46.40	45.46	45.83	46.51	46.66	46.28	46.46	47.68	47.47	46.64	46.71
Al2O3	13.57	13.91	13.76	13.30	13.72	13.97	14.01	16.35	14.02	14.36	14.19	13.87	14.34	14.74	16.15	15.50	15.42	15.24
Fe2O3*	12.06	11.96	11.88	11.58	12.06	12.16	11.96	13.91	12.41	12.24	12.55	13.07	12.36	12.32	11.37	11.90	11.25	11.49
MgO	13.78	13.44	13.65	15.30	13.49	13.36	13.13	8.82	12.59	13.22	11.31	10.69	12.48	12.04	8.90	8.48	9.38	8.73
CaO	9.97	10.00	9.81	9.09	9.40	9.60	9.65	9.27	10.05	9.76	10.54	10.62	10.22	10.32	11.30	10.96	11.48	11.64
Na2O	1.98	2.14	2.11	1.90	2.62	2.20	2.19	3.01	2.55	1.97	2.47	2.69	2.07	2.24	2.46	2.99	2.44	2.36
K2O	0.30	0.39	0.51	0.37	0.45	0.34	0.42	0.45	0.43	0.37	0.40	0.41	0.51	0.42	0.50	0.44	0.46	0.62
TiO2	1.22	1.21	1.22	0.87	1.14	1.15	1.21	1.79	1.31	1.18	1.48	1.64	1.33	1.31	1.26	1.41	1.21	1.31
MnO	0.17	0.18	0.18	0.17	0.18	0.18	0.18	0.18	0.19	0.17	0.19	0.19	0.17	0.17	0.18	0.19	0.17	0.18
P2O5	0.12	0.11	0.12	0.11	0.12	0.12	0.13	0.15	0.15	0.12	0.15	0.17	0.14	0.14	0.15	0.19	0.15	0.18
Total	99.30	99.61	99.89	98.59	99.28	99.85	99.69	100.33	99.17	99.24	99.79	100.01	99.90	100.14	99.94	99.52	98.61	98.46
LOI	3.08	3.2	2.61	4.32	2.62	2.92	1.9	3.57	2.85	2.76	2.12	1.18	3.3	2.84	4.85	1.82	4.64	5.48
Ba	189	299	470	173	161	129	165	101	191	186	158	190	446	169	232	252	229	273
Cr	1246	1180	1176	1010	1048	1018	1007	131	881	973	731	669	841	793	380	314	350	283
Ga	19	19	19	15	17	19	17	18	17	17	19	19	20	15	20	21	19	16
Nb	3.3	4.0	4.4	3.7	3.3	3.8	4.0	4.7	4.7	5.2	6.1	6.5	5.7	5.4	5.2	6.1	5.4	7.8
Ni	450	455	447	463	456	463	437	144	373	410	284	252	348	334	147	130	146	115
Rb	5.0	6.1	10.2	5.2	9.2	7.6	7.2	7.1	7.9	6.5	6.0	5.6	9.2	3.8	6.3	5.5	4.9	7.7
Sc	29	29	29	22	27	26	30	26	30	32	29	29	29	29	28	27	27	28
Sr	277	259	248	256	257	213	239	487	344	271	345	323	346	560	775	408	479	566
V	287	294	292	204	262	268	277	263	282	253	293	320	254	266	256	297	249	267
Y	19	19	18	17	19	20	21	21	21	19	25	26	22	21	21	24	20	23
Zr	83	83	83	65	83	85	87	96	91	83	93	107	88	91	80	95	82	87
La	5.4	3.5	3.8	3.2	5.0	4.8	5.7	6.5	5.9	6.4	8.4	7.7	6.0	9.8	5.3	10.9	5.2	9.3
Ce	17.3	13.2	16.8	10.9	16.8	12.4	15.3	19.5	16.4	18.3	22.9	20.2	16.2	24.0	17.9	26.1	15.4	25.5
Nd	10.3	9.4	12.1	8.0	9.6	10.0	8.6	12.8	10.7	10.3	16.3	13.6	9.3	14.8	12.3	17.3	9.1	18.0

Appendix 4a.i MPG lavas

	BCH41	BCH42	BCH43	BCH44	BCH45	BCH46	BG1	BG2	BG3	BG4	BG5	BG6	BG7	BG8	BHL2	BHL3
SiO2	46.81	46.54	44.35	45.58	44.56	45.61	47.12	45.94	47.75	48.64	48.55	49.32	46.63	46.34	44.24	45.54
Al2O3	16.70	16.63	16.04	16.68	15.89	16.36	16.41	16.65	15.73	14.94	16.15	15.79	17.23	16.92	13.98	14.91
Fe2O3*	12.84	13.09	15.49	15.22	15.27	15.22	13.40	13.51	12.17	12.15	11.89	11.90	15.93	16.27	14.57	13.99
MgO	7.71	7.95	7.52	6.00	7.90	5.96	9.51	10.20	10.41	10.10	8.66	8.11	6.73	7.09	10.66	10.70
CaO	10.61	10.23	8.79	7.93	8.30	7.89	9.27	9.59	9.63	10.53	10.85	10.95	8.53	8.47	8.97	8.65
Na2O	2.77	2.60	3.50	4.28	3.27	3.96	2.43	2.16	2.30	2.56	2.49	2.39	3.27	3.09	3.06	2.67
K2O	0.45	0.46	0.37	0.46	0.24	0.49	0.37	0.39	0.40	0.38	0.38	0.41	0.24	0.25	0.58	0.59
TiO2	1.61	1.76	2.38	2.68	2.37	2.75	1.70	1.77	1.50	1.62	1.63	1.60	2.02	2.09	2.22	2.07
MnO	0.18	0.18	0.18	0.17	0.18	0.17	0.19	0.20	0.19	0.17	0.19	0.20	0.21	0.21	0.20	0.19
P2O5	0.19	0.20	0.29	0.36	0.28	0.37	0.24	0.16	0.18	0.18	0.18	0.17	0.17	0.17	0.21	0.22
Total	99.86	99.64	98.93	99.36	98.26	98.79	100.64	100.57	100.26	101.27	100.97	100.84	100.96	100.90	98.70	99.55
LOI	4.37	5.29	1.86	1.65	2.28	1.97	5.15	5.12	6.55	2.5	3.92	4	1.58	2.01	2.32	4.18
Ba	233	158	73	104	78	123	186	753	189	149	146	322	105	108	130	152
Cr	139	140	23	11	28	4	229	148	450	526	366	385	0	6	326	317
Ga	22	22	22	22	21	18	16	18	14	18	14	19	14	20	19	19
Nb	5.8	6.6	7.9	10.5	8.3	11.0	8.0	6.0	6.6	6.1	5.5	4.8	5.2	6.4	9.6	8.3
Ni	87	85	123	55	123	53	142	229	222	179	123	122	48	49	277	295
Rb	6.3	3.7	7.8	5.3	2.7	4.2	7.0	11.3	7.0	7.7	5.4	5.4	6.1	5.3	11.8	11.7
Sc	28	27	25	21	24	20	25	27	20	31	27	29	25	27	28	28
Sr	575	529	537	754	467	664	341	307	272	313	279	1305	309	299	334	336
V	235	238	225	178	216	169	222	222	226	290	289	279	317	341	249	232
Y	23	23	26	31	27	30	25	23	18	18	20	21	25	25	36	34
Zr	107	111	155	177	159	187	119	100	101	111	105	93	126	131	152	150
La	6.5	8.5	10.5	11.5	10.7	15.5	9.3	7.9	11.1	5.9	7.8	6.2	4.7	5.3	13.1	11.6
Ce	22.9	23.2	29.8	30.3	30.5	39.2	17.4	11.9	18.2	15.1	22.7	12.4	18.6	17.1	26.3	27.2
Nd	15.7	14.9	21.6	24.6	19.8	26.8	17.2	8.2	18.3	13.7	19.4	13.8	17.1	18.3	18.0	18.0

Appendix 4a.i MPG lavas

	BHL5	BHL6	BHL7	BHL8	BHL9	BHL10	BHL11	BHL12	BHL13	BHL14A	BHL14B	BHL15	BHL16	BHL17	BHL18	BHL19	BHL20	BHL21
SiO2	45.40	46.11	44.64	44.92	45.70	46.01	49.11	48.38	47.65	46.36	45.57	47.13	44.07	45.53	46.08	46.36	46.53	46.42
Al2O3	14.76	15.49	14.28	15.35	14.88	15.56	16.60	16.21	17.09	17.49	14.61	14.26	14.94	15.28	15.44	13.66	14.96	16.38
Fe2O3*	14.11	13.83	13.94	14.51	14.90	15.35	10.64	11.06	11.53	14.26	12.80	11.98	13.39	13.43	13.33	11.54	12.11	11.87
MgO	10.99	8.57	11.05	9.64	9.70	6.45	7.61	9.24	8.19	6.91	12.43	13.17	10.72	10.89	10.78	13.55	11.21	8.43
CaO	8.33	9.53	8.46	8.73	8.29	9.98	10.09	10.57	11.18	8.92	10.00	10.51	9.78	9.63	9.70	10.22	10.87	11.55
Na2O	2.58	3.31	2.57	2.24	2.98	2.82	3.17	2.54	2.33	3.18	2.26	1.86	3.19	3.03	2.79	2.08	2.34	2.54
K2O	0.56	0.61	0.51	0.48	0.51	0.66	0.62	0.44	0.34	0.21	0.39	0.20	0.19	0.26	0.26	0.36	0.23	0.21
TiO2	2.04	2.42	2.12	1.97	2.16	2.60	1.30	1.27	1.31	1.88	1.70	1.14	1.67	1.71	1.69	1.06	1.29	1.41
MnO	0.19	0.18	0.20	0.18	0.19	0.16	0.18	0.16	0.17	0.19	0.18	0.17	0.18	0.18	0.18	0.18	0.18	0.17
P2O5	0.21	0.24	0.21	0.21	0.21	0.27	0.15	0.16	0.17	0.17	0.17	0.10	0.18	0.20	0.20	0.11	0.12	0.12
Total	99.17	100.29	97.97	98.23	99.53	99.86	99.47	100.03	99.96	99.56	100.11	100.53	98.31	100.14	100.45	99.11	99.84	99.10
LOI	5.37	4.14	3.12	8.87	6.19	3.69	4.76	5.71	4.58	3.37	2.65	3.99	1.2	1.51	2.64	3.04	4.78	4
Ba	117	141	119	95	97	152	455	217	195	69	171	94	99	156	138	183	123	98
Cr	317	278	354	748	410	331	544	486	686	8	720	875	333	335	337	987	721	321
Ga	19	19	22	17	19	21	17	19	23	23	20	18	22	20	24	14	22	18
Nb	7.8	9.6	9.0	7.4	8.6	10.0	7.0	6.0	6.5	4.2	6.5	3.4	5.0	5.4	5.1	3.6	2.9	3.7
Ni	334	190	278	400	413	299	146	240	231	38	341	375	299	308	294	400	293	160
Rb	10.5	12.0	10.8	8.6	9.9	12.5	8.8	4.5	4.1	3.1	5.9	4.0	4.2	3.8	4.9	6.2	2.5	3.7
Sc	28	28	31	26	28	36	32	30	31	24	27	33	28	28	28	26	28	29
Sr	266	337	283	296	245	314	535	321	287	401	365	198	385	399	373	263	368	388
V	223	261	259	203	221	271	253	254	256	251	282	288	280	278	273	254	279	277
Y	32	39	35	31	34	44	27	25	28	22	23	18	22	22	22	19	18	21
Zr	145	160	147	140	152	184	88	87	88	108	114	76	125	125	120	69	83	84
La	11.6	11.1	11.8	10.0	11.0	14.1	10.0	8.2	11.1	6.7	11.2	5.3	6.5	8.9	7.6	5.8	6.2	5.0
Ce	22.0	32.4	27.0	21.0	24.4	33.9	16.6	17.6	23.1	20.6	23.7	13.2	21.7	24.2	14.0	15.9	14.0	15.0
Nd	14.4	23.0	17.1	15.0	18.0	20.7	17.2	12.5	12.4	13.9	15.6	8.9	16.3	19.1	14.3	10.2	10.0	9.0

	BHL22	BHL23	BHL24	BHL25	BHL26	BHL27	BHL28	BHL29	BHL30	BHL31	BHL32	BHL33	BHL34	BHL35	BHL36	BM1	BM2
SiO2	46.92	45.75	47.70	47.33	47.63	48.11	47.70	45.54	46.51	46.04	45.67	44.93	45.56	46.21	45.52	46.46	46.67
Al2O3	16.59	16.33	15.85	14.93	15.90	15.85	15.85	13.25	14.48	14.05	14.06	13.21	14.18	14.94	16.50	12.55	15.24
Fe2O3*	12.15	16.04	11.76	11.82	11.45	11.65	11.84	12.56	12.76	12.32	12.39	12.50	12.53	12.82	13.66	12.65	13.59
MgO	8.34	6.85	8.23	10.12	8.86	8.95	8.74	13.79	11.42	13.01	13.02	15.23	12.24	11.33	8.53	17.79	11.11
CaO	11.49	8.97	11.84	11.00	11.62	10.84	11.15	9.61	10.45	10.04	9.83	9.98	10.65	10.75	9.92	7.60	9.64
Na2O	2.54	3.19	2.52	2.37	2.32	2.94	2.93	2.09	2.20	2.15	2.09	1.93	2.29	1.99	2.90	1.25	2.41
K2O	0.21	0.35	0.36	0.34	0.37	0.29	0.34	0.32	0.26	0.29	0.29	0.29	0.20	0.20	0.18	0.13	0.18
TiO2	1.52	2.16	1.46	1.36	1.31	1.31	1.27	1.38	1.53	1.32	1.29	1.26	1.43	1.49	1.84	0.90	1.90
MnO	0.17	0.22	0.16	0.16	0.16	0.16	0.18	0.18	0.18	0.18	0.17	0.19	0.19	0.19	0.17	0.17	0.18
P2O5	0.13	0.22	0.15	0.15	0.15	0.13	0.13	0.13	0.14	0.14	0.13	0.12	0.14	0.12	0.12	0.11	0.17
Total	100.04	100.07	100.04	99.60	99.78	100.24	100.12	98.86	99.94	99.53	98.94	99.64	99.41	100.05	99.34	99.61	101.09
LOI	5.54	2.56	5.6	3.4	4.88	4.3	1.86	1.95	3.48	2.39	4.64	2.71	4.68	5.01	4	7.01	3.76
Ba	93	190	154	135	187	143	166	135	131	156	133	387	95	98	60	78	72
Cr	235	14	482	631	406	412	327	1233	807	994	1105	1338	908	1017	54	1630	610
Ga	19	22	17	19	17	18	22	16	17	17	20	13	20	19	22	16	20
Nb	3.8	5.3	4.5	3.4	4.0	3.9	4.6	3.8	4.3	3.8	4.0	4.2	3.8	3.9	4.8	4.0	6.6
Ni	143	79	167	218	135	145	110	458	342	435	470	519	364	354	175	671	291
Rb	4.3	3.4	5.2	4.7	5.0	4.2	5.0	6.9	4.5	6.1	5.0	8.2	3.6	4.1	3.4	3.9	2.5
Sc	30	28	30	30	31	30	28	30	28	30	30	29	31	31	30	20	26
Sr	370	385	422	545	611	287	349	243	254	282	242	347	294	231	343	179	294
V	283	313	288	288	286	289	273	284	301	282	268	271	317	295	296	187	262
Y	21	27	22	20	20	21	21	19	22	20	19	20	21	22	23	17	22
Zr	88	125	91	88	83	84	78	94	93	93	90	81	80	88	93	61	123
La	5.5	8.8	7.0	8.4	6.8	8.3	5.4	7.8	6.9	6.8	4.4	5.0	6.3	4.0	4.8	7.1	6.0
Ce	14.3	24.0	18.6	24.3	25.7	20.6	20.5	12.6	17.4	19.5	13.3	11.4	11.5	10.0	11.6	9.4	18.0
Nd	11.0	16.8	15.0	15.0	13.4	12.8	8.5	13.4	12.2	13.3	11.2	10.4	10.7	8.4	9.2	4.8	16.0

Appendix 4a.i MPG lavas

	BM3	BM4	BM5	BM6	BM7	BM8	BM9	BM10	BM11	BM12	BM13	BM14	BM15	BM16	BM17	BM18	BM19	BM20
SiO2	44.53	47.03	46.22	47.08	46.65	46.73	47.38	44.96	46.90	48.27	47.08	46.35	46.53	46.79	46.92	46.79	46.46	47.22
Al2O3	16.55	14.15	14.69	15.49	15.37	15.30	15.69	11.30	17.04	16.20	13.53	14.18	14.98	14.14	14.47	14.11	16.98	16.98
Fe2O3*	13.80	12.14	12.32	14.03	14.55	12.79	11.98	12.56	13.26	11.33	12.27	12.53	12.75	12.38	12.32	12.02	13.62	13.57
MgO	7.65	13.38	12.00	9.60	8.22	11.74	9.82	19.64	8.53	8.88	12.84	12.68	12.36	13.07	11.84	13.28	9.00	8.84
CaO	10.74	10.54	9.88	8.67	9.70	9.30	10.82	7.57	10.44	11.58	9.74	9.86	9.87	9.83	10.59	9.85	9.54	9.80
Na2O	3.71	2.34	2.67	3.67	3.16	2.43	2.59	1.56	2.66	2.63	2.01	2.36	2.78	2.60	2.25	2.34	2.97	2.95
K2O	0.21	0.21	0.25	0.39	0.28	0.27	0.26	0.27	0.24	0.28	0.30	0.24	0.22	0.29	0.33	0.39	0.17	0.18
TiO2	1.87	1.27	1.43	1.98	1.76	1.28	1.32	0.90	1.69	1.17	1.41	1.34	1.34	1.36	1.37	1.29	1.80	1.82
MnO	0.17	0.18	0.17	0.18	0.19	0.17	0.14	0.18	0.21	0.15	0.18	0.17	0.18	0.17	0.17	0.17	0.17	0.18
P2O5	0.12	0.13	0.14	0.24	0.17	0.13	0.12	0.11	0.13	0.12	0.14	0.14	0.13	0.18	0.17	0.13	0.14	0.15
Total	99.35	101.37	99.77	101.33	100.05	100.14	100.12	99.05	101.10	100.61	99.48	99.85	101.14	100.81	100.45	100.37	100.55	101.69
LOI	7.51	3.31	4.25	2.62	3.98	3.04	4.76	4.47	5.28	4.64	2.86	3.13	8.74	3.07	3.07	2.46		1.56
Ba	66	100	101	138	128	142	128	142	102	122	122	118	111	146	177	170	62	47
Cr	562	1017	794	479	47	602	656	1957	222	389	1234	1100	1266	1173	1033	922	45	65
Ga	21	18	19	19	20	19	20	18	22	19	19	18	16	18	17	15	20	18
Nb	6.0	4.7	5.4	8.2	5.0	5.0	4.0	4.2	4.8	4.1	4.3	4.4	4.1	5.0	6.0	5.1	5.0	4.6
Ni	244	389	345	225	104	326	266	796	139	124	420	429	487	381	322	403	157	160
Rb	2.5	4.8	5.2	9.0	3.5	5.0	4.7	7.1	5.3	4.0	6.9	5.7	4.0	5.6	4.7	5.6	3.0	3.0
Sc	35	31	26	23	28	27	30	19	28	29	30	29	29	28	30	29	32	28
Sr	545	287	306	426	383	295	362	194	294	386	212	239	425	273	326	293	346	324
V	221	265	245	248	317	262	249	191	286	229	276	283	211	269	257	263	287	283
Y	19	18	18	20	20	21	17	14	19	16	17	18	18	18	18	20	21	21
Zr	115	83	96	150	112	83	85	67	99	76	92	93	86	104	103	88	97	101
La	6.0	6.4	7.0	9.8	5.0	8.0	7.2	5.6	7.0	9.0	7.0	8.0	7.4	8.5	7.0	7.0	6.0	6.7
Ce	22.0	16.4	18.0	27.0	19.0	18.0	15.0	8.1	19.0	17.0	12.0	13.0	17.0	15.0	15.0	20.0	33.0	8.7
Nd	12.0	13.0	12.0	17.0	13.0	12.0	13.0	7.0	14.0	12.0	9.0	11.0	13.0	12.0	13.0	10.0	15.0	14.5

Appendix 4a.i MPG lavas

	BM21	BM22	BM23	BM24	BM25	BM26	BM27	BM28	BM29A	BM29B	BM30	BM31	BM32	BM33	BM34	BM35	BM36	BM37
SiO2	46.55	46.46	47.26	46.93	47.73	47.77	47.97	47.51	48.10	48.76	48.69	48.23	48.44	48.91	46.96	46.71	48.12	46.95
Al2O3	16.98	17.08	14.41	14.44	16.18	15.02	15.25	15.02	16.51	16.44	16.52	16.90	16.82	16.92	16.57	16.23	17.25	16.92
Fe2O3*	13.41	13.57	11.85	11.97	11.84	12.16	12.36	12.16	11.80	11.24	11.84	11.67	11.62	11.08	15.00	13.19	12.68	12.78
MgO	9.10	9.26	12.36	12.29	9.26	11.47	10.78	11.32	8.46	8.56	7.78	8.29	8.01	8.49	7.72	9.56	7.50	8.64
CaO	10.22	10.11	10.49	10.30	11.41	10.20	10.17	10.19	11.63	11.98	11.01	10.95	11.12	11.25	8.38	10.73	9.98	10.45
Na2O	2.70	2.76	2.37	2.31	2.38	2.43	2.28	2.62	2.38	2.59	2.98	2.83	2.93	3.06	3.77	2.43	3.30	2.81
K2O	0.19	0.19	0.36	0.32	0.25	0.29	0.29	0.31	0.21	0.21	0.30	0.28	0.35	0.26	0.19	0.14	0.28	0.33
TiO2	1.66	1.66	1.23	1.26	1.34	1.27	1.24	1.27	1.32	1.19	1.46	1.34	1.38	1.18	2.01	1.70	1.70	1.72
MnO	0.18	0.19	0.17	0.17	0.17	0.17	0.17	0.18	0.17	0.17	0.18	0.17	0.17	0.16	0.17	0.19	0.19	0.19
P2O5	0.14	0.15	0.15	0.16	0.15	0.13	0.14	0.15	0.14	0.12	0.19	0.16	0.16	0.14	0.29	0.14	0.24	0.16
Total	101.13	101.43	100.65	100.15	100.71	100.91	100.65	100.73	100.72	101.26	100.95	100.82	101.00	101.45	101.06	101.02	101.24	100.95
LOI	1.71	2.24	2.26	2.55	3.15	2.41	4.52	2.61	5.35	4.91	1.9	4.64	4.8	4.4	4.35	2.42	5.44	5.07
Ba	75	55	176	171	153	112	116	146	115	105	153	146	131	126	107	71	163	210
Cr	84	82	930	882	370	673	656	624	260	240	200	203	203	267	185	235	148	247
Ga	17	19	13	18	16	16	20	17	17	19	20	18	17	17	17	19	21	18
Nb	6.6	5.3	4.8	5.7	6.3	5.0	5.4	6.1	5.1	5.1	5.8	4.1	5.2	5.2	9.3	6.4	8.3	5.8
Ni	157	162	301	318	153	270	299	237	141	136	78	96	94	93	146	174	102	158
Rb	3.0	4.0	6.0	5.0	5.0	6.0	6.0	6.0	3.0	4.0	5.0	4.0	3.0	5.0	3.0	3.0	4.0	5.0
Sc	29	29	28	27	31	29	26	29	26	30	25	26	28	31	20	32	20	28
Sr	272	281	356	277	317	233	224	303	276	288	308	330	360	345	349	247	394	396
V	295	284	263	256	234	230	239	242	236	204	227	215	235	233	205	330	179	262
Y	21	22	17	18	18	20	19	18	19	18	18	17	18	16	19	21	18	22
Zr	102	102	85	87	82	80	79	83	75	65	100	82	87	75	150	99	120	97
La	4.7	6.5	6.2	7.8	10.6	4.7	8.0	7.4	6.4	7.0	7.6	3.2	7.3	7.6	8.4	4.5	6.9	7.0
Ce	9.8	14.4	21.9	16.0	15.3	13.6	9.0	13.1	19.6	16.0	22.1	18.2	18.8	15.9	25.2	10.7	26.5	10.3
Nd	16.0	12.3	17.6	10.6	13.9	14.0	9.0	13.7	12.0	11.3	16.9	14.7	16.6	12.0	25.3	14.8	21.4	16.0

Appendix 4a.i MPG lavas

	BM38	BM39	BM40	BM41	BM42	BM44	BM45	BM46	BM47	BM48	BM49	BM50	BM51	BM52	BM53	BM54	BM55	BM56
SiO2	47.50	47.31	46.61	46.69	46.64	46.57	46.77	47.04	46.33	47.52	45.57	46.65	47.10	46.24	46.46	46.99	47.15	46.37
Al2O3	17.22	15.33	15.46	15.37	15.32	16.08	17.52	16.35	16.92	16.43	16.62	17.50	16.95	16.15	17.07	17.11	16.95	17.20
Fe2O3*	15.10	12.62	12.54	13.16	13.03	14.21	13.73	12.72	13.10	12.65	14.01	13.85	13.73	15.54	15.14	15.66	15.52	15.40
MgO	5.15	10.33	11.15	10.79	10.87	9.25	7.17	9.56	9.88	9.44	9.10	8.29	7.83	7.70	6.07	5.39	6.38	5.77
CaO	7.43	9.63	9.40	10.26	9.66	10.02	10.58	10.38	10.31	10.45	10.22	9.93	10.13	8.75	8.37	8.56	8.49	8.52
Na2O	4.13	3.18	2.31	1.98	2.23	2.29	2.80	2.13	2.13	2.30	2.05	2.44	2.47	2.97	3.63	3.61	3.25	3.52
K2O	0.77	0.55	0.63	0.44	0.53	0.36	0.08	0.66	0.45	0.56	0.25	0.29	0.53	0.19	0.55	0.42	0.19	0.53
TiO2	2.97	1.54	1.51	1.58	1.60	1.94	1.85	1.50	1.55	1.48	1.93	1.91	1.91	2.84	2.74	2.79	2.61	2.73
MnO	0.18	0.19	0.17	0.18	0.18	0.17	0.18	0.18	0.19	0.18	0.20	0.19	0.18	0.17	0.17	0.17	0.19	0.18
P2O5	0.45	0.14	0.17	0.18	0.21	0.21	0.20	0.17	0.17	0.17	0.19	0.21	0.20	0.37	0.38	0.33	0.32	0.34
Total	100.90	100.82	99.95	100.63	100.27	101.10	100.88	100.69	101.03	101.18	100.14	101.26	101.03	100.92	100.58	101.03	101.05	100.56
LOI	3.08	5.5	5.58	6.15	6.11	5.02	5.04	4.96	5.07	9.76	5.7	5.61	4.42	4.39	3.09	2.4	3.25	2.7
Ba	317	388	259	237	244	124	66	200	261	183	100	131	165	103	204	136	65	125
Cr	0	1134	735	725	780	478	154	298	422	313	217	234	198	128	6	4	3	8
Ga	14	15	16	17	15	19	18	17	15	17	17	14	16	18	18	19	16	17
Nb	14.7	5.9	5.7	5.2	5.4	7.3	7.8	6.3	7.2	7.1	7.8	6.8	6.9	14.3	11.1	11.1	10.9	10.5
Ni	44	377	346	349	359	267	110	181	175	167	183	130	123	79	63	30	49	59
Rb	7.2	7.0	7.5	6.1	8.2	5.8	2.0	10.7	7.3	10.8	4.0	4.0	8.9	4.0	6.0	4.0	2.0	7.0
Sc	13	31	19	22	20	29	23	21	19	17	19	21	25	19	17	17	16	16
Sr	590	485	351	310	348	330	268	351	323	335	288	342	328	519	626	507	452	491
V	153	115	201	224	204	214	247	202	222	211	234	239	245	242	205	221	195	196
Y	28	19	19	19	19	20	20	19	19	20	23	22	20	26	25	27	25	26
Zr	229	97	81	88	87	119	114	84	89	88	111	114	117	206	201	200	172	179
La	15.5	7.2	9.3	7.7	6.3	8.0	9.6	6.4	7.1	8.0	7.3	8.4	7.2	11.1	13.2	12.7	9.2	9.8
Ce	41.3	14.3	13.3	17.4	15.3	21.8	19.9	14.0	16.5	12.2	22.0	16.6	21.7	26.4	37.7	36.8	27.0	26.8
Nd	34.7	15.1	10.0	13.2	11.8	15.0	14.0	12.2	14.6	13.3	21.9	14.2	17.0	25.6	31.1	32.4	24.2	25.8

Appendix 4a.i MPG lavas

	BM57	BM58	BM60	BM61	BM62	BM63	BM64	BM65	BM66	BM67	BM68	BM70	BM71	BR1	BR2	BR3	BR4	BR5
SiO2	46.75	46.47	58.41	57.90	58.56	58.61	49.89	49.88	48.78	46.45	46.04	45.97	45.50	45.39	46.46	46.27	47.56	46.43
Al2O3	17.36	17.60	17.94	17.57	17.91	17.93	16.75	16.62	16.18	16.61	16.22	15.26	15.76	15.83	15.92	15.94	15.59	14.45
Fe2O3*	15.41	15.63	7.58	7.84	7.88	7.89	13.30	13.16	14.48	16.19	14.86	14.78	15.00	16.32	16.28	16.62	11.64	12.80
MgO	5.83	6.10	0.58	0.57	0.66	0.65	3.61	3.55	3.89	4.63	6.93	8.65	8.20	6.95	6.74	6.59	9.85	12.51
CaO	8.37	8.59	2.39	2.11	2.15	2.15	6.33	6.30	6.89	7.98	10.28	10.47	10.66	7.67	7.62	7.30	10.99	9.57
Na2O	3.62	3.27	6.33	6.02	6.35	6.39	4.67	4.80	4.32	3.71	2.99	2.37	2.55	3.76	4.08	4.34	2.54	2.56
K2O	0.24	0.23	5.22	5.96	5.25	5.27	2.07	2.09	1.49	0.38	0.54	0.26	0.32	0.24	0.36	0.65	0.50	0.50
TiO2	2.69	2.59	0.46	0.54	0.54	0.54	2.45	2.41	2.81	3.15	2.34	2.49	2.54	2.55	2.60	2.61	1.26	1.42
MnO	0.18	0.20	0.22	0.22	0.22	0.22	0.23	0.25	0.23	0.21	0.16	0.20	0.19	0.20	0.19	0.19	0.16	0.18
P2O5	0.34	0.33	0.24	0.30	0.29	0.29	1.12	1.13	0.99	0.62	0.24	0.30	0.31	0.26	0.27	0.27	0.15	0.15
Total	100.79	101.01	99.37	99.03	99.81	99.94	100.42	100.19	100.05	99.93	100.60	100.75	101.03	99.17	100.52	100.78	100.24	100.57
LOI	2.53	3.32	1.13	1.1	1.13	1.79	1.44	1.55	1.61	2.99	3.23	3.64	3.17	2.62	2.14	2.80	3.52	1.61
Ba	103	126	1658	1908	1896	1816	1125	1130	1106	434	211	247	193	61	75	110	171	151
Cr	2	6	10	2	10	11	25	0	0	8	222	307	364	149	155	119	475	664
Ga	14	13	27	23	27	25	24	18	19	19	17	19	15	16	14	12	15	15
Nb	9.4	10.4	51.7	49.2	49.9	49.0	24.3	26.1	22.0	16.6	9.8	11.1	9.3	8.0	7.7	7.5	5.0	4.0
Ni	48	51	11	9	4	21	7	14	17	29	144	176	180	99	92	74	194	375
Rb	4.0	3.0	77.0	86.7	73.4	67.0	31.2	30.9	21.4	3.0	8.5	6.0	8.0	3.0	3.0	12.0	6.0	9.0
Sc	15	19	8	6	9	8	16	15	13	17	25	21	24	18	18	17	35	32
Sr	498	443	126	141	153	130	729	770	719	588	385	451	406	374	372	732	527	316
V	189	208	3	6	1	0	49	57	71	187	340	306	306	270	266	241	239	316
Y	25	27	60	55	55	55	47	49	45	34	21	21	21	25	24	23	18	18
Zr	173	178	931	879	893	899	365	373	346	255	110	109	114	161	159	165	75	100
La	9.2	10.9	97.6	85.3	87.0	103.0	48.1	46.7	39.5	21.5	8.7	12.1	9.8	7.0	5.0	9.0	7.0	7.0
Ce	32.1	35.3	191.7	166.7	175.2	184.0	107.2	105.1	87.5	54.8	19.9	27.3	24.7	25.0	24.3	24.0	14.0	18.0
Nd	27.8	28.1	102.7	82.0	86.0	85.0	73.0	74.7	58.3	43.5	15.3	24.0	21.2	19.0	15.0	20.0	10.0	12.0

Appendix 4a.i MPG lavas

	BR6	BR7	BR8	BR9	BR10	BR11	BR12	BR13	BR14	BR15	BR16	BR17	BR18	BR19	BR20	BR21	BR22	BR23
SiO2	46.92	47.36	46.79	47.71	47.99	47.19	45.96	46.82	47.56	45.60	46.70	46.74	47.68	47.35	46.35	46.24	45.69	46.77
Al2O3	13.57	14.39	13.49	14.24	15.38	14.52	13.16	13.58	14.36	16.18	16.30	16.63	17.13	17.06	16.74	17.31	16.36	17.20
Fe2O3*	11.96	11.75	12.33	12.28	11.56	11.57	12.25	12.47	11.94	13.30	13.19	13.17	14.46	14.57	14.92	14.68	14.74	15.30
MgO	13.70	11.20	13.49	11.34	9.45	12.19	14.67	13.74	12.59	8.91	9.58	8.12	4.59	5.04	8.36	7.33	9.78	6.32
CaO	9.68	10.47	9.64	10.13	11.03	10.46	10.01	10.05	9.53	9.36	9.19	10.33	6.59	6.72	8.84	9.23	9.22	8.34
Na2O	2.33	2.67	2.42	2.70	2.70	2.48	2.02	2.15	2.97	2.96	3.34	2.74	5.14	5.25	3.04	3.05	2.72	3.83
K2O	0.49	0.51	0.43	0.50	0.46	0.51	0.54	0.30	0.28	0.39	0.32	0.34	1.05	0.84	0.34	0.31	0.22	0.32
TiO2	1.13	1.27	1.22	1.39	1.30	1.18	1.28	1.40	1.21	1.60	1.56	1.66	2.86	2.81	2.21	2.18	1.94	2.60
MnO	0.17	0.17	0.17	0.18	0.17	0.17	0.18	0.18	0.17	0.18	0.17	0.18	0.14	0.14	0.18	0.19	0.19	0.18
P2O5	0.14	0.16	0.16	0.18	0.17	0.16	0.12	0.14	0.15	0.18	0.18	0.18	0.58	0.53	0.28	0.22	0.22	0.32
Total	100.09	99.95	100.14	100.65	100.21	100.43	100.19	100.83	100.76	98.66	100.53	100.09	100.22	100.31	101.26	100.74	101.08	101.18
LOI	2.81	2.10	1.46	2.93	1.92	4.89	2.86	1.48	1.48	4.50	4.48	3.27	2.15	2.62	2.35	3.19	2.34	1.64
Ba	315	312	252	282	255	215	362	115	107	120	98	115	201	197	122	78	66	98
Cr	983	698	991	740	534	759	1470	1333	1231	254	281	168	11	11	25	94	14	20
Ga	16	16	15	15	16	18	15	14	14	16	14	15	17	19	20	14	16	15
Nb	4.5	5.0	5.2	5.1	4.7	4.6	4.3	4.5	5.1	6.1	5.9	5.8	16.6	14.0	9.4	6.0	4.9	10.0
Ni	350	239	350	270	184	270	460	412	332	134	132	67	35	31	134	198	58	32
Rb	6.0	6.0	6.0	7.0	6.0	5.0	13.0	6.0	5.0	6.0	5.0	5.0	12.0	10.0	5.1	4.0	5.0	4.0
Sc	31	33	30	31	33	30	32	39	36	32	31	33	13	15	26	24	28	24
Sr	516	486	304	372	336	634	402	214	267	443	410	358	952	978	500	385	722	508
V	226	236	217	238	230	214	250	275	249	241	230	245	155	148	242	266	301	243
Y	16	18	18	19	18	17	19	21	18	21	20	22	21	21	26	23	25	26
Zr	74	89	90	101	98	91	82	93	104	111	106	112	280	248	151	131	141	187
La	9.0	7.0	9.0	10.0	13.0	10.0	6.0	5.0	8.0	6.0	7.0	8.0	19.0	15.0	8.0	6.0	7.0	15.0
Ce	19.0	16.0	26.0	23.0	25.0	15.0	12.0	14.0	16.0	20.0	19.0	21.0	50.0	49.0	30.0	24.0	28.0	27.0
Nd	12.0	11.0	14.0	15.0	18.0	13.0	10.0	12.0	13.0	13.0	14.0	13.0	31.0	29.0	18.0	13.0	17.0	19.0

Appendix 4a.i MPG lavas

	BR24	BR25	BR26	BR27	BR28	BR29	BR30	BR31	BR32	BR33	C1	C2	C3	C4	C5	CA2
SiO2	46.34	45.90	46.61	47.43	46.96	46.86	46.85	46.67	46.40	46.70	45.51	44.81	45.39	45.04	43.09	47.19
Al2O3	17.12	15.78	16.90	16.58	17.09	16.94	16.99	17.09	17.03	17.33	16.15	14.98	15.10	14.97	18.88	17.45
Fe2O3*	14.85	16.17	15.01	15.19	15.40	15.46	15.37	15.34	15.54	15.56	14.56	14.72	15.09	15.24	16.87	12.42
MgO	5.84	5.32	5.49	5.48	4.88	5.42	5.50	5.69	5.21	5.58	6.69	8.62	8.06	7.85	6.90	6.24
CaO	7.75	7.39	7.57	7.59	7.44	7.75	8.13	7.56	7.68	7.59	8.95	8.45	8.17	9.17	5.56	10.67
Na2O	3.88	4.59	4.12	3.85	4.45	4.35	4.03	4.24	4.02	3.94	3.17	2.87	2.75	2.91	2.73	2.90
K2O	0.36	0.46	0.38	0.67	0.46	0.52	0.39	0.46	0.45	0.48	0.67	0.62	0.65	0.83	0.73	0.31
TiO2	2.68	2.97	2.87	2.68	3.23	3.08	3.03	3.01	3.13	3.15	2.94	2.73	2.71	2.73	3.39	1.06
MnO	0.18	0.19	0.18	0.18	0.18	0.19	0.19	0.18	0.19	0.20	0.20	0.15	0.20	0.23	0.31	0.19
P2O5	0.35	0.43	0.37	0.37	0.50	0.41	0.41	0.39	0.44	0.45	0.37	0.32	0.32	0.32	0.39	0.12
Total	99.35	99.20	99.50	100.02	100.59	100.98	100.89	100.63	100.09	100.98	99.20	98.28	98.43	99.31	97.94	98.55
LOI	2.53	1.66	2.57	2.11	2.39	2.34	1.95	1.96	3.43	3.04	5.44	5.32	5.42	6.07	7.12	4.23
Ba	122	166	145	200	212	128	109	128	141	168	285	233	289	442	234	96
Cr	24	25	30	55	18	9	15	19	14	17	155	283	268	290	197	138
Ga	15	18	15	16	14	14	14	13	14	19	18	20	20	16	22	18
Nb	10.2	6.0	11.0	7.5	13.7	12.3	11.6	10.3	13.1	13.0	9.1	7.7	9.1	14.4	9.2	4.5
Ni	35	29	39	53	41	28	27	31	25	31	109	159	188	229	144	116
Rb	4.0	5.0	5.0	13.0	4.0	9.0	4.0	3.0	5.0	5.0	7.7	7.8	9.4	12.5	10.1	6.0
Sc	24	23	19	26	18	20	21	20	22	24	29	19	22	22	36	35
Sr	782	824	572	417	741	561	655	1050	571	637	619	434	479	538	485	310
V	231	289	232	277	205	223	220	258	238	226	274	246	230	178	299	264
Y	25	26	28	24	30	30	29	28	29	29	32	28	29	26	32	25
Zr	195	245	214	220	265	226	224	222	232	234	178	171	171	166	188	66
La	12.0	13.0	13.0	15.0	15.0	12.0	15.0	12.0	15.0	16.0	18.0	13.1	13.0	10.0	19.9	2.7
Ce	39.0	41.0	32.0	44.0	49.0	44.0	46.0	42.0	48.0	46.0	47.7	40.9	32.3	26.7	30.2	12.2
Nd	24.0	28.0	21.0	27.0	31.0	25.0	27.0	28.0	28.0	31.0	33.6	22.7	28.1	37.2	28.7	4.7

Appendix 4a.i MPG lavas

	CA3A	CA4	CA5	CA6	CA7	CA8	CA9	CA10	CA11	CA18	K1	K3	K4	MR1	MR2	MR3
SiO2	47.68	53.27	47.93	51.43	54.33	56.47	50.95	44.68	54.65	52.21	44.34	46.78	55.03	45.92	45.65	45.93
Al2O3	18.46	16.68	16.44	16.86	17.03	18.11	15.19	18.13	18.56	16.98	16.05	16.96	17.19	16.73	13.91	14.17
Fe2O3*	14.75	12.72	14.03	10.97	10.42	9.55	14.99	13.56	8.22	11.70	14.95	13.88	10.77	15.72	12.58	13.07
MgO	4.56	2.45	3.43	2.58	1.68	1.44	2.85	5.57	1.87	2.48	8.31	6.34	1.16	7.41	14.66	12.53
CaO	6.16	3.92	7.53	5.68	4.00	2.57	5.01	10.30	5.96	5.26	9.69	8.87	3.40	7.88	9.50	10.22
Na2O	4.55	4.32	3.90	4.70	5.87	4.81	5.93	2.91	4.81	4.28	2.69	3.25	5.21	3.17	1.76	2.14
K2O	0.39	3.08	1.95	3.35	3.26	5.13	0.12	0.12	3.63	3.21	0.21	0.53	3.80	0.19	0.22	0.26
TiO2	2.46	2.23	2.79	1.73	1.14	1.08	2.30	2.50	1.50	1.87	2.26	1.53	0.69	2.59	1.28	1.41
MnO	0.28	0.14	0.24	0.22	0.22	0.20	0.36	0.24	0.14	0.19	0.19	0.18	0.29	0.18	0.18	0.19
P2O5	0.41	0.67	0.81	1.31	0.77	0.71	1.42	0.33	0.70	0.75	0.20	0.29	0.55	0.29	0.11	0.15
Total	99.71	99.49	99.05	98.83	98.73	100.07	99.12	98.34	100.05	98.95	98.93	98.63	98.10	100.08	99.85	100.07
LOI	4.03	3.10	3.05	2.17	1.73	2.20	3.73	5.94	3.02	2.70	2.13	0.81	2.47	3.20	3.53	2.97
Ba	432	1232	1197	1215	1303	1799	136	124	2041	1340	60	380	1663	83	85	151
Cr	59	0	0	0	0	0	14	57	15	3	27	20	0	38	1106	902
Ga	26	19	22	24	24	23	26	24	20	22	19	18	32	17	14	16
Nb	14.5	21.7	20.6	26.7	30.7	33.4	15.2	10.1	22.5	20.4	5.3	11.3	42.1	7.9	5.1	4.2
Ni	48	14	1	1	1	0	7	65	6	20	136	52	0	78	441	414
Rb	4.5	38.5	32.2	44.1	44.5	69.9	2.9	3.0	46.8	43.6	5.5	7.3	51.7	4.0	5.7	4.9
Sc	25	18	18	10	6	6	17	30	12	14	27	28	8	21	26	32
Sr	474	324	674	783	613	582	292	473	671	577	321	591	456	453	164	285
V	261	210	57	20	0	0	27	353	84	146	268	170	0	301	262	298
Y	33	47	47	56	55	57	61	24	40	40	31	34	73	25	17	18
Zr	170	215	270	371	516	554	275	113	244	240	136	110	1089	179	75	96
La	26.4	42.4	41.2	72.1	74.6	82.2	56.2	13.7	54.6	52.8	6.2	13.0	102.3	12.0	5.8	8.0
Ce	34.6	71.9	91.3	133.2	120.7	136.6	77.5	34.1	109.0	99.3	24.1	29.9	236.7	21.0	12.0	20.0
Nd	29.3	52.3	60.2	83.5	70.6	85.1	50.8	20.7	59.1	59.0	17.4	17.8	91.3	16.0	9.0	14.0

Appendix 4a.i MPG lavas

	MR4	MR5	MR6	MR7	MR8	MR9	MR10	MR11	MR12	MR13	MR14	MR15	MR16	MR17	MR18	MR19	MR20	MR21
SiO2	49.44	48.60	46.56	46.99	47.61	46.80	46.49	47.81	47.54	46.70	47.45	46.09	46.00	47.02	46.93	45.84	47.34	47.54
Al2O3	15.56	15.38	16.00	13.79	17.01	15.48	14.73	14.94	15.05	14.62	14.95	16.02	15.91	16.18	16.15	16.31	15.07	17.20
Fe2O3*	12.75	12.63	16.29	12.19	12.39	13.08	12.28	11.36	11.27	12.16	11.75	18.09	18.02	15.07	15.10	17.19	11.75	15.54
MgO	7.54	7.85	6.75	12.17	8.65	9.91	12.63	12.01	11.59	11.63	11.61	5.38	5.40	7.47	7.50	6.70	11.80	4.93
CaO	9.70	10.15	8.38	9.85	10.36	10.23	9.58	9.94	10.29	10.18	10.68	7.70	7.43	8.99	9.19	8.16	10.57	7.30
Na2O	2.76	2.65	3.20	2.17	2.40	2.61	2.16	2.33	2.29	2.65	2.24	3.76	4.11	3.41	3.16	3.20	2.31	4.45
K2O	0.58	0.52	0.45	0.36	0.29	0.31	0.31	0.50	0.57	0.28	0.33	0.26	0.33	0.41	0.27	0.27	0.25	0.36
TiO2	1.60	1.49	2.32	1.18	1.52	1.48	1.25	1.13	1.15	1.28	1.23	2.96	2.94	2.29	2.23	2.77	1.10	3.20
MnO	0.14	0.19	0.21	0.17	0.20	0.18	0.17	0.16	0.17	0.17	0.18	0.21	0.21	0.21	0.21	0.22	0.19	0.20
P2O5	0.22	0.20	0.27	0.15	0.14	0.15	0.14	0.14	0.15	0.13	0.14	0.32	0.32	0.30	0.28	0.29	0.11	0.46
Total	100.29	99.66	100.43	99.02	100.57	100.23	99.74	100.32	100.07	99.80	100.56	100.79	100.67	101.35	101.02	100.95	100.49	101.18
LOI	4.11	4.55	3.24	3.53	5.63	1.28	3.33	4.03	3.32	2.03	3.25	1.98	0.87	2.27	1.94	2.29	3.54	2.52
Ba	305	283	223	176	142	170	141	521	318	150	184	131	130	557	161	104	178	161
Cr	226	272	70	1162	432	363	938	669	646	851	585	10	14	122	151	22	685	1
Ga	19	16	21	18	20	19	17	15	15	18	14	15	18	14	17	22	15	14
Nb	5.4	4.5	5.2	5.0	5.2	4.9	5.3	3.7	5.1	5.3	6.1	7.9	9.1	8.6	8.3	6.6	4.4	15.3
Ni	101	128	73	429	150	185	371	305	288	264	246	40	44	93	91	68	251	48
Rb	10.0	8.2	6.0	6.8	4.3	5.4	6.3	12.2	13.0	5.6	6.1	2.7	3.0	9.1	3.0	4.5	4.0	4.0
Sc	28	30	22	27	28	29	29	25	30	26	26	17	17	24	24	24	29	17
Sr	321	308	397	243	251	263	255	339	331	280	324	433	436	375	399	337	586	538
V	306	297	369	250	254	277	254	218	233	284	237	221	224	254	251	335	244	172
Y	20	19	26	18	20	21	18	18	17	17	17	29	29	26	24	28	18	30
Zr	114	108	145	91	93	98	95	82	84	91	76	199	203	148	141	178	63	262
La	11.1	9.0	9.0	9.0	7.1	5.5	5.6	9.0	10.0	7.0	6.3	8.5	7.3	10.9	7.1	6.1	7.3	11.6
Ce	20.0	26.0	21.0	14.0	15.0	21.5	15.1	18.0	20.0	15.3	17.7	25.4	26.3	21.2	30.5	19.0	9.3	39.7
Nd	18.0	13.0	15.0	11.0	12.0	12.7	10.0	12.0	15.0	11.0	13.4	29.1	27.9	20.8	21.8	25.1	8.7	35.1

Appendix 4a.i MPG lavas

	MR22	MR23	MR24	MR25	MR26	MR27	MR28	MR29	MR30	MR31	MR32	MR33	MR34	MR35	MR36	MR37	MR38	MR39
SiO2	47.06	46.90	47.04	47.12	46.73	46.98	51.63	51.12	47.21	46.96	46.99	47.37	46.97	46.40	50.82	50.47	50.14	48.62
Al2O3	17.15	16.81	17.02	17.06	16.56	16.67	17.67	17.70	16.50	16.07	15.68	15.72	17.35	16.73	18.73	18.21	18.17	17.56
Fe2O3*	15.60	15.29	15.52	15.47	16.00	16.04	11.07	11.14	13.12	13.64	13.00	16.58	16.59	16.14	11.15	11.22	11.38	13.93
MgO	5.02	5.64	5.47	4.98	5.52	5.34	3.58	3.42	9.25	8.05	8.66	5.17	4.52	6.49	3.23	3.58	3.17	3.93
CaO	7.35	7.97	7.66	7.84	8.06	7.65	5.80	5.90	10.04	11.01	11.22	7.20	8.26	8.40	7.93	7.74	7.68	7.57
Na2O	4.17	4.15	4.08	4.01	3.74	4.02	5.17	5.20	2.40	2.68	2.29	4.10	3.57	3.36	4.60	4.62	4.78	4.26
K2O	0.38	0.50	0.37	0.50	0.69	0.76	2.03	2.06	0.38	0.36	0.31	0.83	0.56	0.39	1.25	1.22	1.29	1.07
TiO2	3.19	3.08	3.15	3.27	2.81	2.89	2.14	2.14	1.71	1.89	1.62	3.02	2.68	2.46	2.22	2.22	2.28	2.66
MnO	0.20	0.21	0.19	0.21	0.21	0.22	0.20	0.19	0.18	0.17	0.16	0.23	0.17	0.21	0.16	0.17	0.16	0.18
P2O5	0.42	0.44	0.43	0.49	0.41	0.46	1.13	1.14	0.18	0.23	0.20	0.58	0.37	0.32	0.99	1.01	1.03	0.66
Total	100.54	100.99	100.93	100.95	100.73	101.03	100.42	100.01	100.97	101.06	100.13	100.80	101.04	100.90	101.08	100.46	100.08	100.44
LOI	2.99	1.14	3.39	2.39	1.83	1.22	3.05	2.78	5.07	5.27	4.54	2.20	3.96	1.85	2.36	2.02	1.75	3.72
Ba	184	188	159	231	713	467	1361	1395	273	402	286	656	334	284	930	812	828	695
Cr	0	8	3	2	0	0	0	71	298	211	327	11	39	38	2	0	0	0
Ga	17	15	17	19	14	17	18	19	18	17	14	16	21	16	17	16	19	23
Nb	14.9	13.7	14.6	15.3	12.0	12.8	22.8	22.8	8.4	6.4	5.5	9.9	8.6	7.1	11.4	12.3	12.8	11.7
Ni	56	58	51	45	32	38	8	16	161	107	157	39	61	71	9	19	18	23
Rb	4.5	5.0	4.0	5.0	7.5	8.8	27.0	26.5	5.0	4.5	5.2	8.9	5.0	3.4	16.3	16.8	17.8	12.6
Sc	20	17	17	17	23	21	10	12	24	28	26	17	20	19	15	14	20	21
Sr	673	601	486	618	763	598	888	996	1299	1150	700	665	398	403	924	719	720	605
V	171	198	184	169	246	227	41	50	239	237	218	232	319	301	131	137	146	208
Y	28	33	32	34	31	30	46	47	21	21	18	33	29	25	29	29	30	35
Zr	263	266	247	287	215	241	333	342	106	92	77	282	204	153	185	190	203	201
La	13.9	11.3	10.3	12.8	10.7	13.8	43.5	47.0	10.5	10.3	8.0	18.5	11.8	9.5	24.7	28.4	28.6	28.3
Ce	33.9	39.0	31.0	47.7	31.6	41.4	104.6	101.8	19.8	21.4	19.7	52.2	35.5	30.9	69.1	60.9	63.3	50.7
Nd	32.6	35.6	36.1	38.9	28.2	37.7	75.1	76.9	14.8	17.1	14.8	41.8	29.7	24.3	44.6	41.8	39.7	44.8

Appendix 4a.i MPG lavas

	MR40	MR41	T2	T3	T4	T5	T6	T7	T8	T9	T10	T11	T12	T14	T15	T16
SiO2	45.52	46.19	45.79	45.42	45.73	46.06	45.08	45.39	46.71	46.25	45.49	46.49	46.95	47.10	47.50	48.18
Al2O3	16.30	16.67	14.48	14.39	14.76	14.51	14.05	14.31	15.05	14.01	15.72	18.96	13.67	15.94	16.03	17.25
Fe2O3*	15.82	14.55	13.36	13.56	13.14	12.65	13.18	13.52	13.11	13.32	13.97	13.17	12.68	12.10	12.27	11.57
MgO	6.75	7.00	13.32	11.96	12.58	12.07	12.05	12.54	11.42	15.78	10.04	5.63	13.30	7.88	7.54	8.29
CaO	8.89	9.33	9.18	10.02	9.31	9.25	9.34	9.22	8.87	8.15	9.79	10.13	9.38	11.13	10.23	9.68
Na2O	3.32	3.06	2.22	2.29	2.50	2.59	2.64	2.33	2.30	1.66	2.61	3.30	2.10	2.96	3.04	2.92
K2O	0.37	0.37	0.28	0.28	0.24	0.47	0.33	0.27	0.46	0.37	0.26	0.33	0.35	0.48	0.53	0.70
TiO2	3.02	2.57	1.48	1.71	1.47	1.42	1.46	1.52	1.82	1.28	1.75	2.40	1.31	1.65	1.75	1.37
MnO	0.21	0.19	0.20	0.19	0.18	0.19	0.18	0.18	0.19	0.18	0.17	0.20	0.16	0.18	0.18	0.18
P2O5	0.63	0.34	0.17	0.20	0.17	0.18	0.17	0.16	0.23	0.13	0.20	0.20	0.15	0.17	0.20	0.17
Total	100.83	100.97	100.48	100.02	100.09	99.39	98.49	99.45	100.16	101.14	99.99	100.81	100.04	99.60	99.26	100.33
LOI	2.04	2.80	2.57	0.51	3.58	3.39	2.18	2.97	4.10	5.00	3.96	3.21	3.50	3.32	3.70	3.82
Ba	367	584	101	121	92	223	134	129	201	110	129	125	121	171	213	1278
Cr	20	42	843	729	774	762	698	614	670	1136	423	114	437	204	190	102
Ga	19	15	16	17	19	18	20	19	21	17	22	22	19	24	21	18
Nb	8.1	6.4	6.2	7.4	6.6	7.0	6.1	5.8	7.1	4.7	7.6	6.1	4.5	5.1	5.8	5.6
Ni	64	76	405	329	383	309	299	327	321	605	218	83	412	94	109	140
Rb	3.7	4.0	7.0	5.9	5.4	10.0	7.1	4.5	7.1	6.5	3.2	3.9	6.1	9.0	9.1	10.2
Sc	24	25	30	31	29	30	30	32	25	24	32	27	23	27	26	26
Sr	490	1369	292	279	215	310	291	274	302	505	293	626	224	456	318	684
V	304	308	235	275	248	238	259	274	234	236	208	310	250	321	312	265
Y	23	19	27	32	28	26	26	26	26	22	30	34	19	22	25	19
Zr	117	117	100	111	101	104	106	108	132	99	112	120	95	117	123	92
La	9.5	5.1	6.6	7.0	6.7	7.4	8.8	9.8	11.7	6.8	7.3	12.0	8.9	9.6	9.6	7.5
Ce	28.4	15.9	20.3	18.8	20.0	24.9	25.8	22.8	28.2	20.6	20.8	26.3	20.0	31.3	27.0	27.6
Nd	23.2	12.1	11.8	12.9	12.1	12.7	11.6	11.1	16.6	10.3	11.6	21.7	12.1	17.6	15.7	19.3

Appendix 4a.i MPG lavas

	UV2ave	UV3	UV4	UV5	UV6	UV7	UV9	UV10	UV11	W6	W7	EX1	EX2	EX2A	EX2B	EX3
SiO2	49.62	49.39	45.63	48.16	47.12	46.22	46.10	44.88	45.39	46.65	44.54	46.74	46.90	46.96	46.59	46.10
Al2O3	17.28	17.27	14.54	17.09	17.90	15.00	16.96	15.34	16.39	14.58	15.12	15.73	15.78	15.66	15.81	15.19
Fe2O3*	14.06	14.45	12.63	14.49	14.83	12.68	16.00	13.98	15.97	12.92	14.93	13.44	13.47	13.45	13.47	13.73
MgO	3.14	3.83	11.82	4.11	6.01	11.21	6.80	10.84	6.93	12.09	11.13	9.61	9.50	9.52	9.47	9.54
CaO	5.36	6.05	10.12	5.93	8.57	10.04	8.73	10.14	8.84	9.06	9.45	9.70	10.03	9.87	9.92	10.43
Na2O	6.65	5.92	2.52	5.22	3.16	2.35	2.99	2.33	3.27	2.64	2.19	2.18	2.18	2.05	2.27	2.50
K2O	0.77	0.62	0.25	0.67	0.29	0.44	0.25	0.33	0.29	0.38	0.33	0.20	0.20	0.19	0.21	0.19
TiO2	2.31	2.41	1.66	2.45	2.07	1.68	1.99	1.72	2.03	1.44	2.18	1.59	1.66	1.62	1.62	1.63
MnO	0.13	0.13	0.19	0.15	0.17	0.17	0.21	0.19	0.21	0.18	0.18	0.19	0.18	0.18	0.18	0.19
P2O5	0.67	0.62	0.15	0.61	0.17	0.21	0.17	0.17	0.19	0.17	0.23	0.18	0.17	0.19	0.19	0.18
Total	99.98	100.69	99.51	98.88	100.29	100.00	100.20	99.92	99.51	100.24	100.37	99.56	100.08	99.69	99.72	99.67
LOI	2.26	2.58	1.70	3.24	4.19	2.52	2.46	2.66	1.94	5.31	3.49	4.52	4.12	4.14	3.95	4.02
Ba	168	160	**216**	365	80	259	91	101	317	194	132	69	61	56	65	67
Cr	3	2	**751**	67	7	575	5	13	169	858	320	488	433	457	433	479
Ga	26	27	**17**	27	20	21	22	21	21	16	20	17	16	16	17	15
Nb	17.4	17.0	**2.7**	15.0	3.3	5.1	3.1	2.9	4.8	6.0	6.0	5.4	4.8	4.0	4.1	4.1
Ni	11	38	**291**	30	43	247	42	51	236	333	288	248	233	247	226	258
Rb	9.5	8.0	**4.0**	5.8	3.4	5.2	3.3	2.4	3.0	11.0	5.9	3.3	4.0	3.3	4.7	3.6
Sc	8		**31**	13	27	28	31	33	35	29	29					
Sr	1177	1056	**659**	1185	402	382	559	415	376	307	333	259	247	248	250	254
V	52	96	**310**	96	287	283	317	315	294	219	292	251	254	250	269	252
Y	14	13	**20**	16	25	21	26	27	24	24	32	15	15	18	16	18
Zr	389	355	**101**	344	118	122	113	119	110	109	132	101	102	103	101	104
La	24.0	25.0	**5.0**	37.8	7.3	11.7	6.4	7.6	7.5	8.8	9.5	4.4	4.6	6.3	4.0	4.9
Ce	73.0	63.0	**15.0**	73.9	20.6	31.7	22.1	19.6	24.3	17.7	18.4	12.8	18.0	23.2	16.4	21.7
Nd	48.7	40.0	**14.0**	55.4	14.0	19.9	15.8	16.8	15.4	13.8	15.1	10.2	11.7	11.2	11.3	12.0

	EX9	EX10	EX14	EX19	EX20	BM11A	BM11B	BM11C	EBM13A	EBM13B	EBM13C	EBM13D	EBM13E	EBM13F	EBM13G
SiO2	45.56	47.02	46.58	47.62	48.63	47.10	47.28	48.63	46.73	46.43	46.61	45.94	45.80	45.85	45.88
Al2O3	17.27	15.46	14.79	15.36	15.96	16.32	16.62	14.23	13.79	13.76	13.82	13.75	13.63	13.62	13.61
Fe2O3*	14.42	13.76	12.30	12.28	11.13	13.51	13.20	13.81	12.30	12.33	12.16	12.25	12.13	12.08	12.16
MgO	7.67	8.05	11.95	9.41	8.91	8.49	8.48	7.90	12.71	12.90	12.78	12.58	12.91	12.87	12.63
CaO	9.20	8.25	9.99	8.86	9.19	10.92	10.05	8.97	9.94	9.95	9.96	9.89	9.73	9.89	9.93
Na2O	2.68	3.59	2.74	3.10	3.37	2.77	3.31	5.24	2.37	2.49	2.54	2.62	2.56	2.48	2.41
K2O	0.10	0.51	0.35	0.54	0.59	0.23	0.29	0.58	0.34	0.31	0.34	0.31	0.26	0.29	0.30
TiO2	1.76	1.98	1.31	1.42	1.34	1.69	1.69	2.01	1.39	1.37	1.38	1.36	1.35	1.32	1.36
MnO	0.18	0.19	0.18	0.18	0.16	0.19	0.21	0.21	0.17	0.17	0.16	0.17	0.17	0.17	0.16
P2O5	0.14	0.25	0.16	0.17	0.21	0.14	0.14	0.16	0.14	0.13	0.12	0.13	0.12	0.13	0.16
Total	97.83	97.89	100.47	98.94	99.50	101.36	101.27	101.74	99.89	99.84	99.86	99.01	98.66	98.70	98.60
LOI	2.68	3.67	1.88	3.41	2.07	5.36	4.67	5.20	1.78	1.82	1.89	2.21	2.08	2.16	2.38
Ba	52	139	180	185	314	107	127	157	134	138	133	130	126	129	137
Cr	68	351	693	329	339	164	204	294	1204	1223	1178	1055	1029	1005	1022
Ga	18	21	19	22	20	18	16	16	17	15	17	15	15	18	18
Nb	6.6	11.3	5.0	4.1	4.4	6.2	6.8	6.6	3.5	3.1	3.0	5.0	5.0	5.0	6.0
Ni	151	202	318	185	199	138	141	71	395	381	379	378	376	357	357
Rb	3.6	10.6	6.2	5.7	6.2	4.1	5.0	8.3	6.0	7.0	7.0	5.0	4.0	6.0	5.0
Sc	27	25	30	23	27	28	29	34				14	27	26	27
Sr	245	256	300	355	474	289	256	191	248	250	251	223	224	229	225
V	199	292	251	245	268	271	308	404	296	281	282	262	253	257	270
Y	31	29	23	21	21	21	22	27	15	17	15	18	18	18	17
Zr	90	136	88	100	95	87	92	111	89	89	89	81	80	78	80
La	4.6	11.6	8.3	9.1	9.4	8.0	7.0	8.0	5.0	4.0	5.0	6.0	6.0	5.0	8.0
Ce	15.9	23.5	18.0	21.8	30.0	20.0	16.0	22.0	10.0	17.0	13.0	16.0	11.0	8.0	17.0
Nd	6.5	15.3	11.4	12.5	18.0	12.0	11.0	18.0	9.0	12.0	9.0	12.0	11.0	7.0	12.0

Appendix 4a.i MPG lavas

	UV2A	UV2B	UV2C	UV2D	UV2E	UV2F	P12	P35	STA3
SiO2	50.23	48.76	49.73	48.99	49.90	50.09	46.67	47.31	43.32
Al2O3	17.45	17.08	17.16	17.06	17.49	17.45	14.63	14.35	10.74
Fe2O3*	14.19	14.04	14.03	13.96	14.06	14.09	12.03	12.46	14.35
MgO	3.08	3.12	3.02	3.03	3.27	3.30	11.92	13.00	20.72
CaO	5.44	5.42	5.29	5.15	5.35	5.53	9.80	9.38	5.90
Na2O	7.11	6.19	7.14	7.31	6.00	6.14	2.10	2.23	2.34
K2O	0.78	0.75	0.82	0.78	0.75	0.73	0.33	0.40	0.26
TiO2	2.33	2.31	2.30	2.29	2.31	2.31	1.23	1.33	1.08
MnO	0.13	0.13	0.13	0.13	0.13	0.14	0.17	0.18	0.18
P2O5	0.67	0.67	0.68	0.66	0.66	0.66	0.13	0.16	0.12
Total	101.41	98.47	100.30	99.36	99.92	100.44	99.00	100.80	99.31
LOI	2.12	2.51	1.61	2.19	2.64	2.47	2.98	2.12	
Ba	164	173	162	161	167	178	145	216	78
Cr	25	21	20	24	10	0	828	968	1591
Ga	22	22	23	19	24	27	16	15	19
Nb	14.9	16.2	15.1	15.3	18.0	18.0	6.6	7.0	1.9
Ni	9	5	3	6	26	15	324	359	842
Rb	9.9	7.2	10.3	11.4	14.0	8.0	7.0	17.0	6.1
Sc							27	29	28
Sr	1200	1235	1176	1146	1160	1146	252	295	400
V	108	100	102	102	63	57	245	256	198
Y	12	12	13	13	14	14	18	19	18
Zr	377	379	382	376	384	370	77	94	61
La	21.5	22.1	22.7	21.5	29.0	27.0	5.2	8.0	6.0
Ce	73.1	73.3	72.9	71.7	74.0	73.0	14.2	17.0	16.0
Nd	51.0	50.5	54.7	48.7	44.0	43.0	9.9	12.0	8.9

	BCH1	BCH7	BCH7A	BCH7B	B1	B2	W1	W2	W3	W4	W5	C6	C7	C8	T1	A1	A2	STA2	UV1
SiO2	46.52	48.16	48.23	48.16	50.25	49.86	48.41	49.56	47.56	48.53	51.55	53.37	49.49	47.44	48.84	50.01	48.44	49.26	49.05
Al2O3	14.84	16.14	16.00	16.13	15.30	14.78	15.38	15.16	15.10	14.39	14.83	14.76	14.51	14.60	14.34	14.66	15.32	14.66	16.14
Fe2O3*	12.98	12.89	12.85	12.85	12.26	12.61	11.17	12.34	12.28	12.00	12.03	11.67	12.58	12.00	14.58	12.49	12.40	11.61	11.66
MgO	10.78	8.31	8.09	8.12	5.51	5.92	6.63	5.81	6.61	6.60	5.80	6.40	6.81	7.40	5.79	5.62	7.74	5.35	8.81
CaO	10.11	9.49	9.28	9.07	10.24	10.73	12.64	10.57	12.29	11.65	10.42	9.77	11.63	11.90	10.06	10.29	11.58	10.17	9.75
Na2O	2.62	3.21	3.24	3.62	3.27	2.78	2.77	2.99	2.38	2.33	2.73	2.56	2.49	2.51	3.21	3.34	2.53	2.89	3.12
K2O	0.48	0.56	0.60	0.65	0.92	0.80	0.52	0.78	0.33	0.39	0.61	1.04	0.36	0.51	0.76	0.97	0.48	0.94	0.53
TiO2	1.54	1.67	1.67	1.66	1.75	2.16	1.63	1.78	1.77	1.85	2.07	1.02	1.61	1.60	2.35	1.76	1.69	1.54	1.36
MnO	0.18	0.18	0.18	0.18	0.21	0.23	0.58	0.21	0.18	0.20	0.22	0.19	0.20	0.19	0.22	0.20	0.20	0.19	0.16
P2O5	0.17	0.18	0.15	0.24	0.25	0.26	0.19	0.29	0.17	0.20	0.26	0.13	0.15	0.16	0.28	0.28	0.16	0.19	0.22
Total	100.33	100.95	100.47	100.69	99.63	100.18	99.98	99.51	98.73	98.20	100.55	100.91	99.84	98.33	98.43	99.86	100.33	97.02	100.51
LOI	0.79	2.11	2.34	3.49	4.14	3.31	3.02	3.87	3.35	2.60	3.22	3.18	2.37	1.30	1.48	1.61	1.31	3.06	1.88
Ba	188	353	357	397	539	187	191	476	80	119	197	323	165	184	266	591	134	389	354
Cr	539	225	244	225	47	88	201	40	216	213	84	40	48	188	88	36	211	54	339
Ga	19	22	21	22	22	21	20	24	20	31	23	19	22	20	22	22	21	21	19
Nb	5.0	4.0	5.0	5.9	7.0	9.0	5.0	7.0	6.0	8.0	9.0	6.3	5.9	5.8	10.6	6.8	6.0	5.7	4.0
Ni	197	135	164	167	35	20	36	35	78	40	21	26	29	53	39	30	58	27	188
Rb	6.0	5.0	4.0	5.2	11.0	12.0	12.0	6.3	4.0	7.0	26.4	17.9	4.0	10.4	14.0	11.0	11.0	7.9	3.0
Sc	33	24	31	25	35	35	38	37	42	39	38	36	37	35	40	38	39	33	26
Sr	431	479	511	672	475	312	323	496	255	283	345	322	293	319	259	455	243	334	472
V	273	295	310	312	358	394	353	366	366	354	362	302	327	323	400	357	344	305	264
Y	26	23	24	25	37	43	32	35	32	35	41	28	32	31	49	35	31	34	20
Zr	111	108	111	113	141	190	114	150	140	150	190	110	120	107	177	140	123	135	90
La	9.5	12.9	11.4	12.6	19.9	21.9	12.8	20.3	8.7	13.4	28.4	11.7	10.7	8.6	15.8	16.4	11.3	18.8	9.7
Ce	21.8	30.2	28.4	30.7	48.2	54.2	27.2	40.8	21.8	31.2	59.2	25.6	31.7	23.2	45.8	39.8	25.1	41.6	22.2
Nd	13.6	19.0	19.5	20.6	28.6	29.2	20.6	26.4	15.5	19.2	34.0	14.4	17.3	15.8	25.6	25.1	14.2	25.4	17.2

Appendix 4a.ii SMT lavas

	BM73	BM74	BM75	BM76	BM77	BM78	BM79	BM80	BM81	BM82	BM83	BM84	BM85	BM86	BM87	BM88	BM89	BM90	BM91
SiO2	47.03	46.04	46.67	47.10	46.94	46.44	44.24	47.53	45.55	46.80	46.30	46.49	45.90	46.46	44.96	46.58	47.42	45.34	44.84
Al2O3	16.29	16.52	16.29	14.74	15.47	15.91	16.93	15.29	16.82	17.10	16.16	15.80	16.59	15.93	16.73	16.29	15.08	16.70	17.12
Fe2O3*	13.12	13.20	12.60	12.28	12.31	13.96	14.16	12.46	15.01	12.99	13.99	13.13	12.78	13.47	14.58	12.19	12.22	13.58	12.71
MgO	8.75	8.86	10.20	11.78	11.27	9.72	8.98	11.53	7.21	7.58	8.99	10.99	10.88	10.63	10.64	12.47	11.54	8.49	9.39
CaO	11.82	11.61	10.81	11.03	10.67	10.01	10.74	10.88	10.22	11.54	10.69	10.55	10.51	10.30	9.35	9.99	9.33	10.17	10.38
Na2O	2.19	2.23	2.30	1.71	1.73	2.28	2.25	1.87	2.89	2.39	2.29	1.95	2.08	1.89	2.19	1.55	2.84	2.49	2.42
K2O	0.26	0.24	0.21	0.33	0.61	0.16	0.16	0.12	0.56	0.22	0.13	0.11	0.23	0.31	0.42	0.28	0.17	0.27	0.18
TiO2	1.67	1.64	1.70	1.22	1.35	1.85	1.89	1.22	2.19	1.88	1.74	1.35	1.38	1.49	1.57	1.22	1.15	1.49	1.42
MnO	0.18	0.18	0.17	0.18	0.17	0.18	0.18	0.16	0.21	0.20	0.20	0.18	0.17	0.19	0.19	0.18	0.18	0.17	0.18
P2O5	0.15	0.13	0.13	0.13	0.13	0.16	0.18	0.13	0.22	0.20	0.19	0.13	0.12	0.16	0.16	0.12	0.11	0.14	0.14
Total	101.46	100.65	101.08	100.50	100.65	100.67	99.71	101.19	100.88	100.90	100.68	100.68	100.64	100.83	100.79	100.87	100.02	98.84	98.79
LOI	2.56	3.62	3.73	2.88	4.28	3.36	4.45	3.42	4.53	5.52	3.17	2.93	4.60	6.83	6.08	6.65	6.11	5.96	3.94
Ba	77	51	77	77	210	109	129	116	345	114	113	71	107	159	92	111	44	75	60
Cr	557	450	439	842	738	392	356	730	149	117	207	386	433	397	564	722	864	347	301
Ga	19	20	19	17	17	19	21	14	18	21	15	13	16	17	17	14	17	14	19
Nb	7.4	7.2	6.4	6.7	7.3	8.8	7.6	6.5	8.1	8.6	7.6	5.8	6.5	7.2	7.5	6.0	5.1	6.1	5.9
Ni	197	206	236	337	324	215	216	349	95	98	202	298	312	224	353	375	406	273	255
Rb	7.0	5.0	3.5	13.3	11.0	3.7	3.7	2.7	9.0	3.6	2.9	3.1	4.9	6.2	9.0	6.0	4.1	4.7	4.2
Sc	32	32	32	29	27	24	25	31	38	28	23	29	29	30	29	25	31	36	28
Sr	194	236	222	166	179	229	279	207	404	337	185	160	167	168	158	126	189	182	170
V	275	264	264	240	245	278	262	225	324	314	253	254	244	253	272	247	231	239	227
Y	26	23	22	21	21	22	22	23	28	21	27	23	25	25	25	22	23	31	28
Zr	85	79	81	69	71	93	92	69	119	91	85	68	73	76	71	67	67	78	76
La	7.4	7.0	3.9	5.5	10.5	8.0	5.4	8.1	5.2	7.4	6.7	7.3	6.6	6.4	8.3	5.7	3.0	7.2	6.0
Ce	13.6	10.7	10.5	14.1	14.4	12.0	14.1	12.8	26.1	21.1	18.6	12.6	16.0	12.9	9.0	10.0	9.7	15.5	12.2
Nd	15.1	10.9	8.6	13.6	10.6	13.6	13.9	7.6	19.6	14.5	14.4	6.8	11.5	7.2	8.0	8.2	6.8	11.9	8.5

	BM92	BM93	BM94	BM95	BM96	BM97	BM98	BM99	CA2
SiO2	45.90	46.13	46.48	46.04	45.86	45.91	45.92	46.61	47.19
Al2O3	16.68	16.26	16.47	16.08	16.63	17.09	18.10	17.66	17.45
Fe2O3*	12.72	12.45	11.84	12.03	12.02	12.37	14.05	13.20	12.42
MgO	7.94	10.10	9.30	9.45	9.23	8.98	7.62	8.08	6.24
CaO	10.91	10.24	10.63	11.02	10.71	10.33	9.44	9.64	10.67
Na2O	2.12	2.10	2.16	1.91	2.26	2.48	2.44	2.61	2.90
K2O	0.34	0.18	0.40	0.68	0.10	0.24	0.29	0.17	0.31
TiO2	1.80	1.39	1.47	1.34	1.27	1.34	1.74	1.52	1.16
MnO	0.20	0.19	0.21	0.18	0.16	0.18	0.23	0.19	0.19
P2O5	0.18	0.14	0.15	0.13	0.10	0.10	0.13	0.18	0.12
Total	98.79	99.17	99.10	98.85	98.35	99.02	99.96	99.85	98.55
LOI	5.39	3.22	3.12	3.88	3.22	4.02	3.81	3.30	4.23
Ba	60	110	121	103	36	53	30	114	96
Cr	278	157	266	233	243	272	52	21	138
Ga	18	22	18	17	21	17	22	20	18
Nb	6.6	7.9	6.3	6.0	5.3	6.0	6.5	5.6	4.5
Nl	243	114	235	236	222	223	126	107	116
Rb	3.3	6.2	10.0	15.7	3.3	5.2	4.5	3.0	6.0
Sc	31	31	34	28	28	32	31	28	35
Sr	169	181	172	155	185	184	212	279	310
V	257	278	243	215	209	230	257	198	264
Y	28	33	29	26	27	27	33	27	25
Zr	76	89	81	73	70	73	89	75	66
La	5.0	4.8	4.2	4.6	4.6	5.9	6.2	7.2	4.3
Ce	14.7	16.7	16.1	17.8	14.9	16.2	16.9	18.8	12.0
Nd	7.8	9.7	7.7	6.8	7.2	10.5	8.7	7.6	8.3

	CA3B	CA12	CA13	CA14	CA15	CA16	CA17	CA19	CA20	EX7	EX8	EX17
SiO2	47.62	50.77	51.29	52.05	46.94	47.94	47.74	49.18	51.32	47.10	46.17	50.35
Al2O3	21.14	13.16	13.63	13.85	15.29	23.79	14.49	22.26	21.48	13.78	16.84	20.88
Fe2O3*	8.19	16.08	13.51	13.55	12.49	8.21	14.14	9.16	8.62	15.14	13.00	7.44
MgO	5.48	4.43	5.18	5.47	8.09	4.16	5.89	3.65	2.93	6.51	7.58	4.15
CaO	13.21	8.83	9.69	9.32	12.17	11.79	10.44	10.06	10.31	12.06	10.37	10.85
Na2O	2.06	2.80	2.71	2.91	2.22	2.36	2.97	4.17	3.22	2.39	2.46	3.10
K2O	0.07	1.14	0.77	0.24	0.05	0.11	0.41	0.49	0.56	0.12	0.25	0.71
TiO2	0.72	2.32	1.58	1.59	1.07	0.63	1.61	0.80	0.76	1.38	1.13	0.66
MnO	0.13	0.23	0.21	0.22	0.20	0.12	0.22	0.08	0.11	0.24	0.18	0.11
P2O5	0.07	0.22	0.19	0.19	0.09	0.06	0.28	0.07	0.03	0.12	0.12	0.05
Total	98.70	99.97	98.75	99.38	98.61	99.16	98.19	99.91	99.34	100.19	99.72	98.31
LOI	1.88	1.66	1.10	2.59	2.67	5.73	2.18	5.32	4.95	2.04	4.67	3.25
Ba	51	297	287	144	47	101	269	149	170	73	61	331
Cr	229	123	149	132	283	98	200	102	87	126	134	208
Ga	18	22	20	20	17	17	24	14	16	19	19	17
Nb	3.4	10.0	9.9	10.0	5.6	2.5	8.3	2.9	2.9	5.0	4.0	3.6
Ni	77	25	43	40	106	97	54	49	48	97	91	49
Rb	2.2	24.6	9.3	3.7	3.0	3.2	6.9	8.7	12.9	8.8	2.9	18.2
Sc	29	37	43	41	41	23	37	29	29	35	35	25
Sr	219	194	215	218	123	353	348	375	361	203	206	268
V	215	436	345	359	303	177	316	254	132	233	234	163
Y	17	46	41	39	31	13	41	18	16	26	26	15
Zr	41	166	158	156	63	36	109	41	41	61	64	43
La	3.2	16.8	13.8	12.8	4.0	2.1	15.6	2.0	3.0	3.3	4.5	3.0
Ce	7.4	29.5	28.1	24.3	12.2	5.1	33.7	6.9	11.5	12.3	10.3	8.7
Nd	5.5	17.9	15.8	12.1	6.1	4.7	20.8	4.0	5.2	8.2	5.9	6.8

Appendix 4a.iv CMT lavas

	EX16	EX15	EX13	P3	P10	P11	P18	P19	P20
SiO2	48.24	47.47	47.80	61.22	48.08	49.18	60.62	60.37	61.38
Al2O3	14.77	13.59	14.05	17.82	15.75	17.28	17.95	17.97	18.68
Fe2O3*	12.60	15.11	15.55	4.85	15.09	14.62	4.73	4.63	4.74
MgO	7.33	6.70	6.73	0.91	5.36	3.80	1.10	1.01	0.91
CaO	11.89	12.04	11.85	2.35	8.54	5.78	1.51	1.84	1.42
Na2O	2.31	2.57	2.84	7.66	4.39	5.66	6.03	6.88	5.79
K2O	0.12	0.12	0.13	3.99	0.97	0.71	5.33	5.25	5.69
TiO2	1.18	1.37	1.41	0.49	2.26	2.42	0.66	0.65	0.65
MnO	0.20	0.24	0.25	0.19	0.19	0.14	0.21	0.21	0.19
P2O5	0.08	0.12	0.12	0.37	0.34	0.64	0.45	0.45	0.43
Total	98.72	99.33	100.78	99.85	100.99	100.23	98.58	99.25	99.90
LOI	1.52	1.04	2.90	4.42	0.88	2.95	2.08	0.74	2.40
Ba	85	42	33	954	613	179	963	951	861
Cr	310	56	43	4	20	2	2	0	2
Ga	19	20	24	22	20	23	26	24	22
Nb	4.5	3.0	4.0	42.4	6.6	16.6	43.5	45.3	46.6
Ni	88	60	58	7	58	35	10	16	7
Rb	3.6	4.0	3.5	67.9	11.8	10.0	108.4	101.0	116.0
Sc	42	46	43	1	19	5	3	5	3
Sr	180	119	111	106	538	1095	149	145	120
V	290	384	396	1	359	87	10	12	8
Y	29	39	39	40	26	13	47	44	45
Zr	64	75	75	905	182	335	822	793	846
La	2.3	3.1	11.6	42.7	22.1	19.8	90.8	72.3	94.0
Ce	12.6	7.5	1.8	89.4	41.6	61.8	175.6	166.1	176.0
Nd	5.1	6.9	5.7	49.3	29.7	57.4	96.2	85.9	81.0

Appendix 4a.v plugs intrusions

	SK974	JE208	SK906	SK971	SK940	(CD)124	(CD)123	(CD)44	(CD)17a	MS184#
SiO2	48.14	60.91	45.20	46.86	44.35	45.65	46.38	45.02	44.88	51.06
Al2O3	14.53	17.91	16.44	16.66	15.57	24.41	17.84	17.47	17.00	14.03
Fe2O3*	11.26	4.25	15.92	13.03	15.40	6.33	11.47	10.10	11.20	14.40
MgO	10.96	0.89	7.44	7.91	8.28	6.97	7.23	10.54	10.61	4.57
CaO	10.27	1.59	8.42	9.71	9.05	14.21	13.01	11.85	11.32	9.82
Na2O	2.16	6.42	3.12	3.19	2.98	1.62	1.60	1.29	1.38	3.21
K2O	0.58	5.18	0.21	0.40	0.30	0.06	0.28	0.11	0.11	0.40
TiO2	1.14	0.83	2.60	1.40	2.63	0.41	0.96	0.66	0.80	1.96
MnO	0.17	0.14	0.19	0.18	0.20	0.09	0.18	0.16	0.18	0.26
P2O5	0.15	0.29	0.26	0.17	0.28	0.06	0.06	0.06	0.07	0.36
Total	99.36	98.41	99.80	99.51	99.04	99.86	99.10	97.35	97.64	100.15
LOI	2.99	1.40	2.06	1.11	1.45	2.95	3.77	4.01	5.50	1.35
Ba	293	3298	50	265	65	16	776	61	60	345
Cr	825	35	51	105	403	164	236	227	245	43
Ga	16	22	20	20	20	17	17	17	17	20
Nb	2.8	24.1	6.7	2.7	6.5	1.9	1.4	1.5	1.5	7.8
Ni	298	0	76	118	135	125	97	164	266	33
Rb	8.0	77.4	3.1	2.8	3.2	3.1	8.3	3.9	2.6	5.8
Sc	28	3	25	32	27	22	35	30	29	43
Sr	348	277	452	422	600	239	281	132	135	250
V	268	18	292	259	317	119	273	192	189	309
Y	17	33	29	25	25	9	19	15	15	50
Zr	87	488	180	87	200	30	47	37	42	195
La	9.0	117.7	10.5	6.5	13.7	1.0	1.0	1.0	2.0	22.9
Ce	15.7	224.2	29.7	23.5	36.0	5.0	2.0	5.0	8.0	47.0
Nd	13.6	112.2	21.6	14.2	27.3	4.5	5.0	5.0	6.0	28.7

MS184 - Mull lava (originally analysed by Morrison 1980)

	Tiree Lewisian															
	P36	P37	P38	P39	P39A	P40	P41	P42	P43	P44	P45	P47	P48	P49	P50	P51
SiO2	55.85	62.39	69.47	46.70	49.73	77.20	50.00	69.41	72.07	54.41	89.85	73.25	48.42	71.84	72.89	65.30
Al2O3	16.54	19.13	15.36	13.77	14.53	12.35	15.70	14.39	14.25	19.29	5.99	14.80	13.19	14.21	14.15	16.53
Fe2O3*	10.96	2.50	1.80	16.55	16.56	0.98	10.42	2.33	1.70	8.20	0.32	0.83	17.47	0.75	0.65	2.53
MgO	4.38	0.99	0.66	6.95	6.83	0.65	8.37	1.10	0.59	3.66	0.42	0.47	4.99	0.50	0.50	0.54
CaO	3.33	1.89	1.58	10.41	9.09	2.57	9.01	2.09	0.86	6.70	0.57	0.81	8.56	0.63	0.75	0.88
Na2O	3.29	3.22	1.12	2.56	1.74	3.87	3.82	4.98	3.21	5.51	1.58	4.20	2.70	2.51	2.84	5.21
K2O	2.21	7.70	8.82	1.19	0.67	1.02	1.21	4.20	5.40	1.35	1.85	5.24	1.11	8.25	6.81	5.89
TiO2	0.74	0.44	0.19	1.19	1.31	0.18	0.75	0.29	0.18	0.67	0.03	0.07	1.78	0.08	0.09	0.40
MnO	0.14	0.01	0.04	0.19	0.26	0.00	0.15	0.02	0.00	0.11	0.00	0.00	0.26	0.01	0.00	0.13
P2O5	0.08	0.16	0.07	0.09	0.13	0.03	0.30	0.13	0.09	0.46	0.02	0.04	0.27	0.03	0.03	0.17
Total	98.70	98.42	99.10	99.67	100.92	98.85	99.79	98.95	98.36	100.40	100.65	99.72	98.81	98.80	98.72	97.57
LOI	1.06	0.84	2.96	2.52	2.02	0.57	0.81	0.50	0.43	0.59	0.37	0.47	0.67	0.26	0.43	2.04
Ba	683	2994	2160	323	56	335	487	1388	6881	928	1024	587	212	3467	3825	262
Cr	371	89	32	220	150	0	460	22	18	24	0	18	85	27	17	18
Ga	21	19	14	20	19	18	19	17	14	23	9	16	23	14	14	22
Nb	6.0	7.0	5.0	6.0	6.0	5.0	6.0	4.0	2.0	3.0	3.0	4.0	10.0	3.0	2.0	53.0
Ni	111	26	13	115	105	13	73	19	5	22	16	11	64	12	8	5
Rb	84.0	189.0	182.0	26.0	25.0	21.0	10.0	101.0	72.0	16.0	21.0	132.0	48.0	90.0	125.0	115.0
Sc	27	6	2	59	49	3	32	5	3	14	1	1	45	1	2	5
Sr	414	758	246	227	121	632	561	541	822	1315	381	285	307	504	565	112
V	219	76	41	334	337	12	222	35	28	130	2	5	355	9	13	5
Y	35	10	2	26	27	0	21	5	1	11	1	1	33	1	1	28
Zr	97	11	45	66	77	181	75	98	63	54	36	37	125	50	14	895
La	28.0	24.0	7.0	5.0	5.0	8.0	21.0	31.0	1.0	36.0	2.0	9.0	19.0	3.0	2.0	105.0
Ce	43.0	50.0	2.0	7.0	10.0	2.0	42.0	55.0	1.0	78.0	1.0	10.0	22.0	1.0	1.0	206.0
Nd	18.0	22.0	1.0	6.0	5.0	1.0	24.0	22.0	2.0	37.0	2.0	6.0	14.0	2.0	3.0	72.0

	Permo-Carb lamprophyres		Moine			Iona Lewisian		
	L1	L2	P32	P58A	P58B	P60	P61	P62
SiO2	43.57	44.21	91.11	65.04	62.52	78.70	62.44	51.18
Al2O3	15.96	13.28	4.66	15.38	16.83	10.96	19.98	14.87
Fe2O3*	12.97	13.01	0.26	7.21	8.32	1.01	2.10	10.86
MgO	6.90	11.72	0.01	2.52	2.26	0.17	0.43	9.62
CaO	11.42	9.09	0.39	1.55	2.33	0.86	1.73	4.39
Na2O	3.40	2.55	0.80	4.19	3.11	2.22	7.17	2.65
K2O	1.88	1.38	2.26	2.42	3.19	4.82	4.35	2.98
TiO2	2.50	2.23	0.04	0.62	0.97	0.04	0.22	1.48
MnO	0.20	0.24	0.00	0.10	0.12	0.00	0.02	0.10
P2O5	0.76	0.52	0.18	0.20	0.19	0.02	0.08	1.50
Total	99.56	98.23	99.72	99.22	99.84	98.80	98.52	99.63
LOI	4.31	7.14	0.19	1.19	1.08	0.43	0.82	2.30
Ba	817	548	1260	406	888	1229	2955	2696
Cr	48	459	18	54	82	28	25	65
Ga	19	16	4	19	21	13	18	25
Nb	62.0	30.7	3.1	13.5	18.9	2.1	2.6	16.7
Ni	86	314	15	41	35	0	1	14
Rb	48.0	28.0	27.0	128.2	132.8	34.3	61.1	57.4
Sc	22	24	0	7	13	0	0	13
Sr	1042	702	157	266	288	265	827	890
V	287	239	3	102	135	7	37	155
Y	28	23	0	29	39	3	4	22
Zr	204	124	4	244	276	76	105	360
La	44.0	34.1	0.0	87.0	59.9	9.0	24.9	206.6
Ce	85.0	53.1	4.0	120.0	103.0	19.9	42.9	295.3
Nd	40.0	33.6	4.0	49.0	51.5	10.4	18.8	150.1

Appendix 4b

ICP-MS data

Sample localities are given in Appendix 1 and XRF analyses in Appendix 4a. Rock/magma type is given below each sample name;

Abbreviations

MPG - Mull Plateau Group

SMT - Staffa Magma sub-Type

CGMT - Coire Gorm Magma Type

CMT - Central Mull Tholeiites

PM - Preshal More type (Skye)

Lew - Lewisian crust

P-C - Permo-Carboniferous lamprophyre

	BR1	BR2	BR3	BR4	BR5	BR6	BR8	BR9	BR10	BR11
Type	MPG	MPG	MPG	MPG	MPG	MPG	MPG	MPG	MPG	MPG
Pb	1.11	1.37	1.31	1.05	1.40	1.58	1.61	1.72	2.03	1.53
Th	0.55	0.65	0.73	0.25	0.34	0.20	0.22	0.27	0.25	0.20
U	0.16	0.18	0.18	0.07	0.11	0.06	0.07	0.12	0.13	0.06
La	6.58	7.23	7.20	4.55	5.50	6.03	6.83	8.71	8.34	6.86
Ce	18.68	19.86	20.60	11.78	14.10	14.81	16.87	20.32	20.09	16.71
Pr	3.14	3.39	3.41	1.92	2.31	2.22	2.56	3.02	3.05	2.52
Nd	16.84	17.40	18.02	9.71	11.32	11.15	12.01	14.45	13.89	11.76
Sm	5.17	5.25	5.27	3.00	3.26	3.00	3.27	3.71	3.56	3.17
Eu	1.88	1.98	1.91	1.07	1.18	1.05	1.13	1.27	1.31	1.14
Gd	5.57	5.55	5.62	3.39	3.64	3.35	3.61	4.09	4.07	3.40
Tb	0.87	0.86	0.83	0.53	0.60	0.53	0.59	0.65	0.63	0.51
Dy	4.77	4.84	4.70	3.30	3.58	3.11	3.36	3.67	3.71	2.97
Ho	0.90	0.91	0.90	0.69	0.69	0.60	0.66	0.80	0.75	0.66
Er	2.41	2.47	2.32	1.88	1.89	1.74	1.77	1.98	2.07	1.81
Tm	0.32	0.34	0.33	0.29	0.29	0.25	0.28	0.27	0.34	0.25
Yb	2.05	2.07	2.02	1.70	1.66	1.59	1.65	1.75	1.81	1.55
Lu	0.30	0.30	0.28	0.25	0.26	0.23	0.23	0.28	0.30	0.23

	BR12	BR13	BR14	BR16	BR17	BR18	BR19	BR21	BR22	BR23
Type	MPG	MPG	MPG	MPG	MPG	MPG	MPG	MPG	MPG	MPG
Pb	1.02	1.21	1.33	1.21	1.24	2.09	2.06	1.05	1.06	1.47
Th	0.20	0.24	0.29	0.34	0.39	0.88	0.82	0.30	0.26	0.64
U	0.07	0.09	0.10	0.10	0.12	0.28	0.25	0.10	0.07	0.19
La	3.26	4.78	4.63	5.27	5.40	15.96	15.09	5.57	4.86	9.48
Ce	9.51	13.05	12.79	14.43	15.07	43.90	41.34	16.01	15.60	26.65
Pr	1.62	2.12	2.02	2.28	2.43	6.69	6.38	2.73	2.82	4.20
Nd	8.64	11.04	10.78	12.01	12.46	32.11	30.32	14.22	15.12	21.21
Sm	2.58	3.32	3.21	3.55	3.91	7.67	7.38	4.34	4.82	5.70
Eu	1.05	1.21	1.12	1.32	1.45	2.55	2.53	1.53	1.78	2.06
Gd	3.12	3.69	3.48	3.80	4.23	6.55	6.33	4.63	5.19	5.95
Tb	0.51	0.62	0.58	0.60	0.70	0.79	0.87	0.73	0.84	0.93
Dy	3.03	3.70	3.27	3.77	4.32	4.04	4.26	4.45	4.96	5.46
Ho	0.64	0.75	0.68	0.75	0.86	0.67	0.67	0.88	0.97	1.01
Er	1.67	2.09	1.85	2.14	2.50	1.62	1.77	2.47	2.55	2.69
Tm	0.27	0.31	0.27	0.30	0.37	0.22	0.23	0.35	0.35	0.41
Yb	1.52	1.85	1.73	1.91	2.35	1.28	1.40	2.20	2.23	2.42
Lu	0.23	0.25	0.23	0.31	0.35	0.19	0.21	0.32	0.32	0.36

	BR24	BR25	BR27	BR28	BR29	BR30	BR31	BR32	BR33	BM2
Type	MPG	MPG	MPG	MPG	MPG	MPG	MPG	MPG	MPG	MPG
Pb	1.56	2.04	2.50	1.90	1.75	1.65	1.64	1.91	1.82	1.07
Th	0.65	0.50	0.74	0.94	0.80	0.78	0.77	0.81	0.82	0.31
U	0.20	0.15	0.19	0.32	0.25	0.23	0.24	0.25	0.27	0.13
La	10.70	10.77	13.20	13.94	11.28	10.89	10.95	13.49	11.91	5.03
Ce	28.63	33.26	35.00	38.28	32.04	31.41	30.38	36.80	33.51	15.02
Pr	4.50	5.50	5.50	6.06	5.03	5.03	4.88	5.83	5.32	2.65
Nd	22.18	29.32	27.13	29.09	24.66	24.92	24.06	27.51	25.73	13.66
Sm	6.04	7.84	7.27	7.54	6.79	6.68	6.44	7.24	6.92	4.51
Eu	2.19	2.72	2.37	2.67	2.36	2.31	2.25	2.57	2.34	1.63
Gd	6.12	7.70	6.97	7.17	6.33	6.33	6.20	7.03	6.69	4.54
Tb	0.94	1.05	0.99	1.14	0.99	0.98	1.01	1.08	1.01	0.71
Dy	5.38	5.49	5.47	6.21	5.70	5.73	5.73	6.18	6.10	4.31
Ho	1.04	1.02	0.98	1.28	1.13	1.13	1.10	1.22	1.16	0.85
Er	2.81	2.47	2.50	3.33	3.12	3.04	2.90	3.41	3.13	2.17
Tm	0.34	0.34	0.34	0.48	0.44	0.42	0.42	0.43	0.44	0.34
Yb	2.38	1.95	2.21	2.72	2.62	2.72	2.53	2.91	2.92	1.92
Lu	0.37	0.28	0.30	0.39	0.40	0.41	0.40	0.45	0.45	0.28

	BM4	BM5	BM6	BM17	BM21	BM28	BM35	BM40	BM48	BM56
Type	MPG	MPG	MPG	MPG	MPG	MPG	MPG	MPG	MPG	MPG
Pb	1.11	1.38	1.97	1.21	1.31	1.21	0.58	1.05	1.20	1.50
Th	0.30	0.34	0.94	0.29	0.35	0.36	0.24	0.42	0.56	0.64
U	0.13	0.11	0.25	0.12	0.14	0.08	0.10	0.08	0.19	0.20
La	4.42	5.34	8.96	6.66	3.77	5.86	3.57	6.25	6.81	10.43
Ce	11.97	14.49	22.92	16.53	11.42	14.20	10.65	15.24	17.57	27.84
Pr	1.90	2.32	3.44	2.48	1.96	2.19	1.95	2.33	2.57	4.13
Nd	10.16	11.99	17.30	12.61	10.81	11.01	11.42	13.01	13.11	21.26
Sm	3.10	3.61	4.78	3.33	3.87	3.28	4.07	4.24	4.38	6.23
Eu	1.14	1.25	1.60	1.24	1.28	1.16	1.37	1.48	1.23	1.92
Gd	3.47	3.58	4.80	3.75	4.40	3.74	4.87	4.12	4.28	5.53
Tb	0.55	0.59	0.73	0.57	0.66	0.57	0.75	0.65	0.61	0.97
Dy	3.42	3.15	3.89	3.50	3.96	3.70	4.62	3.92	3.69	5.08
Ho	0.72	0.65	0.78	0.77	0.86	0.74	0.86	0.81	0.69	1.02
Er	1.92	1.73	1.96	1.82	2.39	2.16	2.34	2.25	2.05	2.66
Tm	0.29	0.26	0.28	0.28	0.35	0.32	0.39	0.37	0.35	0.42
Yb	1.76	1.50	1.68	1.73	2.14	1.88	2.59	2.09	2.30	2.71
Lu	0.28	0.21	0.23	0.25	0.36	0.25	0.36	0.28	0.31	0.43

	BM62	BM66	MR2	MR9	MR16	MR23	MR27	MR38	MR41	UV1
Type	MPG	MPG	MPG	MPG	MPG	MPG	MPG	MPG	MPG	MPG
Pb	14.08	5.45	1.24	1.45	1.29	1.72	2.08	3.96	1.20	2.99
Th	4.40	1.72	0.38	0.44	0.58	0.90	0.79	1.20	0.40	0.42
U	1.28	0.59	0.17	0.10	0.16	0.31	0.25	0.39	0.18	0.22
La	80.67	37.64	4.25	6.10	9.00	12.97	15.58	27.54	7.68	9.73
Ce	165.15	87.31	10.25	15.59	25.33	35.28	40.40	62.66	18.85	22.22
Pr	18.86	12.20	1.66	2.42	4.21	5.31	6.05	8.65	3.01	3.42
Nd	71.58	53.59	10.03	12.11	22.49	26.45	30.63	41.53	15.06	17.16
Sm	13.55	12.35	3.56	4.61	6.73	8.10	8.50	9.35	5.05	4.44
Eu	3.62	3.80	1.16	1.41	2.36	2.34	2.78	2.91	1.76	1.55
Gd	11.71	11.30	4.05	4.75	6.71	7.62	8.89	8.44	5.04	4.02
Tb	1.63	1.50	0.64	0.71	1.13	1.21	1.07	1.15	0.61	0.64
Dy	9.00	8.56	3.59	4.41	6.00	6.25	6.45	5.80	4.05	3.63
Ho	1.79	1.74	0.76	1.01	1.15	1.29	1.26	1.12	0.79	0.84
Er	5.39	4.21	2.12	2.56	2.76	2.92	3.00	2.95	1.98	1.83
Tm	0.84	0.66	0.35	0.38	0.44	0.47	0.51	0.50	0.32	0.31
Yb	5.82	4.35	2.13	2.28	2.61	3.02	3.24	2.95	1.98	1.82
Lu	0.88	0.66	0.30	0.34	0.41	0.47	0.45	0.47	0.29	0.29

	UV2E	CA4	CA8	CA10	CA12	CA14	BHL2	BHL36	C3	T4
Type	MPG	MPG	MPG	MPG	MPG	MPG	MPG	MPG	MPG	MPG
Pb	3.11	7.14	13.23	2.57	6.92	5.99	2.76	0.85	2.84	1.03
Th	1.43	2.79	2.70	0.63	3.30	2.32	1.03	0.25	0.74	0.33
U	0.45	0.68	0.88	0.28	1.03	0.80	0.37	0.09	0.23	0.08
La	22.17	34.95	67.45	12.62	18.53	16.24	10.00	4.51	13.34	6.33
Ce	61.55	93.53	183.67	33.02	43.46	38.08	27.95	13.24	34.48	16.91
Pr	9.43	11.25	17.47	4.45	5.17	4.48	3.87	2.11	4.84	2.57
Nd	47.76	47.57	69.57	21.50	24.16	20.49	18.52	11.09	23.33	12.35
Sm	11.71	10.28	13.18	5.44	6.55	5.10	5.34	3.45	6.25	3.73
Eu	3.52	3.31	4.25	2.02	2.31	1.75	2.00	1.30	2.17	1.39
Gd	8.25	10.24	13.53	6.62	7.15	5.22	6.52	3.84	7.33	4.50
Tb	1.22	1.37	1.68	0.78	1.25	0.97	0.89	0.56	0.92	0.65
Dy	4.81	8.10	9.42	4.43	7.73	6.31	5.52	3.58	5.20	4.15
Ho	0.65	1.38	1.69	0.78	1.57	1.29	0.99	0.62	0.83	0.77
Er	1.34	4.11	5.00	2.11	4.56	3.94	2.81	1.82	2.21	2.15
Tm	0.18	0.49	0.64	0.26	0.60	0.54	0.34	0.23	0.25	0.28
Yb	0.80	3.58	4.88	1.83	4.28	3.72	2.53	1.52	1.57	1.91
Lu	0.11	0.45	0.65	0.23	0.56	0.49	0.31	0.21	0.20	0.24

	BB7B	BB9	BB10A	AM2A	STA3	UV1	W3	W4	BM74
Type	MPG	MPG	MPG	MPG	MPG	SMT	SMT	SMT	CGMT
Pb	1.05	1.03	1.56	1.81	1.55	2.99	3.29	4.19	0.69
Th	0.26	0.19	0.37	0.82	0.44	0.42	1.79	3.19	0.46
U	0.10	0.07	0.14	0.30	0.08	0.22	0.44	0.73	0.14
La	6.13	4.82	10.63	9.45	6.28	9.73	8.68	13.38	4.00
Ce	18.36	14.75	32.72	24.39	16.58	22.22	21.80	31.25	9.96
Pr	2.80	2.49	4.89	3.43	2.16	3.42	3.26	3.95	1.74
Nd	14.54	13.37	24.88	17.07	9.79	17.16	15.48	19.21	9.16
Sm	4.33	4.22	7.06	5.14	2.69	4.44	4.67	5.65	3.06
Eu	1.67	1.59	2.51	1.92	1.00	1.55	1.83	1.85	1.29
Gd	4.93	4.61	7.82	5.92	3.34	4.02	6.46	5.61	4.61
Tb	0.71	0.67	1.02	0.88	0.45	0.64	0.87	0.90	0.70
Dy	4.20	4.35	6.01	5.58	2.92	3.63	5.73	6.08	4.37
Ho	0.78	0.77	1.09	1.02	0.55	0.84	1.03	1.25	1.01
Er	2.16	2.22	3.02	2.96	1.59	1.83	3.20	3.17	2.55
Tm	0.27	0.28	0.37	0.37	0.22	0.31	0.54	0.50	0.44
Yb	1.91	1.97	2.63	2.62	1.51	1.82	2.97	3.34	2.71
Lu	0.25	0.25	0.31	0.32	0.19	0.29	0.49	0.49	0.35

	BM79	BM83	BM85	CA3B	CA15	CA16	CA19	CD124	CD44
Type	CGMT	CGMT	CGMT	CMT	CMT	CMT	CMT	PM	PM
Pb	1.26	0.86	0.79	1.08	1.44	1.24	1.28	0.48	0.50
Th	0.56	0.70	0.66	0.24	0.31	0.40	0.31	0.06	0.05
U	0.27	0.26	0.17	0.09	0.12	0.17	0.10	0.03	0.02
La	6.40	6.21	4.89	1.99	3.29	3.57	3.09	0.88	1.24
Ce	14.46	14.67	11.49	5.64	8.20	8.32	7.43	2.57	3.68
Pr	2.35	2.04	1.61	0.93	1.27	1.13	1.06	0.44	0.62
Nd	12.74	12.14	9.80	4.71	7.30	5.29	5.34	2.46	3.68
Sm	4.17	4.16	3.39	1.84	2.83	1.57	1.75	0.91	1.42
Eu	1.74	1.58	1.45	0.77	1.20	0.59	0.71	0.39	0.62
Gd	4.75	4.60	4.28	2.22	3.95	2.08	2.51	1.20	2.00
Tb	0.78	0.87	0.71	0.38	0.68	0.33	0.39	0.19	0.32
Dy	4.33	5.57	5.10	2.72	4.62	2.14	2.70	1.34	2.27
Ho	0.98	1.13	1.10	0.52	0.95	0.41	0.54	0.28	0.44
Er	2.54	3.07	2.92	1.50	2.92	1.26	1.69	0.82	1.31
Tm	0.36	0.59	0.49	0.20	0.40	0.19	0.24	0.11	0.18
Yb	2.39	3.32	2.84	1.49	2.90	1.28	1.64	0.75	1.29
Lu	0.39	0.53	0.40	0.19	0.38	0.16	0.22	0.10	0.17

Sample	P40	P43	P50	P42	P61	L1
Type	Lew	Lew	Lew	Lew	Lew	P-C
Pb	5.81	9.39	14.07	13.49	10.05	3.06
Th	0.45	0.09	0.86	3.99	1.25	4.57
U	0.09	0.07	0.12	0.26	0.09	1.17
La	12.01	6.31	9.02	38.17	35.61	38.52
Ce	13.98	8.20	10.28	74.48	60.87	77.46
Pr	1.01	0.90	0.86	6.62	4.80	8.84
Nd	3.04	3.48	2.78	23.08	15.50	40.93
Sm	0.64	1.08	0.81	3.94	2.62	8.44
Eu	0.86	3.20	1.95	1.29	0.93	2.85
Gd	0.49	1.16	0.95	3.03	2.11	7.45
Tb	0.07	0.10	0.09	0.23	0.14	1.05
Dy	0.39	0.50	0.49	1.03	0.62	5.73
Ho	0.10	0.11	0.12	0.15	0.09	1.01
Er	0.31	0.31	0.41	0.42	0.25	2.69
Tm		0.05	0.08	0.05	0.03	0.40
Yb	0.39	0.47	0.55	0.35	0.21	2.58
Lu	0.05	0.05	0.06	0.05	0.02	0.37

Appendix 4c

Radiogenic isotope ratios

The following table gives radiogenic isotope ratios (with 2σ errors) for Sr, Nd and Pb. 'i' denotes age corrected (60Ma) ratios, (decay constants are the same as those used by Dickin 1981) and it is these corrected values that have been used in section 4.4. All the analysed samples are basalts, with the exception of P42, P43 & P50 which are Lewisian crustal material.

	87Sr/86Sr	(87Sr/86Sr)i	143Nd/144Nd	(143Nd/144Nd)i	206Pb/204Pb	(206Pb/204Pb)i	207Pb/206Pb	(207Pb/206Pb)i	208Pb/204Pb	(208Pb/204Pb)i
BR1	0.702858±6	0.702851	0.513094±4	0.512974	17.874±3	17.759	15.413±2	15.408	37.609±6	37.497
BR8	0.704235±7	0.704218	0.512153±5	0.512046	15.138±2	15.111	14.921±2	14.920	34.916±4	34.812
BR10	0.704244±7	0.704229	0.512138±4	0.512037	15.148±3	15.105	14.958±3	14.956	35.009±6	34.905
BR13	0.704118±7	0.704094	0.512625±5	0.512507	16.322±1	16.272	15.127±1	15.125	36.072±3	35.965
BR18	0.703118±7	0.703107	0.512986±8	0.512893	17.789±1	17.699	15.382±1	15.378	37.482±3	37.371
BR24	0.703054±7	0.703050	0.513014±3	0.512907	17.747±1	17.661	15.370±1	15.366	37.410±3	37.299
BM2	0.703156±7	0.703149	0.512948±4	0.512819	17.022±2	16.942	15.267±2	15.263	36.772±5	36.663
BM4	0.704105±7	0.704091	0.512620±6	0.512500	16.609±1	16.531	15.200±1	15.196	36.377±3	36.269
BM17	0.704057±7	0.704045	0.512442±5	0.512338	16.193±3	16.129	15.119±3	15.116	35.996±8	35.889
MR2	0.704125±7	0.704095	0.512613±12	0.512458	16.346±4	16.253	15.141±4	15.137	36.359±9	36.251
P42	0.723478±7	0.723319	0.510588±4	0.510499	14.590±0	14.583	14.845±0	14.845	35.409±1	35.304
P43	0.710025±7	0.709950	0.510577±4	0.510364	14.506±1	14.501	14.9025±1	14.902	34.363±2	34.260
P50	0.722260±7	0.722071	0.510451±4	0.510345	14.043±0	14.038	14.737±0	14.737	34.483±1	34.380

Appendix 4c Isotopes

Appendix 4d

Electron Microprobe Analyses

4d.i	-	Olivines
4d.ii	-	Pyroxenes
4d.iii	-	Feldspars
4d.iv	-	Oxides

Abbreviations used in the data tables:

B - basalt, **H** - hawaiite, **B-H** - basaltic-hawaiite, **M** - mugearite, **T** - trachyte, **SMT** - Staffa Magma sub-Type, **CMT** - Central Mull Tholeiite. **gmass** - groundmass crystal, **p core** - phenocryst core, **p rim** - phenocryst rim.

Sample	BM10	BM10	BM10	BM10	BM10	BM10	BM10 core	BM10 rim	BM10 core	BM10 rim	BM10	BM10	BR5 core	BR5 rim	BR5 rim	BR5 core	BR5 core	BR5 core	BR5
Lithology	B	B	B	B	B	B	B	B	B	B	B	B	B	B	B	B	B	B	B
SiO2	38.41	39.18	39.65	39.51	39.29	38.66	41.05	39.01	39.91	37.73	37.65	40.90	40.57	40.07	39.69	40.03	39.68	39.35	39.67
TiO2	0.00	0.07	0.07	0.05	0.06	0.03	0.12	0.00	0.04	0.00	0.05	0.09	0.10	0.00	0.12	0.11	0.00	0.00	0.00
Al2O3	0.26	0.31	0.15	0.28	0.12	0.21	0.22	0.31	0.03	0.00	0.03	0.16	0.00	0.09	0.04	0.28	0.42	0.00	0.29
Cr2O3	0.00	0.07	0.06	0.00	0.16	0.05	0.03	0.12	0.23	0.02	0.00	0.12	0.53	0.00	0.10	0.07	0.00	0.02	0.13
FeO	21.31	14.61	14.63	14.48	16.71	17.41	14.47	19.89	13.67	21.74	18.74	14.27	11.54	13.31	14.64	11.82	12.00	11.38	13.01
MnO	0.41	0.16	0.37	0.42	0.37	0.29	0.19	0.33	0.28	0.38	0.34	0.28	0.18	0.36	0.33	0.03	0.31	0.37	0.20
NiO	0.11	0.16	0.26	0.39	0.47	0.11	0.00	0.22	0.34	0.18	0.00	0.25	0.32	0.16	0.35	0.31	0.17	0.38	0.23
MgO	38.70	43.45	44.29	44.45	42.13	41.50	45.94	40.89	45.01	37.93	39.21	45.58	46.98	45.30	43.63	45.95	44.77	44.91	45.34
CaO	0.30	0.30	0.29	0.28	0.31	0.38	0.30	0.43	0.35	0.20	0.39	0.35	0.30	0.33	0.38	0.30	0.24	0.34	0.30
Na2O	0.13	0.16	0.00	0.11	0.00	0.16	0.08	0.14	0.15	0.01	0.00	0.24	0.22	0.08	0.00	0.36	0.11	0.00	0.13
K2O	0.03	0.00	0.00	0.00	0.02	0.01	0.21	0.54	0.08	0.00	0.00	0.00	0.00	0.00	0.03	0.00	0.00	0.00	0.16
SUM	99.66	98.47	99.77	99.97	99.63	98.80	102.61	101.88	100.09	98.19	96.41	102.23	100.74	99.70	99.31	99.24	97.71	96.74	99.46
Atoms per four Oxygens																			
Si	1.000	1.001	0.999	0.994	1.002	0.997	1.002	1.000	0.999	1.000	0.999	1.002	1.002	1.003	1.005	1.000	1.009	1.008	0.996
Ti	0.000	0.001	0.001	0.001	0.001	0.001	0.002	0.000	0.001	0.000	0.001	0.002	0.002	0.000	0.002	0.002	0.000	0.000	0.000
Al	0.008	0.010	0.005	0.008	0.004	0.006	0.006	0.009	0.001	0.000	0.010	0.005	0.000	0.002	0.001	0.008	0.012	0.000	0.009
Cr	0.000	0.001	0.001	0.000	0.003	0.001	0.001	0.003	0.005	0.000	0.000	0.002	0.001	0.000	0.002	0.001	0.000	0.000	0.003
Fe2+	0.464	0.299	0.308	0.305	0.356	0.375	0.295	0.426	0.286	0.482	0.416	0.292	0.238	0.279	0.310	0.247	0.254	0.244	0.275
Mn	0.009	0.003	0.008	0.009	0.008	0.006	0.004	0.007	0.006	0.009	0.002	0.006	0.004	0.008	0.007	0.001	0.007	0.008	0.004
Ni	0.002	0.003	0.005	0.008	0.010	0.002	0.000	0.004	0.007	0.003	0.000	0.005	0.006	0.003	0.007	0.006	0.003	0.008	0.005
Mg	1.502	1.660	1.663	1.667	1.601	1.595	1.672	1.529	1.679	1.499	1.551	1.664	1.729	1.690	1.649	1.711	1.693	1.715	1.696
Ca	0.008	0.008	0.008	0.007	0.009	0.011	0.008	0.012	0.009	0.006	0.011	0.009	0.008	0.009	0.010	0.008	0.007	0.009	0.008
Na	0.006	0.008	0.000	0.005	0.000	0.008	0.004	0.007	0.007	0.000	0.000	0.012	0.011	0.004	0.000	0.017	0.006	0.000	0.006
K	0.001	0.000	0.000	0.000	0.001	0.000	0.001	0.002	0.003	0.000	0.000	0.000	0.000	0.000	0.001	0.000	0.000	0.000	0.001
Total	3.000	2.994	2.998	3.004	2.995	3.002	2.995	2.999	3.003	2.999	2.990	2.999	3.001	2.998	2.994	3.001	2.991	2.992	3.003
Fo%	76.40	84.74	84.37	84.53	81.81	80.96	85.00	78.21	85.45	75.67	78.85	85.07	87.90	85.83	84.18	87.39	86.95	87.54	86.05

Appendix 4d.i olivines

Sample	BR5	BR5	BR5	BR5	BR5	BR5	BR5	BR19	BR19	BR19	BR19	BR19	BM1	BM1	BM1	BM5	BM5	BM5	BM5
Lithology	B	B	B	B	B	B	B	H	H	H	H	H	B	B	B	B	B	B	B
SiO2	39.38	39.65	39.01	41.01	40.18	39.15	38.78	37.37	36.26	37.11	37.07	36.67	40.94	40.46	41.52	38.88	38.75	39.09	38.33
TiO2	0.01	0.00	0.17	0.11	0.00	0.00	0.05	0.00	0.01	0.32	0.11	0.09	0.10	0.06	0.07	0.00	0.01	0.01	0.06
Al2O3	0.10	0.24	0.18	0.17	0.07	0.09	0.69	0.45	0.00	0.92	0.66	0.71	0.23	0.20	0.20	0.15	0.00	0.20	0.09
Cr2O3	0.01	0.03	0.16	0.03	0.06	0.00	0.18	0.00	0.00	0.06	0.00	0.00	0.12	0.08	0.23	0.03	0.06	0.00	0.06
FeO	13.23	15.87	19.88	12.78	11.02	19.52	22.57	29.10	32.19	30.25	30.87	30.37	12.65	12.62	13.04	24.01	22.79	17.07	24.60
MnO	0.13	0.28	0.12	0.09	0.12	0.33	0.23	0.38	0.49	0.39	0.59	0.40	0.21	0.29	0.08	0.29	0.40	0.21	0.33
NiO	0.48	0.23	0.00	0.23	0.42	0.23	0.11	0.03	0.11	0.13	0.00	0.00	0.25	0.12	0.00	nd	nd	nd	0.23
MgO	43.50	42.65	39.66	46.82	47.17	41.51	38.46	30.84	29.48	28.80	29.75	29.48	47.20	45.83	46.45	38.26	38.63	41.84	37.54
CaO	0.22	0.39	0.40	0.28	0.29	0.25	0.39	0.35	0.50	0.60	0.63	0.51	0.33	0.37	0.39	0.28	0.32	0.31	0.31
Na2O	0.19	0.22	0.00	0.02	0.00	0.00	0.00	0.37	0.20	0.65	0.20	0.27	0.09	0.29	0.32	0.09	0.00	0.00	0.00
K2O	0.00	0.02	0.00	0.00	0.00	0.00	0.02	0.00	0.00	0.10	0.07	0.11	0.00	0.00	0.00	0.00	0.00	0.01	0.00
SUM	97.25	99.58	99.58	101.53	99.33	101.08	101.48	98.89	99.25	99.33	99.94	98.60	102.12	100.32	102.29	102.00	100.95	98.73	101.55
Atoms per four Oxygens																			
Si	1.011	1.006	1.006	1.003	0.999	0.995	0.994	1.017	0.996	1.014	1.013	1.010	0.996	1.003	1.008	0.999	1.001	1.004	0.994
Tl	0.000	0.000	0.003	0.002	0.000	0.000	0.002	0.000	0.014	0.007	0.003	0.002	0.002	0.001	0.001	0.000	0.000	0.000	0.002
Al	0.003	0.007	0.005	0.005	0.003	0.004	0.031	0.014	0.000	0.030	0.021	0.023	0.007	0.006	0.006	0.005	0.000	0.006	0.004
Cr	0.000	0.001	0.003	0.001	0.002	0.000	0.005	0.000	0.000	0.001	0.000	0.000	0.002	0.002	0.004	0.001	0.001	0.000	0.002
Fe2+	0.289	0.337	0.434	0.261	0.229	0.415	0.484	0.663	0.740	0.695	0.694	0.699	0.258	0.262	0.265	0.516	0.492	0.367	0.533
Mn	0.003	0.006	0.003	0.002	0.003	0.007	0.005	0.009	0.011	0.009	0.013	0.009	0.004	0.006	0.002	0.006	0.009	0.005	0.007
Ni	0.010	0.005	0.000	0.004	0.008	0.005	0.002	0.001	0.002	0.003	0.002	0.000	0.005	0.002	0.000	-	-	-	0.005
Mg	1.670	1.613	1.530	1.707	1.749	1.572	1.470	1.259	1.209	1.180	1.229	1.210	1.713	1.694	1.681	1.465	1.487	1.602	1.450
Ca	0.006	0.011	0.011	0.007	0.008	0.007	0.011	0.010	0.015	0.017	0.018	0.015	0.009	0.010	0.010	0.008	0.009	0.009	0.009
Na	0.010	0.011	0.000	0.001	0.000	0.000	0.000	0.020	0.011	0.034	0.011	0.014	0.004	0.014	0.015	0.000	0.000	0.000	0.000
K	0.000	0.001	0.000	0.000	0.000	0.000	0.001	0.000	0.000	0.004	0.002	0.004	0.000	0.000	0.000	0.000	0.000	0.000	0.000
Total	3.002	2.998	2.995	2.993	3.001	3.005	3.006	2.993	2.998	2.994	3.006	2.986	3.000	3.000	2.992	3.000	2.999	2.993	3.006
Fo%	85.25	82.72	77.90	86.74	88.41	79.12	75.23	65.50	62.03	62.93	63.91	63.38	86.91	86.61	86.38	73.95	75.14	81.36	73.11

Appendix 4d.i olivines

Sample	BM5	MR9 core	MR9 core	MR9 rim	MR9 core	MR9 core	MR9 rim	MR9 core	MR9 rim	BM2	BM2	BM2	BM2	BM2	BR27	BR27	BR27	BR27	BR27
Lithology	B	B	B	B	B	B	B	B	B	B	B	B	B	B	B-H	B-H	B-H	B-H	B-H
SiO2	37.70	39.61	39.61	39.21	39.77	38.66	38.03	37.85	37.29	38.88	39.80	40.36	39.89	39.65	35.19	35.25	35.98	37.11	36.20
TiO2	0.09	0.05	0.00	0.00	0.38	0.00	0.00	0.00	0.06	0.00	0.03	0.04	0.00	0.00	0.05	0.13	0.12	0.09	0.07
Al2O3	0.08	0.19	0.04	0.42	0.20	0.08	0.06	0.15	0.09	0.17	0.02	0.12	0.22	0.30	0.27	0.56	0.49	0.20	0.13
Cr2O3	0.02	0.05	0.00	0.07	0.06	0.00	0.00	0.08	0.02	0.00	0.11	0.00	0.11	0.16	0.00	0.00	0.00	0.03	0.08
FeO	24.69	20.67	20.34	21.13	20.89	19.55	22.08	19.20	24.09	17.30	14.94	14.51	15.79	14.12	32.39	33.53	33.40	32.22	31.90
MnO	0.30	0.36	0.39	0.33	0.30	0.29	0.28	0.30	0.33	0.17	0.13	0.35	0.17	0.12	0.70	0.61	0.61	0.69	0.51
NiO	0.20	nd	nd	nd	nd	0.25	0.11	0.14	0.08	0.35	0.29	0.27	0.50	0.28	0.00	0.30	0.08	0.01	0.00
MgO	36.43	40.87	40.82	38.73	41.05	41.94	36.86	41.05	36.41	41.33	43.82	44.07	43.77	44.73	27.86	27.31	27.61	31.14	29.40
CaO	0.29	0.35	0.33	0.62	0.29	0.38	0.47	0.32	0.41	0.29	0.34	0.37	0.21	0.29	0.49	0.40	0.39	0.46	0.35
Na2O	0.00	0.00	0.00	0.07	0.02	0.00	0.00	0.00	0.00	0.17	0.04	0.09	0.35	0.02	0.22	0.22	0.24	0.25	0.29
K2O	0.00	0.00	0.02	0.00	0.02	0.02	0.01	0.01	0.01	0.05	0.00	0.00	0.04	0.00	0.00	0.06	0.00	0.00	0.00
SUM	99.80	102.13	101.55	100.58	102.98	101.17	97.90	99.10	98.79	98.71	99.50	100.17	101.03	99.66	97.16	98.36	98.90	102.20	98.91
Atoms per four Oxygens																			
Si	0.996	0.999	1.004	1.008	0.999	0.984	1.011	0.983	0.994	1.003	1.005	1.009	0.998	0.996	0.996	0.994	1.004	0.993	1.002
Ti	0.004	0.001	0.000	0.000	0.001	0.000	0.000	0.000	0.002	0.000	0.001	0.001	0.000	0.000	0.001	0.003	0.002	0.002	0.001
Al	0.004	0.006	0.001	0.013	0.006	0.004	0.003	0.007	0.004	0.005	0.000	0.003	0.006	0.009	0.010	0.019	0.016	0.006	0.005
Cr	0.001	0.001	0.000	0.002	0.001	0.000	0.000	0.002	0.001	0.000	0.002	0.000	0.002	0.003	0.000	0.000	0.000	0.001	0.002
Fe2+	0.546	0.436	0.431	0.454	0.439	0.416	0.491	0.417	0.537	0.373	0.317	0.306	0.330	0.297	0.788	0.791	0.780	0.721	0.739
Mn	0.007	0.008	0.008	0.007	0.006	0.006	0.006	0.007	0.007	0.004	0.003	0.007	0.004	0.003	0.018	0.015	0.014	0.016	0.012
Ni	0.004	-	-	-	-	0.005	0.002	0.003	0.002	0.007	0.005	0.005	0.010	0.006	0.000	0.007	0.002	0.000	0.000
Mg	1.435	1.537	1.542	1.484	1.537	1.583	1.461	1.580	1.446	1.589	1.650	1.648	1.633	1.676	1.157	1.148	1.149	1.243	1.214
Ca	0.008	0.009	0.009	0.017	0.008	0.010	0.013	0.009	0.012	0.008	0.009	0.010	0.006	0.008	0.016	0.012	0.012	0.013	0.010
Na	0.000	0.000	0.000	0.003	0.001	0.000	0.000	0.000	0.000	0.009	0.002	0.004	0.017	0.001	0.014	0.012	0.013	0.013	0.015
K	0.000	0.000	0.001	0.000	0.001	0.001	0.000	0.000	0.000	0.002	0.000	0.000	0.001	0.000	0.000	0.002	0.000	0.000	0.000
Total	3.004	2.997	2.996	2.988	2.999	3.009	2.989	3.008	3.006	3.000	2.994	2.993	3.007	2.999	2.997	3.003	2.992	3.008	3.000
Fo%	72.45	77.90	78.16	76.57	77.78	79.19	74.84	79.12	72.92	80.99	83.88	84.34	83.19	84.95	59.49	59.21	59.56	63.29	62.16

Appendix 4d.i olivines

Sample	MR2	MR2	MR2	MR2	MR2	MR2	MR2	MR2	MR2 core	MR2 core	MR2 rim	BR22	BR22	BR22	BR22	BM8 core	BM8 rim	BM8 core	BM8 core
Lithology	B	B	B	B	B	B	B	B	B	B	B	B	B	B	B	B	B	B	B
SiO2	39.75	39.00	38.70	37.89	39.21	37.91	38.49	38.23	39.13	37.67	36.63	37.04	37.24	36.10	36.12	40.35	40.30	40.53	40.33
TiO2	0.00	0.00	0.08	0.08	0.00	0.09	0.00	0.07	0.00	0.33	0.04	0.00	0.11	0.13	0.09	0.02	0.13	0.12	0.00
Al2O3	0.10	0.00	0.00	0.22	0.12	0.11	0.03	0.01	0.06	0.00	0.00	0.16	0.20	0.58	0.53	0.13	0.68	0.19	0.00
Cr2O3	0.16	0.09	0.13	0.11	0.13	0.05	0.09	0.03	0.01	0.10	0.00	0.09	0.06	0.02	0.04	0.02	0.09	0.03	0.08
FeO	16.38	16.65	16.91	24.14	16.80	24.67	17.91	20.35	17.50	25.76	31.33	31.44	29.80	34.06	34.09	12.94	14.40	12.28	11.23
MnO	0.20	0.23	0.27	0.55	0.20	0.52	0.28	0.39	0.18	0.33	0.53	0.29	0.37	0.45	0.61	0.24	0.22	0.17	0.28
NiO	0.33	0.34	nd	nd	nd	nd	0.19	0.13	0.20	0.17	0.04	nd	nd	nd	nd	0.25	0.40	0.31	0.37
MgO	42.73	42.68	41.94	36.06	43.02	36.82	41.90	38.81	42.29	35.27	30.93	31.38	32.29	27.78	27.79	44.51	43.37	45.99	46.32
CaO	0.32	0.32	0.26	0.47	0.29	0.36	0.30	0.30	0.35	0.35	0.33	0.55	0.50	0.51	0.57	0.47	0.53	0.31	0.21
Na2O	0.00	0.01	0.00	0.15	0.08	0.00	0.00	0.00	0.00	0.00	0.00	0.23	0.10	0.00	0.05	0.36	0.50	0.38	0.02
K2O	0.00	0.00	0.04	0.03	0.02	0.03	0.02	0.00	0.00	0.00	0.00	0.00	0.00	0.01	0.00	0.00	0.00	0.04	0.00
SUM	99.98	99.30	98.33	99.70	99.87	100.56	99.21	98.31	99.72	99.98	99.83	101.18	100.67	99.64	99.88	99.27	100.61	100.34	98.83
Atoms per four Oxygens																			
Si	1.004	1.001	1.000	1.000	0.995	0.994	0.991	1.005	0.999	0.999	1.000	0.997	0.999	1.001	1.000	1.013	1.005	1.004	1.005
Ti	0.000	0.000	0.002	0.002	0.000	0.002	0.000	0.003	0.000	0.013	0.002	0.000	0.002	0.003	0.002	0.000	0.002	0.002	0.000
Al	0.003	0.000	0.000	0.007	0.004	0.003	0.001	0.000	0.003	0.000	0.000	0.005	0.006	0.019	0.017	0.004	0.020	0.005	0.008
Cr	0.003	0.002	0.003	0.002	0.003	0.001	0.003	0.001	0.000	0.003	0.000	0.002	0.001	0.001	0.001	0.000	0.002	0.001	0.001
Fe2+	0.359	0.358	0.365	0.533	0.357	0.541	0.386	0.447	0.374	0.571	0.716	0.710	0.669	0.790	0.789	0.272	0.300	0.254	0.296
Mn	0.004	0.005	0.006	0.012	0.004	0.012	0.006	0.009	0.004	0.007	0.012	0.006	0.008	0.010	0.014	0.005	0.005	0.004	0.007
Ni	0.007	0.007	-	-	-	-	0.004	0.003	0.004	0.004	0.001	-	-	-	-	0.005	0.008	0.006	0.007
Mg	1.604	1.618	1.615	1.419	1.628	1.439	1.608	1.520	1.609	1.394	1.259	1.260	1.292	1.148	1.147	1.665	1.613	1.697	1.648
Ca	0.008	0.008	0.007	0.013	0.008	0.010	0.008	0.008	0.010	0.010	0.010	0.016	0.014	0.015	0.017	0.013	0.014	0.008	0.011
Na	0.000	0.000	0.000	0.007	0.004	0.000	0.000	0.000	0.000	0.000	0.000	0.012	0.005	0.000	0.003	0.017	0.024	0.018	0.016
K	0.000	0.000	0.001	0.001	0.001	0.001	0.001	0.000	0.000	0.000	0.000	0.000	0.000	0.000	0.000	0.000	0.000	0.001	0.001
Total	2.992	2.999	2.999	2.996	3.004	3.003	3.009	2.995	3.001	3.001	3.000	3.008	2.996	2.987	2.990	2.994	2.993	3.000	3.000
Fo%	81.71	81.88	81.57	72.69	82.02	72.68	80.65	77.26	81.15	70.93	63.76	63.96	65.88	59.24	59.25	85.96	84.32	86.98	84.77

Appendix 4d.i olivines

Sample	BM8 core	BM8 rim	BM8 core	BM8 rim	AM5	AM5	STA3	STA3	BM4	BM4	BM4	BCH2 core	BCH2 rim	BCH2 core	BCH2 rim	BCH2 core	BCH2 rim	BCH2 core	BCH2 core
Lithology	B	B	B	B	B	B	B	B	B	B	B	B	B	B	B	B	B	B	B
SiO2	39.87	40.91	40.75	40.73	39.04	38.76	38.81	39.99	37.51	36.68	36.31	37.02	38.86	39.77	37.10	38.92	37.05	39.73	37.03
TiO2	0.00	0.11	0.08	0.06	0.00	0.03	0.00	0.03	0.00	0.07	0.07	0.04	0.01	0.00	0.07	0.00	0.04	0.00	0.04
Al2O3	0.00	0.21	0.29	0.73	0.08	0.11	0.06	0.06	0.07	0.00	0.07	0.01	0.03	0.06	0.06	0.00	0.03	0.03	0.01
Cr2O3	0.00	0.07	0.08	0.04	0.04	0.03	0.04	0.02	0.01	0.00	0.00	0.08	0.06	0.03	0.02	0.05	0.05	0.07	0.02
FeO	10.46	14.43	11.44	14.54	20.07	18.93	15.24	17.36	25.40	30.13	29.97	19.17	19.51	17.53	26.71	15.12	29.47	15.07	28.60
MnO	0.32	0.33	0.16	0.34	0.30	0.21	0.22	0.30	0.39	0.46	0.50	0.26	0.28	0.25	0.37	0.28	0.31	0.23	0.45
NiO	0.34	0.34	0.34	0.48	0.21	0.19	0.28	0.30	0.14	0.14	0.18	0.22	0.21	0.24	0.19	0.27	0.16	0.23	0.12
MgO	46.49	45.17	46.88	44.03	41.01	41.77	43.82	41.85	35.58	32.56	31.78	40.57	40.41	42.23	35.11	44.24	33.24	45.23	33.46
CaO	0.34	0.32	0.31	0.60	0.32	0.25	0.30	0.35	0.35	0.35	0.38	0.28	0.30	0.35	0.30	0.34	0.35	0.30	0.42
Na2O	0.26	0.04	0.56	0.49	0.06	0.00	0.00	0.00	0.00	0.00	0.00	0.00	0.00	0.30	0.01	0.05	0.00	0.00	0.00
K2O	0.00	0.02	0.06	0.00	0.01	0.03	0.00	0.00	0.00	0.00	0.19	0.00	0.00	0.00	0.03	0.00	0.01	0.02	0.01
SUM	98.08	101.95	100.95	102.03	101.14	100.31	98.77	100.26	99.45	100.39	99.45	97.65	99.67	100.76	99.97	99.27	100.71	100.91	100.16
Atoms per four Oxygens																			
Si	1.003	1.003	1.000	1.003	0.994	0.991	0.992	1.013	0.999	0.991	0.991	0.978	1.002	1.003	0.990	0.989	0.993	0.991	0.995
Ti	0.000	0.002	0.001	0.001	0.000	0.001	0.000	0.001	0.000	0.003	0.003	0.002	0.000	0.000	0.003	0.000	0.002	0.000	0.002
Al	0.000	0.006	0.008	0.021	0.004	0.005	0.003	0.003	0.003	0.000	0.003	0.000	0.001	0.003	0.003	0.000	0.001	0.001	0.000
Cr	0.000	0.001	0.002	0.001	0.001	0.001	0.001	0.001	0.000	0.000	0.000	0.003	0.002	0.001	0.001	0.002	0.002	0.002	0.001
Fe2+	0.220	0.296	0.235	0.299	0.427	0.405	0.326	0.368	0.566	0.681	0.684	0.424	0.421	0.370	0.596	0.321	0.661	0.314	0.643
Mn	0.007	0.007	0.003	0.007	0.006	0.005	0.005	0.006	0.009	0.010	0.012	0.006	0.006	0.005	0.008	0.006	0.007	0.005	0.010
Ni	0.007	0.007	0.007	0.009	0.004	0.004	0.006	0.006	0.003	0.003	0.004	0.005	0.004	0.005	0.004	0.006	0.003	0.005	0.003
Mg	1.744	1.651	1.715	1.616	1.556	1.591	1.669	1.582	1.412	1.311	1.293	1.582	1.553	1.587	1.396	1.676	1.328	1.682	1.340
Ca	0.009	0.008	0.008	0.016	0.009	0.007	0.008	0.009	0.010	0.010	0.011	0.008	0.008	0.009	0.009	0.009	0.010	0.008	0.012
Na	0.013	0.017	0.026	0.023	0.003	0.000	0.000	0.000	0.000	0.000	0.000	0.000	0.000	0.015	0.001	0.002	0.000	0.000	0.000
K	0.000	0.000	0.002	0.000	0.000	0.001	0.000	0.000	0.000	0.000	0.007	0.000	0.000	0.000	0.001	0.000	0.000	0.001	0.000
Total	3.003	2.998	3.007	2.996	3.006	3.009	3.008	2.989	3.001	3.009	3.009	3.007	2.998	2.997	3.010	3.011	3.007	3.009	3.005
Fo%	88.80	84.80	87.95	84.39	78.45	79.72	83.67	81.14	71.40	65.82	65.39	78.88	78.68	81.11	70.08	83.91	66.78	84.25	67.58

Appendix 4d.i olivines

Sample	BM1	BM1	BM1	BM1	BR5	BM10	BM10	BM10	BM10	BM10	BM10	BR19	BM5	BM5	BM5 core	BM5 rim	BM5	BM5	MR9
Lithology	B	B	B	B	B	B	B	B	B	B	B	H	B	B	B	B	B	B	B
SiO2	49.85	52.78	51.67	51.10	50.14	50.08	49.98	51.50	52.75	49.20	52.07	48.09	49.43	52.18	52.36	50.55	51.12	49.75	47.84
TiO2	0.62	0.49	0.65	1.21	1.56	1.62	1.30	1.49	0.86	2.39	0.88	3.19	1.67	0.94	0.88	1.31	0.97	1.58	2.15
Al2O3	3.52	2.35	1.87	1.91	3.93	2.59	3.61	3.51	1.98	3.59	1.97	4.70	3.73	2.07	2.20	2.95	2.29	3.46	3.53
Cr2O3	0.81	0.83	0.18	0.00	0.07	0.06	0.63	0.50	0.37	0.12	0.35	0.07	0.92	0.51	0.62	0.31	0.69	0.30	0.00
FeO	5.85	6.11	6.56	13.16	8.33	8.55	6.34	6.97	6.04	7.74	6.07	8.52	8.04	7.52	7.57	8.46	7.49	7.52	13.67
MnO	0.15	0.16	0.24	0.41	0.31	0.02	0.19	0.25	0.14	0.08	0.24	0.30	0.05	0.29	0.14	0.22	0.34	0.14	0.38
MgO	15.92	17.32	16.15	14.37	14.50	14.24	15.05	15.68	16.23	14.54	16.11	11.51	14.35	15.64	15.65	14.67	15.28	14.32	10.88
CaO	19.75	20.33	19.83	18.80	20.61	19.34	20.55	20.97	20.66	20.21	20.67	21.53	22.18	21.41	21.21	20.81	21.28	21.77	20.19
Na2O	0.49	0.44	0.37	0.54	0.70	0.50	0.42	0.56	0.41	0.72	0.46	1.24	0.24	0.29	0.21	0.33	0.16	0.33	0.36
K2O	0.00	0.00	0.00	0.00	0.00	0.00	0.01	0.00	0.00	0.00	0.00	0.05	0.02	0.01	0.00	0.01	0.03	0.00	0.01
Total	96.96	100.80	97.52	101.50	100.15	96.99	98.08	101.43	99.44	98.59	98.82	99.20	100.63	100.87	100.83	99.61	99.65	99.17	99.01
Per six Oxygens																			
Si	1.887	1.923	1.947	1.923	1.860	1.915	1.881	1.875	1.946	1.856	1.937	1.823	1.838	1.919	1.923	1.891	1.907	1.869	1.848
Ti	0.018	0.013	0.018	0.030	0.042	0.046	0.037	0.040	0.024	0.068	0.025	0.090	0.046	0.026	0.024	0.037	0.027	0.045	0.062
Al	0.156	0.101	0.083	0.081	0.170	0.117	0.160	0.149	0.086	0.155	0.086	0.210	0.164	0.090	0.095	0.130	0.100	0.153	0.160
Cr	0.024	0.024	0.005	0.000	0.002	0.002	0.019	0.014	0.011	0.004	0.010	0.002	0.028	0.015	0.018	0.009	0.019	0.009	0.000
Fe2+	0.185	0.186	0.207	0.401	0.255	0.273	0.199	0.212	0.186	0.242	0.189	0.270	0.250	0.231	0.233	0.265	0.233	0.236	0.441
Mn	0.005	0.005	0.008	0.012	0.010	0.001	0.006	0.008	0.004	0.002	0.008	0.010	0.002	0.009	0.004	0.007	0.011	0.004	0.013
Mg	0.900	0.940	0.907	0.783	0.802	0.812	0.844	0.848	0.892	0.816	0.894	0.649	0.796	0.858	0.857	0.817	0.848	0.802	0.627
Ca	0.803	0.794	0.800	0.735	0.818	0.792	0.828	0.815	0.817	0.815	0.823	0.873	0.880	0.844	0.835	0.834	0.851	0.876	0.836
Na	0.036	0.031	0.027	0.039	0.048	0.037	0.031	0.040	0.029	0.052	0.033	0.090	0.018	0.021	0.015	0.024	0.011	0.024	0.027
K	0.000	0.000	0.000	0.000	0.000	0.000	0.001	0.000	0.000	0.000	0.000	0.002	0.000	0.000	0.000	0.000	0.002	0.000	0.000
Total	4.014	4.017	4.002	4.004	4.007	3.995	4.006	4.001	3.995	4.010	4.005	4.019	4.022	4.013	4.004	4.014	4.009	4.018	4.014
En	47.5	48.8	47.2	40.5	42.5	43.2	45.0	45.0	47.0	43.5	46.7	36.0	41.3	44.2	44.4	42.5	43.6	41.8	32.7
Fs	10.0	9.9	11.2	21.4	14.1	14.6	10.9	11.7	10.0	13.0	10.3	15.5	13.1	12.4	12.3	14.1	12.6	12.5	23.7
Wo	42.4	41.2	41.6	38.1	43.4	42.2	44.1	43.3	43.0	43.5	43.0	48.4	45.6	43.5	43.3	43.4	43.8	45.7	43.6

Appendix 4d.ii pyroxenes

Sample	MR9 core	MR9 rim	MR9 core	MR9	MR9	MR9	MR9	BM2	BM2	BM2	BM2	BM51	BM51	BM51	BM51	BM51	BM51	BR27	BR27
Lithology	B	B	B	B	B	B	B	B	B	B	B	B	B	B	B	B	B	B-H	B-H
SiO2	49.01	48.89	48.69	47.76	48.83	48.85	46.87	48.17	48.83	47.23	47.23	50.25	51.59	47.82	47.63	47.44	47.48	48.97	47.38
TiO2	1.52	1.73	1.32	1.66	1.51	1.31	2.62	2.41	1.94	2.51	2.54	1.55	1.67	2.43	3.17	2.56	2.97	2.51	3.60
Al2O3	4.46	3.43	4.58	3.26	4.12	4.07	3.83	3.51	4.48	5.07	5.05	1.71	1.73	4.65	4.16	4.79	4.84	3.32	4.31
Cr2O3	1.05	0.00	1.17	0.16	0.55	0.73	0.00	0.07	0.73	0.61	0.88	0.03	0.00	0.00	0.08	0.00	0.00	0.00	0.00
FeO	7.54	10.33	7.29	9.84	8.02	6.57	12.59	10.12	8.11	8.28	8.28	11.25	11.66	9.86	11.07	10.29	11.18	10.41	10.83
MnO	0.00	0.20	0.20	0.12	0.25	0.09	0.39	0.19	0.10	0.31	0.24	0.19	0.27	0.18	0.36	0.09	0.16	0.07	0.35
MgO	13.81	12.26	13.65	12.52	14.21	14.29	11.17	11.62	13.62	12.61	12.78	12.03	12.80	11.96	11.45	11.82	11.57	11.88	10.75
CaO	21.20	21.28	21.38	21.06	20.27	21.43	19.90	20.48	21.79	20.65	20.43	20.87	21.55	21.33	20.69	20.77	21.16	21.26	20.94
Na2O	0.37	0.48	0.39	0.27	0.31	0.27	0.48	0.87	0.43	0.50	0.65	0.24	0.50	0.43	0.67	0.54	0.63	0.88	0.92
K2O	0.05	0.00	0.00	0.04	0.04	0.05	0.02	0.04	0.06	0.00	0.02	0.03	0.02	0.03	0.06	0.00	0.00	0.00	0.00
Total	99.02	98.59	98.66	96.68	98.11	97.66	97.87	97.47	100.09	97.77	98.11	98.14	101.79	98.70	99.34	98.29	99.97	99.30	99.08
Per six Oxygens																			
Si	1.844	1.870	1.840	1.864	1.848	1.857	1.829	1.863	1.820	1.809	1.808	1.933	1.916	1.823	1.818	1.818	1.803	1.862	1.815
Tl	0.043	0.050	0.037	0.049	0.043	0.037	0.077	0.070	0.054	0.072	0.068	0.045	0.047	0.070	0.091	0.074	0.085	0.072	0.104
Al	0.198	0.155	0.204	0.149	0.184	0.182	0.176	0.160	0.199	0.229	0.228	0.077	0.076	0.209	0.187	0.217	0.217	0.149	0.195
Cr	0.031	0.000	0.035	0.005	0.015	0.022	0.000	0.002	0.022	0.019	0.027	0.001	0.000	0.000	0.002	0.000	0.000	0.000	0.000
Fe2+	0.237	0.331	0.231	0.311	0.253	0.209	0.411	0.327	0.253	0.265	0.265	0.362	0.362	0.315	0.354	0.331	0.355	0.331	0.347
Mn	0.000	0.006	0.006	0.004	0.008	0.003	0.013	0.006	0.004	0.010	0.008	0.006	0.009	0.006	0.012	0.003	0.005	0.002	0.011
Mg	0.775	0.699	0.769	0.729	0.802	0.809	0.650	0.670	0.757	0.720	0.730	0.690	0.709	0.680	0.651	0.676	0.655	0.674	0.614
Ca	0.855	0.873	0.866	0.880	0.841	0.873	0.832	0.849	0.870	0.847	0.838	0.860	0.858	0.871	0.846	0.854	0.861	0.866	0.860
Na	0.027	0.035	0.028	0.021	0.023	0.020	0.036	0.065	0.032	0.037	0.048	0.018	0.036	0.032	0.050	0.040	0.046	0.065	0.068
K	0.002	0.000	0.000	0.002	0.002	0.002	0.001	0.002	0.003	0.000	0.000	0.002	0.001	0.002	0.003	0.000	0.000	0.000	0.000
Total	4.012	4.019	4.016	4.014	4.019	4.015	4.025	4.014	4.014	4.008	4.020	3.994	4.014	4.008	4.014	4.013	4.027	4.021	4.014
En	41.5	36.6	41.1	37.9	42.1	42.7	34.1	36.2	40.2	39.1	39.7	36.0	36.6	36.3	34.9	36.3	34.9	36.0	33.5
Fs	12.7	17.7	12.7	16.4	13.7	11.2	22.2	18.0	13.6	14.9	14.8	19.2	19.1	17.1	19.6	17.9	19.2	17.8	19.5
Wo	45.8	45.7	46.3	45.7	44.2	46.1	43.7	45.8	46.2	46.0	45.5	44.8	44.3	46.5	45.4	45.8	45.9	46.2	46.9

Appendix 4d.ii pyroxenes

Sample	BR27	MR2	MR2	MR2	MR2	MR2	MR2	MR2	BR22	BR22	BM8 core	BM8	BM8	BM8	BM8	BCH2	BCH2	AM5	AM5
Lithology	B-H	B	B	B	B	B	B	B	B	B	B	B	B	B	B	B	B	B	B
SiO2	48.79	50.42	50.47	50.54	51.37	51.08	51.48	51.09	47.45	47.89	50.09	51.43	49.86	50.47	50.03	49.31	49.90	46.75	47.99
TiO2	2.58	0.77	1.23	1.28	0.97	0.73	0.86	1.19	2.86	2.74	1.26	1.50	1.25	1.45	1.41	1.85	1.46	3.32	2.77
Al2O3	3.05	2.82	3.40	3.23	2.74	2.78	2.63	2.49	3.88	4.39	4.44	2.61	4.76	4.69	3.99	3.62	1.82	4.53	4.54
Cr2O3	0.00	1.01	0.38	0.77	0.47	0.67	0.47	0.11	0.07	0.22	0.00	0.02	0.01	0.42	0.22	0.12	0.04	0.00	0.22
FeO	10.17	6.17	7.22	6.88	6.73	5.61	6.18	6.92	12.52	11.59	7.56	13.15	6.98	7.24	9.16	8.75	10.99	9.86	9.02
MnO	0.38	0.13	0.26	0.17	0.06	0.21	0.08	0.11	0.23	0.17	0.09	0.38	0.18	0.28	0.17	0.24	0.22	0.17	0.18
MgO	11.49	14.81	14.50	14.51	14.92	15.34	15.33	15.18	12.28	12.30	14.83	12.39	14.23	14.45	13.37	13.52	12.63	11.75	12.58
CaO	21.21	21.66	21.90	21.92	22.05	21.90	21.38	21.56	19.28	20.41	20.87	19.65	21.35	21.21	21.17	21.28	20.66	21.09	21.94
Na2O	0.92	0.13	0.31	0.25	0.54	0.24	0.29	0.28	0.03	0.73	0.76	0.66	0.60	0.49	0.34	0.37	0.32	0.48	0.46
K2O	0.00	0.00	0.00	0.00	0.01	0.00	0.16	0.00	0.00	0.00	0.00	0.00	0.00	0.00	0.00	0.00	0.00	0.00	0.00
Total	98.59	97.91	99.66	99.56	99.83	98.56	98.86	98.93	98.61	100.43	99.89	101.79	99.21	100.69	99.86	99.06	98.04	97.95	99.70
Per six Oxygens																			
Si	1.870	1.904	1.882	1.885	1.907	1.910	1.920	1.911	1.806	1.808	1.859	1.913	1.854	1.858	1.873	1.863	1.920	1.803	1.812
Ti	0.074	0.022	0.034	0.036	0.027	0.021	0.024	0.033	0.082	0.077	0.035	0.042	0.035	0.040	0.040	0.053	0.042	0.096	0.079
Al	0.138	0.126	0.149	0.142	0.120	0.123	0.116	0.110	0.174	0.194	0.194	0.114	0.209	0.203	0.176	0.161	0.083	0.206	0.202
Cr	0.000	0.030	0.011	0.023	0.014	0.020	0.014	0.003	0.002	0.007	0.000	0.001	0.000	0.012	0.007	0.004	0.001	0.000	0.007
Fe2+	0.326	0.195	0.225	0.215	0.209	0.175	0.193	0.217	0.398	0.365	0.234	0.409	0.217	0.223	0.287	0.276	0.354	0.318	0.285
Mn	0.013	0.004	0.008	0.005	0.002	0.007	0.003	0.003	0.008	0.006	0.003	0.012	0.006	0.009	0.005	0.008	0.007	0.006	0.006
Mg	0.657	0.834	0.806	0.807	0.825	0.855	0.852	0.846	0.709	0.691	0.795	0.687	0.788	0.793	0.746	0.761	0.724	0.676	0.708
Ca	0.871	0.877	0.875	0.876	0.877	0.878	0.854	0.864	0.788	0.824	0.830	0.783	0.851	0.837	0.849	0.861	0.852	0.872	0.888
Na	0.068	0.009	0.022	0.018	0.039	0.017	0.021	0.020	0.051	0.052	0.054	0.048	0.043	0.035	0.025	0.027	0.024	0.036	0.034
K	0.000	0.000	0.000	0.000	0.000	0.000	0.008	0.000	0.001	0.000	0.000	0.000	0.000	0.000	0.000	0.000	0.000	0.000	0.000
Total	4.017	4.001	4.012	4.007	4.020	4.007	4.006	4.009	4.019	4.024	4.004	4.009	4.003	4.010	4.008	4.016	4.008	4.015	4.021
En	35.2	43.7	42.1	42.4	43.1	44.7	44.8	43.8	37.3	36.6	42.7	36.3	42.3	42.6	39.5	39.9	37.4	36.1	37.5
Fs	18.2	10.4	12.2	11.6	11.0	9.5	10.3	11.4	21.3	19.7	12.7	22.3	12.0	12.5	15.5	14.9	18.6	17.3	15.4
Wo	46.7	45.9	45.7	46.0	45.8	45.8	44.9	44.8	41.4	43.7	44.6	41.4	45.7	45.0	45.0	45.2	44.0	46.6	47.1

Appendix 4d.ii pyroxenes

Sample	C4	C4	MR37	MR29	MR29	BM61	BM61	BM61	W4	W4	W4	CA3B	CA3B
Lithology	B	B	H	M	M	T	T	T	SMT	SMT	SMT	CMT	CMT
SiO2	45.57	44.45	48.85	49.43	50.36	48.71	49.14	49.30	50.51	51.78	50.50	50.16	52.10
TiO2	3.57	4.87	2.48	2.08	1.85	0.67	0.73	0.49	1.18	0.67	1.12	0.84	0.45
Al2O3	5.85	6.14	4.32	2.99	2.36	2.07	2.18	1.78	2.38	2.28	4.07	3.59	1.92
Cr2O3	0.00	0.02	0.02	0.00	0.00	0.03	0.02	0.00	0.03	0.27	0.88	0.00	0.07
FeO	12.30	10.42	10.18	8.94	9.16	17.02	17.36	16.50	10.14	6.91	7.16	7.49	7.25
MnO	0.22	0.22	0.17	0.25	0.29	0.60	0.60	0.53	0.17	0.19	0.15	0.18	0.18
MgO	10.97	10.18	12.54	12.82	12.71	6.75	6.85	7.19	14.03	16.60	16.19	15.02	16.86
CaO	18.82	21.46	21.24	21.55	21.42	21.04	20.57	20.89	19.72	20.40	19.05	21.09	20.35
Na2O	0.73	0.69	0.86	0.82	1.05	1.11	1.18	0.94	0.20	0.21	0.24	0.25	0.16
K2O	0.06	0.00	0.00	0.03	0.04	0.00	0.00	0.04	0.00	0.00	0.00	0.04	0.00
Total	98.09	98.45	100.66	98.91	99.24	98.00	98.63	97.66	98.36	99.31	99.36	98.66	99.34
Per six Oxygens													
Si	1.769	1.722	1.824	1.877	1.906	1.941	1.944	1.962	1.919	1.922	1.873	1.886	1.933
Ti	0.104	0.142	0.070	0.059	0.053	0.020	0.022	0.015	0.034	0.019	0.031	0.024	0.013
Al	0.268	0.280	0.189	0.134	0.105	0.097	0.102	0.084	0.107	0.100	0.178	0.159	0.084
Cr	0.000	0.001	0.001	0.000	0.000	0.001	0.001	0.000	0.001	0.008	0.026	0.000	0.002
Fe2+	0.399	0.338	0.316	0.284	0.290	0.567	0.574	0.549	0.322	0.214	0.222	0.235	0.225
Mn	0.007	0.007	0.005	0.008	0.009	0.020	0.020	0.018	0.005	0.006	0.005	0.006	0.006
Mg	0.635	0.588	0.698	0.726	0.717	0.401	0.404	0.426	0.795	0.918	0.895	0.841	0.932
Ca	0.783	0.891	0.849	0.877	0.869	0.898	0.872	0.891	0.803	0.811	0.757	0.849	0.809
Na	0.055	0.052	0.062	0.060	0.077	0.086	0.091	0.073	0.015	0.015	0.017	0.018	0.011
K	0.003	0.000	0.000	0.001	0.002	0.000	0.000	0.002	0.000	0.000	0.000	0.002	0.000
Total	4.022	4.021	4.014	4.027	4.028	4.033	4.029	4.019	4.001	4.013	4.003	4.021	4.017
En	34.8	32.2	37.4	38.3	38.0	21.2	21.6	22.6	41.3	47.1	47.6	43.6	47.3
Fs	22.3	18.9	17.2	15.4	15.9	31.1	31.8	30.1	17.0	11.3	12.1	12.5	11.7
Wo	42.9	48.9	45.4	46.3	46.1	47.6	46.6	47.3	41.7	41.6	40.3	44.0	41.0

Appendix 4d.ii pyroxenes

Sample	BM10	BR5	BR5	BR5	BR5	MR9	MR9	MR9	MR9	MR9	MR9	BM2	BM2	BM2	BM2 gmass	BM51	BM51
Lithology	B	B	B	B	B	B	B	B	B	B	B	B	B	B	B	B	B
SiO2	56.97	50.17	50.76	52.59	55.23	50.20	52.50	51.25	49.81	48.71	56.97	49.44	49.91	49.51	52.15	53.77	54.29
TiO2	0.25	0.05	0.07	0.04	0.13	0.06	0.13	0.09	0.07	0.06	0.25	0.00	0.12	0.02	0.10	0.13	0.12
Al2O3	25.86	30.49	30.55	28.93	26.41	28.99	28.47	28.74	30.68	31.27	25.86	28.81	27.49	29.47	26.53	25.73	26.11
FeO	0.68	0.81	0.86	0.98	0.71	1.53	0.62	0.91	0.68	0.45	0.68	0.81	1.83	0.89	0.90	0.88	0.83
MnO	0.00	0.02	0.03	0.00	0.00	0.13	0.16	0.07	0.00	0.03	0.00	0.01	0.00	0.03	0.00	0.14	0.00
MgO	0.17	0.39	0.18	0.29	0.15	0.43	0.30	0.35	0.18	0.01	0.17	0.61	0.72	0.35	0.55	0.67	0.40
CaO	9.22	13.90	14.32	12.33	9.79	14.06	12.98	13.53	13.26	15.37	9.22	13.83	12.32	14.61	10.85	11.02	11.21
Na2O	6.20	3.66	3.71	4.42	5.04	3.30	4.40	3.77	3.83	3.08	6.20	3.25	3.89	3.22	4.82	4.76	4.63
K2O	0.31	0.10	0.18	0.02	1.26	0.05	0.09	0.16	0.09	0.13	0.31	0.00	0.15	0.08	0.21	0.23	0.17
SUM	99.67	99.59	100.66	99.58	98.70	98.75	99.64	98.86	98.60	99.11	99.67	96.76	96.43	98.18	96.11	97.32	97.76
Per Eight Oxygens																	
Si	2.570	2.295	2.305	2.394	2.533	2.324	2.401	2.370	2.306	2.255	2.574	2.320	2.370	2.307	2.441	2.507	2.516
Ti	0.008	0.002	0.002	0.001	0.004	0.002	0.004	0.003	0.002	0.002	0.008	0.000	0.004	0.001	0.004	0.004	0.004
Al	1.376	1.644	1.635	1.550	1.428	1.582	1.535	1.566	1.674	1.707	1.377	1.589	1.539	1.620	1.463	1.413	1.425
Fe2+	0.026	0.030	0.033	0.037	0.027	0.059	0.024	0.035	0.026	0.017	0.026	0.031	0.071	0.035	0.041	0.035	0.032
Mn	0.000	0.001	0.001	0.000	0.000	0.005	0.006	0.003	0.000	0.001	0.000	0.000	0.000	0.001	0.000	0.005	0.000
Mg	0.012	0.026	0.012	0.020	0.010	0.030	0.021	0.024	0.012	0.001	0.012	0.042	0.051	0.024	0.037	0.047	0.028
Ca	0.446	0.679	0.695	0.598	0.481	0.697	0.636	0.670	0.658	0.762	0.446	0.699	0.626	0.730	0.544	0.551	0.559
Na	0.543	0.323	0.326	0.388	0.448	0.296	0.390	0.338	0.344	0.276	0.543	0.297	0.357	0.290	0.437	0.429	0.415
K	0.018	0.006	0.010	0.027	0.073	0.003	0.005	0.009	0.005	0.008	0.018	0.000	0.009	0.005	0.012	0.013	0.010
Total	4.999	5.006	5.019	5.015	5.004	4.998	5.022	5.018	5.029	5.031	5.008	4.978	5.027	5.013	4.979	5.004	5.004
An	44.3	67.4	67.4	59.0	46.0	70.0	61.7	65.9	65.3	72.8	44.3	70.2	63.1	71.2	54.8	55.4	56.8
Ab	53.9	32.0	31.6	38.3	44.7	29.7	37.8	33.2	34.1	26.4	53.9	29.8	36.0	28.3	44.0	43.2	42.2
Or	1.8	0.6	1.0	2.7	7.3	0.3	0.5	0.9	0.5	0.7	1.8	0.0	0.9	0.5	1.2	1.3	1.0

Appendix 4d.iii feldspars

Sample	BM51	BM51 p core	BM51 p core	BM51 p core	BM51 p rim	BM51 gmass	MR2	MR2	MR2	MR2	MR2	MR2	MR2	MR2	BR22	BR22	BR22
Lithology	B	B	B	B	B	B	B	B	B	B	B	B	B	B	B	B	B
SiO2	54.77	49.95	51.13	50.83	55.31	55.10	49.26	50.17	49.34	49.36	51.47	53.41	51.12	51.43	50.11	50.59	52.03
TiO2	0.21	0.10	0.00	0.01	0.21	0.23	0.19	0.07	0.05	0.06	0.08	0.17	0.10	0.13	0.21	0.03	0.23
Al2O3	26.29	29.38	30.21	29.78	26.74	26.16	29.95	28.43	30.34	31.15	30.27	28.15	30.17	29.99	28.65	29.13	29.51
FeO	0.81	0.60	0.45	0.54	1.35	1.33	1.16	1.11	0.85	0.76	0.55	0.90	0.64	0.69	0.85	0.53	0.72
MnO	0.00	0.00	0.13	0.06	0.00	0.00	0.00	0.00	0.00	0.00	0.00	0.00	0.00	0.00	0.05	0.00	0.00
MgO	0.45	0.22	0.39	0.36	0.83	0.63	0.27	0.27	0.22	0.48	0.03	0.03	0.14	0.08	0.25	0.14	0.18
CaO	11.21	13.99	14.25	14.03	11.44	11.23	14.89	13.51	15.07	14.95	13.04	10.73	13.28	13.44	13.54	14.34	13.55
Na2O	4.44	3.53	3.38	3.75	5.02	5.02	2.86	3.55	2.75	3.11	4.00	5.15	4.08	4.18	3.72	3.50	3.76
K2O	0.29	0.97	0.00	0.04	0.31	0.24	0.12	0.20	0.16	0.12	0.19	0.27	0.16	0.12	0.16	0.06	0.16
SUM	98.47	98.73	99.94	99.39	101.19	99.94	98.69	97.30	98.78	99.99	99.63	98.81	99.69	100.06	97.54	98.31	100.14
Per Eight Oxygens																	
Si	2.518	2.332	2.333	2.336	2.485	2.505	2.290	2.359	2.290	2.265	2.352	2.435	2.339	2.345	2.347	2.350	2.369
Ti	0.007	0.003	0.000	0.000	0.007	0.009	0.007	0.002	0.002	0.002	0.003	0.006	0.003	0.004	0.008	0.001	0.008
Al	1.423	1.617	1.625	1.610	1.418	1.401	1.642	1.576	1.659	1.685	1.631	1.513	1.628	1.612	1.584	1.595	1.584
Fe2+	0.031	0.023	0.017	0.020	0.051	0.051	0.045	0.044	0.033	0.029	0.021	0.034	0.024	0.026	0.034	0.021	0.027
Mn	0.000	0.000	0.005	0.002	0.000	0.000	0.000	0.000	0.000	0.000	0.000	0.000	0.000	0.000	0.002	0.000	0.000
Mg	0.031	0.015	0.026	0.023	0.055	0.043	0.018	0.019	0.015	0.033	0.002	0.002	0.010	0.005	0.017	0.010	0.012
Ca	0.553	0.700	0.697	0.690	0.549	0.547	0.742	0.681	0.749	0.735	0.638	0.524	0.651	0.657	0.679	0.713	0.661
Na	0.397	0.320	0.299	0.333	0.437	0.443	0.258	0.323	0.247	0.277	0.355	0.455	0.362	0.370	0.337	0.315	0.332
K	0.017	0.006	0.000	0.002	0.018	0.014	0.007	0.012	0.010	0.007	0.011	0.016	0.009	0.007	0.010	0.003	0.009
Total	4.977	5.016	5.002	5.016	5.020	5.013	5.009	5.016	5.005	5.033	5.013	5.022	5.029	5.031	5.018	5.008	5.002
An	57.2	68.2	70.0	67.3	54.7	54.5	73.7	67.0	74.5	72.1	63.6	52.7	63.7	63.6	66.2	69.2	66.0
Ab	41.1	31.2	30.0	32.5	43.5	44.1	25.6	31.8	24.6	27.2	35.3	45.7	35.4	35.8	32.8	30.6	33.1
Or	1.8	0.6	0.0	0.2	1.8	1.4	0.7	1.2	1.0	0.7	1.1	1.6	0.9	0.7	1.0	0.3	0.9

Appendix 4d.iii feldspars

Sample	BR22 p core	BR22 p rim	BM8	BM8	BM8	AM5	AM5	C4	C4	BR27	BR27	BR27	BR27	BR19	BR19	MR37 p rim	MR37 p core
Lithology	B	B	B	B	B	B	B	B	B	B-H	B-H	B-H	B-H	H	H	H	H
SIO2	52.18	49.49	48.95	49.98	51.45	49.86	51.79	50.55	54.62	53.45	54.52	53.00	54.91	55.36	54.54	56.94	56.84
TIO2	0.00	0.21	0.13	0.10	0.07	0.05	0.11	0.12	0.17	0.16	0.22	0.29	0.12	0.26	0.34	0.10	0.30
AI2O3	23.31	28.51	29.51	29.55	29.73	31.06	30.42	30.44	28.02	26.28	27.53	26.08	26.41	27.02	24.25	27.85	27.45
FeO	0.44	0.47	1.63	0.79	0.91	0.41	0.47	0.53	0.62	0.70	0.58	0.48	0.55	0.53	2.84	0.52	0.53
MnO	0.03	0.00	0.09	0.01	0.05	0.03	0.04	0.01	0.00	0.00	0.00	0.08	0.11	0.01	0.00	0.00	0.00
MgO	0.34	0.02	1.66	0.62	0.59	0.10	0.11	0.12	0.04	0.13	0.34	0.07	0.35	0.15	0.78	0.21	0.15
CaO	13.17	14.14	14.17	13.83	14.26	14.78	13.13	13.66	10.69	10.34	11.04	10.38	9.92	9.58	7.95	10.71	10.56
Na2O	4.19	3.21	2.84	3.29	3.55	3.27	4.30	3.57	5.66	5.24	5.28	5.40	5.61	5.81	6.12	5.51	5.32
K2O	0.00	0.08	0.01	0.14	0.08	0.15	0.20	0.10	0.27	0.21	0.15	0.24	0.22	0.31	0.91	0.39	0.36
SUM	93.64	96.13	98.98	98.29	100.67	99.71	100.57	99.10	100.09	96.49	99.66	96.01	98.19	99.02	97.73	102.24	101.51
Per Eight Oxygens																	
SI	2.405	2.348	2.267	2.322	2.338	2.288	2.347	2.325	2.472	2.504	2.475	2.499	2.523	2.521	2.533	2.521	2.519
TI	0.000	0.008	0.004	0.003	0.002	0.002	0.004	0.004	0.006	0.005	0.008	0.010	0.004	0.009	0.010	0.004	0.009
AI	1.538	1.595	1.611	1.618	1.592	1.680	1.625	1.651	1.495	1.451	1.473	1.449	1.430	1.450	1.325	1.440	1.447
Fe2+	0.017	0.018	0.063	0.031	0.035	0.016	0.018	0.020	0.023	0.027	0.022	0.019	0.021	0.020	0.110	0.019	0.020
Mn	0.001	0.000	0.004	0.001	0.002	0.001	0.002	0.000	0.000	0.000	0.000	0.003	0.004	0.000	0.000	0.000	0.000
Mg	0.023	0.002	0.115	0.043	0.040	0.007	0.007	0.008	0.003	0.009	0.023	0.005	0.024	0.010	0.049	0.013	0.009
Ca	0.650	0.719	0.703	0.688	0.694	0.727	0.638	0.673	0.518	0.519	0.537	0.524	0.488	0.468	0.395	0.508	0.505
Na	0.374	0.296	0.253	0.297	0.312	0.291	0.378	0.318	0.497	0.476	0.464	0.494	0.499	0.513	0.540	0.473	0.465
K	0.000	0.005	0.000	0.008	0.004	0.009	0.012	0.006	0.016	0.012	0.009	0.015	0.013	0.018	0.055	0.023	0.020
Total	5.008	4.991	5.020	5.011	5.019	5.020	5.031	5.007	5.030	5.003	5.011	5.018	5.006	5.009	5.017	5.001	4.995
An	63.5	70.5	73.5	69.3	68.7	70.8	62.1	67.5	50.3	51.5	53.2	50.7	48.8	46.8	39.9	50.6	51.0
Ab	36.5	29.0	26.5	29.9	30.9	28.3	36.8	31.9	48.2	47.3	45.9	47.8	49.9	51.4	54.5	47.1	47.0
Or	0.0	0.5	0.0	0.8	0.4	0.9	1.1	0.6	1.5	1.2	0.9	1.5	1.3	1.8	5.6	2.3	2.0

Appendix 4d.iii feldspars

Sample	MR37	MR37	MR37	MR37	MR37	MR37	MR37	MR37	MR29	MR29	BM61	BM61	BM61	BM61	BM61	BM61
	p core	p core	p core	p core	p rim	p core	p rim	p core	gmass	gmass						
Lithology	H	H	H	H	H	H	H	H	M	M	T	T	T	T	T	T
SiO2	56.12	55.28	56.31	56.50	55.99	54.90	54.73	55.50	63.61	62.89	64.16	65.67	64.55	64.57	65.36	66.00
TiO2	0.04	0.08	0.05	0.17	0.27	0.18	0.17	0.08	0.21	0.10	0.04	0.04	0.05	0.03	0.05	0.08
Al2O3	27.22	27.11	25.97	26.55	25.84	26.95	25.16	27.13	23.55	21.24	24.67	21.47	19.45	18.40	19.64	19.78
FeO	0.35	0.47	0.44	0.58	1.02	0.53	1.37	0.50	0.52	0.26	0.44	1.74	0.43	0.30	0.29	0.34
MnO	0.02	0.06	0.00	0.00	0.06	0.14	0.01	0.00	0.06	0.00	0.03	0.03	0.00	0.00	0.01	0.02
MgO	0.37	0.36	0.22	0.36	0.34	0.20	0.52	0.29	0.00	0.00	0.04	0.00	0.00	0.00	0.00	0.00
CaO	10.75	10.61	9.52	9.82	9.55	10.67	9.09	10.55	4.13	4.19	1.24	0.55	0.17	0.10	0.25	0.25
Na2O	5.52	5.58	5.79	5.77	5.88	5.35	5.61	5.55	7.09	5.88	8.79	5.27	2.64	6.02	5.56	5.33
K2O	0.33	0.39	0.45	0.24	0.37	0.28	0.33	0.32	1.61	3.62	0.90	5.28	12.70	8.39	8.92	7.66
SUM	100.72	99.94	98.75	99.99	99.31	99.20	96.99	99.92	100.78	98.18	100.31	100.05	99.99	97.81	100.08	99.46
Per Eight Oxygens																
Si	2.516	2.503	2.567	2.546	2.550	2.504	2.550	2.514	2.796	2.854	2.806	2.920	2.954	2.981	2.952	2.971
Ti	0.001	0.003	0.002	0.006	0.009	0.006	0.006	0.003	0.007	0.003	0.001	0.001	0.002	0.001	0.002	0.003
Al	1.439	1.447	1.395	1.411	1.387	1.449	1.382	1.448	1.220	1.136	1.272	1.125	1.049	1.001	1.046	1.050
Fe2+	0.013	0.018	0.017	0.022	0.039	0.020	0.054	0.019	0.019	0.010	0.016	0.065	0.016	0.012	0.011	0.013
Mn	0.001	0.002	0.000	0.000	0.002	0.006	0.001	0.000	0.002	0.000	0.001	0.001	0.000	0.000	0.000	0.001
Mg	0.025	0.024	0.015	0.024	0.023	0.013	0.036	0.020	0.000	0.000	0.003	0.000	0.000	0.000	0.000	0.000
Ca	0.516	0.515	0.465	0.474	0.466	0.522	0.454	0.512	0.195	0.204	0.058	0.026	0.008	0.005	0.012	0.012
Na	0.480	0.490	0.512	0.504	0.519	0.473	0.507	0.469	0.604	0.517	0.745	0.454	0.234	0.539	0.487	0.465
K	0.019	0.022	0.026	0.014	0.021	0.016	0.019	0.019	0.090	0.210	0.050	0.299	0.741	0.494	0.514	0.440
Total	5.010	5.024	4.999	5.001	5.016	5.009	5.009	5.004	4.934	4.937	4.954	4.893	5.007	5.034	5.024	4.954
An	50.8	50.1	46.4	47.8	46.3	51.6	46.3	51.2	21.9	21.9	6.8	3.4	0.8	0.5	1.2	1.3
Ab	47.3	47.7	51.0	50.8	51.6	46.8	51.7	46.9	68.0	55.6	87.3	58.3	23.8	51.9	48.1	50.7
Or	1.9	2.1	2.6	1.4	2.1	1.6	1.9	1.9	10.2	22.5	5.9	38.4	75.3	47.6	50.7	48.0

Appendix 4d.iii feldspars

Sample	W4	W4	W4	W4	W4	CA3B	CA3B	CA3B	CA3B	CA3B	CA3B	CA3B	CA19	CA19	CA19	CA19
	p core	p core	p core	gmass	gmass	p core	p rim	p core	p rim	gmass	gmass	gmass	p core	p rim	p core	p rim
Lithology	SMT	SMT	SMT	SMT	SMT	CMT	CMT	CMT	CMT	CMT	CMT	CMT	CMT	CMT	CMT	CMT
SiO2	47.23	46.10	46.48	50.43	50.41	45.69	49.03	46.51	54.80	49.89	51.28	50.31	50.56	47.51	48.63	48.86
TiO2	0.01	0.05	0.03	0.06	0.08	0.00	0.04	0.07	0.09	0.09	0.14	0.03	0.00	0.04	0.02	0.04
Al2O3	33.14	34.40	33.49	30.67	31.18	35.54	31.06	32.52	28.00	31.32	29.94	30.39	28.49	32.73	31.68	32.32
FeO	0.52	0.09	0.47	0.39	0.51	0.52	0.56	0.42	0.87	0.80	0.82	0.67	0.38	0.35	0.44	0.46
MnO	0.04	0.07	0.01	0.00	0.00	0.00	0.00	0.00	0.00	0.05	0.02	0.00	0.01	0.02	0.01	0.17
MgO	0.18	0.09	0.18	0.17	0.21	0.20	0.21	0.14	0.09	0.11	0.17	0.25	0.22	0.14	0.16	0.16
CaO	17.05	17.60	17.69	14.30	14.26	17.90	15.52	16.93	10.96	14.75	13.50	14.18	14.61	16.55	15.34	15.64
Na2O	1.80	1.29	1.73	3.37	3.29	1.42	2.74	1.82	5.52	3.18	3.67	3.51	1.96	1.97	2.89	2.86
K2O	0.06	0.05	0.06	0.17	0.18	0.04	0.05	0.00	0.17	0.05	0.07	0.08	0.07	0.04	0.04	0.07
SUM	100.03	99.74	100.14	99.56	100.12	101.31	99.21	98.41	100.50	100.24	99.61	99.42	96.30	99.35	99.21	100.58
Per Eight Oxygens																
Si	2.173	2.125	2.142	2.312	2.284	2.081	2.265	2.174	2.458	2.279	2.347	2.312	2.382	2.195	2.246	2.229
Ti	0.000	0.002	0.001	0.002	0.003	0.000	0.001	0.002	0.003	0.003	0.005	0.001	0.000	0.001	0.001	0.001
Al	1.797	1.870	1.819	1.658	1.666	1.908	1.692	1.792	1.480	1.687	1.615	1.647	1.583	1.782	1.725	1.738
Fe2+	0.020	0.003	0.018	0.015	0.019	0.020	0.022	0.016	0.033	0.031	0.031	0.026	0.015	0.014	0.017	0.018
Mn	0.001	0.003	0.000	0.000	0.000	0.000	0.000	0.000	0.000	0.002	0.001	0.000	0.000	0.001	0.000	0.007
Mg	0.012	0.006	0.012	0.012	0.014	0.014	0.014	0.010	0.006	0.007	0.012	0.017	0.015	0.010	0.011	0.011
Ca	0.840	0.869	0.873	0.703	0.692	0.874	0.768	0.848	0.527	0.722	0.662	0.698	0.738	0.819	0.759	0.764
Na	0.161	0.115	0.155	0.300	0.289	0.125	0.245	0.165	0.480	0.282	0.326	0.313	0.179	0.176	0.259	0.253
K	0.004	0.003	0.004	0.010	0.010	0.002	0.003	0.000	0.010	0.003	0.004	0.005	0.004	0.002	0.002	0.004
Total	5.010	4.997	5.026	5.011	5.005	5.027	5.011	5.010	5.028	5.016	5.005	5.021	4.918	5.002	5.022	5.028
An	83.7	88.0	84.7	69.4	69.8	87.2	75.6	83.7	51.8	71.7	66.8	68.7	80.1	82.1	74.4	74.8
Ab	16.0	11.7	15.0	29.6	29.1	12.5	24.1	16.3	47.2	28.0	32.8	30.8	19.4	17.7	25.4	24.8
Or	0.4	0.3	0.3	1.0	1.0	0.2	0.3	0.0	1.0	0.3	0.4	0.5	0.5	0.2	0.2	0.4

Appendix 4d.iii feldspars

	Chrome spinels								
	MR9	BR5	BR5	BR5	STA3	BM5	BM5	MR9	MR9
Lithology	B	B	B	B	B	B	B	B	B
SiO2	1.67	0.18	0.00	0.00	0.00	3.39	0.04	0.33	0.20
TiO2	0.85	13.25	0.34	0.37	4.22	5.72	15.57	0.68	0.67
Al2O3	31.78	4.64	15.61	15.47	21.42	22.19	6.89	37.87	35.80
Cr2O3	23.60	8.62	41.97	41.94	25.98	14.82	12.48	19.76	20.62
FeO	17.56	35.19	20.39	19.44	25.74	32.04	37.32	18.77	17.71
Fe2O3	7.74	29.56	9.25	7.60	10.94	10.91	18.85	7.57	9.37
MnO	0.11	0.40	0.27	0.28	0.30	0.21	0.38	0.14	0.29
NiO	0.00	0.15	0.15	0.15	0.23	0.02	0.26	0.10	0.08
MgO	13.20	5.09	8.31	8.35	7.49	6.32	5.24	12.55	12.52
CaO	0.11	0.07	0.00	0.02	0.04	1.88	0.03	0.00	0.00
Na2O	0.18	0.00	0.00	0.00	0.00	0.00	0.00	0.00	0.07
K2O	0.05	0.00	0.00	0.01	0.06	0.00	0.00	0.02	0.02
Total	96.83	97.15	96.29	95.23	96.42	97.50	97.06	97.79	97.35
Per 32 Oxygens									
Si	0.403	0.053	0.000	0.000	0.000	0.882	0.011	0.078	0.048
Ti	0.154	2.909	0.069	0.077	0.842	1.120	3.365	0.121	0.121
Al	9.062	1.597	4.986	5.061	6.701	6.809	2.335	10.564	10.109
Cr	4.513	1.989	8.989	9.201	5.450	3.050	2.836	3.696	3.904
Fe2+	3.553	8.591	4.619	4.512	5.712	6.975	8.971	3.715	3.548
Fe3+	1.409	6.492	1.886	1.587	2.185	2.137	4.076	1.347	1.688
Mn	0.022	0.099	0.062	0.066	0.067	0.046	0.093	0.028	0.059
Ni	0.000	0.035	0.033	0.033	0.049	0.004	0.060	0.019	0.015
Mg	4.758	2.214	3.355	3.453	2.962	2.452	2.244	4.426	4.469
Ca	0.029	0.022	0.000	0.006	0.011	0.524	0.009	0.000	0.000
Na	0.083	0.000	0.000	0.000	0.000	0.000	0.000	0.000	0.033
K	0.015	0.000	0.000	0.004	0.020	0.000	0.000	0.006	0.006
Total	24.000	24.000	24.000	24.000	24.000	24.000	24.000	24.000	24.000

Appendix 4d.iv oxide minerals

	Magnetites										Ilmenites					
	MR9	BM2	BM2	BR22	C4	MR37	MR29	BM61	BM61	BM61	BM10	BM10	MR2	MR2	MR2	MR29
Lithology	B	B	B	B	B	H	M	T	T	T	B	B	B	B	B	M
SiO2	1.65	1.21	3.38	3.83	0.20	3.55	0.67	0.60	0.39	0.50	7.20	2.51	1.57	0.19	0.19	0.31
TiO2	29.38	28.20	27.52	23.62	28.49	23.52	2.49	1.16	14.72	8.63	37.90	47.56	48.10	53.30	51.97	47.42
Al2O3	1.71	1.50	2.57	3.42	2.40	2.19	2.38	0.15	0.26	0.18	1.80	0.74	0.45	0.01	0.00	0.21
Cr2O3	0.00	0.26	0.31	0.20	0.46	0.27	0.00	0.01	0.03	0.00	0.10	0.11	0.00	0.00	0.01	0.00
FeO	53.93	53.63	53.40	52.90	51.62	49.70	31.34	29.73	37.16	34.71	27.99	35.46	36.99	39.45	41.06	33.89
Fe2O3	2.78	8.11	4.24	9.86	5.57	12.42	57.98	61.89	34.76	46.00	11.29	1.85	4.50	1.17	0.00	9.68
MnO	2.14	0.50	0.84	0.96	1.92	1.05	0.28	0.43	4.16	2.30	0.57	1.21	0.55	0.59	0.51	1.49
NiO	0.00	0.00	0.00	0.00	0.02	0.00	0.03	0.00	0.00	0.00	0.00	0.11	0.00	0.01	0.00	0.05
MgO	0.48	1.55	1.89	0.43	1.08	1.79	0.70	0.00	0.00	0.00	6.28	4.04	3.55	4.46	0.32	4.14
CaO	0.14	0.11	0.48	0.75	0.02	0.44	0.14	0.08	0.27	0.18	0.48	0.35	0.42	0.07	0.02	0.10
Na2O	0.36	0.24	0.54	0.47	0.09	0.57	0.00	0.15	0.00	0.00	0.32	0.27	0.15	0.00	0.00	0.00
K2O	0.01	0.01	0.03	0.07	0.02	0.06	0.20	0.09	0.40	0.07	0.27	0.03	0.01	0.02	0.00	0.02
Total	94.35	95.32	95.17	96.51	92.98	95.57	96.21	94.29	92.15	92.57	94.21	94.23	96.29	99.27	94.08	97.31
Per 32 oxygens											Per 6 oxygens					
Si	0.517	0.369	1.011	1.139	0.063	1.062	0.209	0.195	0.128	0.164	0.177	0.064	0.040	0.005	0.005	0.008
Ti	6.948	6.470	6.185	5.284	6.797	5.296	0.584	0.283	3.622	2.132	0.703	0.913	0.915	0.985	1.030	0.898
Al	0.634	0.539	0.905	1.199	0.898	0.773	0.876	0.057	0.100	0.070	0.052	0.022	0.013	0.000	0.000	0.006
Cr	0.000	0.063	0.072	0.047	0.116	0.064	0.000	0.003	0.008	0.000	0.002	0.002	0.000	0.000	0.000	0.000
Fe2+	14.183	13.684	13.348	13.158	13.695	12.444	8.180	8.069	10.168	9.534	0.577	0.757	0.782	0.811	0.905	0.713
Fe3+	0.658	1.862	0.953	2.206	1.329	2.800	13.617	15.116	8.559	11.368	0.209	0.035	0.086	0.022	0.000	0.183
Mn	0.570	0.128	0.211	0.241	0.516	0.267	0.074	0.118	1.153	0.640	0.012	0.026	0.012	0.012	0.011	0.032
Ni	0.000	0.000	0.000	0.000	0.005	0.000	0.008	0.000	0.000	0.000	0.000	0.002	0.000	0.000	0.000	0.001
Mg	0.223	0.703	0.841	0.191	0.511	0.799	0.326	0.000	0.000	0.000	0.231	0.154	0.134	0.163	0.013	0.155
Ca	0.048	0.036	0.152	0.239	0.007	0.142	0.047	0.028	0.095	0.063	0.013	0.010	0.011	0.002	0.001	0.003
Na	0.218	0.139	0.311	0.270	0.055	0.329	0.000	0.094	0.000	0.000	0.015	0.013	0.007	0.000	0.000	0.000
K	0.002	0.005	0.011	0.027	0.008	0.024	0.080	0.037	0.167	0.029	0.009	0.001	0.000	0.001	0.000	0.001
Total	24.000	24.000	24.000	24.000	24.000	24.000	24.000	24.000	24.000	24.000	2.000	2.000	2.000	2.000	1.965	2.000

DURHAM

Appendix 4d.iv oxide minerals

Sodium contamination of fused X-ray Fluorescence discs; a Departmental soap.

A.C. Kerr and R. Hardy

Sodium has always been a notoriously difficult element to analyse by XRF. Analysts have for years struggled with poor sodium calibration lines and as a result obtained many dubious sodium values.

It is well known fact that, due to perspiration, human skin surfaces possess significant amounts of sodium. Exactly how much of this sodium gets on to fusion discs (even with careful handling) had not really been quantified. In Durham, attempts to clean the analytical surfaces of standard glass fusion discs with organic solvents did not improve the calibration line. However it was pointed out to one of us (RGH) that organic solvents would not remove all the contaminating sodium, it being mostly present, on skin, in the form of NaCl. It was suggested to us that we use distilled water (with or without a commercial washing-up liquid*) to clean the analytical surfaces of our fusion discs. Twenty international standard fusion discs were wiped with distilled water and dried, the result was a near perfect sodium calibration line of count rates vs. standard values.

Quantifying the contamination

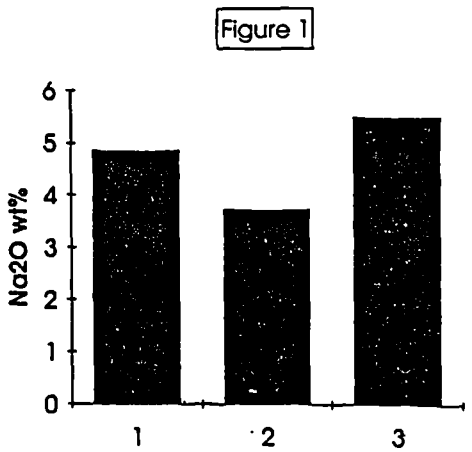
The fused disc of a sample of basalt from the Isle of Mull, Scotland (BR1), which had been analysed several times before, was again analysed without cleaning using this new calibration, and gave a sodium value of 4.86%. The disc was then cleaned with distilled water, dried and analysed again, whereupon it gave a sodium value of 3.70%. This disc was then deliberately contaminated, by handling the analytical surface for several minutes and analysed again, giving a value of 5.46%, a total 1.8% higher than the cleaned disc. (Fig 1)

All the other major elements with the exception of potassium and possibly phosphorus are for the most part unaffected by handling the analytical surfaces. Contact with skin results in the addition of potassium to the analytical surface, with the result that potassium varies from 0.30% on contaminated discs to 0.22% on cleaned discs. (Fig 2)

Conclusions

Fused glass XRF discs are particularly susceptible to sodium and potassium contamination from skin surfaces. Consequently care should always be taken to avoid touching the analytical surfaces of fused glass discs. Discs which are analysed regularly e.g. international standards should be cleaned with distilled water or a detergent solution on a frequent basis.

* RGH (the elder author) prefers the use of "Fairy Liquid" and water, as it is also kind to his hands; and has nothing whatsoever to do with the fact that he has a relation who works for Proctor and Gamble!



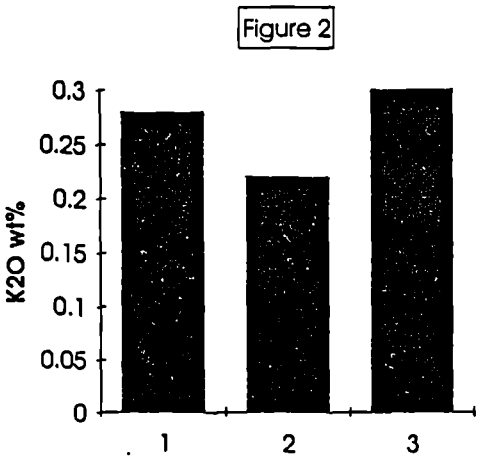


Figure 1 showing sodium analyses for three XRF runs. 1; Uncleaned disc, 2; Disc surface cleaned with distilled water, 3; Disc surface deliberately handled.

Figure 2 showing potassium analyses for the same three XRF runs as fig. 1.

This copy belongs to A.C. Kerr Thesis, Durham Univ 1993

Journal of the Geological Society, London, Vol. **150,** 1993, pp. 763–769, 7 figs. Printed in Northern Ireland

Elemental evidence for an enriched small-fraction-melt input into Tertiary Mull basalts, Western Scotland

A. C. KERR

Department of Geological Sciences, University of Durham, South Road, Durham, DH1 3LE, UK

Abstract: Continental basalts enriched in the incompatible trace elements have recently been interpreted as mixtures of depleted asthenospheric melt and an enriched small-fraction-melt lithospheric component. Hebridean Tertiary basalts are relatively depleted in incompatible trace elements, and it has been suggested that this is because the enriched lithospheric component had already been extracted beneath that region, during the Permo-Carboniferous. It was therefore not widely available to contaminate Tertiary magmas. A flow-by-flow geochemical study of the Mull lava succession has nevertheless revealed the presence of lava flows relatively enriched in the incompatible trace elements, at the base of the succession, in some parts of the island.

Fractional crystallization, contamination by Archean and Moinian crust, variation in the degree of mantle melting and an asthenospheric, ocean island basalt-like source, have all been ruled out as possible mechanisms of enrichment in favour of 5–10% contamination by an enriched, fusible, small-fraction-melt from the lithospheric mantle. The overall lack of basalts enriched in trace elements in the British Tertiary Igneous Province, argues strongly against the *widespread* presence of an enriched Tertiary lithospheric mantle below the Hebrides. The origin of the a sodic (rather than potassic) contaminant within the Hebridean lithosphere is also discussed.

Recent studies on continental mafic magma genesis have focused on the importance of small, low-temperature, melt fractions that are relatively enriched in incompatible trace elements. These are thought, through time, to have migrated from the convecting asthenosphere into the cold rigid continental lithosphere and solidified there (McKenzie 1989). Subsequent extension of the lithosphere, with some extra heating, may cause asthenospheric upwelling and decompression melting. This leads to the generation of basaltic magma in the asthenosphere, which migrates upwards through the lithosphere to the surface. In several parts of the world these magmas have been shown to pick up some of this enriched small-fraction-melt from the lithospheric mantle, thus modifying their asthenospheric compositions (e.g. Gibson *et al.* 1991; Ellam & Cox 1991).

The British Tertiary Igneous Province (BTIP)

Tertiary magmatism in western Britain is believed to have been caused by the arrival of a mantle plume below the North Atlantic region (White 1988). Most early volcanism occurred predominantly in regions, such as western Britain, where the lithosphere had already been substantially thinned in pre-Tertiary times (Thompson & Gibson 1991). The volcanism associated with these pre-existing, lithospheric thinspots ultimately led to a series of igneous centres along the west coast of Britain (Fig. 2a).

The basalts of the British Tertiary Igneous Province display a wide variation in the concentrations and ratios of incompatible trace elements and Sr, Nd, Ce and Pb isotopes (e.g. Thompson *et al.* 1982, 1986). This range has previously been attributed to a combination of varying degrees of mantle fusion and varying amounts of crustal contamination. Those basalts of the Province which show little geochemical evidence of crustal assimilation are relatively depleted in incompatible trace elements, when compared to other basalts erupted in continental settings, e.g. the Snake River Plain, western USA (Fig. 1). The reason for this depletion is probably because most of the enriched small-fraction-melt had already been extracted by magmatism associated with minor extension during the Permian and Carboniferous (Morrison *et al.* 1980). It was not therefore widely available as a potential input to the British Tertiary Igneous Province magmas, unlike many of the basalts in the western USA, which have a geochemical signature of an enriched lithospheric component (Fitton *et al.* 1991; Gibson *et al.* 1991; Fig. 1).

In the Hebrides, the youngest pre-Tertiary, low-temperature, small-volume, melts are preserved as a series of Permo-Carboniferous, lamprophyric dykes (mostly camptonites and monchiquites) in western Scotland (Morrison *et al.* 1987; Baxter 1987). These dykes are relatively enriched in incompatible trace elements, such as Ba, Rb, K, Nb and the LREE, when compared with Tertiary lavas (e.g. L1 in Table 1). Thompson & Morrison (1988) proposed that the Permo-Carboniferous melts had been extracted from the uppermost asthenosphere, and that some of this depleted, residual material subsequently became coupled to the overlying lithosphere, which had been thinned by the extension associated with the Permo-Carboniferous magmatic event. Subsequent convective overturn of this region would be very slow, due to the predominance of conductive heat transfer processes and so it could retain a depleted geochemical signature over significant periods of time. The Tertiary magmas were probably derived through heating by the plume and decompression melting at the base of this depleted lithosphere.

The Mull lava succession

The Isle of Mull (Fig. 2b) represents the eroded basal remnant of one of the British Tertiary Igneous Province volcanoes. The earliest manifestation of igneous activity, the

UNIV DURHAM

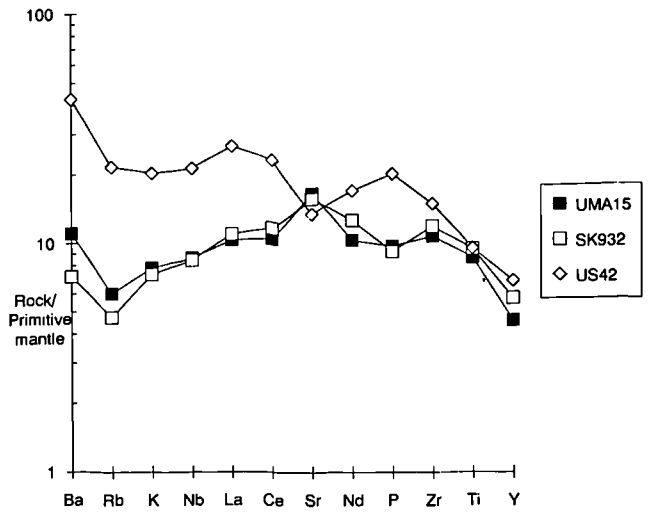


Fig. 1. Multi-element variation diagram normalized to the primitive mantle of Sun & McDonough (1989). UMA15, an average of 15 Mull basalts, which lack geochemical evidence for crustal contamination. (Kerr unpublished data). SK932, an uncontaminated basalt from Skye (Thompson *et al.* 1982). US42, basalt from the Snake River Plain, western USA (Thompson *et al.* 1983).

lava flows, today cover an area of over 900 km^2 and attain a maximum thickness of approximately 1000 m, on the highest peak on the island, Ben More. Intruded into these lava flows is a central complex comprising a wide variety of igneous rocks.

The excellent exposure on Mull has enabled extensive flow-by-flow sampling of this lava succession, from the coast to 1000 m above sea level. The hydrothermal alteration of lava flows associated with central intrusive complexes is a well-known phenomenon, and Mull is no exception. A study of the amygdale mineral assemblage by Walker (1970) revealed the presence of alteration zones grading outwards with decreasing intensity, from greenschist-facies alteration, close to the central complex (Fig. 2b), to lower grade zeolite-facies alteration, in the western coastal regions of the island. A further study on the Mull basalts (Morrison 1978, 1979) focused attention on the mobility of elements, both at lower and higher grades of alteration. The chief conclusions of this study were that most elements were relatively 'immobile' at low zeolite-facies grades, but at higher grades of alteration only Ti, Zr, Y, P, Nb and the REE were effectively 'immobile'. In accordance with the suggestions of Morrison (1979) samples have, where possible, been collected from the solid centres of flows and not the more altered vesicular margins.

New geochemical data (Kerr, unpublished) on 500 samples, have confirmed that previously published petrogenetic models for the Skye Main Lava Series (Thompson *et al.* 1982, 1986) can also be applied to the Mull Plateau Group. These models proposed that small amounts of crustal contamination were largely confined to the most Mg-rich (hottest) magmas during their turbulent ascent. The postulated contamination source was a fusible acidic fraction of lower crustal Lewisian material. This process of contamination is thought to have occurred in thin, poorly connected, dyke- and sill-like magma chambers, with high surface-to-volume ratios. The present work has shown that packets of flows with a distinctive chemistry (either contaminated or uncontaminated) interleave up the stratigraphic succession, thus supporting the idea of small unconnected magma chambers.

On Fig. 1 the average normalized incompatible element abundances for 15 uncontaminated Mull Plateau Group basalts is displayed along with the same data for SK932, a Skye Main Lava Series basalt which has been shown to be elementally and isotopically uncontaminated with continental crust or lithospheric mantle (Thompson *et al.* 1982). These two patterns are remarkably similar, strongly suggesting that Mull Plateau Group basalts with low levels of Ba, K and Rb are relatively free from a crustal input. Such a sequence of uncontaminated basalts (BM2-7), depleted in incompatible elements, has been found on the slopes of Ben More, within the lower third of the lava pile (Table 1, Figs 2b & 3). BM6 which occurs among these depleted and uncontaminated flows is nevertheless, relatively enriched in the incompatible trace elements (Fig. 3).

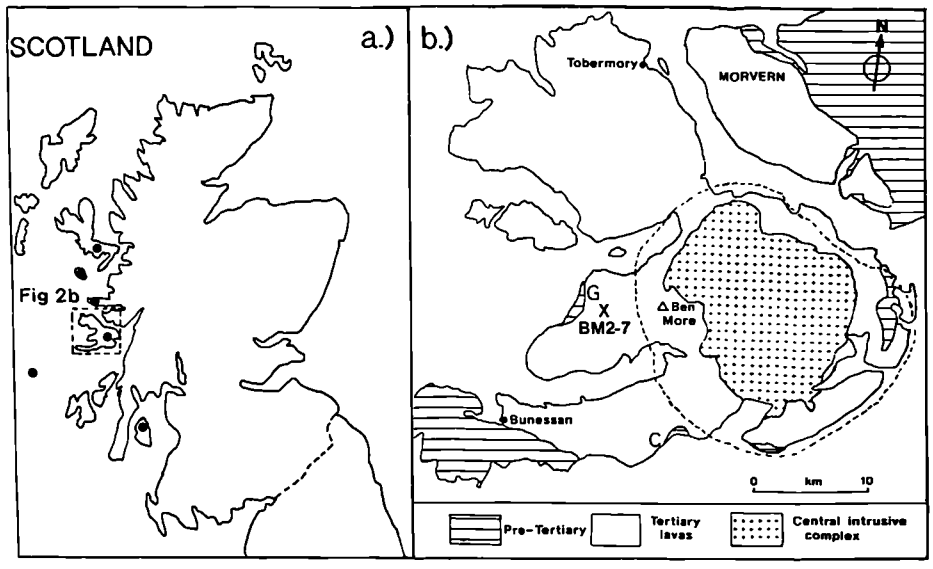


Fig. 2. (**a**) The location of the Isle of Mull and the Scottish Tertiary igneous centres (black circles). (**b**) The Mull lava field, showing the sample location of BM2-7 (**X**), The locations of the enriched flows at Gribun and Carsaig are denoted by **G** and **C** respectively. Note the outer limit of the central greenschist zone of alteration represented by the dashed line (Walker 1970).

Table 1. *Whole rock chemical analyses of some of the Mull lavas and potential contaminants*

	BM2	BM3	BM4	BM5	BM6	BM7	AM1	C2	L1	P-ave	T-ave
Major elements wt. %											
SiO_2	46.67	44.53	47.03	46.22	47.08	46.65	44.63	44.81	43.57	45.25	70.62
TiO_2	1.90	1.87	1.27	1.43	1.98	1.76	2.10	2.73	2.50	2.82	0.23
Al_2O_3	15.42	16.55	14.15	14.69	15.49	15.37	14.51	14.98	15.96	13.44	14.62
Fe_2O_3*	13.59	13.80	12.14	12.32	14.03	14.55	14.58	14.72	12.97	12.83	2.12
MnO	0.18	0.17	0.18	0.17	0.18	0.19	0.20	0.15	0.20	0.18	0.02
MgO	11.11	7.65	13.38	12.00	9.60	8.22	11.67	8.62	6.90	10.05	0.99
CaO	9.64	10.74	10.54	9.88	8.67	9.70	9.40	8.45	11.42	10.14	1.76
Na_2O	2.41	3.71	2.34	2.67	3.67	3.16	2.68	2.87	3.40	2.62	3.24
K_2O	0.18	0.21	0.21	0.25	0.39	0.28	0.37	0.62	1.88	1.76	5.51
P_2O_5	0.17	0.12	0.13	0.14	0.24	0.17	0.21	0.32	0.76	0.89	0.12
Total	101.01	99.78	101.29	100.24	101.78	100.05	100.37	98.28	99.56	99.99	99.21
LOI	3.76	7.51	3.31	4.25	2.62	3.98	2.14	5.32	4.31	6.37	0.76
Trace elements ppm											
Ba	72	74	100	98	138	128	161	233	817	815	2584
Cr	610	526	1017	794	479	47	357	282	48	389	27
Ga	20	21	18	19	19	20	20	20	19	—	16
Nb	6	6	5	5	8	5	8	10	62	51	4
Ni	291	244	389	345	225	104	305	159	86	225	15
Rb	3	3	5	5	9	4	9	8	48	42	103
Sc	26	35	31	26	23	28	30	19	22	23	4
Sr	294	305	287	306	426	383	313	434	1042	956	602
V	262	221	265	245	248	317	260	246	287	224	38
Y	22	19	18	18	20	20	32	28	28	28	4
Zr	123	115	83	96	150	112	139	171	204	224	45
La	5	6	4	5	9	5	12	36	44	50	13
Ce	15	20	12	15	22	19	25	23	85	101	22
Nd	14	16	10	12	17	15	18	14	40	50	11
La/Nb	0.83	1.00	0.8	1.00	1.10	1.00	1.5	3.6	0.70	0.98	3.25
$(La/Ce)_n$	0.68	0.78	0.86	0.86	1.06	0.68	1.24	0.96	1.34	1.28	1.53

Major element values recalculated to 100% on a volatile free basis.

* Total Fe determined as Fe_2O_3.

BM2–7, Mull lavas, lower slopes of Ben More (NM486317). AM1, the first lava from the base of the succession at Gribun (NM454328). C2, lava from near the base of the succession at Malcolms Point, near the Carsaig Arches (NM501187). L1, Permo-Carboniferous camptonite dyke, Morvern (NM782595). P-ave, average of Permo-Carboniferous dykes in western Scotland (Morrison *et al.* 1987; Baxter 1987) T-ave, average of 10 evolved Lewisian rocks, from the Isle of Tiree. $(La/Ce)_n$—normalized to the primitive mantle of Sun & McDonough (1989).

At Gribun at the base of the succession, 2 km north of the BM2-7 section, a series of eight flows exist which are all, like BM6, relatively enriched in the incompatible trace elements (Table 1). Five similarly enriched flows also occur, at the base of the succession at Carsaig (Fig. 2b). Nevertheless, this enrichment of the basal flows is by no means a universal feature of the Mull lava succession and in Morvern and north of Tobermory (two other places where the base of the succession is definitely exposed) no flows enriched in incompatible elements have been found. BM2-7 lie stratigraphically immediately above the enriched flows at Gribun and because BM6 is directly underlain by a primitive (high MgO) flow BM5, which shows little evidence of crustal contamination, the latter has been chosen as a starting point for modelling the composition of BM6. Table 1 shows representative analyses of the enriched flows at Gribun and Carsaig as well as BM2-7.

BM6 and the other enriched flows are not significantly petrographically different from BM2-7; most are fine-to-medium grained with variable quantities of well-formed olivine microphenocrysts. The groundmass consists principally of plagioclase and interstitial pale brown/lilac clinopyroxene, with smaller amounts of Fe/Ti oxides, olivine and secondary alteration products including zeolites and chlorite. The enriched flows show a tendency towards more lilac coloured clinopyroxene, which is undoubtedly a reflection of the higher bulk Ti content in these lavas.

Chemically, however these basalts are much more distinctive, and as has been noted above, contain higher levels of the incompatible trace elements (Table 1, Fig. 3). La/Ce ratios which have been normalized using the primitive mantle values of Sun & McDonough (1989) are also shown in Table 1. It can be seen that the incompatible element enriched flows have $(La/Ce)_n$ values >0.95, whereas BM2-5 & 7 have values <0.90. The major element compositions of the lava flows in Table 1 strongly suggest that the magmas last equilibrated at quite high pressures, and indeed the lavas plot close to the 9 kbar cotectic on the normative *di, hy, ol, ne* and *Q* diagram of Thompson (1982, Fig. 2).

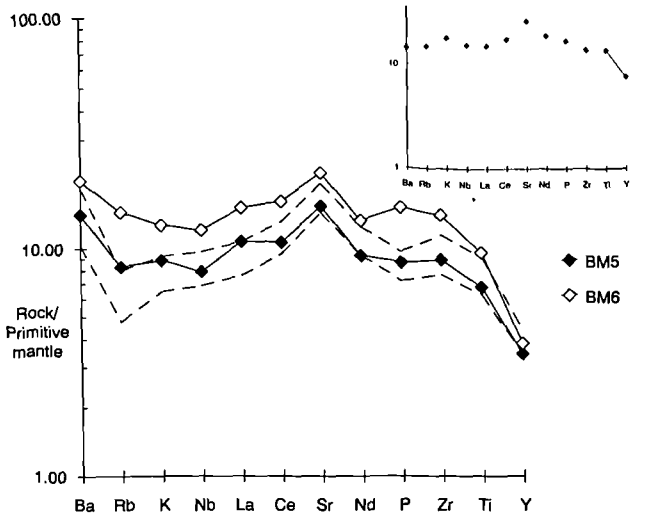


Fig. 3. Multi-element variation diagram showing the incompatible element enrichment of flow BM6. The area between the dotted lines represents the compositional range of BM2-5 & 7. The inset shows the incompatible element abundances for BM5 normalized using the values of Thompson (1982), which previous studies on the geochemistry of the BTIP have used. The two normalization patterns for BM5 are very similar, with the exception of Ba, a point which is discussed by Thompson (1982, appendix 1 and references therein).

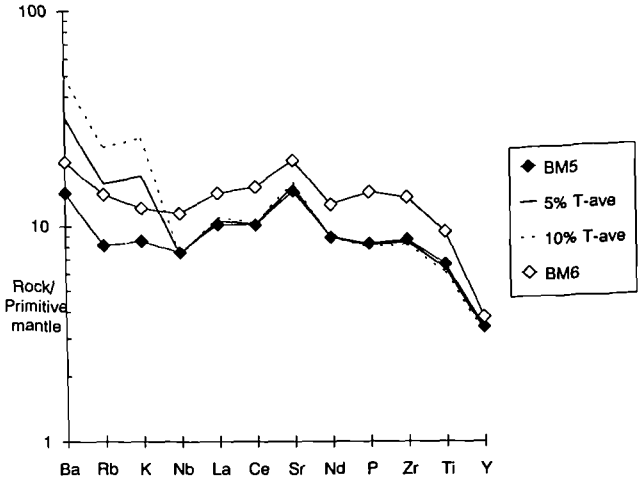


Fig. 4. Multi-element variation diagram showing the chemical effect of adding 5 & 10% lower crustal material (T-ave), to an uncontaminated lava, BM5 The enriched flow BM6 is shown for comparison

Discussion

Several possible reasons may be advanced in attempting to explain the relative enrichment of incompatible elements in flow BM6 and the other enriched flows;

Fractional crystallization

BM5, the flow below BM6, is slightly more primitive (higher MgO content) and obviously fractional crystallization must therefore be regarded as a contender to explain the relative enrichment of the latter. However, this process is rejected for two reasons. (1) Two other flows in the same succession, (BM3 & 7) are more evolved (lower MgO content) than BM6 and yet they contain lower levels of incompatible elements (Table 1; Fig. 3). (2) Petrogenetic modelling with the TRACE program (Nielsen 1988), using BM5 as a starting composition, requires 40% fractional crystallization of olivine, plagioclase and clinopyroxene to produce the observed relative enrichment of K, Ba and Nb in BM6. This calculated liquid composition contains under 7% MgO and less than 100 ppm Cr and Ni. It is therefore too evolved to represent flow BM6 and so fractional crystallization is dismissed as the *sole* cause of the observed enrichment.

Crustal contamination

Lewisian granulite and amphibolite facies rocks, which may be taken to represent the majority of the lower and upper crust beneath Mull (Thompson *et al.* 1986), have recently been collected from the Isle of Tiree, 30 km west of Mull. An average analysis of some of the more acidic samples (T-ave) is given in Table 1. Simple mixing of variable amounts of this crustal material with BM5, produces a multi-element variation pattern (Fig. 4) which, although it is enriched in Ba, Rb and K, has a pronounced Nb trough, unlike BM6 which has no significant trough at Nb. Moine schists form the uppermost crust beneath Mull and Thompson *et al.* (1986) have shown that the tholeiitic Staffa Type lavas, near the base of the lava succession, interacted with them. Addition of a Moine schist to BM5 has much the same effect on the incompatible element pattern as adding Lewisian crust.

This is further confirmed by incompatible element variation diagrams (e.g. Fig. 7) which suggest that, like the Skye Main Lava Series, some of the Mull Plateau Group lavas have suffered contamination by a small amount of acidic Lewisian crust. But BM6 does not plot towards this acidic crustal material and it is therefore highly improbable that the addition of crustal material is responsible for the relative enrichment in flow BM6.

Asthenospheric, OIB (Ocean Island Basalt)-like source

Thompson & Morrison (1988) reported that the youngest Tertiary dykes on Skye, the Beinn Dearg Mhor swarm, were enriched in the incompatible trace elements. The concentrations and ratios of incompatible elements in these dykes were found to be very similar to typical North Atlantic Ocean Island basalt (OIB) compositions. They postulated that the Tertiary Beinn Dearg Mhor dykes were derived chiefly from an asthenospheric (convecting mantle) OIB-like source, after extensive melting had stripped away a significant amount of the lithosphere during the earlier Tertiary magmatism. Therefore in the later stages of the evolution of the Skye igneous centre, asthenospheric magma batches were able to traverse the (by now) refractory lithospheric mantle, with little contamination.

With this in mind, it is possible to suggest that the enrichment of the Tertiary lava flows, at the base of the Mull lava succession, could be explained by invoking an asthenospheric source region for the magmas, similar to the postulated source for the Beinn Dearg Mhor dykes. Early batches of enriched asthenospheric melt could have passed through the lower lithospheric mantle, and suffered little contamination from it, simply because the lithosphere had not yet been warmed up by the massive influx of Tertiary magmas.

North Atlantic OIB and the Beinn Dearg Mhor dykes

have quite distinctive La/Nb ratios of <0.95, and one would therefore expect, that if the enriched Mull basalts had been derived from an OIB-like source, then they should have similar low La/Nb ratios. This is not the case and the enriched Mull flows have La/Nb >1.0 (Table 1). It would therefore seem highly unlikely that an enriched, asthenospheric, OIB-like source could have been the cause of the enriched flows at the base of the Mull Plateau Group.

Variable partial melting of the mantle

In an attempt to explain the slight variation of incompatible element abundances and ratios in primitive, uncontaminated Hebridean lavas, Morrison *et al.* (1980) proposed a model which involved varying degrees of mantle fusion. Thus, the possibility that the enrichment in flow BM6 is simply due to a smaller degree of mantle partial melting than BM2-5 & 7, should also be considered, and in this respect it is useful to look at $(La/Ce)_n$ ratios. The $(La/Ce)_n$ values for BM2-7 are given in Table 1 and, as was noted above, the enriched flows (AM1, C2 & BM6) have higher, (>0.95) $(La/Ce)_n$ values than the rest of the flows [$(La/Ce)_n < 0.9$]. Melt modelling (Fig. 5) shows that, in the calculated liquids, this normalized incompatible element ratio hardly changes above 1–2% partial melting of a spinel peridotite. Nevertheless, below 1–2% partial melting $(La/Ce)_n$ increases dramatically.

Therefore such a change in the ratios of two highly incompatible elements, such as La and Ce, which is observed between BM5 and BM6, cannot be produced by a slight variation in the amount of melting, with moderate degrees (2–5%) of mantle fusion. But a possible way to explain this increase in $(La/Ce)_n$, is to invoke the addition of a small-fraction-melt (<2% melting), to a lava such as BM5.

Contamination by an enriched small-degree-melt fraction

Much of the small-degree, low-temperature melt fraction, had probably been extracted from the uppermost asthenosphere below Mull, in the Permo-Carboniferous. As has been noted above, some of this depleted residuum became coupled to the base of the thinned lithosphere at the end of the Permo-Carboniferous magmatic event and ultimately became a major source region for the Tertiary magmas. But a small proportion of the enriched Permo-Carboniferous melt probably remained frozen within the upper lithospheric mantle, perhaps in localized, disseminated pockets. Support for this contention is provided by the work of Morrison *et al.* (1987) who suggested that few of the Permo-Carboniferous dykes fed surface lava fields, and that significant volumes may have been frozen within the lower crust and upper lithospheric mantle.

The massive influx of Tertiary magmas into the upper lithosphere could have remobilized this enriched material and led to its incorporation into some of the Tertiary magmas. One would predict that such occurrences would be quite rare and restricted to some of the earliest lava flows, due to the extraction of most of the enriched melt in the Permo-Carboniferous.

A Permo-Carboniferous camptonite dyke (L1) from Morvern has been analysed and its chemical composition compares favourably with an average of previously analysed Permo-Carboniferous dykes, (Table 1; Morrison *et al.* 1987; Baxter 1987). These dykes represent the closest approximation to the small-melt fraction [$(La/Ce)_n$ - 1.34] sparsely available within the Tertiary lithospheric mantle below the Hebrides. When 5–10% of L1 are added to BM5 (Fig. 6) the multi-element variation pattern of BM6 can be reproduced for most of the elements.

The disagreement between the observed and modelled values for Ti, Zr and P may cause slight concern, but elsewhere in the world these elements are highly variable in rocks of lamprophyric composition (Rock 1991). Baxter (1987) has shown that the Permo-Carboniferous lamprophyre dykes of Scotland are no exception and have incompatible element values which are extremely erratic, and he attributed this to a localized hetrogeneity of the Permo-Carboniferous mantle. Thus the mismatch between modelled and observed values probably reflects some local heterogeneity and this is clearly demonstrated in Fig. 7,

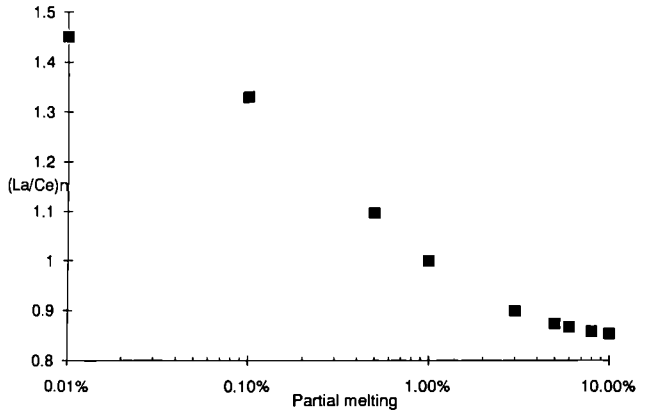


Fig. 5. Modelled $(La/Ce)_n$ values at varying degrees of non-modal batch melting of MORB-source spinel lherzolite. Note the relatively constant values of $(La/Ce)_n$ above 1–2% melting, in contrast to the elevated values at lower degrees of partial melting. Spinel lherzolite phase compositions, elemental abundances, melting proportions and partition coefficients used in the calculations are taken from Kostopoulos & James (1992). $(La/Ce)_n$—normalized as in Table 1.

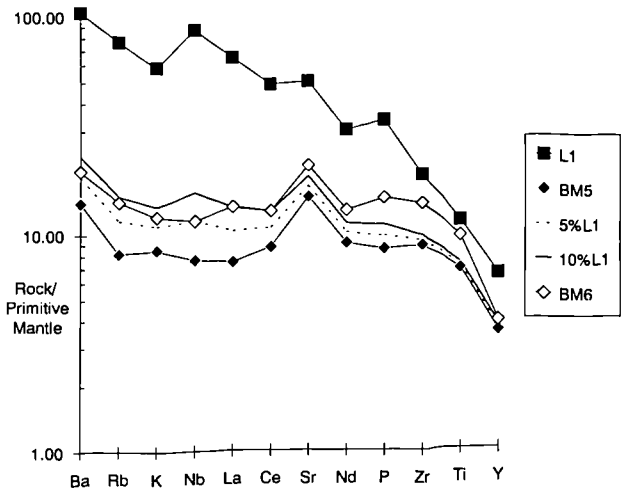


Fig. 6. Multi-element variation diagram to show how adding 5–10% of an enriched component, L1, to BM5 can reproduce the pattern of the enriched lava BM6 for most elements. The mismatch for P, Ti and Zr is discussed in the text.

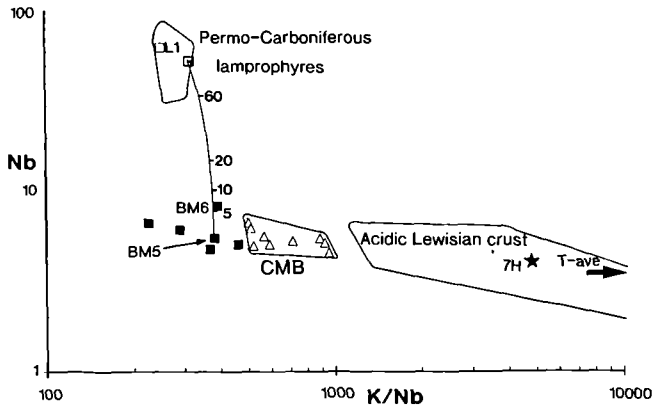


Fig. 7. Nb v. K/Nb, showing a mixing line between BM5 and an average Permo-Carboniferous lamprophyre, P-ave. The ticks on the mixing line represent the addition of 5, 10, 20, and 60%. BM5 needs addition of 5–10% lamprophyre to produce the composition of BM6. The fields for Permo-Carboniferous lamprophyres, (Morrison *et al.* 1987; Baxter 1987) and acidic Lewisian crust, (Weaver & Tarney 1980, 1981) are shown along with crustally contaminated Mull basalts (CMB) (open triangles) (Kerr unpublished data), the solid squares represent BM2-7. L1 is discussed in the text, 7H from Thompson *et al.* (1982).

which shows a wide range of compositions for Permo-Carboniferous dykes from NW Scotland. Therefore the enriched material available for sampling at the surface may not necessarily be an exact representation of the enriched melt fraction available either (a) at depth and/or (b) in the Tertiary period. The variability of the small-fraction-melt contaminant is borne out by the incompatible element variations of the three enriched lavas in Table 1, which come from two different localities 20 km apart.

The mixing line on Fig. 7 clearly shows that the addition of 5–10% variably enriched Permo-Carboniferous melt to flow BM5 can produce the observed relative enrichment of flow BM6 but, for the reasons outlined above, it is difficult to quantify precisely the amount of enriched fraction involved.

It is also important to consider the possible magmatic processes involved in the incorporation of an enriched melt fraction into a Tertiary basalt. First of all, it is the hottest and thus most primitive magmas which have the greatest chance of assimilating fusible material, whether from the crust or the lithospheric mantle. The lavas BM2-7 are, however, all relatively primitive (8–13% MgO) and yet they show little evidence for a crustal input. This strongly implies that any fractionation during uprise took place at sub-crustal levels, within the largely refractory lithosphere, probably just beneath the density discontinuity represented by the Moho (major element compositions also suggest that these magmas last equilibrated at approximately 9 kbar). This was followed by rapid ascent to the surface in thin cracks and fissures. Since these lavas are well within the bottom third of the succession, the crust would still have been quite cold when these magmas passed through them, thus minimising the role of crustal assimilation. (Primitive uncontaminated lavas have also been discovered near the base of the lava pile elsewhere on Mull).

It is envisaged that small localized concentrations of highly fusible, enriched melt material existed within the lithospheric mantle during the Tertiary. These small-scale concentrations may have been a remnant of the Permo-Carboniferous magmatic event or they may have accumulated subsequent to it; bleeding from the underlying asthenosphere. These frozen, enriched melt fractions would have been relatively easy to re-mobilize because (a) they probably took the form of thin dykes and veins which would require minimal heat to melt them and, (b) they contained a reasonably high volatile content, as is evidenced by the presence of abundant kaersutitic amphibole and biotite in the Permo-Carboniferous dykes. This would have lowered their solidus temperature, so making them much more fusible than the anhydrous parts of the lithospheric mantle.

The fact that an enriched lithospheric input to British Tertiary Igneous Province lavas has hitherto been unreported, in the published literature, is testament in itself to the scarcity of an enriched lithosphere beneath western Scotland during the Tertiary. Menzies *et al.* (1986, 1987) noted the occurrence of a Tertiary monchiquite dyke containing enriched mantle xenoliths, at Loch Roag, on the Isle of Lewis, over 150 km northwest of Mull. This isolated dyke cannot, however, be interpreted as evidence for the *widespread* existence of an enriched lithospheric mantle below western Scotland. The great weight of evidence from the British Tertiary Igneous Province as a whole, with its depleted basic igneous rocks, argues very strongly against the presence of such an enriched mantle. Rather, the Loch Roag dyke probably represents the remelting of a small pocket of an enriched, low-temperature, small-fraction-melt, similar to the proposed pockets of enriched material which contaminated the lower Mull basalts.

The Permo-Carboniferous dykes of western Scotland have mostly been 'dated' by their directional trends and distinctive lamprophyric geochemistry, with the Loch Roag dyke being the only noted example of a British Tertiary Igneous Province lamprophyre. Yet, in the western USA, where a small-melt input into basaltic magma has been proposed, the enriched lithospheric contaminants are associated with the same magmatic event as the lavas (Gibson *et al.* 1991). No Tertiary lamprophyre dykes have been found which cut the Mull lavas and this is hardly surprising since the enriched small-melt component would have been mobilized early in the magmatic event, when the lava field would not have been very thick or extensive. But the experience of other lava fields suggests that Tertiary lamprophyre dykes should exist and dating of the assumed Permo-Carboniferous dykes of western Scotland may well reveal that some of them are of Tertiary age.

It is also worth noting that the proposed lithospheric contaminant of the Mull lavas is of a sodic composition, whereas the enriched lithospheric contaminants invoked by Gibson *et al.* (1991) and Ellam & Cox (1991) are of an ultra-potassic nature. The exact reason for this difference is not clear but it may well reflect something of the past tectonic and magmatic history of western Scotland. The magmatism in the western USA has been strongly influenced by a relatively recent subduction event, but in western Scotland the most recent subduction appears to have been associated with the closure of the Iapetus ocean in the Silurian/Ordovician. The chemical difference therefore, would seem to be dependent on whether the small-fraction melt, migrating into the lithosphere from below, contained a subduction related component or not. The ten or so enriched basaltic flows discovered on Mull can be classified as belonging to a sub-type of the Mull Plateau Group. Three sub-types of the group have been identified; (1) basalts which are uncontaminated with either crust or a small-fraction, lithospheric melt; (2) basalts which contain a

significant crustal component; and (3) basalts which have been contaminated with a small-fraction-lithospheric melt.

Conclusions

(1) The anomalous enriched incompatible trace element signature of BM6, and the basal Mull Plateau Group basalts at Gribun and Carsaig, can be attributed to the interaction of a Tertiary magma batch with 5–10% of an enriched, low temperature, small-fraction-melt from the lithosphere.

(2) Most of the small-melt fraction seems to have been extracted by the Permo-Carboniferous magmatic event, but small pockets of enriched melt probably froze in the upper lithospheric mantle and, because of their low solidus temperatures, the earliest Tertiary lavas found them relatively easy to melt and to mix with.

(3) While small disseminated veins and pockets of fusible, enriched melt may have existed within the refractory, upper lithospheric mantle during the Tertiary, the great weight of evidence from the British Tertiary Igneous Province *does not support* the argument for a widespread enriched lithospheric mantle, below western Scotland during the Tertiary.

(4) The fact that the proposed small-melt-lithospheric contaminant in the Hebrides is of a sodic-alkaline nature, as opposed to potassic or ultra-potassic, may well be due to the absence of a subduction event in western Scotland since Ordovician times.

I would like to thank R.N. Thompson, S.A. Gibson, H. Emeleus and R. England for numerous discussions on the geology of the British Tertiary Igneous Province, and for invaluable comments on earlier drafts of this paper. Many thanks also go to R. Hardy for help with XRF procedures and J. Wills for assistance with the ICP-MS work at Royal Holloway. The financial support of the Dept. of Education for Northern Ireland, by way of a Postgraduate Research Studentship is gratefully acknowledged. The constructive and detailed comments of H. Downs and A. Morrison greatly improved the finished manuscript.

Analytical procedures

All the samples were crushed in a jaw crusher and powdered in an agate Tema mill. Both major and trace elements were determined by XRF techniques at the University of Durham, using commercially available Philips software. Major element analyses have been performed on fused glass discs, using lithium metaborate flux and ignited rock powder, whereas trace elements have been analysed on pressed powder pellets. Additionally Nb, Rb and REE have been analysed by ICP-MS at Royal Holloway and Bedford New College, after dissolution of the samples with a HNO_3 and HF mixture.

References

BAXTER, A. N. 1987. Petrochemistry of late Palaeozoic alkali lamprophyre dykes from N Scotland. *Transactions of the Royal Society of Edinburgh: Earth Sciences*, **77** (for 1986), 267–277.

ELLAM, R. M. & COX, K. G. 1991. An interpretation of Karoo picrite basalts in terms of interaction between asthenospheric magmas and mantle lithosphere. *Earth and Planetary Science Letters*, **105**, 330–342.

FITTON, J. G. , JAMES, D. & LEEMAN, W.P. 1991. Basic magmatism associated with late Cenozoic extension in the western United States: compositional variations in space and time. *Journal of Geophysical Research*, **96, B8**, 13693–13711.

GIBSON, S. A., THOMPSON, R.N., LEAT, P. T., MORRISON, M. A., HENDRY, G. L. & DICKIN, A. P. 1991. The Flat Tops Volcanic field 1. Lower Miocene open-system, multisource magmatism at Flander, Trappers Lake. *Journal of Geophysical Research*, **96, B8**, 13609–13627.

KOSTOPOULOS, D. K. & JAMES, S. D. 1992. Parameterization of the melting regime of the shallow upper mantle and the effects of variable lithospheric stretching on mantle modal stratification and trace-element concentrations in magmas. *Journal of Petrology*, **33**, 665–691.

MCKENZIE, D. P. 1989. Some remarks on the movement of small melt fractions in the mantle. *Earth and Planetary Science Letters*, **95**, 53–72.

MENZIES, M. A., HALLIDAY, A. N., HUNTER, R.H., MACINTYRE, R. M. & UPTON, B.G.J. 1986. The age, composition and significance of a xenolith-bearing monchiquite dyke, Lewis, Scotland. *Proceedings of the 4th International Kimberlite Conference, Vol. 2*. Geological Society of Australia, Special Publication, **14**, 843–852.

——, ——, PALACZ, Z., HUNTER, R.H., UPTON, B.G.J., ASPEN, P. & HAWKESWORTH, C. J. 1987. Evidence from mantle xenoliths for an enriched lithospheric keel under the outer Hebrides. *Nature*, **325**, 44–47.

MORRISON, M. A. 1978. The use of 'immobile' trace elements to distinguish the palaeotectonic affinities of metabasalts: applications to the Palaeocene basalts of Mull and Skye, NW Scotland. *Earth and Planetary Science Letters*, **39**, 407–416.

——. 1979. *Igneous and metamorphic geochemistry of Mull lavas*. PhD thesis University of London.

——, THOMPSON, R. N., GIBSON, I. L. & MARRINER, G. F. 1980. Lateral chemical heterogeneity in the Palaeocene upper mantle beneath the Hebrides. *Philosophical Transactions of the Royal Society; London*, **A297**, 229–244.

——, HENDRY, G. L. & LEAT, P. T. 1987. Regional and tectonic implications of parallel Caledonian and Permo-Carboniferous lamprophyre dyke swarms from Lismore, Ardgour. *Transactions of the Royal Society of Edinburgh: Earth Sciences*, **77** (for 1986), 279–288.

NIELSEN, R.L. 1988. A model for the simulation of combined major and trace element liquid lines of descent. *Geochimica et Cosmochimica Acta*, **52**, 27–38.

ROCK, N.M.S. 1991. *Lamprophyres*. Blackie, Glasgow.

SUN, S.-S & MCDONOUGH, W. F. 1989. Chemical and isotopic systematics of oceanic basalts: implications for mantle compositions and processes. *In*: SAUNDERS, A.D. & NORRY, M.J., (eds) *Magmatism in the Ocean Basins*, Geological Society, London, Special Publication, **42**, 313–345.

THOMPSON, R. N. 1982. Magmatism of the British Tertiary Volcanic Province. *Scottish Journal of Geology*, **18**, 49–107.

—— & GIBSON, S. A. 1991. Subcontinental mantle plumes, hot spots and pre-existing thin spots. *Journal of the Geological Society, London*, **148**, 973–977.

—— & MORRISON, M. A. 1988. Asthenospheric and lower-lithospheric mantle contributions to continental extentional magmatism: an example from the British Tertiary Province. *Chemical Geology*, **68**, 1–15.

——, DICKIN, A. P., GIBSON, I. L. & MORRISON, M.A. 1982. Elemental fingerprints of isotopic contamination of Hebridean Palaeocene mantle derived magmas by Archean sial. *Contributions to Mineralogy and Petrology*, **79**, 159–168.

——, MORRISON, M. A., DICKIN, A. P. & HENDRY, G. L. 1983. Continental flood basalts ... Arachnids rule OK? *In*: HAWKESWORTH, C. J. & NORRY, M. J. (eds) *Continental Basalts and Mantle Xenoliths*, Shiva Publishing, 158–185.

—— ——, ——, GIBSON, I. L. & HARMON, R. S. 1986. Two contrasting styles of interaction between basic magmas and continental crust in the British Tertiary Volcanic Province. *Journal of Geophysical Research*, **91, B6**, 5985–5995.

WALKER, G. P. L. 1970. The distribution of amygdale minerals in Mull and Morvern (western Scotland). *In*: MURTY, T. V. V. G. R. K. & RAO, S. S. (eds) *Studies in Earth Sciences (West Commemoration Volume)*, Univ. Saugar.

WEAVER, B. L. & TARNEY, J. 1980. Rare earth geochemistry of Lewisian granulite facies gneisses, NW Scotland: Implications for the petrogenesis of Archean lower continental crust. *Earth and Planetary Science Letters*, **51**, 279–286.

—— & —— 1981. Lewisian gneiss geochemistry and Archean crustal development models. *Earth and Planetary Science Letters*, **55**, 171–180.

WHITE, R. S. 1988. A hot-spot model for early Tertiary volcanism in the North Atlantic. *In*: MORTON, A. C. AND PARSON, L. M. (eds) *Early Tertiary Volcanism and the Opening of the NE Atlantic*. Geological Society, London, Special Publication, **39**, 3–13.

Received 20 July 1992; revised typescript accepted 2 November 1992.

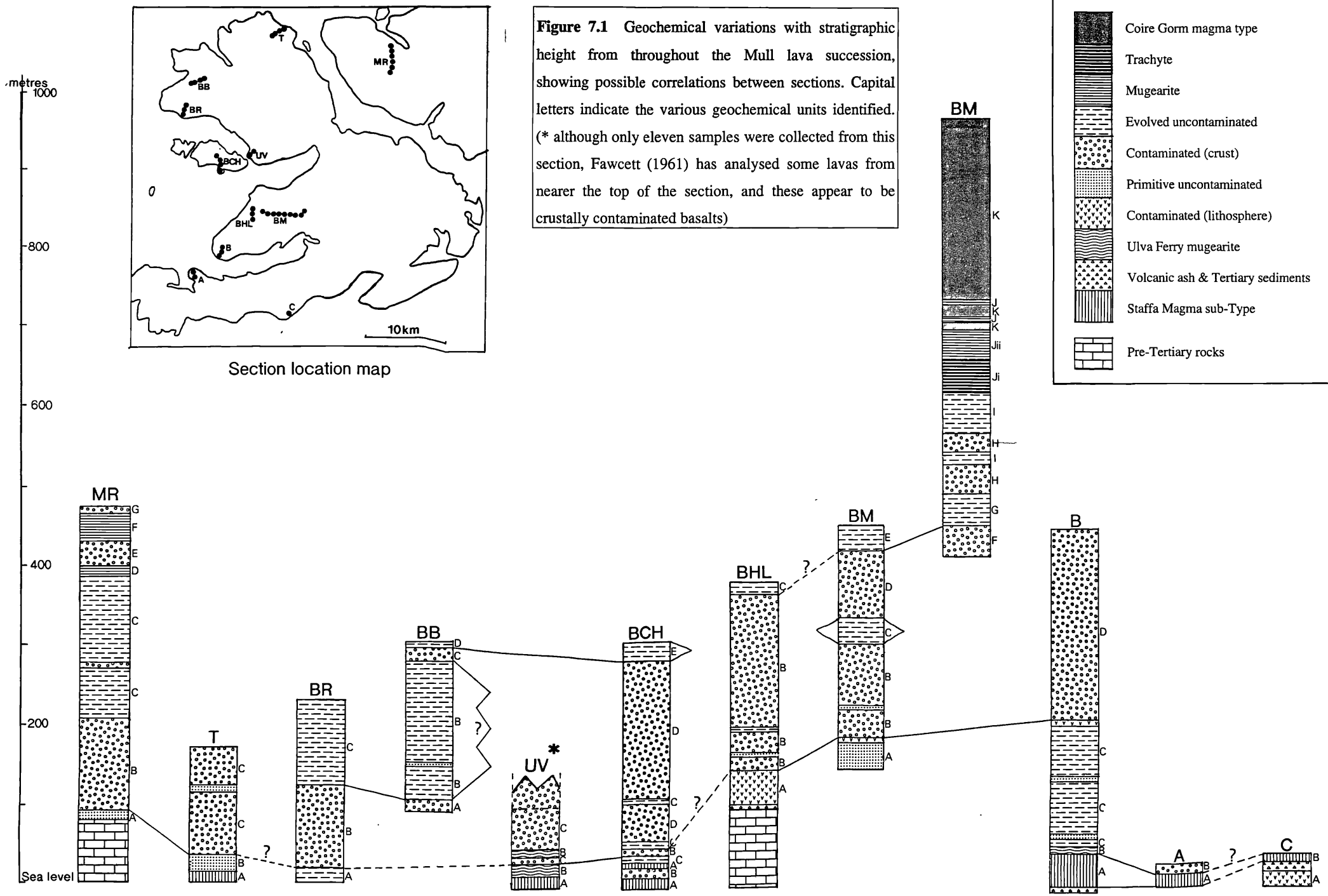


Figure 7.1 Geochemical variations with stratigraphic height from throughout the Mull lava succession, showing possible correlations between sections. Capital letters indicate the various geochemical units identified. (* although only eleven samples were collected from this section, Fawcett (1961) has analysed some lavas from nearer the top of the section, and these appear to be crustally contaminated basalts)